

ELECTRO-OPTICAL SYSTEMS, INC.

A Subsidiary of Xerox Corporation
300 N. Halstead Street, Pasadena, California

N66 27243

(ACCESSION NUMBER)

371

(PAGES)

OP-75370

(NASA CR OR TMX OR AD NUMBER)

(THRU)

1

(CODE)

03

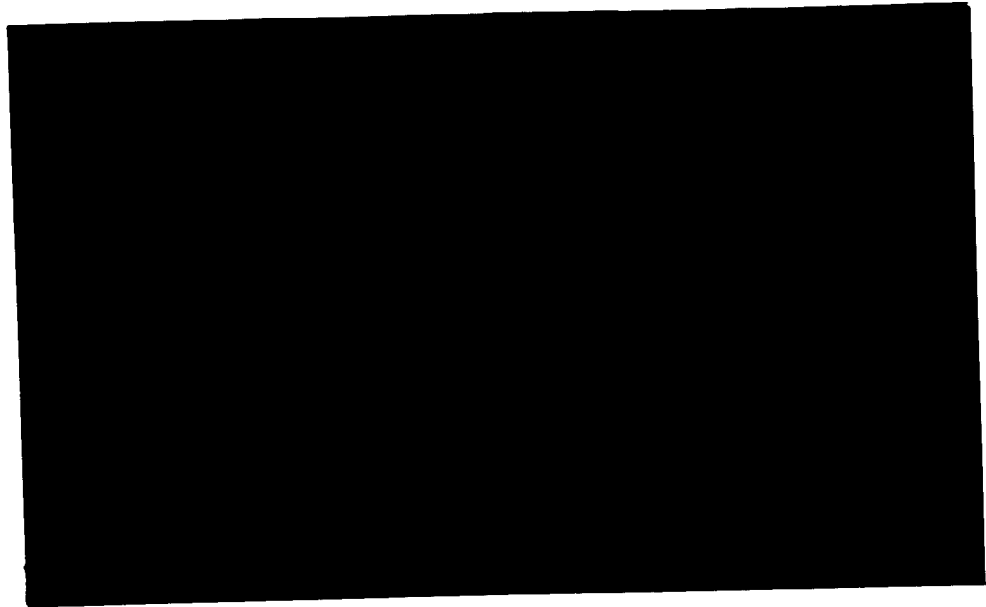
(CATEGORY)

GPO PRICE \$ _____

CFSTI PRICE(S) \$ _____

Hard copy (HC) 7.00

Microfiche (MF) 2.00



Interim Design Report

DEVELOPMENT OF LIGHTWEIGHT RIGID SOLAR PANEL

Prepared for
NASA Headquarters
Office of Advanced Research & Technology
Office of Solar & Chemical Power Systems

Contract NAS7-428

EOS Report 7027-IDR

18 May 1966

Prepared by Staff

Approved by



W. Menetrey, Manager
Power Systems Division

ELECTRO-OPTICAL SYSTEMS, INC. - PASADENA, CALIFORNIA
A Subsidiary of Xerox Corporation

ABSTRACT

This document is the Interim Design Report for Contract NAS7-428, entitled "Development of Lightweight, Rigid Solar Panels". The contract is between NASA Headquarters, Office of Advanced Research and Technology, Office of Solar and Chemical Power Systems and Electro-Optical Systems, Inc. This Interim Report is a summary of the work accomplished during the first four months of a ten-month contract with an effective starting date of 1 January 1966.

This document will be followed by a Final Report to be released on 1 December 1966.

The final solar array studied in this program will use an aluminum alloyed electroformed substrate and a beryllium frame using technology which is being developed at present under separate contracts. Solar array design is based on the use of a 4-mil silicon solar cell with an air mass zero efficiency of 9.6 percent at 28°C; this efficiency has been demonstrated in several cases.

A 10.4 kW array has been designed which will fit within an Atlas/Centaur shroud and will provide power on a Jupiter flyby mission. Array equilibrium temperature ranges from +145°C at 0.6 AU to -128°C at 5.2 AU. Voltage output at earth is 100V nominal. The specific weight of the array, using aluminum alloy electroforming and beryllium frames, is 27.4 lb/kW based on power output at earth and including all mechanisms. The 10.4 kW array is self-deploying, using a series of spacecraft commands to release pyrotechnic devices.

The same array, using a nickel substrate and aluminum frame, would weigh 42.4 lb/kW using 3-mil cover glass on the solar cells. This weight includes all necessary adhesives, paint, mechanisms, cabling, and other items to make a complete solar array.

The basic objective of the program is to demonstrate the ability to fabricate and use large photovoltaic solar arrays with specific weight capability of 25 to 50 lb/kW. The primary design emphasis is being placed on structures and mechanisms, as these areas are most critical in producing large weight reductions. The array concepts studied in this program incorporate a completely rigid structure, in contrast to other arrays being studied which use semirigid or flexible solar cell support structures. Feasibility of the 25 to 50 lb/kW

array will be demonstrated by design analysis and a demonstration solar panel, approximately 25 sq ft, which will be subjected to Atlas/Centaur launch environmental tests. Much of the design analysis is summarized in this report.

The demonstration panel will use an electroformed nickel substrate supported by an aluminum frame. The substrate structure has a double curvature and uses a hollow core or honeycomb configuration. The electroforming process offers an advantage in being able to form thin gage material of integral metal structures into complex shapes. Silicon solar cells with thicknesses of 4 and 8 mils shall be used to demonstrate compatibility with the structure.

CONTENTS

1.	INTRODUCTION	1-1
1.1	Organization of Program Effort	1-1
1.2	Demonstration Panel Design Highlights	1-3
1.3	Program Objectives	1-4
1.4	Summary of Results	1-6
1.5	Conclusions	1-6
1.6	Activity Summary for Remainder of Program	1-8
2.	PROGRAM DESIGN CRITERIA AND REQUIREMENTS	2-1
2.1	Introduction	2-1
2.2	Definitions	2-2
2.3	Mission Assumptions	2-5
2.4	Spacecraft Envelope Requirements	2-5
2.5	Solar Array Structural and Environmental Design Criteria	2-7
2.5.1	Ground Handling	2-7
2.5.2	Launch Configuration	2-7
2.5.3	Deployed Configuration	2-12
2.5.4	Cruise Array Dynamic Characteristics	2-12
2.6	Material Selection Criteria	2-12
2.6.1	Simulated Environments	2-12
2.6.2	Structural Materials Criteria	2-13
2.6.3	Adhesive Criteria	2-13
2.7	Electrical Power Criteria	2-14
2.7.1	Solar Cell Modules	2-15
2.7.2	Conductors	2-16
2.7.3	Conductor Insulation	2-17
2.7.4	Electrical Terminals	2-17

CONTENTS (contd)

2.7.5	Installation	2-18
2.7.6	Electroexplosive Devices	2-18
2.7.7	Electrical Connectors	2-18
2.8	Mechanism Restraints	2-19
2.8.1	Prelaunch and Launch Environments	2-19
2.8.2	Space Environments	2-20
2.8.3	Checkout	2-20
2.9	Reliability	2-20
2.9.1	Structural Reliability	2-20
2.9.2	Mechanical Reliability	2-21
2.9.3	Electrical Reliability	2-21
2.10	Interfaces	2-21
2.10.1	Structural Interfaces	2-21
2.10.2	Spacecraft Interfaces	2-22
3.	DEMONSTRATION PANEL AND SAMPLE PANEL DESCRIPTION	3-1
3.1	Hardware Item Descriptions	3-1
3.1.1	Demonstration Panel	3-1
3.1.2	Sample Panels	3-2
3.2	Demonstration Panel Details	3-2
3.3	Sample Panel and Specimen Details	3-4
4.	JUPITER FLYBY SOLAR ARRAY SYSTEM	4-1
4.1	Atlas/Centaur 10 kW Array	4-2
4.1.1	Structure	4-2
4.1.2	Electrical Layout	4-4
4.1.3	Mechanisms	4-5
4.1.4	Solar Array Weight & Power Predictions	4-8
4.2	Atlas/Agena 5 kW Array	4-8

CONTENTS (contd)

5.	COMMENTS ON COMPONENT STATUS	5-1
5.1	Solar Cells	5-1
5.2	General Properties of N-P Solar Cells	5-8
5.3	Projected Technology of Silicon Solar Cells	5-12
5.4	Cover Glass and its Effect on Cell Characteristics and Array Weight	5-16
5.4.1	General	5-16
5.4.2	Integrated Cover Glass	5-20
5.5	Solar Array Weight	5-22
6.	SOLAR ARRAY STRUCTURAL TRADE STUDIES	6-1
6.1	Selection of Array Packaged and Deployed Configuration	6-1
6.2	Comparison of Substrate Structure	6-11
6.2.1	Corrugated Sandwich Construction	6-11
6.2.2	Prestressed Tape Concept	6-14
6.2.3	Prestressed Diaphragm Concept	6-14
6.2.4	Honeycomb Construction	6-14
6.2.5	Biconvex Hollow Core	6-14
6.3	Hollow Core Design Optimization for Minimum Specific Weight	6-19
7.	DESIGN ANALYSIS	7-1
7.1	Weight Estimate of Demonstration Panel and 10.4 kW Array	7-1
7.1.1	Structural Assembly	7-1
7.1.2	Electroformed Nickel Substrate	7-5
7.1.3	Mechanical Assembly	7-5
7.1.4	Photovoltaic Assembly	7-5
7.2	Structure Stress and Dynamic Analysis	7-7
7.3	Panel Thermal Analysis	7-11
7.3.1	Thermal Considerations	7-11
7.3.2	Methods of Analysis	7-14
7.3.3	Characteristics of Hollow Core Structure	7-15

CONTENTS (contd)

7.3.4	Thermal Coatings	7-18
7.4	Solar Array Characteristics as a Function of Mission Trajectory	7-19
7.5	Solar-Electric Propulsion Power Conditioning	7-41
7.5.1	System Operational Modes	7-41
7.5.2	Power Conditioning Design Approach	7-45
7.6	Structural Material Evaluations	7-46
8.	MANUFACTURING OF THE DEMONSTRATION PANEL	8-1
8.1	Hollow Core Structure Development	8-2
8.2	Status of Program	8-4
9.	TESTS, TEST PLANS, AND DATA SUMMARY	9-1
9.1	Thermal Tests	9-1
9.1.1	Purpose	9-1
9.1.2	Apparatus	9-2
9.1.3	Procedure	9-2
9.2	Dynamic Tests	9-3
9.2.1	Modal Test of Substrate	9-3
9.2.2	Sinusoidal and Random Vibration Hard Mount Tests	9-3
9.3	Static Strength Tests	9-4
9.3.1	Buckling Tests of Hollow Core Substrate	9-4
9.4	Photovoltaic Tests	9-14
9.4.1	Solar Cell Grading	9-14
9.4.2	Solar Cell 3-Quadrant Characteristics Test	9-14
9.4.3	Low and High Intensity Solar Cell Tests	9-19
9.4.4	Low and High Temperature Solar Cell Tests	9-20
9.4.5	Demonstration and Sample Panel Electrical Tests	9-20
9.5	Material Tests	9-21
9.5.1	Tensile Test of Electroformed Nickel	9-21
9.5.2	Bonding of Thermal Control Paint, (RTV-60), and Dielectric Adhesive to Nickel and H-Film	9-21

CONTENTS (contd)

9.6	Electroforming	9-22
9.6.1	Phase I - Fabrication of Buckling Specimens	9-23
9.6.2	Phase II - Full-Scale Plating Tests	9-32
9.6.3	Phase III - Model Demonstration Panel	9-33
9.7	Structural Bond (Frame to Frame and Substrate to Clip Bracket)	9-33
APPENDIX A - MANUFACTURING PROCESS SPECIFICATION OUTLINES		
APPENDIX B - ANALYSIS OF STRUCTURAL CONCEPTS (TRADE STUDIES)		
APPENDIX C - STRUCTURAL ANALYSIS OF HOLLOW CORE SUBSTRATE		
APPENDIX D - EQUATION DERIVATIONS FOR STRUCTURAL ANALYSIS OF DEMONSTRATION PANEL		
APPENDIX E - DYNAMIC ANALYSIS AND EQUATION DERIVATIONS		
APPENDIX F - THERMAL ANALYSIS AND DERIVATIONS		
APPENDIX G - PROGRAM DRAWING LIST AND DETAIL DRAWINGS		

ILLUSTRATIONS

1-1	Typical Panel Structure	1-2
1-2	Program Objectives and Schedule	1-7
1-3	EOS Configuration 10 kW Solar Array Jupiter Flyby	1-9
2-1	Nomenclature Definition	2-3
2-2	Solar-Electric Mission, Jupiter Orbit, 1971 - 800 Days	2-6
2-3	Atlas/Centaur Nose Fairing - Surveyor	2-8
2-4	Atlas/Agena Shroud for Mariner IV	2-9
2-5	Atlas/Centaur, Atlas/Agena Acoustic Environment	2-11
3-1	Solar Panel Assembly, Demonstration	3-7
3-2	Substrate Assembly Demonstration Panel	3-9
3-3	Demonstration Panel Electrical Layout	3-11
3-4	Sample Solar Panel Assembly	3-13
4-1	Configuration of 10 kW Solar Panel for Jupiter Flyby	4-11
4-2	Mechanical Module Size	4-13
4-3	Packaging of Subpanel	4-15
4-4	EOS Configuration 10 kW Solar Array Jupiter Flyby	4-17
4-5	Electrical Module Layout for 10 kW Array	4-19
4-6	Stowed Configuration 10 kW Array	4-21
4-7	Solar Panel Deployment 10 kW Array	4-23
4-8	Assembly Stowed Configuration 10 kW Array	4-25
4-9	Stowed Configuration 5 kW Solar Array	4-27
4-10	Assembly Stowed Configuration with Band 10 kW Array	4-29
4-11	Pin Puller	4-31
4-12	Hinge - Spring-Damper Configuration 10 kW Array	4-33
5-1	Typical Conventional Solar Cell	5-2
5-2	Contact Variations of Silicon Solar Cells	5-4

ILLUSTRATIONS (contd)

5-3	Typical Wrap-Around Solar Cell	5-6
5-4	Typical N-P Cell, Relative Spectral Response	5-9
5-5	Spectrum Response, Typical N-P Cell	5-10
5-6	Typical E/I Curve Limits	5-11
5-7	Temperature Effects on Solar Cell Characteristics	5-13
5-8	Solar Cell Temperature Characteristics	5-14
5-9	Solar Cell Power Output Versus Temperature	5-17
5-10	Absorptivity Characteristics, Silicon Solar Cell	5-18
5-11	Absorptivity Characteristics, Cell with 6-mil Glass and Antireflectivity Coating	5-19
5-12	Solar Array Specific Weight History and Predictions	5-23
6-1	Array Studies 10 kW Array	6-3
6-2	Array Studies 10 kW Array	6-5
6-3	Assembly Stowed Configuration with Band 10 kW Array	6-9
6-4	Sketch of Panel Showing Corrugated Sandwich Construction	6-13
6-5	Prestressed Tape Concept	6-15
6-6	Prestressed Diaphragm Concept	6-16
6-7	Honeycomb Construction	6-17
6-8	Sketch Showing Biconvex Hollow Core Concept	6-18
6-9	Geometry Parameter Biconvex Substrate	6-20
6-10	Hollow Core Specific Weight vs Thickness (square pattern)	6-22
6-11	Hollow Core Specific Weight vs d/a Ratio (square pattern)	6-23
6-12	Hollow Core Specific Weight vs Width (square pattern)	6-24
6-13	Hollow Core Specific Weight vs Slope (square pattern)	6-25
6-14	Hollow Core Resonant First Mode Frequency (square pattern)	6-26
6-15	Hollow Core Critical Pressure and Inertia Load Pressure (square pattern)	6-27
6-16	Biconvex Hollow Core Solar Panels - Panel Structure Weight vs Panel Width	6-29
6-17	Hollow Core Specific Weight (slanted pattern) vs d/a Ratio and Skin Thickness	6-30
6-18	Hollow Core Land Dimension (slanted pattern) vs d/a Ratio and Skin Thickness	6-31

ILLUSTRATIONS (contd)

7-1	Solar Panel — Substrate-to-Frame Interconnection	7-10
7-2	Moulding, Proposed Cross Section	7-12
7-3	Moulding, Proposed Cross Section	7-13
7-4	Temperature Distribution of Hollow Core Substrate	7-16
7-5	Characteristic E/I Curve for Silicon Solar Cell	7-20
7-6	E/I Characteristics	7-21a
7-6	Power/Voltage Characteristics	7-21
7-7	E/I Characteristics	7-23a
7-7	Power/Voltage Characteristics	7-23
7-8	E/I Characteristics	7-25a
7-8	Power/Voltage Characteristics	7-25
7-9	E/I Characteristics	7-27a
7-9	Power/Voltage Characteristics	7-27
7-10	E/I Characteristics	7-29a
7-10	Power/Voltage Characteristics	7-29
7-11	E/I Characteristics	7-31a
7-11	Power/Voltage Characteristics	7-31
7-12	E/I Characteristics	7-33a
7-12	Power/Voltage Characteristics	7-33
7-13	E/I Characteristics	7-35a
7-13	Power/Voltage Characteristics	7-35
7-14	E/I Characteristics	7-37a
7-14	Power/Voltage Characteristics	7-37
7-15	E/I Characteristics	7-39a
7-15	Power/Voltage Characteristics	7-39
7-16	Power/Voltage Curve for Jupiter Flyby Solar Array	7-42
7-17	Thruster Parameter Input Power Profiles	7-43
7-18	Stress/Strain Curves for Electroplated Nickel	7-48
7-19	Tensile Characteristics of Various Thickness of Kapton H-Film and Fiber Glass	7-49
7-20	Thermal Characteristics 5-mil Fiber Glass and 1-mil Kapton H-Film	7-50

ILLUSTRATIONS (contd)

8-1	Aluminum Mandrel for Fabrication of Hollow Core Structure	8-1
8-2	Electroforming Setup - Hollow Core Structure	8-3
8-3	Substrate Construction - Hollow Core Structure	8-5
9-1	Buckling Test Sample Sketch and Critical Dimensions	9-6
9-2	Photo Showing Specimen Readied for Test	9-7
9-3	Instron Pressure Testing Machine	9-8
9-4	Sample Data Sheet	9-9
9-5	Load/Time Strain Relations - Typical Sample	9-10
9-6	Photo Showing Buckling of Specimen	9-13
9-7	Sample Solar Panel Assembly	9-15
9-8	Demonstration Panel Electrical Layout	9-17
9-9	Plating Mandrel - Hollow Core Sample	9-24
9-10	Plating Mandrel Hollow Core Samples for Pattern No. S-U-4	9-25
9-11	Plating Mandrel - Hollow Core Sample Pattern for Part No. S-C-4	9-26
9-12	Plating Mandrel - Hollow Core Samples Hex Pattern H-H-4	9-27
9-13	Plating Mandrel - Hollow Core Samples Hex Pattern H-H-8	9-28
9-14	Electroforming Bath Setup - Buckling Specimens	9-29
9-15	Nickel Hollow Core Structure After Cutting and Etching	9-30
9-16	Nickel Hollow Core Buckling Specimen Ready for Test	9-31

CONTRIBUTORS

<u>Name</u>	<u>Program Area</u>
J. (Al) Carlson	Structural Dynamics and Material Evaluation
S. A. Friedlander	Photovoltaics Analysis
R. N. Hanson	Electroforming Process and Fabrication
L. A. Inners	Structural Engineering Design
G. A. Jelley	Mechanisms Analysis
K. K. Knapp	Thermal Analysis
H. A. Kuitens	Mechanisms Engineering Design
R. L. Moore	Program Management
R. Osuna	Photovoltaics Design and Fabrication
B. A. Thorstensen	Structural Strength Analysis

1. INTRODUCTION

Under Contract NAS7-428, EOS intends to demonstrate the feasibility of producing lightweight, large-area photovoltaic arrays to be used as power sources for the Jupiter flyby mission and other electric propulsion deep-space probes. This demonstration will be accomplished in the latter phase of the contract by the design, assembly, and test of a representative cellular panel with a weight-to-power ratio of 25 to 50 lb/kW. Based on the individual panel capability, an entire array could be assembled (using similar panels as array sections) at the same overall weight-to-power ratio to provide 5 to 10 kW of electrical power in earth-space environments.

The panel design analysis tends to emphasize the use of a rigid curved-shell structure made of electroformed material in a unique hollow core configuration, as shown in Fig. 1-1. (This is in contrast to semi-rigid and flexible structures proposed by other studies in the past.) Very thin silicon photovoltaic cells, connected in series and parallel, are mounted on the rigid panel. This forms a power-source section with the required equivalent weight-to-power ratio of 25 to 50 lb/kW. The studies documented in this report have been based on use of Atlas/Agna or Atlas/Centaur combinations as ultimate launch vehicles for a complete solar array.

1.1 Organization of Program Effort

The program described herein is primarily development-oriented, and is subdivided into discrete tasks, defined as follows:

1. Task I - Perform tradeoff analyses and produce a solid, workable design for a representative photovoltaic cellular panel. (This interim report marks completion of this task.)

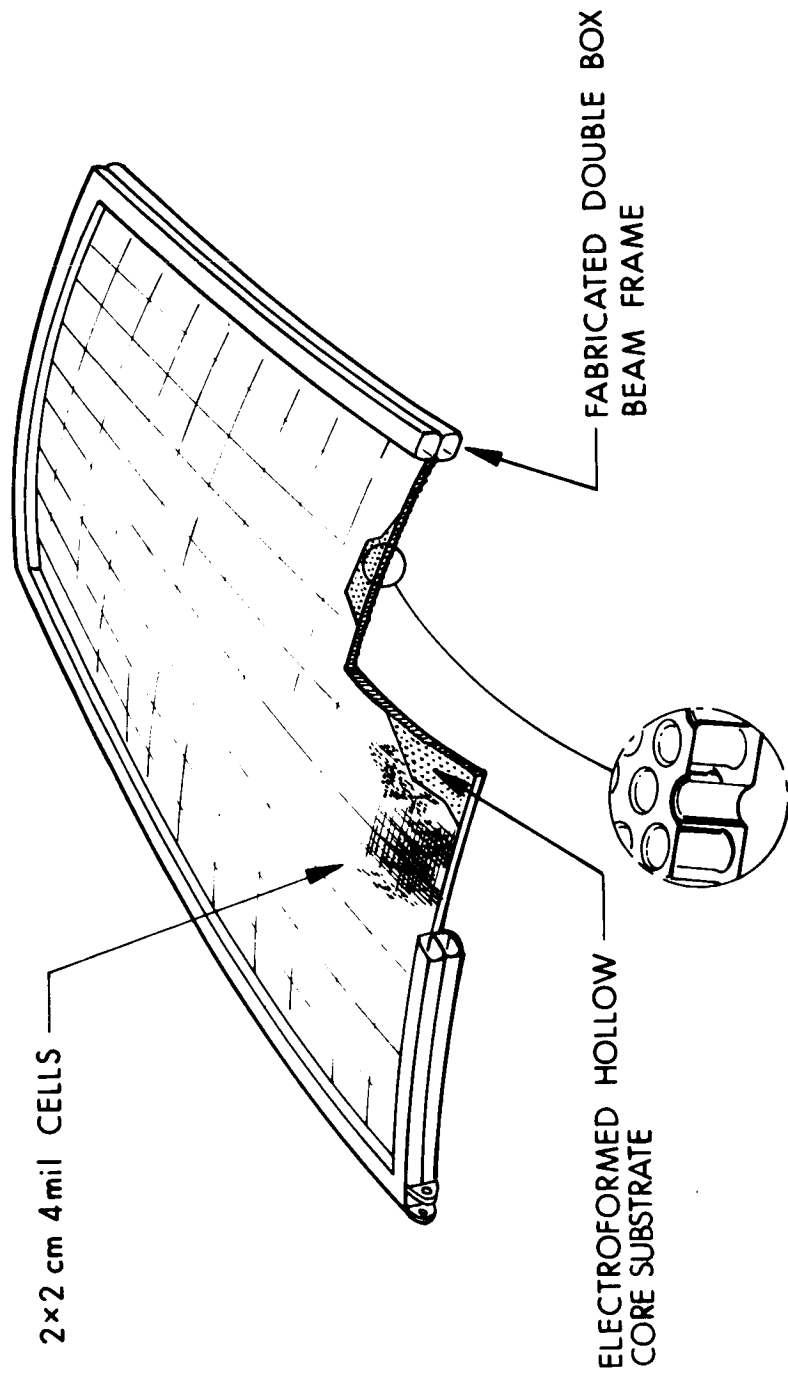


FIG. 1-1 TYPICAL PANEL STRUCTURE

2. Task II - Fabricate a demonstration panel model including assembly of structure, attachments, photovoltaic (or solar) cells, and filters (cover glass). (This task will be completed in the seventh month.)
3. Task III - Complete testing and evaluation of demonstration panel. Tests include thermal/vacuum, acoustics, shock and vibration, and performance demonstration. (These tests, defined in this report, will be completed during the ninth month.)
4. Task IV - Interpret data obtained from panel tests, and extrapolate design criteria for applicability to multikilowatt arrays.

1.2 Demonstration Panel Design Highlights

Fabrication of the demonstration panel commences during the fifth month of the contract; the completed panel will be available for the Task III test effort during the seventh month. Special panel design features are listed below.

1. Panel is constructed in a curved biconvex configuration with an area of approximately 25 sq ft. The all-metal structure employs electroformed nickel on a hollow core substrate with an aluminum frame.
2. Very thin (4 to 8 mils) lightweight silicon solar cells are used with a 3-mil cover glass.
3. Attachments are placed on the panel structure to simulate the holding mechanisms employed during launch and deployment of panel. These attachments will be used during the evaluation tests to simulate actual flight conditions.

The design of the demonstration panel and the feasibility study of the 5 to 10 kW arrays are predicted on the performance definition of 10 W/ft^2 (at 1 AU, AMO, and 55°C) for a 4-mil solar cell with a 1-mil integral cover glass. This defines the weight and power capabilities of the solar cell stack used in the analysis and design.

The effect of radiation degradation on the performance of cell and integral cover glass are not considered when calculating the solar array mission performance. The solar array is electrically rated for day one operation.

The majority of the contract effort is directed toward achieving extremely lightweight (specific weight of 0.1 to 0.2 lb/ft²) structure and mechanisms design. Consequently, detailed trades were not accomplished in panel electrical design. With the improvements made in performance because of higher production quantities and innovations in design (such as wrap-around contacts), the specific power value of 10 W/ft² is potentially achievable with 4-mil cells.

1.3 Program Objectives

The singular objective of the Task I effort was to produce a sound engineering design for a demonstration panel with a weight-to-power ratio which verifies the feasibility of a 25- to 50 lb/kW solar array for deep-space applications. (This design is presented in this report.)

The engineering design studies of the first task concentrated on variations of electroformed biconvex structures and the interaction of these structures with the solar cells. Trade studies included comparison of the rigid curved structure to flat panel configurations. The studies clearly indicated the superiority of the electroformed structure by virtue of its high stiffness-to-weight ratio (allowing 1- to 2-mil skin thicknesses in a one-piece metal structure).

Parameters which were varied in the studies for design of the 25 to 50 lb/kW array include degree of curvature, edge constraints, attachment points, skin thicknesses, hole size (for hollow core structure), input loads, and cell stack weight.

The major steps of Task II (demonstration panel fabrication effort) are:

1. Tooling design
2. Fabrication of the structure
3. Cell and filter procurement and submodule preparation
4. Panel assembly

The objectives of Task III are to define test requirements and conduct necessary engineering tests to prove compliance of the panel with the program design goals. Major steps for this task are:

1. Test equipment preparation
2. Definition, preparation, and conduction of performance tests
3. Formulation and conduction of thermal/vacuum, vibration, acoustic, and other environmental tests

The objectives of Task IV are to summarize program results and to submit recommendations for a follow-on development effort.

Major steps of Task IV are:

1. Interpretation of test results and correlation of data to relate results to Task I analysis.
2. Provide recommendations for design, fabrication, and test of a 5 to 10 kW array (or portion thereof). Documentation includes a breakdown of tasks in a logical sequence of design effort, component development, and tests necessary to develop an array structure, schedule, cost milestone, and a plan for ground support equipment and related test requirements.
3. Preparation and submittal of a summary of characteristics for a 5 to 10 kW array, including data gleaned from studies of weight/mass/power tradeoffs, reliability, redundancy requirements, reparability and maintenance, and electrical design.

An overview of the program is presented in the schedule of Fig. 1-2, which shows major objectives, tasks, documentation requirements, and reviews, as well as projected completion dates.

1.4 Summary of Results

The engineering analysis of Task I has resulted in:

1. The design of the demonstration panel. The panel contains an electroformed nickel hollow core substrate and an aluminum frame.
2. The design of a 10.4 kW array using the concepts of the demonstration panel to achieve a weight-to-power ratio of 42 lb/kW. Adoption of design modifications presented in the report will decrease the array weight-to-power ratio to 27 lb/kW. The structure for this design is an electroformed aluminum hollow core and a beryllium frame.
3. Testing of sample hollow core samples to verify the structural analysis.
4. Optimizing the technique for electroforming the hollow core substrate.

The array design (shown in Fig. 1-3) contains a two-quadrant panel arrangement with 8 subpanels per quadrant. The subpanels are nested in a box arrangement which is secured by pyrotechnic "pin puller" holding devices. For deployment, the spring-loaded hinges are released by a special command sequence. Deployment is completed by engagement of the frame latches shown.

1.5 Conclusions

The specific result of this contract effort is the fabrication, assembly, and test of the lightweight biconvex hollow core structure and thin solar cells. The subpanel will be measured to show that it meets certain minimum weight values and through analysis will show an electrical output for standard conditions. The assembled demonstration panel is to be subjected to specified environmental tests; these will confirm:

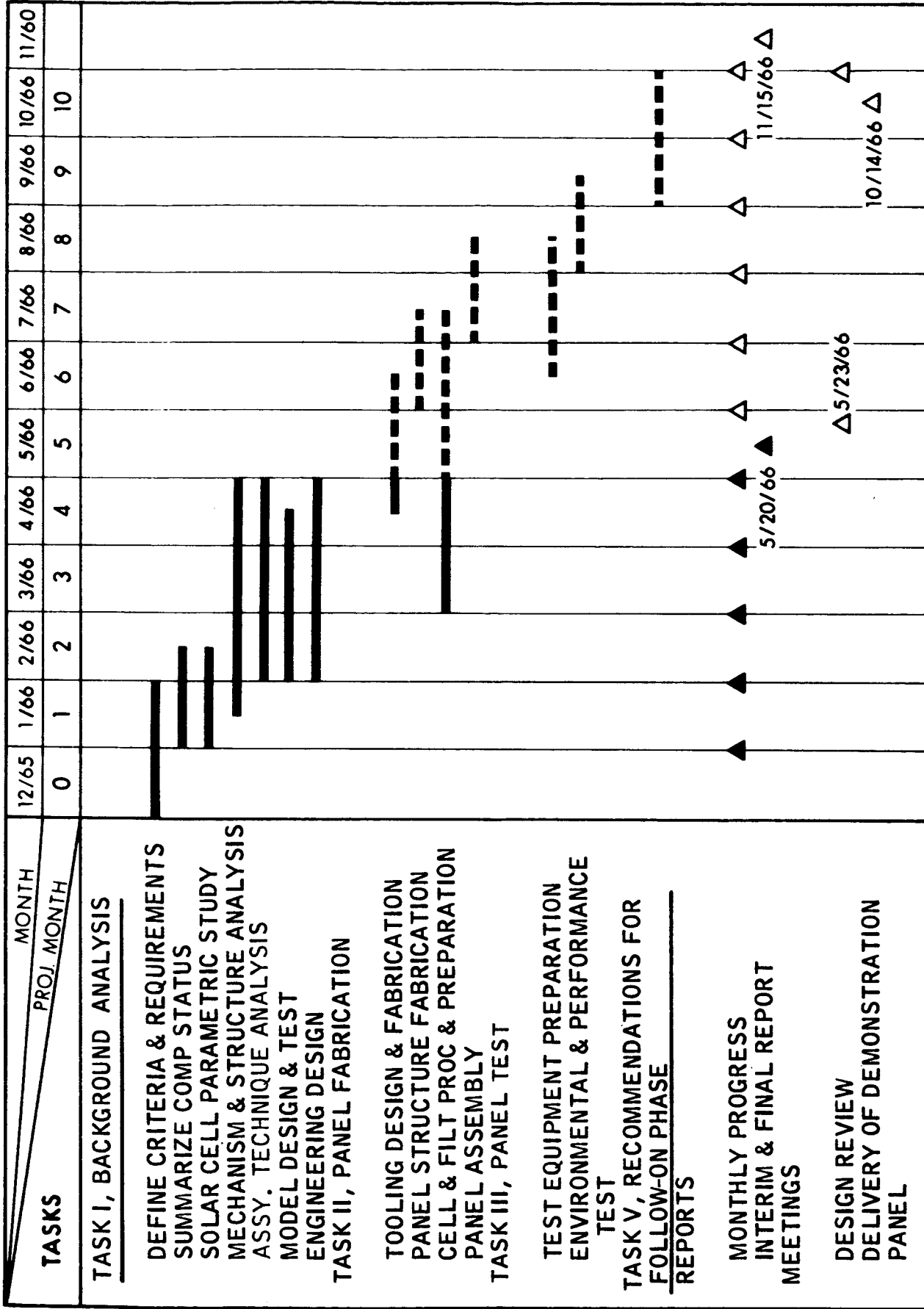
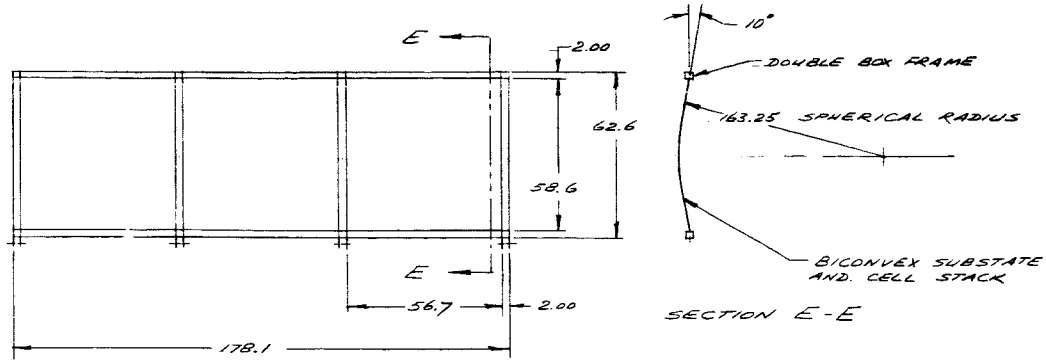


FIG. 1-2 PROGRAM OBJECTIVES AND SCHEDULE

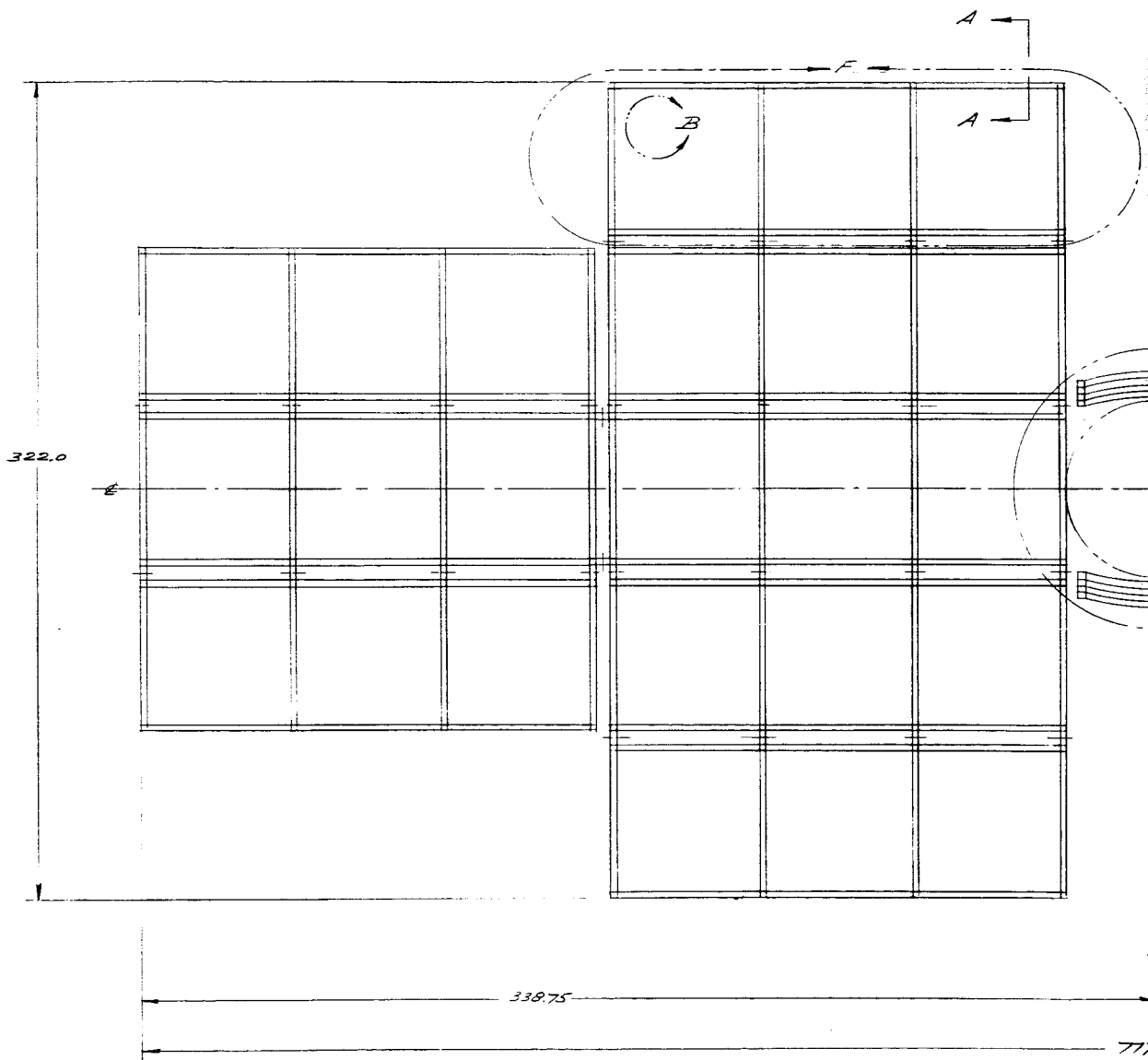
1. The structure is capable of supporting the design loads without failure.
2. The subpanel exhibits the frequency and stiffness requirements defined by the specification.
3. The structure and cells are compatible in thermal and dynamic environments.

1.6 Activity Summary for Remainder of Program

The activities for the remainder of the contract period are defined by Tasks II, III, and IV. Certain subtasks have already been started. The lead time requirements for the manufacture of the thin cells have dictated that they be ordered early in the program. Material and tooling preparation for the electroforming of the 25-sq-ft hollow core substrate has been initiated.

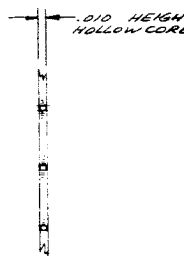
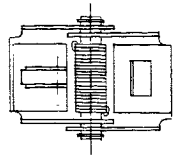
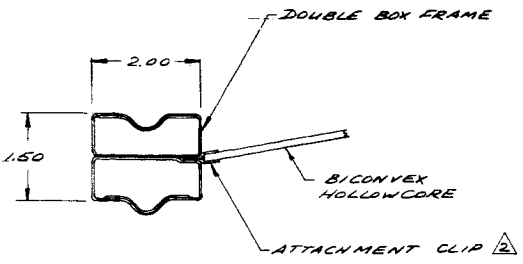


DETAIL F SUB PANEL CONFIGURATION

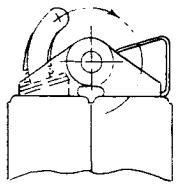


ARRAY CONFIGURATION Δ
 PANEL ASSEMBLY DEPLOYED

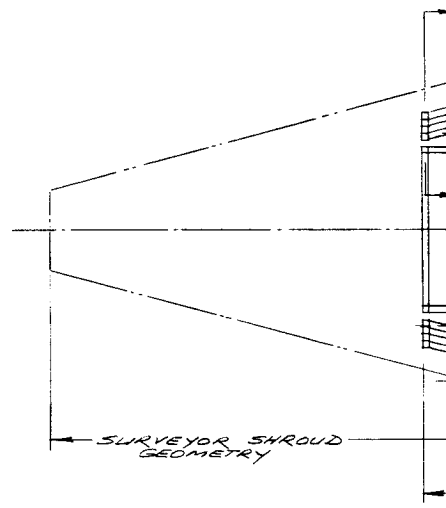
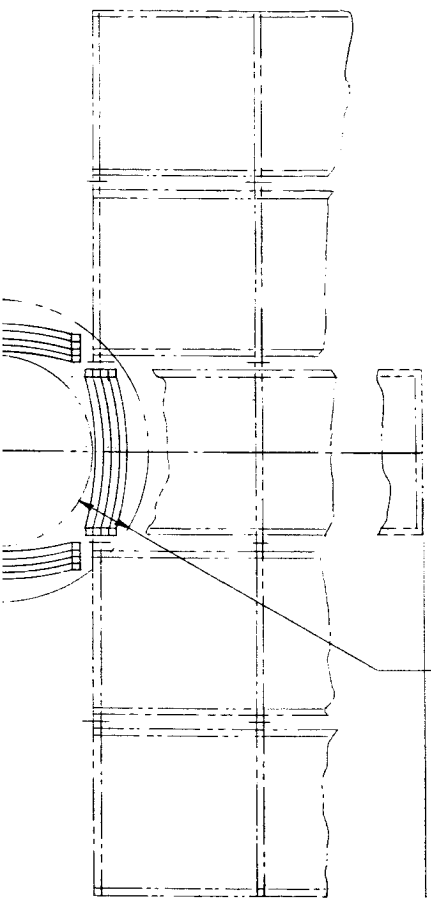
1-9 ①



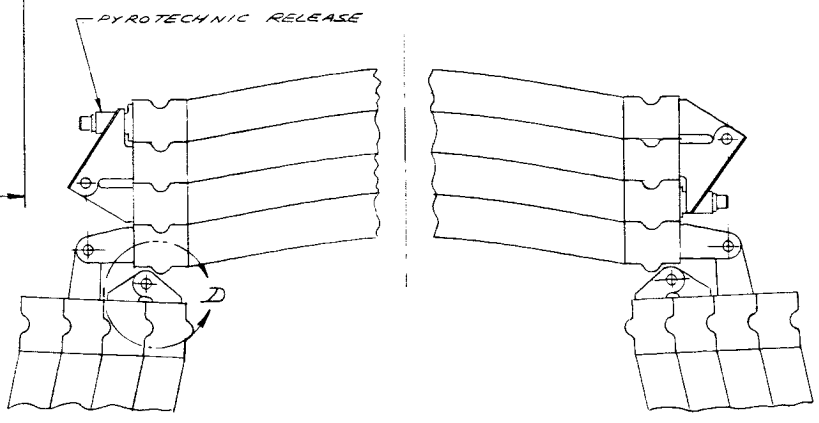
SECTION A-A
(TYPICAL FRAME CROSS SECTION.)



DETAIL D
TYPICAL HINGING

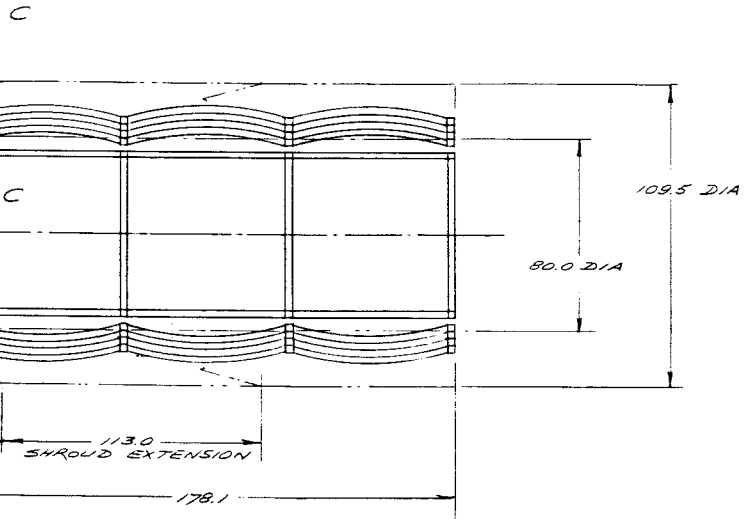
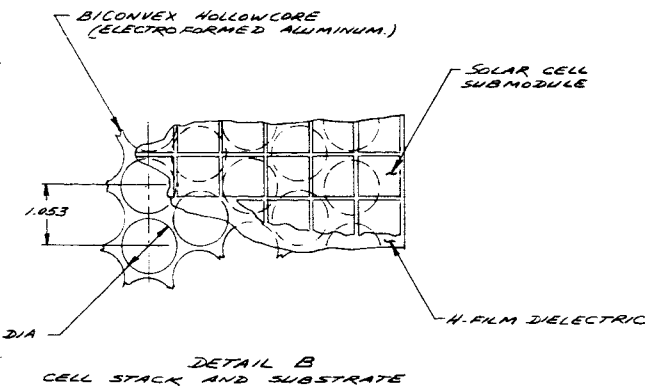


ARRAY CONFIGURATION AND
PANEL ASSEMBLY



SECTION C-C
LATCHING CONCEPT

- \triangle CLIP AND
- \triangle CELL SUBSTRATE GROSS
- (a) SURVEYOR SHROUD
- (b) HOLLOW CORE
- (c) ATTACHMENT CLIP
- BUYER'S OFFICE
- BETWEEN
- NOTES



END SHROUD GEOMETRY UNSTOWED.

1100350

ROUNDED TO HOLLOWCORE SUBSTRATE
 RIVETED TO FRAME
 SURFACE (a) AREA 1080 SQ. FT.
 SURFACE (b) AREA 1100 " "
 SURFACE (c) AREA 12 " "
 SURFACE AREA OF 291.920 EACH 2x2 CM CELLS
 HOLLOWCORE BICONVEX SUBSTRATE AREA.
 PRINTING FOR FRAME SURFACE AREA
 DOES NOT INCLUDE SPACING
 BETWEEN SUB PANELS
 UNLESS OTHERWISE SPECIFIED.

REV	DATE	BY	CHK	APP	DESCRIPTION	QTY	UNIT	REMARKS
LIST OF MATERIALS								
UNLESS OTHERWISE NOTED					ELECTRO-OPTICAL SYSTEMS, INC.			
1. QUANTITY					Pasadena, California A Subsidiary of Kaman Corp.			
2. MATERIAL					EOS CONFIGURATION			
3. FINISH					10 KW SOLAR ARRAY			
4. DIMENSIONS					JUPITER FLYBY			
5. TOLERANCES					PART NUMBER			
6. SURFACE FINISH					1100350			
7. WEIGHT					12705			
8. OTHER					REV 1/01			
9. ORIGINAL APPLICATION					W.O. 7027 NAS 7-428			

FIG. 1-3

2. PROGRAM DESIGN CRITERIA AND REQUIREMENTS

2.1 Introduction

This section defines the design criteria and requirements of the solar array power subsystem. The information presented here is used as the ground rules for the preliminary design of two solar photovoltaic arrays which provide primary electrical power for electrically propelled Jupiter flyby spacecrafts. The preliminary designs are a portion of this contract to be ultimately used in design, assembly, and test of the demonstration solar panel. The program purpose is to indicate the feasibility of erecting large-area, 25-to-50-lb-per-kW arrays.

One design, for an array on a spacecraft launched by the Atlas/Centaur, provides 10 kW at a sun-probe distance of one astronomical unit. The second array, for a spacecraft launched by the Atlas/Agena, is designed to provide 5 kW at a sun-probe distance of one astronomical unit.

Data for this specification were obtained from the following references:

1. Electro-Optical Systems, Inc., "Design Requirements and Constraints for SPEP Spacecraft Solar Array"; Interim Report 4816-IR-1, Jun 1965, Air Force Contract No. AF 33(615)-1530
2. "Fabrication Feasibility Study of a 20 Watts per Pound Solar Array"; Bimonthly Report No. 3, Aug 1965, JPL Contract 951132 (Subcontract under NASA)
3. A. Smith, meeting at EOS to define technical aspects of NASA Contract NAS7-428, Jan 1966

2.2 Definitions

Nomenclature used in this report is shown with an illustrated solar array in Fig. 2-1. Specific definitions of terms are given below.

Solar Array Electrical Power

The solar array electrical power is unregulated direct current (at specified voltages) supplied by solar cells. The solar array power is rated at 100 percent load at standard conditions (q.v.).

Electrical Load

The electrical load is the maximum power output capability at a specified average cell temperature and solar intensity in a space environment. It is the operating spacecraft power requirements measured upstream from the power conditioning system.

Nominal System Voltage

This is the voltage supplied under 100 percent electrical load at specified conditions of cell temperature and solar intensity. It is measured upstream from the power conditioning system.

Voltage Range

This is the upper and lower nominal system voltage limits the solar array produces as a function of the mission environmental changes and their effect on solar cell temperature and solar intensity.

Source Impedance

The source impedance is the electrical resistance measured and rated at the solar array output terminals under standard conditions. It is a percentage value which depends on solar intensity, temperature of the solar cells, and amount of electrical load.

Solar Array

A solar array is defined as a complete multicellular assembly for one spacecraft composed of all structural and mechanical mechanisms (actuators, latches, dampers, etc.) and electrical parts and equipment, including the devices for attaching the array to the spacecraft.

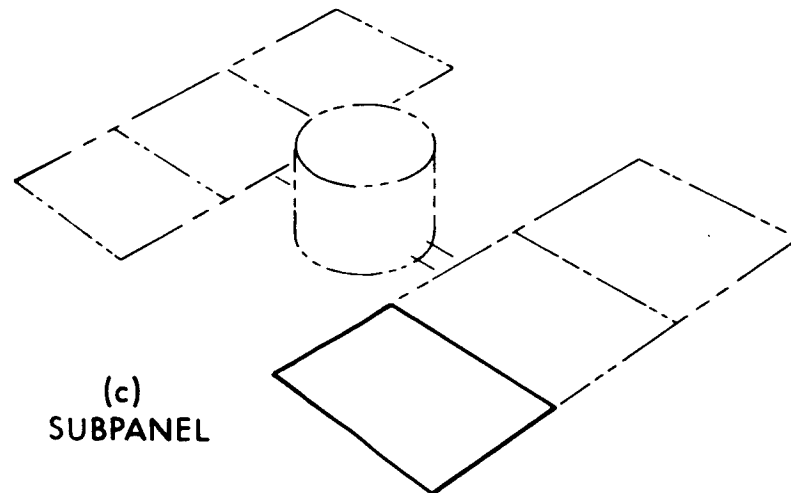
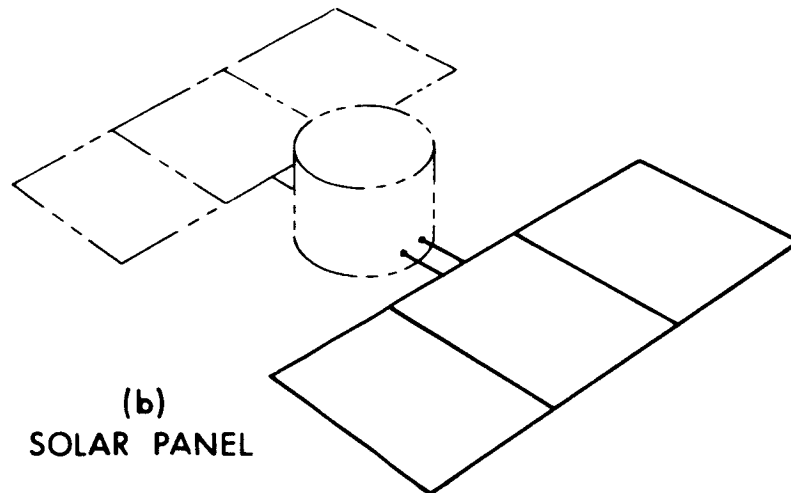
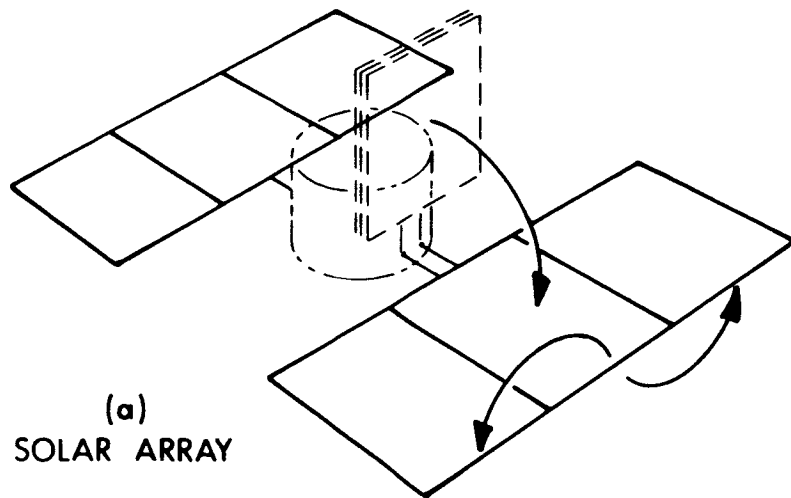


FIG. 2-1 NOMENCLATURE DEFINITION

Electrical lines to the array spacecraft interface are included, but spacecraft cabling between the electrical power conditioning and the interface units are not.

Solar Panel

The largest element of the solar array which can be independently attached to the spacecraft.

Subpanel

The largest structural element that can be independently attached or removed from a solar panel.

Solar Cell Module

A module is the minimum group of solar cells which will independently produce the electrical subsystem voltage at the output terminals of the cell group. Modules will assume various physical outlines as required by the configuration of the structural support and the power system current and voltage requirements. Electrical power output of a module will vary with the number of solar cells used in the module.

Solar Cell Submodule

A group of solar cells interconnected in parallel by a continuous strip or bus bar. A number of submodules connected in series form the solar cell module.

Solar Cell

The smallest current-producing element of the submodule.

Electrical Bus

Metallic conductors which provide electrical continuity between solar cell modules and between each solar panel assembly and the spacecraft.

Bus Crossovers

Flexible or hinge electrical buses which provide electrical continuity across solar panel, subpanel or solar array hinge points.

Standard Condition

The standard conditions for rating solar photovoltaic and solar array characteristics are:

$$\text{Solar Intensity } (S_o) = 130 \text{ watts/ft}^2$$

$$\text{Temperature } (T_o) = 328^\circ\text{K}$$

2.3 Mission Assumptions

Spacecraft

Mariner Series Spacecraft (no midcourse maneuver).

Mission

Solar-electric propulsion spacecraft for Jupiter flyby. Assume a "toward-the-sun-kick" type trajectory which reaches 0.6 astronomical units. (See Fig. 2-2.)

Duration

Eight hundred days typical mission duration for material evaluation.

Launch Vehicles

Atlas/Agena for 5 kW array.

Atlas/Centaur for 10 kW array.

Launch Period

Not specified. Solar Proton Equivalent Year also not defined since radiation degradation was not included in study.

Solar Alignment

Array is fixed with respect to the spacecraft whose attitude control system is capable of a pointing accuracy of ± 1 degree.

2.4 Spacecraft Envelope Requirements

The physical constraints placed on the packaging of the solar array are functions of configurations for the spacecraft, antennas, instrumentation or experiment booms and the vehicle shroud. These configurations are established through mission analysis which is beyond

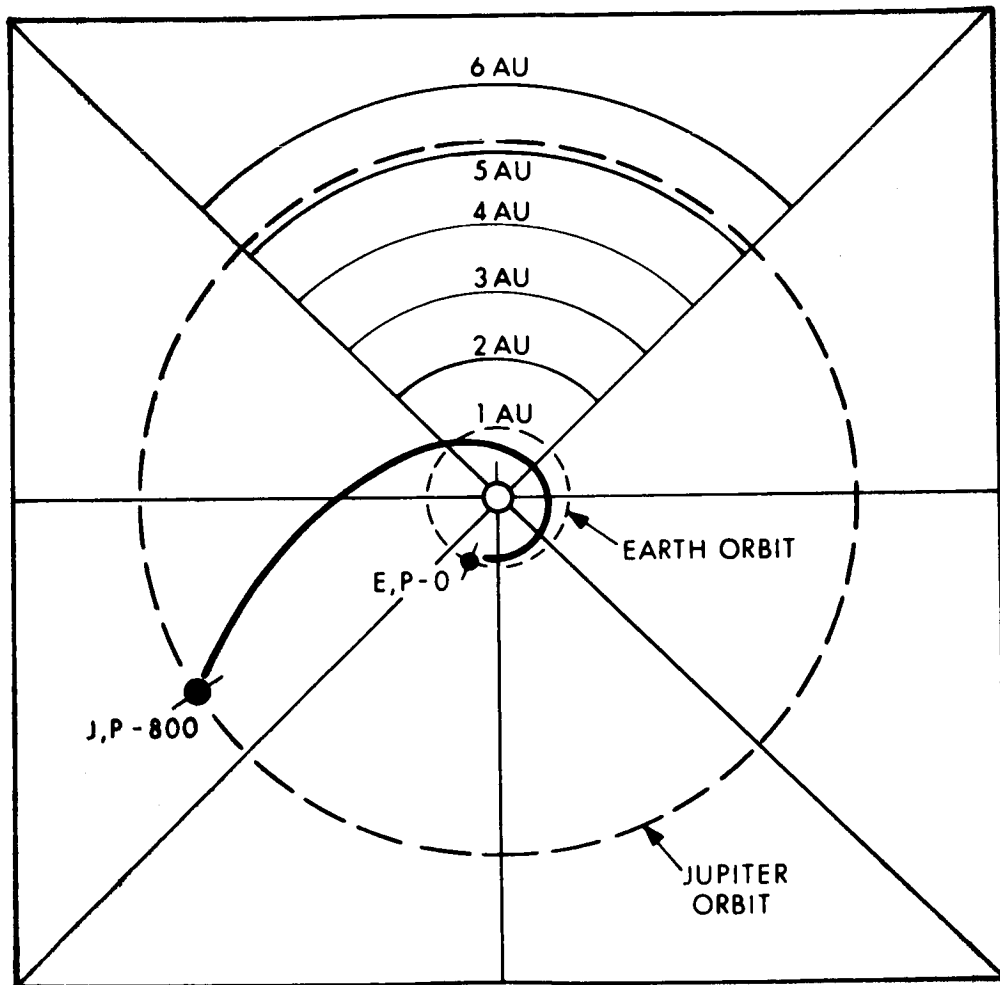


FIG. 2-2 SOLAR-ELECTRIC MISSION, JUPITER ORBIT, 1971 - 800 DAYS

the scope of this study. The envelopes presented here are ground rule configuration limitations extracted from the referenced documents and previous spacecraft missions.

Figures 2-3 and 2-4 define the gross envelope geometry for typical shrouds used with Atlas/Centaur and Atlas/Agna launch vehicles. The envelope restrictions for the stowed solar array are defined from the dynamic envelope shown in the figures, but the packaging study assumed the facility for insertion of a cylindrical section in the shroud to increase its overall length.

The points of attachment between the solar array and the spacecraft are not defined for this study. The spacecraft is assumed to be a cylinder of the diameter indicated in the figures; attachment can be assumed anywhere along the spacecraft length.

2.5 Solar Array Structural and Environmental Design Criteria

2.5.1 Ground Handling

The solar array structural performance shall not be degraded due to assembly or disassembly of solar cells, submodules, or modules.

The solar array structural and electrical performance shall not be degraded due to transporting a suitably packaged array from the manufacturing area to the spacecraft launch area. The ground handling transportation test specification shall be equivalent to the applicable portions of MIL-STD-810A, dated 23 June 1964, and shall be applied to the outside of the container in its transportable condition.

The ground handling requirement for solar arrays shall place no restrictions on the array design. Method of transportation shall assure that arrays experience load conditions less than those defined herein.

2.5.2 Launch Configuration

The solar array in the stowed configuration shall be capable of withstanding without structural, electrical, or mechanical

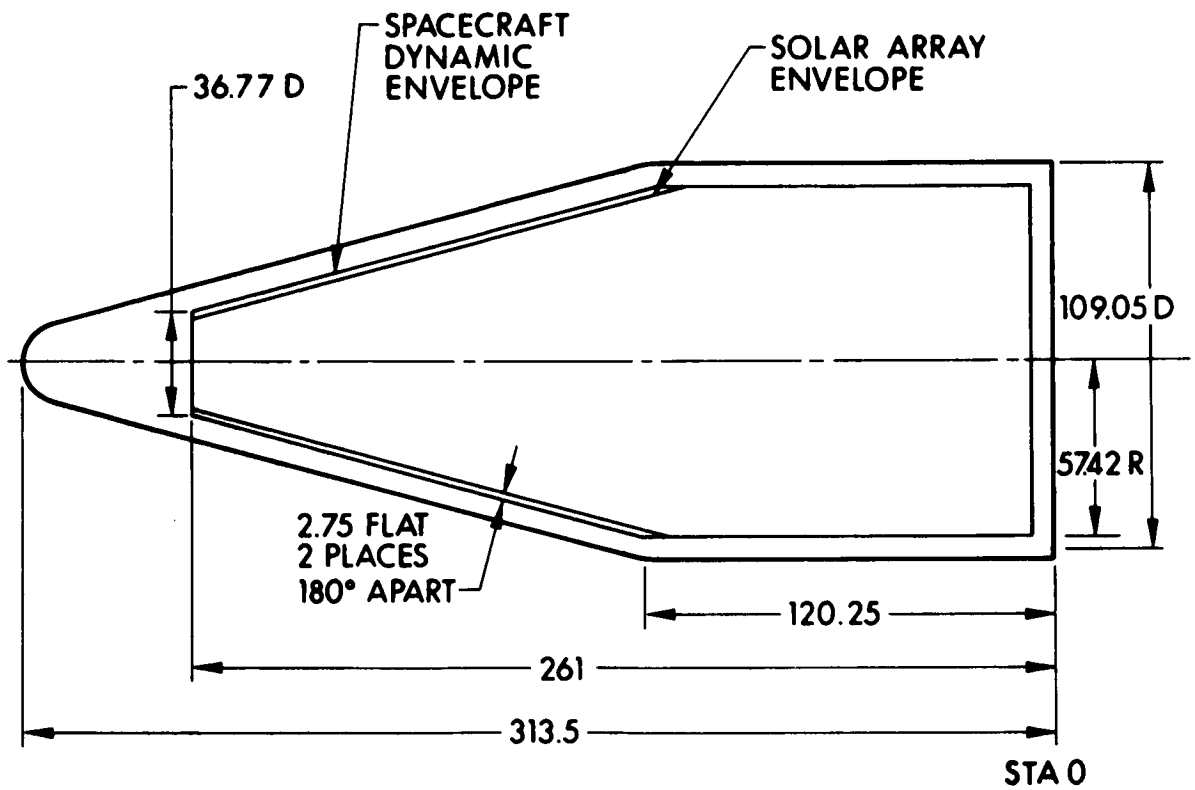


FIG. 2-3 ATLAS/CENTAUR NOSE FAIRING - SURVEYOR

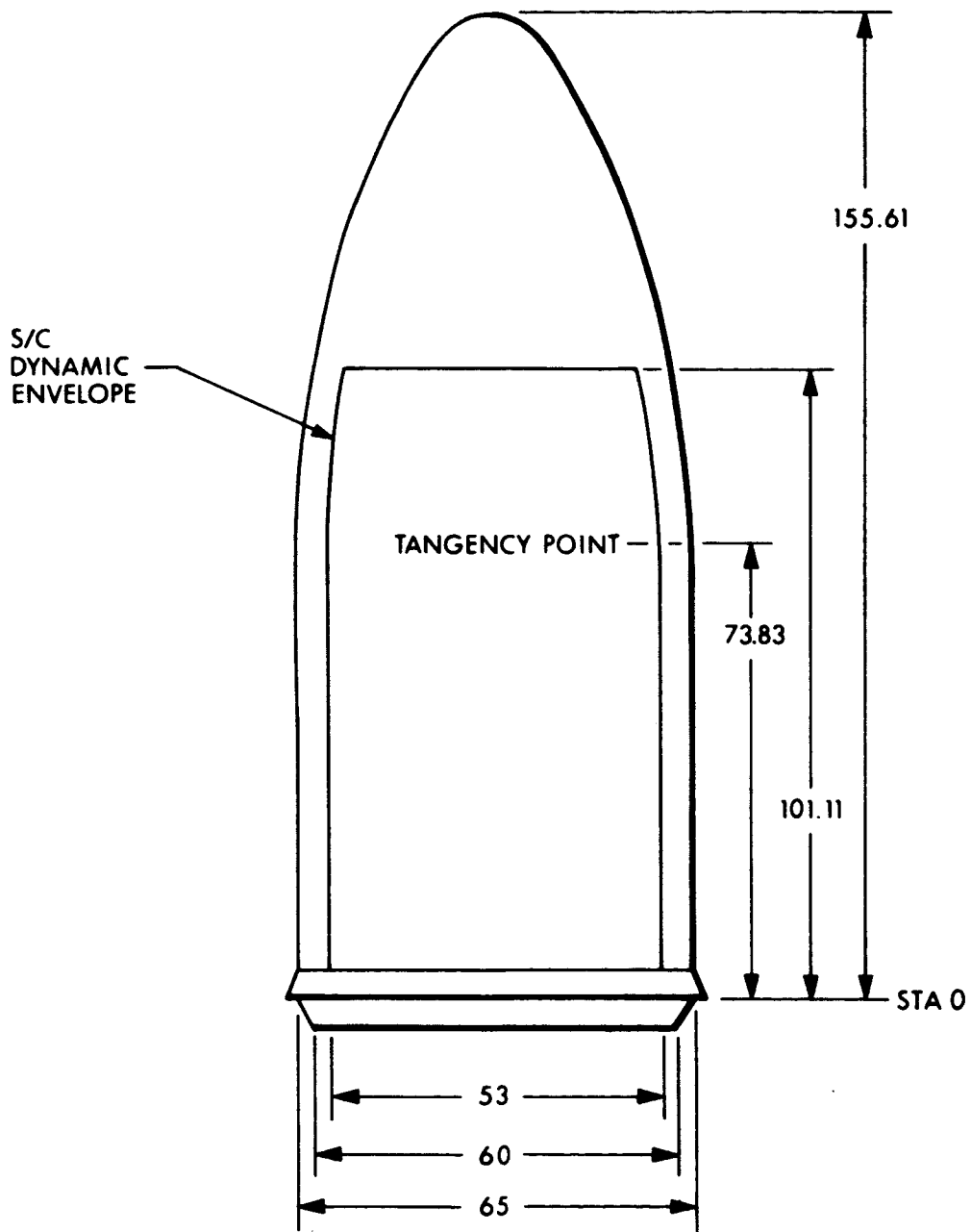


FIG. 2-4 ATLAS/AGENA SHROUD FOR MARINER IV

degradation, the following structural load environment. The solar array shall not be required to withstand the dynamic load environment superimposed upon the static load environment.

2.5.2.1 Vibration Environment

2.5.2.1.1 Sinusoidal Sweep at 1.0 Min/Octave.

The sinusoidal vibration input shall be swept three times from 2 to 200 Hz, first normal to the plane of the stowed array, and then parallel to the plane in a lateral direction. The two vibration inputs shall not be applied simultaneously.

<u>Frequency</u>	<u>Forward Attachment Point</u>	<u>Aft Attachment Point</u>
$2 \leq f < 10$	1.5g (rms)	1.5g (rms)
$10 \leq f < 20$	8.5g (rms)	1.5g (rms)
$20 \leq f < 50$	5.0g (rms)	1.5g (rms)
$50 \leq f < 200$	5.0g (rms)	2.0g (rms)

2.5.2.1.2 Random Gaussian Vibration. Random gaussian vibration shall consist of three minutes vibration at $0.2g^2$ per Hz band-limited between 200 and 2000 Hz.

2.5.2.2 Static Environment

The static loads shall consist of a steady-state acceleration of 18g directed along the spacecraft longitudinal axis and a 1g steady-state acceleration directed normal to the spacecraft longitudinal axis.

2.5.2.3 Dynamic Characteristics

The first mode resonant frequency of the stowed array shall be less than 10 Hz or greater than 25 Hz.

2.5.2.4 Acoustic Environment

The stowed arrays shall withstand without degradation the flight acoustic environments specified in Fig. 2-5 during the launch phase.

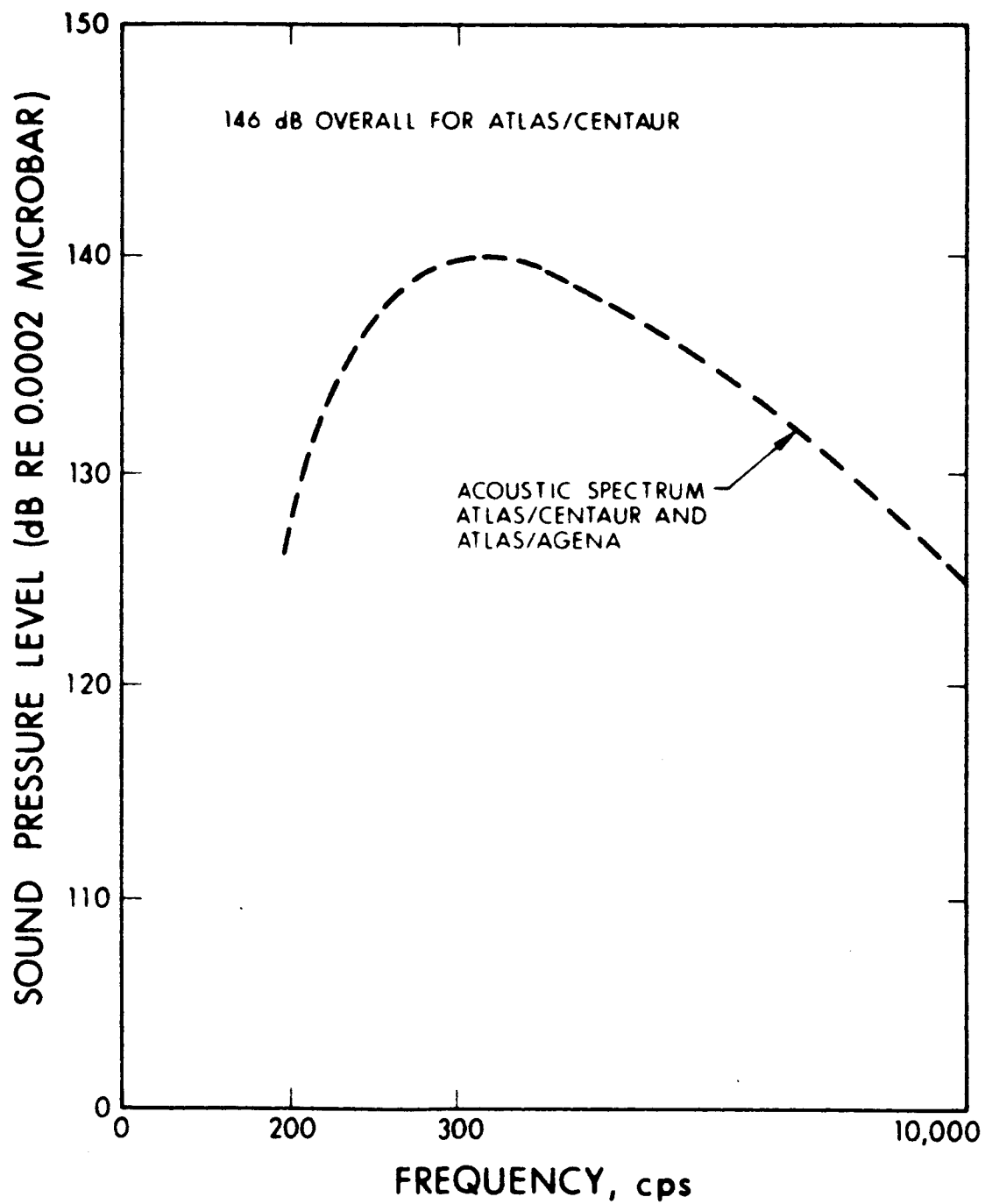


FIG. 2-5 ATLAS/CENTAUR, ATLAS/AGENA ACOUSTIC ENVIRONMENT

2.5.2.5 Thermal Environment

The array shall withstand the transients due to thermal dynamic heating during boost and shroud ejections without structural or electrical degradation.

2.5.3 Deployed Configuration

The solar array shall be capable of full deployment without interference between the array elements and between the array and the spacecraft. The solar array shall be so designed that no structural or electrical degradation will occur due to or during the following conditions:

1. The thermal gradients that will develop between the sun and shade sides of the array due to solar illumination between 400 mW/cm^2 and 5 mW/cm^2 intensity.
2. A steady-state acceleration of $3 \times 10^{-5} \text{ g}$ directed at 45 degrees to the plane of the array. This loading simulates that imposed by the cruise engines.
3. Repeated discrete applications to the entire array of a square-wave pulse with durations not less than 13.0 sec or more than 5 min and maximum amplitude of $2 \times 10^{-5} \text{ radians/sec}^2$ pitch angle accelerations.

2.5.4 Cruise Array Dynamic Characteristics

The first mode resonant frequency of the entire deployed array shall be greater than 0.04 Hz and less than 10 Hz.

2.6 Material Selection Criteria

2.6.1 Simulated Environments

The structural, electrical, thermal control, and lubricant materials used in the solar arrays must withstand exposure to the following simulated environments without a loss in any critical design property. These requirements are to be used for material selection purposes only and not for design.

1. Storage at 95 percent relative humidity at 30°C for 50 hours.
2. One hundred and fifty thermal cycles between -20°C to 60°C at a rate of change that permits temperature stabilization without excessive thermal shock.
3. Ten thermal cycles between -200°C and 90°C at 10⁻⁷ torr with a one-hour cycle and a temperature stabilization dwell at the extreme temperatures.
4. The materials must also resist the flight environment without releasing any condensing gases which would decrease the solar cell efficiency or cause electrical shorts, or cause any degradation to spacecraft systems operation.

2.6.2 Structural Materials Criteria

The structural components of the various configurations and arrays should have a reliability of 0.999+ with a confidence level of above 90 percent. To meet this requirement, the material selection and design configuration must consider not only the load conditions of launch and space maneuvers, but the loads induced by thermal excursions.

The use of state-of-the-art materials and processes shall be a requirement, but their use shall not restrict the design if near state-of-the-art performance can be demonstrated.

2.6.3 Adhesive Criteria

2.6.3.1 Structural

The structural adhesive must be resistant to all of the mechanical, vibrational, and thermal loads induced on the array. A prime requirement of any selected adhesive system is the feasibility of processing and the compatibility of processing procedures with the elements being bonded.

2.6.3.2 Solar Cell Adhesives

This program has a solar cell stack defined as a 4-mil silicon solar cell with an integral 1-mil cover glass. This definition limits the solar cell adhesive study only to that which

bonds the cell to the substrate; there is no need of an adhesive to attach the cover glass to the cell.

The major adhesive criterion is the selection of a material that has the following properties: high thermal conductivity, low outgassing in the vacuum environment, a modulus of elasticity compatible with the thermal motion of the cells and structure, and repairability during fabrication phase.

2.6.3.3 Thermal Control Coatings

These coatings must be resistant to the ultraviolet and particulate radiation of the flight environment such that no significant decrease will occur in the design values of emittance.

2.6.3.4 Bearings and Lubricants

The bearings and lubricants for use on the various array configurations must function a minimum of 10 times in an earth environment (1g) without failure or part replacement. The bearing materials must resist the thermal excursions and particulate radiation of the flight environment without a change in the critical dimensions or the release of any condensing gases.

2.7 Electrical Power Criteria

Design criteria are presented for solar cells, solar cell modules, cell connections, buses and termination, and installations. Discrete values are given wherever possible, but in some cases the exact values will be the result of a trade study. Voltage and power requirements for this study are defined as follows:

1. Atlas/Centaur solar array shall be capable of delivering 10 kW at 100V.*
2. Atlas/Agena solar array shall be capable of delivering 5 kW at 100V.*

* Requirements are at 1 astronomical unit (AU), 130.11W per ft², 55°C, and maximum power point.

2.7.1 Solar Cell Modules

The solar cell modules will be designed and evaluated in accordance with the criteria and assumptions outlined in the following subsections.

2.7.1.1 Power Output Determination

Power output of the array in the vicinity of earth will be determined by the following equation and assumed design constants:

$$P = (\phi)(A)(\eta_p) [1 - (T_c - 55^\circ\text{C})(K)]$$

where

P = power output in watts

ϕ = defined electrical power at maximum power point per unit area of solar cell as 10 watts/ft² for AMO, 1 AU and 55°C

A = gross area of panel in square feet

η_p = ratio of active cell area to gross panel area

T_c = cell temperature in degrees centigrade

K = temperature efficiency coefficient = 0.4 percent/°C

2.7.1.2 Cell Efficiency

Power output calculations will be based on a hypothetical N-P cell having an efficiency of 10.1 percent air/mass zero.

2.7.1.3 Electrical Insulation

The electrical insulation between the solar cells and the metallic substrate or the ground plane will provide a minimum breakdown strength in air at standard temperatures and pressure conditions greater than three times the open circuit voltage of the panel. Leakage resistance under the same test conditions will be greater than 10⁹ ohms per cm² on cell area.

2.7.1.4 Packing Factor

The spacing between adjacent solar cells connected in parallel shall not exceed 0.01 inch. Spacing between series-connected modules will not exceed 0.03 inch with front-connected cells or 0.01 inch with back-connected cells. The number of 2 cm^2 solar cells per square foot of gross area shall not be less than 217 front-connected cells or 221 back-connected cells.

2.7.1.5 Interconnections

The cells will be interconnected both in parallel and in series by metallic conductors. The conductors shall be designed to minimize both thermal and flex stresses on the cell. The resistance of the interconnection plus solder shall not exceed 2 percent of the total series resistance of the cell. The joint shall have a strength equal to or greater than the strength of the bond between the silicon and the ohmic contacts. The joining materials shall exhibit stable physical and electrical characteristics in both space and terrestrial environments.

2.7.1.6 Solar Cell Characteristics

Power output as a function of temperature will be evaluated using the definition noted in Subsection 2.7.1.1.

2.7.1.7 Cover Glasses and Filters

Stack design will be initially based on the use of 1- to 2-mil integral cover glass. Alternate material to be considered will include 2- to 3-mil microsheet.

2.7.2 Conductors

Spacecraft raw electrical power for the solar array is provided by one or more two-wire, ungrounded conductors from each solar cell module.

The configuration of electrical conductors shall be determined with regard to the following considerations:

1. Minimum possible weight
2. Minimum resistivity
3. Minimum magnetic field
4. Mechanical strength to endure launch environment
5. Allowable voltage drops (to be determined by trade studies)
6. Exterior finish to be resistant to natural and induced environments
7. Process adaptability
8. Redundancy
9. Thermal expansion coefficient considerations

2.7.3 Conductor Insulation

Selection of conductor insulating materials shall be made with regard to the following considerations:

1. Broad spectrum radiation resistance
2. Heat resistance (to be compatible with manufacturing and assembly processes)
3. Mechanical strength
4. Notch sensitivity
5. Flexibility
6. Dielectric characteristics
7. Ease of forming or fabricating
8. Cost
9. Flight thermal considerations

2.7.4 Electrical Terminals

Terminals shall be used to facilitate maintenance (including repair and replacement) of electrical components. The following requirements shall be observed:

1. Voltage drop across any terminal shall not exceed 25 mV at rated load.
2. The terminal shall withstand 50 cycles of manual mating and unmating without replacement of parts.
3. The terminal shall be accessible for ease of wiring and for factory or field checkout.

4. It shall be rigidly attached to primary or secondary structure.
5. It shall have minimum possible weight consistent with other design specifications.
6. Exterior finish of the terminal shall be resistant to both natural and induced environments.

2.7.5 Installation

The installation of wires, terminals, electrical connectors, and buses shall conform to the following requirements:

1. Buses and other wiring shall be installed to minimize magnetic fields.
2. Installation shall withstand rigors of normal handling and transportation as well as launch and operational maneuvers.
3. Installation shall be designed to facilitate service and repair activities.

2.7.6 Electroexplosive Devices

The design, installation and test of wires which control the initiation of electroexplosive devices shall meet requirements of AFETRP 80-2, "General Range Safety Plan," Volume 1, Paragraphs 3 and 4 of Appendix A.

2.7.7 Electrical Connectors

2.7.7.1 Total Connector

Electrical connectors shall conform to the following requirements:

1. All electrical connectors shall have removable crimp-type contacts which shall be removed from the back of the connector.
2. They shall have cable strain-relief provisions.
3. They shall have positive moisture seals at the wire entry and at the mating interface.

2.7.7.2 Socket Connector Halves

Each connector half which contains the socket contacts shall have the following characteristics:

1. The exposed insert insulator shall be made of hard plastic material.
2. Socket contact entry shall be protected by the hard plastic insulator.

2.7.7.3 Pin Connector Halves

Each connector half which contains the pin contacts shall have a rubber insulator at the mating interface.

2.7.7.4 Finish Requirements

The exterior finish of each electrical connector shall withstand the following conditions:

1. All common terrestrial environmental conditions listed in NAS 1599, Connectors, General Purpose, Electrical, Environment Resisting.
2. Exposure to zero mass/air density for 1 year without sublimation.
3. Fuels used as propellants in launch vehicles.

2.8 Mechanism Restraints

2.8.1 Prelaunch and Launch Environments

The solar array, including release and deployment mechanisms, must fit within the solar array envelope specified for the applicable configuration.

In the stowed configuration, the solar array must be protected from any damage which could be caused by shock and vibration during launch, and must be supported in such a way that shock and vibration loads are transferred to spacecraft structure.

Release and deployment mechanisms must withstand the launch environment without damage, and upon command and in proper sequence, must release solar array restraints and extend and lock the array into its deployed position.

2.8.2 Space Environments

In the deployed configuration, under steady-state conditions, the solar array must have sufficient rigidity so that by controlling the attitude of the spacecraft, the array can be oriented and maintained in a plane normal to the direction of the sun within ± 10 degrees. (This tolerance shall include deflections from static spacecraft load inputs and thermal gradients, but shall not include deflections due to dynamic load inputs.)

Release, deployment, and locking mechanisms must withstand and be capable of functioning mechanically in the space environment after launch and 4 hours of space flight. They shall function structurally for the duration of the mission.

Release, deployment, and locking of the solar array shall not cause release of loose parts or gases which could damage or impair the function of the solar array or other spacecraft subsystems.

2.8.3 Checkout

Release, deployment, and locking mechanisms shall be designed so that, with suitable test equipment, their operating function can be checked in a lg environment. Mechanisms shall be capable of operating a minimum of 10 times in a lg field in a vacuum of 10^{-5} torr without failure or part replacement.

2.9 Reliability

2.9.1 Structural Reliability

The structural reliability has a probability of 0.999 of successfully functioning under all loading conditions. This will be achieved by defining the design load criteria as noted below.

The stresses resulting from the design loads shall be compared to the allowable stresses of the materials with the following conditions to be satisfied:

$$MS = \frac{YS}{DL} - 1 > 0$$

or

$$MS = \frac{AS}{1.25 (DL)} - 1 > 0$$

where

MS = margin of safety

YS = yield stress (F_{t_y})

AS = allowable stress (F_{t_u} , F_{c_o} , and F_{c_c})

DL = design limit stress (f)

The allowable stresses are defined as: the ultimate stress (F_{t_u}), the critical buckling stress (F_{c_o}), and the crippling stress (F_{c_c}). Yield and ultimate stress values shall be the minimum guaranteed values for the appropriate material.

2.9.2 Mechanical Reliability

The probability that the mechanisms successfully deploy 100 percent of the array one time is 0.999 or greater.

2.9.3 Electrical Reliability

The electrical reliability is established at 0.98 for a power loss of 5.0 percent. The reliability for the electrical buses and connections is 0.998.

2.10 Interfaces

Interface coordination is required to establish compatibility between the spacecraft and the array in the following areas.

2.10.1 Structural Interfaces

The following are requirements governing spacecraft/array structural interfacing:

1. The solar array design shall be compatible with the solar array to spacecraft attachment points.
2. The solar array structural materials shall be compatible with the spacecraft materials, spacecraft instrumentation, and the mission requirements.
3. The spacecraft/array thermal interaction shall be considered on a system basis so as to provide the most efficient combination capable of performing the mission.

4. The solar array design shall not be unilaterally restricted by the spacecraft thermal control requirement.
5. The deployed array shall experience no shadowing from the earth, moon, other planetary bodies or spacecraft subsystems prior to Jupiter rendezvous.
6. The solar array structural design shall be such that dynamic coupling of the solar array with the spacecraft guidance and control equipment is minimized by meeting the frequency restrictions.
7. The solar array shall be designed so that displacement of the vehicle mass center due to solar pressure, thermal gradients, and array temperatures are minimized consistent with other array requirements.

2.10.2 Spacecraft Interfaces

Design of the array and spacecraft shall take into consideration the following interface problems:

1. Clearance with the exhaust from attitude control jets and electric thrusters.
2. Satisfactory antenna view angles for communication with earth.
3. View angles for cameras or sensors on the spacecraft.
4. Electrical, magnetic, and radiofrequency interference limits.
5. Space envelope interface, for both storage and deployment between the arrays, spacecraft, booster, and shroud.
6. The spacecraft attitude control system shall maintain the solar array plane normal to the sun line within ± 1 degree.

3. DEMONSTRATION PANEL AND SAMPLE PANEL DESCRIPTION

This section delineates the hardware items to be fabricated and assembled during this contract and includes drawings, descriptions, and a discussion of each unit's purpose. Hardware items are sample panels and a demonstration panel.

3.1 Hardware Item Descriptions

3.1.1 Demonstration Panel

The demonstration panel is a 5-foot-square structural model of the subpanel used in the 10 kW array. Three demonstration panels with frame modifications and no change to the hollow core substrate make up the subpanel. It differs also in that only 5 percent of the substrate area is covered with live cells; the remainder contains aluminum chips for mass mockup.

The purposes of the demonstration panel are:

1. Verify, through tests, the engineering analysis and the qualification of the design.
2. Demonstrate the photovoltaic structure assembly procedures.
3. Demonstrate the structural fabrication procedures.

Demonstration of electroforming techniques will be accomplished first on full-size test specimens similar to the demonstration panel substrate. The difference between the test specimen substrates and that of the demonstration panel is that the specimen substrates will be electroformed on a mandrel made from a commercially available aluminum perforated sheet. This mandrel will not have the hole spacing, hole diameter, thickness, and surface finish required of the demonstration panel.

3.1.2 Sample Panels

The sample panel size ranges from 5 in. square to 5 ft square. The sample panel consists of a section of hollow core substrate on which cells and other material may be assembled. The large sample panel also serves the purpose described previously. To date, 40 of the smaller sample panels have been fabricated and three of the large panels are planned.

The purposes of the sample panel are:

1. Demonstrate electroforming technique (see Section 8).
2. Serve as the model for tensile strength tests (see Sections 8 and 9).
3. Serve as the model for thermal tests (see Section 9).
4. Serve as the model for substrate buckling tests (see Section 9.3).
5. Demonstrate fabrication and assembly techniques.

3.2 Demonstration Panel Details

Figure 3-1 shows the final assembly for the demonstration solar panel to be fabricated and assembled in this program. Figure 3-2 depicts the hollow core biconvex substrate. Drawings of detailed structures are contained in Appendix G of this report.

The substrate is an electroformed-nickel hollow core structure having a biconvex shape. The hollow core geometry is as follows:

1. Panel thickness--0.10 in.
2. Panel radius of curvature (both directions)--163 in.
3. Skin thickness (for facing and cylinder)--0.002 in.
4. Wall diameter, cylinders (also defined as holes)--1.0 in.
5. Spacing between centers of triangular-pattern holes--1.05 in.
6. Open area of hollow core surface--92 percent.

The substrate's rear surface (opposite to cell surface) is coated with 2 to 3 mils of Laminar X-500, a commercially available thermal control paint. The substrate is joined to the frame by Y-shaped aluminum alloy clips. The clip is bonded to the substrate with a viscoelastic adhesive similar to FM-1000 and is riveted to the

frame. The front surface of the substrate is covered with a 1-mil sheet of H-film that is attached by a 1- to 2-mil adhesive similar to RTV-60. The H-film adhesive covers only 18 percent of the total substrate surface area because it is applied only to the hollow core surface.

The frame is composed of a pair of stacked box sections. The frame material is 6061-T5 aluminum with a gage thickness of 0.010 in. Each of the two box sections is fabricated from curved U sections (one inverted with respect to the other). The flanges are bonded together with the viscoelastic adhesives.

The four corners of the frame contain formed 0.020 gage sheet-metal corner brackets that join the four peripheral box beams. Four 0.062 gage hinge brackets are inserted into the bracket at each corner. These simulate the hinges between subpanels and will be the means for mounting the demonstration panel to the various test fixtures.

Figure 3-3 shows the photovoltaic assembly of the demonstration panel. The panel will contain three different cell stacks with two live electrical sections. The 2 x 2-cm cell stacks are: (1) a 4-mil cell and a 3-mil cover glass, (2) 8-mil cell and 3-mil cover glass, and (3) a mass mockup (thin anodized aluminum wafer) of a 4-mil cell with a 1-mil integral cover glass. The two electrical sections will contain six cell submodules in a series string of 35 submodules. The mass mockups will cover the remainder of the substrate area. The spacing between submodules will account for the front contact cells, but the mass mockups will be spaced assuming simulation of a wrap-around contact.

The cells and mockups are bonded to the H-film with RTV-60 and the cover glass is bonded to the live cell with RTV-602. The cell interconnection is accomplished with silver bus bars.

The demonstration solar panel assembly will be used to confirm the techniques necessary to obtain a large, lightweight solar

array capable of supplying electrical power at a weight-to-power ratio of less than 50 lb/kW. The panel will undergo environmental testing as defined in Section 9 to confirm the integrity of the cells and their attachment mechanisms, the structural integrity when subject to a specified environment and the structural design analysis by measurement of such characteristics as resonant frequencies, stiffness, etc. The solar-photovoltaic performance will be measured to determine degradation of electrical power output related to environmental testing.

3.3 Sample Panel and Specimen Details

The tensile property test specimens are described in Section 9; their purpose is defined in Section 8. Briefly, these are typical flat-strip tensile specimens that are tested to ASTM E-8. The data defines the material properties of the electrodeposited nickel.

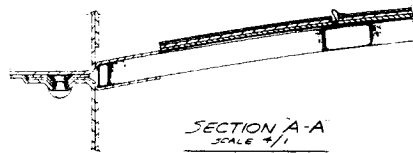
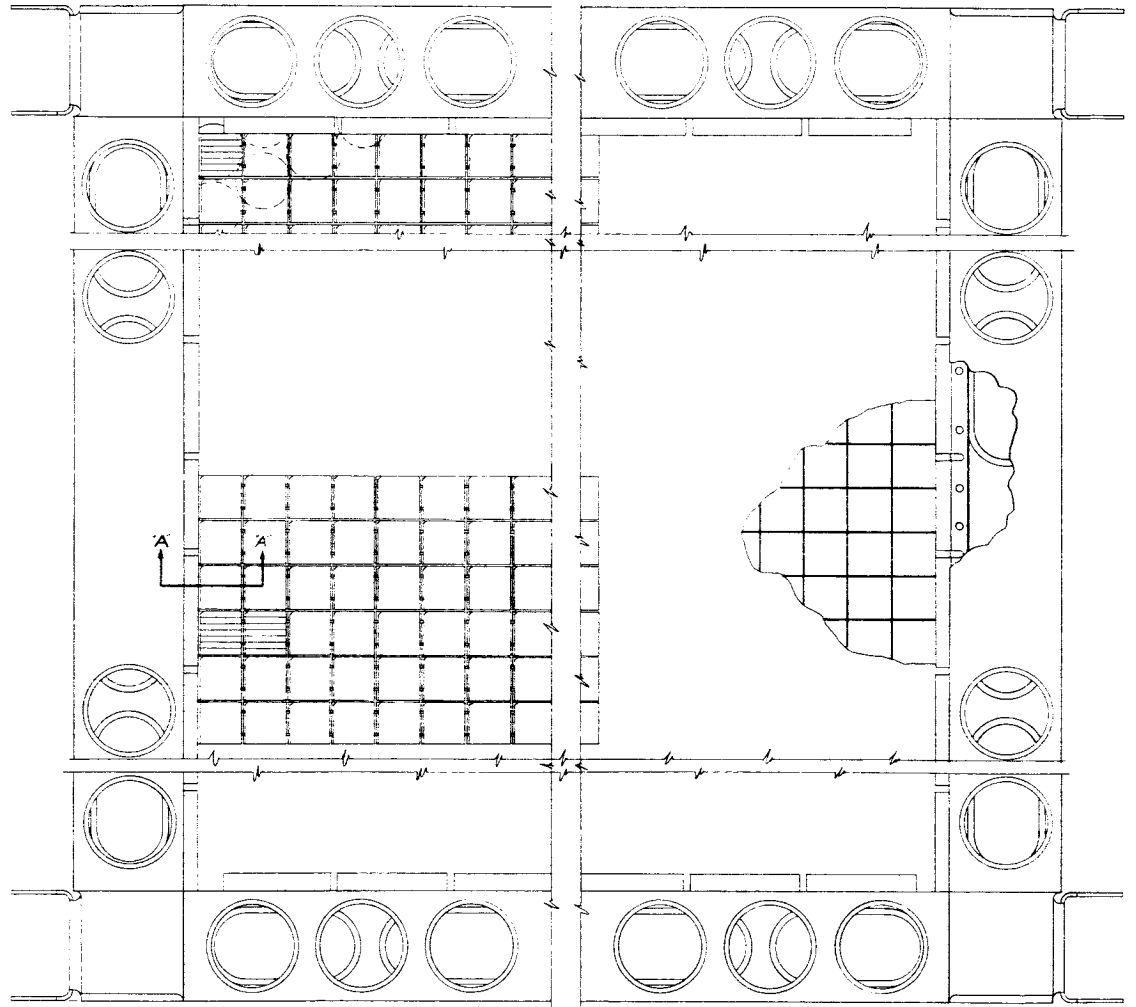
The properties of the nickel can be varied by the electroplating process techniques. For this structural concept, high values of modulus of elasticity are preferred; through these specimens, the electroplating procedure can be controlled so as to achieve this requirement.

The description and purpose of the buckling test samples are discussed in detail in Section 9. The importance of these samples to the hollow core substrate design and analysis is in the ability from test results to show the mode of failure and obtain empirical buckling coefficients. This data can then be converted into design curves for buckling coefficients as a function of hollow core geometry.

The thermal test samples are also used for verification of photovoltaic assembly techniques. Tests will be conducted on samples in a thermal/vacuum environment to verify thermal analysis. Figure 3-4 illustrates the thermal samples to be assembled. There are three 5 x 5-in. substrates (two are hollow core samples and the other is aluminum sheet stock) that will be covered with solar cells; one with 4-mil cells plus 3-mil microsheet cover glass, and the other two with 8-mil cells and 3-mil microsheet cover glass. The tests and expected results from these samples are detailed in Section 9.

The large size, 5-foot-square sample panels will be used for verification of the photovoltaic assembly techniques. The H-film dielectric will first be applied to these panels to work out techniques and procedures before this task is accomplished on the demonstration panel. The same will be true for the thermal control paint.

BLANK PAGE 3-6



2. ALL SPOTWELDS PER MIL. W. 6858, EDGE DISTANCE AND CENTER TO CENTER LOCATION OF SPOTS PER SPECIFICATION.
 1. ASSEMBLE PER EOS SPECIFICATION.

NOTES:

3-7

W107087 NAS 7-428

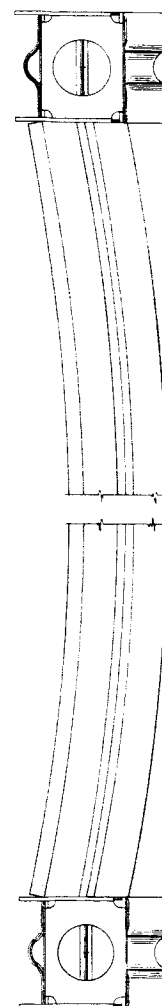
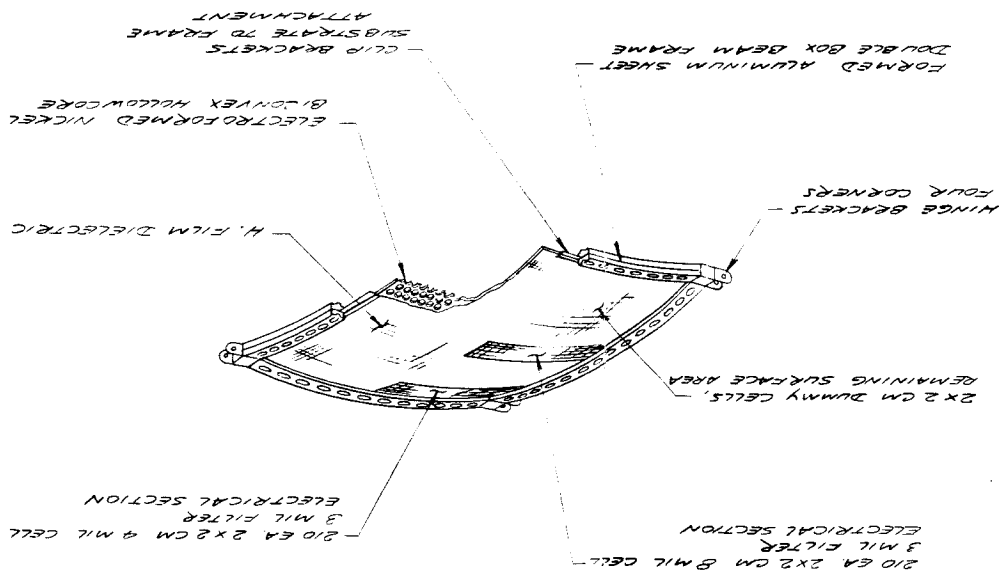
1100300		1100300	
SOLAR PANEL ASSEMBLY DEMONSTRATION			
ELECTRO-DYNAMIC SYSTEMS, INC.			
LIST OF MATERIALS			

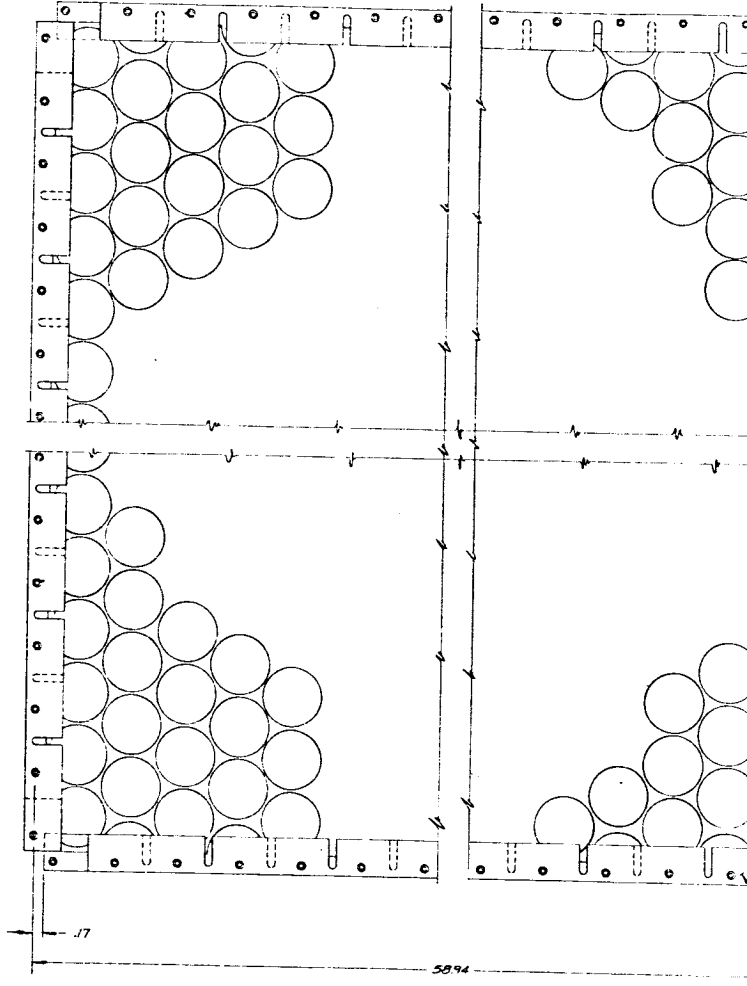
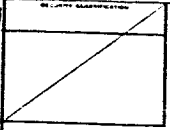
QTY	DESCRIPTION	UNIT
1	1100301 SUBSTRATE ASSY	
1	1100302 UPPER FRAME ASSY	
1	1100303 LOWER FRAME ASSY	
4	1100310 HINGE BRACKET	
1	1100322 PANEL	

1100300

QTY	DESCRIPTION	UNIT
228	1100322 PANEL	

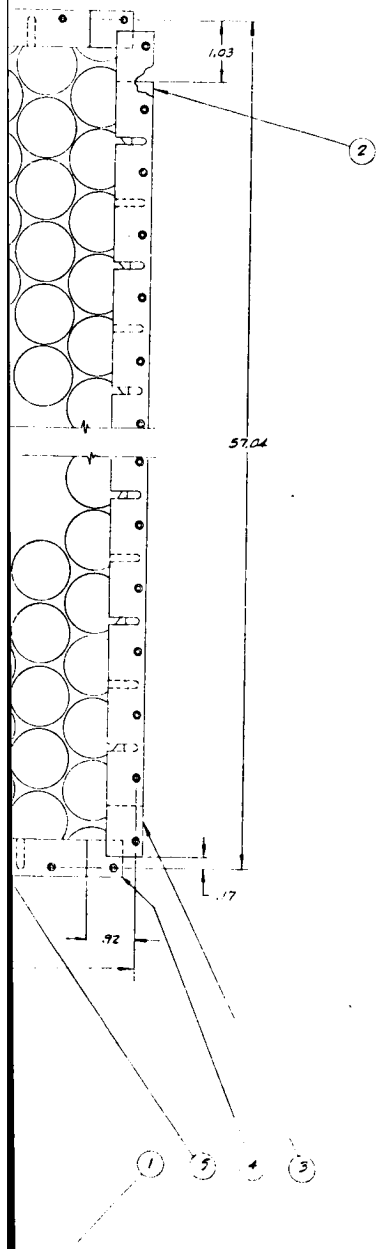
ISOMETRIC VIEW OF DEMONSTRATION SOLAR PANEL





ADHESIVE AND SANDING PROCEDURE
 TO BE SPECIFIED BY
 COGNIZANT ENGINEER

REVISIONS			
NO.	DATE	DESCRIPTION	BY



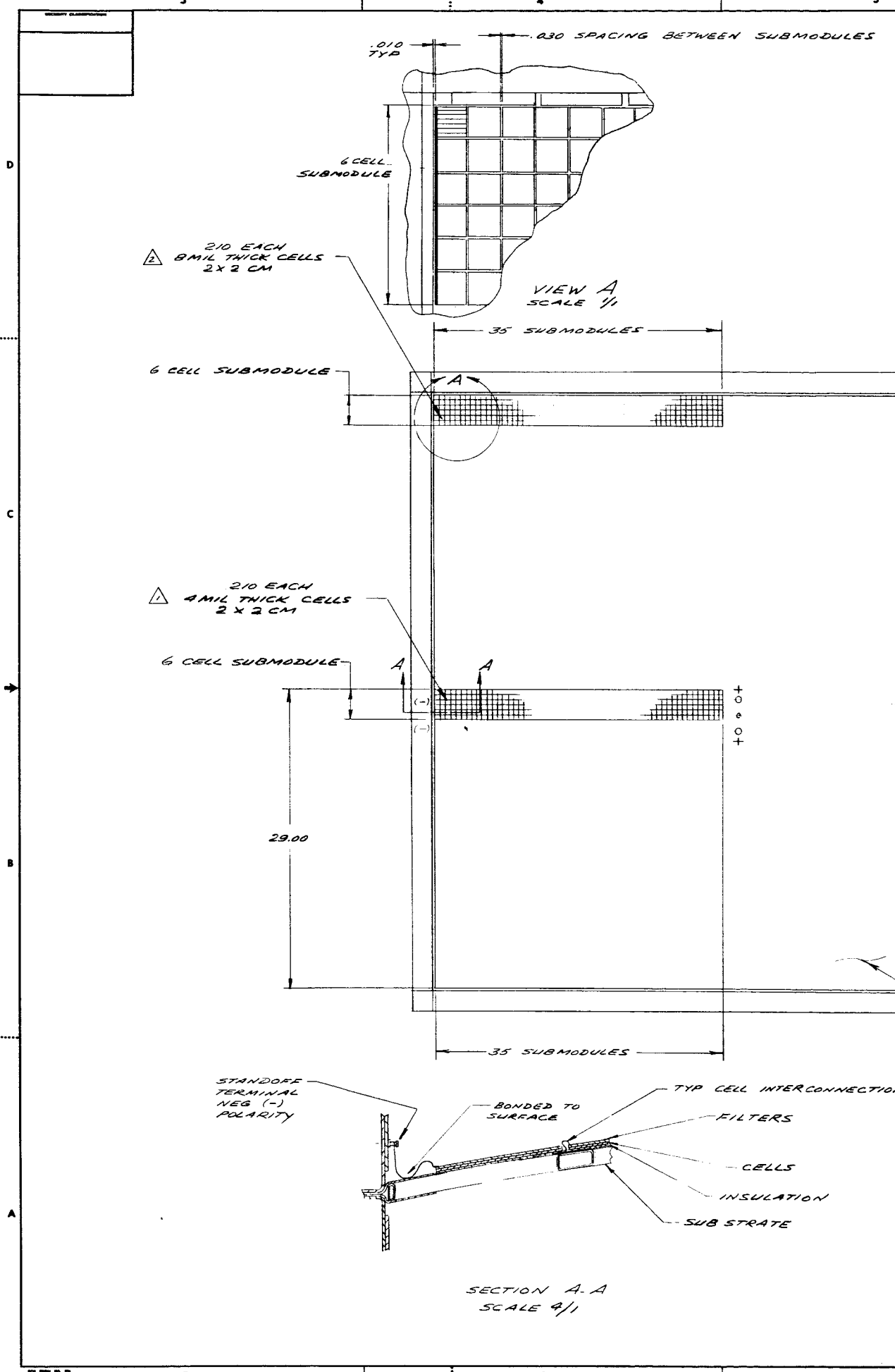
D
C
B

1100301 -

QTY	UNIT	DESCRIPTION	REMARKS
2	5	1100301 CLIP-UPPER, SB6	
2	4	1100305 CLIP-LOWER, SB6	
2	3	1100306 CLIP-UPPER, SW7	
2	2	1100355 CLIP-LOWER, SW7	
1	1	1100317 HOLLOW CORE	

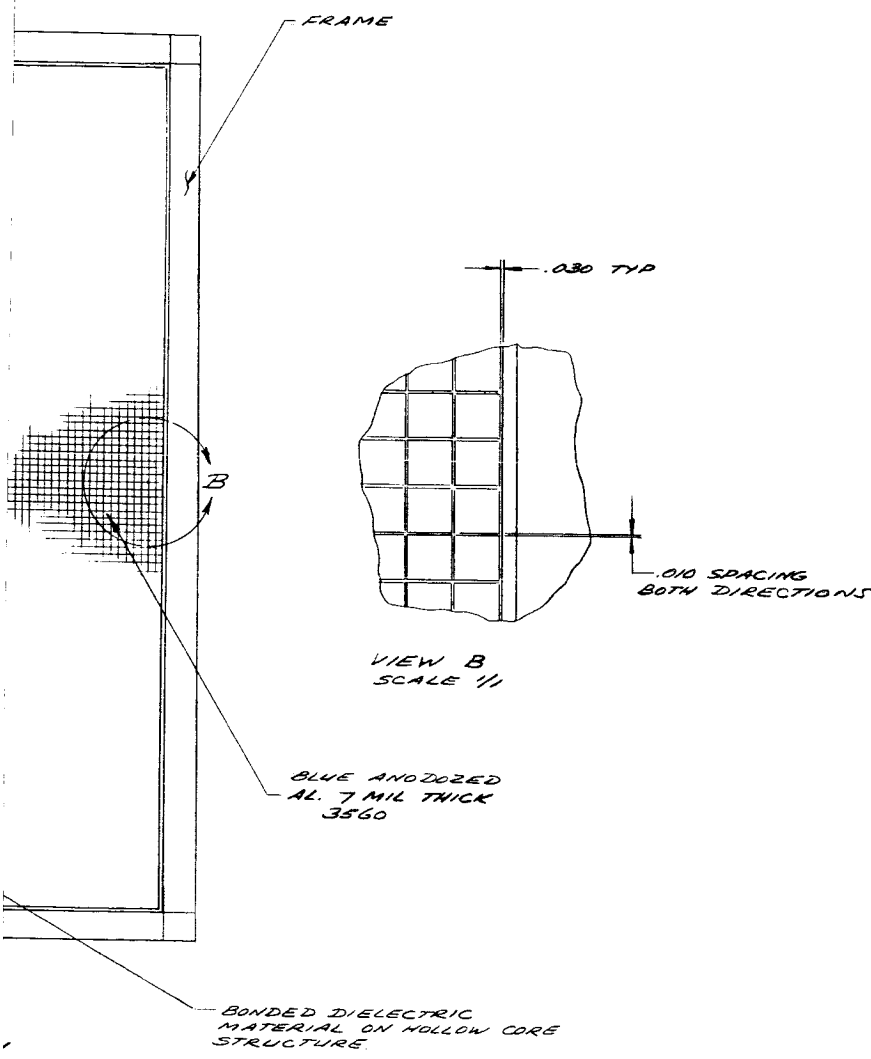
UNLESS OTHERWISE NOTED: 1. DIMENSIONS ARE IN INCHES. A. DECIMALS FRACTIONS ANGLES B. 1/8 1/16 1/32 1/64 3/32 1/4 5/16 3/8 7/16 1/2 5/8 3/4 7/8 1 1 1/8 1 1/4 1 1/2 1 3/4 2 2 1/4 2 1/2 3 3 1/4 3 1/2 4 4 1/4 4 1/2 5 5 1/4 5 1/2 6 6 1/4 6 1/2 7 7 1/4 7 1/2 8 8 1/4 8 1/2 9 9 1/4 9 1/2 10 10 1/4 10 1/2 11 11 1/4 11 1/2 12 12 1/4 12 1/2 13 13 1/4 13 1/2 14 14 1/4 14 1/2 15 15 1/4 15 1/2 16 16 1/4 16 1/2 17 17 1/4 17 1/2 18 18 1/4 18 1/2 19 19 1/4 19 1/2 20 20 1/4 20 1/2 21 21 1/4 21 1/2 22 22 1/4 22 1/2 23 23 1/4 23 1/2 24 24 1/4 24 1/2 25 25 1/4 25 1/2 26 26 1/4 26 1/2 27 27 1/4 27 1/2 28 28 1/4 28 1/2 29 29 1/4 29 1/2 30 30 1/4 30 1/2 31 31 1/4 31 1/2 32 32 1/4 32 1/2 33 33 1/4 33 1/2 34 34 1/4 34 1/2 35 35 1/4 35 1/2 36 36 1/4 36 1/2 37 37 1/4 37 1/2 38 38 1/4 38 1/2 39 39 1/4 39 1/2 40 40 1/4 40 1/2 41 41 1/4 41 1/2 42 42 1/4 42 1/2 43 43 1/4 43 1/2 44 44 1/4 44 1/2 45 45 1/4 45 1/2 46 46 1/4 46 1/2 47 47 1/4 47 1/2 48 48 1/4 48 1/2 49 49 1/4 49 1/2 50 50 1/4 50 1/2 51 51 1/4 51 1/2 52 52 1/4 52 1/2 53 53 1/4 53 1/2 54 54 1/4 54 1/2 55 55 1/4 55 1/2 56 56 1/4 56 1/2 57 57 1/4 57 1/2 58 58 1/4 58 1/2 59 59 1/4 59 1/2 60 60 1/4 60 1/2 61 61 1/4 61 1/2 62 62 1/4 62 1/2 63 63 1/4 63 1/2 64 64 1/4 64 1/2 65 65 1/4 65 1/2 66 66 1/4 66 1/2 67 67 1/4 67 1/2 68 68 1/4 68 1/2 69 69 1/4 69 1/2 70 70 1/4 70 1/2 71 71 1/4 71 1/2 72 72 1/4 72 1/2 73 73 1/4 73 1/2 74 74 1/4 74 1/2 75 75 1/4 75 1/2 76 76 1/4 76 1/2 77 77 1/4 77 1/2 78 78 1/4 78 1/2 79 79 1/4 79 1/2 80 80 1/4 80 1/2 81 81 1/4 81 1/2 82 82 1/4 82 1/2 83 83 1/4 83 1/2 84 84 1/4 84 1/2 85 85 1/4 85 1/2 86 86 1/4 86 1/2 87 87 1/4 87 1/2 88 88 1/4 88 1/2 89 89 1/4 89 1/2 90 90 1/4 90 1/2 91 91 1/4 91 1/2 92 92 1/4 92 1/2 93 93 1/4 93 1/2 94 94 1/4 94 1/2 95 95 1/4 95 1/2 96 96 1/4 96 1/2 97 97 1/4 97 1/2 98 98 1/4 98 1/2 99 99 1/4 99 1/2 100 100 1/4 100 1/2		ELECTRO-OPTICAL SYSTEMS, INC. Pasadena, California A Subsidiary of Sperry Corp. SUBSTRATE ASSEMBLY DEMONSTRATION PANEL PART NO. 1100301 QUANTITY 1 DATE 1-1-57
---	--	---

1100301 - 1100301 - 1100301 -



3-11

REVISIONS			
NO.	DATE	DESCRIPTION	BY



1100332

- ② AREA CONTAINS 210 EACH 5 MIL CELLS, CONVENTIONAL CONTACT, AND 3 MIL COVER GLASS
- ③ AREA CONTAINS 210 EACH 4 MILL CELLS, CONVENTIONAL CONTACT, AND 3 MIL COVER GLASS

ITEM NO.	QUANTITY	DESCRIPTION	UNIT	REMARKS								
LIST OF MATERIALS												
UNLESS OTHERWISE NOTED:												
1.		Lot# 111										
2.		Lot# 111										
<table border="1" style="width: 100%;"> <tr> <td>DATE</td> <td>BY</td> <td>APP'D</td> <td>DATE</td> </tr> <tr> <td> </td> <td> </td> <td> </td> <td> </td> </tr> </table>					DATE	BY	APP'D	DATE				
DATE	BY	APP'D	DATE									
ORIGINAL APPLICATION												

DATE	BY	APP'D	DATE

DATE	BY	APP'D	DATE

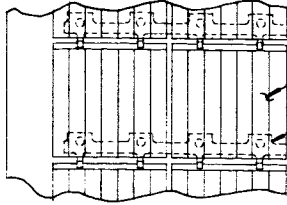
DATE	BY	APP'D	DATE

ELECTRO-OPTICAL SYSTEMS, INC.	
Pasadena, California - A Subsidiary of Xerox Corp.	
DEMONSTRATION PANEL ELECTRICAL LAYOUT	
SECURITY CLASSIFICATION	
E	1100332
DATE	12705

FIG. 3-3

3

SECURITY CLASSIFICATION



210 (REF) POSITIVE (NEAR SIDE)

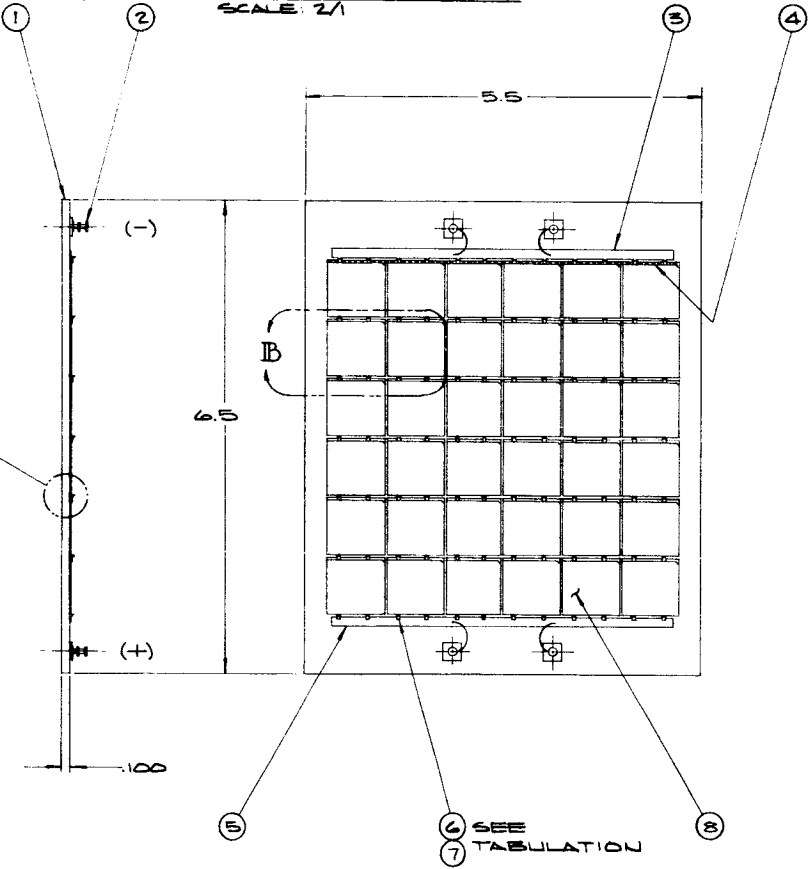
67 (REF) NEGATIVE (FAIR SIDE)

DETAIL B
 SOLAR CELL ORIENTATION & POLARITY
 (SHOW PRIOR TO APPLYING FILTER)
 SCALE: 2/1

C

B

A



SEE TABULATION

6 SEE
7 TABULATION

1 REF

13

DETAIL
 TYPICAL SOLAR
 INTERCONNECT
 SCALE

3

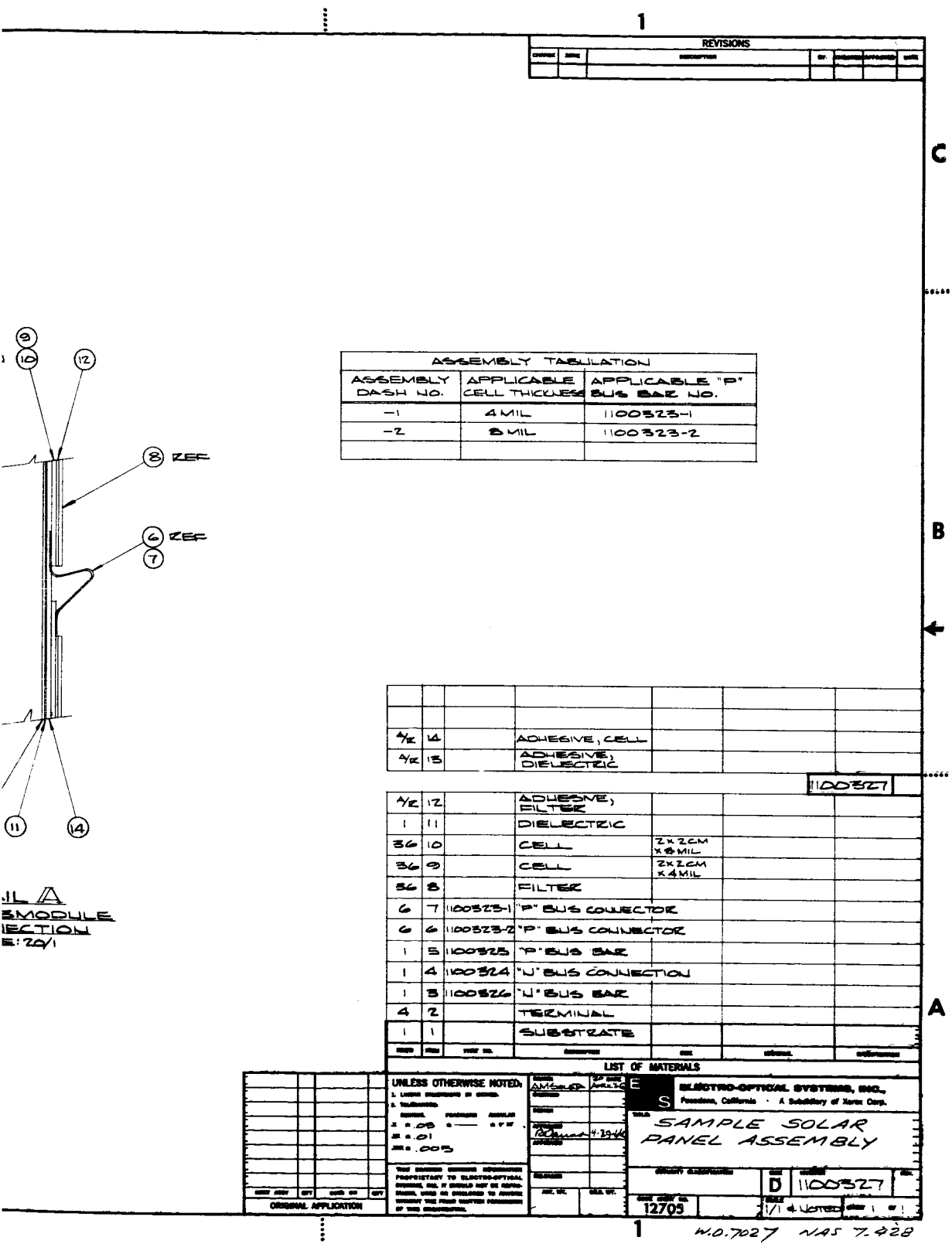


FIG. 3-4

4. JUPITER FLYBY SOLAR ARRAY SYSTEM

This section presents conceptual drawings and descriptions of the 5 kW and 10 kW solar arrays for a Jupiter flyby mission.

The 5 kW array tradeoffs have not been completed at this time; a full discussion will be incorporated in the final report. The 10 kW array is capable of experiencing the environment of an Atlas/Centaur launch, stowed within a shroud similar to the OAO nose fairing. The design discussed in this section is for a unit capable of producing 10.4 kW electrical power at earth's distance from the sun.

The projected weight of the array is equivalent to 27.4 lb/kW, including mechanisms for deployment. This weight is based on the use of aluminum electroformed structures, beryllium frames, 1-mil integral cover glass and silicon solar cells 0.004 in. thick with capability of 10 W/ft². All of these items are under development and should be available for incorporation into a demonstration panel in early 1967. The first demonstration panel to be assembled in this program will use a nickel electroformed structure, aluminum frames, 3-mil cover glass, and currently available 4-mil solar cells. Use of the first demonstration panel, of a 10.4 kW array, could result in an overall array weight of 42.4 lb/kW, including mechanisms. The following items represent some of the more significant structural design modifications which will be examined to decrease array weight:

1. Hollow core electroformed from aluminum.
2. Panel frame structure fabricated from beryllium.
3. Incorporation of thermal control surfaces into the metallic substrate by anodizing.
4. Incorporation of the major electrical cables into the frame design so that this material serves the dual purpose of conducting current and adding to the structural strength.
5. Use of better production techniques to decrease adhesive weight.

Another modification relates to decreasing the solar cell stack weight by developing 4-mil cells with 1-mil cover glass capable of producing 10 W/ft² at standard conditions.

4.1 Atlas/Centaur 10 kW Array

The configuration of the 10 kW array is shown in Fig. 4-1. The array contains 241,920 2-cm-squared solar cells, with a cell surface of 1040 sq ft. The gross surface area, including the subpanel frames but not including spacing between subpanels, is 1239 sq ft. The area of the substrate, not including frames is 1100 sq ft. Using the specific power value of 10 W/ft² the Atlas/Centaur array will generate 10.4 kW of raw power at standard conditions and 100 percent electrical load.

4.1.1 Structure

The design concept of the Atlas/Centaur solar panel assembly was governed mainly by the power requirement of 10 kW. This requirement demands an array of greater than 1000 sq ft.

The additional requirements governing the array design and layout are:

1. Environmental conditions
2. Spacecraft limitations
3. Spacecraft support arrangements
4. Electrical arrangement
5. Stowed position
6. Deployment and deployed condition

The most critical environmental condition occurs during the boost phase of the flight, when vibrations and steady-state acceleration subject the solar panel package to high loading conditions. These conditions require supporting arrangement such that the inertia loads can be transferred into the spacecraft.

After solar panel deployment and during the transit phase of flight the mechanical loading conditions associated with the

small steering and attitude corrections are insignificant and do not influence the design. A condition which can be significant is the thermal stress and distortion caused by either steady-state thermal gradients or material that includes composite metals with different coefficients of thermal expansion. The relative differential expansions between subpanels of different temperatures due to the influence of the spacecraft can be accommodated by allowing axial travel in all but one of the subpanel hinges. The intrapanel loading due to dissimilar metal in the structure design can be handled primarily by a choice of material with similar coefficients of thermal expansion, compliance in the method of attachment, and adequate structural strength to survive the worst-case loading condition. This design employs a compliant attachment between the substrate and frame.

A further factor affecting structural design is the resonant frequency limit of 0.4 Hz for the deployed array. The frame design itself is the principal contributing factor in conveying stiffness to the deployed array. By selecting a deployed array configuration that minimizes the cantilever length, the frame stiffness requirement is lessened. The dynamic analysis of Subsection 7.3.3.1 derives the array resonant frequencies.

Because of the increase in dynamic loading conditions for increasing station numbers along the spacecraft (see Subsection 2.5.2) the attachment between the array and spacecraft is located at the aft attachment point. No other attachment along the spacecraft is made.

The electrical requirement of 100V resulted in a mechanical module size of 56.5 x 58.4 in. Three mechanical modules are contained in each subpanel. (See Fig. 4-2.)

The stowed package of the solar panels must fit within the dynamic envelope. This requirement determines the maximum solar panel frame size and the solar panel curvature rise. By designing the mechanical modules so that each module's surface has a 10-degree slope

at its periphery, maximum usage could be made of the packaging volume (see Fig. 4-3). This constitutes a curvature rise of 3 inches.

The stowed package is strapped down to form a rigid unit. This allows transfer of boost loads from subpanel to subpanel. Providing the frame assembly with a tongue-and-groove design achieves this design requirement at little additional weight.

Deployment of the array causes loadings on the frame structure; to minimize this, considerable effort was expended on deployment sequencing and limiting the closing loads to those acceptable to the design.

The following items summarize the structural concept findings:

1. The optimum subpanel contains 3 mechanical modules with a total area of 69 sq ft.
2. The mechanical module (consistent with electrical requirements and packaging envelope) is 58.4 x 56.5 in.
3. The stowed subpanels are arranged 4 to a quadrant, as shown in Fig. 4-4.
4. By overlapping the subpanels in two of the quadrants, an interlocked package is obtained with considerable load restraint.

4.1.2 Electrical Layout

The electrical module layout is illustrated in Fig. 4-5. The figure delineates dimensions of this integral unit of the total array and shows the number of cells and spacing between cells in the 10.4 kW array. A typical series string of cells consists of 280 2-cm-square solar cells with a spacing of 10 mils between cells in both directions. The basic solar cell submodule consists of 6 cells in parallel with a total of 18 cells in parallel for the electrical module. The resulting power module (comprising 5.184 cells) supplies approximately 216W (100V at 2.16A) of useful electrical power based on the requirement of 10 W/ft².

The submodule is made up of a 2-cm-square solar cell (4 mils thick) and a 1-mil integral cover glass. The cell has a 10.6 percent conversion efficiency at AM0, 28°C. The cell has wrap-around around contacts and is interconnected with a silver bus bar.

4.1.3 Mechanisms

The array concept shown in this section is a two-sector system developed from the arrangements evaluated in Section 6. The selected pattern has the merit of providing the lowest mass moment and can be deployed without superimposing significant torsional moments on the spacecraft. If trapezoidal panels were adopted for the design, complex problems would occur in fabrication and analysis, which would make the array unjustifiably complex. Thus, only rectangular panels were considered for further study.

The rectangular panels for the 10 kW array can be packaged in a standard OAO shroud. (The Surveyor shroud with its conical envelope was found to yield a less effective package.) It was necessary to modify the aerodynamic shape of the selected package for this study. Figure 4-6 shows the variations which have taken place in the evolution from a four- to a two-quadrant array, together with the variations proposed for the aerodynamic envelope.

Modification of the envelope is justified by the fact that the main purpose is the development of a lightweight demonstration panel and it was required that the geometry be defined very early in the program. Further studies indicated that the array design would require a shroud modification.

The deployment sequence adopted for the selected array is shown in Fig. 4-7 and Fig. 4-8. The sequence starts with the outer panels, which are referenced in Fig. 4-8 as 4, 8, 5, 7, sector 1; and 9, 13, 10, 12, sector 2. This sequence allows the overlapped panels to be deployed with minimum disturbance to the spacecraft; all rotational moments cancelling. Following this maneuver, the latch devices constraining panels 2, 6 and 11, 15 are activated, allowing deployment

of all but the remaining four panels (1, 3 and 14, 16) to take place. To complete the array pattern, the stow latches are triggered to allow movement of panels 1, 3, 14, and 16.

The panels are latched after successful deployment by spring-biased pawls situated at the same locations as the drive springs. There are two power sources and latching mechanisms per panel together with signaling microswitches.

The objective in the stowed configuration is to allow the panels to rest together with minimum space and provide shear paths through the panel frames for the vibratory loads experienced during the launch. Figure 4-9 (as well as Fig. 4-6 and Fig. 4-8) shows the manner in which the array is overlapped to obtain a symmetrical stacking arrangement, allowing the hinge brackets to be in the vacant corner spaces. Because of the biconvex structural design, the maximum diameters and tangential points to the spacecraft dynamic envelope occur at the panel centers.

The panels will be self-supporting and are not connected to the spacecraft structure other than at station 0, thus minimizing vibration amplitude gain effects.

Figure 4-10 illustrates the stowed configuration with banding and spring ejectors superimposed on the latched panels. The banding would be used as an additional constraint if subsequent analysis discloses buckling of the panels due to longitudinal environmental loading during launch modes.

Initially, one of the requirements was to package the 5 kW array within the dynamic envelope of the Atlas/Agena nose fairing, and package the 10 kW array in the Atlas/Centaur nose fairing. During the development, however, it was clearly seen that this would restrict the design concepts; since the prime effort is in lightweight array study and development, restrictions of exact space for packaging were considered unimportant at this stage.

The Surveyor shroud has a severe taper commencing at 120 in. beyond station 0, which had to be extended by 113 in. Alternatively, the aerodynamic shape could be modified to encompass the stowed array (Fig. 4-7).

In the stowed condition, the panels are subjected to the vibrations introduced by the spacecraft's launch vehicle. These increase in magnitude along the spacecraft structure due to the system gain. Rigid connection to the spacecraft structure (remote from the spacecraft/launch vehicle interface) was not considered because such mounting would tend to accentuate transmission of high-amplitude vibration to the panel. A better approach is to nest the frames and mechanically lock them at either end with latches of the retractable-shaft type. Using this technique the retractable pin absorbs the shear loads, yet retains the features of reliability and lightness of weight.

Figure 4-11 illustrates the releasing device adopted; improvements already have been attempted in the design by providing a means of repeatedly retracting the pin by manually pulling the end of the shaft. (It is shown in the drawing in various stages of deployment.) This feature reduces the requirement for either actuation of the initiator or removal of the device (impossible if the components are welded to save the bolt weight). Internally, there is a soft aluminum bolster pad which absorbs most of the firing impact by becoming distorted. The result is that the frame on which the components are mounted receives an attenuated pulse of insignificant proportions.

With the demand for reliable lightweight actuators, springs were selected and the application modified in an attempt to achieve some control over the panel velocity. The approach adopted in this study (shown in Fig. 4-12) is to allow the spring to be deployed beyond its normal free condition. With this approach, the springs begin to exert a resisting force which increases in magnitude as the panel reaches full deployment. Theoretically, an absolute balance is possible neglecting friction and constraints of positive latching

when deployed. As a result, a compromise is necessary; thus, a limiting factor was established on the basis of the impact loads which could be tolerated by the structure. Weight of one motor is approximately 5.5 oz; spring weight is 3 oz.

4.1.4 Solar Array Weight & Power Predictions

Table 4-I presents the weight and power predictions of the 10.4 kW array. Column 1 summarizes the weight of the array using the same materials and techniques as will be used in the demonstration panel.

Column 2 gives the weight of the array based on technology which is under development including the use of beryllium framework and aluminum electroformed structures.

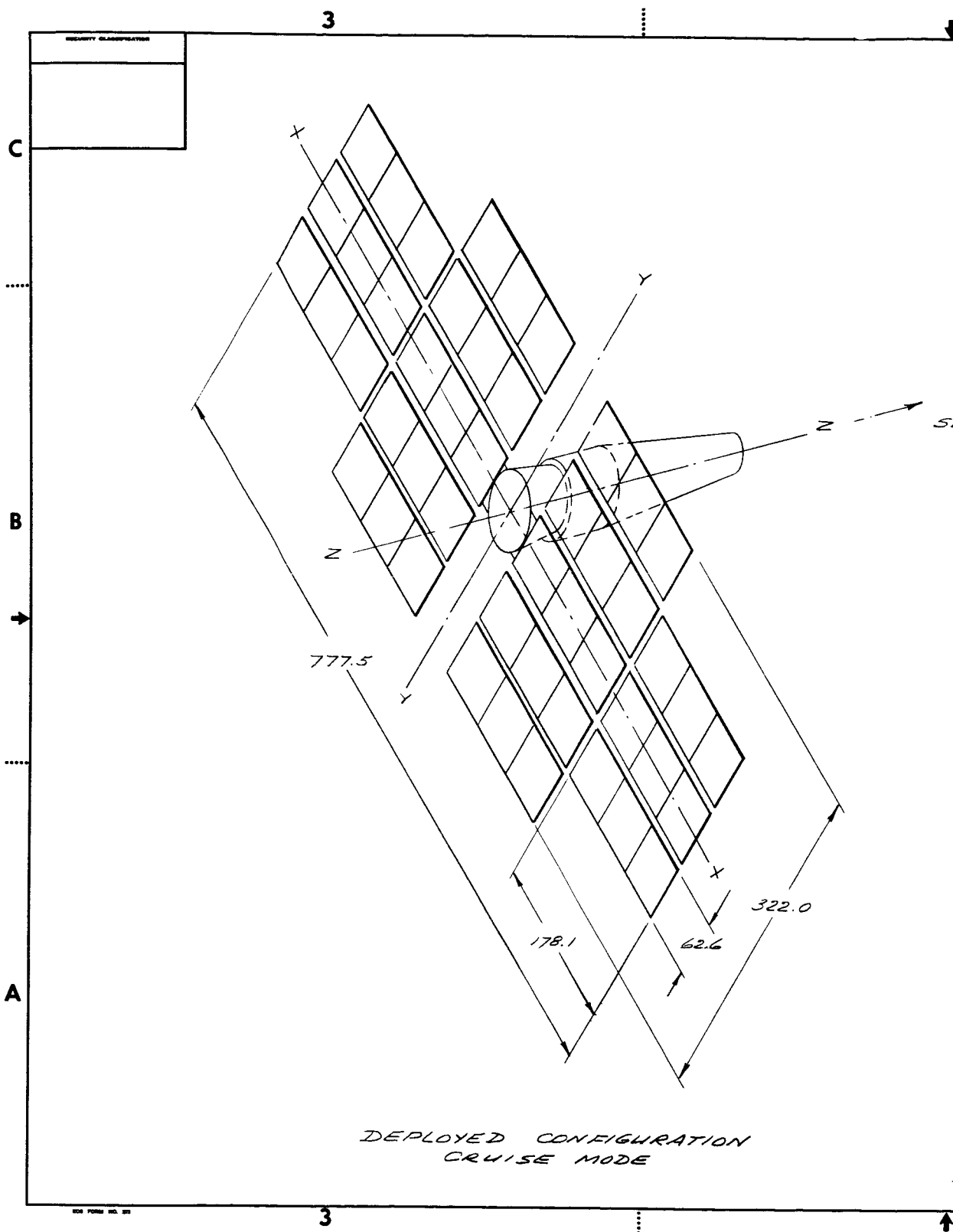
4.2 Atlas/Agna 5 kW Array

Engineering emphasis to date has been placed on the 10 kW array. Design and discussion of the 5 kW array will be incorporated into the final report.

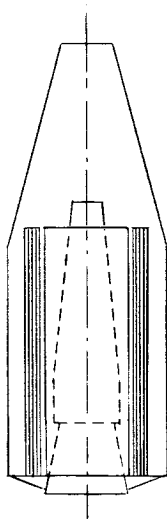
TABLE 4-I
PROJECTED WEIGHT AND POWER CHARACTERISTICS, 10.4 kW ARRAY

Item	Description	Demonstration Panel Design		Array Design	
		lb/ft ²	lb	lb/ft ²	lb
Cover glass	3 mil microsheet 2 x 2 cm	0.0394	41.0		
	1 mil integral cover glass 2 x 2 cm			0.0131	13.7
Filter Adhesive	2 mil RTV-602	0.0096	10.0		
	none			-----	-----
Solar Cell	4 mil conventional contact 2 x 2 cm	0.0530	55.1		
	4 mil wrap-around contact 2 x 2 cm			0.0530	55.1
Interconnector	Bus bar & solder	0.0200	20.8		
	Printed circuit back contact			0.0100	10.4
Cell Adhesive	4 mil RTV-40	0.0207	22.8		
	Same			0.0207	22.8
Dielectric	1 mil H-film	0.0072	7.9		
	Same			0.0072	7.9
Dielectric Adhesive	2 mil RTV-40, 18% of area	0.0037	4.1		
	Same			0.0037	4.1
Thermal Control Paint	3 mil laminar X-500	0.0240	29.7		
	None, anodized substrate			-----	-----
Cabling & Hardware	Separate cable bundles	0.0228	28.2		
	Major cabling incorporated in frame			0.0050	6.2
Mechanisms	See Section 7.1.2	0.0376	46.7		
	Same			0.0376	46.7
Substrate	2 mil electroformed nickel	0.0664	73.0		
	Electroformed aluminum alloy			0.0464	51.1
Frame	10 mil aluminum box beam	0.0815	101.0		
	Beryllium frame			0.0538	66.7
Sum Total	lb		440.3		285.0
Specific Power	Watt/ft ²		10W/ft ²		10W/ft ²
Array Power	Watt		10400W		10400W
Weight/Power	lb/kW		42.4 lb/kW		27.4 lb/kW

BLANK PAGE 4-10



REVISIONS					
NO.	DATE	DESCRIPTION	BY	APPROVED	REMARKS



MODIFIED ATLAS/CENTAUR
LAUNCH CONFIGURATION

1100347

REV	DATE	DESCRIPTION	BY	APPROVED	REMARKS

LIST OF MATERIALS					

UNLESS OTHERWISE NOTED: 1. LAUNCH CONFIGURATION IS SHOWN. 2. TOLERANCES 3. DIMENSIONS 4. ALL DIMENSIONS ARE IN INCHES UNLESS OTHERWISE SPECIFIED.		DRAWN: <i>HK</i> CHECKED: <i>5/22/66</i> DATE: <i>5/22/66</i> BY: <i>5/22/66</i>	PART NO.: <i>1100347</i> QUANTITY: <i>1</i> UNIT: <i>1</i>	MANUFACTURER: ELECTRO-OPTICAL SYSTEMS, INC. Pasadena, California - A Subsidiary of Korea Corp.	TITLE: CONFIGURATION OF 10 KW SOLAR PANEL FOR JUPITER FLY BY
THIS DRAWING AND/OR INFORMATION IS PROPRIETARY TO ELECTRO-OPTICAL SYSTEMS, INC. IT SHOULD NOT BE REPRODUCED, COPIED OR DISCLOSED TO ANYONE WITHOUT THE WRITTEN PERMISSION OF THIS ORGANIZATION.		MATERIAL: <i>55/66</i>	SECURITY CLASSIFICATION: D	PART NO.: 1100347	REV: 1
ORIGINAL APPLICATION		DATE: 12705	CLASS: 1	QUANTITY: 1	UNIT: 1

W.O. 7027 NAS 7-428

FIG. 4-1

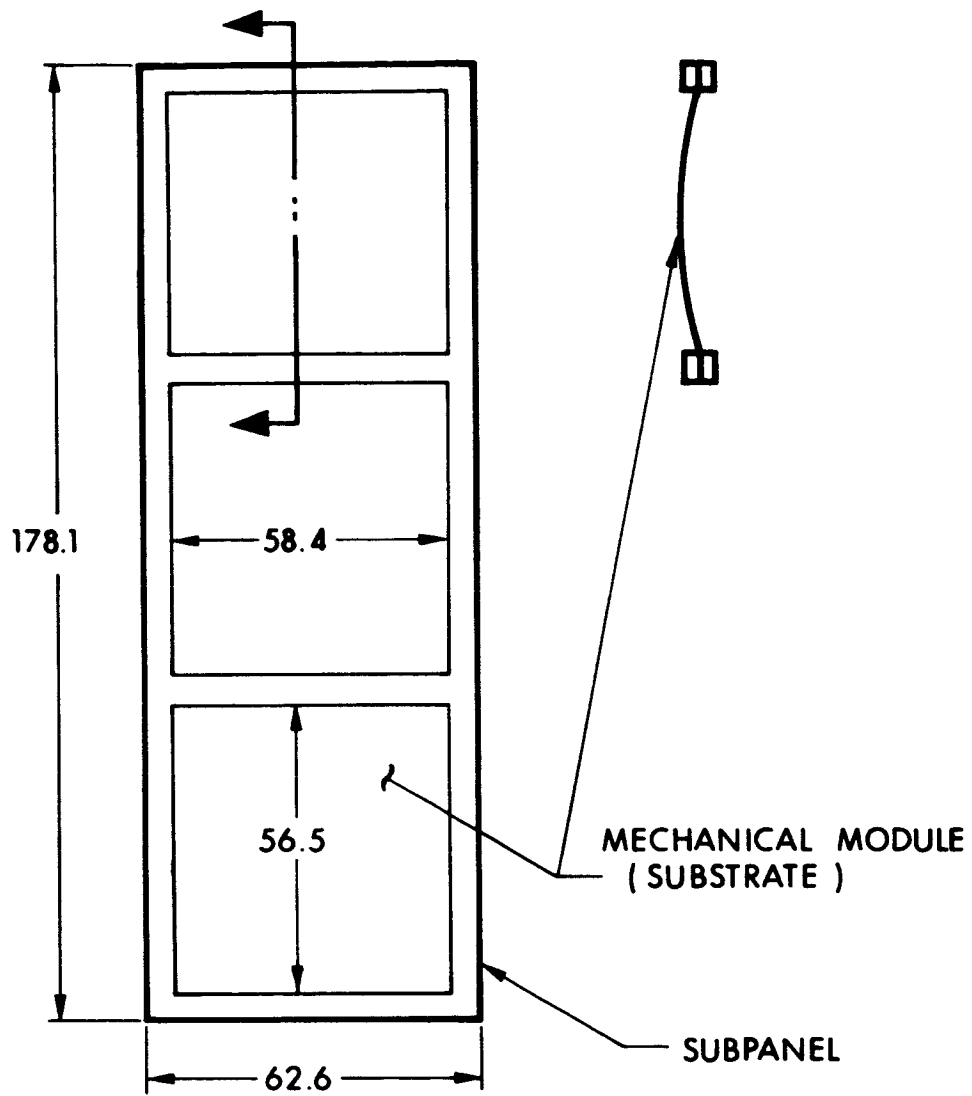


FIG. 4-2 MECHANICAL MODULE SIZE

BLANK PAGE 4-14

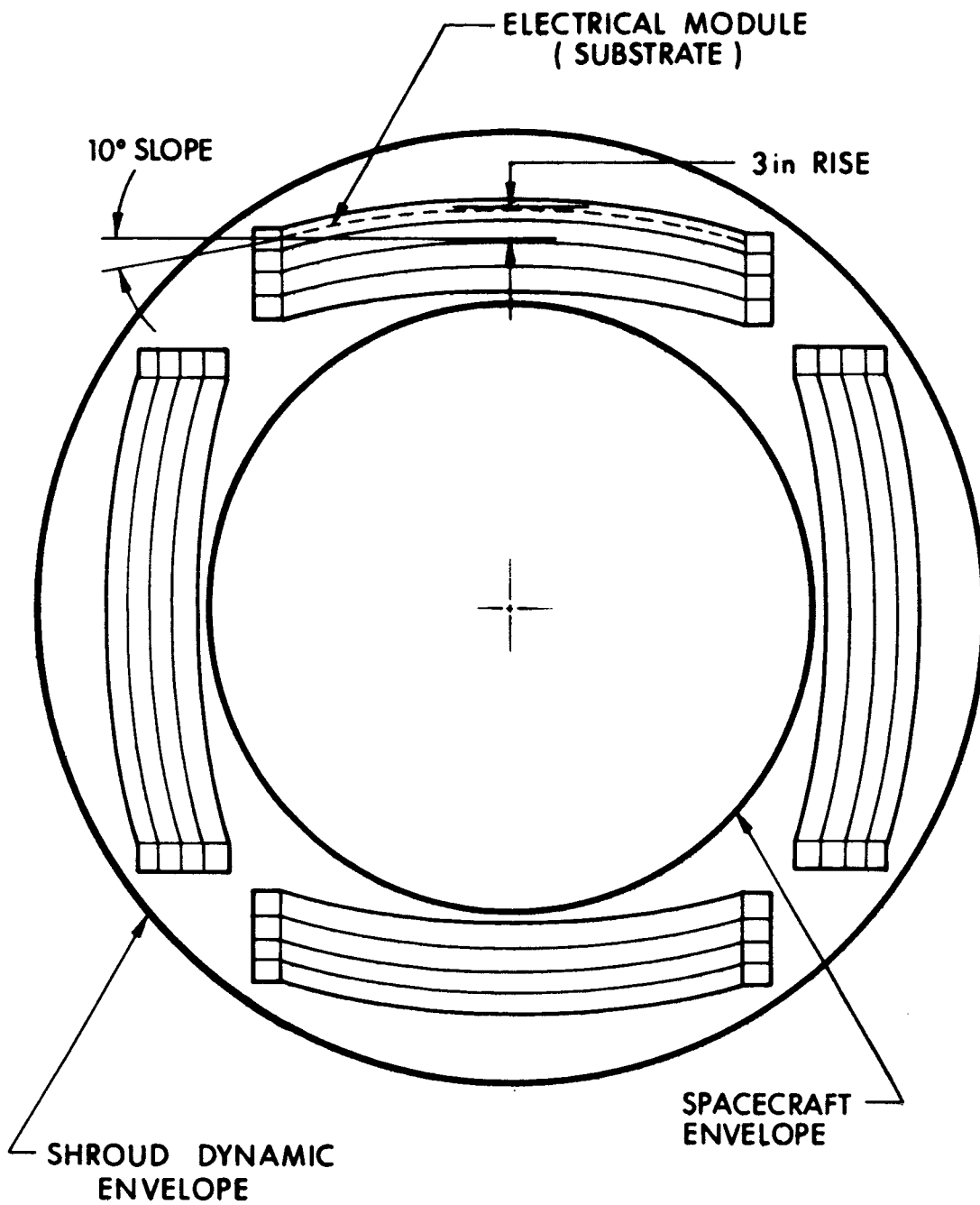
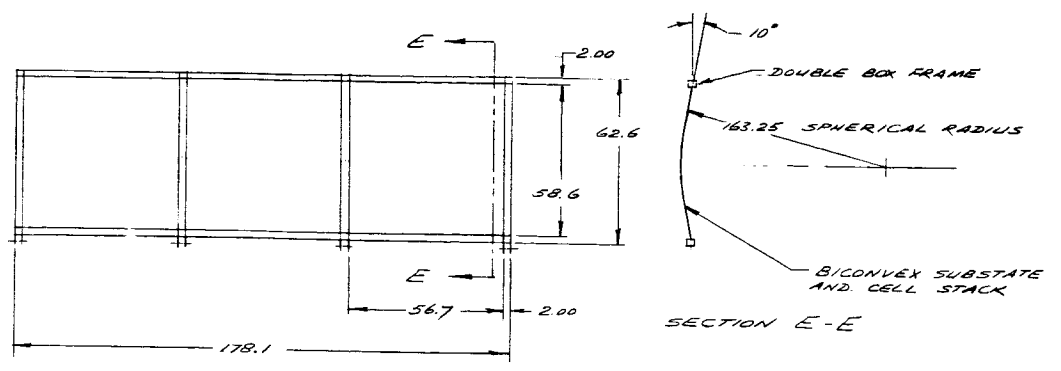
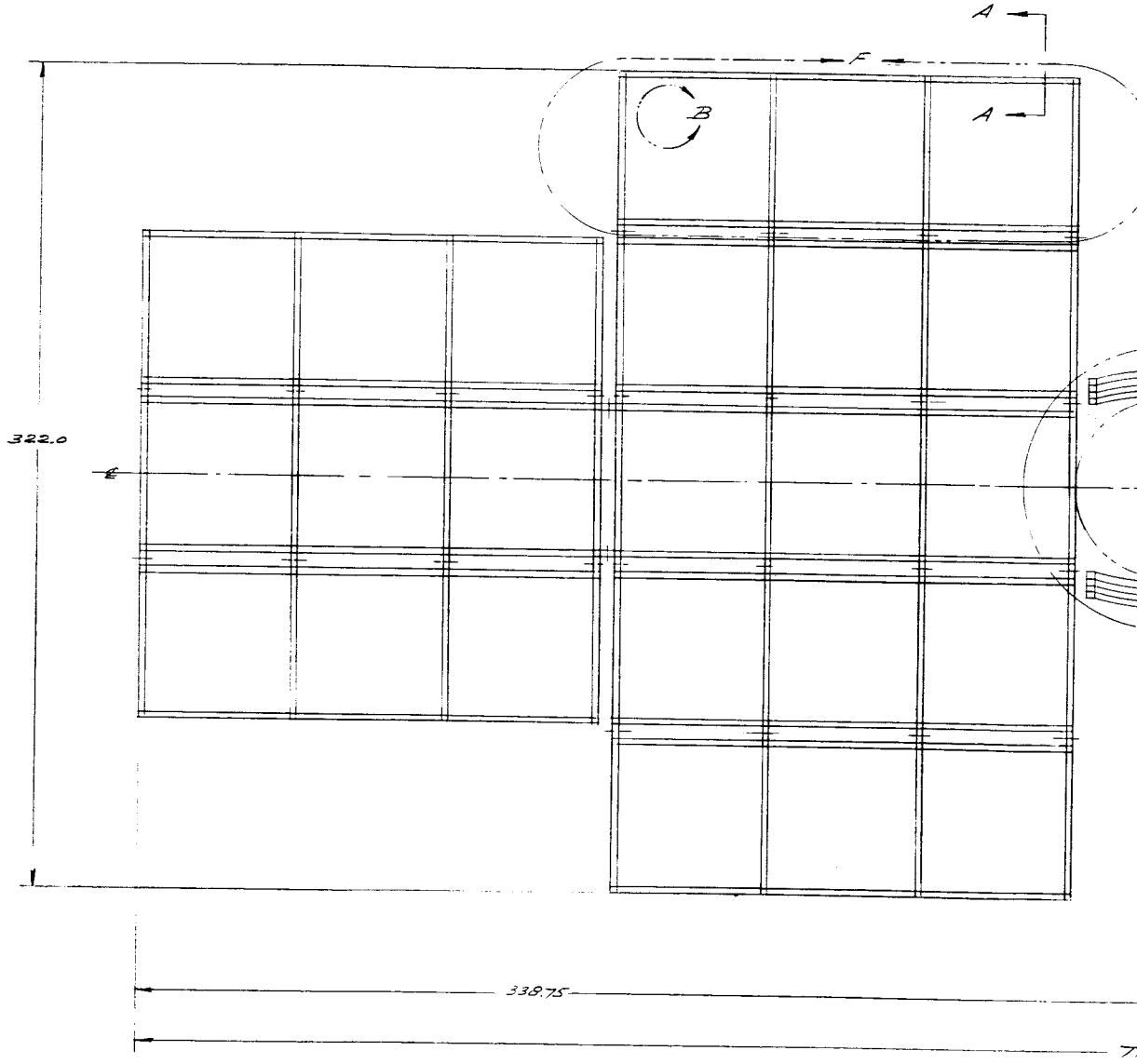


FIG. 4-3 PACKAGING OF SUBPANEL

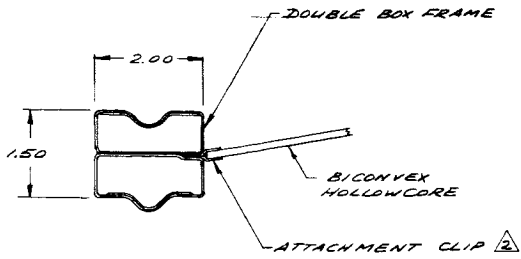
BLANK PAGE 4-16



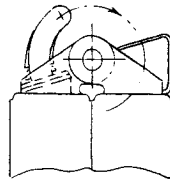
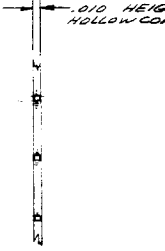
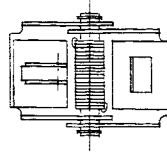
DETAIL F SUBPANEL CONFIGURATION



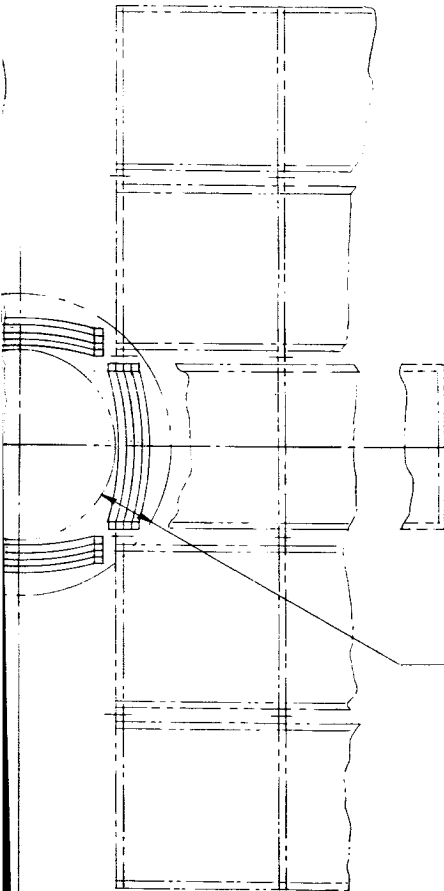
ARRAY CONFIGURATION
 PANEL ASSEMBLY DEPLOYED



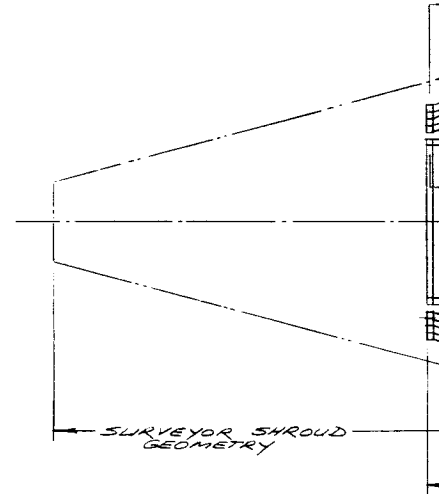
SECTION A-A
(TYPICAL FRAME CROSS SECTION)



DETAIL D
TYPICAL HINGING

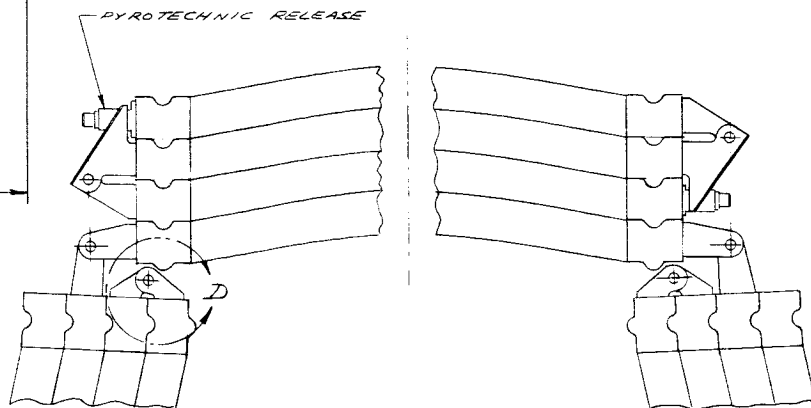


SOLAR ARRAY ENVELOPE



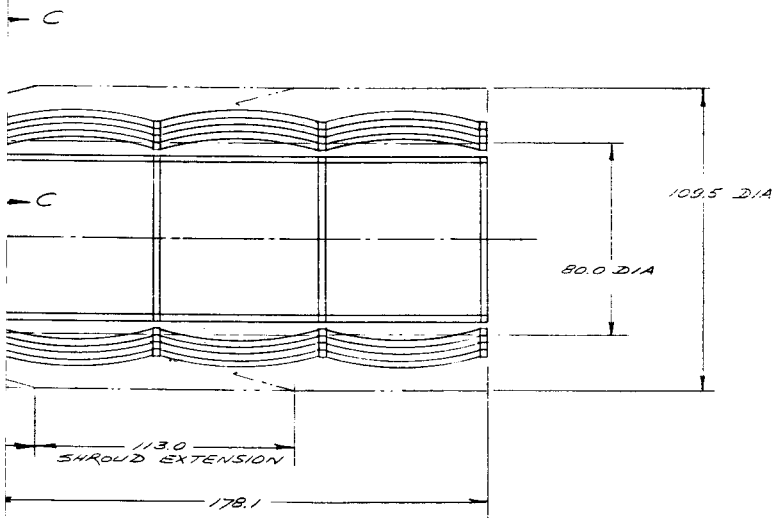
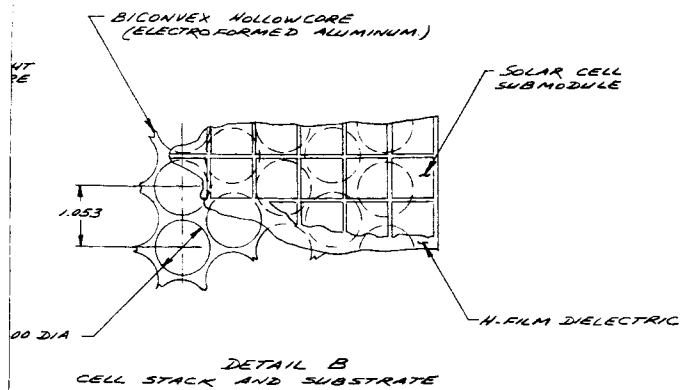
SURVEYOR SHROUD GEOMETRY

ARRAY CONFIGURATION
PANEL ASSEMBLY



SECTION C-C
LATCHING CONCEPT

- △ CLIP AND
- △ CELL SUBSTRATE GROSS
- (a) SURFACE
- (b) HOLLOW CORE
- (c) ATTACHMENT CLIP
- BU
- BETWEEN
- NOTES



AND SHROUD GEOMETRY
BY STOWED.

1100350

BONDED TO HOLLOWCORE SUBSTRATE
RIVETED TO FRAME

SURFACE (a) AREA 1040 SQ. FT.
SURFACE (b) AREA 1100 " "
SURFACE (c) AREA 12 " "

FACE AREA OF 291,920 EACH 2x2 CM CELLS
HOLLOWCORE BICONVEX SUBSTRATE AREA.
COUNTING FOR FRAME SURFACE AREA
IT DOES NOT INCLUDE SPACING
BETWEEN SUB PANELS
UNLESS OTHERWISE SPECIFIED.

DATE	FILE	REV. NO.	DESCRIPTION	BY	CHKD.	APPROVED
LIST OF MATERIALS						
UNLESS OTHERWISE NOTED:						
1. ALL DIMENSIONS IN INCHES.						
2. FINISHES:						
A	AS	AS	AS	AS	AS	AS
B	AS	AS	AS	AS	AS	AS
C	AS	AS	AS	AS	AS	AS
D	AS	AS	AS	AS	AS	AS
E	AS	AS	AS	AS	AS	AS
THIS DRAWING AND ALL INFORMATION CONTAINED HEREIN IS UNCLASSIFIED EXCEPT WHERE SHOWN OTHERWISE AND IS RELEASED TO THE PUBLIC WITHOUT LIMITATION OF ANY RESTRICTIONS.						
DATE	BY	JOB NO.	REV.	DATE	BY	DATE
ORIGINAL APPLICATOR				ELECTRO-OPTICAL SYSTEMS, INC. Pasadena, California - A Subsidiary of Xerox Corp. EOS CONFIGURATION 10 KW SOLAR ARRAY JUPITER FLYBY		
				DRAWING NO. J 1100350 REV. 12705 SHEET 1 OF 1		

W.O. 7037 NAS 7-428

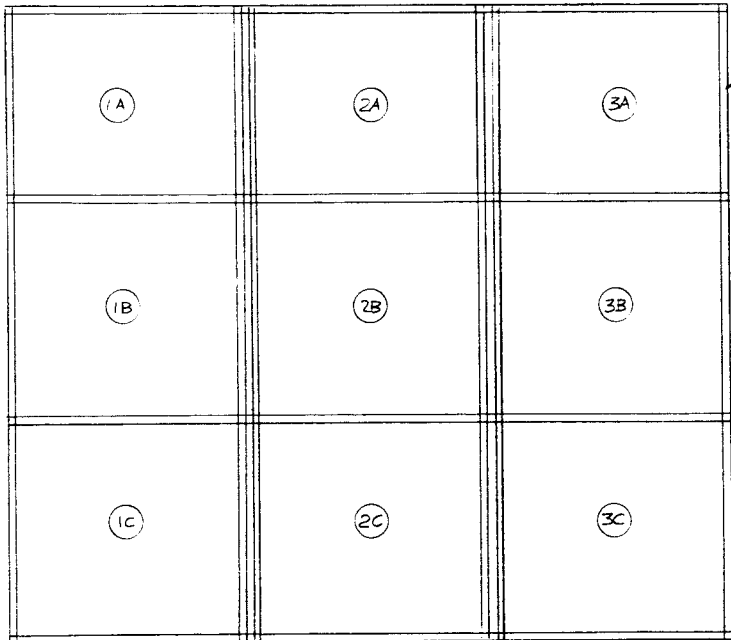
FIG. 4-4

② 4-18

SECURITY CLASSIFICATION

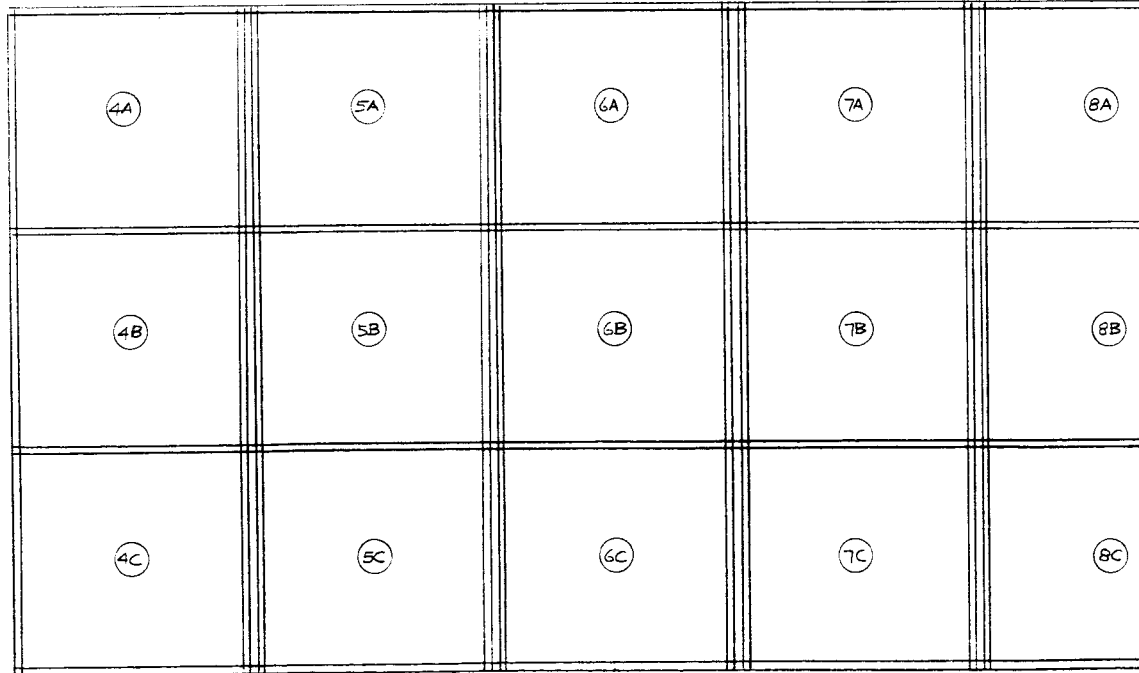
3

C



DE
TYP
FOR

B



A

SPACECRAFT

EOS FORM NO. 271

3

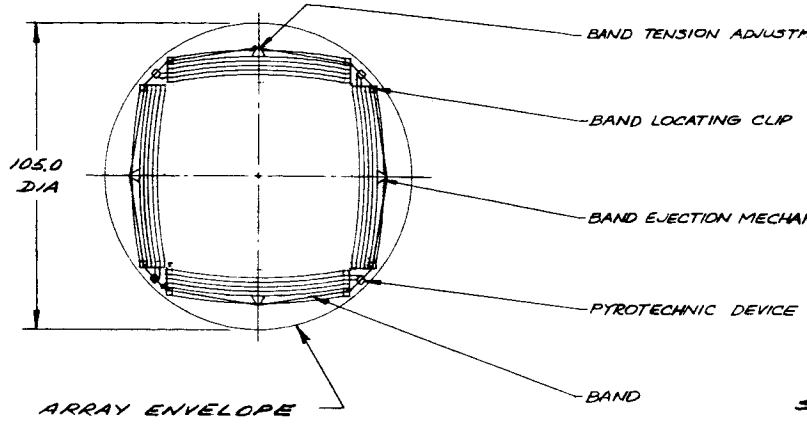
4-19

7027-IDR

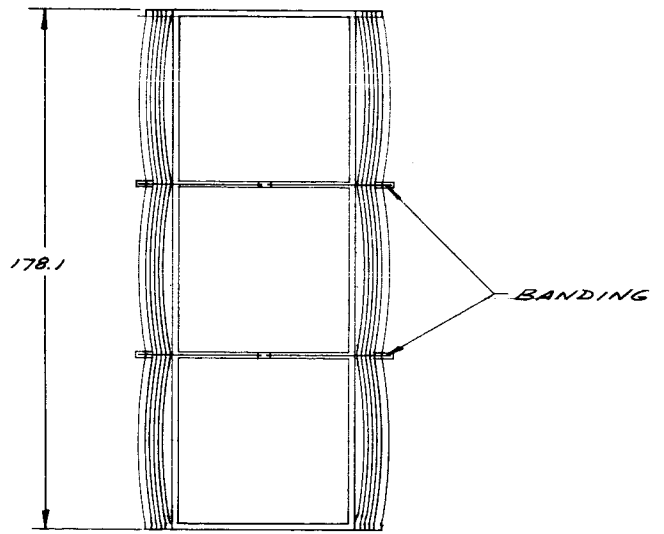
SECURITY CLASSIFICATION

C

3



B

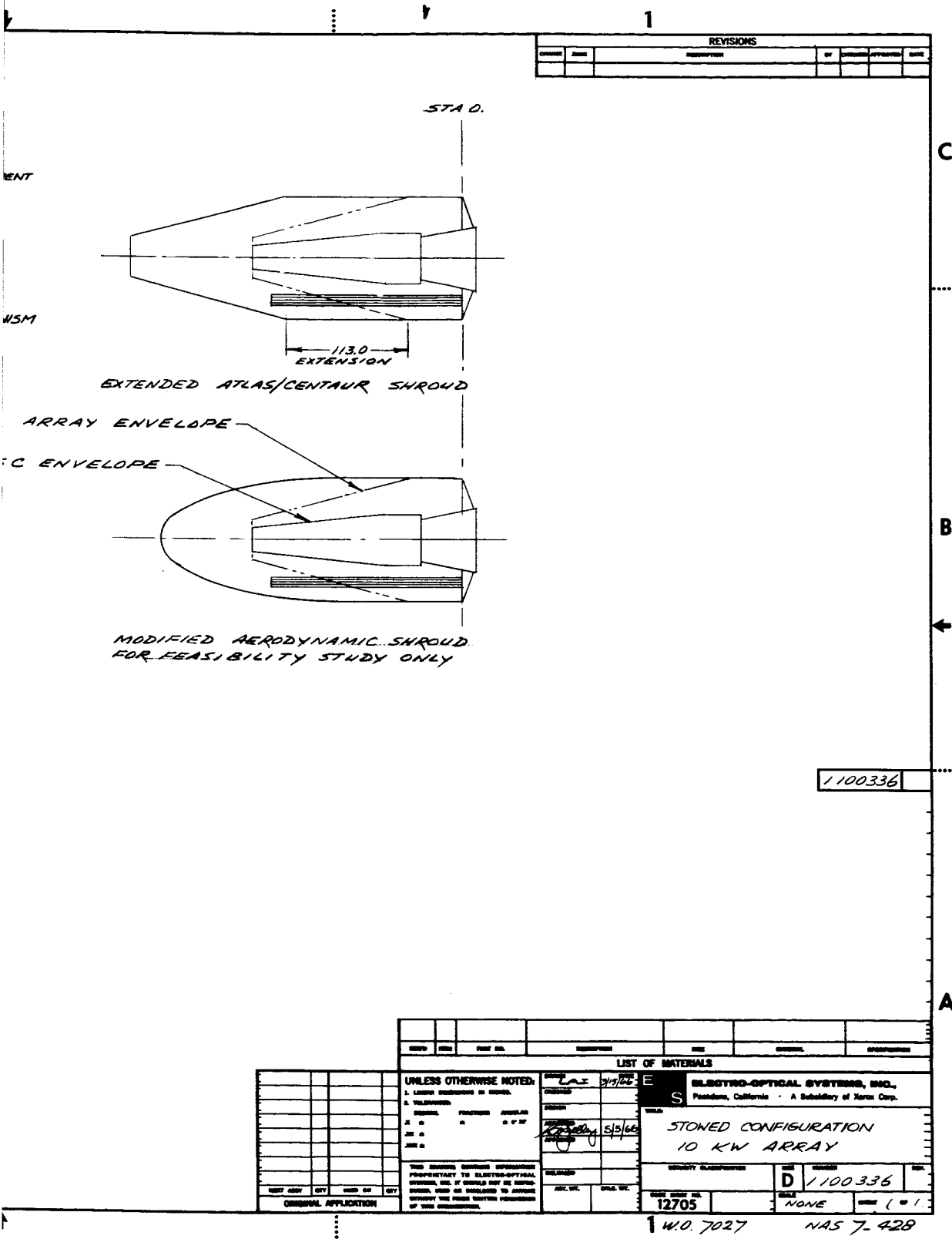


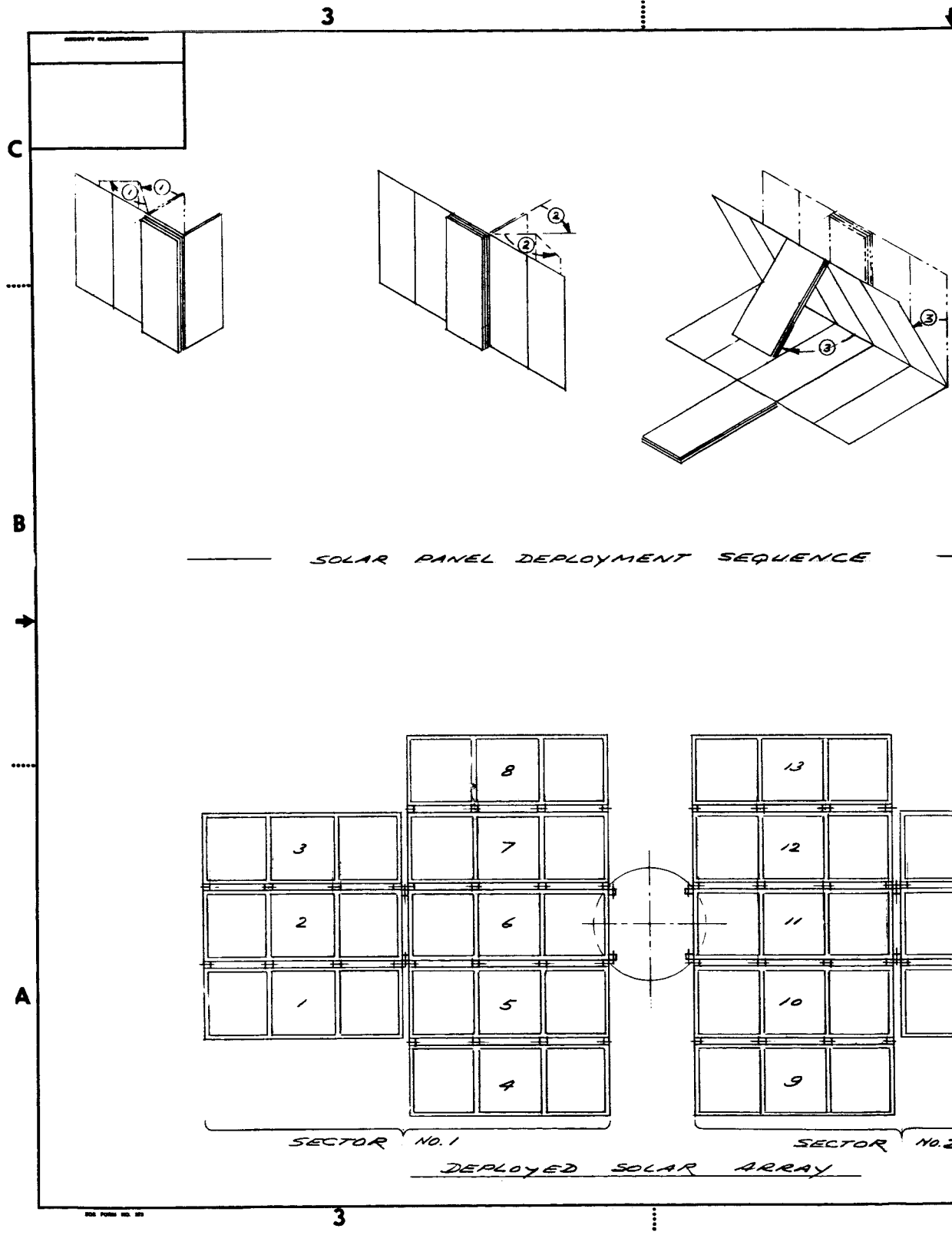
A

3

4-21

7027-IDR



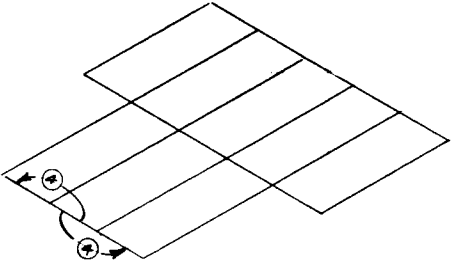


7027-IDR

4-23

1

REVISIONS						
CHANGES	DATE	DESCRIPTION	BY	APPROVED	DATE	



C

B

A

1100337

16	
15	
14	

ITEM	QTY	UNIT	DESCRIPTION	DATE	REMARKS	OPERATIONS
LIST OF MATERIALS						
UNLESS OTHERWISE NOTED:			E ELECTRO-OPTICAL SYSTEMS, INC., Pasadena, California - A Subsidiary of Honey Corp.			
1. LINES INDICATED BY DASHES.			S SOLAR PANEL DEPLOYMENT 10 KW ARRAY			
2. TOLERANCES:			FINISH: <i>Handwritten: 5/16/66</i> DIMENSIONS: <i>Handwritten: 5/16/66</i>			
3. MATERIALS:			SECURITY CLASSIFICATION: D 1100337			
4. FINISH:			DATE: 12705 CODE: NONE ORDER: 101			
5. COLOR:			110.7027 NAS 7.428			
6. WEIGHT:			ORIGINAL APPLICATION			
7. OTHER:			THE DRAWING SHOWS INFORMATION PROPRIETARY TO ELECTRO-OPTICAL SYSTEMS, INC. IT SHOULD NOT BE REPRODUCED, USED OR INCORPORATED IN ANY MANNER WITHOUT THE WRITTEN PERMISSION OF THIS ORGANIZATION.			

FIG. 4-7

5

4

3

PROPERTY CLASSIFICATION

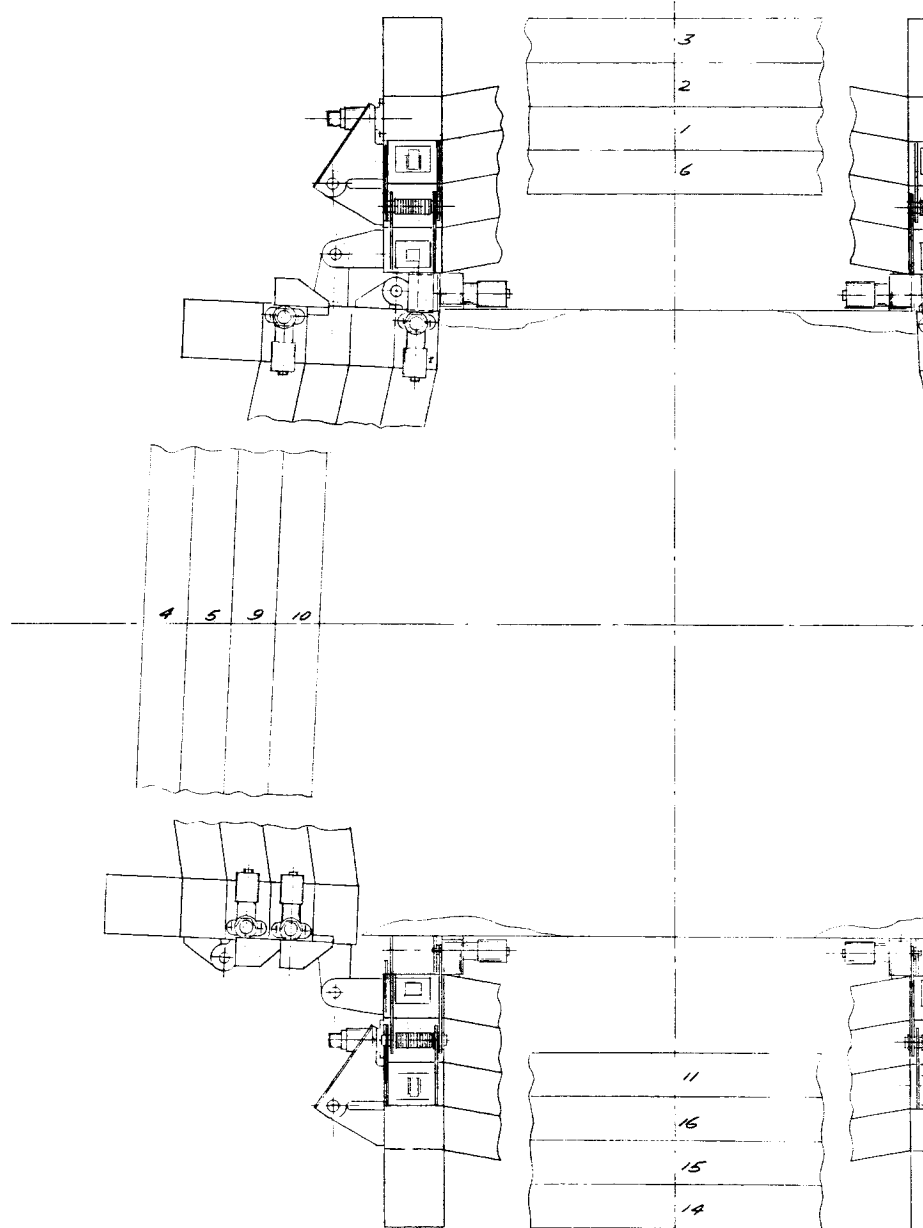
D

SECTOR NO. 1

C

B

A



SECTOR NO. 2

5

4

3

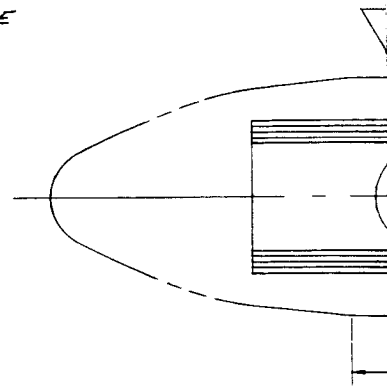
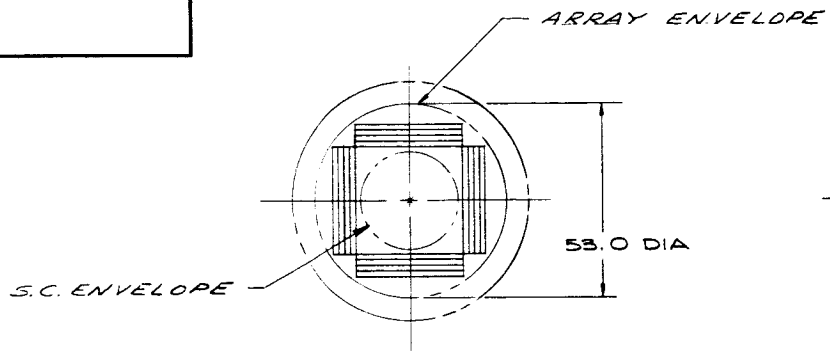
4-25

7027-IDR

SECURITY CLASSIFICATION

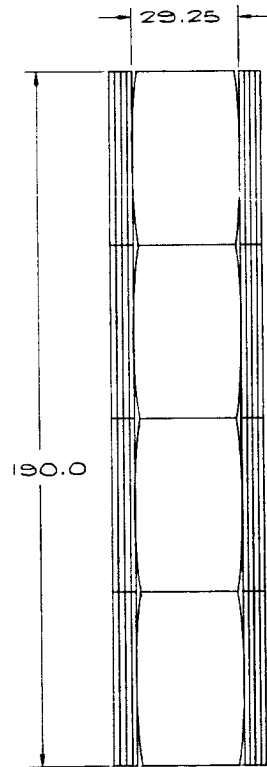
3

C



EXTEN

B



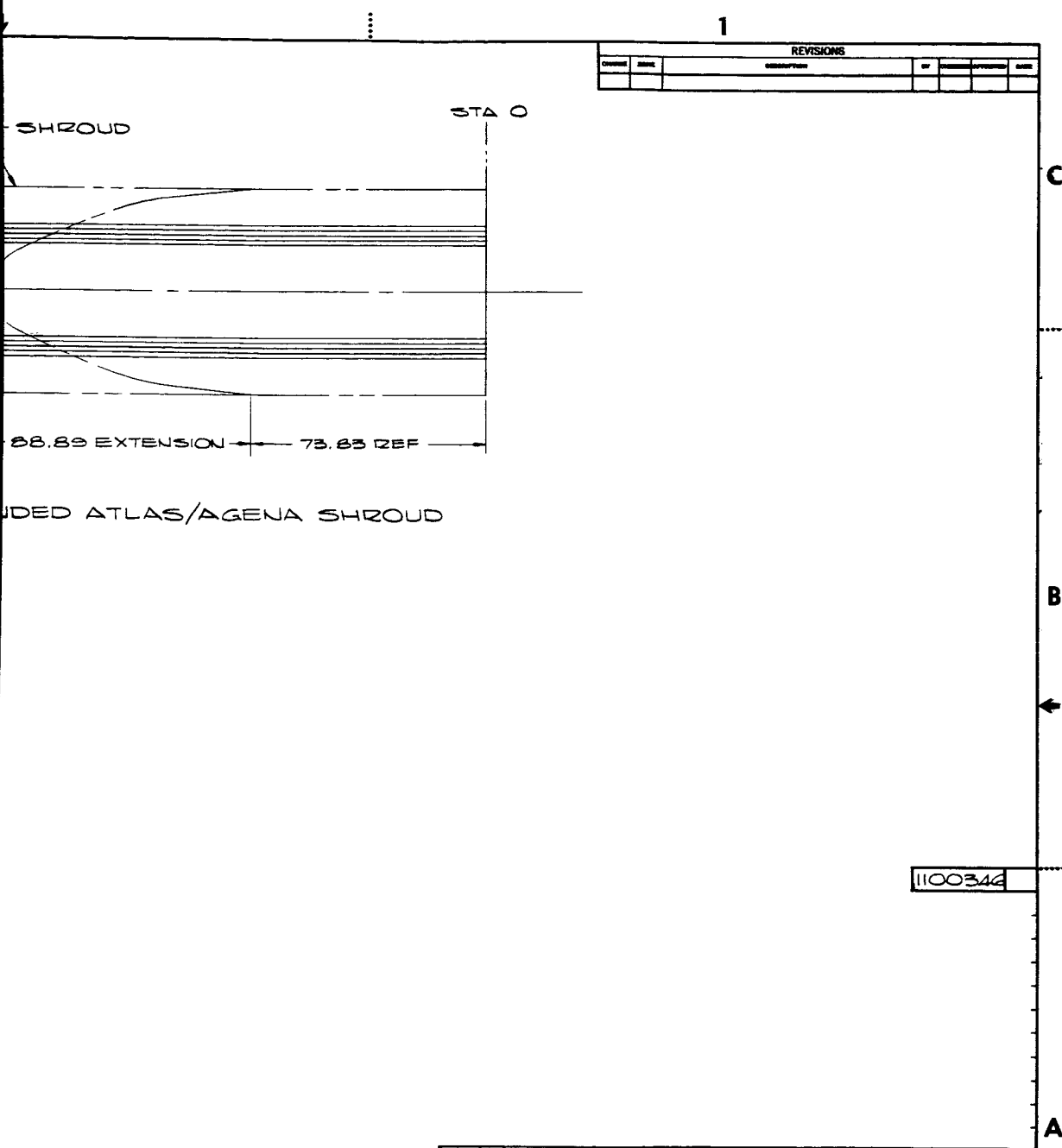
A

SEE FIGURE NO. 21

3

4-27

7027-IDR



REVISIONS			
CHANGE	DATE	DESCRIPTION	BY

PROVIDED ATLAS/AGENA SHROUD

1100346

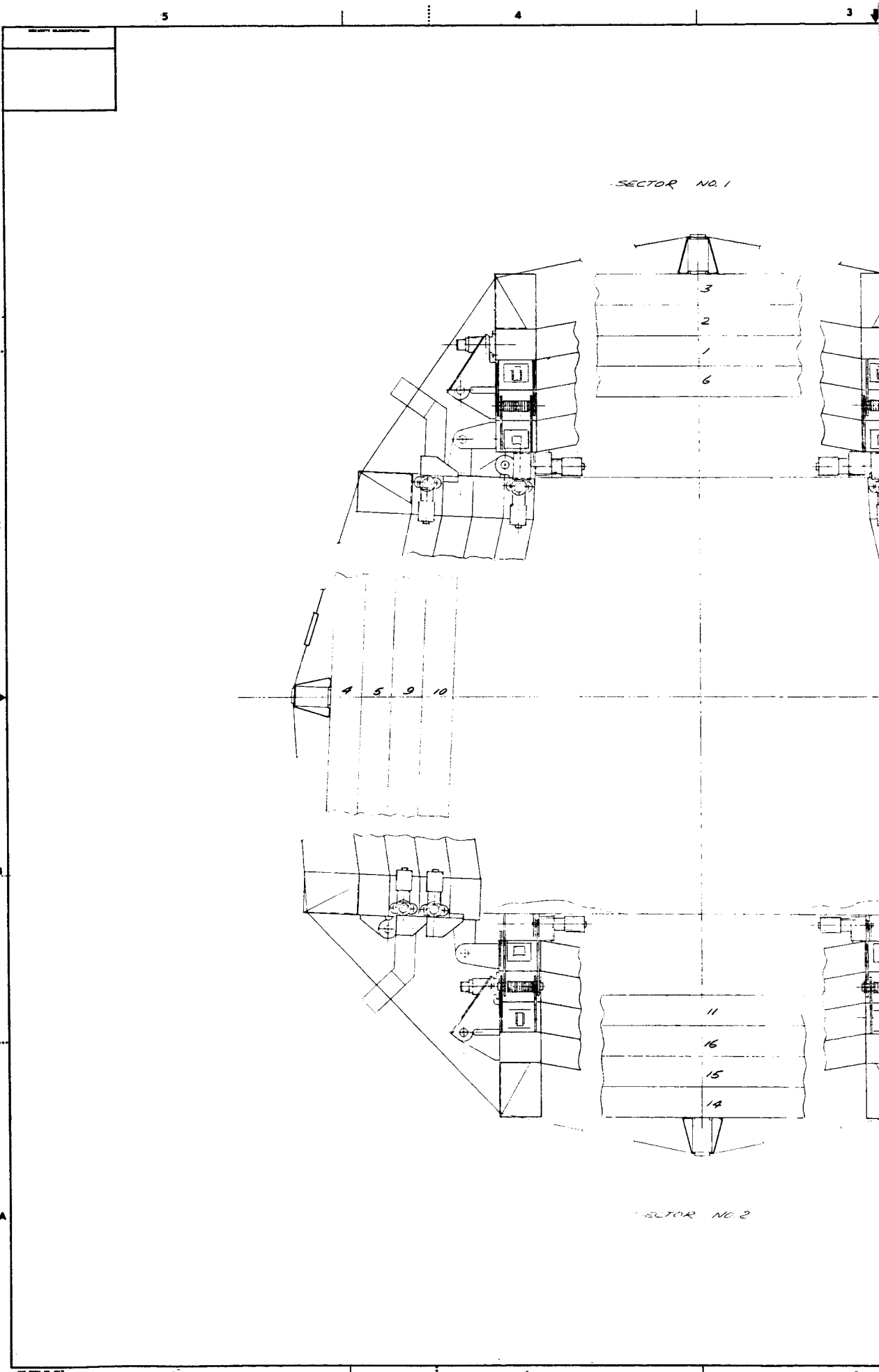
ITEM	QTY	UNIT	DESCRIPTION	DATE	REVISION

UNLESS OTHERWISE NOTED:	
1. LISTED DIMENSIONS IN INCHES	DATE: 5/5/66
2. TOLERANCES:	
FRACTIONAL DECIMAL ANGULAR	
± .010 ± .005 ± .010	
± .015 ± .005 ± .010	

LIST OF MATERIALS	

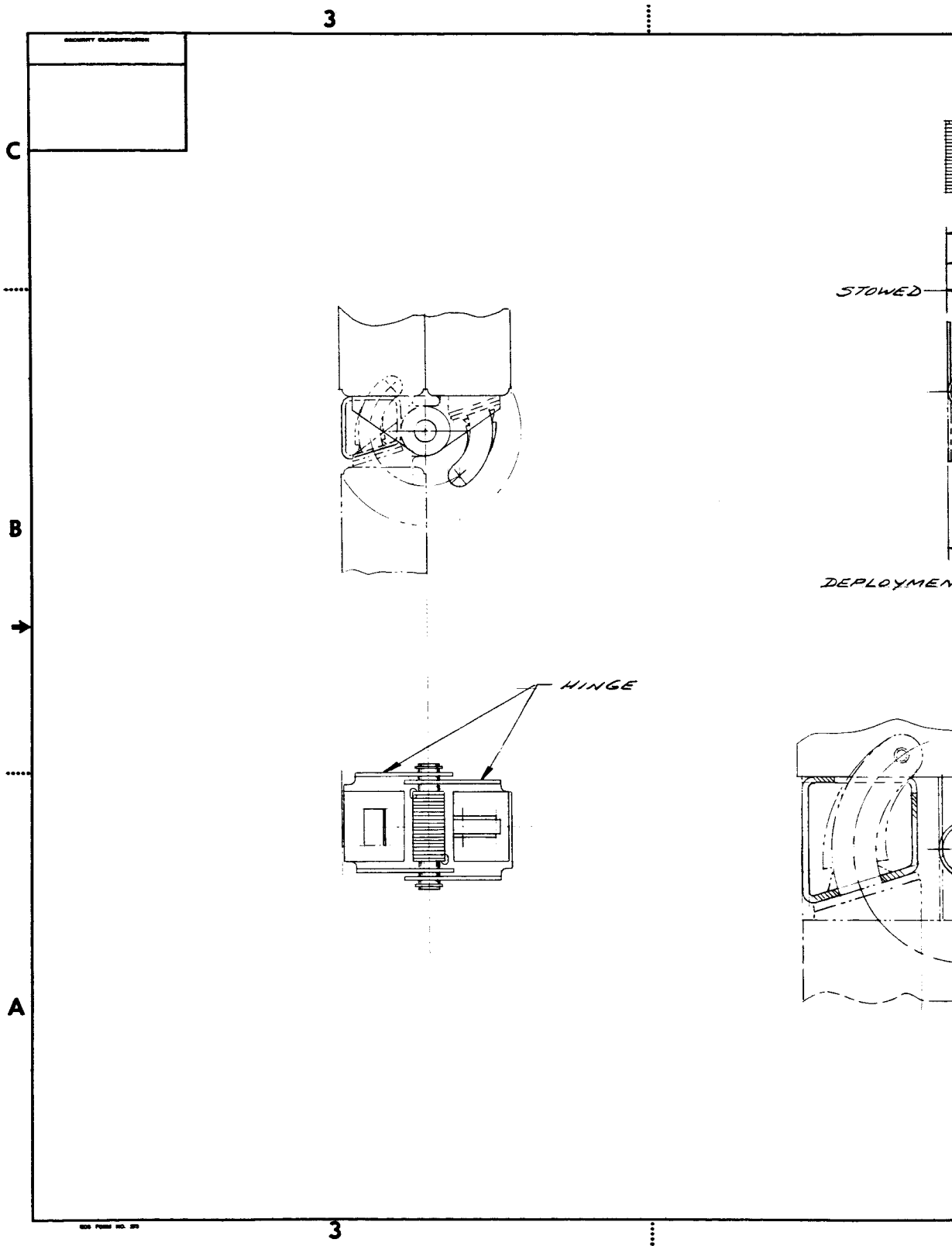
<p>THIS DRAWING CONTAINS INFORMATION PROPRIETARY TO ELECTRO-OPTICAL SYSTEMS, INC. IT SHOULD NOT BE REPRODUCED, COPIED OR DISCLOSED TO ANYONE WITHOUT THE WRITTEN PERMISSION OF THIS ORGANIZATION.</p>	<p>ELECTRO-OPTICAL SYSTEMS, INC. Freedom, California - A Subsidiary of Aero Corp.</p>
<p>STOWED CONFIGURATION 5 KW SOLAR ARRAY</p>	<p>SECURITY CLASSIFICATION: D DATE: 11/00346 SCALE: 1/20 SHEET: 1 OF 1</p>
<p>DATE: 12705</p>	<p>W.A. 7027 NAS 7-428</p>

FIG. 4-9



4-29

BLANK PAGE 32



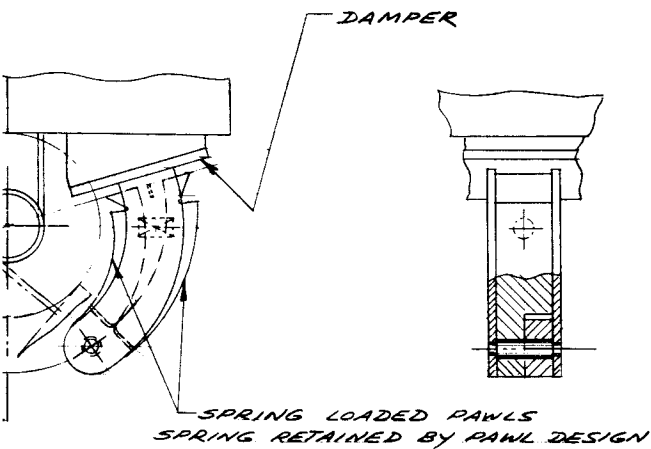
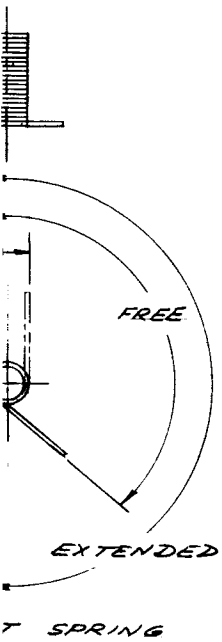
4.33

1

REVISIONS			
NO.	DATE	DESCRIPTION	BY

DEPLOYMENT SPRINGS

	LOCATION	NO. REPS	ACTIVE TURNS	DEPLOYMENT ANGLE	WIRE DIA.	MATERIAL	WT./SPRING
1	MAIN HINGE	2	7	90°	.053	Be Cu	.0122
2	SECONDARY	2	6	180°	.039	"	.0059
3	DOUBLE PANEL DEPL.	4	7	180°	.031	"	.00919
4	SINGLE PANEL DEPL.	8	7	180°	.026	"	.00294



1100338

SCALE 2/1

REV.	DATE	REV. NO.	DESCRIPTION	BY	APPROVED	DATE

UNLESS OTHERWISE NOTED:		LIST OF MATERIALS	
1. LEADERS PRESENTED IN ORDER	2. DIMENSIONS	3. FINISHES	4. TOLERANCES
5. MATERIALS	6. PARTS	7. ASSEMBLY	8. OTHER
9. JOINTS	10. SURF. FIN.	11. COAT.	12. OTHER
THIS DRAWING SHOWS EXPANSION PROPRIETARY TO ELECTRO-OPTICAL SYSTEMS, INC. IT SHOULD NOT BE REPRODUCED, USED OR DISCLOSED TO ANYONE WITHOUT THE WRITTEN PERMISSION OF THIS CORPORATION.		ELECTRO-OPTICAL SYSTEMS, INC., Pasadena, California - A Subsidiary of Jetco Corp.	
TITLE: HINGE - SPRING - DAMPER CONFIGURATION 10 KW ARRAY		QUANTITY: 1	
DRAWN: [Signature]		DATE: 11/00/338	
CHECKED: [Signature]		SCALE: 2/1	
APPROVED: [Signature]		PART NO: 12705	
ORIGINAL APPLICATION		W.O. 7027 NAS 7-428	

FIG. 4-12

5. COMMENTS ON COMPONENT STATUS

The program goal of a 5 to 10 kW solar array with a weight-to-power ratio of 25 to 50 lb/kW requires that the specific weight of each of the array components be minimized. The cell stack, power cabling, structures, and mechanisms are the prime components of the array. Each of these items requires design improvements if the overall specific weight is to be reduced. The decrease in specific weight of one unit without a corresponding decrease in another will not achieve a lightweight solar array.

This section projects the present and future status of cell stack components. In the early 1960's, the Ranger spacecraft design had a solar array with a specific weight of 1.9 lb/ft². At present, solar array specific weights have decreased to approximately 1 lb/ft². By the mid-1970's, flight hardware can be decreased to approximately 0.25 lb/ft².

5.1 Solar Cells

At present, phosphorous diffused n-p solar cells are the only cells being used on solar-powered spacecraft (except in specific instances requiring the higher voltages of the p-n cells). The discussion in this section is limited to silicon n-p solar cells.

The lightest weight silicon solar cells presently available in production quantities are 12-mil chips with an area of 1 x 2 or 2 x 2 cm, containing solderless sintered silver-titanium ohmic contacts as shown in Fig. 5-1. The specific weight of the cell is typically 0.16 lb/ft². Cells can be obtained in quantities up to 11.3 percent AMO, 28°C minimum average efficiency. The typical cost for these solar cells ranges from perhaps \$10 per cell for 2 cm squares (11.3 percent AMO efficiency) to \$5 per cell for the same size at 10.5 percent AMO efficiency.

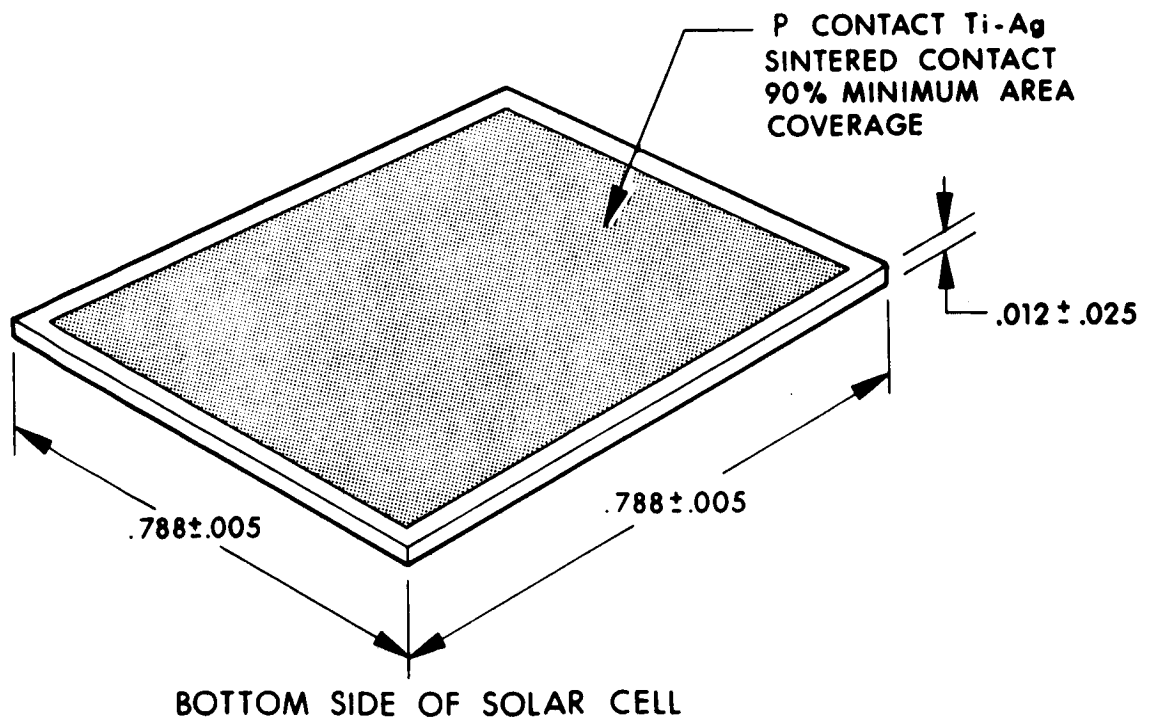
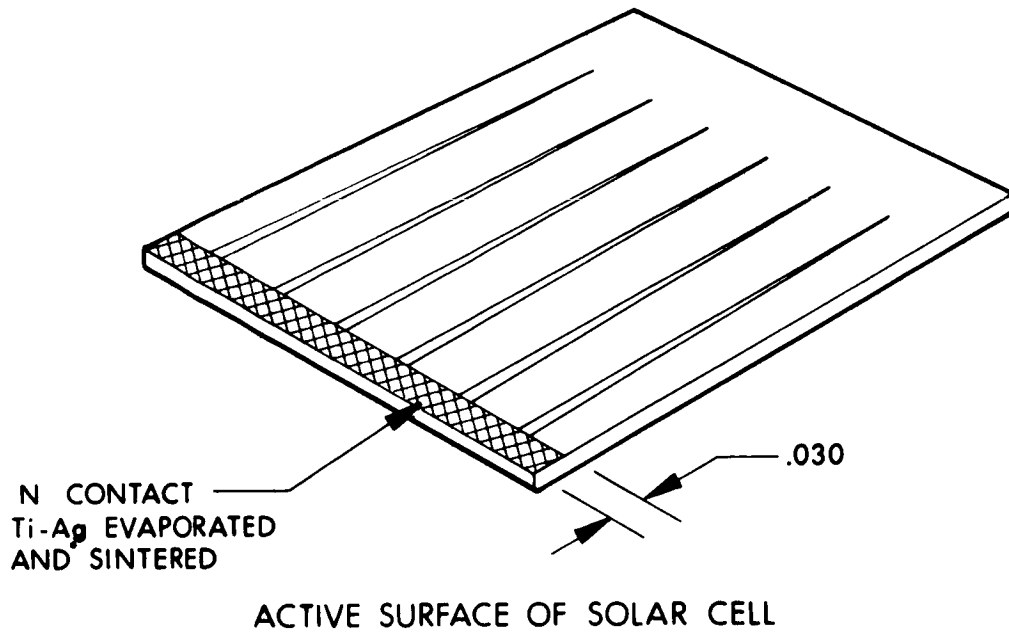


FIG. 5-1 TYPICAL CONVENTIONAL SOLAR CELL

Silicon solar cells available in limited quantities for experimental use include the following variations. (See Fig. 5-2 and Table 5-I.)

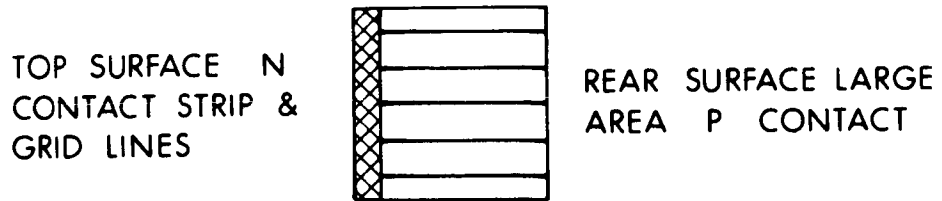
1. Back-contact or wrap-around cells
2. Front-contact cells
3. Dendritic cells up to 30 cm length using either normal or wrap-around contacts.
4. Larger area silicon cells (up to 3 cm squares)
5. Aluminum- and lithium-doped silicon cells
6. Thin solar cells

The wrap-around contacts shown in Fig. 5-3 offer several interesting features:

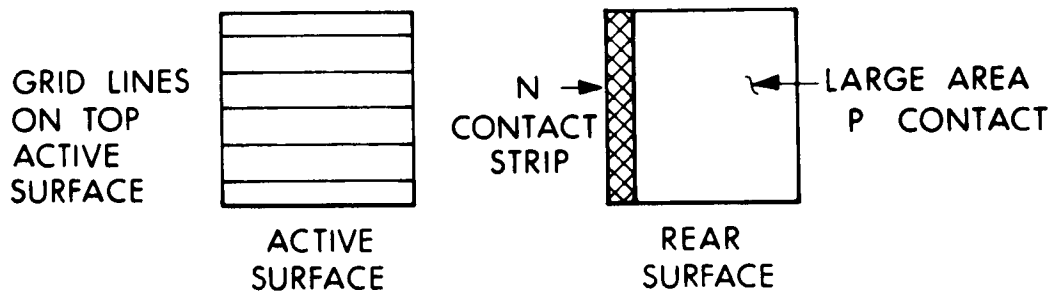
1. The cell permits connection of both the positive and negative contacts on the rear surface of the cell. A better packaging factor is possible, thereby permitting closer spacing of the cells.
2. Absence of the contact strip from the active surface increases the active cell area, thereby increasing the power output per cell.
3. A disadvantage of the wrap-around cell is the replaceability limitation. Removal of a single failed cell from the array is prohibited since none of the soldered connections are visible or accessible.
4. Limited data indicates that a 5-percent loss in power occurs during the fabrication of wrap-around cell arrays.

Very little costing data is available on 1 x 2 cm and 2 x 2 cm wrap-around cells, but it is expected that these cells would soon be in the same general price range as the normal-contact silicon n-p solar cells. The front-contact solar cell offers the same active area as a normal-contact cell; but since both contacts are on the top surface, fabrication and repair is simplified. Since all soldered connections are visible, any damage to the contacts can be easily

1. NORMAL CONTACT SOLAR CELL



2. WRAP-AROUND SOLAR CELL



3. FRONT CONTACT SOLAR CELL

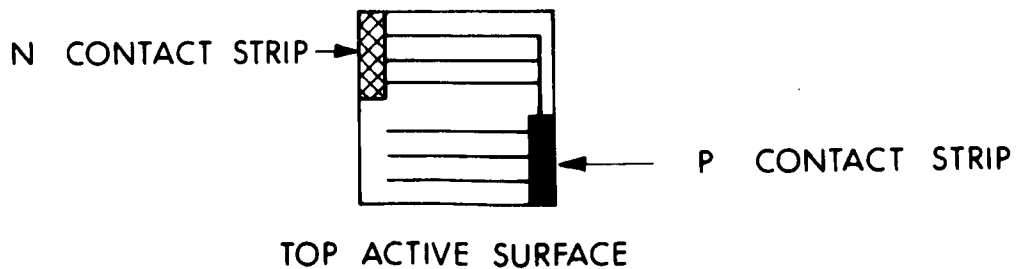


FIG. 5-2 CONTACT VARIATIONS OF SILICON SOLAR CELLS

TABLE 5-I

AVAILABLE VARIATIONS IN SOLAR CELL FABRICATION

1. Contacts:
 - a) Normal contacts (with ohmic strip and grid lines on n side of cell and large area contact on p side of cell).
 - b) Wrap-around contacts (with both n strip and large area p contact on rear side of solar cell). Grid lines are on top active surface.
 - c) Front contacts (with both n and p contact strips and grid on top active surface of cell).
2. Surface Area:

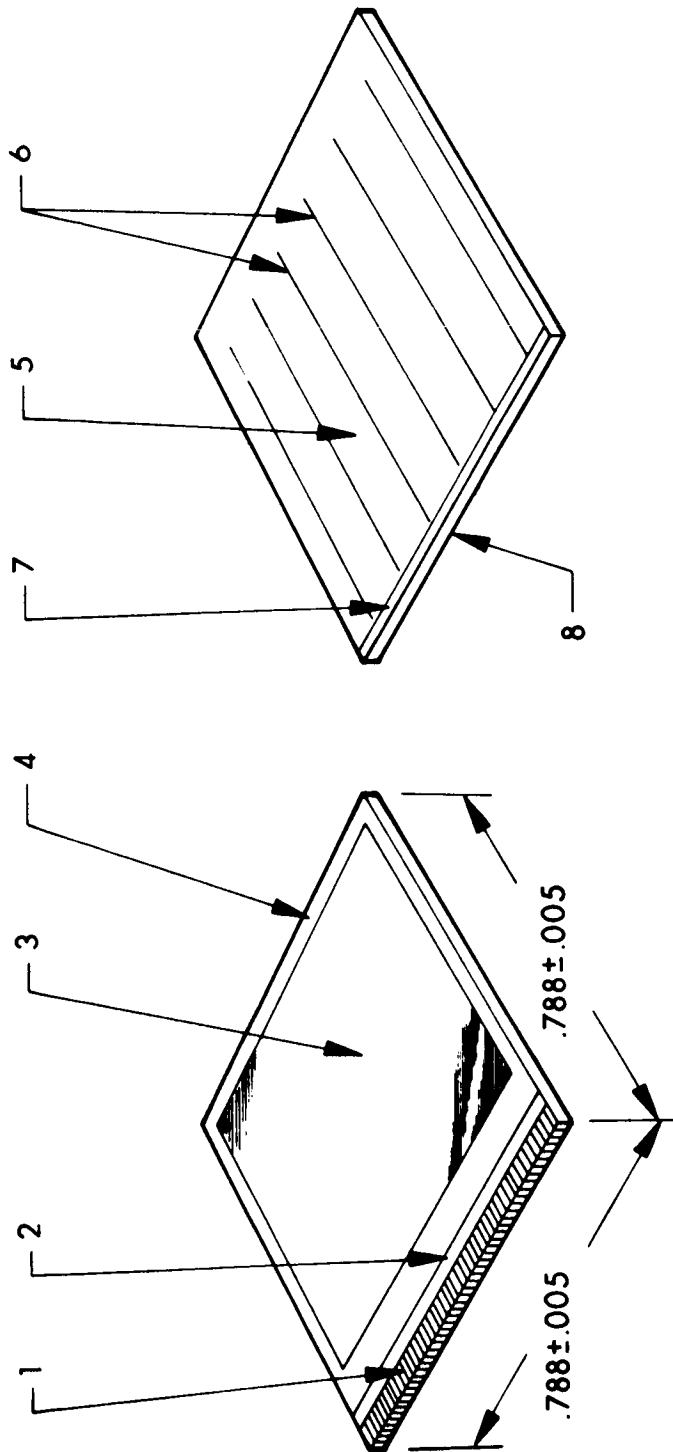
In production: 1 x 2 cm; 2 x 2 cm.

In development: 2 x 3 cm, 3 x 3 cm, 1 x 30 cm, 2 x 30 cm, 3 x 30 cm, 1 x 13 cm.
3. Dopant:

Phosphorus -- Present n-p silicon solar cell.

Aluminum -- Under development to produce radiation-resistant p-n cells.

Lithium -- Low-concentration dopant used in conjunction with phosphorus to obtain a cell that has low-temperature radiation annealing properties.
4. Thickness: 18 mils to 4 mils.
5. Internal Properties: With and without drift fields.



N Side of Cell (Active Surface)

- 5. N-sensitive area
- 6. Conventional grid lines
- 7. Connecting assurance bus bar
- 8. Ti-Ag contact evaporated & sintered over N region of cell

N & P Side of Cell (Rear Surface)

- 1. Ti-Ag sintered contact on N region
- 2. Void area
- 3. P-contact
- 4. "Picture Frame" around 3 sides of cell

FIG. 5-3 TYPICAL WRAP-AROUND SOLAR CELL

located. The cost of these cells should eventually fall into the same price range as the normal-contact silicon cells now on the market.

The large-area dendritic solar cells under investigation by Westinghouse Company and others have been fabricated with AMO efficiencies ranging up to 9 percent. Solar cells measuring 1 x 15 cm and 1 x 30 cm with drift field structures have been fabricated. The ohmic contacts on these dendritic cells are similar to those of the top contact n-p silicon solar cells. Costing data, again, is not readily available due to the limited number of cells presently being manufactured.

Larger-area top-contact silicon cells, 3 x 3 cm, are available in limited quantities; these have the same general properties of the smaller cells. The use of the larger cell reduces the number of intercell spaces required and permits packaging factors of up to 97 percent if wrap-around contacts are used.

Preliminary costing data have been obtained for 3-cm-square cells. For small quantity production, the cost ranges from \$13 per cell for an 8-mil cell (with 11.2 percent average AMO efficiency) to \$18 per cell for a 6-mil cell (at 10.4 percent average AMO efficiency). These efficiencies are rated at 28°C, 0.14 W/cm². It is expected that the cost per cell will decrease as production quantities become available.

The aluminum-doped p-n solar cells are presently under investigation, and samples are available in very limited quantities. This type of cell appears to have improved radiation-resistant properties compared to the boron-doped p-n solar cell. Characteristics of aluminum-doped cells are currently being investigated.

The lithium-doped solar cell is under investigation at NASA/Goddard under the direction of Dr. Fang. This type cell appears to have excellent low-temperature radiation annealing properties. Data indicate complete recovery in 24 hours (at 28°C) after radiation has ceased. Investigation is continuing to determine annealing effects at high temperatures under continuing radiation bombardment.

Progress in the development of thin solar cells has led to a presently obtainable 4-mil solar cell with an AMO efficiency of between 7.5 and 8.5 percent. The efficiency of thin solar cells will probably always be less than that obtainable with thicker cells due to transmission losses through the thin cells, but predicted AMO efficiencies for the 1970-1985 period range from 9.5 to 10.5 percent. The development of thin cells is now accelerating due to the increasing demand for large, lightweight solar arrays. A major problem, at present, is the reduction of cell costs. The thin solar cell is high-priced due to high cell attrition rates during cell and array fabrication. In addition, development costs are still being included in the basic cell price.

5.2 General Properties of N-P Solar Cells

The spectral response of a typical n-p solar cell is shown in Fig. 5-4. The spectral response of a solar cell shows at what wavelengths the solar cell operates and indicates the relative output at these wavelengths. Thus, a typical n-p solar cell operates between 0.3 and 1.1μ . The rest of the incident spectrum (less than 0.37 and greater than 1.1μ) is either reflected from the surface, transmitted through the cell without creating electron hole pairs, or reradiated from the cell in the form of heat. Figure 5-5 shows the spectrum response of a typical n-p silicon solar cell in relation to the spectrum of incident sunlight.

The electrical characteristic curve of a typical n-p silicon solar cell is shown in Fig. 5-6. The curves show the typical limits encountered in the operation of solar cells in space at various temperatures.

The open-circuit voltage per cell ranges from approximately 0.55V at 25°C to 0.39V at 100°C . The voltage of a solar cell can be assumed to be independent of the efficiency of the cells and the impinging solar intensity, but it is very dependent upon the cell temperature and internal series resistance. The cell current is a direct

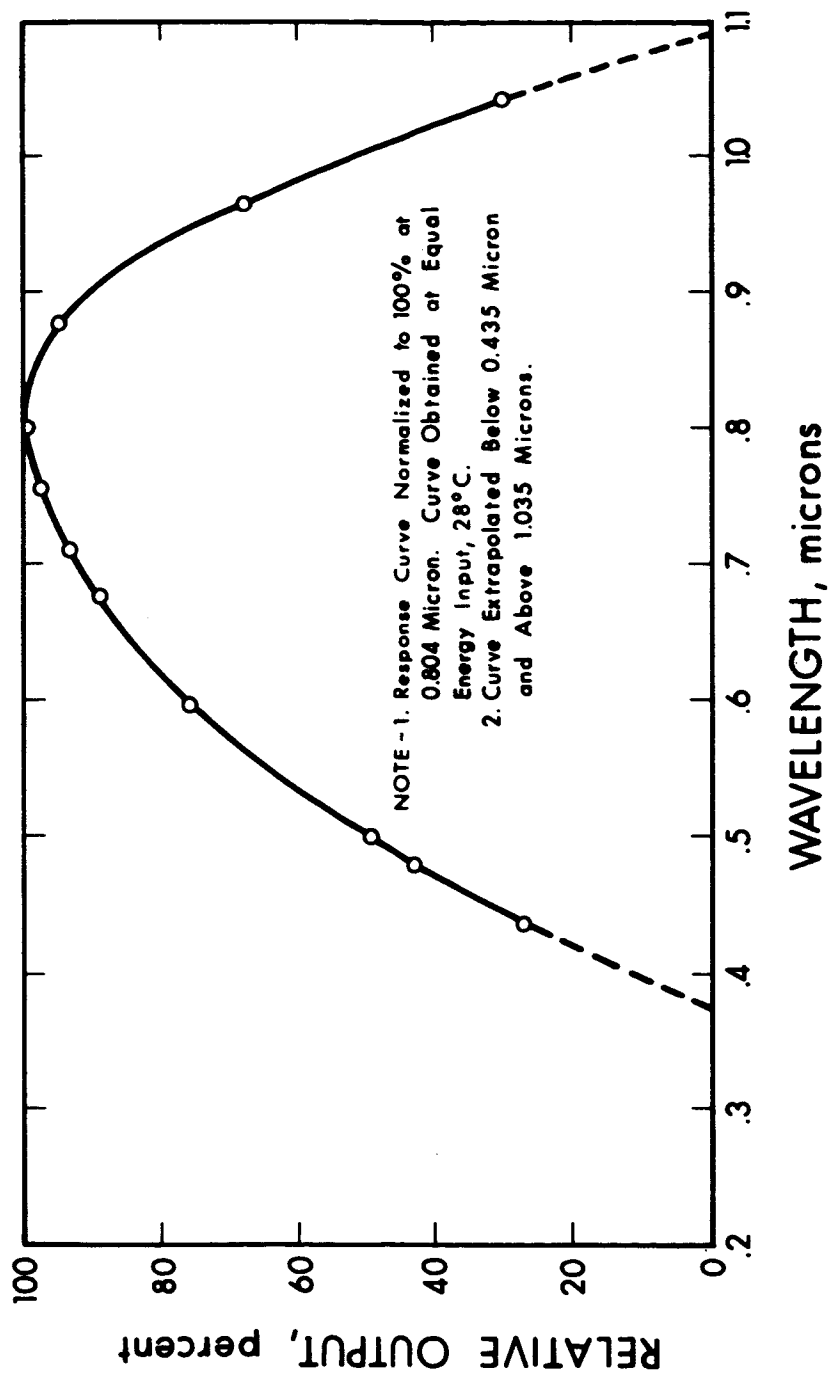


FIG. 5-4 TYPICAL N-P CELL, RELATIVE SPECTRAL RESPONSE

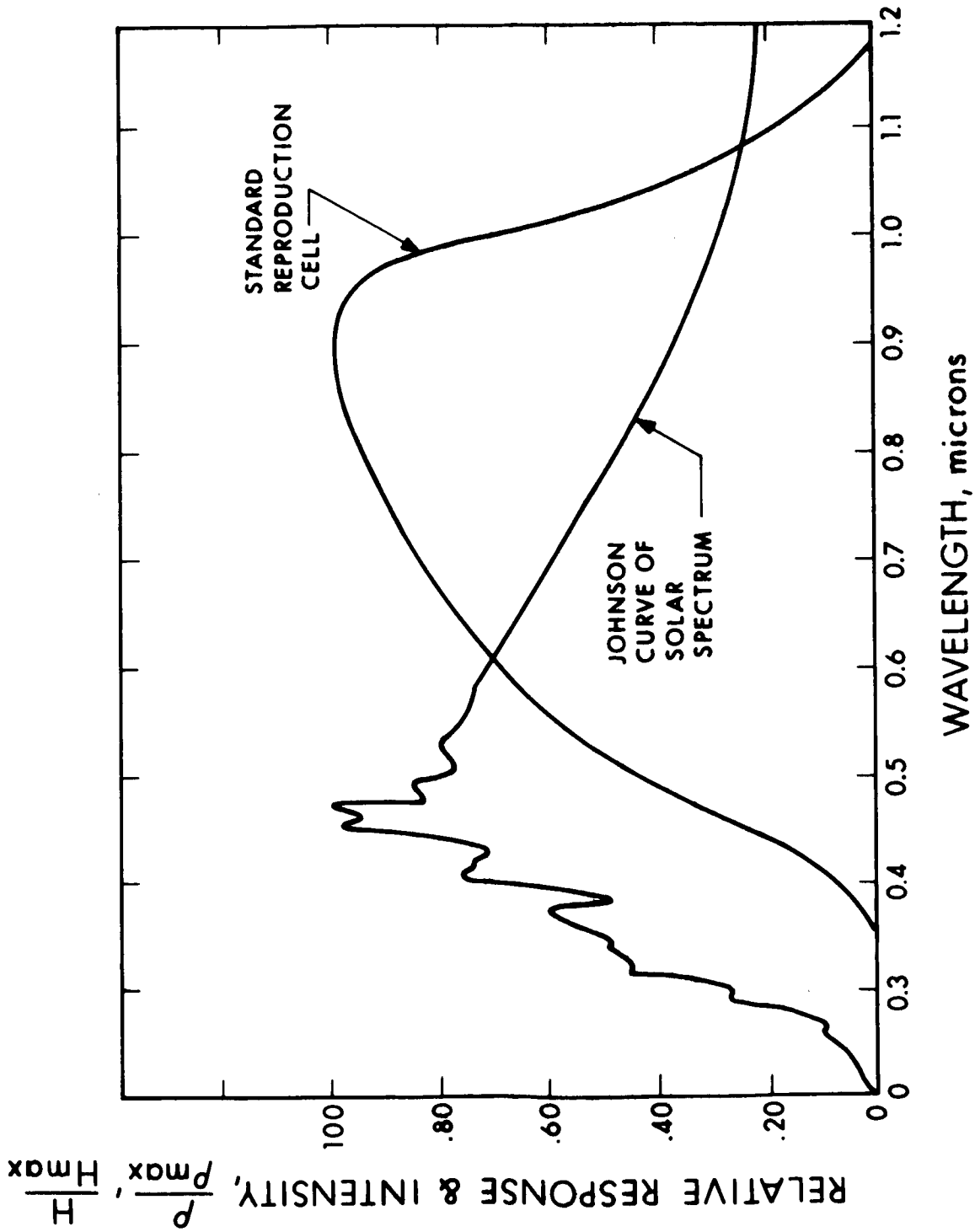


FIG. 5-5 SPECTRUM RESPONSE, TYPICAL N-P CELL

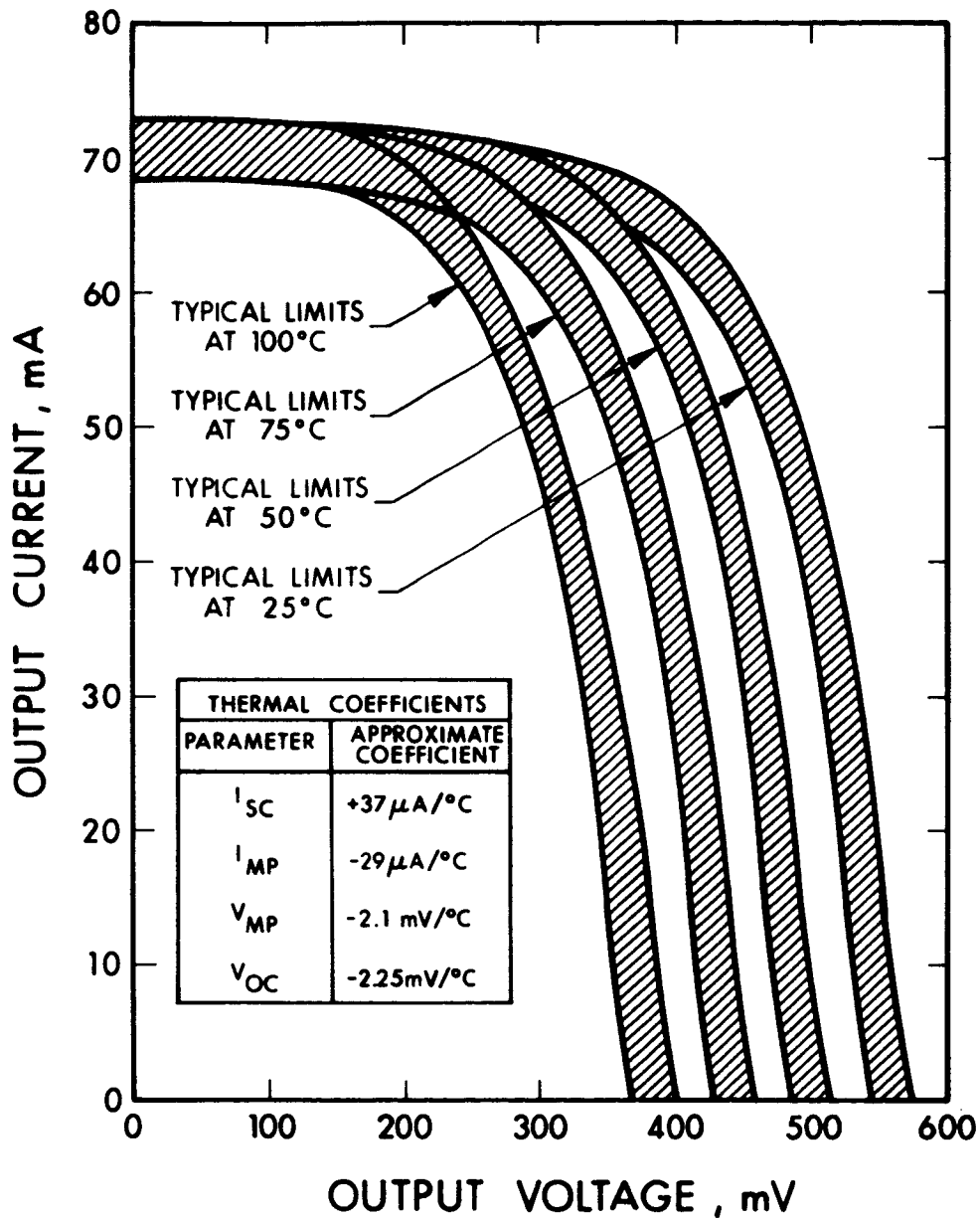


FIG. 5-6 TYPICAL E/I CURVE LIMITS

function of the solar intensity and cell efficiency; it is relatively independent of the cell temperature and internal series resistance.

The fact that a solar cell is a semiconductive device indicates that some of the cell characteristics are affected by temperature and intensity. These effects are shown in Fig. 5-7. These curves are typical for n-p solar cells of present manufacture and are probably typical for cells to be manufactured in the future. The combined effects of the temperature-dependent parameters result in significant changes in the cell operating power. Thus, temperature effects must be considered in the system analysis. For present cells, the output power decreases from 0.3 percent per $^{\circ}\text{C}$ to 0.5 percent per $^{\circ}\text{C}$ for increases in temperature. Figure 5-8 summarizes the effects of both temperature and intensity on current (under short-circuit conditions), voltage (under open-circuit conditions), and maximum power output of a solar cell.

5.3 Projected Technology of Silicon Solar Cells

Table 5-II shows the predicted silicon cell general characteristics from the present to the 1970-1980 time period. The relative improvement of efficiency for thin solar cells (less than 12 mils thick) will exceed that obtained for the thicker cells over the next 10 years. The efficiency of the 4-mil cells should be expected to be improved to approximately 9.5-10.5 percent in 1970 to 1980, for about a 25 percent increase in efficiency. Two other expected major improvements in silicon solar cell technology during the next 10 years will be (1) the enlargement of the basic cell size to a maximum of approximately $3 \times 30 \text{ cm}$ ($90\text{-}100 \text{ cm}^2$), and (2) a projected lowering of bare cell costs from $\$2/\text{cm}^2$ at present to approximately $\$1.50/\text{cm}^2$ in the 1970 time period. It is also expected that some improvements will be made in increasing the radiation resistance of n-p silicon solar cells by possibly changing the dopant material used to obtain the p material, improving the drift field cells presently under development, or by changing the material used in the contacts to the solar cell.

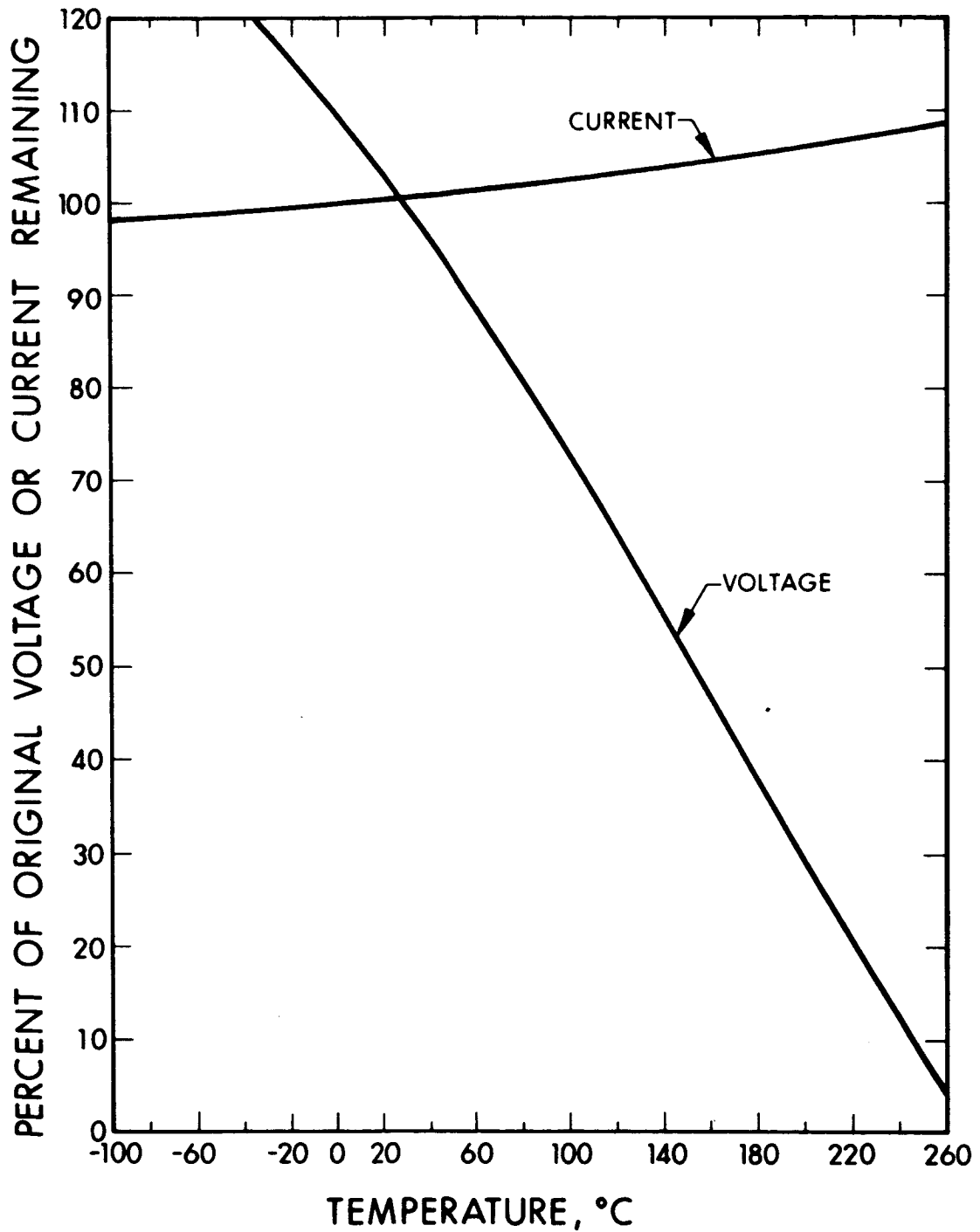


FIG. 5-7 TEMPERATURE EFFECTS ON SOLAR CELL CHARACTERISTICS

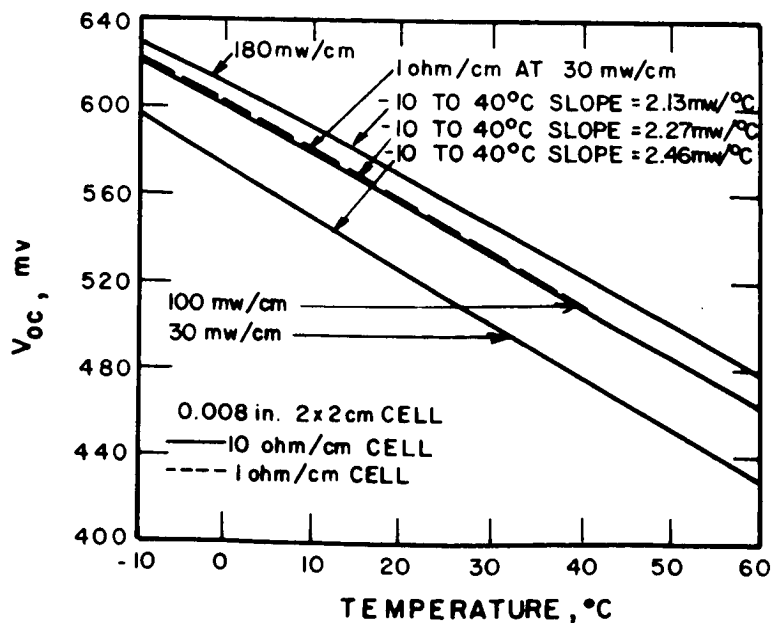
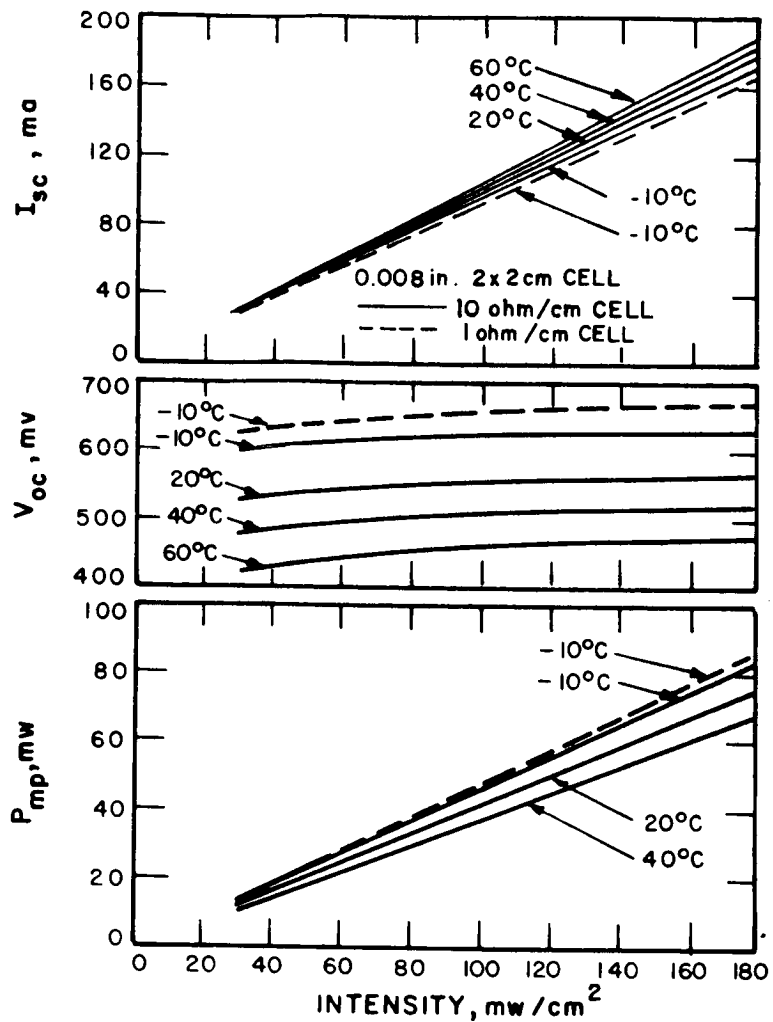


FIG. 5-8 SOLAR CELL TEMPERATURE CHARACTERISTICS

TABLE 5-II
 PREDICTED SILICON SOLAR CELL CHARACTERISTICS

	<u>Present (1966)</u>	<u>1970-1980</u>
Type	n-on-p	n-on-p drift field
Ohmic Contact	Top-solderless Silver-titanium	Wrap-around A_g-T_i
Thickness	12 mils	12, 8, 4 mils
Weight	0.07 gm/cm ²	0.023 gm/cm ² for 4 mils thick
Base Resistivity	1-10 ohm-cm	1-25 ohm cm
Size	1 cm x 2 cm 2 cm x 2 cm	Same, also 3 x 3 cm 1 cm x 30 cm 2 cm x 30 cm 3 cm x 30 cm
Power Output at 55°C for 12-mil cell	13.1 mW/cm ²	14.6 mW/cm ²
Total Cell Efficiency at 28°C (Average Production)	10.5% (12 mils) 9.5% (8 mils) 7.5-8.5% (4 mils)	11.7% (12 mils) 11.0% (8 mils) 9.5-10.5% (4 mils)
Cost/cm ²	\$2.00/cm ²	\$1.50/cm ²

In summary, it is expected that the n-p silicon solar cell technology in the 1975-1985 time period will provide a solar cell capable of producing approximately 11 W/ft^2 . This power will be produced at a cost of approximately \$100 per watt based on bare cell costs. The silicon solar cell will continue to be the prime source of electrical power in space for missions requiring power up to approximately 50 kW, since the solar cell is a proved piece of space hardware capable of supplying reliable power at reasonable cost and specific weights.

5.4 Cover Glass and Its Effect on Cell Characteristics and Array Weight

5.4.1 General

The chief function of the cover glass on the solar cell is to provide a surface with a high thermal emission to permit the cell to operate at a lower temperature and higher performance level (see Fig. 5-9). The front surface of a typical bare solar cell has an absorptivity curve as shown in Fig. 5-10. It has an α_s of 0.935 (absorptivity) and an ϵ (emissivity) of 0.368 at 127°C , yielding α_s/ϵ of 2.54 and an in-space temperature of 85°C (assuming the rear surface is radiating with an ϵ of 0.9). This results in a relative power output of only 77 percent of the power capability at 28°C .

By the addition of a glass cover with a deposited antireflective coating to the surface of the solar cell, the absorptivity characteristics of the unit can be improved as shown in Fig. 5-11. The antireflective coating reduces transmission losses related to the index of refraction of the cover material. The cell with added cover glass now has an α_s of 0.813 and an ϵ of 0.835 at 60.2°C , yielding an α_s/ϵ ratio of 0.974 and an in-space temperature of 36°C (assuming the rear surface is radiating with an ϵ of 0.9). This results in a power output equivalent to 92 percent of the power capability at 28°C . A net gain of 15.8 percent over the bare cell is shown, including transmission losses from the antireflective coating. This covered cell provides the most favorable power gain.

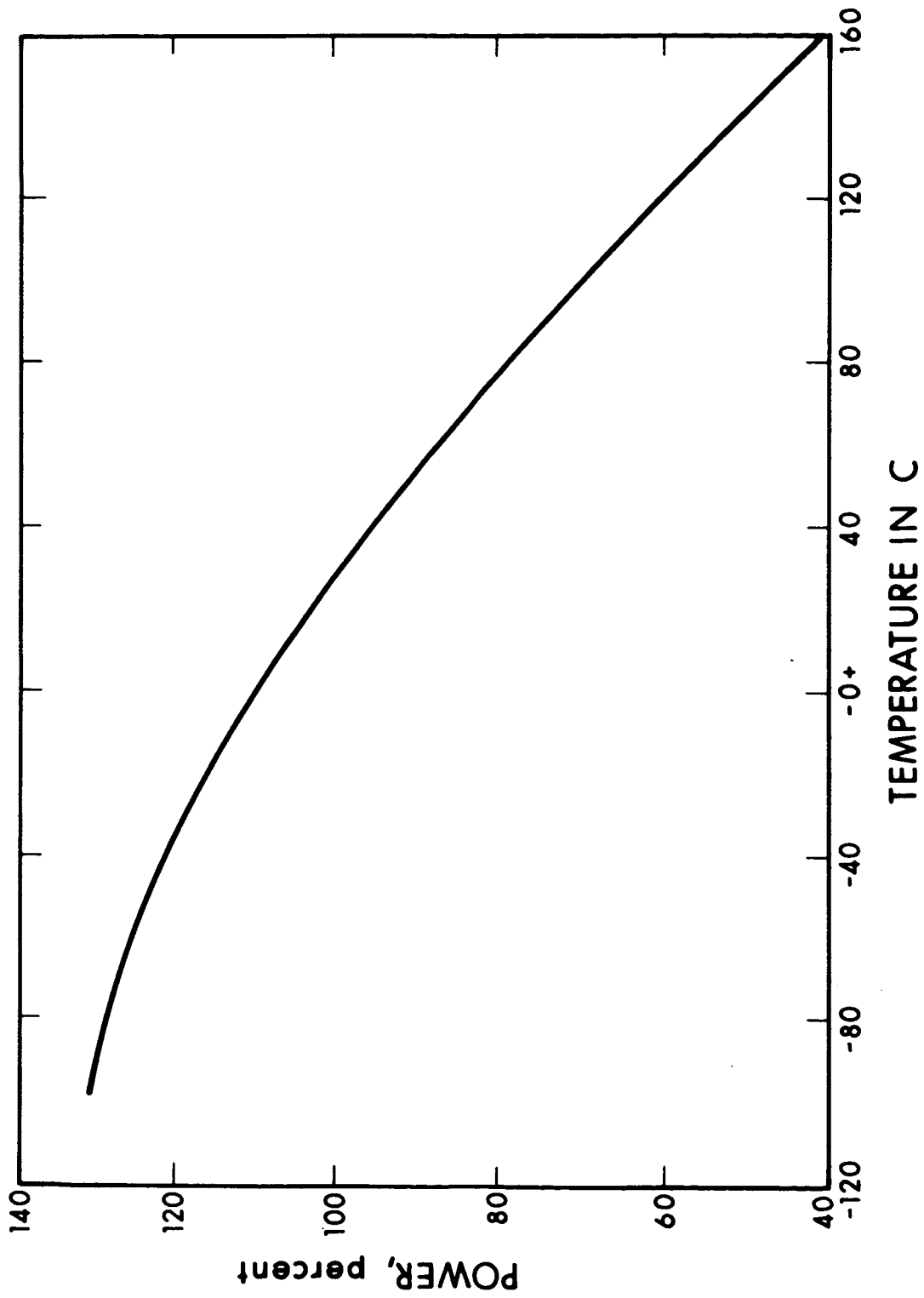
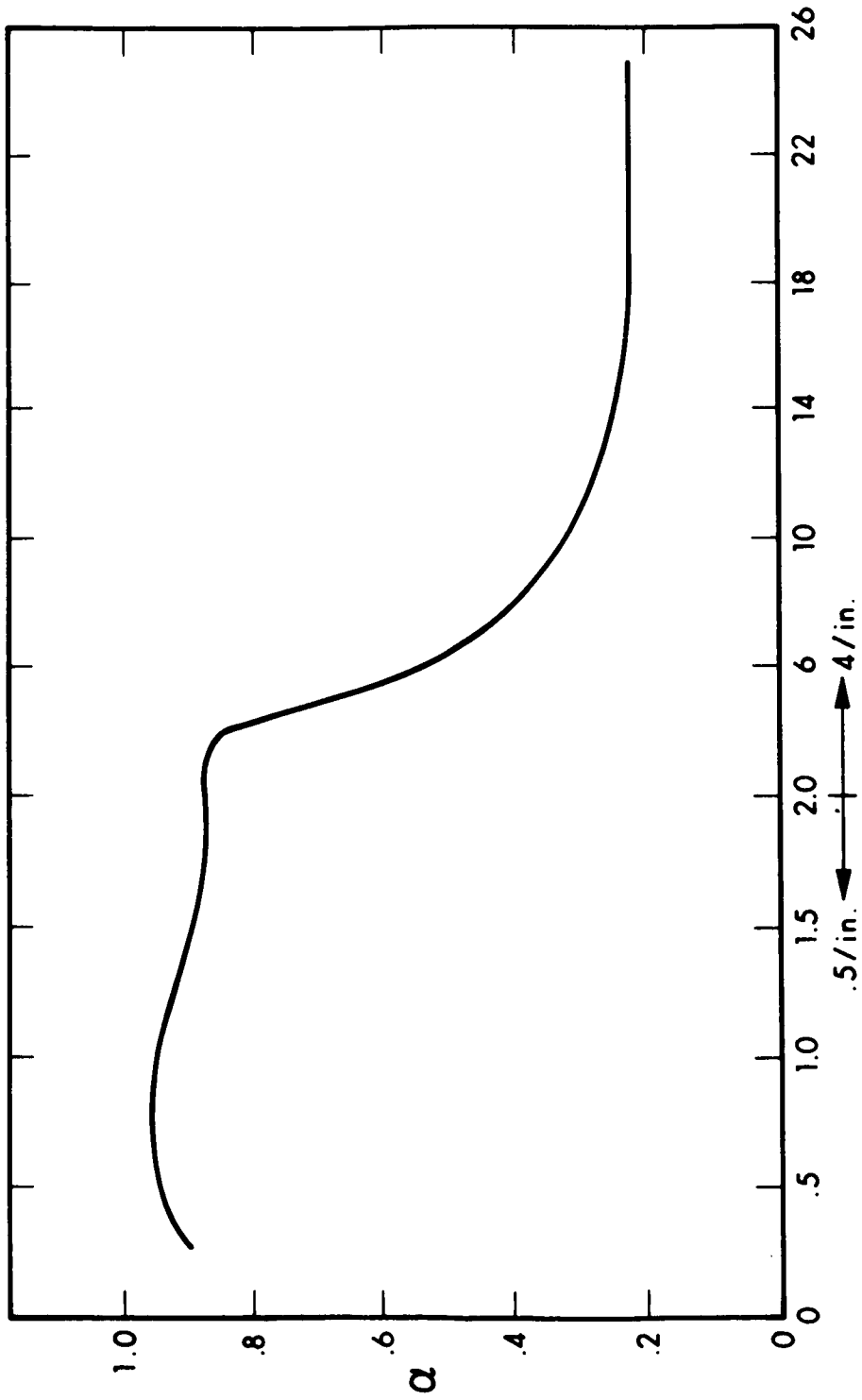


FIG. 5-9 SOLAR CELL POWER OUTPUT VERSUS TEMPERATURE



WAVELENGTH, microns

FIG. 5-10 ABSORPTIVITY CHARACTERISTICS, SILICON SOLAR CELL

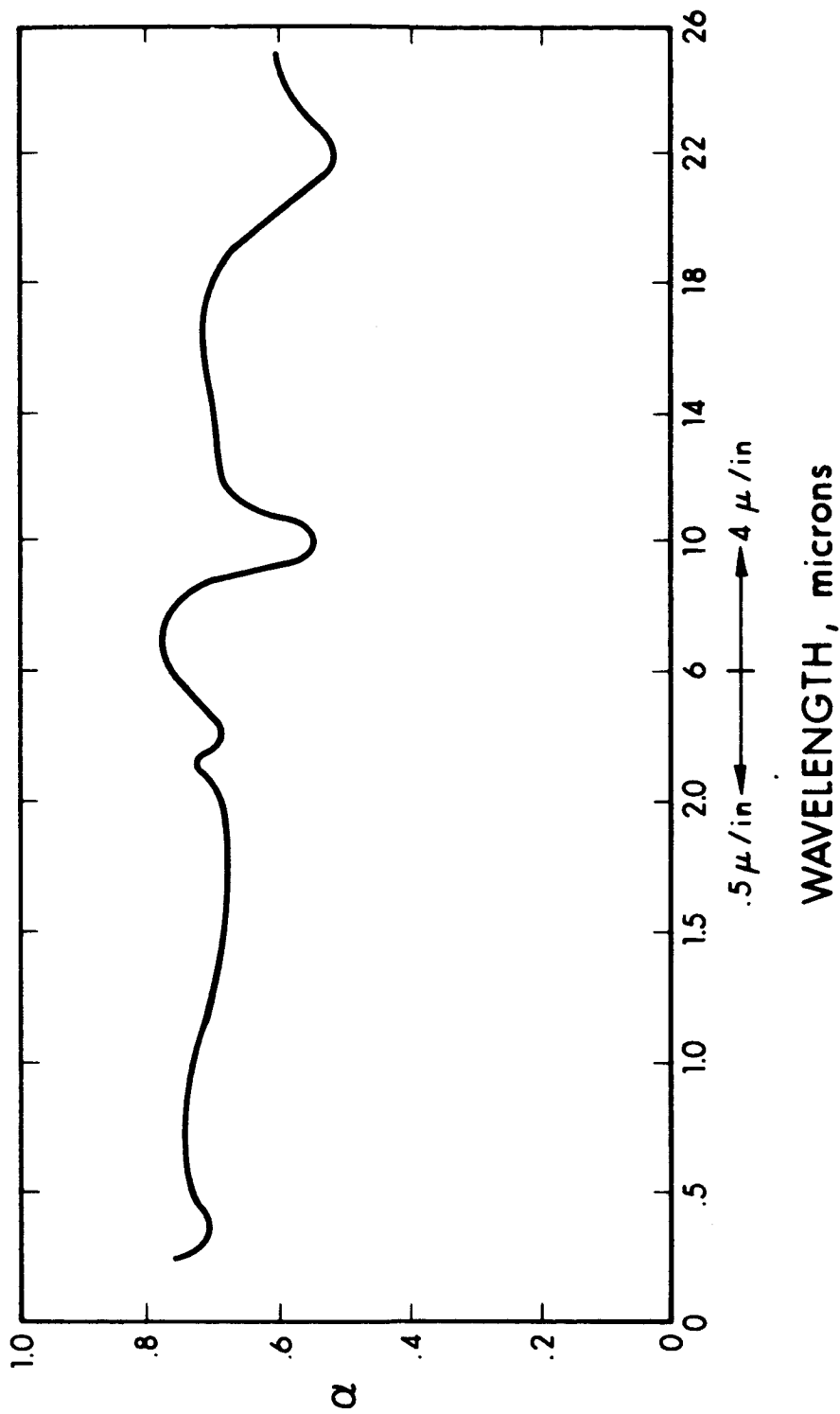


FIG. 5-11 ABSORPTIVITY CHARACTERISTICS, CELL WITH 6-MIL GLASS AND ANTIREFLECTIVITY COATING

The type of filter shown has been used extensively and is readily available in large quantities. A red cutoff coating (which can be used to further cool the cells by reflecting the unusable light in the red region) does not provide any appreciable gain over the blue filtered cover since for the Jupiter mission the panels are already operating at a low temperature thermal equilibrium as a result of the low illumination levels. The addition of a red filter would also increase the cover glass cost with no significant increase in power capability. Information on spectral filters is summarized in Table 5-III.

One characteristic of the film filters is that when the temperature is increased, the blue filter will shift to the longer wavelengths; as the temperature is decreased, the filter will shift to shorter wavelengths. The wavelength shift of these filters is essentially a linear function of the film temperature, because the materials which form the various layers have indexes of refraction which vary linearly with temperature. As a result, the optical thickness of adjacent layers can be perfectly matched at only one temperature (called the design temperature). In general, these filters retain their transmission and cutoff shape characteristics over a wide temperature range, but serious transmission losses may occur at filter temperatures exceeding 100°C . In the case of the Jupiter mission, this will be no problem except during that part of the trajectory where the array is swinging in towards the sun and high temperatures (190°C) may be reached. For the portion of the orbit where temperatures are less than 100°C , no measurable change in transmission loss will occur due to filtering shifts.

5.4.2 Integrated Cover Glass

The need for reducing the weight and complexity of solar cell assemblies led to the development of the process for incorporating an integrated cover glass directly on the silicon solar cell without the use of an intervening adhesive. This development

TABLE 5-III
SPECTRAL FILTER CHARACTERISTICS

<u>Cells & Modifications</u>	α	ϵ	α/ϵ	<u>T</u>	% Power at 28°C	% Power Gain From Bare Cell
Ideal cell	0.700	1.000	0.700	28°C	100%	-
Bare cell	0.935	0.368	2.540	85°C	77%	-
Cell with 1.11 SiO coating	0.874	0.642	1.360	63°C	86%	4.3%
Cell with thin glass and anti-reflective coating	0.813	0.835	0.974	46°C	92%	15.8%
Cell with thin glass, 1.15 red and antireflective coating	0.700	0.835	0.840	35°C	96%	11.2%

has enabled solar cell manufacturers to decrease the cover glass thickness to less than 1 mil while eliminating the cover glass adhesive weight and the subsequent degradation in adhesive transmission properties due to the space environment. The major problem in the application of integrated cover glass, both of the boron and phosphor silicates and slurried or sputtered quartz, is the decreased optical transmission through the cover glass. The present cover and adhesive combination has a combined transmission-loss factor of 0.94 while the integrated cover glass has a transmission loss factor of 0.91. This leads to a subsequent 3 percent decrease in solar array power output, but the weight-to-power ratio for the integrated cover glass is equal to or less than that for the cover-adhesive combination. This is because of the thinner cover glass obtainable with the integrated process and because the cover glass adhesive is eliminated.

The spectral filtering and transmission properties of the integrated cover glass can be made equivalent to that of the cover-adhesive combination; therefore, only the specific power (watts per lb) need be investigated in comparing the integrated cover glass to the cover-adhesive combination. This comparison, summarized in Section 6, indicates the integrated cover glass has definite advantages over the presently used cover-adhesive combination.

5.5 Solar Array Weight

The specific weight of both the entire solar array and its components is steadily decreasing; the expected trends are shown in Fig. 5-12. The lower curve shows the specific weight of the substrate/frame (without solar cells). As shown, in 1962 the capability was approximately 1.2 lb/ft^2 (Ranger). Specific weights have been decreasing until at the present time a specific weight of about 0.5 lb/ft^2 is obtainable (Mariner '64). The specific weight of the substrate/frame is expected to decrease as newer substrate designs are introduced.

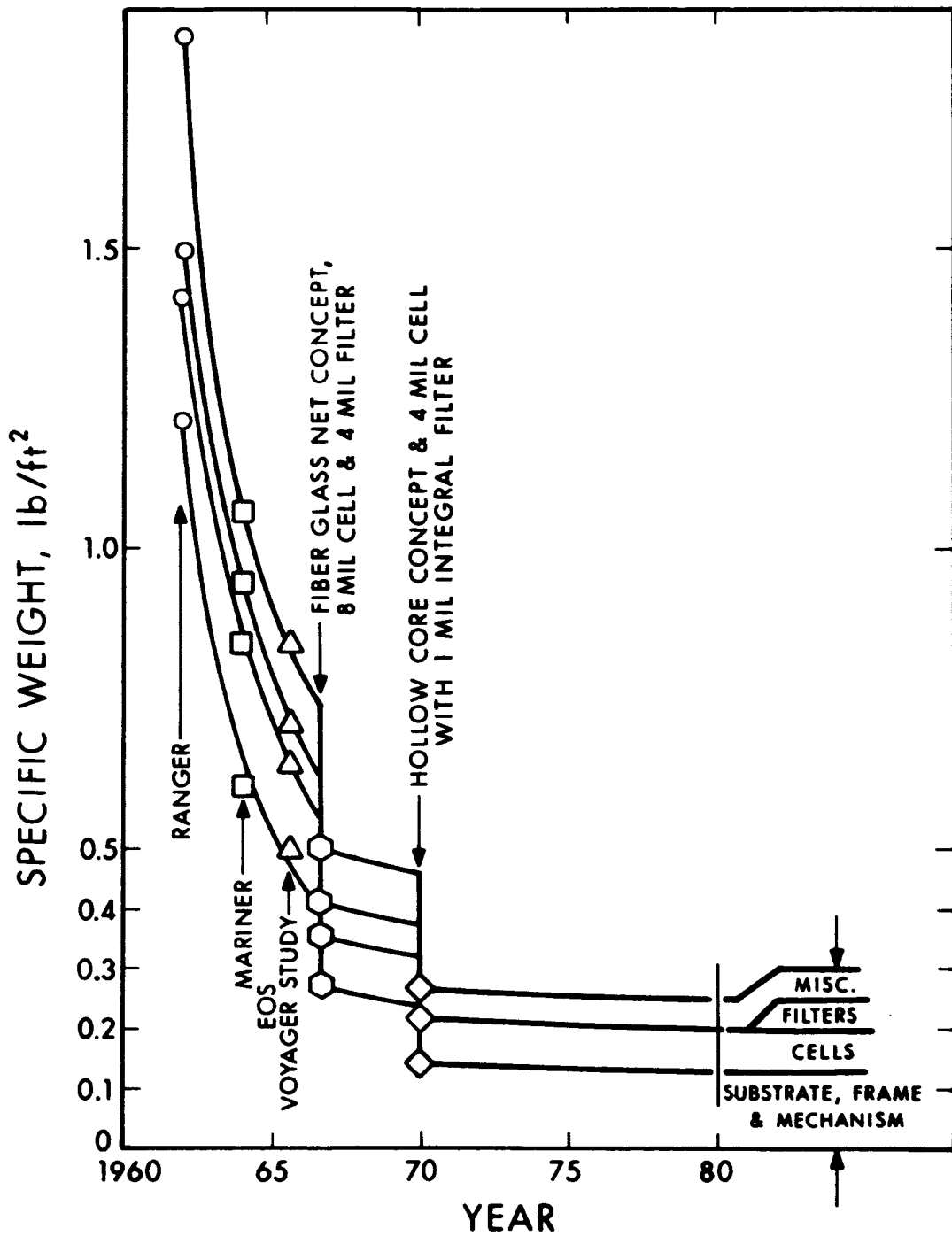


FIG. 5-12 SOLAR ARRAY SPECIFIC WEIGHT HISTORY AND PREDICTIONS

The second curve in Fig. 5-12 shows the expected decrease in solar cell specific weight as thin cells with increased efficiency are developed. The probable minimum practical thickness for silicon solar cells is 4 mils (equivalent to a specific weight of 0.053 lb/ft^2).

The third curve shows the expected decrease in cover glass weight after about 1970 when cells with integrated cover glass become items of standard use. At present, the minimum glass thickness is 4 mils. This gives minimum radiation protection but practical thermal control. The thin (2 mils or less) integrated cover glass will give the same thermal control. The expected minimum specific weight for cover glass will be approximately 0.02 lb/ft^2 .

The top curve shows the expected trend in total array specific weight including such items as adhesives, bus bar, solder, paints, hardware, cabling, etc. The specific weight of these miscellaneous items, taken as a group, is expected to decrease uniformly from a maximum value of 0.32 lb/ft^2 in 1962 to approximately a 0.050 lb/ft^2 by 1970. Improvements are also expected in decreasing hardware requirements and minimizing cooling weights by improved designs. The trend in specific weight indicates that expected minimum total array specific weight after 1970 could be 0.25 lb/ft^2 .

6. SOLAR ARRAY STRUCTURAL TRADE STUDIES

The development of a lightweight solar array requires that each of its components be designed to achieve minimum specific weight without significantly decreasing the photovoltaic conversion efficiency. Large lightweight array development requires structural/mechanical design that minimizes packaging volume and has minimal influence on spacecraft design. EOS's program is primarily directed toward developing a lightweight structure that can be used in a large array. The cell and cover glass combination with its specific power characteristics was defined early in the program. The major portion of the trade study analysis is therefore directed toward development of a biconvex hollow core structure of minimum practical weight. Since the demonstration panel is designed to be a section of a larger array, it was necessary to define subpanel configuration and establish package dimensions. This was accomplished as a result of trade studies comparing the advantages of various configurations in both stowed and deployed states. The areas of evaluation in these trade studies included:

1. Analysis of package requirements in stowed and deployed state
2. Comparison of structural concepts
3. Comparison of performance and design criteria of biconvex hollow core structure versus other practical structures

6.1 Selection of Array Packaged and Deployed Configuration

Studies were conducted to determine structural planform sizes and compare methods of latching the stowed array. One result of the study was the definition of the demonstration panel geometry.

The array's planform arrangement was established after the study of basic alternatives shown in Figs. 6-1 and 6-2. Competing characteristics considered are: exposed area, shroud size and shape,

BLANK PAGE 62

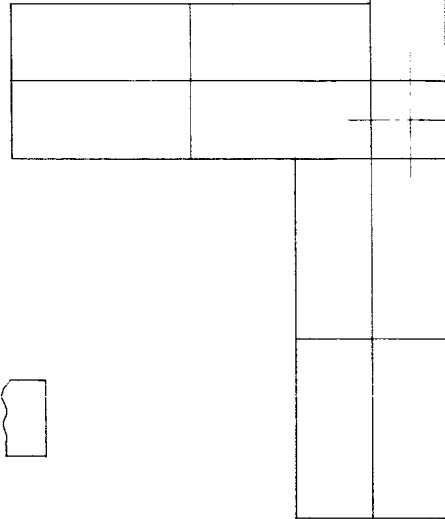
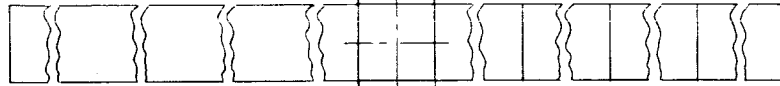
SECURITY CLASSIFICATION

D

C

B

A



250 SQ. FT.
4 PLACES
1

250 SQ. FT.
4 PLACES
2

5

4

3

5

4

3

6-3

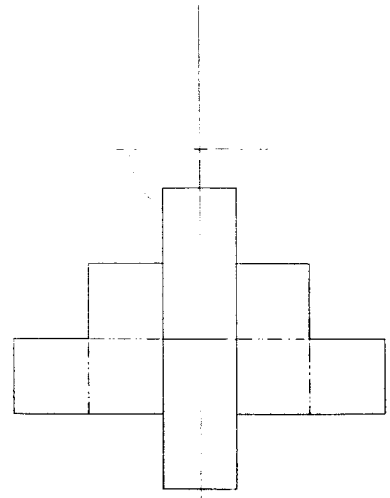
SECURITY CLASSIFICATION

D

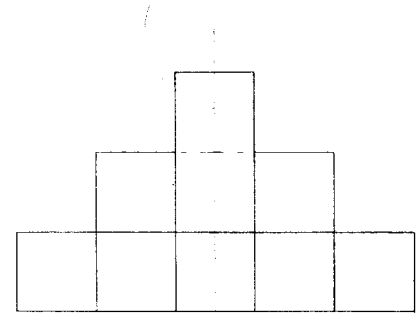
C

B

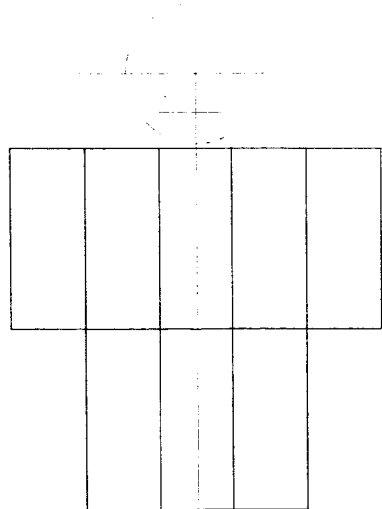
A



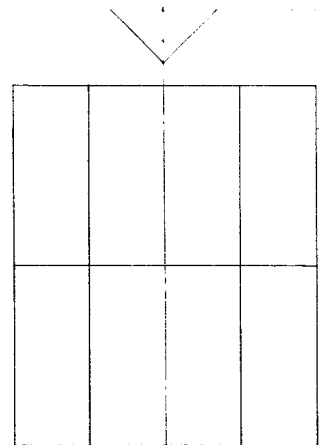
250 FT²
4 PLACES



250 FT²
4 PLACES
2



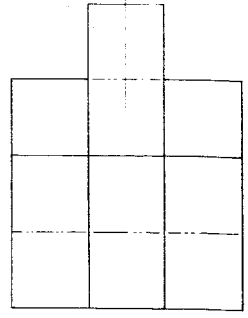
500 FT²
2 PLACES
3



500 FT²
2 PLACES
4

REVISIONS			
NO.	DATE	DESCRIPTION	BY

D
C
B
A



250 FT²
4 PLACES
5

1100322

NO.	DATE	DESCRIPTION	BY

LIST OF MATERIALS			
NO.	DATE	DESCRIPTION	BY

UNLESS OTHERWISE NOTED:
 1. LATEST REVISION IS SHOWN.
 2. THE DESIGNER.
 3. CHECKED BY: *5/19/66*
 4. DATE: *5/19/66*

THIS DRAWING IS THE PROPERTY OF ELECTROOPTICAL SYSTEMS, INC. IT IS TO BE KEPT IN CONFIDENCE AND IS TO BE RETURNED TO THE COMPANY WHEN REQUESTED TO DO SO.

BLINDING-OPTICAL SYSTEMS, INC.
 Pasadena, California - A Subsidiary of Spac Corp.

ARRAY STUDIES
 10 KW ARRAY

SECURITY CLASSIFICATION: E
 1100322

12705

14.0.7027 HAS 7.428

FIG. 6-2

limits of the biconvex structure, and stability of the spacecraft. The four-quadrant approach established the requirements for a "spider" tie pattern or trapezoidal panels due to the limited space available close to the spacecraft. A spider, or cruciform, array of small size presents minor problems for deployment and cabling. However, as the array area increases, deployment becomes more complex. Spacecraft stability when subjected to attitude control accelerations is a major consideration. Trapezoidal panels would be desirable for easier packaging within the tapering shroud. However, with the adoption of the biconvex approach for panel structural rigidity and lightness, the complications involved with trapezoidal panels are undesirable. These complications include determination of points of intersection of compound curves for manufacture, hinging, and latching. Consequently, the rectangular shape panel was retained.

The need for a rigid structure during launch with distribution of panel latching points around the array resulted in the compact approaches illustrated in Fig. 6-2. As shown, the concept of a symmetrical two-sector array was selected both for the 5 and 10 kW arrays.

An alternative method of constraining movement of the panels is by banding the array. The release mechanisms considered for this application were guillotine cable cutters. In addition to the banding, however, individual release devices would be required to allow for sequential deployment with additional weight. Another reason which influenced the decision in favor of individual release units was the uncertainty of clearing the severed banding from the array. One approach would be to propel the pieces away from the panels by means of the stored energy from springs. Figure 6-3 illustrates the concept.

Estimates of weights and reliability were the deciding factors in formulating the decision to proceed with the retractable pin devices.

BLANK PAGE 6-8

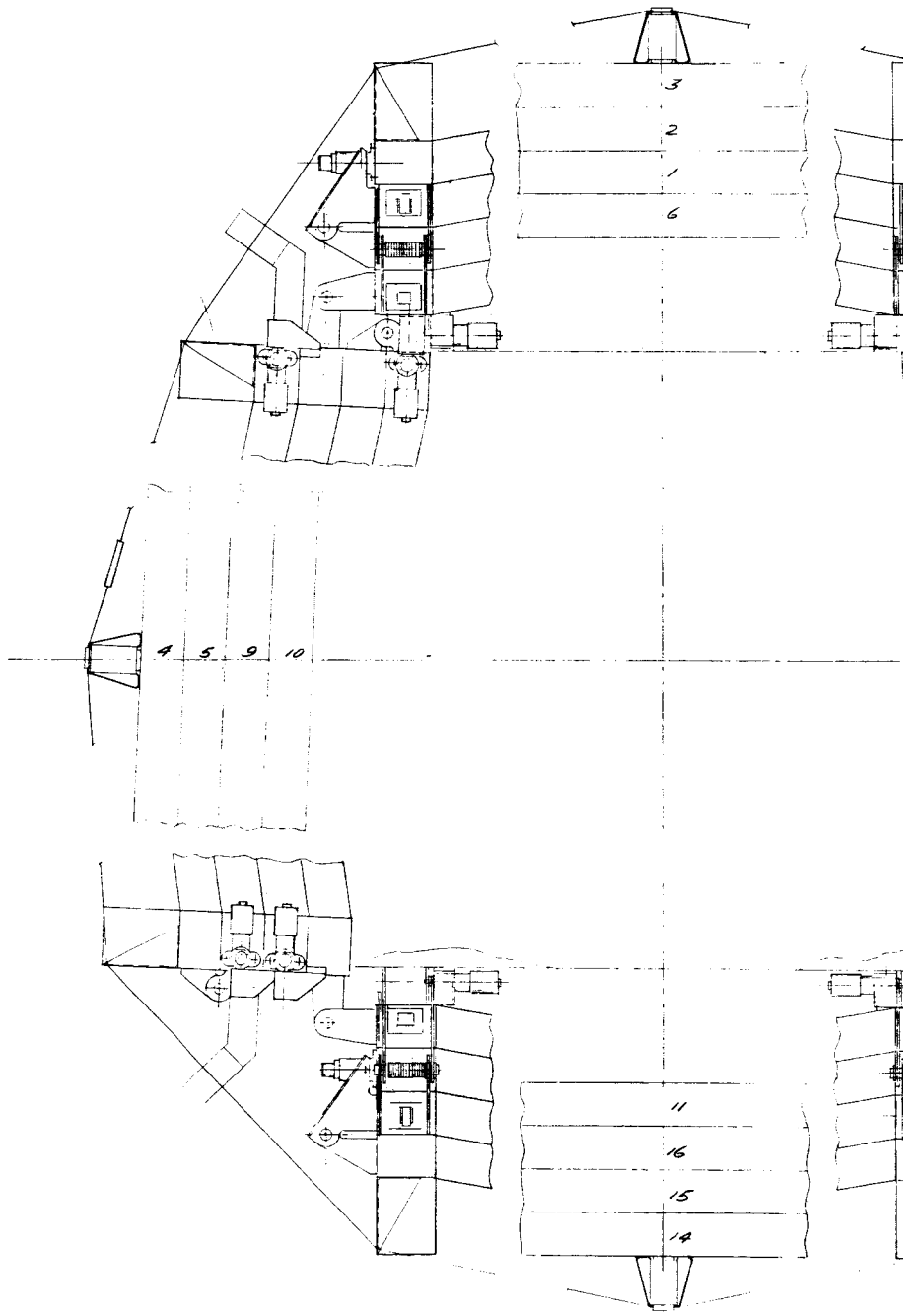
D

SECTOR NO. 1

C

B

A



SECTOR NO. 2

6.2 Comparison of Substrate Structure

This trade study was performed to determine the biconvex hollow core structure's potential as a lightweight array concept by approximate comparison with several other types of substrate.

At the beginning of the program a selection was made of potential structural concepts that would meet the lightweight criteria. From these concepts 5 candidates were selected for further study.

They are:

1. Conventional flat plate sandwich design with structural beams
2. Prestressed tapes
3. Prestressed diaphragm
4. Honeycomb flat plate design
5. Hollow core biconvex design

The detailed analysis of the study may be found in Appendix C.

The study indicated that the hollow core design had a weight advantage (as did the prestressed tape and prestressed diaphragm) over the more conventional corrugated and honeycomb concepts. The specific weight values are shown in Table 6-I.

The study ground rules for substrate structure comparison were to use the same criteria and requirements. They are:

1. Design loading condition
2. Cell stack weight (0.16 lb/ft^2)
3. Surface dimensions (subpanel width of 58.6 in.)
4. Gain factors (40 for substrate, 10 for frame)

The one variable in the analysis was the attachment points. Each concept had the attachment points at the position that best suited its design.

6.2.1 Corrugated Sandwich Construction

The corrugated sandwich structure is shown in Fig. 6-4. Earlier work on a similar program had produced design curves to optimize the structure; these were used in the analysis. The results of the study defined a 0.265-in. high beryllium corrugation and a $1 \times 1.5 \text{ in.}^2$ box beam.

TABLE 6-I

SUMMARY OF STRUCTURAL CONCEPTS COMPARISON

Concept Component	Corrugated (lb/ft ²)	Prestressed Tape (lb/ft ²)	Prestressed Diaphragm (lb/ft ²)	Honeycomb (lb/ft ²)	Biconvex* Hollow Core (lb/ft ²)
Substrate	0.1292	0.0150	0.0109	0.1332	0.0770
Frame	<u>0.1236</u>	<u>0.1740</u>	<u>0.1740</u>	<u>0.1236</u>	<u>0.1137</u>
Total	0.2528	0.1890	0.1849	0.2548	0.1907

* This biconvex hollow core concept uses electroformed nickel for the substrate and aluminum for the frame.

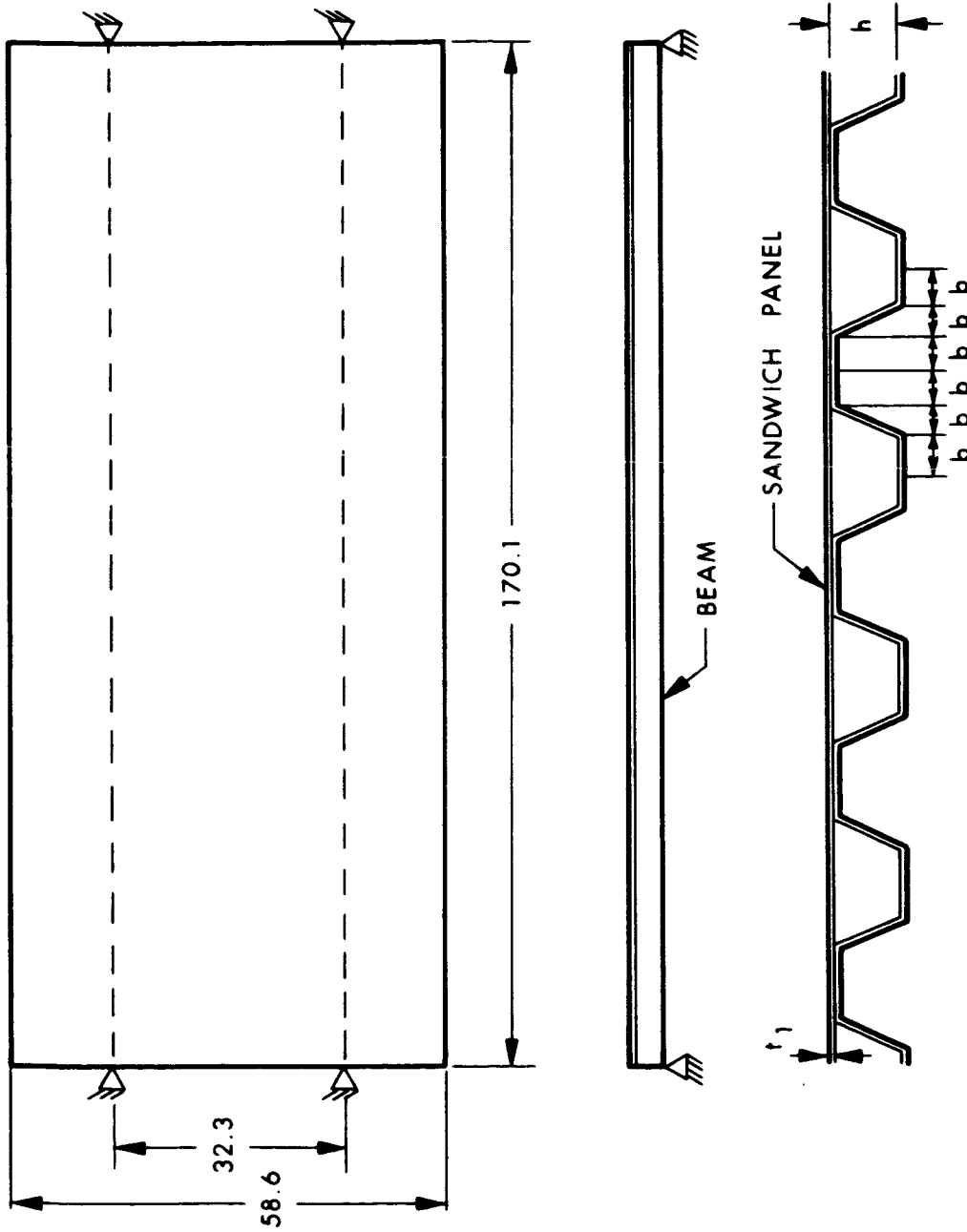


FIG. 6-4 SKETCH OF PANEL SHOWING CORRUGATED SANDWICH CONSTRUCTION

6.2.2 Prestressed Tape Concept

Figure 6-5 shows a sketch of the prestressed tape concept. The 0.2-in. wide by 0.003-in. thick fiberglass tapes are stretched over a beryllium frame to a pretension of 84 lb/in. Because of the high prestress the frame must be reinforced with stiffeners. The frame consists of two identical halves, one upper and one lower. Thus, the tapes can be inserted between the frame halves. The analysis shows a need of a 2 x 0.75 x 0.014 in.² box section for the frame and a 0.75 square box section for the stiffeners. The stiffeners are located as shown on the figure. A significant problem area would be relaxation of the tapes during the flight caused by creep. This creeping would tend to lower the natural frequency.

6.2.3 Prestressed Diaphragm Concept

The prestressed diaphragm concept (shown in Fig. 6-6) is similar to the one described above, except that a thin membrane is used instead of the tapes. The membrane is made of 0.001-in.-thick beryllium foil. The frame is the same as in the tape design even though a smaller size could be used due to the smaller membrane loads. The metal diaphragm will perform better since creep is not a problem.

6.2.4 Honeycomb Construction

The honeycomb concept shown in Fig. 6-7 is similar to the corrugated sandwich construction.

Study of the design indicates that a panel height of 0.5 in. and facing sheets of 0.002 in. will produce the lightest weight design. Beryllium facing sheets are bonded to an aluminum honeycomb core. The core is fabricated from 0.0005-in. foil, with 1/8-in. openings.

6.2.5 Biconvex Hollow Core

The biconvex hollow core concept, shown in Fig. 6-8, has been given a thorough analysis (see Section 7). The concept uses an electroformed spherical cap which has been perforated with holes to remove approximately 81.5 percent of the top surface. The membrane is

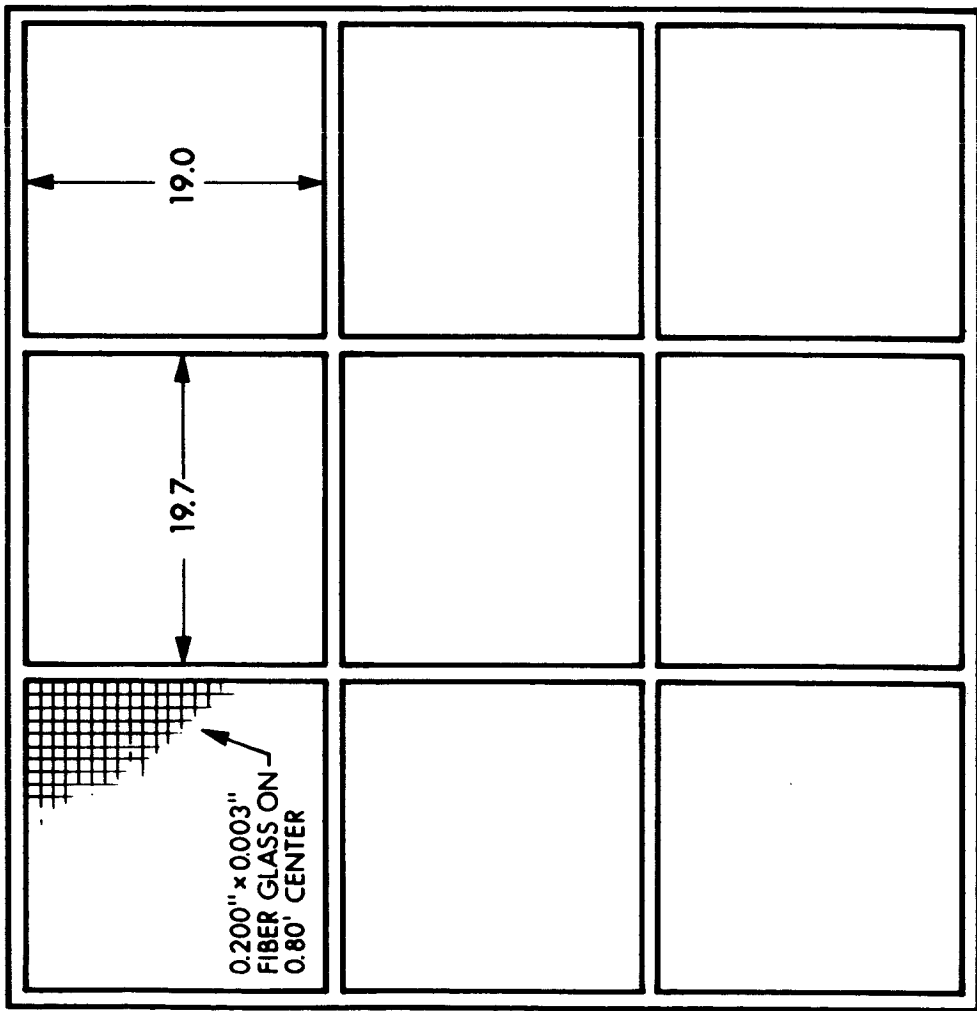
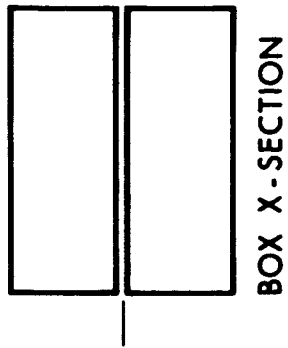


FIG. 6-5 PRESTRESSED TAPE CONCEPT

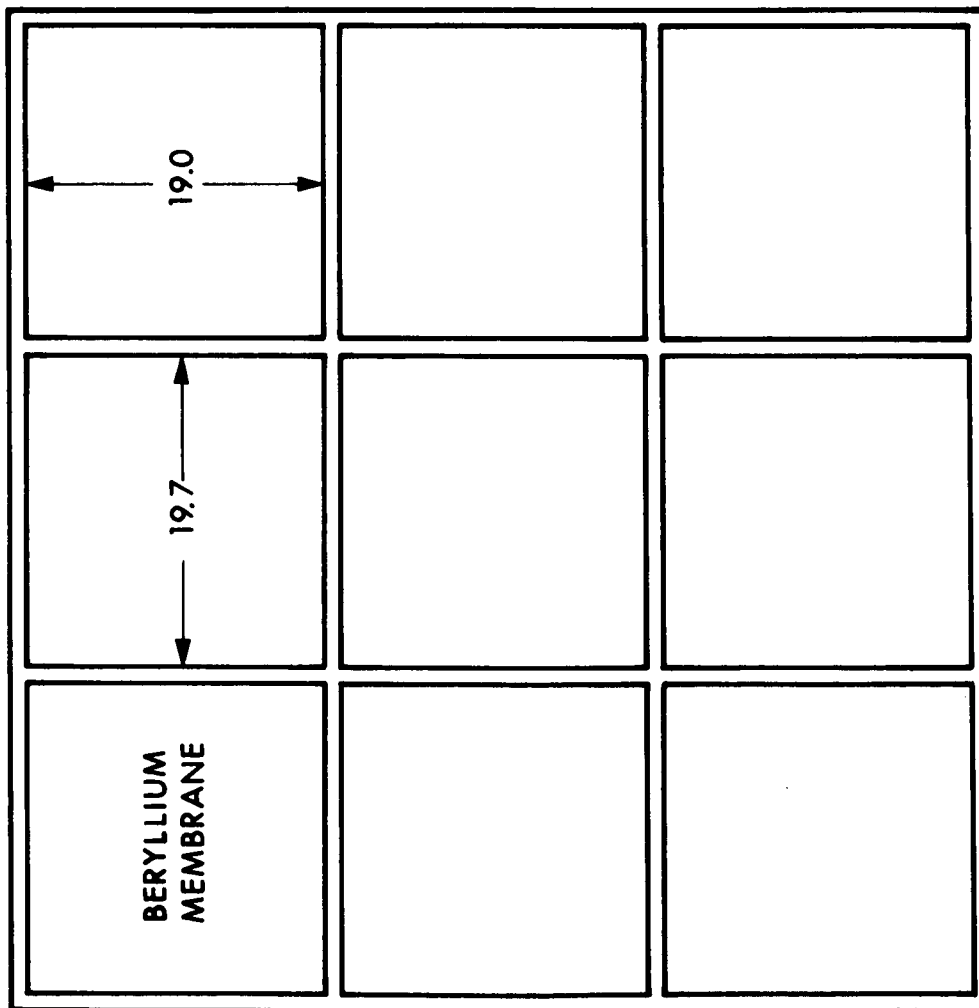
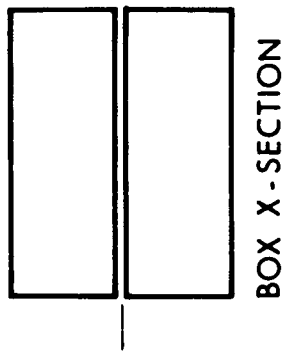


FIG. 6-6 PRESTRESSED DIAPHRAGM CONCEPT

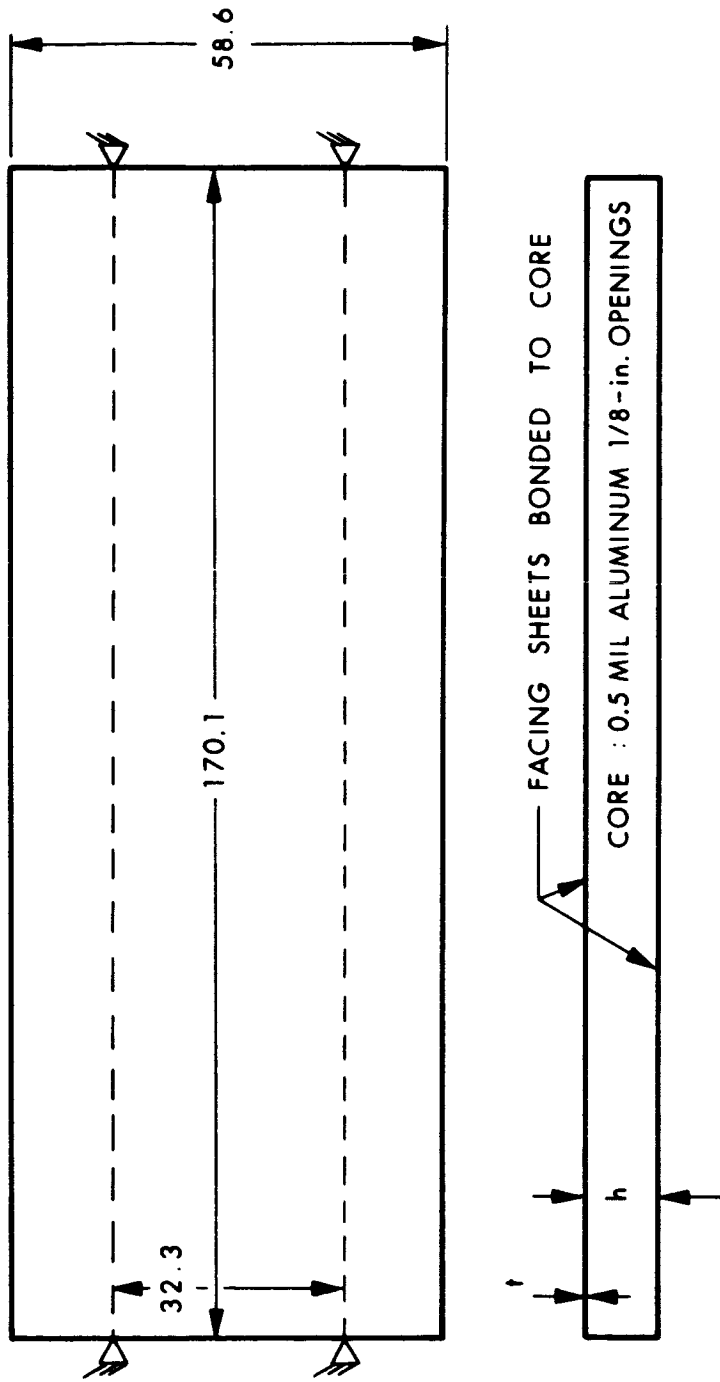


FIG. 6-7 HONEYCOMB CONSTRUCTION

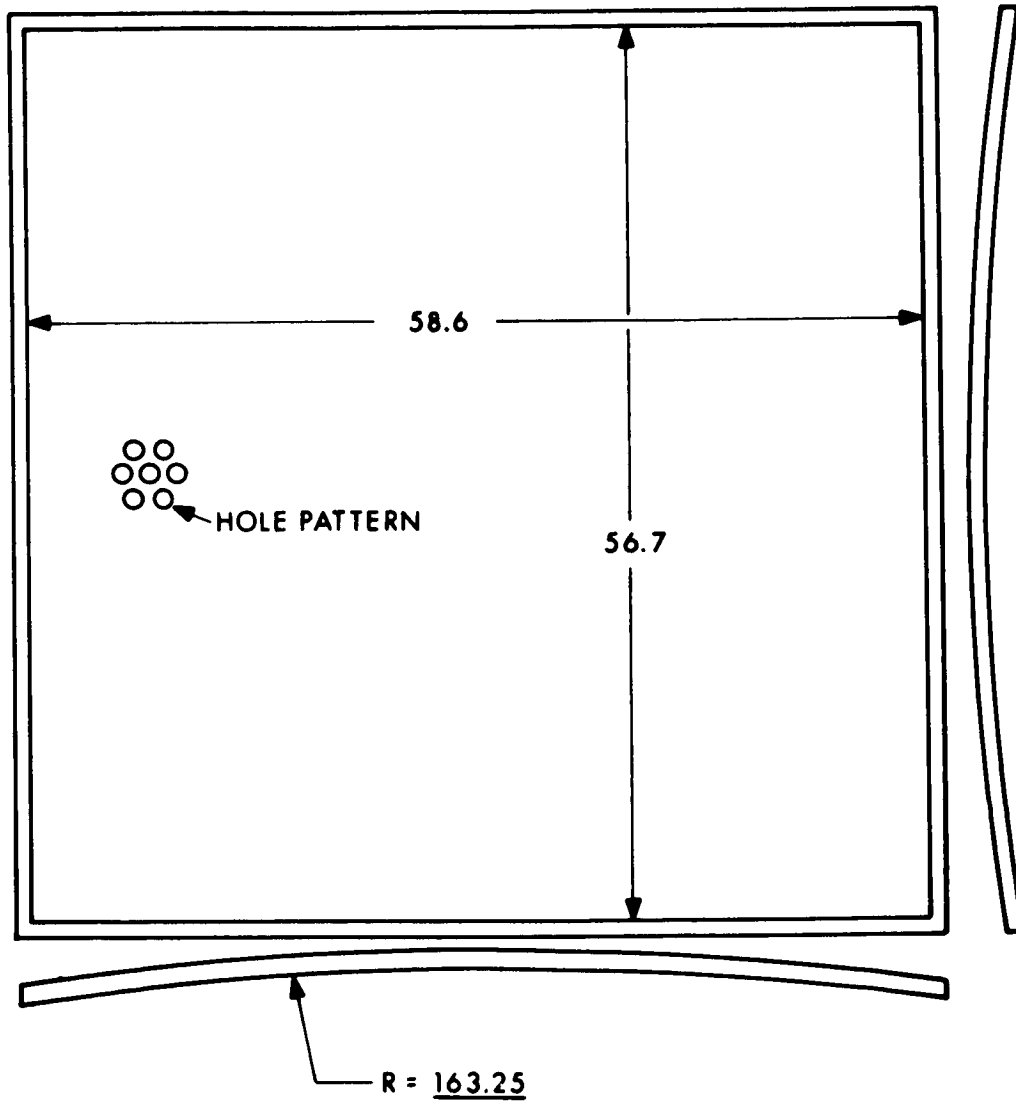


FIG. 6-8 SKETCH SHOWING BICONVEX HOLLOW CORE CONCEPT

essentially a top and bottom skin supported by cylinders with the skin removed within the cylinders. The curvature increases the buckling strength and the natural frequency.

The material used is nickel substrate and aluminum frame. By using aluminum substrate and beryllium frame further reduction in the weight may be obtained.

6.3 Hollow Core Design Optimization for Minimum Specific Weight

Equations used to obtain the data and information in this trade study are shown in Appendix E.

Many factors affect the hollow core design. Figure 6-9 shows the geometry parameters. The parameters considered are:

1. Solar cell weight -- W_{sc} (this includes cells, coverglass, dielectric, adhesives, etc.)
2. Input inertia effect -- $g_o - g_{stat}$ (dynamic and static environment)
3. Structure gain -- q (dynamic magnification factor)
4. Radii describing the curvature and size of the panel -- R_1, R_2 .
5. Half-angles of the curved surfaces -- α, β
6. Density of the structural material -- ρ
7. Skin thickness -- t
8. Hole pattern
9. Hole spacing -- $2a$ (diagonal distance across square hole pattern)
10. Hole size -- d
11. Panel material

All of these parameters must be evaluated before an optimum design can be found. Essentially, the parameters can be grouped as: (1) geometry, (2) dead-load and loading conditions, and (3) material.

A computer program was used to study the biconvex hollow core design because of the large number and range of variables to be considered. The program was derived from the equilibrium equations shown in Appendix E. The equations were simplified to lessen the program complexity, but the results are representative of the trends. The demonstration panel design was analyzed to the equations given.

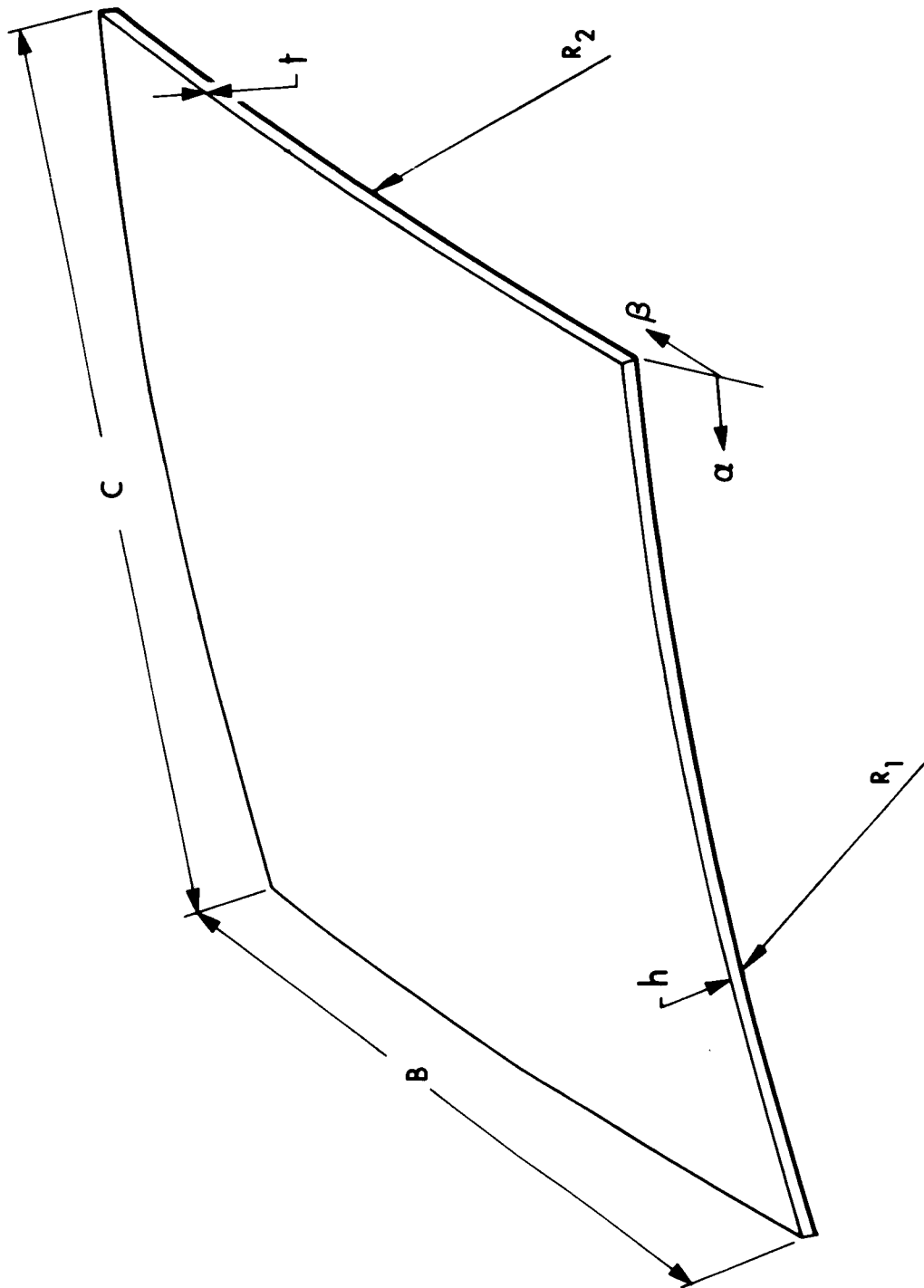


FIG. 6-9 GEOMETRY PARAMETER BICONVEX SUBSTRATE

This section contains a series of graphs which summarize the results of the computer study. Each graph considers a specific cell stack weight of 0.16 lb/ft^2 and a square hole pattern. The remaining significant parameters are noted.

The first graph, Fig. 6-10, shows relative comparisons between substrate specific weight and: (1) depth of section, and (2) material gage. The thinner section depths indicate a minimum, and if the range of thickness of material had been computed beyond 0.002 in., the thicker section depth would also show the same trend. It is expected that section depths thinner than 0.1 in. would soon show a reversal in specific weight, but fragility of the electroforming mandrel dictated this value as a minimum thickness.

Figure 6-11 defines specific weight for: (1) variations in hole diameter/spacing (d/a) ratio, and (2) depth of section. The d/a ratio has an upper limit of 1.4, which is the value where the holes are touching. This curve indicates that depth of section is the more critical parameter for minimum specific weight.

The third graph, Fig. 6-12, shows the relationships of specific weight to: (1) substrate span and (2) section depth. The biconvex substrate is shown to have a small increase in specific weight for a large change in span.

Figure 6-13 considers the specific weight variations due to the change in curvature of the biconvex substrate. The curve shows a drastic increase at small angles. This range is where the curved structure approaches a flat plate.

The fifth graph, Fig. 6-14, defines the first mode resonant frequency of the biconvex structure as a function of: (1) substrate span, (2) section depth, and (3) hole geometry. The curve shows the high-stiffness value of this structural concept.

Figure 6-15 shows the critical buckling pressure and inertia loading pressure as a function of: (1) substrate span, and (2) section depth. These critical buckling pressures are defined as the pressure

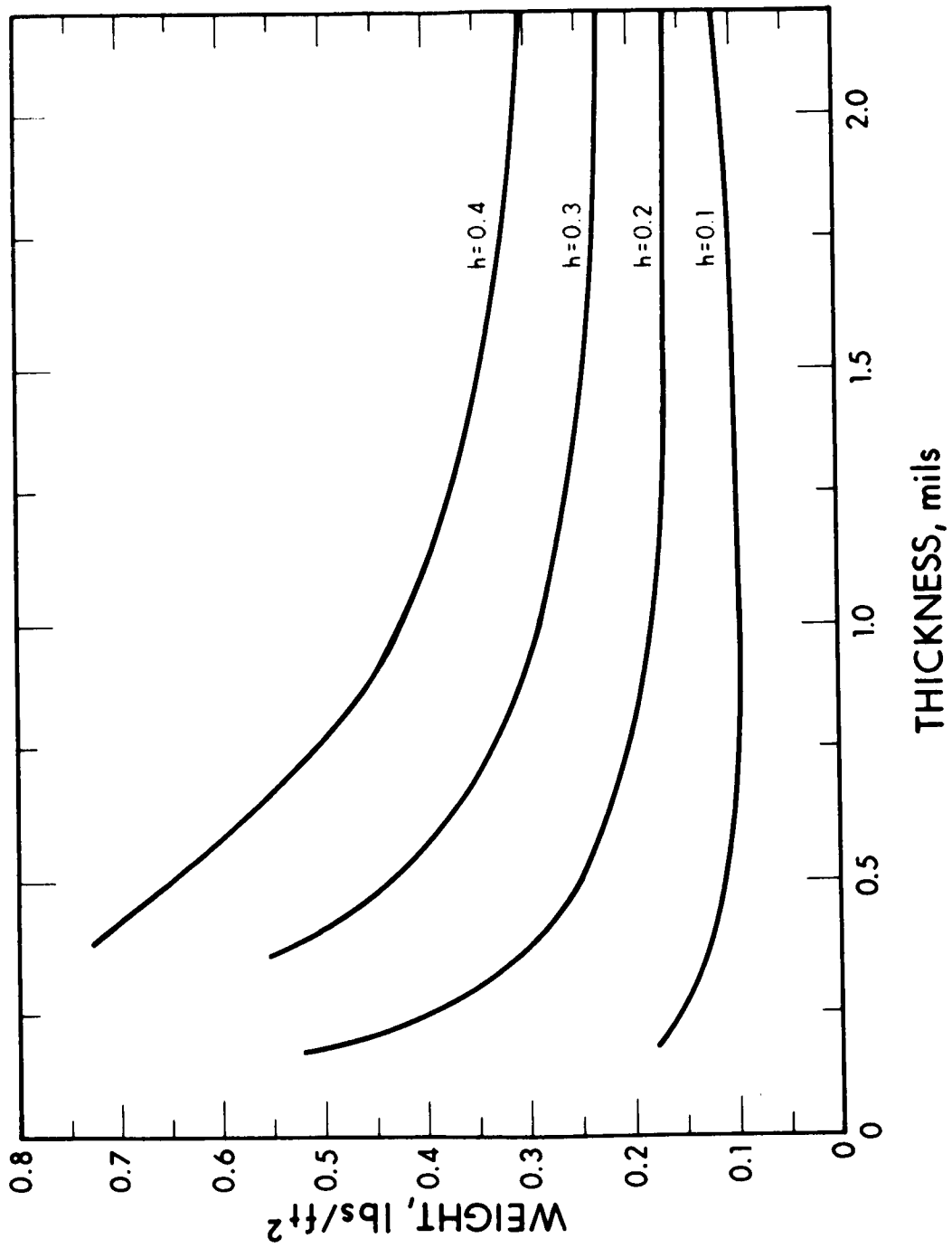


FIG. 6-10 HOLLOW CORE SPECIFIC WEIGHT VS THICKNESS (square pattern)

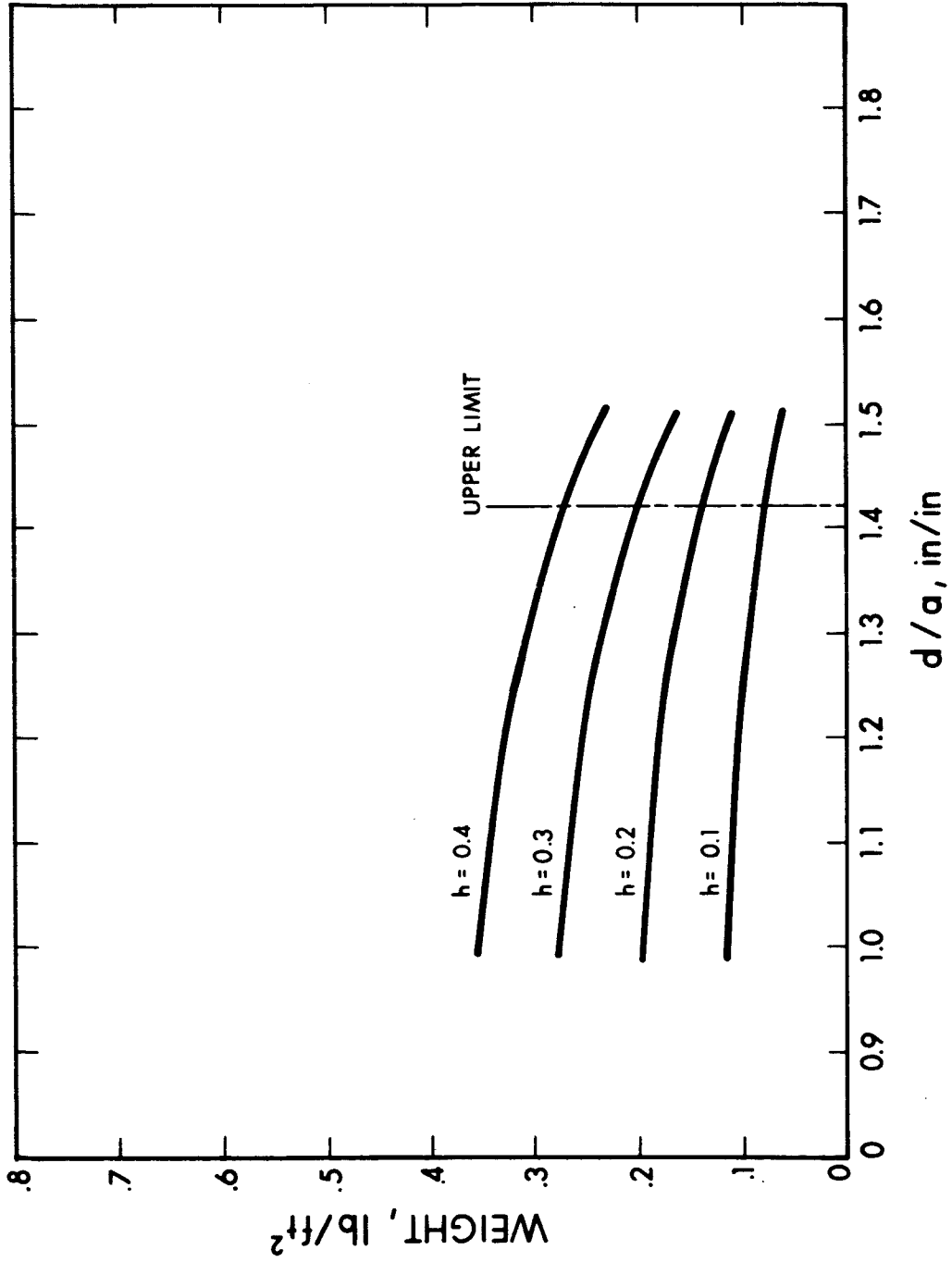


FIG. 6-11 HOLLOW CORE SPECIFIC WEIGHT VERSUS d/a RATIO (square pattern)

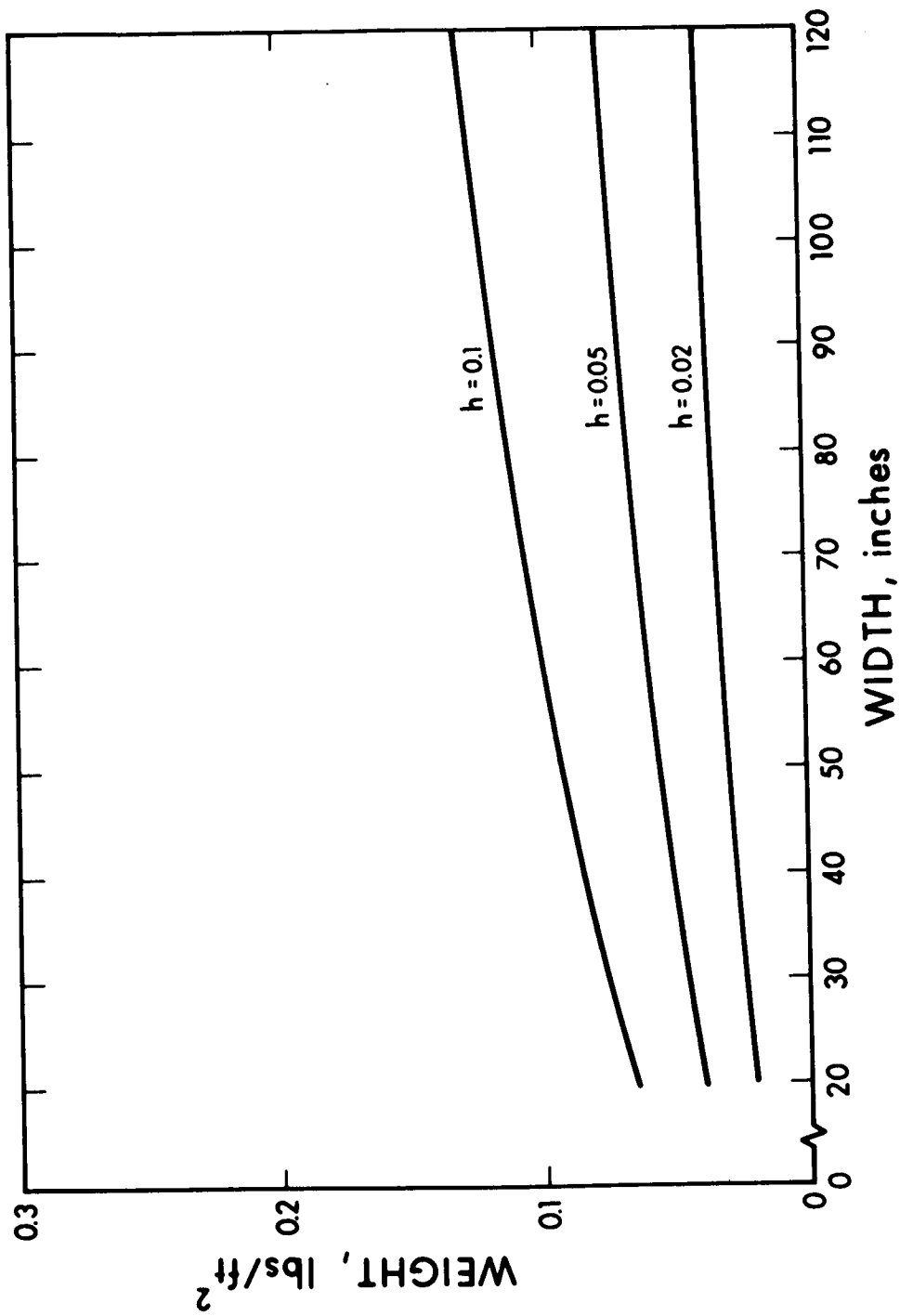


FIG. 6-12 HOLLOW CORE SPECIFIC WEIGHT VS WIDTH (square pattern)

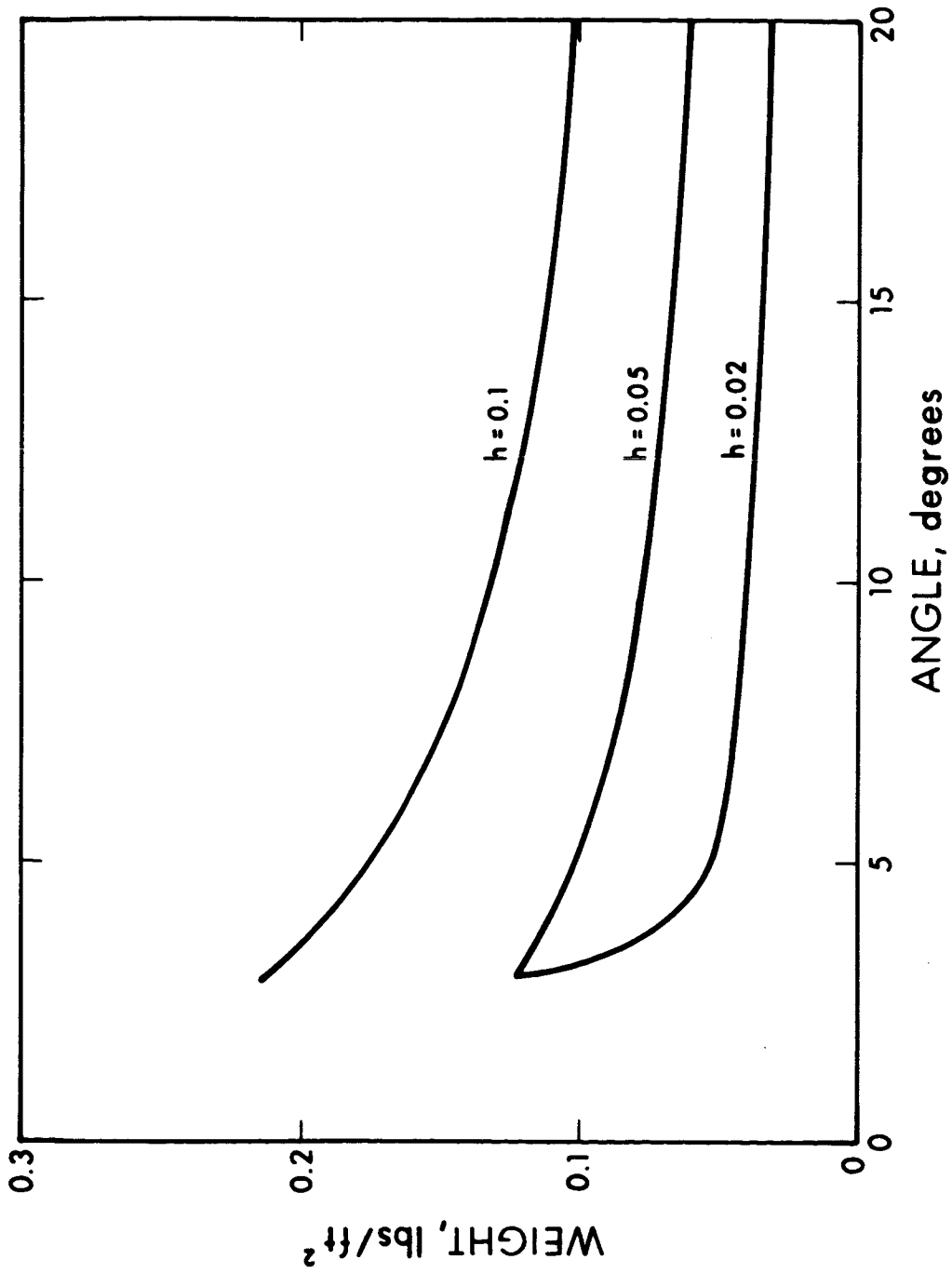


FIG. 6-13 HOLLOW CORE SPECIFIC WEIGHT VERSUS SLOPE (SQUARE PATTERN)

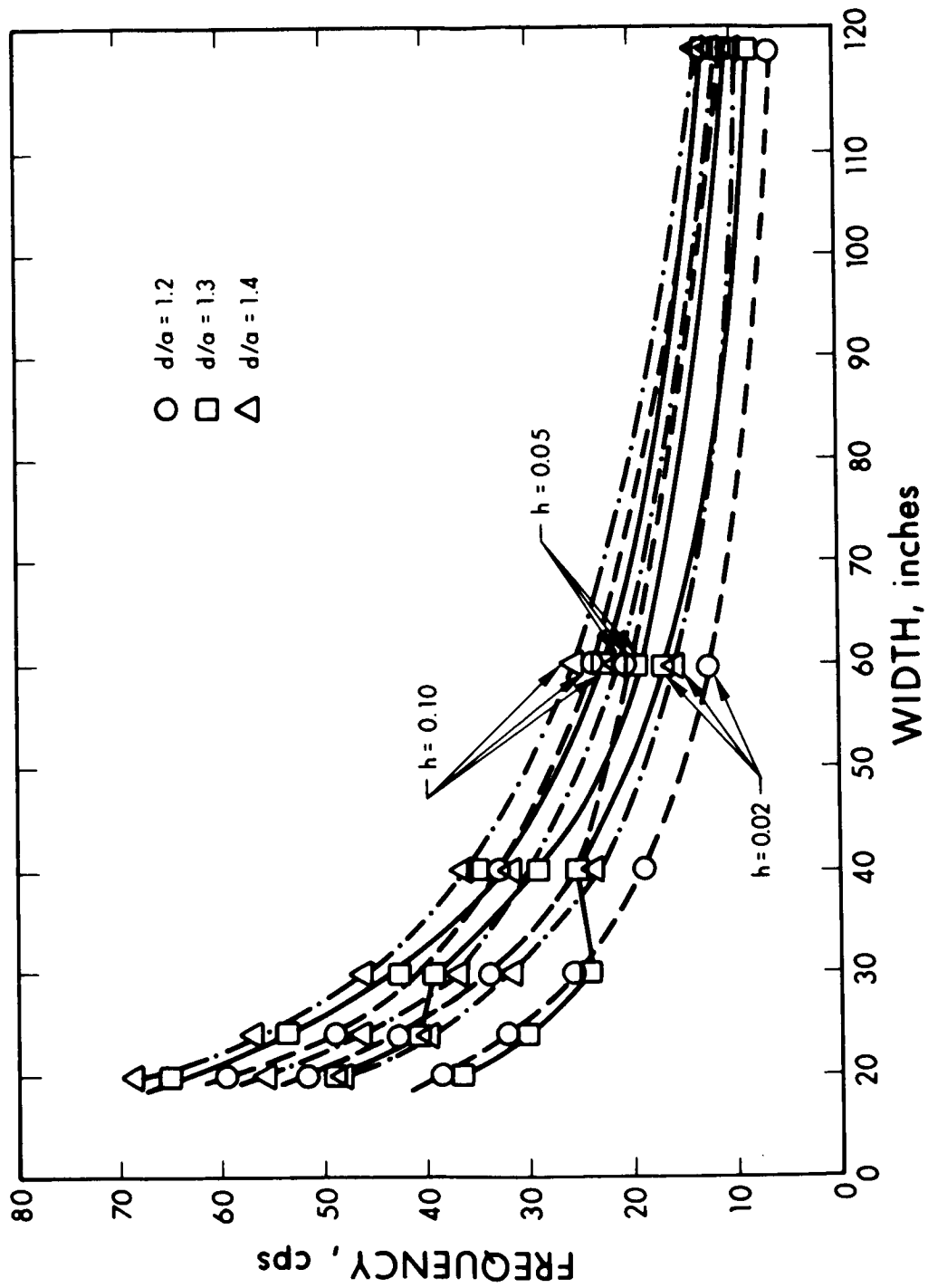


FIG. 6-14 HOLLOW CORE RESONANT FIRST MODE FREQUENCY (square pattern)

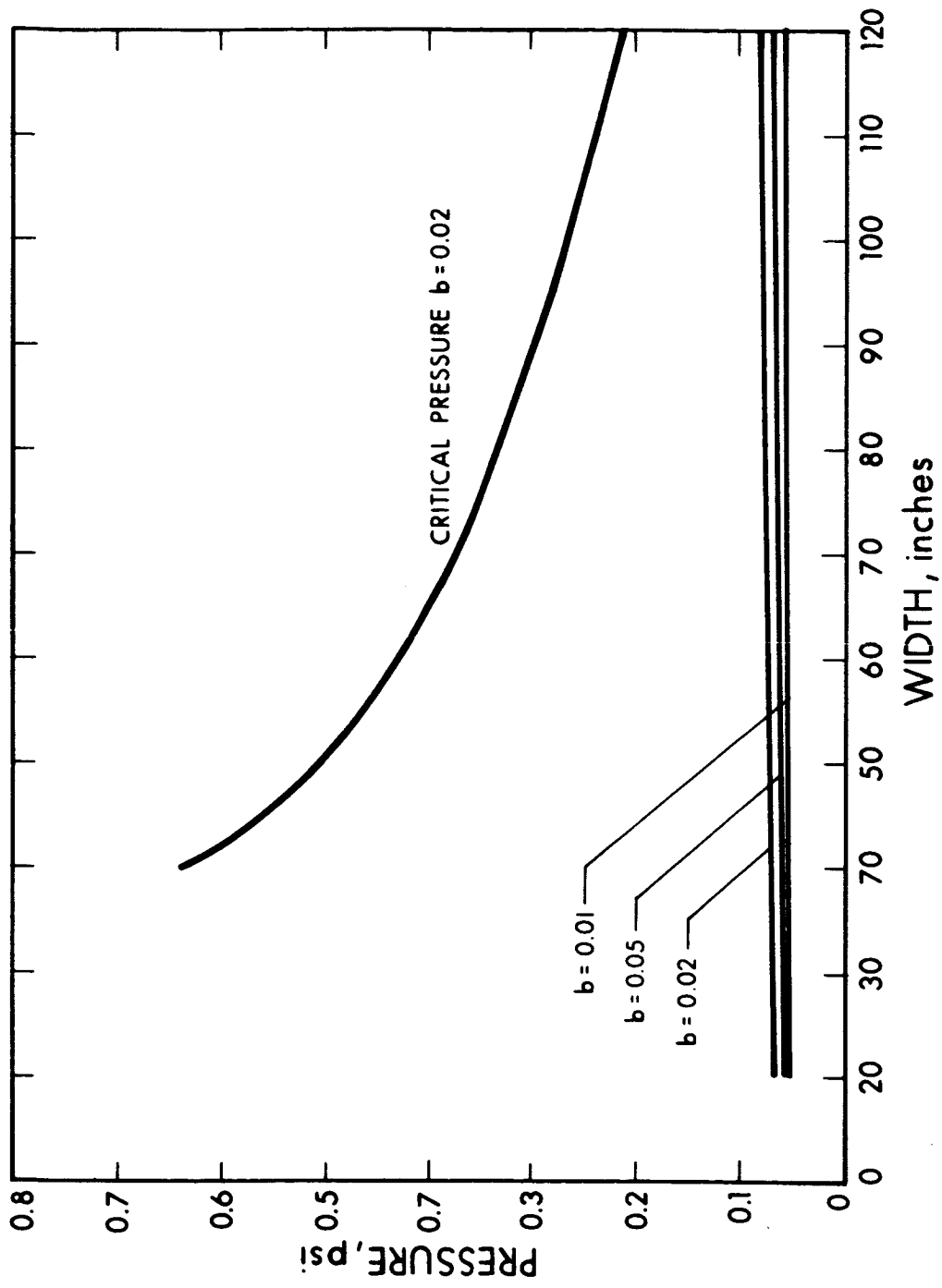


FIG. 6-15 HOLLOW CORE CRITICAL PRESSURE AND INERTIA LOAD PRESSURE (square pattern)

at which the substrate buckles. This is not the local crippling of the hollow core surface. The curve indicates the large margin between applied and critical pressures.

The seventh graph, Fig. 6-16, defines the specific weight of the hollow core structure as a function of: (1) structural material and (2) dynamic magnification factor. Comparison of curves 2 and 4 shows that an aluminum substrate is half the weight of a nickel substrate. Curves 2 and 3 show that decreasing the assumed magnification factor by two decreases the specific weight by 30 percent.

Figures 6-17 and 6-18 define the relationship between substrate specific weight (slanted hole pattern) and: (1) land dimension, (2) skin thickness, and (3) hole diameter/spacing ratio. Practical limits on mandrel fabrication require a land dimension (the distance between edges of adjacent holes) of at least 0.05 in. for a hole diameter of about 1 in. Using this limit, Fig. 6-17 shows the minimum specific weight is 0.066 lb/ft^2 for a hole diameter/spacing ratio of 1.9.

The trade study indicates that the structure can be thin (panel height) and still have large radius of curvature before structure will become critical for any given size.

For a panel size as needed in the demonstration panel, the study indicates an optimum configuration of:

Size:	$58.6 \times 56.7 \text{ in.}^2$
Hole diameter:	1.00 in.
Hole spacing:	1.05 in.
Radius of curvature:	$R = 163.25 \text{ in.}$
Panel thickness:	$h = 0.100 \text{ in.}$
Skin thickness:	$t = 0.002 \text{ in.}$

With this configuration, the structure weighs 0.066 lb/ft^2 .

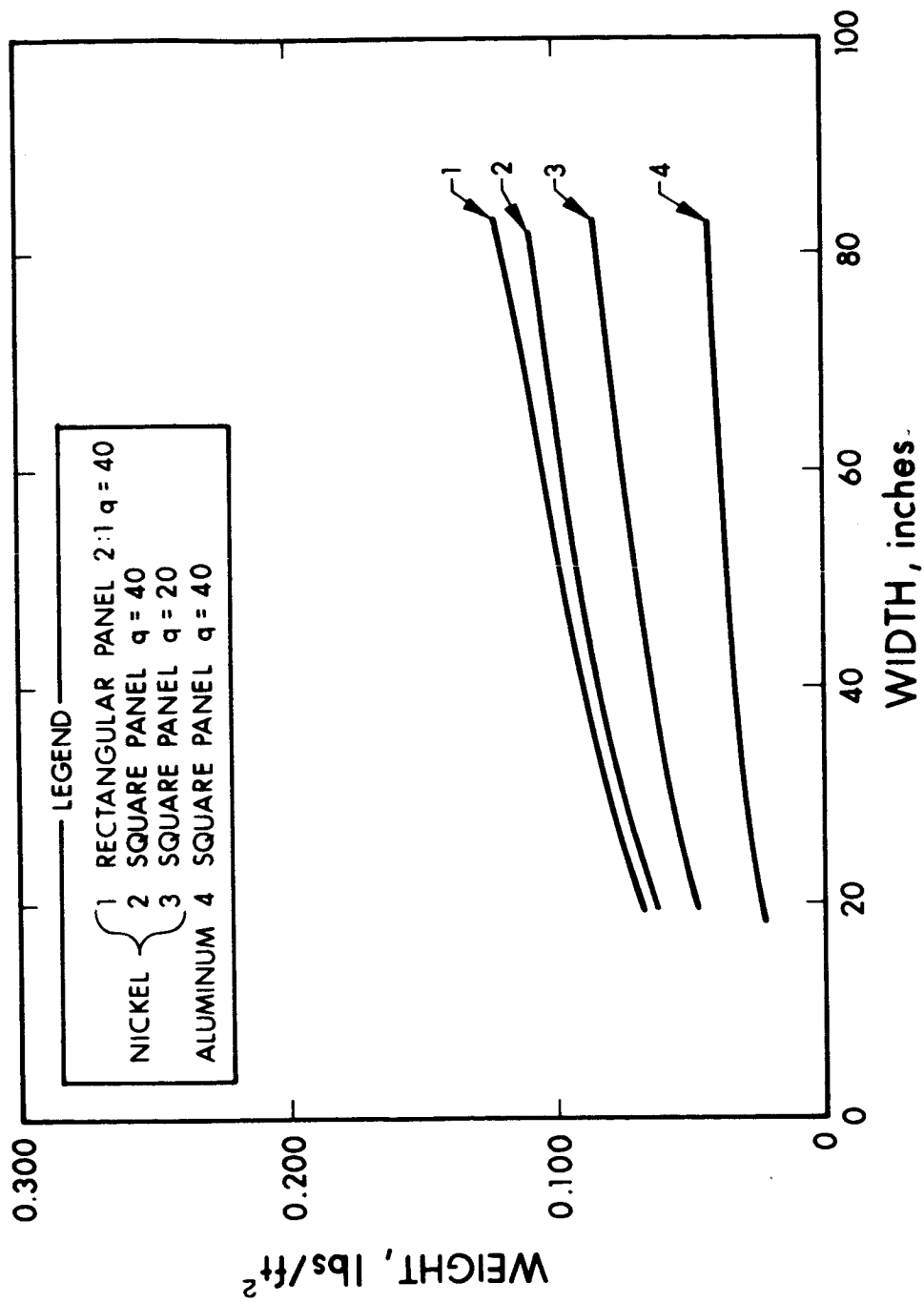


FIG. 6-16 BICONVEX HOLLOW CORE SOLAR PANELS -- PANEL STRUCTURE WEIGHT VERSUS PANEL WIDTH

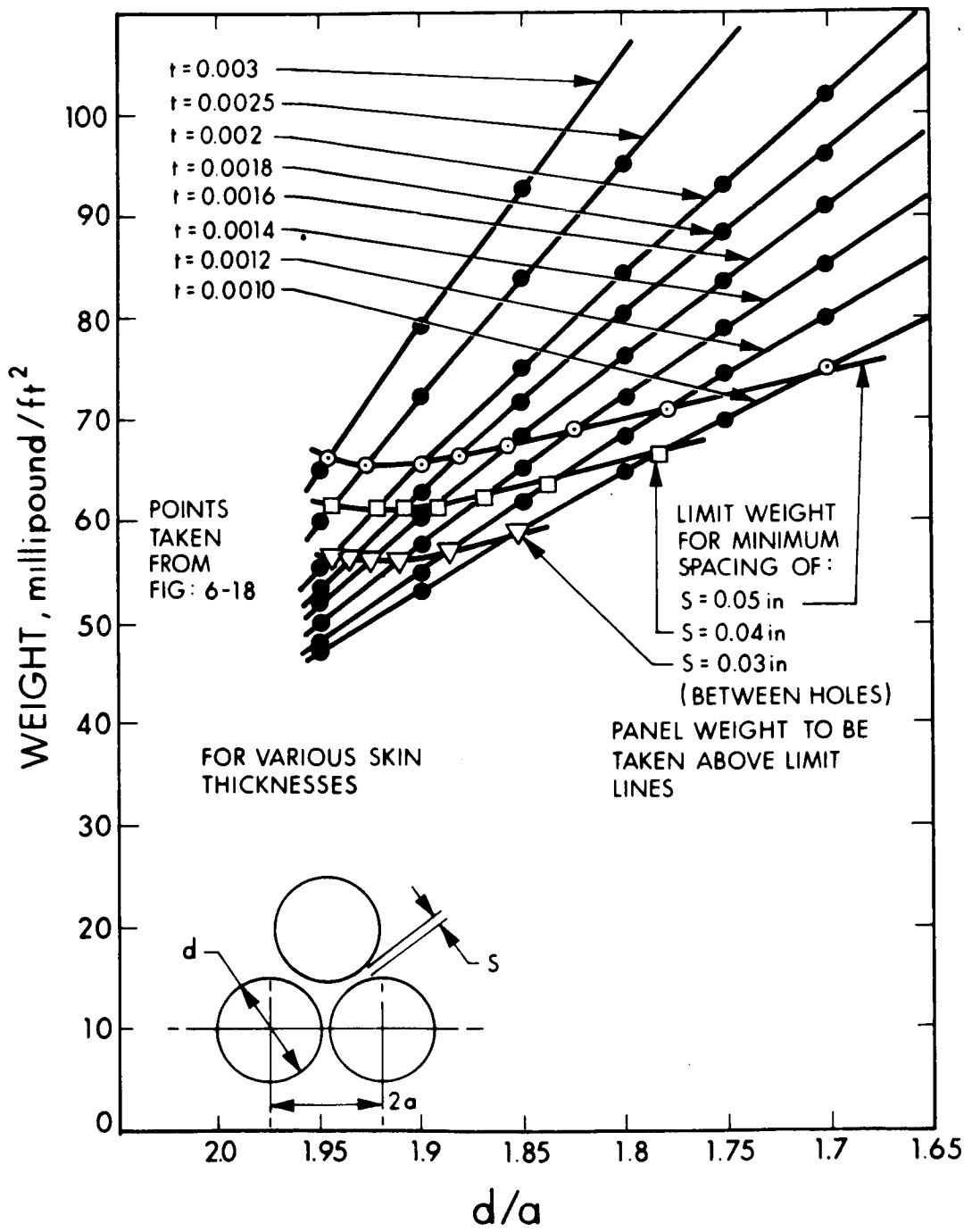


FIG. 6-17 HOLLOW CORE SPECIFIC WEIGHT (SLANTED PATTERN) VERSUS d/a RATIO AND SKIN THICKNESS

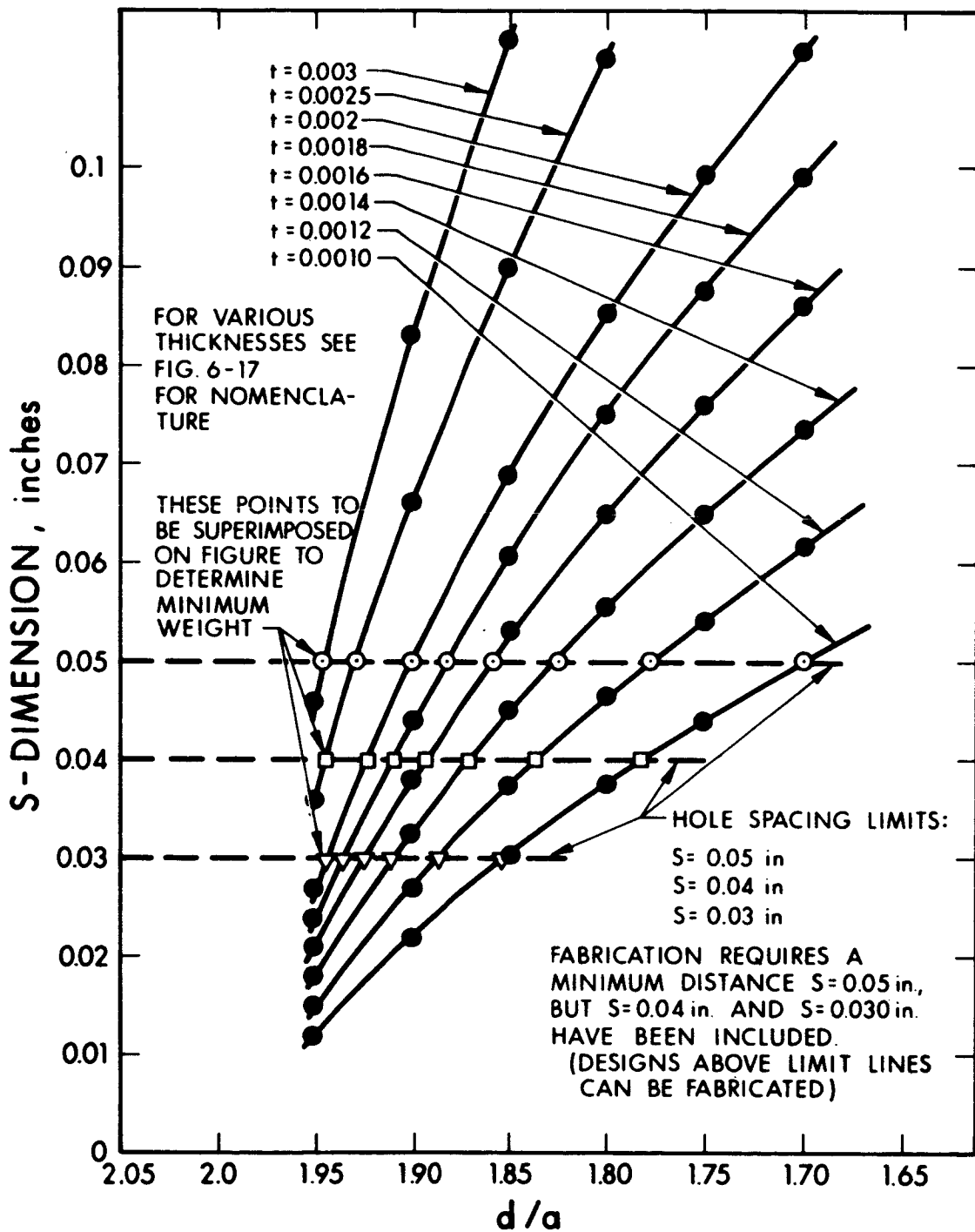


FIG. 6-18 HOLLOW CORE LAND DIMENSION (SLANTED PATTERN) VERSUS d/a RATIO AND SKIN THICKNESS

7. DESIGN ANALYSIS

This section outlines the engineering analysis used to develop and design the demonstration panel and the feasibility study for a 10.4 kW solar array. The study areas discussed are:

1. Weight estimates of demonstration panel and 10.4 kW array.
2. Structural and dynamic analysis of demonstration panel and 10.4 kW array.
3. Thermal analysis of hollow core substrate.
4. Solar cell characteristics in a Jupiter mission environment.
5. Solar-electric propulsion power conditioning.

7.1 Weight Estimate of Demonstration Panel and 10.4 kW Array

The weights of the demonstration panel and the 10 kW array are shown in Table 7-I. The completed demonstration panel will weigh 7.2 lb and will have a structure specific weight of 0.168 lb/ft^2 . The demonstration panel weight, when revised to include mechanisms and cabling, will increase to 9 lb. A weight-to-power ratio is not shown for the actual demonstration panel because of the various cell stack combinations. Also shown in Table 7-I is an estimate of the weight of the 10.4 kW array with the same design features as the demonstration panel, but using materials and components which should be available in 1967.

7.1.1 Structural Assembly

The structural assembly consists of the following components:

1. Hollow core substrate
2. Box beam frame members
3. Joining clip
4. Bonding adhesives and mechanical fasteners

BLANK PAGE 7-2

TABLE 7-1

ESTIMATE OF SPECIFIC WEIGHT, SPECIFIC POWER AND POWER DENSITY

Item	Description		DEMONSTRATION PANEL			10 kW ARRAY (1967 Technology)			
	No.	Size	Remarks	Specific Weight lb/ft ²	Total Weight lb	Projected Improvements	Remarks	Specific Weight lb/ft ²	Total Weight lb
Cover glass	480	2 x 2 cm x 3 mil	Microsheet	0.0394	0.0799	1 mil integrated SiO ₂	See cell	-	-
Filter adhesive		2 mil	RTV-602	0.0096	0.0198	None required		-	-
Solar cell	240	2 x 2 cm x 4 mil	Solderless conventional contact	0.0530	0.0547	4 mil wrap-around with integral filter	241,920 cells	0.0662	68.93
		2 x 2 cm x 8 mil	Solderless conventional contact	0.1060	0.1094	NA	NA	-	-
Dummy cell stack	3548	2 x 2 cm x 7 mil	Aluminum wafers (1)	0.0987	1.5071	NA	NA	-	-
Interconnector	480	2 mil	Bus bar and solder	0.0150	0.0310	Printed circuit		0.0100	10.41
Cell adhesive		56 x 57.9 x 4 mil	RTV-40	0.0207	0.4660	Same		0.0207	22.37
Dielectric		56.5 x 58.4 x 1 mil	H-film	0.0072	0.1649	Same		0.0072	7.92
Dielectric adhesive	10%	56.5 x 58.4 x 2 mil	RTV-40	0.0207	0.0948	Same	Covers 20% area	0.0207	4.10
Thermal control paint		62.6 x 60.7 x 3 mil	Laminar X-500	0.0240	0.6333	None, anodize substrate and pigmented H-film		-	-
Substrate		2 mil	Nickel hollow core	0.0660	1.5230	2 mil aluminum hollow core		0.0512	51.17
Frame		10 mil	Aluminum box beams	0.1098	2.5260	10 mil beryllium box beams		0.0538	66.69
SUBTOTAL					7.210				
Cabling			Separate cable bundles	0.0300	0.7917	Main electrical bus incorporated into frame		0.0050	6.20
Mechanism				0.0376	1.0000	Same		0.0376	46.70
TOTAL					9.00				285.0
Total area		ft ²			26.0				1239
Power		watts			(2)				10,400
Weight/power ratio		lb/kW							27.4

(1) Sized for 4 mil wrap-around cell and 1 mil microsheet cover glass
 (2) To be determined by test

BLANK PAGE 7-4

7.1.2 Electroformed Nickel Substrate

The electroformed nickel substrate has a specific weight of 0.066 lb/ft² as determined by analysis (see Appendix D). The trade study in Section 6 shows that by changing to electroformed aluminum the specific weight will decrease to 0.051 lb/ft².

Using aluminum as the frame material gives a specific weight of 0.110 lb/ft², but the use of beryllium results in a specific weight of 0.054 lb/ft². The specific weight values include the weight of the joining clips, adhesives, and mechanical fasteners.

7.1.3 Mechanical Assembly

The mechanical assembly consists of the following components with specific weights as shown:

	<u>Specific Weight</u>
1. Hinges and deployment springs	0.005 lb/ft ²
2. Deployed position latches	0.003 lb/ft ²
3. Pyrotechnic release devices	0.016 lb/ft ²
4. Signaling circuits	0.011 lb/ft ²
5. Interpanel electrical cables	0.003 lb/ft ²
Total	0.038 lb/ft ²

7.1.4 Photovoltaic Assembly

The photovoltaic assembly consists of the following components:

1. Cover glass
2. Cover glass adhesive
3. Solar cell
4. Interconnector
5. Cabling
6. Cell adhesive
7. Dielectric
8. Dielectric adhesive
9. Thermal control paint

For a spacecraft operating outside the earth's radiation belts, a typical cover glass is approximately 6 mils of micro-sheet (7094 quartz). The cover used for this program is 3 mils thick. Test data shows that 1 to 2 mils of glass can be deposited directly on a cell with only a 3-percent decrease in power-producing capability of the cell at the end of one year (as compared to using a 6 mil cover). The use of integrated cover glass for interplanetary probe missions will greatly reduce the weight, complexity, and cost of fabricating a solar photovoltaic array.

The panel specific weight decreases by an additional 0.0096 lb/ft^2 if an integrated cover glass is used which eliminates the requirement for the cover glass adhesive.

Typical bus bar weight is approximately 0.03 lb/ft^2 , which is a small part of the total array weight. It is expected that the use of the wrap-around solar cell will minimize bus bar interconnections and decrease the weight and complexity.

The power cabling for typical current array designs use printed circuits to interconnect electrical section and copper-jacketed wire for the main power leads. The specific weight in the 10.4 kW array using this cabling concept is 0.300 lb/ft^2 . Preliminary designs indicate it is possible to incorporate the main power leads into the frame structure as flat strips. An alternate method would be to insulate certain frame members and use them as the conductors. The cabling weight is decreased significantly since most of the cabling is included in the structure weight; the remainder is estimated to have a specific weight of 0.005 lb/ft^2 . The dielectric uses a 1-mil H-film with a specific weight of 0.0072 lb/ft^2 . No improvements are expected in reducing the weight of the dielectric, either film or paint, in the near future.

The adhesive to be used to bond the cell to the dielectric and the dielectric to the substrate on the demonstration panel will be RTV-40, a silicone adhesive which will have an approximate

thickness of 4 mils when used to bond the cell to the dielectric and 2 mils when bonding the dielectric to the substrate. The specific weights for this adhesive are 0.0207 lb/ft^2 and 0.0072 lb/ft^2 . The dielectric adhesive covers only 10 percent of the substrate area.

The thermal control surface for the demonstration panel will be a 3-mil organic paint with a specific weight of 0.024 lb/ft^2 . The thermal control surface for the 10.4 kW array will be incorporated into the substrate by anodizing the aluminum hollow core and pigmenting the H-film.

7.2 Structure Stress and Dynamic Analysis

Theoretical equations have been developed to enable structural analysis of the solar panel structural members. Since instability is the main contributing factor, empirical data have been used to arrive at the analytical expressions. The empirical data has been extracted from NASA publications (such as NASA TN 3781), and has been proved in numerous practical applications. It was necessary to confirm the failure mode of the hollow core substrate before the tests defined in Section 9 were performed. These tests confirmed that the failure mode was crippling of the surfaces between holes. The tests showed that even after crippling, the structure was able to carry full load, with a column-type failure as a secondary effect.

The demonstration panel was analyzed utilizing the equilibrium equations defined in Appendix D. It was found structurally sound for the most critical loading condition.

The results of the structural analysis on the demonstration panel showed that the substrate will meet design loads with local crippling as the most probable failure mode. The interconnection indicates a minimum margin of 2.5. The frame was determined to have a critical margin of safety of 0.23, with local buckling of the frame surface as the failure mode. Section 9 describes this analysis.

The dynamic analysis of the biconvex hollow core structure has not been completed. The exact solution of the equation for dynamic response is yet to be solved.

The theory for the dynamic analysis of the biconvex hollow core substrate is contained in Appendix C. The first mode resonant frequency was determined from these equations to be 84.7 Hz. The substrate center-point displacement is calculated to be a maximum of 1.47 in. at resonance. The deployed array is estimated to have a first torsional resonance of 0.038 Hz. This is the lowest deployed array frequency.

Appendix C contains a discussion of the incorporation of viscoelastic adhesives for increasing structural damping. The present demonstration panel design is being evaluated to determine what design gains can be made in the specific weight by incorporating the viscoelastic adhesive. This study will be reported in the final report.

The biconvex hollow core construction demands continuous support along the edges to prevent panel instability. This means that to assure that the boundary conditions (assumed in the analysis) hold true, a support structure of sufficient rigidity must be designed. Several frame constructions have been investigated. Principal evaluation criteria are as follows:

1. The frame must provide ample strength to prevent excessive distortion during maximum loading.
2. It must possess good torsional stiffness.
3. It must have the ability to restrain combined loading (vertical and horizontal).

The requirements above dictate a box cross section; to assure minimum torsional effects, the box is split to form a double box so that the substrate panel can be attached to the center of the box cross section.

Because of the need for tongue-and-groove construction for packaging of the array, the box cross section derives additional reinforcing against column and buckling instability. The demonstration panel frame is fabricated from 10-mil aluminum sheet stock.

The demonstration panel design produces a frame that will weigh on the order of 2.5 lb.

The basic theory of the biconvex hollow core concept demands strict adherence to the boundary conditions. If the boundary conditions change, a substantial change in the hollow core characteristic may take place. One may therefore set as governing factors, for both the frame and the interconnection, the following:

1. The hollow core edges must remain in place for all loading conditions, within elastic limits.
2. The edge restraint caused by the interconnection must approach that of simple support, minimizing moment input to the hollow core.
3. The interconnection must transfer the loading equally from both top and bottom skins of the hollow core.
4. The interconnection must transfer the load uniformly along the edges, minimizing stress concentrations.
5. The interconnection must minimize the effect of differential growth of frame and hollow core substrate, caused by environment or fabrication.
6. The effect of deviation from the nominal curvature of both mating edges shall be reduced in the interconnection.

Point one concerns itself mainly with the frame, even though the tangential rigidity of the interconnection enters into overall action. The column length is so short that stability is not of concern. (Substrate-to-frame interconnection is shown in Fig. 7-1.)

Points (2) and (3) state that the interconnection must approach a hinge, with very small flexural rigidity, assuring freedom of the edges to rotate. The interconnection must be bonded to the top and bottom skins such that the membrane loading can be distributed evenly. Point (4) indicates that the interconnection must run the full length of the hollow core boundary.

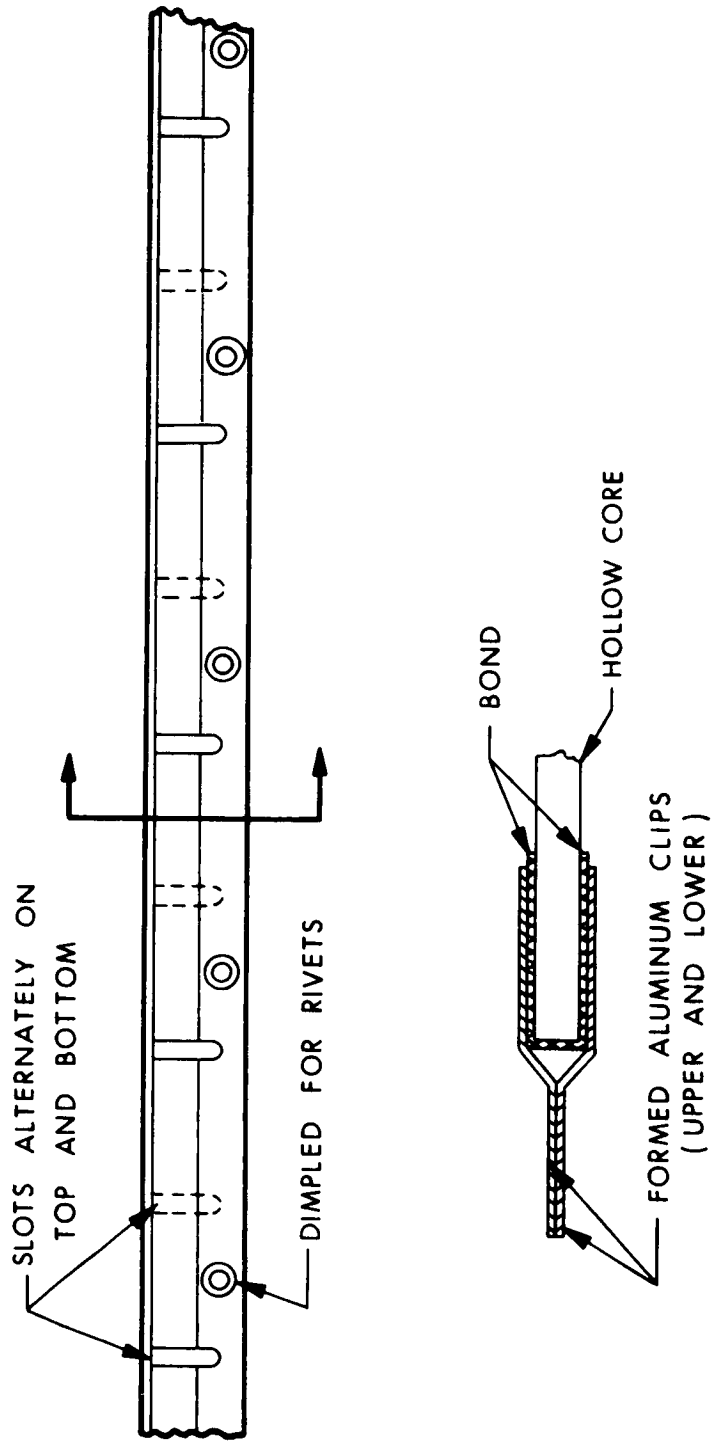


FIG. 7-1 SOLAR PANEL - SUBSTRATE-TO-FRAME INTERCONNECTION

The established method for attachment of the two mating parts is through an adhesive bond. Most adhesives need curing for long periods of time at elevated temperatures. The interconnection must therefore be constructed such that the thermal growth loads are minimized at the interface. The interconnection will be attached to the hollow core structure and then the assembly is attached to the frame assembly by ambient temperature means, such as mechanical fasteners. There is going to be some difference in the thermal growth of the interconnection and the hollow core, but this loading can be relieved by milling slots in the interconnection surfaces bonding to the hollow core. The difference in thermal growth existing during the casting period, can be relieved by some distortion of the hollow core; i.e., edge loading.

To tolerate normal fabrication deviations, it is necessary to make the interconnection pliable or flexible radially conforming to the contour of the two mating parts. Thus, the edges may be fit to each other with a minimum of stress input or buildup.

Many schemes have been considered for the interconnection. Two concepts are shown in Fig. 7-2 and 7-3. Nonmetallic molded sections have been studied, but their use was omitted because of the uncertainty in space operation (outgassing and its temperature sensitivity).

One may obtain one added benefit from the adhesive bond material between clip and substrate, and that is a certain amount of viscoelastic damping in the joint.

7.3 Panel Thermal Analysis

7.3.1 Thermal Considerations

The efficiency of silicon solar cells decreases with increasing temperature. A 2°C temperature increase lowers the electrical output by 1 percent. In order to maximize the electrical power and minimize solar array weight and area, it is necessary to maintain the solar cells at the lowest possible temperature while absorbing a large percentage of the incident solar radiation.

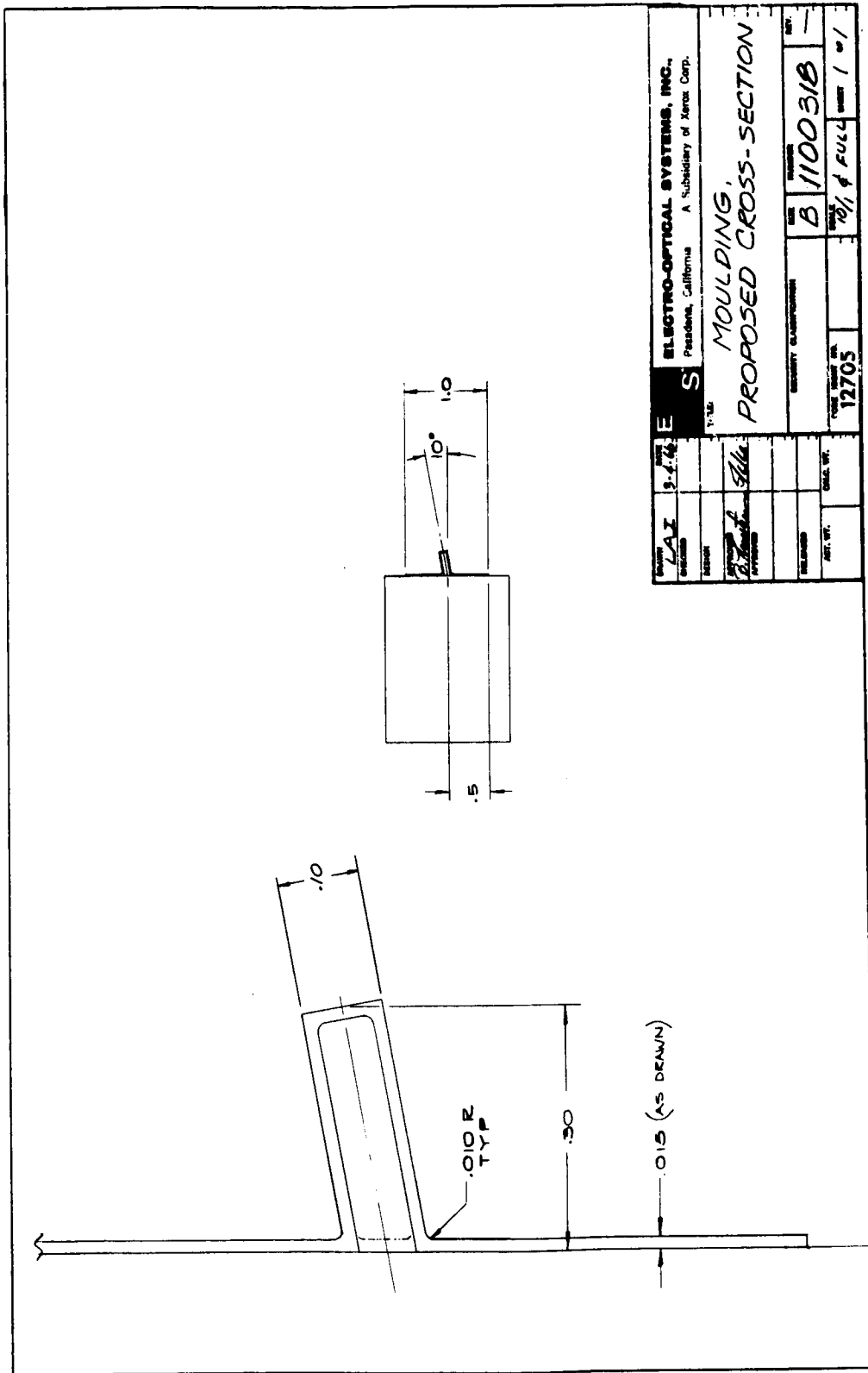


FIG. 7-2

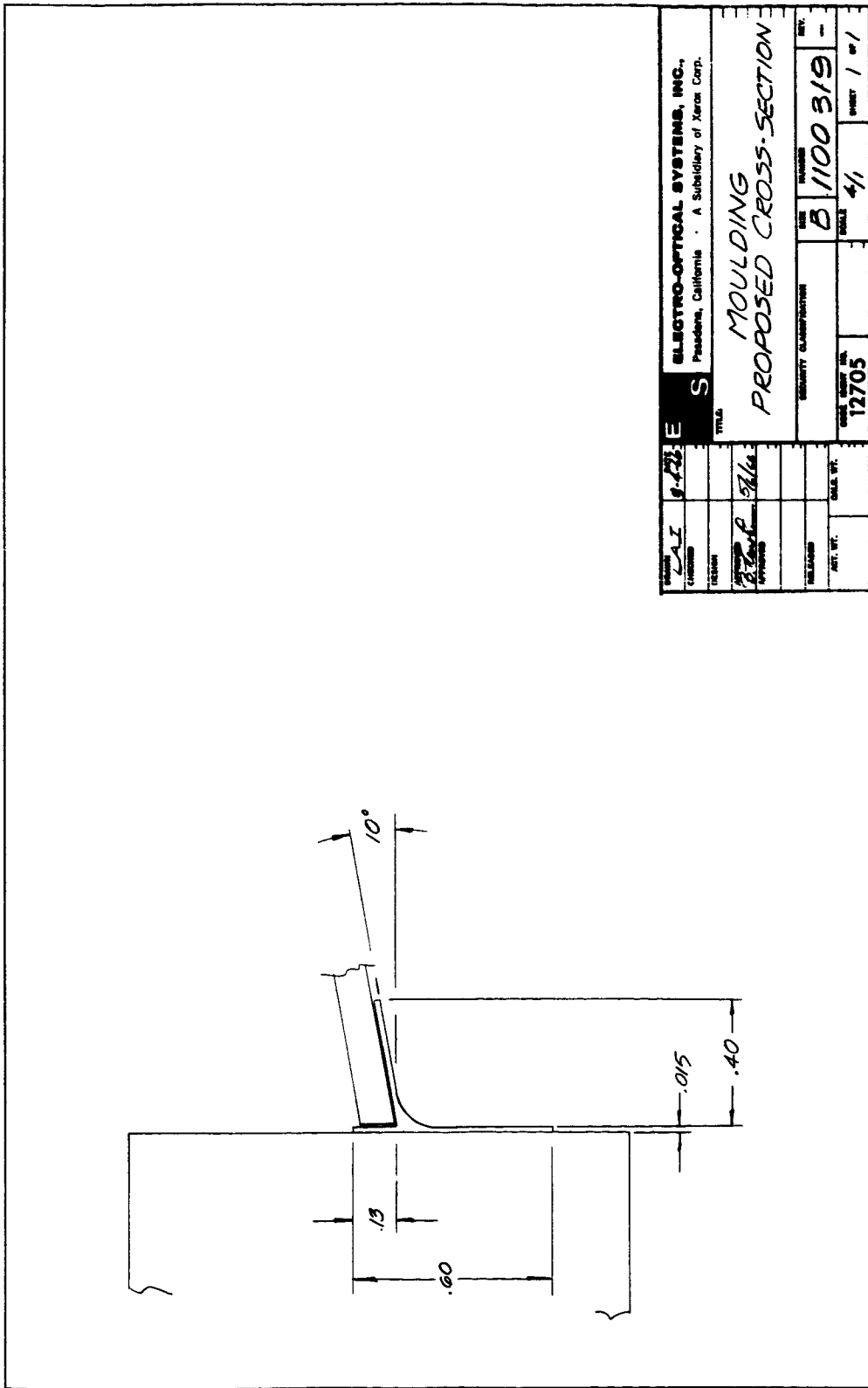


FIG. 7-3

The control of solar panel temperatures is passive and is accomplished by the use of thermal coatings on both sides of the panel. Once thermal coatings have been selected, the temperature of a sun-facing solar panel varies primarily with the intensity of solar radiation. The construction of the panel substrate and supporting frame, as well as interactions with the spacecraft bus and with an adjacent planet during orbit, will also affect the average steady-state temperature and the detailed distribution of temperature throughout the panel assembly.

Changes in the solar radiation intensity incident on solar panels during transit occur slowly enough to enable thermal analysis to be based on quasi steady-equilibrium conditions. The primary concern of this analysis is the effect of the substrate construction on solar cell temperatures. An ideal solar array would absorb only that part of the solar spectrum which can be converted to electrical power and would radiate infrared from both sides via an isothermal black plate. Since approximately half the absorbed solar radiation must be conducted through the substrate before being radiated to space from the back surface of the panel, the front (cell side) of the panel is normally slightly hotter than the back side.

7.3.2 Methods of Analysis

The temperature drop through a simple laminated substrate (such as a flat aluminum plate or membrane including cells, filter covers, etc.) can be calculated on the basis of a one-dimensional model. Approximately 8 percent of the absorbed radiation is converted to electrical power, and the remaining energy is radiated to space from the top surface (filter covers) and from the bottom surface (black paint). The bottom surface is thermally connected to the top through several thermal resistances in series.

The temperature distribution through a substrate structure which is more complicated than described above must take into account conduction in directions other than normal to the cell

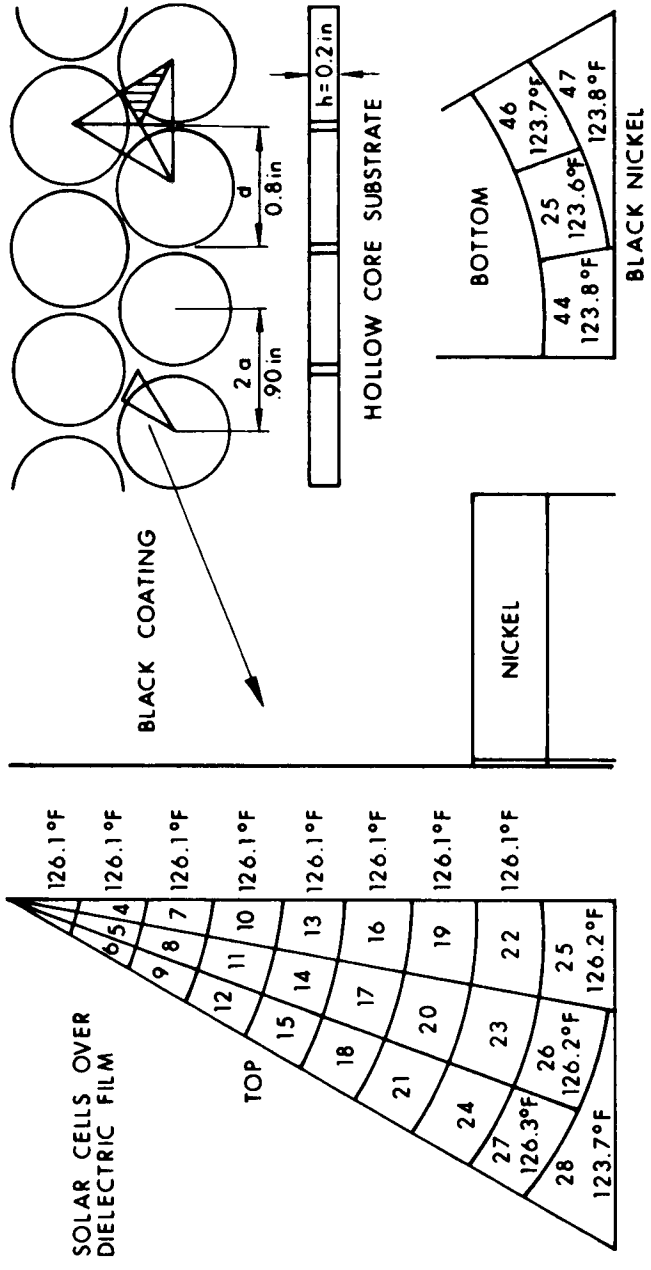
surface. Thermal radiation between members of the thermal substrate is significant only in designs where large temperature variations occur between the panel surfaces (an undesirable situation from the standpoint of solar cell efficiency). In the case of lightweight structures, the conductivity of the solar cells parallel to the panel surface may be a significant part of the thermal circuit.

The hollow core substrate structure under consideration represents a complex geometrical problem for the thermal analyst. As a result, a digital computer program, which takes into consideration both radiation and conduction heat transfer, has been used to compute the temperature distribution for the hollow core substrate. Through a study of the symmetry of the hexagonal hole pattern for the hollow core substrate, a triangular section (Fig. 7-4) was selected as representative of the structure for thermal analysis. The boundaries of this segment have no heat flow through them. This section can be divided into four distinct segments: (1) a pie-shaped dielectric skin with cells attached and an open back surface; (2) an irregularly shaped nickel segment of the front-cell surface which has a closed back; (3) a cylindrical nickel segment which forms part of the hole wall; and (4) a bottom segment of black-coated nickel which is shaped identical to the second item.

The thermal model described here was then subdivided into 47 nodal areas for the purposes of digital computation. The node-to-node conductances and the radiation coefficients were computed for input to the program, and matrix information was tabulated so that the computer could solve the 47 simultaneous algebraic equations by a numerical iteration process. The energy absorbed by the top surface of the panel was computed as heat sources for each of the nodes involved.

7.3.3 Characteristics of Hollow Core Structure

A detailed digital computer analysis of the hollow core structure has been completed. The example discussed here is for a 1-mil electroformed nickel substrate with 0.8-in. holes and a spacing



31	30	29
126.1°F	126.1°F	126.0°F
34	33	31
125.8°F	125.7°F	125.7°F
37	36	35
125.4°F	125.4°F	125.4°F
40	39	38
125.1°F	125.1°F	125.1°F
43	42	41
124.8°F	124.8°F	124.8°F

FIG. 7-4 TEMPERATURE DISTRIBUTION OF HOLLOW CORE SUBSTRATE

of 0.1-in. between holes ($d/a = 1.8$). The panel thickness was assumed as 0.2-in.; 4-mil cells with 2-mil filter covers were considered (each with a 1-mil dielectric skin between cells and substrate). This example is considered to be a conservative one, as the thermal resistances will be higher than, for example, substrates with heavier walls and smaller panel thicknesses.

The following assumptions concerning the surface properties of the completed panel were used in this analysis: Solar absorptivity of top surface, $\alpha_s = 0.8$; total thermal emissivity of top surface, $\epsilon_t = 0.8$; thermal emissivity of bottom surface, $\epsilon_b = 0.9$. (The power converted by the cells into electricity was neglected in this case.) Further, it was assumed that only the horizontal surfaces of the back surface were coated with black paint, leaving the sides of the cylindrical holes with a specularly reflective, natural finish.

The results of the analysis for earth-space solar radiation intensity, ($S = 444 \frac{\text{Btu}}{\text{hr ft}^2}$) show a maximum difference of 5.5°F between the hottest spot on the front surface and the coldest spot on the rear surface. The average effect on solar cell temperatures is to raise their temperatures less than 2°F compared with a perfectly conducting system.

The only apparent uncertainty in the analysis is the assumption that the cells effectively contributed to the transverse conduction of the assembly when they in fact are not joined in a continuous sheet. An examination of the data shows that this might influence the temperatures in a relatively small region where the hollow core structure shields the back of the cell top surface. Assuming that the silicon did not contribute at all to the conduction increases the predicted temperature of the hottest spot by approximately 2°F .

It appears from this analysis that the hollow core structure, when used as the open structure under consideration here, has excellent thermal characteristics from the standpoint of solar cell efficiency. A lightweight structure of this type would be very easily influenced by transient changes in the thermal environment. However,

since it is a good conducting system internally there should be no difficulty with thermal stresses due to temperature gradients within the substrate. Differential expansions or contractions between materials with differing properties or between the panel and its frame are a potential source of concern. These will be examined later for a particular case.

7.3.4 Thermal Coatings

The primary function of the filter, or cover glass, conventionally applied to the top of a silicon solar cell is to increase the thermal emissivity of the topside of the solar panel without appreciably decreasing the transmission of energy at useful wavelengths. In a lightweight panel the cover glass may be a significant contributor to the panel weight if used in normal thicknesses. However, a coating of SiO less than 2 mils thick will double the emissivity of a bare cell (from 0.35 to 0.70), and a thin cover glass (0.002 in.) can be expected to produce an emissivity of at least 0.8. The use of blue and infrared reflective coatings can also reduce cell temperatures by lowering the amount of energy absorbed at wavelengths which cannot be converted to electric power by the cells.

A black paint coating will be used on the back side of the solar panel to maximize the emissivity of that surface and minimize the solar cell temperatures. Several durable, stable, and space-proved black coatings (such as Laminar X-500) are available. Most appear to require a minimum thickness of approximately 2 mils to obtain a full value of their thermal emissivity, which will vary between 0.85 and 0.95 for the temperature in an earth-space environment. The emissivity value obtained will depend upon the brand, the batch, and the application process. An examination of the thermal circuit of the hollow core structure reveals that there is a slight advantage in not coating the walls of the cylindrical holes on the bottom of the panel. Although the effect is not important for cylinders with a large d/a ratio, reflective walls allow the end of the cylinder (the coated back of the

dielectric skin) to radiate to space with geometric view factor of 1.0. If the walls of the cylinder are black, additional conduction must take place before all of the heat is radiated.

7.4 Solar Array Characteristics as a Function of Mission Trajectory

Assuming that a solar cell output of 10 W/ft^2 is desired (at 55°C and 1 AU) to a cell efficiency (at air mass zero and 28°C) of 9.5 percent (active area efficiency of 10 percent). This efficiency includes cover glass losses (0.94 loss factor) and fabrication/mismatch losses (0.965 loss factor). It also includes an approximate temperature coefficient of power of 0.4 percent per degree Celsius.

Figure 7-5 shows the characteristic curve for a 10.6 percent efficient 2-cm-square solar cell with a resistivity of 5 to 10 ohms/cm. This curve has been incorporated into a computer program to calculate a total array output at sun-probe distances bearing 0.6 to 5.2 AU. Figures 7-6 through 7-15 give E/I characteristics and the P/E characteristics for a 10.4 kW solar array operating from 0.6 to 5.2 AU. In most cases where the array is either close to or far from the sun, (i.e., not in near-earth space), the shape of the E/I and P/E curves at the higher voltages appears to be distorted. This is due to the manner in which the curves are obtained by linear extrapolation of the current and voltage axes as a function of the temperature intensity at which the array is operating. Very little data is presently available in the quadrants which the axes must be extrapolated to expand or decrease the solar cell characteristic curves. An important result of this analysis is the requirement for data to be taken on the operation of solar cells in the second and fourth quadrant in order to expand the E/I curves beyond the short-circuit current and open-circuit voltage point into the negative-voltage and negative-current regions. This will enable the computer to extrapolate using known data points to the new operating conditions without obtaining apparently distorted characteristic curves.

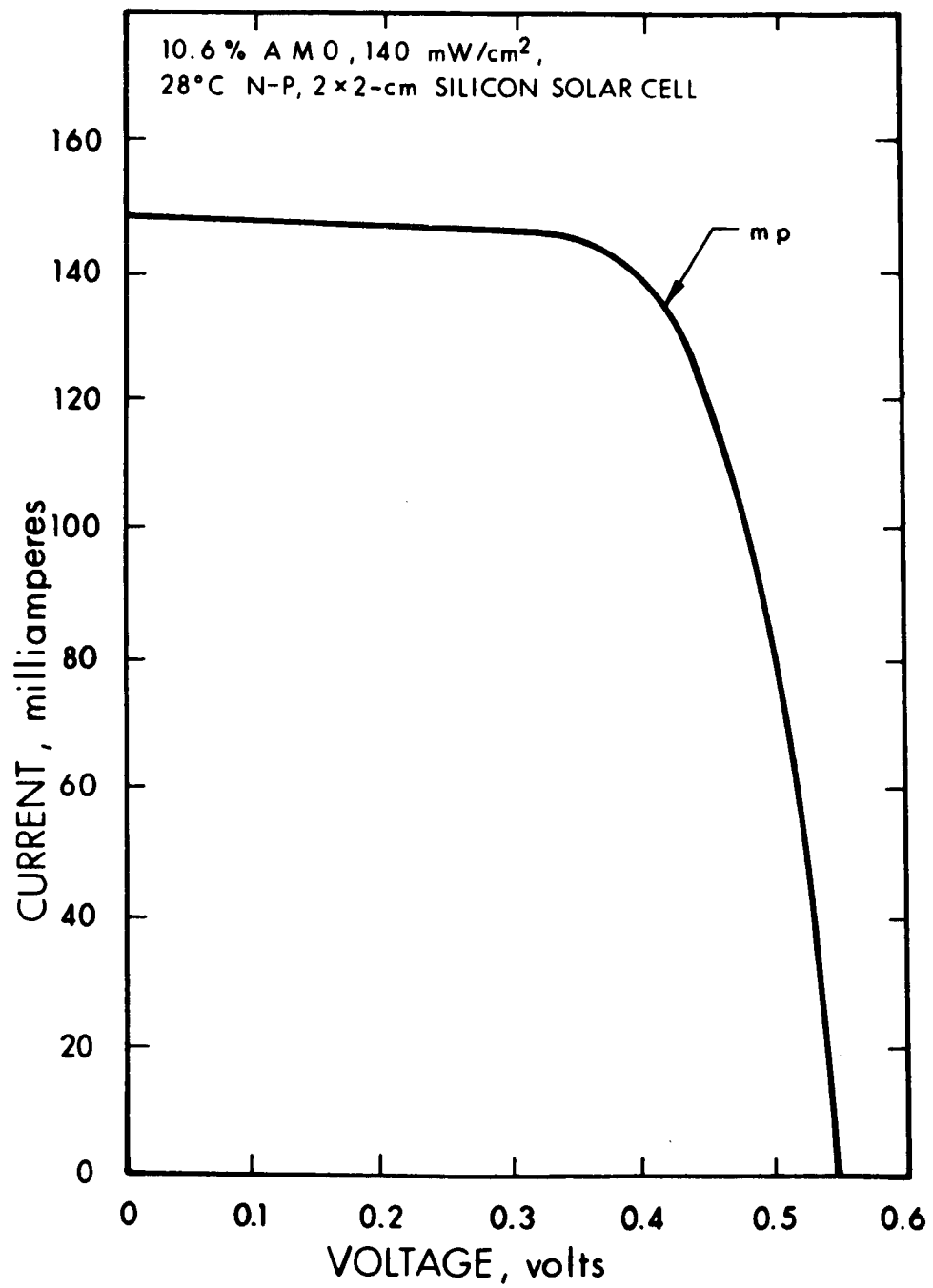


FIG. 7-5 CHARACTERISTIC E/I CURVE FOR SILICON SOLAR CELL

TEMP. (DEG. C) 55.00
JNT. (MW/STRIK) 140.00

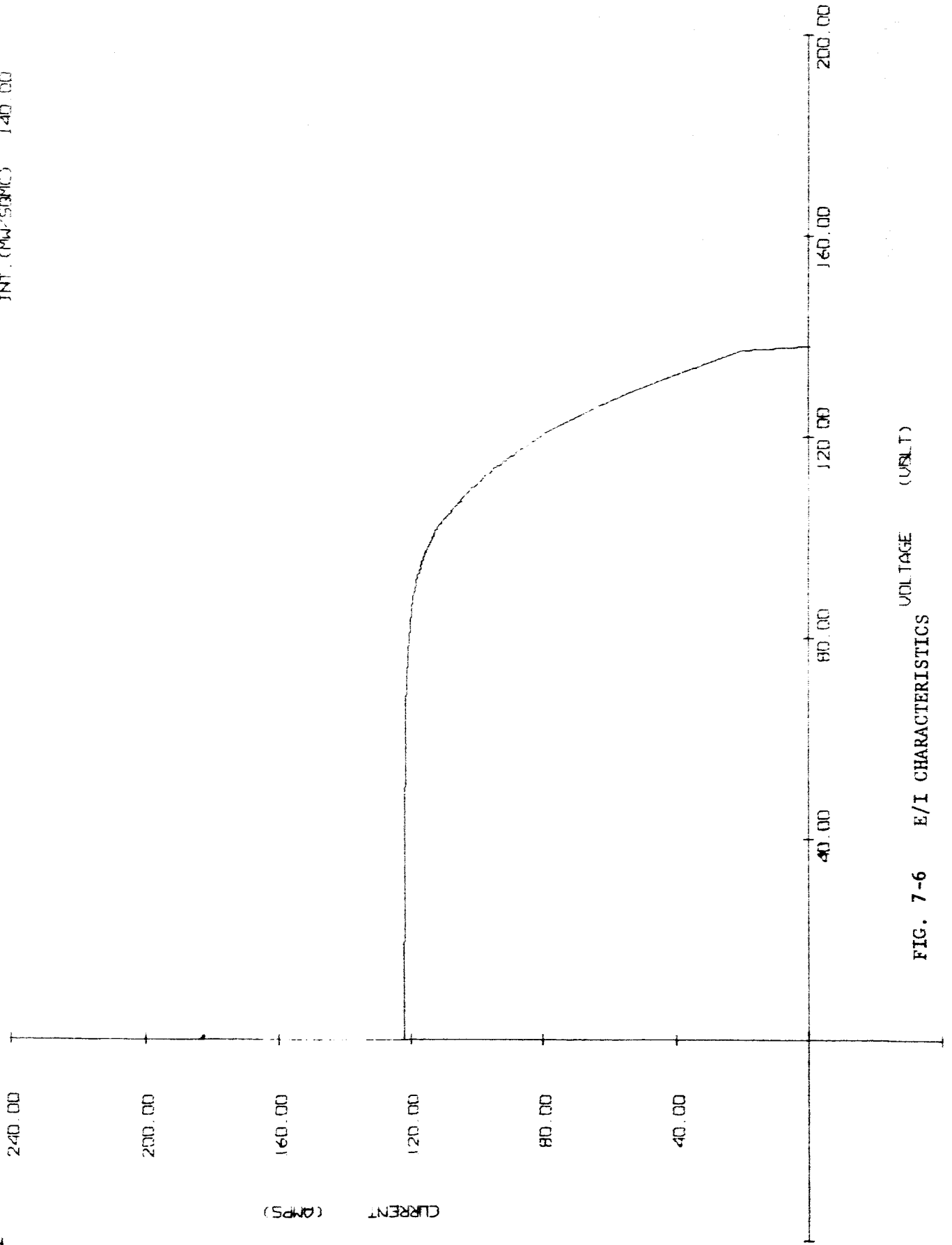


FIG. 7-6 E/I CHARACTERISTICS VOLTAGE (VSLT)

PL01 02

7027-IDR

7-21a

TEMP. (DEG. C) 55.00
JNT. (MW/50MC) 140.00

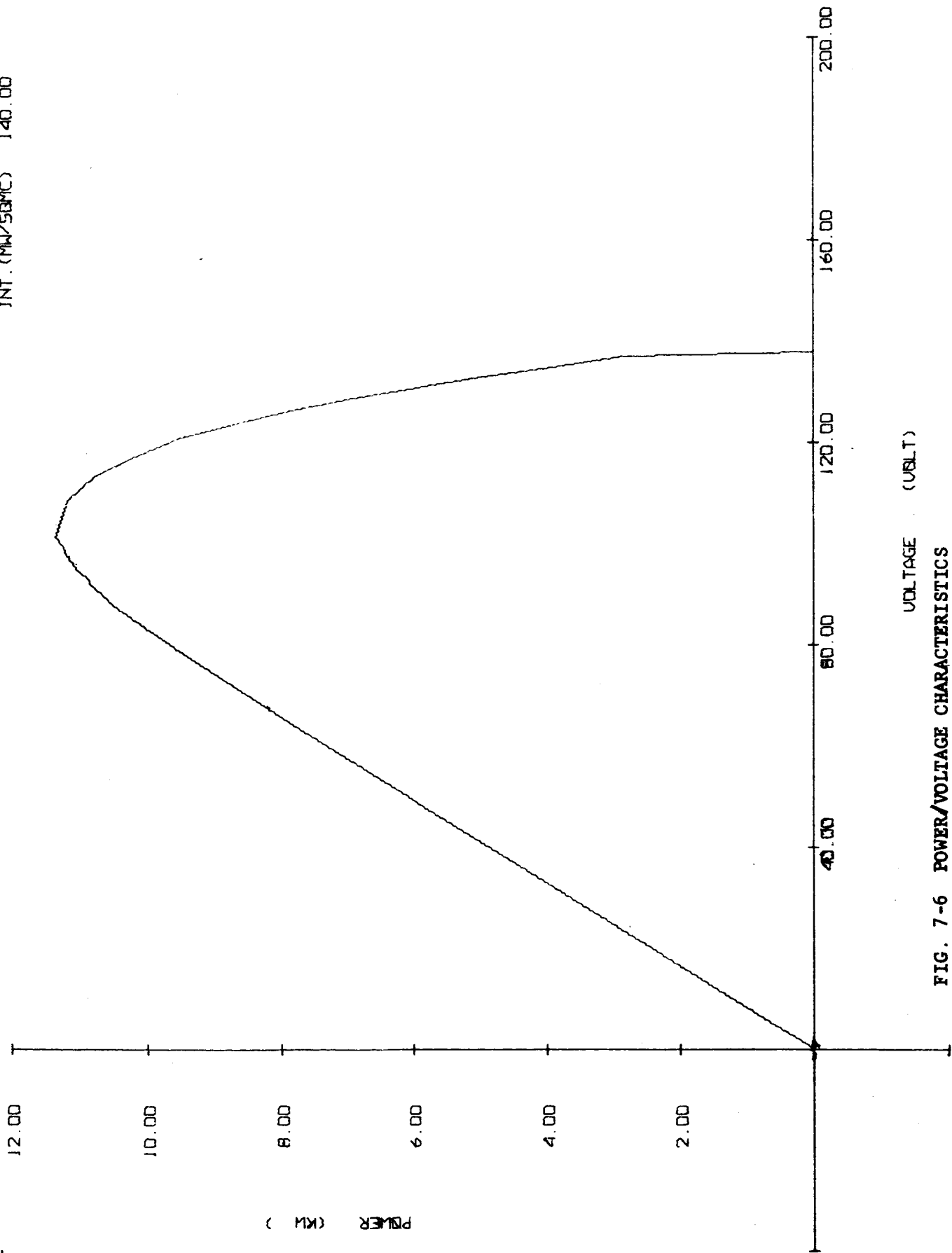


FIG. 7-6 POWER/VOLTAGE CHARACTERISTICS

BLANK PAGE 7-22

PL01 04

7027-IDR

7-23a

TEMP. (DEG C) 110.00
INT. (MM/50MC) 269.00

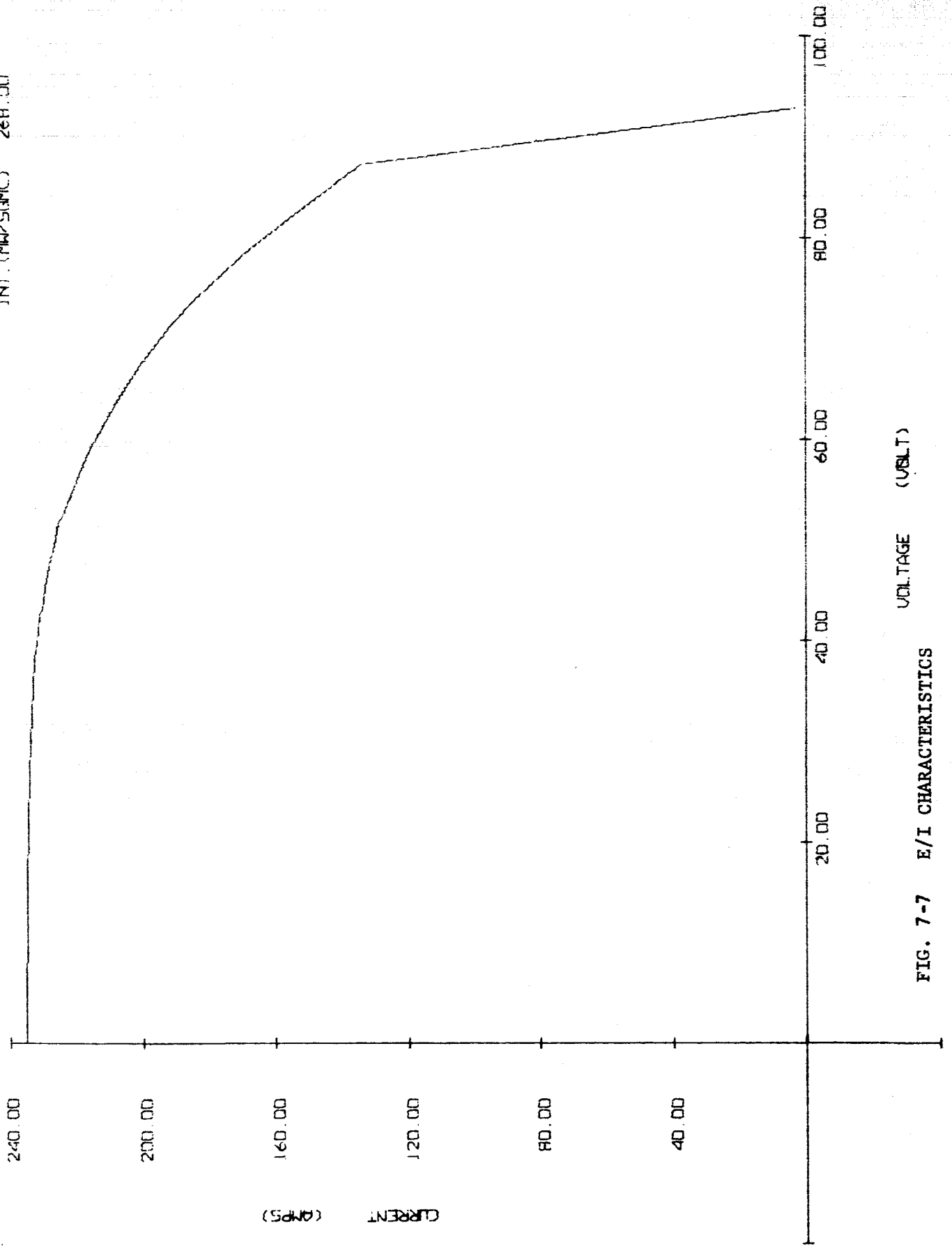


FIG. 7-7 E/I CHARACTERISTICS

VOLTAGE (VOLT)

CURRENT (AMPS)

TEMP. (DEG. C) 110.00
INT. (MW/SQCM) 268.00

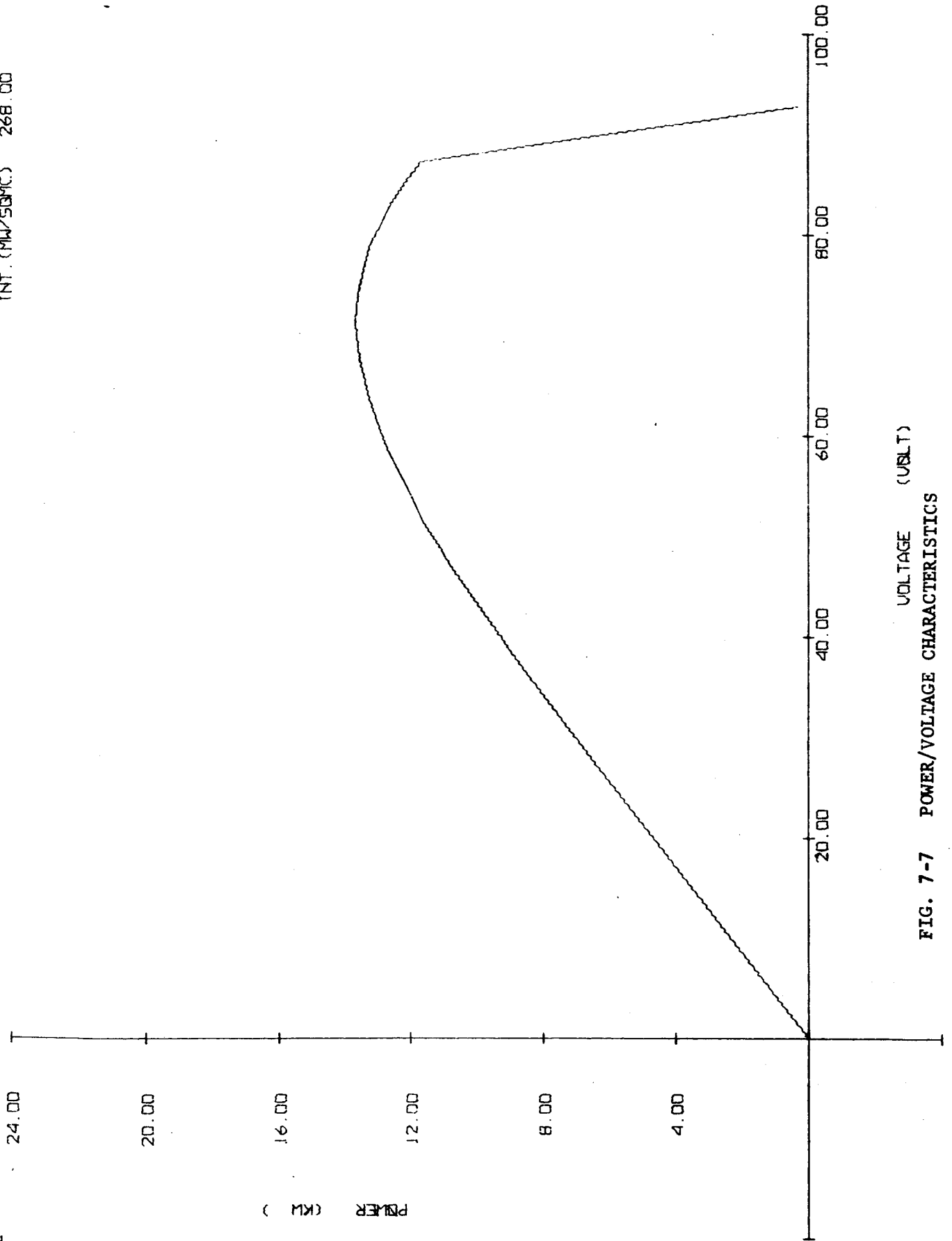
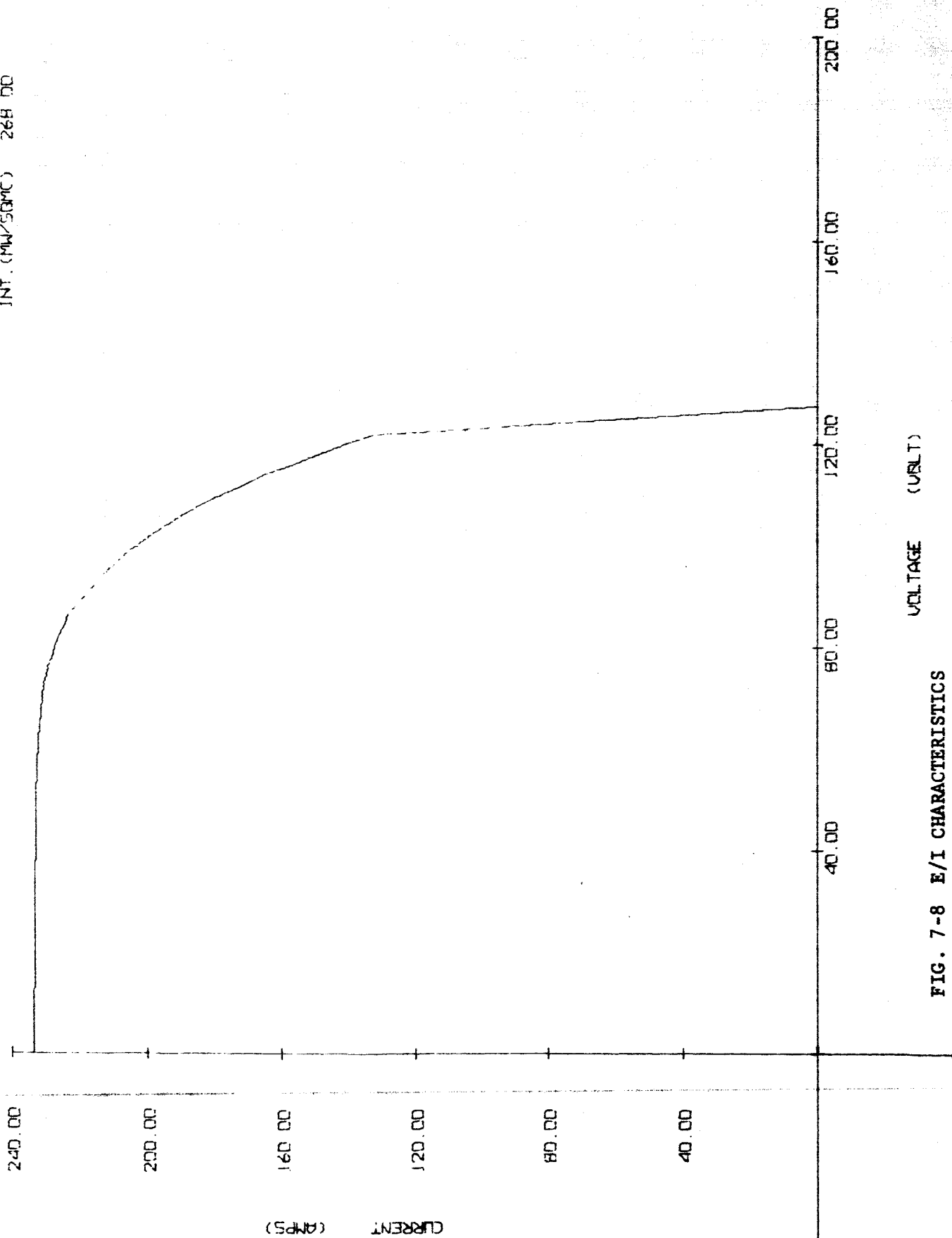


FIG. 7-7 POWER/VOLTAGE CHARACTERISTICS

7-
BLANK PAGE 24

TEMP. (DEG. C) : 55.00
JNT. (MM/50MC) : 268.00



PLT 06

7027-IDR

7-25a

VOLTAGE (VOLT)

FIG. 7-8 E/I CHARACTERISTICS

TEMP. (DEG. C) 55.00
INT. (MW/50MIC) 268.00

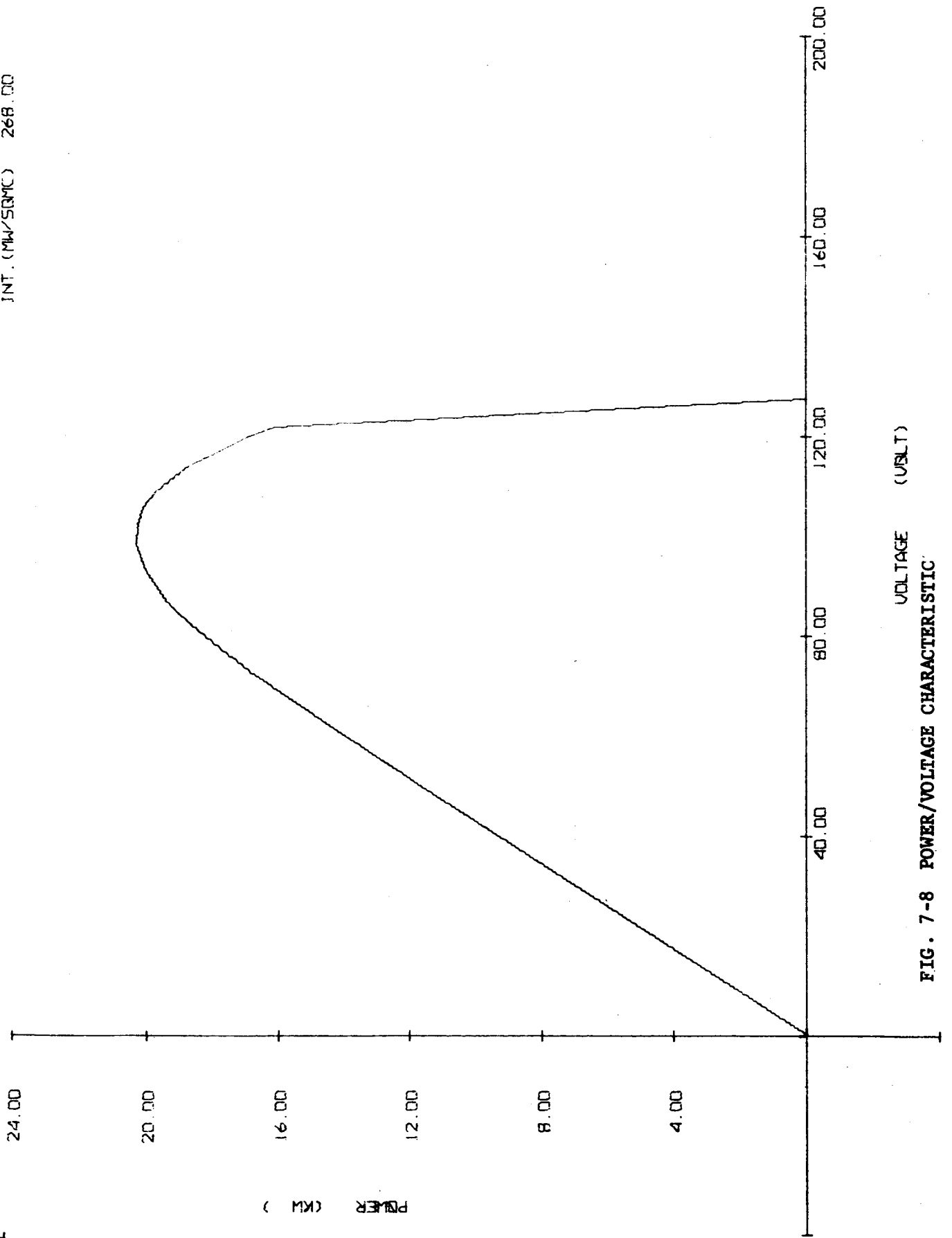


FIG. 7-8 POWER/VOLTAGE CHARACTERISTIC

BLANK PAGE

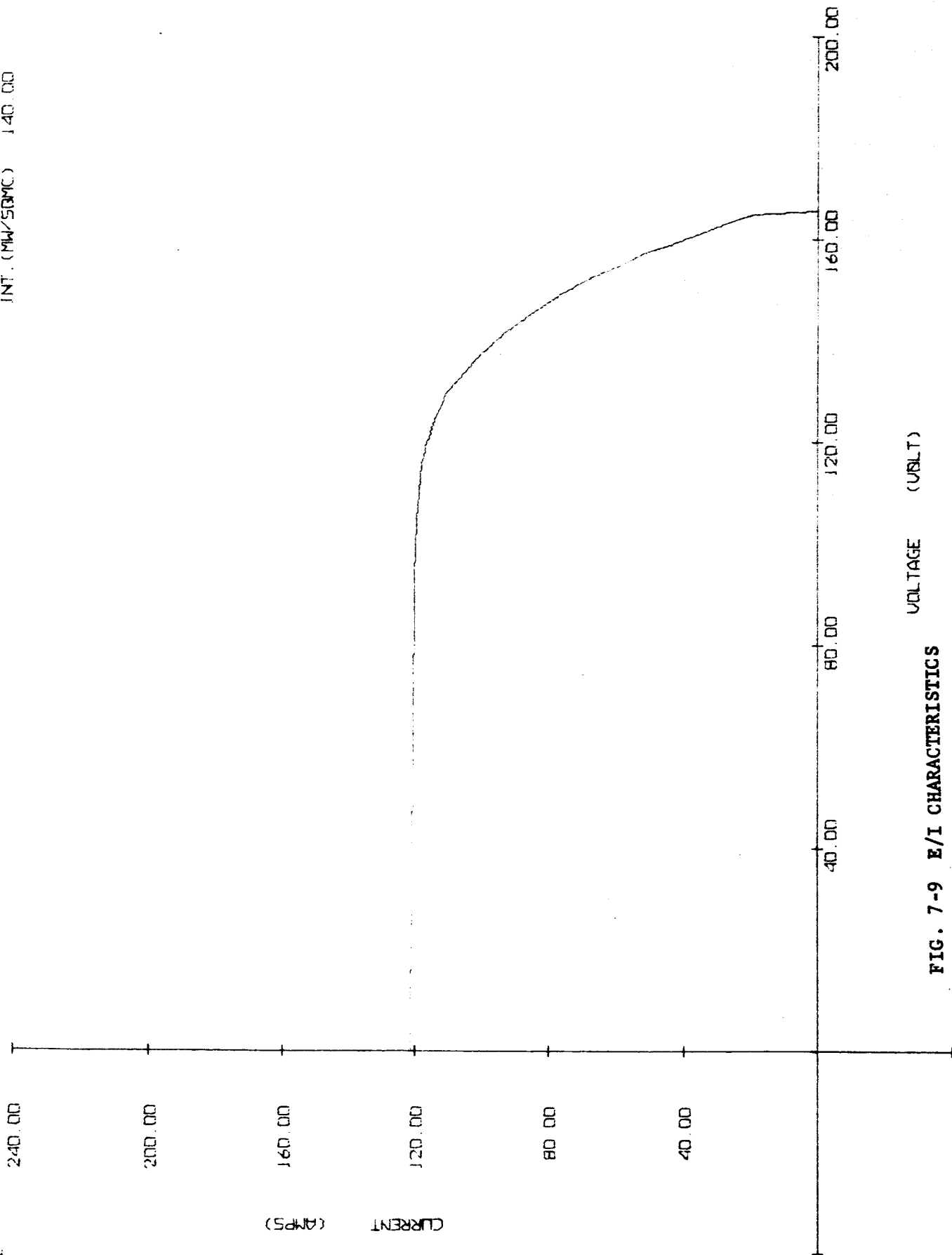
7-26

PLT 08

7027-IDR

7-27a

TEMP. (DEG. C) 6.00
INT. (MW/50MC) 140.00



VOLTAGE (VBLT)

FIG. 7-9 E/I CHARACTERISTICS

TEMP. (DEG. C) 6.00
INT. (MW/50MC) 140.00

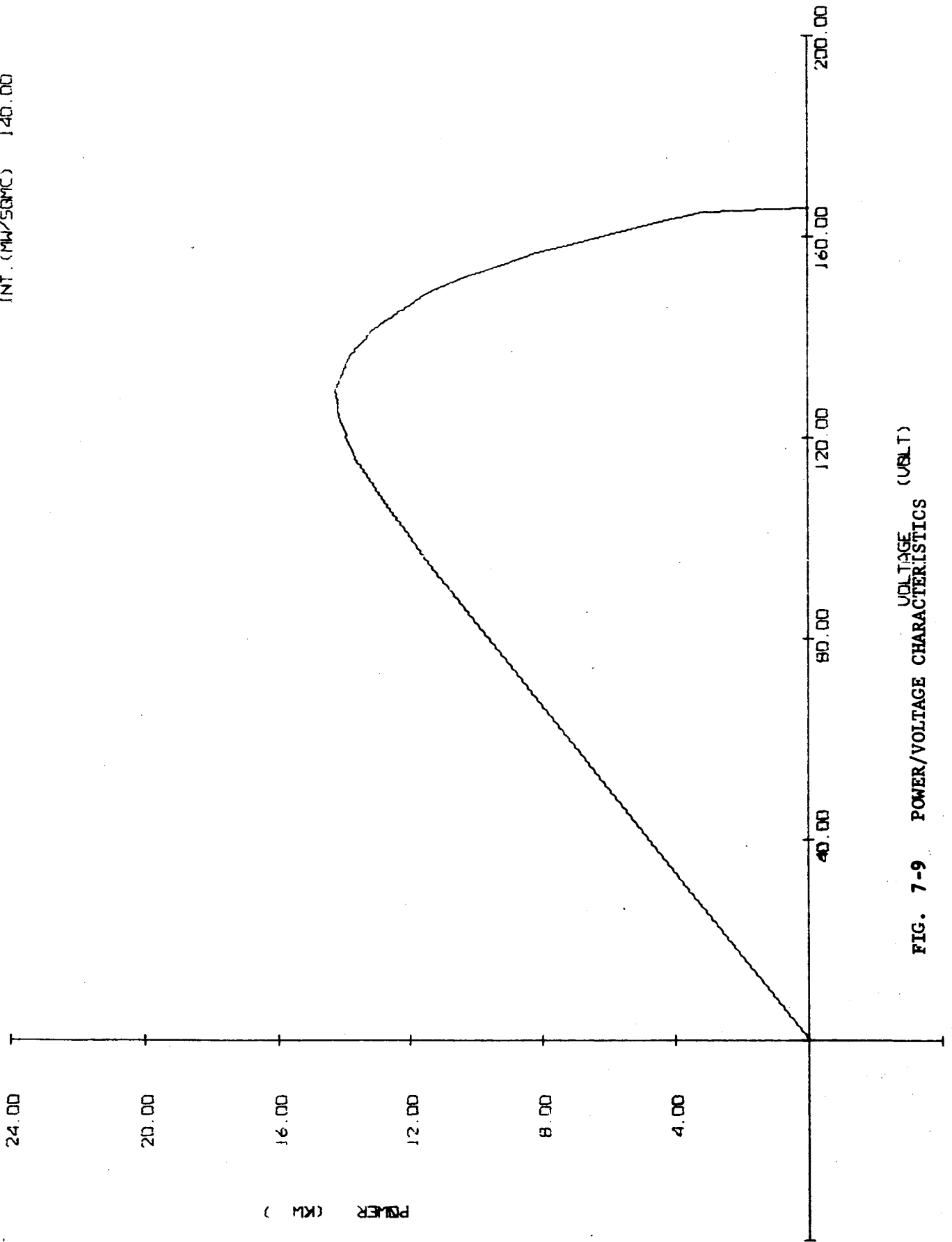


FIG. 7-9 POWER/VOLTAGE CHARACTERISTICS (VBLT)

BLANK PAGE 28

PLT 10

7027-IDR

7-29a

TEMP. (DEG. C) - 55.00
JNT. (MW/50MC) 22.00

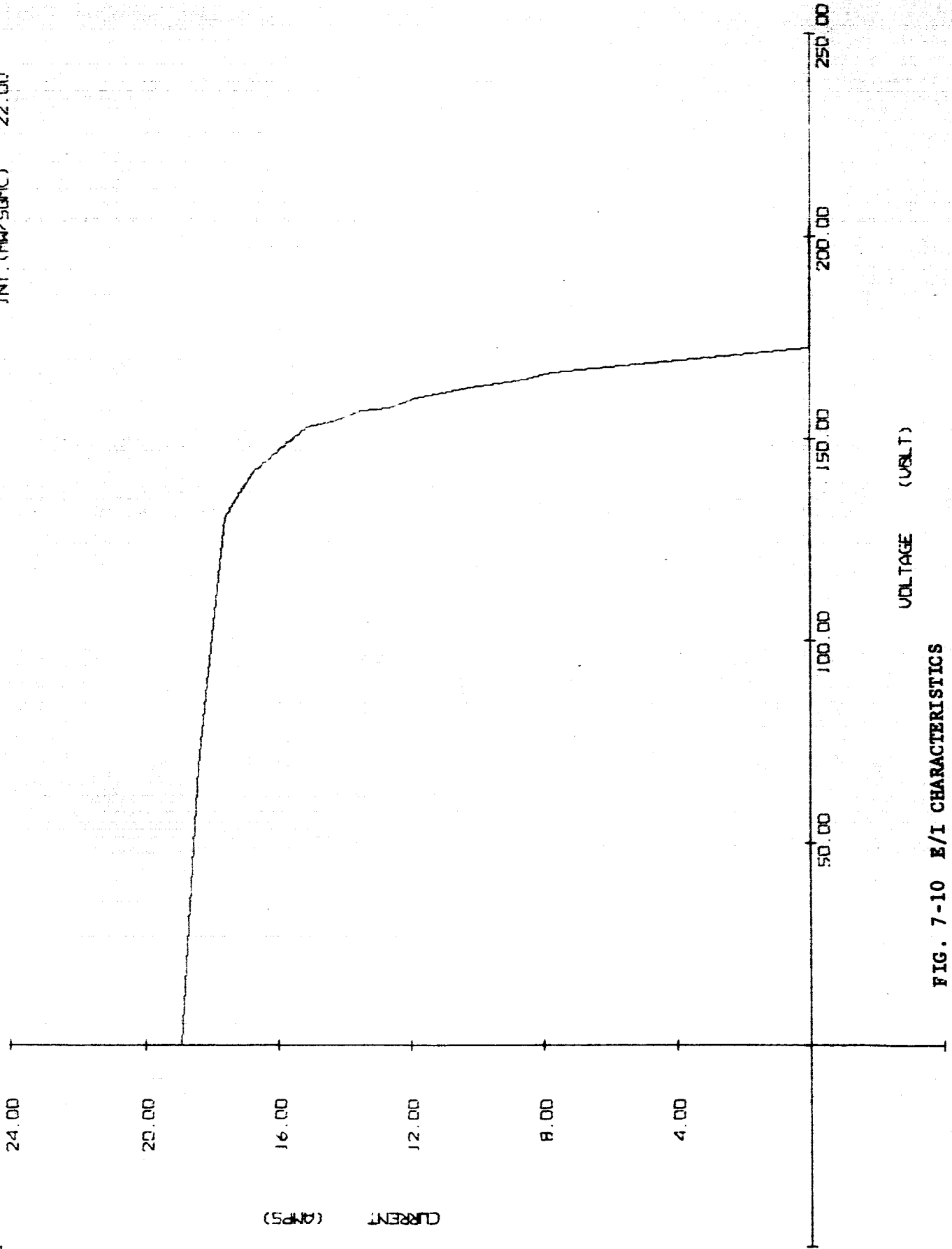


FIG. 7-10 E/I CHARACTERISTICS

PLNT 09

7027-IDR

7-29

TEMP. (DEG. C) - 55.00
INT. (MW/50MC) 22.00

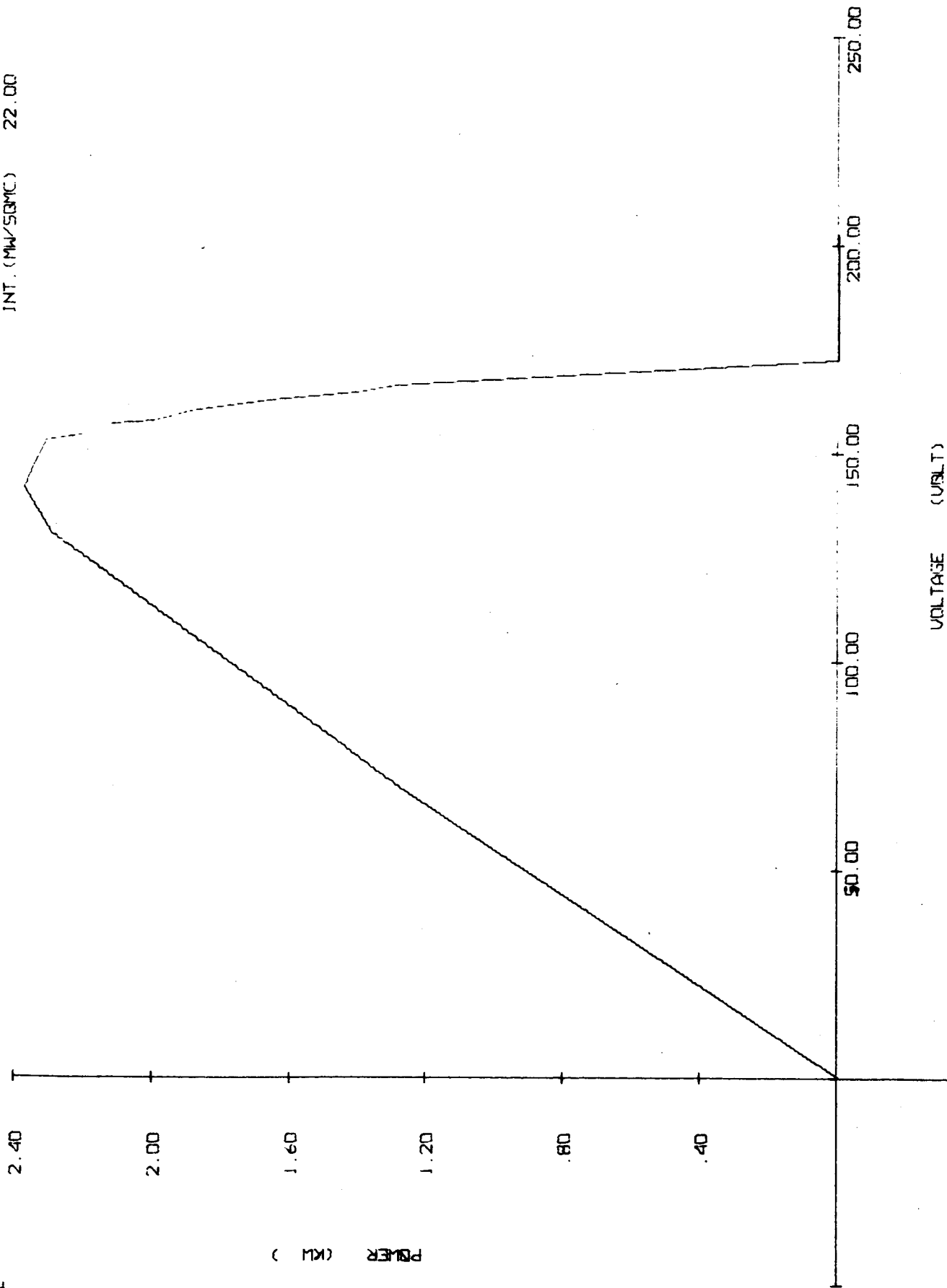
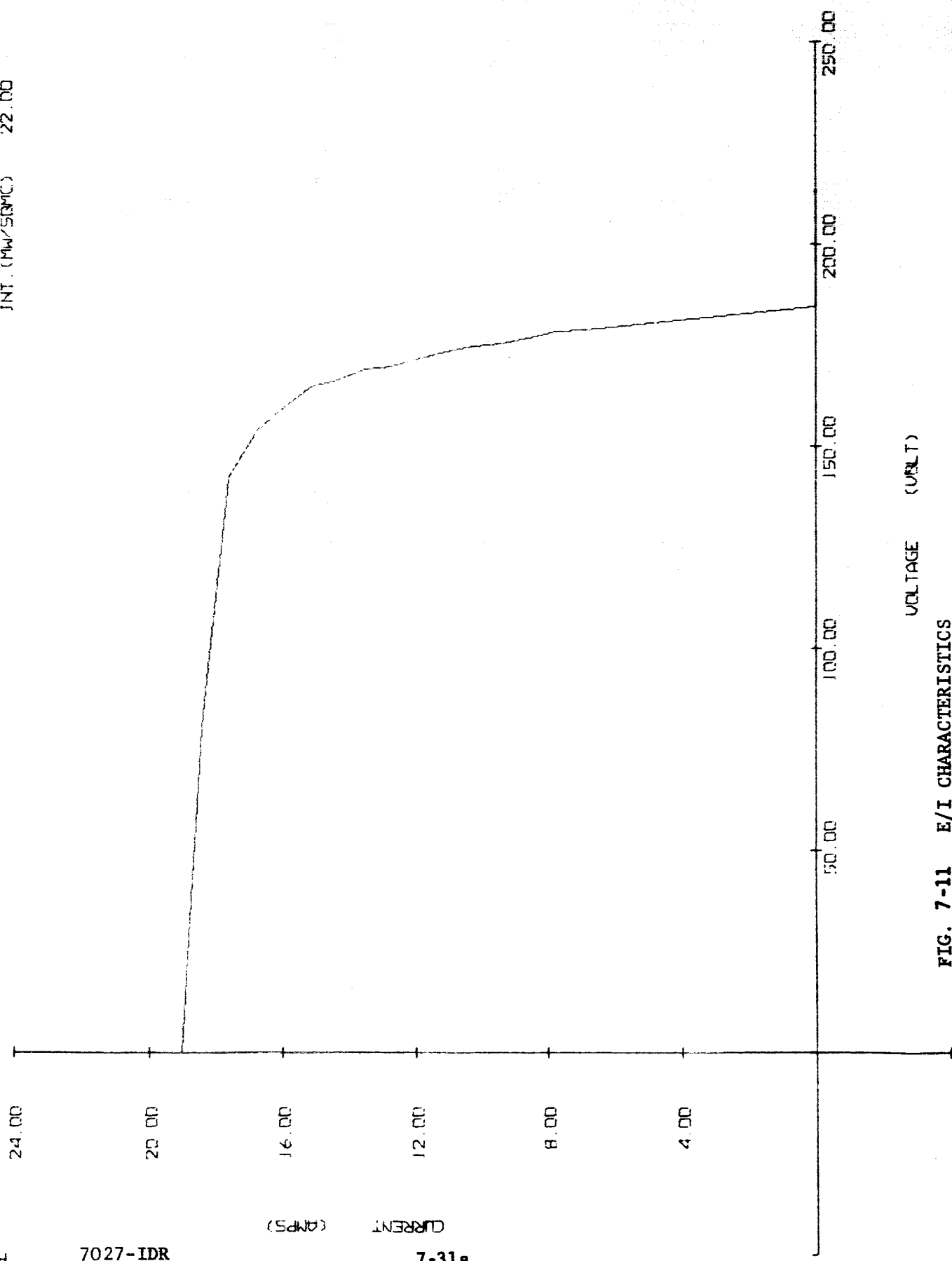


FIG. 7-10 POWER/VOLTAGE CHARACTERISTICS

TEMP. (DEG. C) - 86.00
JNT. (MW/50MC) 22.00



PLOT 12

7027-IDR

7-31a

FIG. 7-11 E/I CHARACTERISTICS

TEMP. (DEG. C) - 86.00
INT. (MW/50MC) 22.00

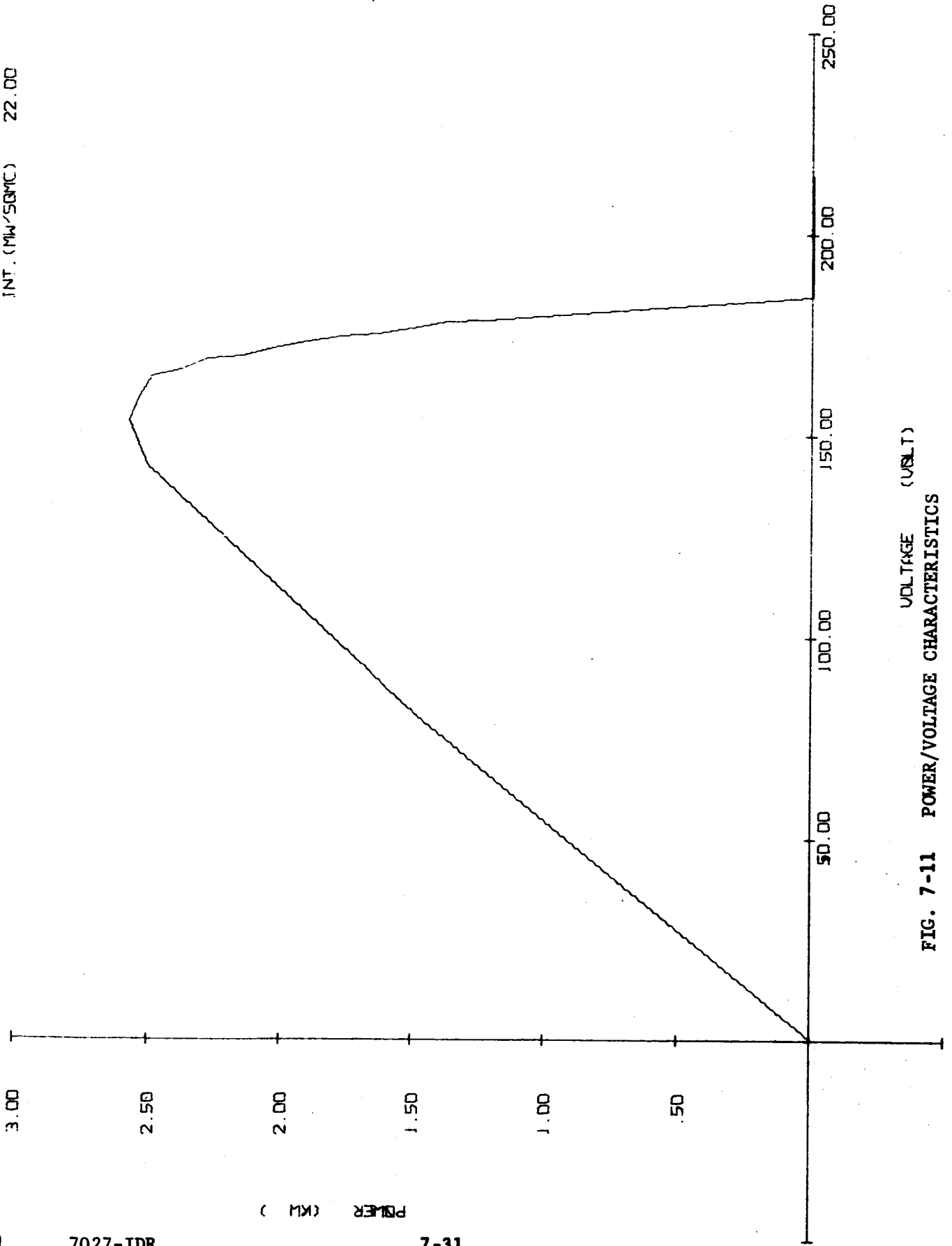


FIG. 7-11 POWER/VOLTAGE CHARACTERISTICS

TEMP. (DEG. C) - 86.00
INT. (MW/SBMC) 5.00

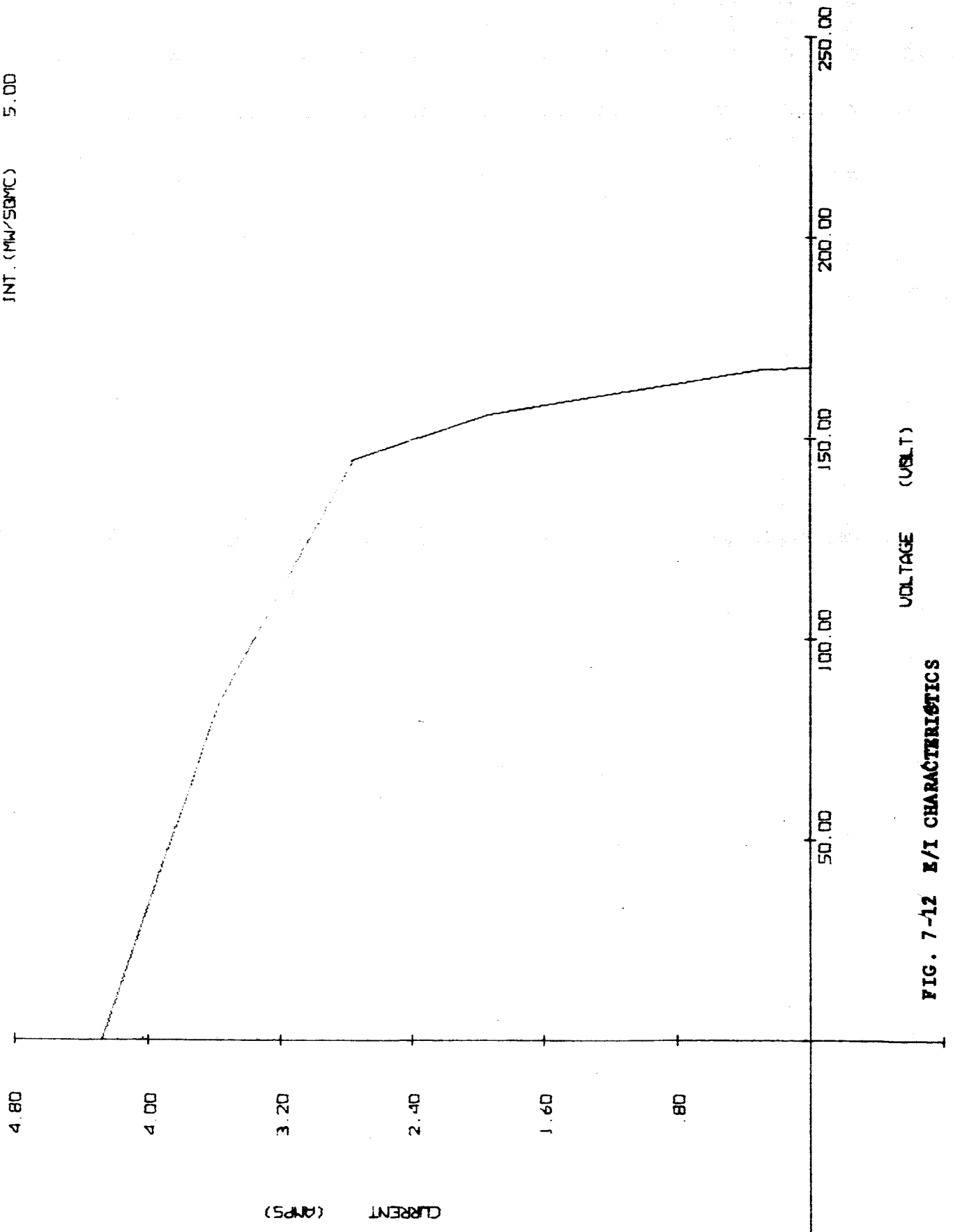


FIG. 7-12 E/I CHARACTERISTICS

TEMP. (DEG. C) = 86.00
INT. (MW/SQCM) = 5.00

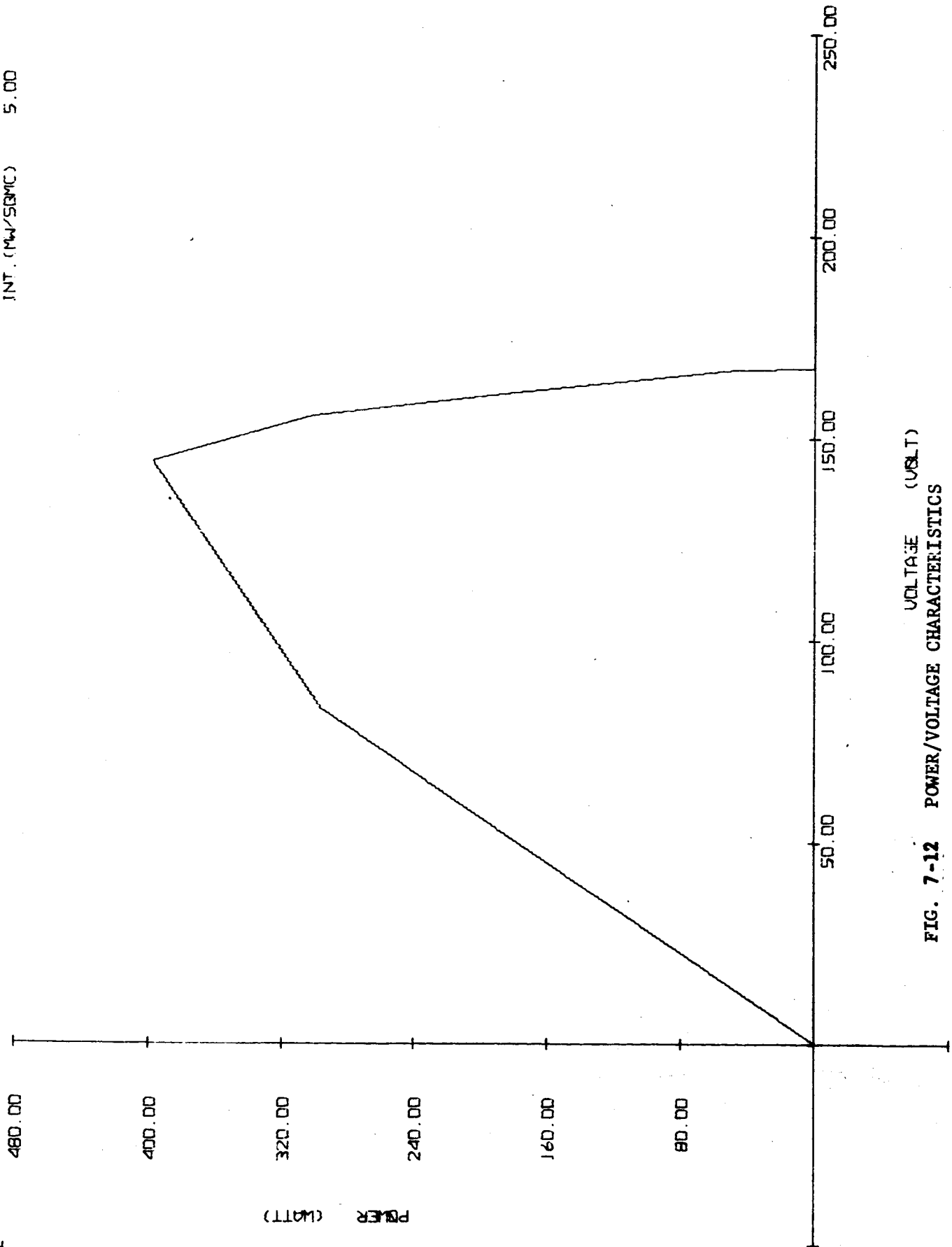


FIG. 7-12 POWER/VOLTAGE CHARACTERISTICS

BLANK PAGE 34

TEMP. (DEG. C) - 135.00
INT. (MW/SQCM) 5.00

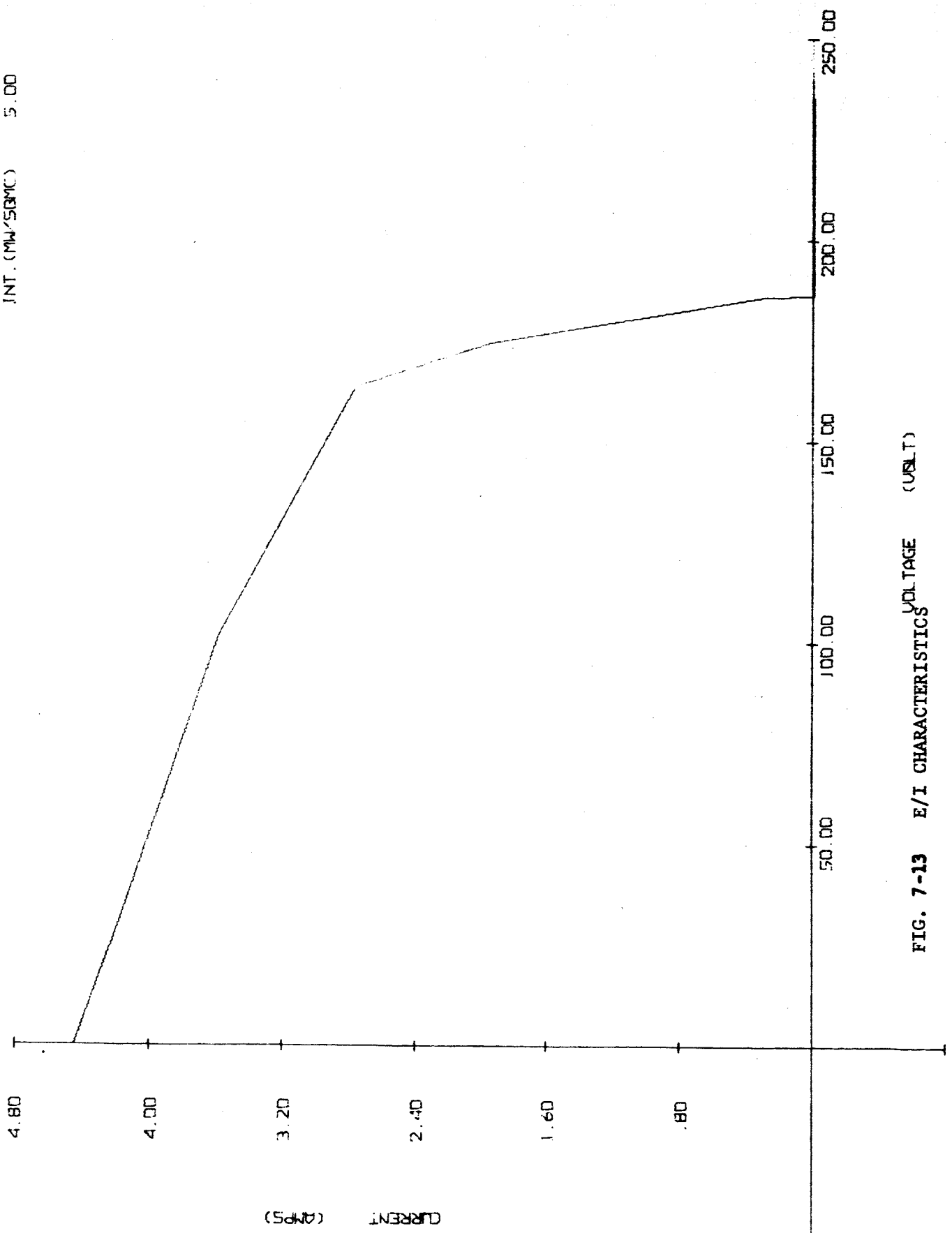


FIG. 7-13 E/I CHARACTERISTICS (USLT)

TEMP. (DEG. C) - 135.00
INT. (MW/SQCM) 5.00

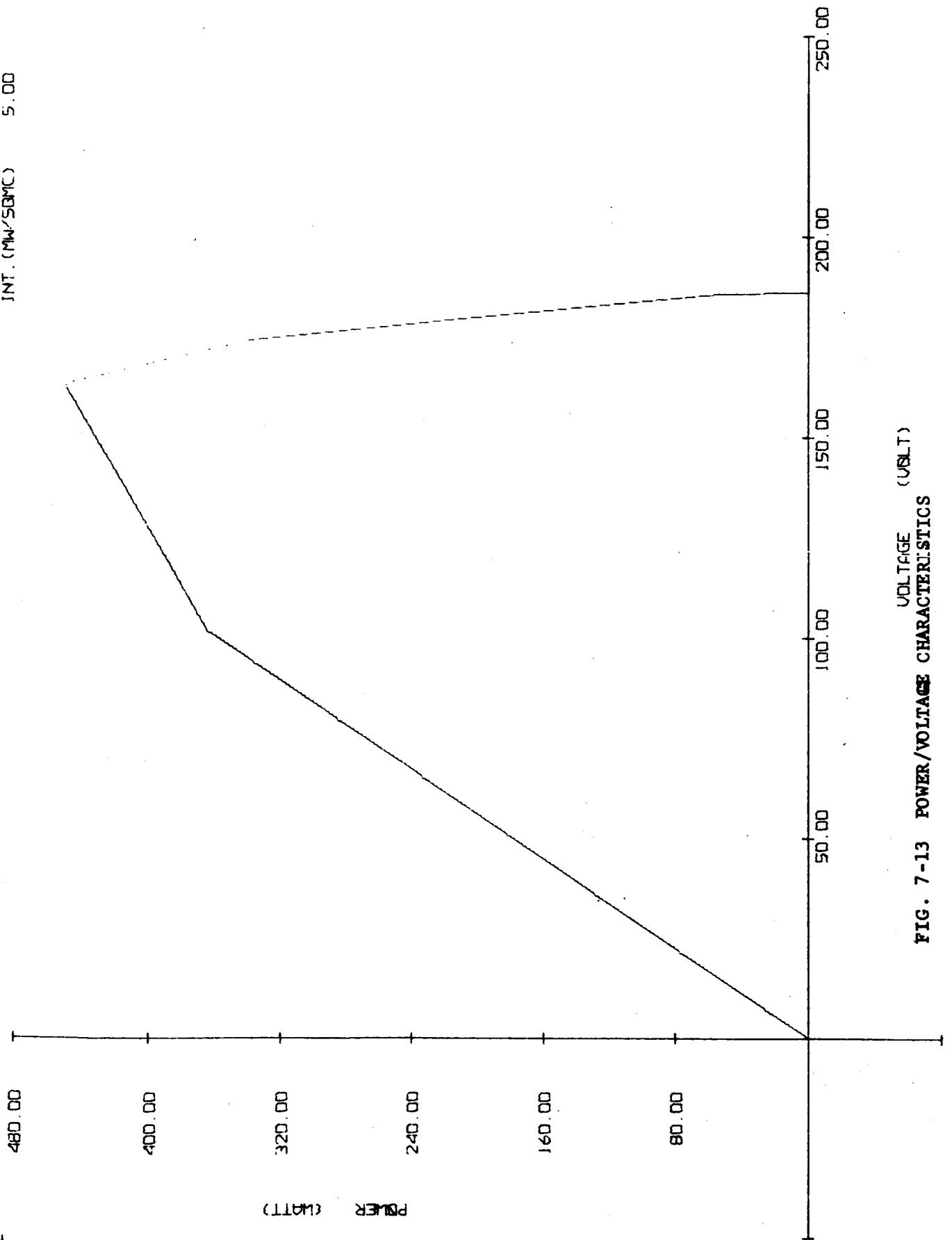


FIG. 7-13 POWER/VOLTAGE CHARACTERISTICS

BLANK PAGE 7-36

TEMP. (DEG. C) 145.00
INT. (MW/SQCM) 389.00

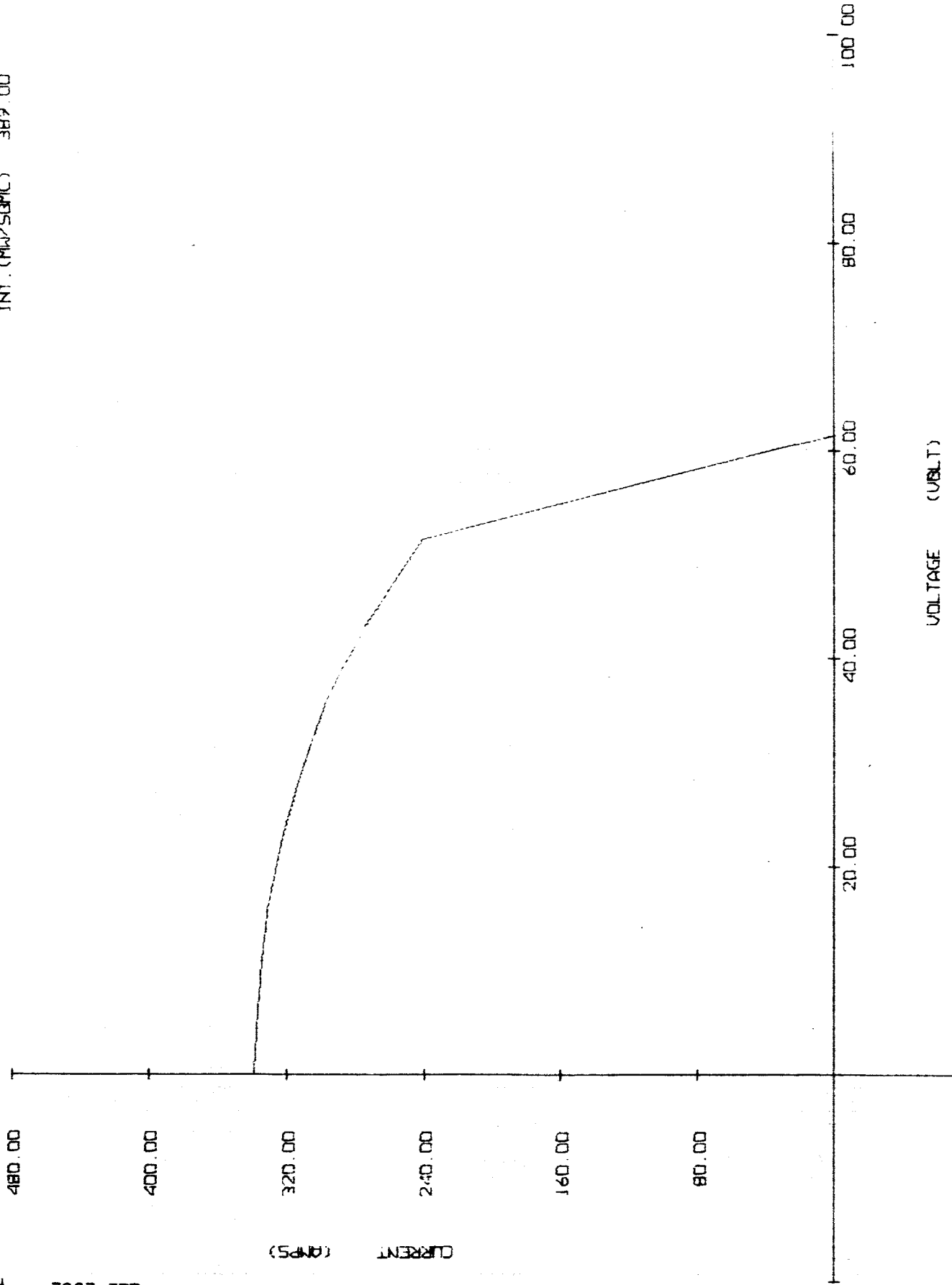
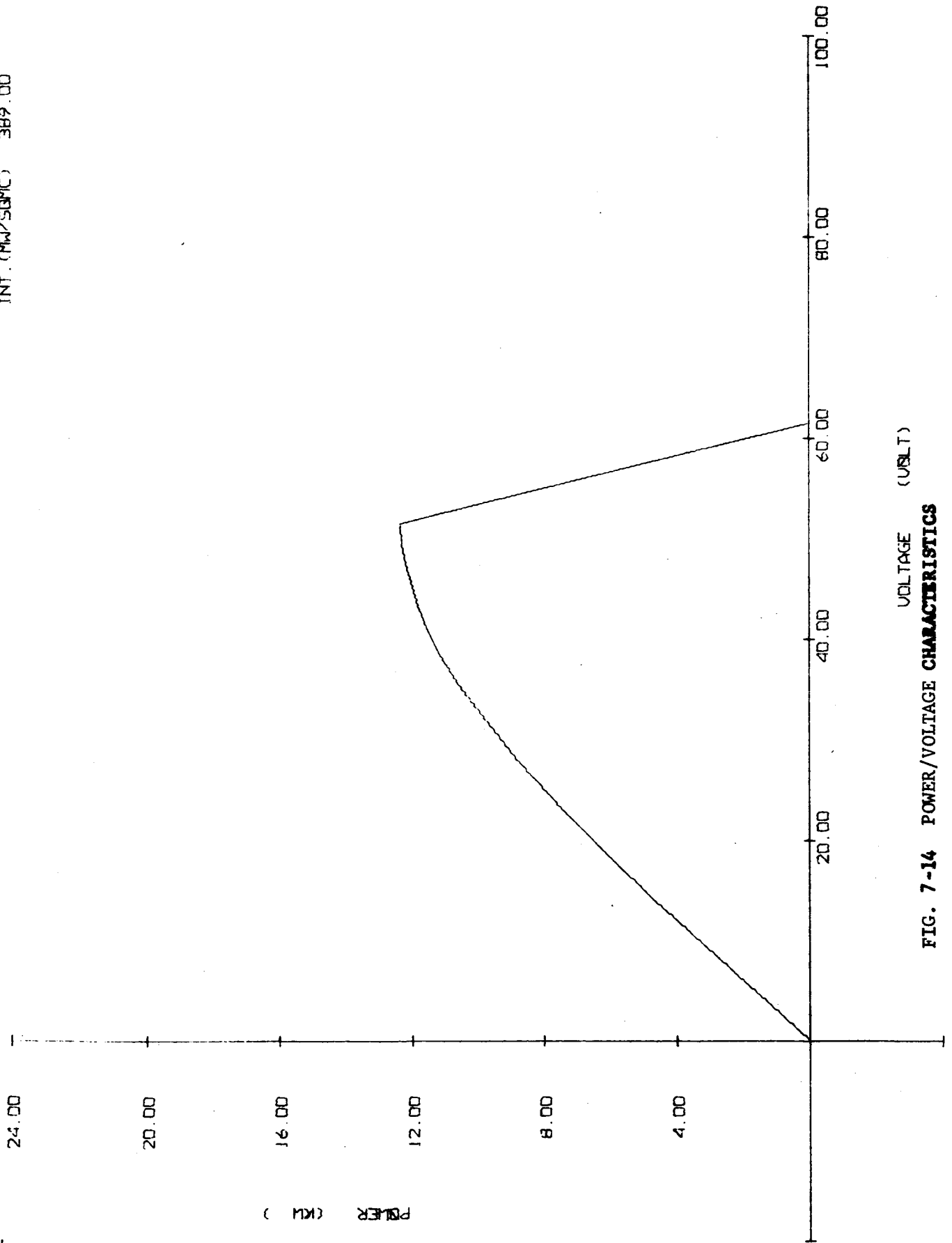


FIG. 7-14 E/I CHARACTERISTICS

TEMP. (DEG. C) 145.00
INT. (MW/50MC) 389.00

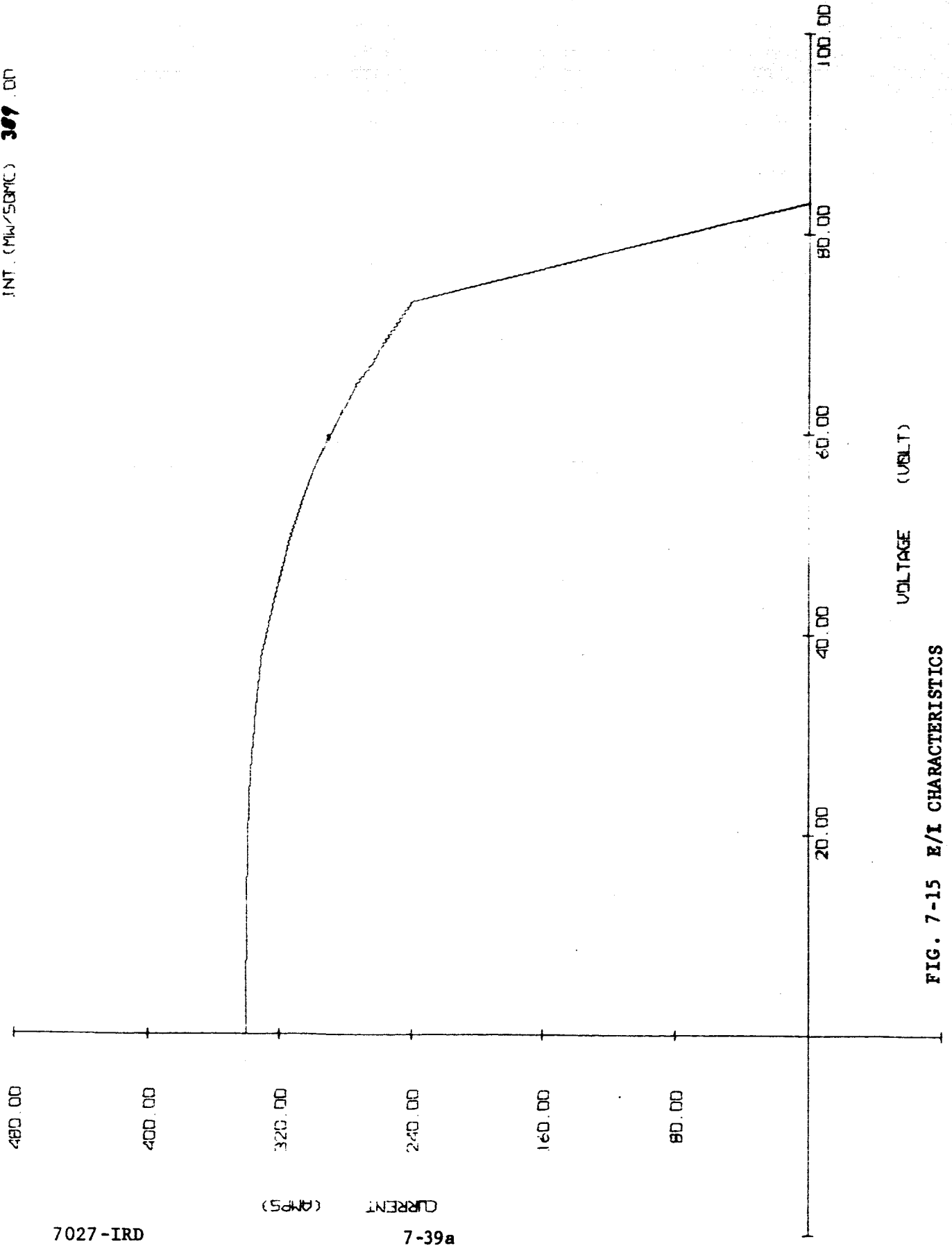


VOLTAGE (VOLT)

FIG. 7-14 POWER/VOLTAGE CHARACTERISTICS

BLANK PAGE 7-38

TEMP. (DEG. C) 110.00
INT. (MIN/SEC) 309.00



7027-IRD

7-39a

FIG. 7-15 E/I CHARACTERISTICS

TEMP. (DEG. C) 110.00
INT. (MW/SBMC) 309.00

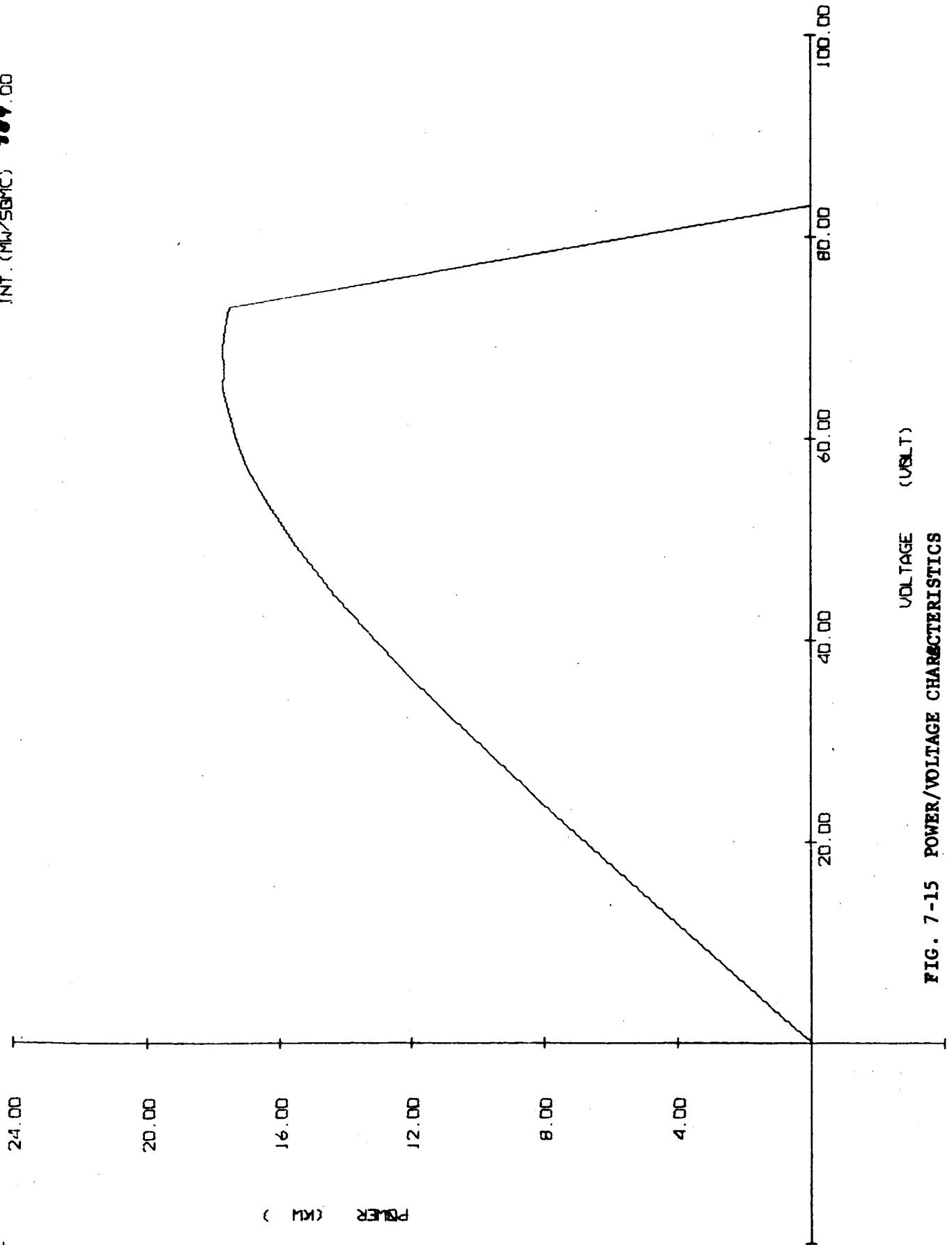


FIG. 7-15 POWER/VOLTAGE CHARACTERISTICS

BLANK PAGE

7-
40

7.5 Solar-Electric Propulsion Power Conditioning

Figure 7-16 is a nominal power-versus-voltage characteristic curve for the 10-kW Jupiter flyby solar array. This figure and the previous E/I curves illustrate the severe electrical mating problems involved in solar-electric propulsion. In order to define the power conditioning and control subsystem mating requirements (and thus the design approach), the solar-electric propulsion system operational modes must first be defined.

7.5.1 System Operational Modes

The thrust profile that can be followed over the trajectory may be either one that varies with the power actually available (thus being somewhat unpredictable and possibly requiring one or more impulsive midcourse corrections), or one that is preprogrammed as a function of available power to eliminate the need for impulsive corrections.

In the case of preprogrammed thrust, several thrust profiles can be considered. Under most operating conditions, the mass flow and specific impulse can be varied in the thruster to produce the programmed thrust value employing the full available power rather than the predicted value. However, the relationship

$$46 \quad \eta P = F I_{sp} \quad (1)$$

shows that if the I_{sp} is near a value for which the efficiency varies linearly with I_{sp} it will not be possible to maintain the required thrust when P changes. Such a lack of controllability is exhibited at an I_{sp} of about 4000 sec for the contact ion engine, 3000 sec for the Cs bombardment engine and 2000 sec for the Li-H arc jet. Operation on programmed thrust should be carried out with I_{sp} values at least 1000 sec above these values, or else the power profile should also be programmed at a conservative value throughout the thrusting phase. Figure 7-17 illustrates some of the choices of thrust and power profiles.

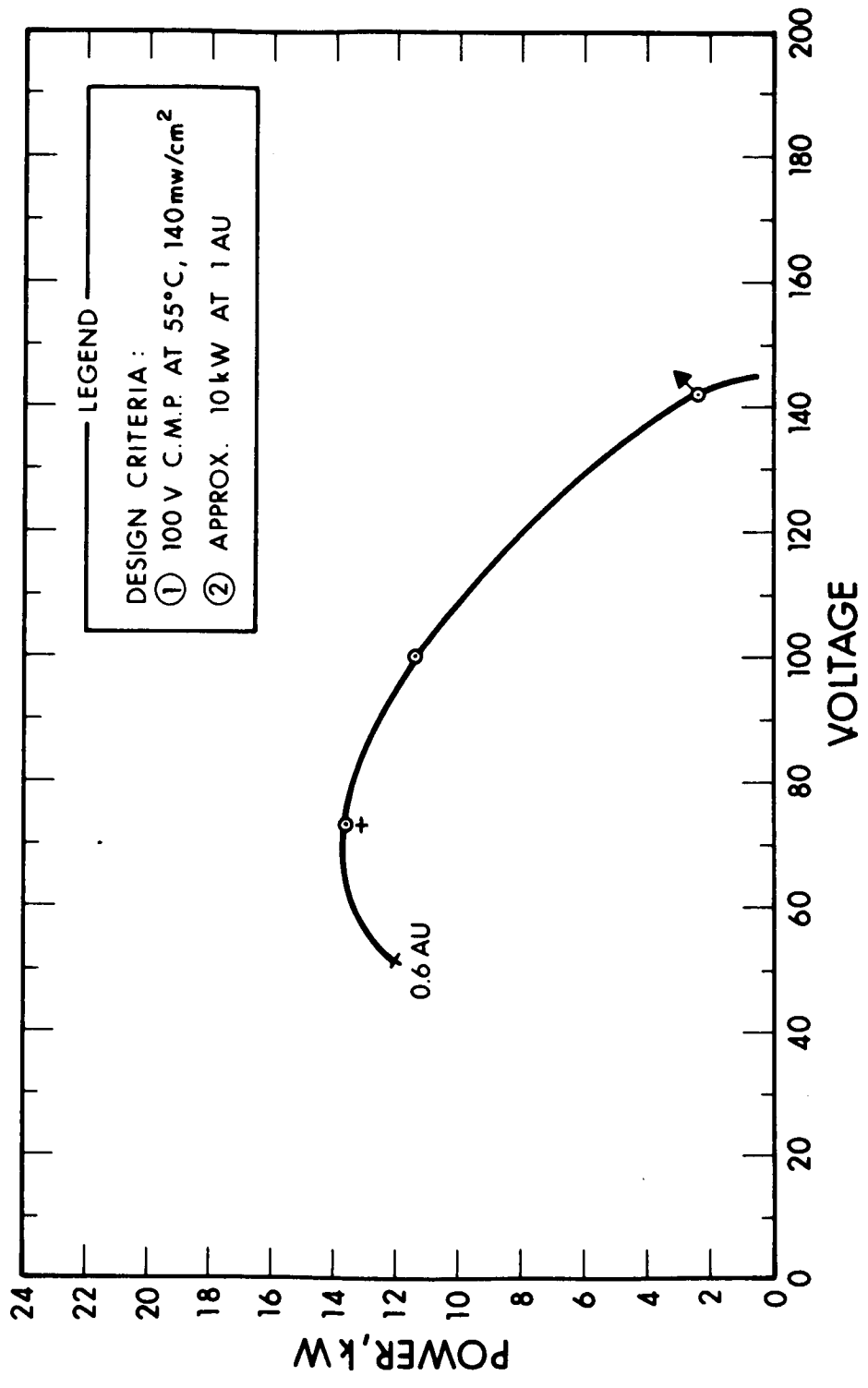


FIG. 7-16 POWER/VOLTAGE CURVE FOR JUPITER FLYBY SOLAR ARRAY

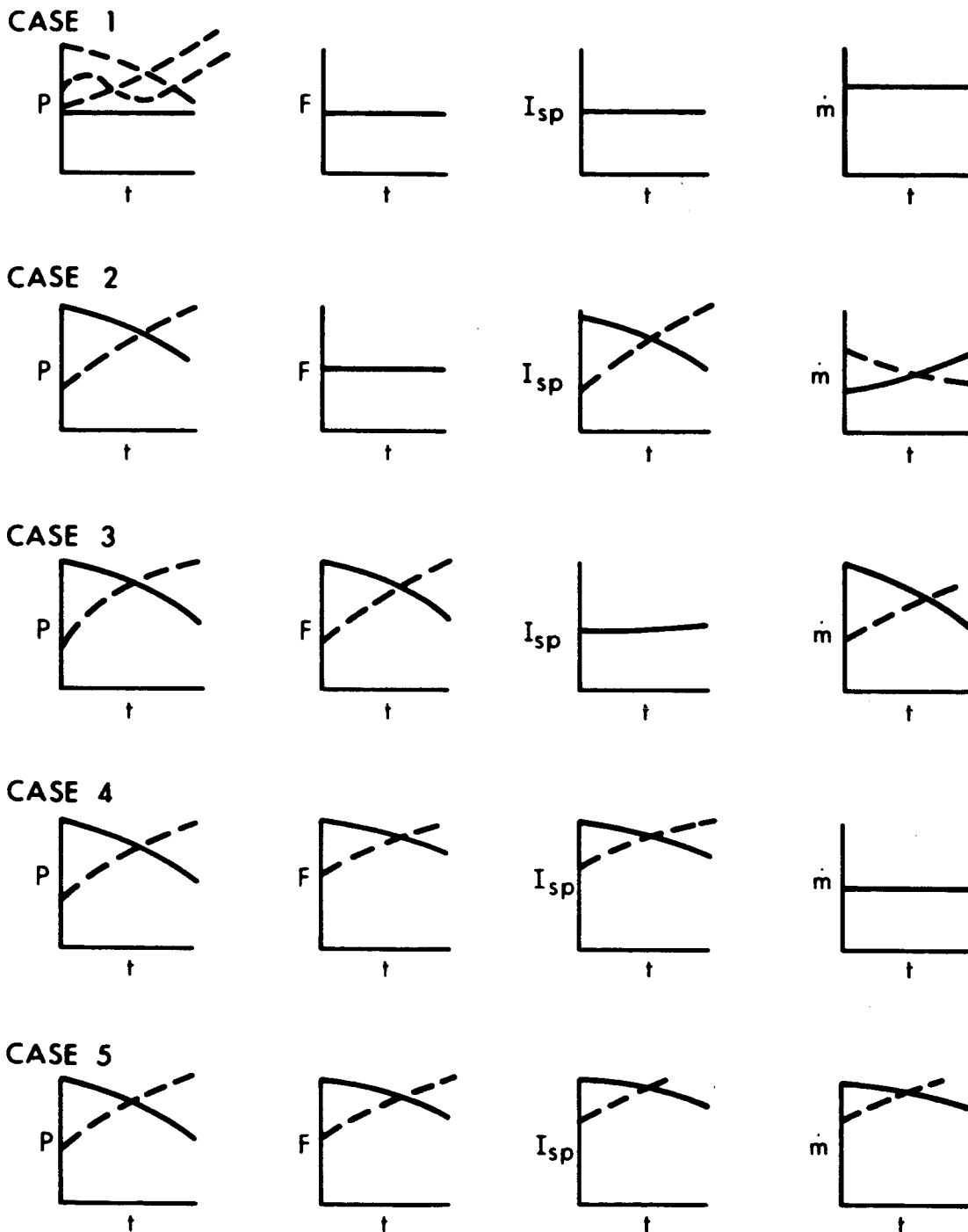


FIG. 7-17 THRUSTER PARAMETER INPUT POWER PROFILES

With a second equation,

$$F = \dot{m} g I_{sp} , \quad (2)$$

it can be seen that only one of the variables of F , \dot{m} , I_{sp} is independent if P is fixed.

Case 1 corresponds to operating at constant power, chosen conservatively at a value which can be assured with sufficient reliability throughout the thrust phase. Note that thrust control will require simultaneous changes in \dot{m} and I_{sp} to correct for errors in P or changes in η . This case represents simplicity in power conditioning but a large loss in available energy.

Case 2 uses the available power profile to give constant thrust. If the variations in power output are large, as could be the case with solar energy sources, this mode of operation is unattractive. The basic problem is the linear variation of efficiency with I_{sp} at the lower I_{sp} values as discussed previously.

Case 3 uses a thrust profile that tracks the nominal power profile, with I_{sp} maintained essentially constant. Such operation is particularly suitable for the bombardment engine and the Li-H arc jets. The contact engine will suffer a small efficiency loss with falling mass flow. A variation of this case that is quite attractive for all thruster types is to select two or more levels of constant power, switching in or out thruster modules as power level changes.

Case 4, based on constant mass flow, requires both F and I_{sp} to vary as $(P \eta)^{1/2}$ where η depends on I_{sp} . There appear to be no special advantages for operating in this mode.

Case 5 is particularly attractive for the contact ion engine. It uses a linear relationship $\dot{m} = I_{sp}$ which has been found to give near-maximum efficiency at each I_{sp} for the contact engine. The mass flow and specific impulse will vary as $(P \eta)^{1/3}$ and thrust as $(P \eta)^{2/3}$. As before, the thrust profile will be maintained by varying I_{sp} and \dot{m} to utilize the available power.

For the mission under consideration, the case 1 operational mode could be used effectively provided that it met trajectory requirements without undue loss of available power. Integration with payload power requirements is also another important consideration.

The initial problem associated with using all or a fixed percentage of the available source power in the other operational modes concerns the determination of that power. Preprogramming as a function of time could possibly be used. If the unit thruster size was relatively small (e.g., 1 - 2 kW), direct programming as a function of the rate of charge and magnitude of source voltage and current could be utilized. After the source electrical capabilities are determined, the load can be varied accordingly as a function of thruster preprogramming. An example would be thruster module changes (case 3). The output voltage excursions required for maximum use of available photovoltaic system power, however, are much larger than the excursions for case 1, the constant power profile. Thus, case 3 regulation requirements will be greater than those for case 1.

7.5.2 Power Conditioning Design Approach

With the exception of regulation requirements, case 1 and case 3 operational modes could use the same power conditioning design approach. There are three basic design approaches that could be used. The first would use a single power conditioning subsystem for each unit thruster. The second could use a single power conditioning subsystem for several thrusters, and the third would use a modularized power conditioning and control subsystem for each thruster.

Based on engineering considerations such as redundancy/reliability, heat rejection, fabrication, logistics, stability, available component capabilities, and control, the third approach is by far the most attractive. This is substantiated by the results of a past modularized power conditioning development program. The results of this program indicate that power conditioning including controls, radiators, and redundancy could be presently fabricated at 8 lb/kW at 90 percent efficiency for a 2.5 kW cesium electron bombardment thruster.

One of the basic problems that is eliminated with this approach is the stability problem with high efficiency regulation. In the modular approach the output voltage for 80 percent of the engine power requirements is regulated by switching in and out open-loop dc-to-dc converter modules. Thus, the stability problem is reduced considerably.

The selection of transistors versus silicon-controlled rectifiers for control and switching involves consideration of the power, forward current, and breakdown voltage ratings of available semiconductors.

Without using hybrid parallel-series combinations of these active devices, which would require compensation circuitry, present transistors have sufficient ratings for the modular approach. The single power conditioning unit approach would require SCR's. SCR dc-to-dc converters would have to be operated at lower switching frequencies than the transistor approach. This would result in additional magnetic component weight. The SCR approach also requires considerable commutating circuitry.

7.6 Structural Material Evaluations

Aluminum will be used in the frame and interconnection structure for the demonstration panel; all pertinent mechanical properties can be found in MIL-HBK-5.

The demonstration panel materials requiring developmental testing to establish their physical properties are:

1. Electroformed nickel
2. Structural adhesive
3. Dielectric film

Section 9 defines the procedures to perform this testing. Testing of the electroformed nickel has been completed.

The electroformed nickel tensile test samples were found to have an ultimate strength between 146,000 to 150,000 psi with 10 percent elongation in 1-in. gage length. The 2 mil/in. yield strength is 104,000 to 109,000 psi. The stress-strain curve shown

in Fig. 7-18 does not show a true elastic behavior, but in the lower range of the curve the slope approximates the modulus of nickel. Thus, for analytical purposes, one can use $E = 31.10^6$ psi. The ultimate strength of 80,000 psi and yield strength of 50,000 psi used in the analysis is conservative.

Several structural adhesives have been tested and will be given further testing. They are:

1. A nylon-epoxy adhesive film (FM-1000).
2. Several epoxies (Epon 919, 934)

A procedure will be developed from these tests to obtain the required cleanness. Tooling is being designed to apply the correct bond pressures. The cure cycle, heating rate, cure temperature, and other parameters are also being determined from the tests.

The dielectric materials being considered for the demonstration panel are fiber glass and DuPont Kapton H-film. The fiber glass is a flight-proved material, having been used on Ranger and Syncom-3. The recently developed Kapton H-film has been shown to maintain its physical, electrical, and mechanical properties over a wide temperature range. The H-film can be used from -269° to $+400^{\circ}\text{C}$ without adverse effects. In comparison, the fiberglass dielectric is limited to operation between -65°C and $+85^{\circ}\text{C}$.

The tensile properties of the Kapton H-film and fiber glass are shown in Fig. 7-19, while the thermal characteristics of each are shown in Fig. 7-20. As shown, the H-film has a higher thermal conductivity than fiber glass, thus aiding to cool the panel during the part of the mission where the trajectory is near the sun.

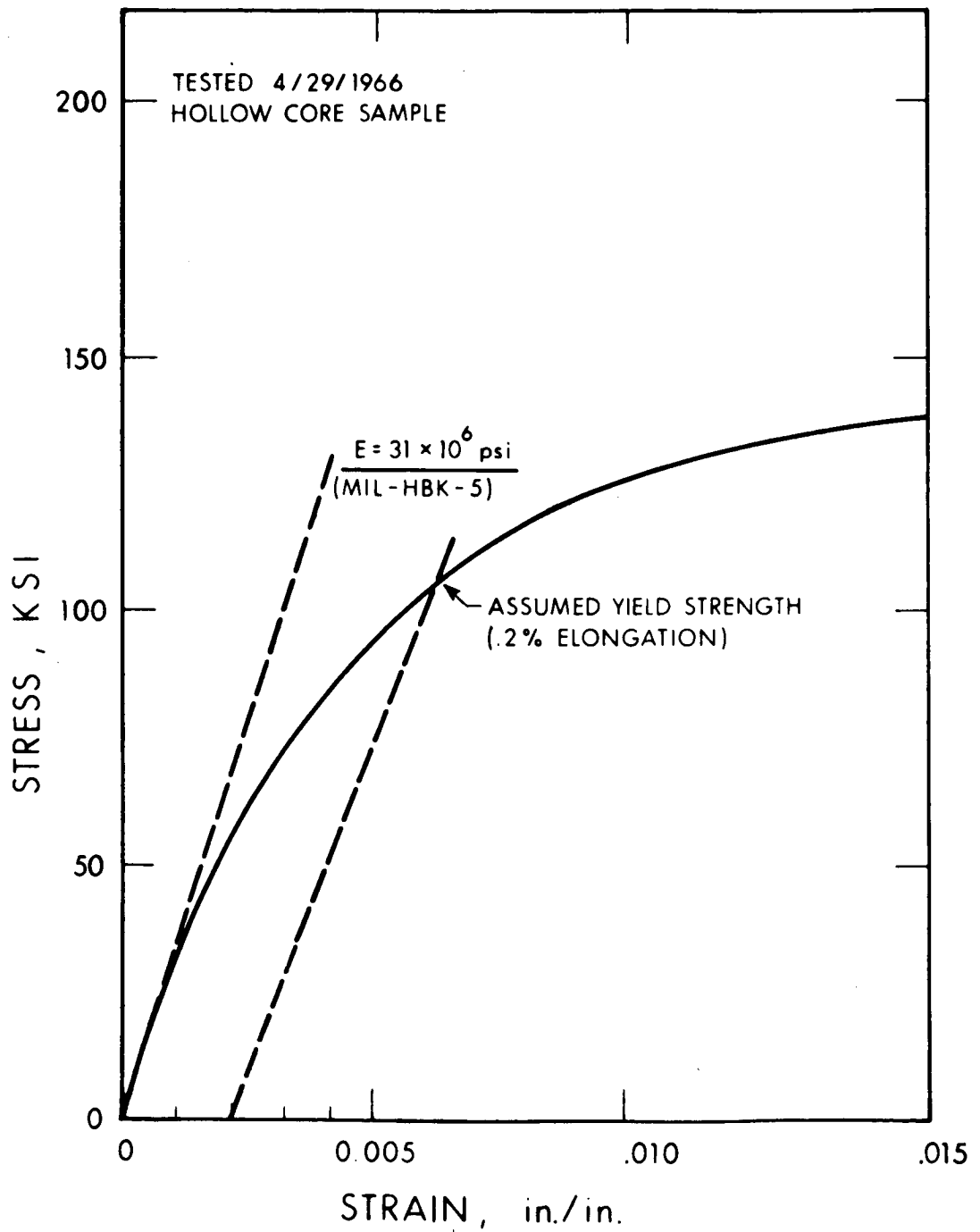


FIG. 7-18 STRESS/STRAIN CURVES FOR ELECTROPLATED NICKEL

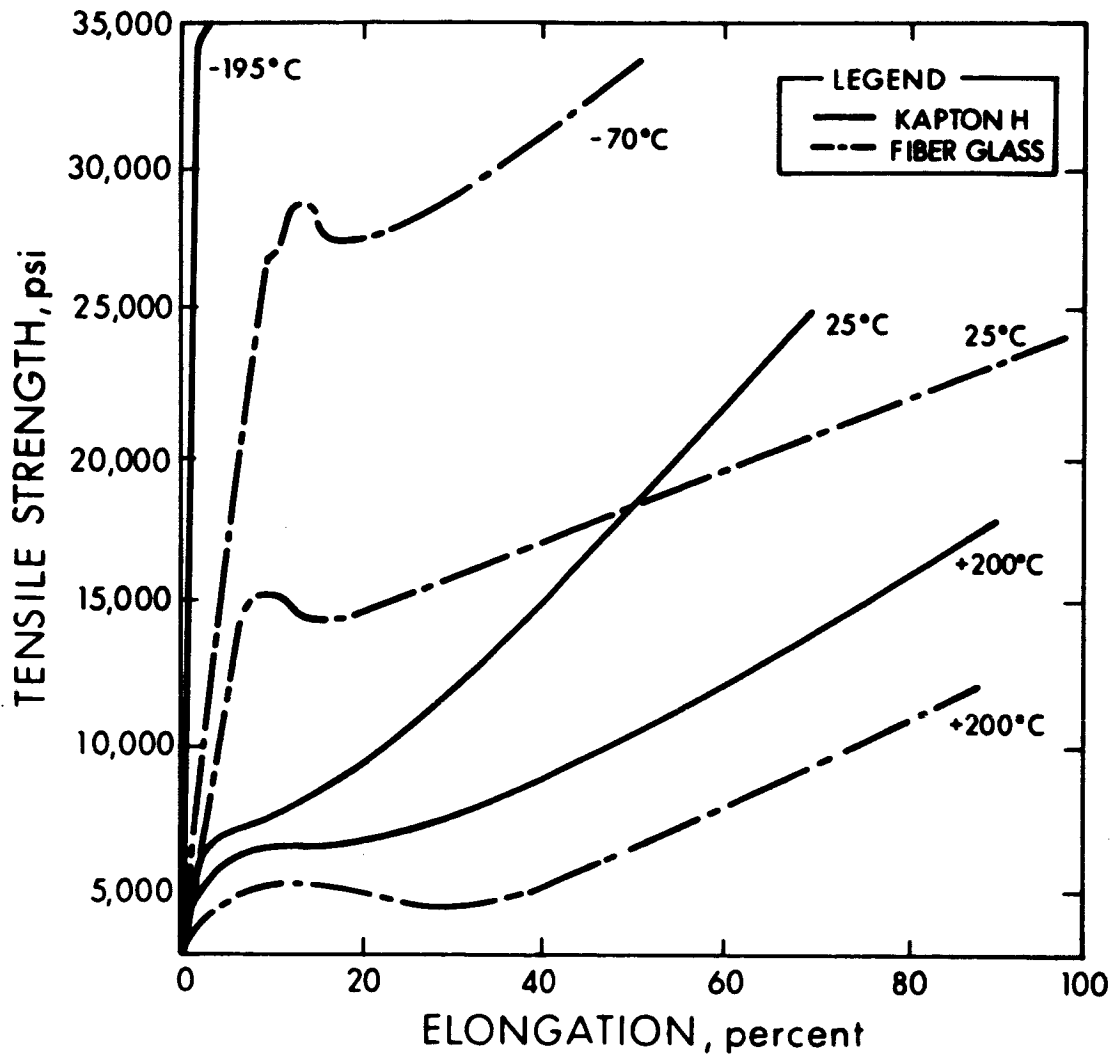


FIG. 7-19 TENSILE CHARACTERISTICS OF VARIOUS THICKNESS OF KAPTON H-FILM AND FIBER GLASS

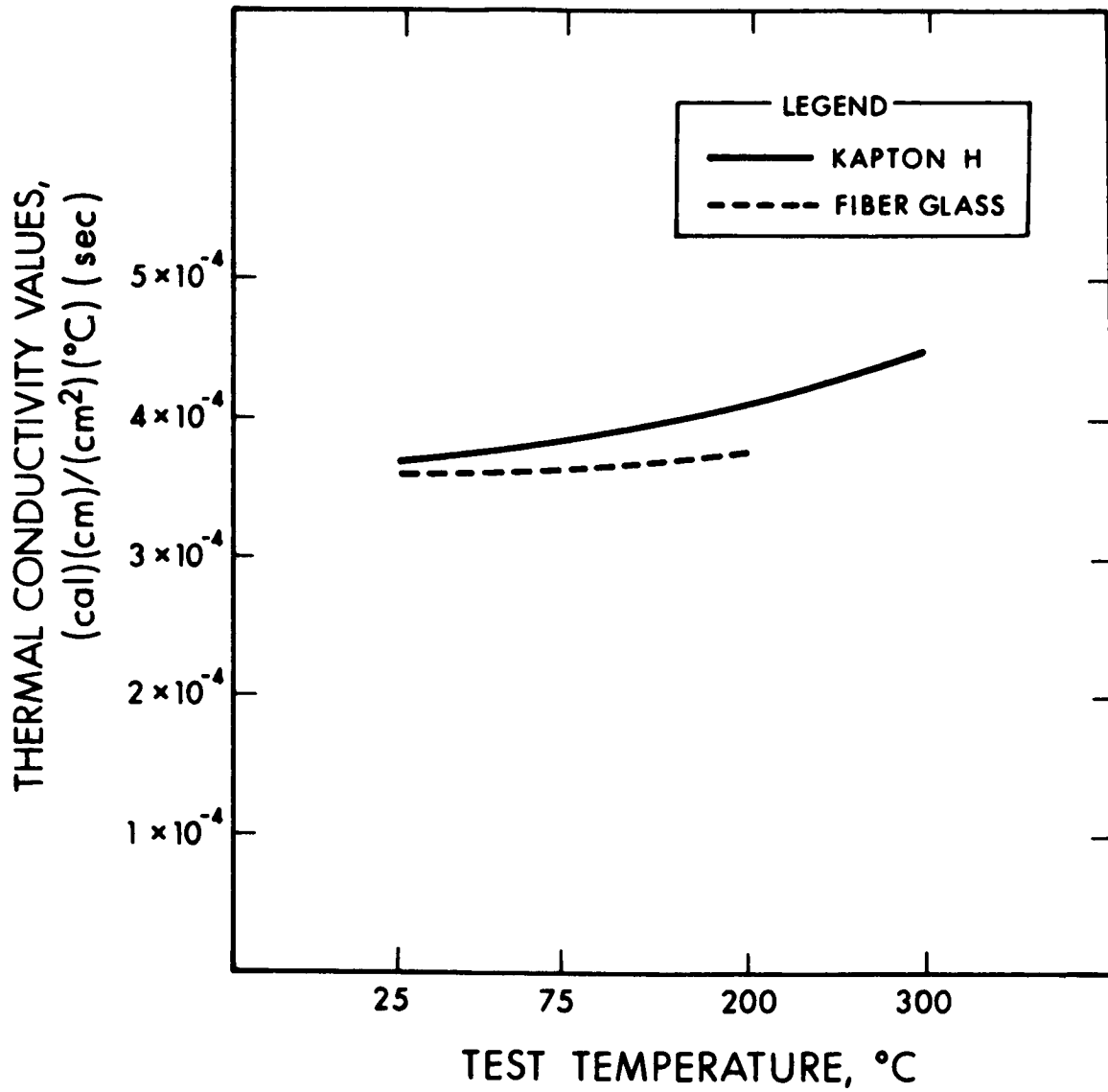


FIG. 7-20 THERMAL CHARACTERISTICS 5-MIL FIBER GLASS AND 1-MIL KAPTON H-FILM

8. MANUFACTURING OF THE DEMONSTRATION PANEL

This section defines the manufacturing plans and processes to be used in fabrication and assembly of the demonstration panel. These processes are being developed in the sample panel program. For this report, the discussion is limited to the hollow core structure development. The final report will cover the photovoltaic assembly, frame, and other areas.

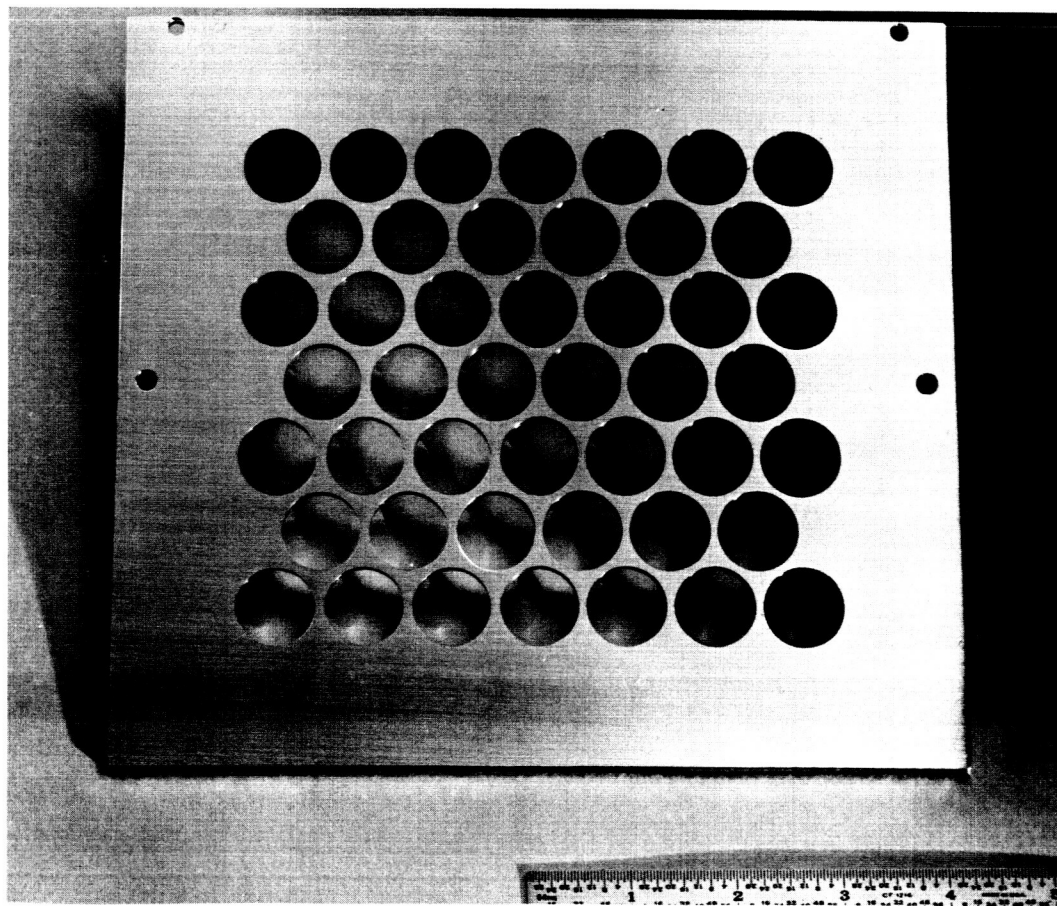


FIG. 8-1 ALUMINUM MANDREL FOR FABRICATION OF HOLLOW CORE STRUCTURE

8.1 Hollow Core Structure Development

The hollow core structure which supports the solar cells will be fabricated by the electroforming process. Electroforming is defined as the production or reproduction of articles by electrodeposition upon a mandrel or mold that is subsequently separated from the deposit.

With the use of the electroforming process an extremely lightweight and relatively stiff structural element can be fabricated economically. The process permits the fabrication of the hollow core structure as an integral unit, without welded or bonded joints.

The hollow core structure is fabricated by preparing an aluminum mandrel similar to the one shown in Fig. 8-1. Flat aluminum sheet stock is set up and drilled to the required hole pattern. In extremely lightweight structures (such as the solar panel) the holes in the mandrel are very close together, and aluminum in the T-6 condition is used to prevent tearing of the material between the holes during drilling. After drilling, each hole is reamed and chamfered. These operations are required to produce an even, electroformed surface; the process will replicate exactly even the smallest surface irregularity. Special tooling is required to insure hole uniformity.

After the mandrel has been cleaned and prepared, it is mounted in a reciprocator and electroformed in a nickel sulfamate electrolyte. A sketch of the electroforming setup is shown in Fig. 8-2. As shown, the mandrel is mounted in the electroforming bath between two anode baskets. Between each basket and the aluminum mandrel, there is a fiber glass profile mask. The purpose of this mask is to reduce the effect of the high current density that develops at the edge of the mandrel. As the thickness of the electroformed deposit is directly related to current density, the thickness at the edge of the mandrel would be greater if the part were plated without a mask. The mask acts as a resistance in the flow path of the nickel from the anode to the cathode; proper sizing permits a uniform thickness to be obtained. Reciprocation of the mandrel is used to minimize

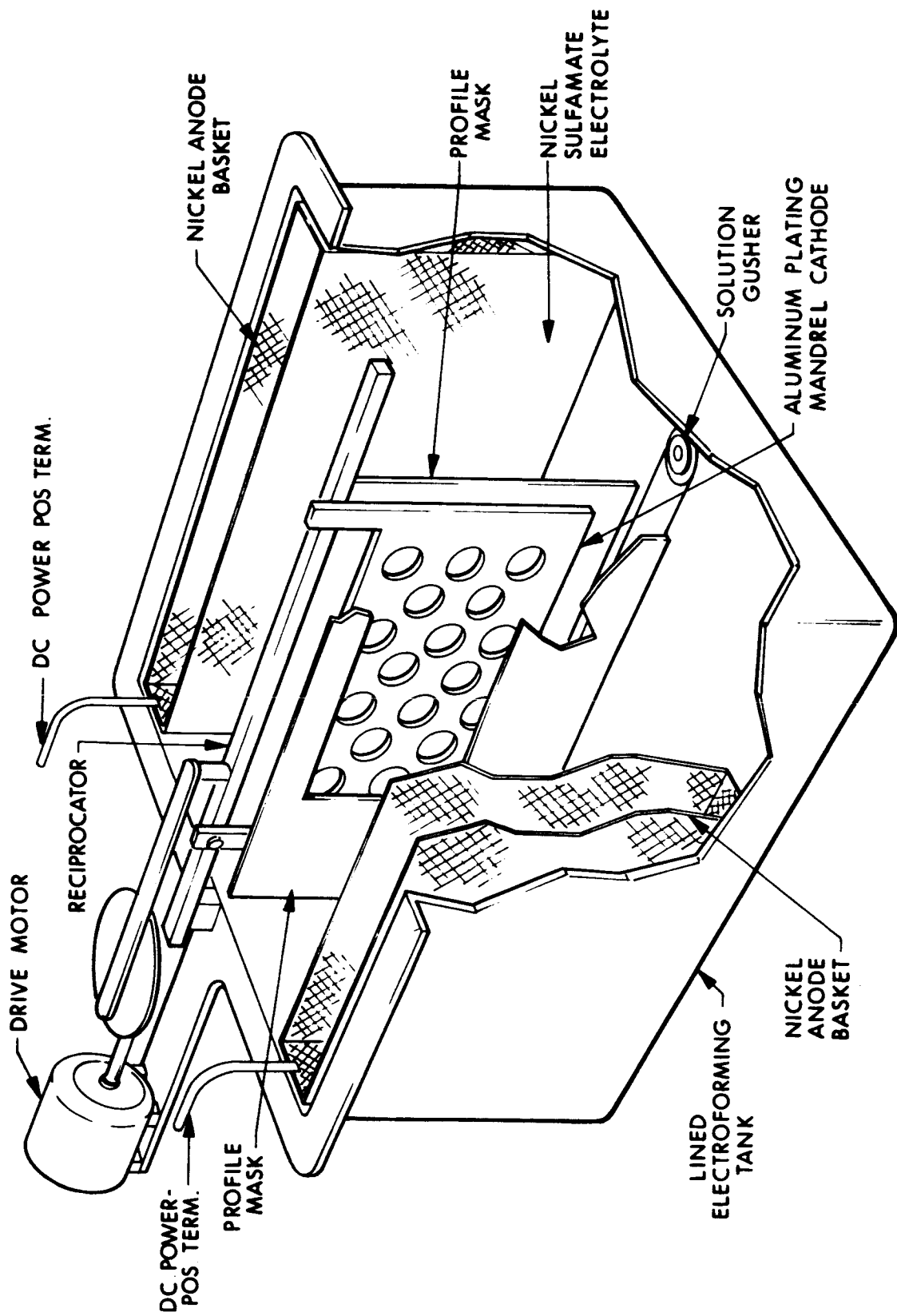


FIG. 8-2 ELECTROFORMING SETUP - HOLLOW CORE STRUCTURE

variations in the current density distribution in the bath. The gusher provides bath agitation which reduces pitting and removes hydrogen gas from the cathode.

After the required thickness of nickel has been deposited on the mandrel, the aluminum is removed by etching with diluted hydrochloric acid. The resulting hollow core structure is shown in Fig. 8-3.

8.2 Status of Program

Several types of extremely lightweight hollow core structures have been successfully fabricated by EOS. The weight requirement for this part of the solar panel is 0.066 lb/ft^2 , which requires an 82-percent open area. As this requires a structure that had not previously been fabricated, a three-phase development study has been established to verify the design and fabrication process for the hollow core structure. The three phases are:

1. Fabrication of buckling specimens (Phase I)
2. Full-scale plating tests (Phase II)
3. Fabrication of demonstration panel (Phase III)

To date, only the Phase I study has been completed. It was the purpose of this study to verify on a small scale the fabrication procedures and provide test data to verify the design analysis of the structure. Both of these objectives were met. A hollow core sample of the required weight was fabricated to successfully carry the design loads. The results of these tests are detailed in Section 9.

Phase II (full-scale plating tests) is currently in progress to establish the exact masking and electroforming parameters for the full-scale panel.

Phase III (actual fabrication of the demonstration panel) will only be attempted after the full-scale plating tests have been completed. Each of these process development tests is described in detail in Section 9.

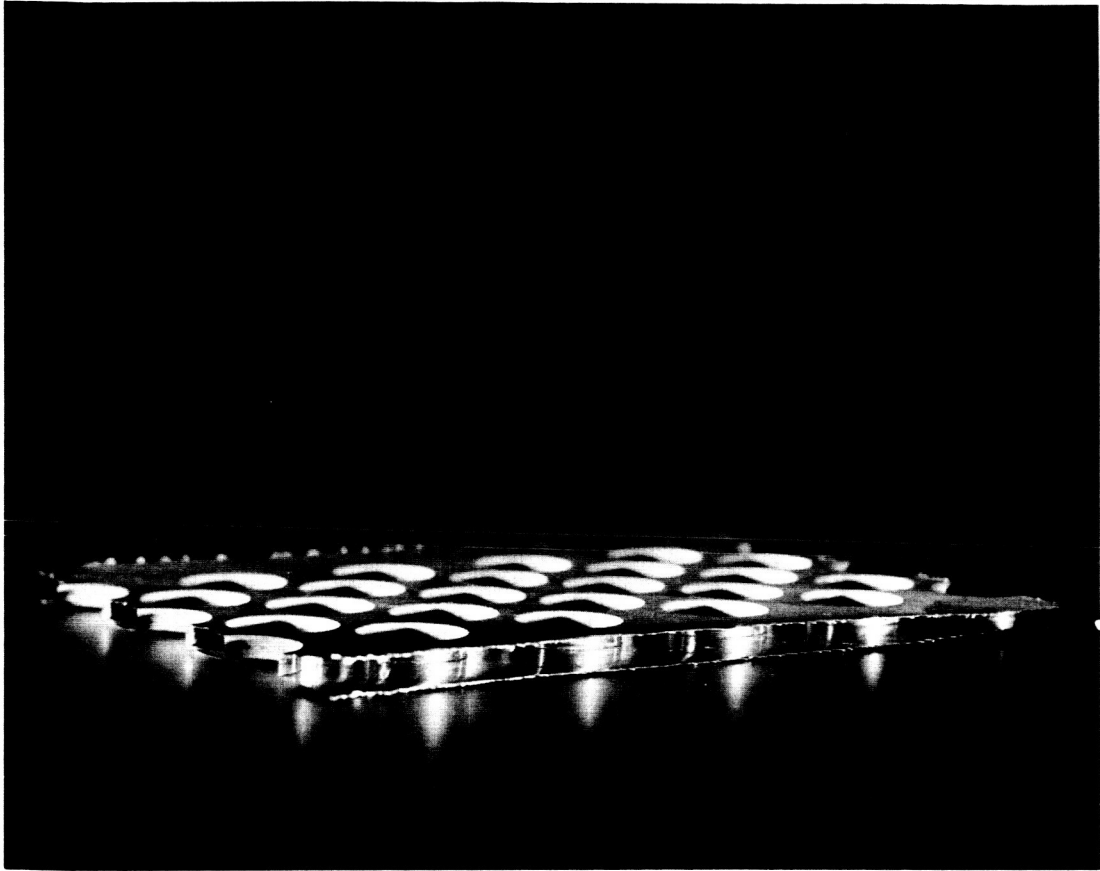


FIG. 8-3 SUBSTRATE CONSTRUCTION — HOLLOW CORE STRUCTURE

The development studies are necessary because the electroforming process is affected by several variables which must be fixed for each type of structure, then closely maintained to insure successful fabrication.

The proper combination of the following parameters must be established and maintained:

1. Bath composition (chemical analysis)
2. pH
3. Current density
4. Plating temperature
5. Masking
6. Agitation
7. Reciprocation
8. Deposit stress

The methods and results of these interactions have been documented by several investigators, but without much agreement. The proper combination of these variables will be developed during the process studies of Phase I and Phase II. This will result in a process specification to be used for the Phase III demonstration panel.

In general, the fabrication process for the full-scale hollow core structure will be as follows:

1. Drill, ream, and chamfer 6061-T6 aluminum plating mandrel to the proper pattern.
2. Form mandrel to the final panel contour and trim to size.
3. Surface-finish mandrel as required.
4. Electroform mandrel to required thickness using parameters established under Phase I and Phase II studies.
5. Remove aluminum mandrel by etching.
6. Bond to supporting frame.

9. TESTS, TEST PLANS, AND DATA SUMMARY

This section defines the tests and test plans for the demonstration panel, sample panels, and solar cell. The tests are conducted to qualify the demonstration panel design, verify the structural analysis and determine the electrical characteristics of individual cells and electrical modules. The section discusses the results of tests conducted to date and indicates what data will be obtained from tests yet to be conducted.

A formal test specification will be developed before the start of the demonstration panel test and will amplify and bring together the material contained in different parts of this section.

9.1 Thermal Tests

9.1.1 Purpose

The purpose of the planned thermal tests is to make a comparative experimental measurement of the effects of the lightweight hollow core substrate structure on solar cell performance. The proposed method involves the measurement of open-circuit cell voltages under illumination intensities similar to the earth-space environment. A direct comparison will be made between a completed sample of the hollow core solar panel and another completed sample with identical cells and coatings using a flat aluminum sheet as substrate. A series of calibration tests will be conducted to establish precision in the tests.

The analysis of the temperature distribution (see Subsection 7.4) does not indicate that a thermal penalty on cell performance is probable. These tests will be conducted to verify that conclusion. Although it will be difficult if the temperature gradients are as small as predicted, the tests may give an indication of

the average effect of the local temperature variations in the celled surface on the electrical output of the array. Although the effect of changing the temperature of an isothermal panel has been accurately determined, the effect of scattered local "hot spots" is not well understood at the present time.

9.1.2 Apparatus

The thermal tests will be conducted in a 2 ft³ vacuum chamber in which black liquid-nitrogen-cooled walls have been placed. Illumination will be provided by high temperature incandescent lamps or an arc source with a significant percentage of radiation in the band between 0.7 and 1.0 μ . The solar panel samples, complete with silicon cells and thermal coatings, will be instrumented for nominal temperature. No attempt will be made to measure the detailed temperature due to the thinness of the nickel hollow core substrate walls. Cold wall temperatures, lamp power, and chamber pressure will also be measured during the test. A radiometer survey will be conducted to determine the uniformity of illumination, which will be adjusted if necessary.

9.1.3 Procedure

The basic procedure will consist of measuring the open-circuit voltage of the cells on a hollow core substrate and a flat plate substrate while both are being illuminated at the same time. The lamp power will be adjusted so that the samples are operating at a steady-state temperature similar to that predicted for the earth-space environment. A series of calibration tests will be conducted to establish precision in the comparison. The two samples will be tested with the backs insulated to calibrate the cells. Each test will be rerun with the two sample positions reversed to eliminate dissimilarities in the illumination.

9.2 Dynamic Tests

9.2.1 Modal Test of Substrate

The purpose of the modal tests of the substrate will be to verify the natural frequencies and mode shapes predicted in Subsection 7.3.1 and to determine the damping coefficients for the significant modes of natural vibration.

The doubly curved substrate panel, supported in the manner which best approximates the boundary conditions assumed in the analysis, will be excited by at least two electromagnetic shakers driven by the same oscillator. These shakers will drive the panel by coupling with eddy currents generated in the panel surface and will not be mechanically attached to the panel. The natural modes will be tuned in by (1) placing the shakers at locations where maximum amplitudes in the mode of interest are expected and (2) adjusting the frequency and amplitude of the excitation until the excitation is in phase with the velocity of the response, which is the condition for resonance. The nodal patterns will be detected by sprinkling a mixture of polyvinylchloride (PVC) pellets (Monsanto Chemical Company, Opalon 300 FM resin) and magnesium stearate powder in a ratio of 10 parts PVC to 1 part Mg stearate. This mixture will stick to the curved surface and tend to gather the nodes of the vibrating shell.

Each time a natural mode is tuned in, the structural damping coefficient for that mode will be determined by placing a displacement pickup (preferably of the capacitance or microwave type) at a point of large amplitude vibration in the mode and recording the decay of the vibration when all excitation is shut off simultaneously. The damping can be estimated by applying the logarithmic decrement method to the record of the decay.

9.2.2 Sinusoidal and Random Vibration Hard Mount Tests

The purpose of the sinusoidal and random test will be primarily to verify that the demonstration panel can meet the requirements specified in the Design Criteria and Requirements Specification. For the present design, these requirements are:

1. Three sweeps of sinusoidal vibration from 2 to 200 Hz at 1.0 min/octave with levels of 1.5g rms from 2 to 50 Hz and 2.0g rms from 50 to 200 Hz.
2. Three minutes of gaussian vibration at $0.2g^2/Hz$, band-limited between 200 and 2000 Hz.

A secondary purpose of the sinusoidal tests, which will be accomplished first in the testing sequence, will be to verify by low level tests that the gains used to establish the design loads for the panel were conservative and that positive margins of safety will exist when the environments above are applied.

9.3 Static Strength Tests

9.3.1 Buckling Tests of Hollow Core Substrate

9.3.1.1 Objective of Tests

The objective of the tests is to confirm the mode of failure and the empirical buckling coefficients used in the analysis of the hollow core substrate.

9.3.1.2 Summary of Results

The tests confirmed that the primary failure made in the hollow core structure is crippling of the small flat surfaces between the cylinders, followed by secondary column-type failure of the total substrate. The tests also confirmed that the empirical buckling coefficients assumed in the analysis are safe to use.

9.3.1.3 Test Specimens and Their Preparation

The test specimens are electroformed to the same procedure as those for the demonstration solar panel, with respect to current densities, electrode arrangement, etc. More than one specimen is electroformed from each mandrel. After removal of mandrel, the specimen is visually checked for structural soundness.

Epoxy shoes are cast on each side of the specimen. The specimen is aligned such that its mid-plane is coincident with the shoe center line. The epoxy shoe surface is machined

so that the load surfaces are parallel. A 1/8-inch radius mill is used for this operation. (See Fig. 9-1 for dimensions.) The specimen is shown ready for test in Fig. 9-2.

9.3.1.4 Test Plan

The Instron testing machine used for the compression tests is shown in Fig. 9-3. The machine has a range of 0-20,000 lb. The strain rate is maintained at a constant rate of 5.0 in./min until buckling has occurred, and a maximum load-carrying capacity has been reached.

Before each test series, the machine is calibrated over the anticipated loading range, providing a permanent record for data reduction. A dead weight is used for this purpose. The test fixture is mounted in the testing machine during calibration.

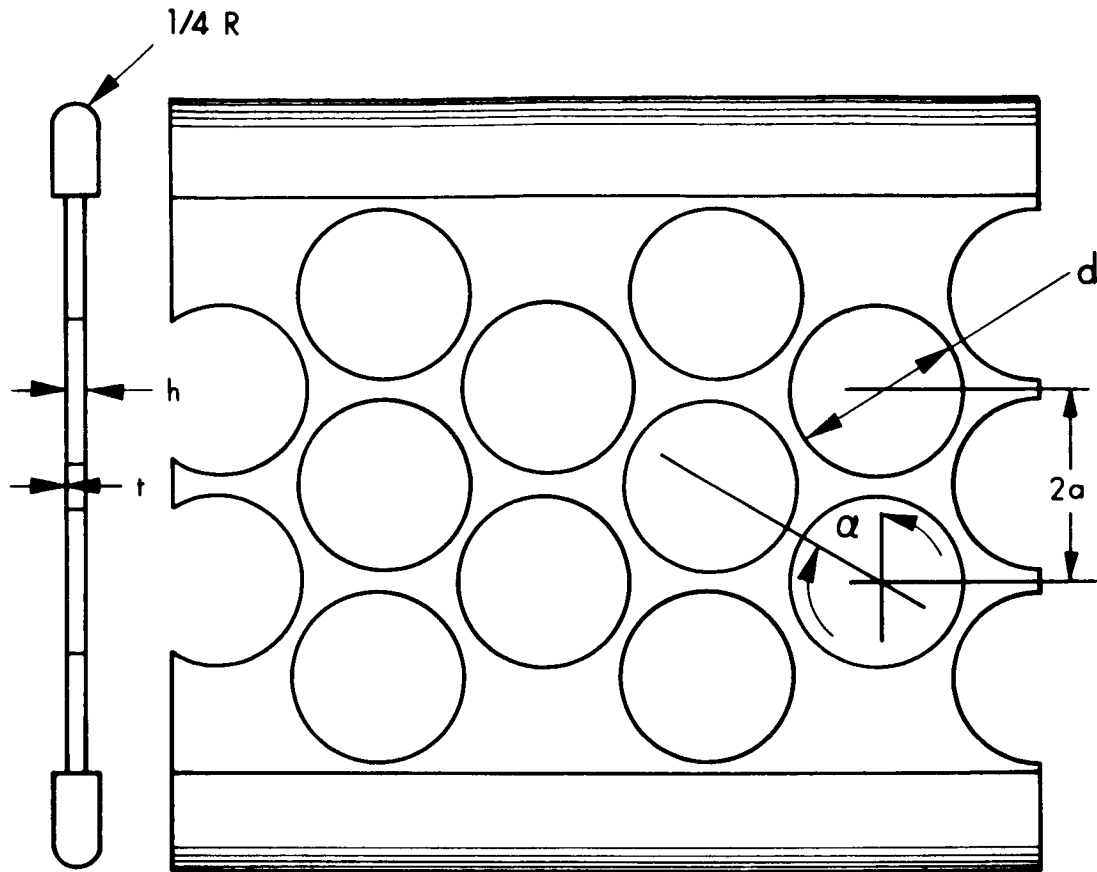
The test fixture is so constructed that it assures uniform loading over the length. The contact surface is cylindrical, assuring line contact and a minimum eccentricity. The two fixture halves are visually aligned in the testing machine before each run, assuring a line load transfer.

After fixture mounting and calibration, the test specimen is inserted into the fixture and aligned until specimen is vertical and has full-length contact.

The zero load point is marked before testing. The test is initiated and continued past crippling and secondary column-type failure until the load starts to drop off, then the load is released and the zero point remarked on the record. The record is labeled with specimen number and remarks of the test procedure and result.

9.3.1.5 Test Results

The test results were derived from 21 hollow core samples. The table in Fig. 9-1 defines the geometry variations of the samples. Figure 9-4 shows typical data documentation; load strain relations for one of the samples are shown in the chart of Fig. 9-5.



NO.	d	2a	α	h	t
S-V-4	0.50	0.848	45°	0.1	0.002
H-H-2-2	0.250	0.350	60°	0.1	0.002
S-C-4-2	0.500	0.600	60°	0.1	0.002
H-H-6-2	0.750	0.850	60°	0.1	0.002
No. 1 - No. 9	1.000	1.050	60°	0.1	0.002

FIG. 9-1 BUCKLING TEST SAMPLE SKETCH AND CRITICAL DIMENSIONS

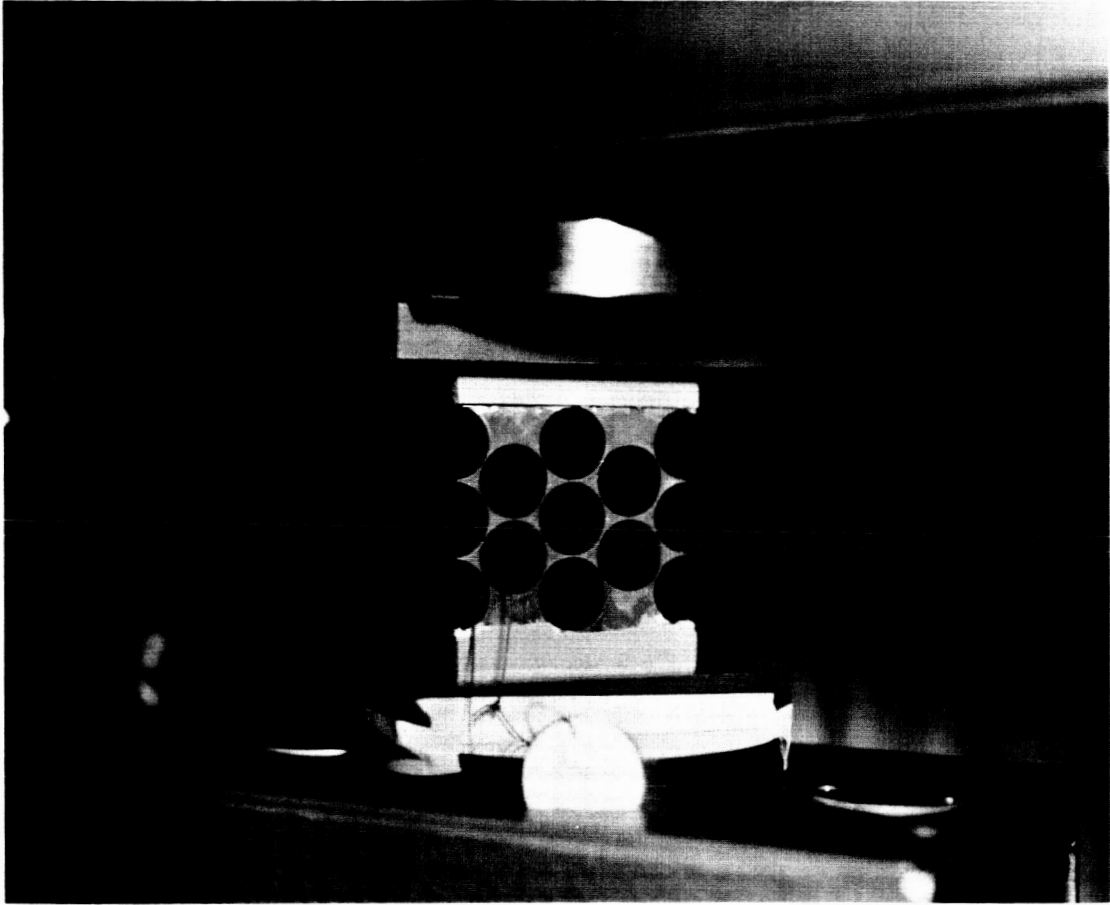


FIG. 9-2 PHOTO SHOWING SPECIMEN READIED FOR TEST

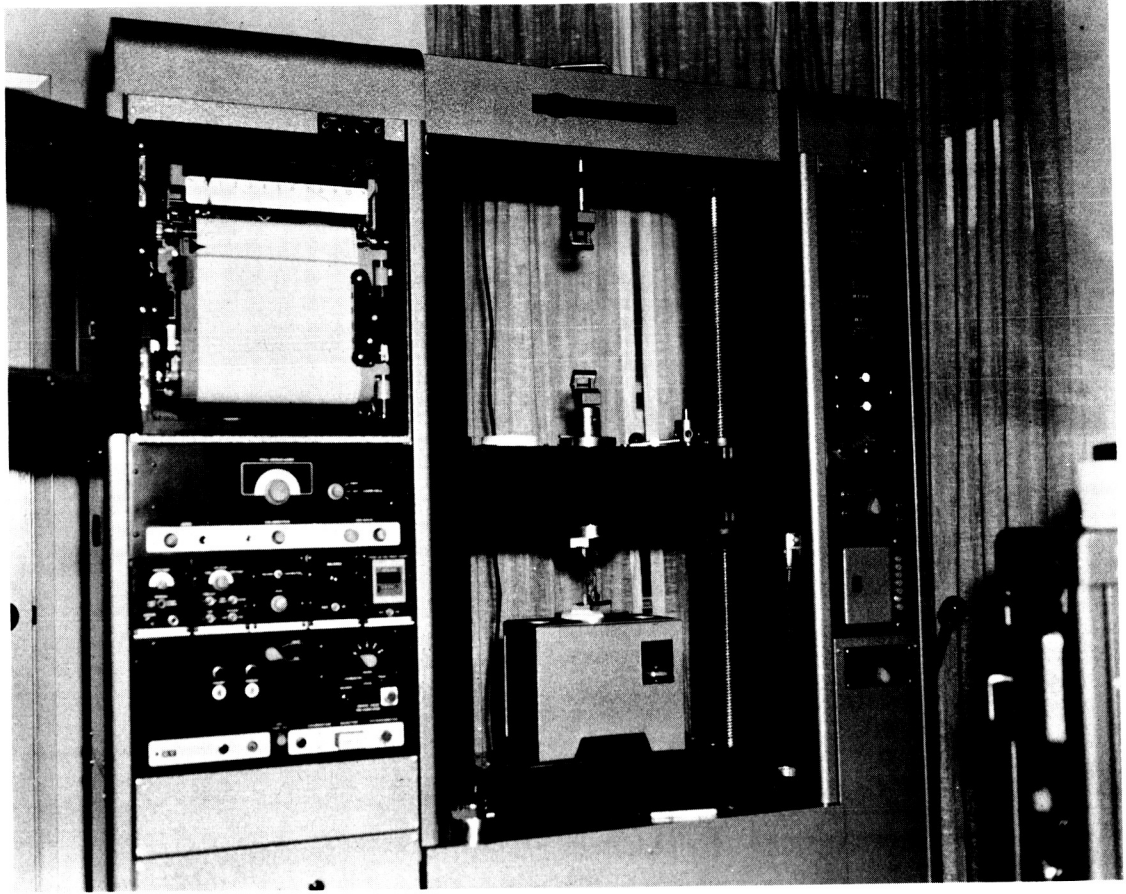



FIG. 9-3 INSTRON PRESSURE TESTING MACHINE

FIG. 9-4 SAMPLE DATA SHEET

<u>PROJECT:</u> <u>BICONVEX HOLLOW CORE</u>	DATE <u>Y-27-66</u>
<u>SOLAR PANELS</u>	W.A. <u>7027-01-01</u>
<u>TEST:</u> <u>COMPRESSION TEST OF HOLLOW CORE SAMPLES</u>	
<u>TO DETERMINE THE BUCKLING COEFFICIENT</u>	
<u>TEST FACILITY:</u> <u>METALLURGICAL TESTING CORP</u>	
<u>1246 S. ANAHEIM-PUENTE ROAD INDUSTRY</u>	
<u>EQUIPMENT USED:</u>	
TESTING MACHINE: <u>INSTRON</u>	
<u>RANGE</u>	LOAD: <u>0-20 000 LBS</u> TEMPERATURE: <u>AMP</u>
	RATE: <u>0.05 IN/MIN</u> CALIBRATION N ^o <u>A 3</u>
	DATA: <u>10.0 IN/MIN</u>
<u>INSTRUMENTATION:</u> <u>NONE</u>	
<u>TEST SPECIMEN</u> N^o # <u>4</u>	
SIZE:	<u>W = 4.9g</u>
LENGTH: <u>2.62 INCHES</u>	
WIDTH: <u>3.27 INCHES</u>	
PANEL THICKNESS: <u>0.100 INCHES</u>	
SKIN THICKNESS: <u>0.002 INCHES</u>	
HOLE PATTERN: <u>TRIANGULAR</u>	<u>ORIENTATION:</u> 
HOLE SIZE: <u>1.0 IN.</u>	
HOLE SPACING: <u>1.05 IN</u>	
MATERIAL: <u>NICKEL</u>	STRENGTH: <u>?</u> PSI
<u>REMARKS ON TEST:</u> <u>STANDARD PERFORMANCE</u>	
ATTAINED: $\frac{20.5}{2.62} = \underline{7.8} \#/IN$	COLUMN TYPE BUCKLING AFTER
CALCULATED = $\underline{7.4} \#/IN$	INITIAL CRIPPLING, WITH
$E_{SLOPE} : \frac{9.28}{0.00025} \#/IN$	CONSIDERABLE LOAD CARRYING
	CAPABILITY AFTER CRIPPLING
	SEE FIG. 9.3.16
MAXIMUM LOAD: <u>LBS 20.5</u>	RATE: <u>7</u> #/SEC
APPROVAL SIGNATURES	EOS OBSERVER: <u>Ragnar Thorsen</u>
	TEST FACILITY: _____

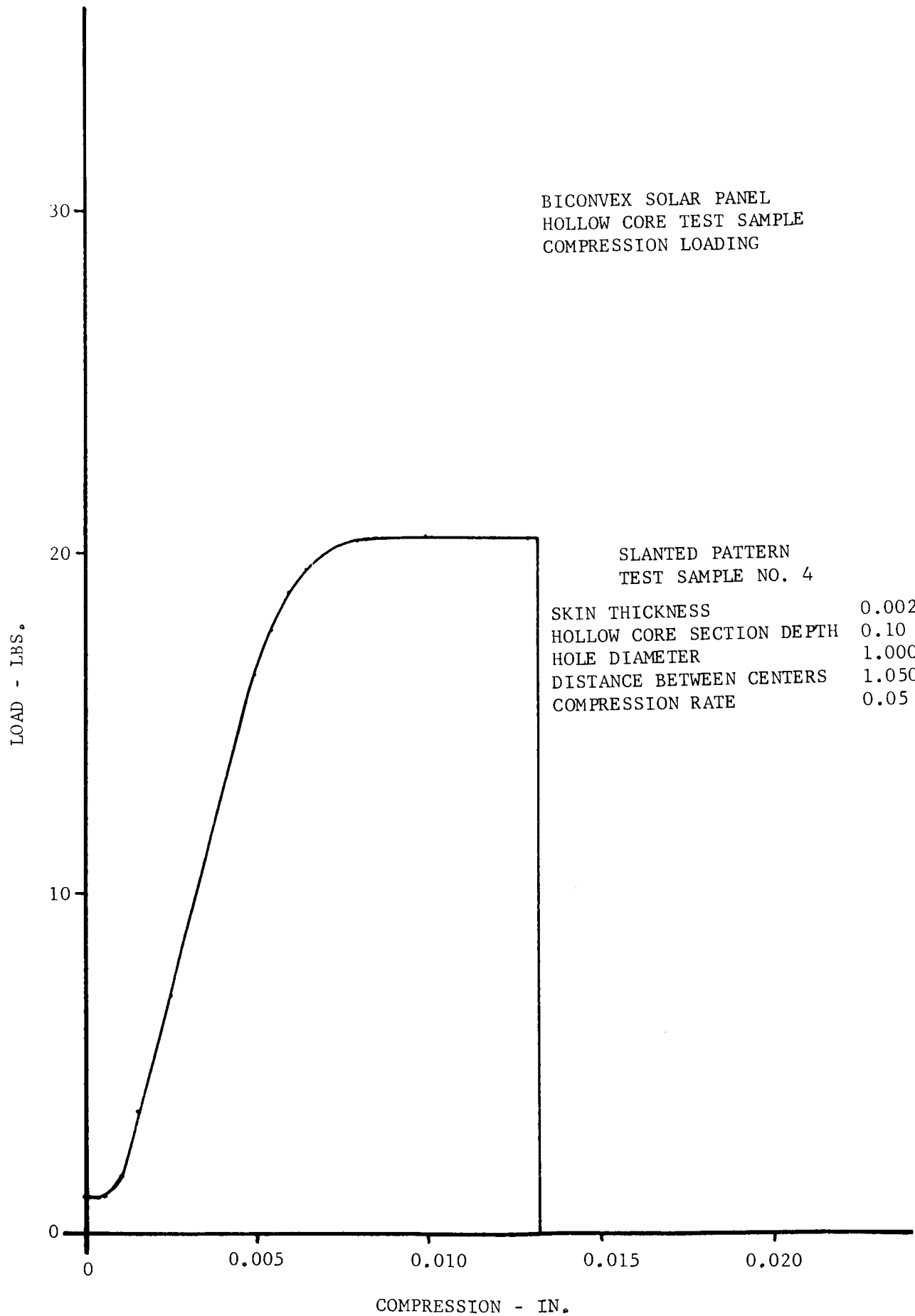


FIG. 9-5 LOAD/TIME STRAIN RELATIONS - TYPICAL SAMPLE

The results of the tests have been a confirmation of the anticipated failure mode and the assumed buckling strengths. One must take into consideration such things as the edge effects, the sections deviating from the hollow core design (sections without holes), shrinking stress from the epoxy shoes. All of these effects reduce the overall strength. These latter effects explain the variation in the load-strain curve within the same design. One may, therefore, expect higher strength in the structure hollow core, where the restraining factors have been eliminated.

The tests have confirmed that the crippling coefficients are

$$K = 6.98 \text{ for square pattern}$$

$$K = 12.00 \text{ for triangular pattern for unidirectional loading}$$

9.3.1.6 Anticipated Failure Loads

The formula for flat plate failure is

$$\tau_{cR} = \frac{K \pi^2 E}{12(1 - \nu^2)} \left(\frac{t}{b}\right)^2$$

For square pattern (0.5-in. diam, 0.848-in. centers):

$$F_{cR} = \frac{9.6 \cdot \pi^2 \cdot 25 \cdot 10^6}{12[1 - (0.3)^2]} \left(\frac{0.002}{0.848 - 0.500}\right)^2$$

$$F_{cR} = 7150 \text{ psi}$$

$$P_{cr} = F_{cR} \times A$$

$$P_{cR} = 7150 \times 0.0021 = 15.1 \text{ lb/in.}$$

For triangular hole spacing:

$$F_{CR} = \frac{12 \cdot \pi^2 \cdot 25 \cdot 10^6}{12[1 - (0.3)^2]} \left(\frac{0.002}{(4a - 1.732d)} \right)^2$$

$$= \frac{1085}{(4a - 1.732d)^2}$$

d = 0.250	F _{cR} = 15220	P _{cR} = 34.8 lb/in.
d = 0.500	F _{cR} = 9720	P _{cR} = 13.0 lb/in.
d = 0.750	F _{cR} = 6740	P _{cR} = 6.3 lb/in.
d = 1.000	F _{cR} = 8010	P _{cR} = 4.6 lb/in.

The crippling is caused by average stress rather than local stress. For this reason the average cross section is used.

$$A_{\text{mean}} = \left(2 - \frac{d}{a} \cos\theta + \frac{h}{a} \right) t$$

$$P_{CR} = F_{CR} \cdot A_{\text{mean}}$$

d	P _{cr}
0.250	40.6 lb/in.
0.500	17.3 lb/in.
0.750	9.5 lb/in.
1.000	7.4 lb/in.

It can be seen that the test results and the calculated failure strengths correspond. The tests also indicated that even though the structure crippld, it is still capable of carrying the full load. The deformation must be extremely high to arrive at a significant drop in load-carrying capacity. Figure 9-6 shows one of the specimens exhibiting a bowed condition under load.

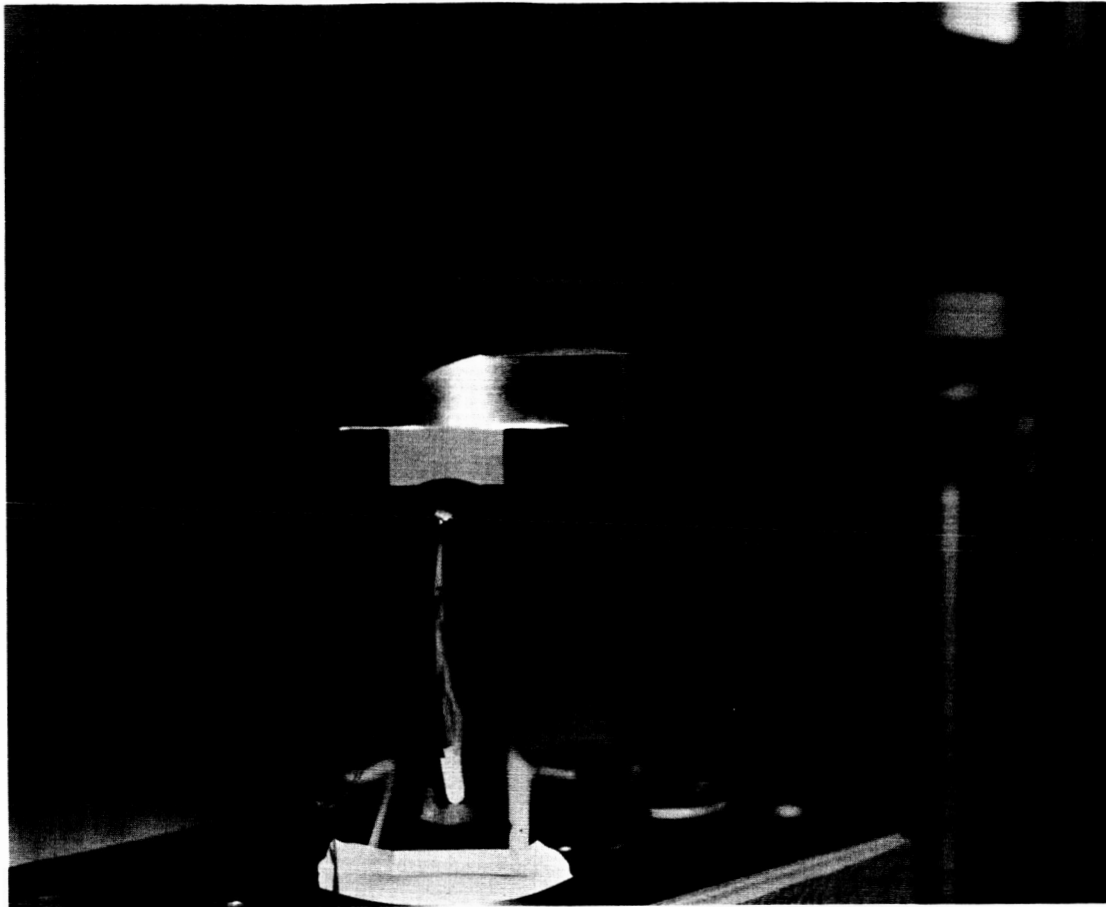


FIG. 9-6 PHOTO SHOWING BUCKLING OF SPECIMEN

9.4 Photovoltaic Tests

9.4.1 Solar Cell Grading

Solar cells used in the fabrication of the two sample panels (5 in.²) and for the large demonstration panel (5 ft²) shall be of two types: (1) 8 mils thick, 2 cm², with 3-mil microsheet coverslides and an average efficiency of 11.6 percent AMI, and (2) 4 mils thick, 2 cm², with 3-mil microsheet coverslides and an average efficiency of 9.8 percent AMI (see Figs. 9-7 and 9-8).

A representative cell from each cell thickness shall be calibrated at the Table Mountain test site, and used as a standard in the electrical testing of the cells and arrays.

A cell and submodule test fixture will be designed to prevent damaging the thin solar cells and to obtain optimum ohmic contact to the cells and submodules.

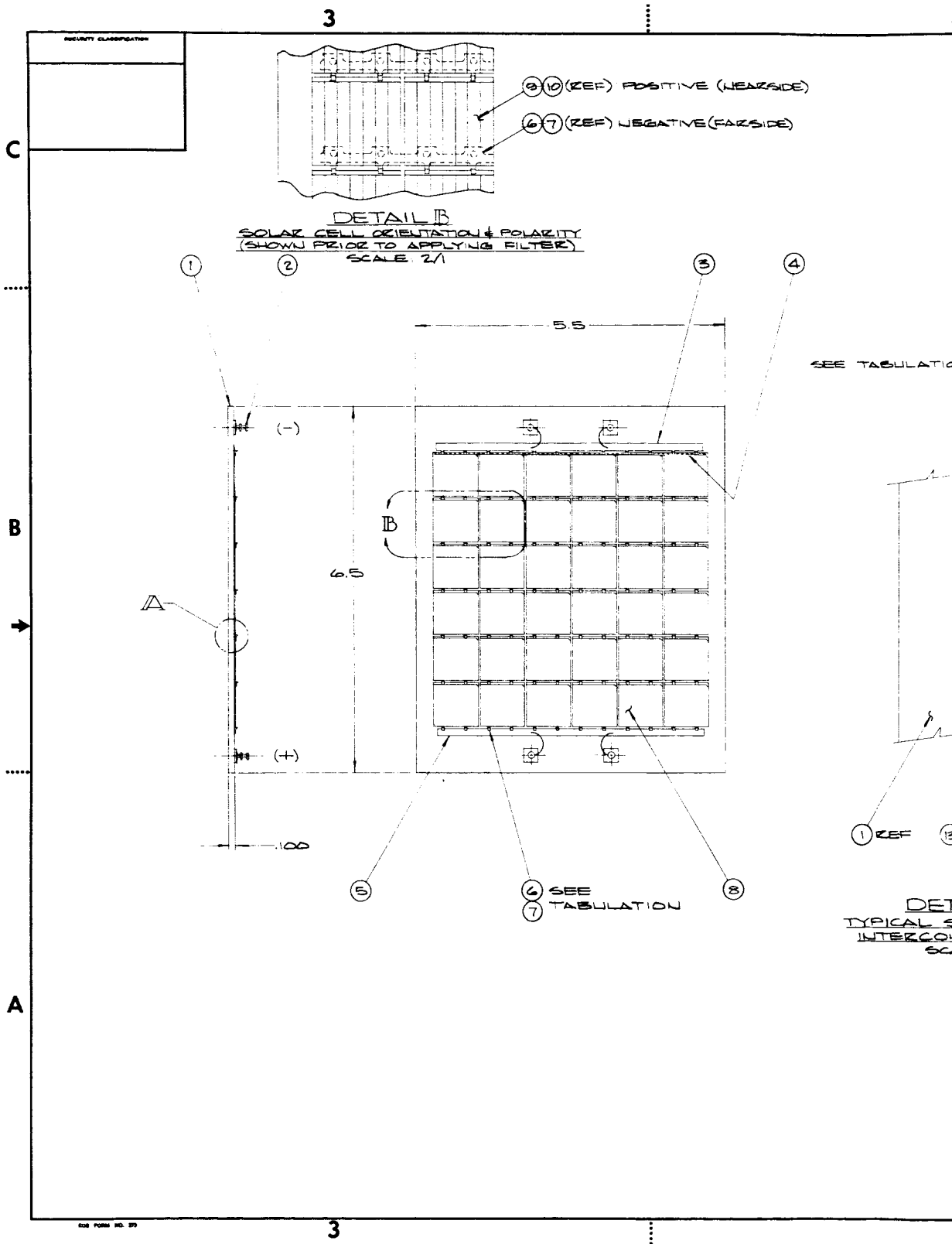
The cells will be tested at 28 (±2)°C at 100 mW/cm² with a tungsten light source. They will be graded with respect to current output at a constant voltage of 450 mV. The cells will be grouped in a matrix of equal current outputs and the matrix will be used to select 6 cells with the same current outputs to form 6 cell submodules.

The 6 cell submodules shall be tested at 28 (±2)°C at 100 mW/cm² with a tungsten light source, similar to the test described above.

A test log of cell grouping and submodule test data will be maintained to allow compilation of the degradation values of submodule fabrication.

9.4.2 Solar Cell 3-Quadrant Characteristics Test

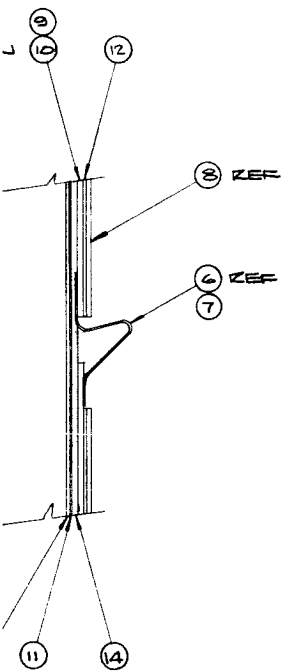
The characteristic of the solar cell E/I curve in the negative voltage and current region is not presently well known. Because of this lack of data, extrapolation into these regions leads to approximations which give deformed characteristic curves. It is the purpose of the 3-quadrant characteristic test to determine the E-I



9-15

REVISIONS				
DATE	BY	DESCRIPTION	BY	DATE

ASSEMBLY TABULATION		
ASSEMBLY DASH NO.	APPLICABLE CELL THICKNESS	APPLICABLE "P" BUS BAR NO.
-1	4 MIL	1100323-1
-2	8 MIL	1100323-2



SECTION
MODULE
SECTION
LE: 241

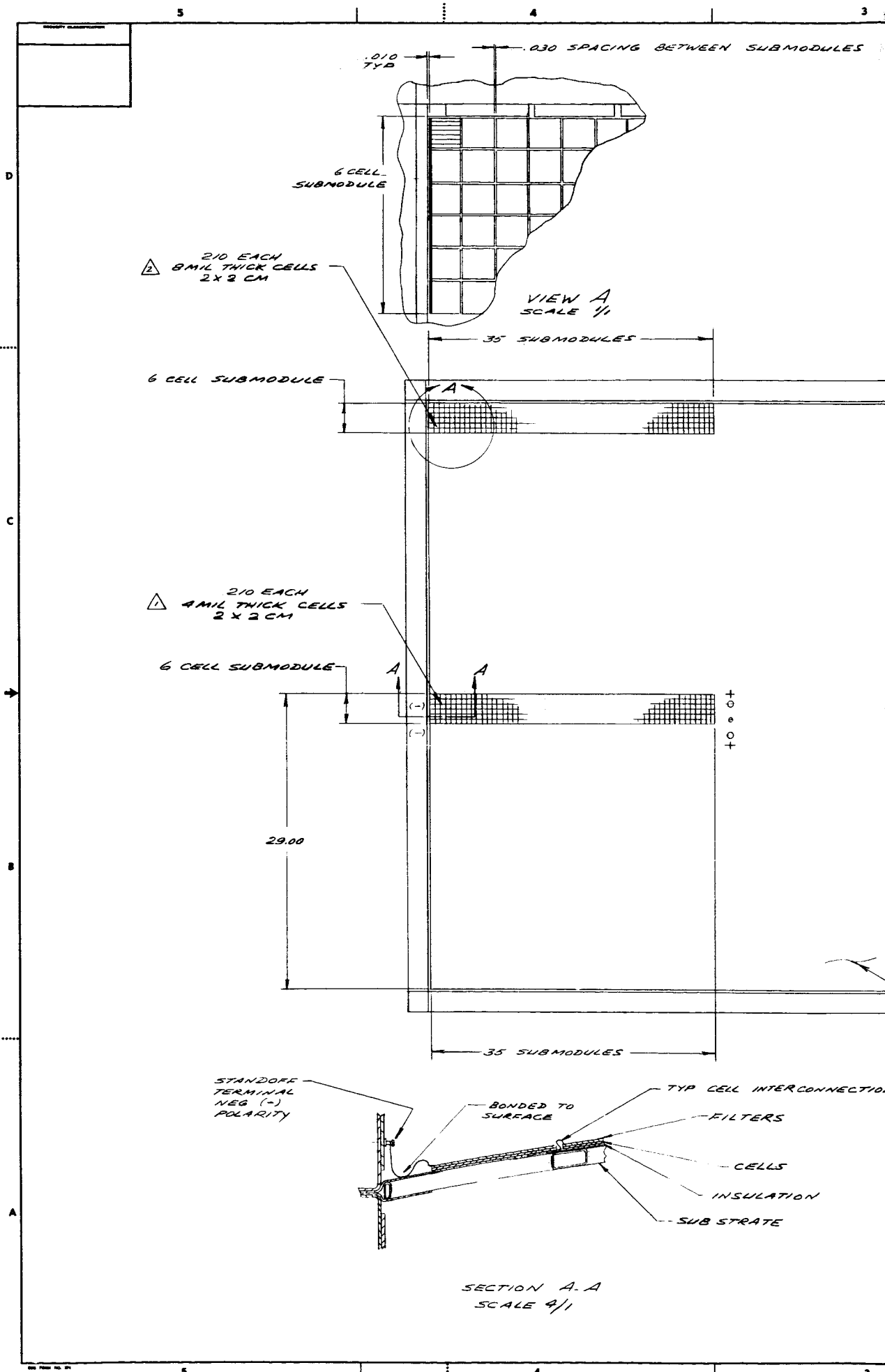
4x	14	ADHESIVE, CELL			
4x	15	ADHESIVE, DIELECTRIC			
					1100327
4x	12	ADHESIVE, FILTER			
1	11	DIELECTRIC			
36	10	CELL	2x2CM		
36	9	CELL	2x2CM		
36	8	FILTER	4MIL		
6	7	1100323-1 "P" BUS CONNECTOR			
6	6	1100323-2 "P" BUS CONNECTOR			
1	5	1100323 "P" BUS BAR			
1	4	1100324 "N" BUS CONNECTION			
1	3	1100326 "N" BUS BAR			
4	2	TERMINAL			
1	1	SUBSTRATE			

LIST OF MATERIALS

UNLESS OTHERWISE NOTED: 1. LISTED DIMENSIONS IN DECIMALS 2. TOLERANCES 3. GENERAL FINISHES UNLESS SPECIFIED 4. DIMENSIONS IN INCHES 5. DIMENSIONS IN MILLIMETERS		QUANTITY 12705 DATE 12705	PART NO. 1100327 REV. D	ELECTRO-OPTICAL SYSTEMS, INC., Pasadena, California - A Subsidiary of Xerox Corp. SAMPLE SOLAR PANEL ASSEMBLY
THIS DRAWING OR ANY INFORMATION CONTAINED HEREIN IS PROPRIETARY TO ELECTRO-OPTICAL SYSTEMS, INC. IT SHOULD NOT BE REPRODUCED, COPIED OR DISCLOSED TO ANYONE WITHOUT THE WRITTEN PERMISSION OF THIS CORPORATION.		ORIGINAL APPLICATION	12705	1100327 1/1

NO. 7027 HAS 7.428

FIG. 9-7



curve in the first, second, and fourth quadrant in order to obtain values which can be incorporated into computer programs to allow extrapolations over wide temperature and intensity ranges. These large scale extrapolations using known data points will enable the computer to obtain E-I characteristic curves which maintain a continuous form from the short-circuit to the open-circuit condition without step deformations.

The test plan for the 3-quadrant characteristic test will be generated during the period between the interim report and the final report; the test itself will also be conducted during this period.

9.4.3 Low and High Intensity Solar Cell Tests

In conjunction with the 3-quadrant characteristic test, the solar cell characteristic curve at low intensities, down to 5 mW/cm^2 , and at high intensities, up to 400 mW/cm^2 , will be obtained in order to verify the extrapolation methods performed by the computer. Again, very little data is presently available on the performance of solar cells at either very low or very high intensities (especially of solar cells that have not been fabricated for the specific operation at these particular intensities). It will be the purpose of these tests to measure standard N-P silicon solar cells with the standard number of grid lines (5 or 6) at low and high intensities, using both a tungsten light source and solar simulator to obtain cell characteristic curves over a wide range of intensities. The temperature of the cell will be kept constant at 28°C in order to eliminate the temperature as a variable parameter. These tests should lead to a better understanding of the operation of silicon solar cells over wide intensity ranges. They will culminate in preparation of a theoretical model which can be incorporated into a computer to aid in analyzing a solar photovoltaic that must operate over large ranges of intensity.

The test procedure will be formulated in the period following the interim report; the test itself will also be performed in this time period.

9.4.4 Low and High Temperature Solar Cell Tests

It will be the purpose of these tests to determine the changes in the solar cell operating parameters such as open-circuit and maximum output voltage, short-circuit and maximum-drain current, and maximum output power as a function of temperature over a large temperature range (-150 to +200°C). Very little data is available covering extremes of temperature which can be encountered in a solar photovoltaic array (0.6 to 5.2 AU). It will be the purpose of this test to measure the characteristics of a solar cell operating at a constant intensity but varying temperature in order to obtain values over large temperature ranges which can be incorporated into the computer program to aid in analyzing the performance of a solar photovoltaic array operating from 0.6 to 5.2 AU.

The test plan (and test itself) will be formulated and performed in the period between the interim and final report.

9.4.5 Demonstration and Sample Panel Electrical Tests

The purpose of the electrical tests on the assembled demonstration and sample panels is to determine by comparative measurement the effect of assembly procedures and environmental testing on electrical performance. The results of these tests will indicate any electrical degradation experienced by the celled panels. Measurements will be taken of current and voltage value for the various electrical sections when exposed to sunlight. The sunlight tests are to be conducted after electrical assembly and before and after each of the design qualification tests.

The test site is to be the sun deck facility at EOS. A calibrated cell (reference Subsection 9.4.1) is to be used as the standard by which to check the solar intensity.

The results of these tests are not meant to give prediction of the power performance of the electrical module hollow core substrate design, as this is beyond the scope of the effort; it will, however, provide a basis for performance definition. The intent of the test is to show (by absence of change in electrical output of the panel after each test) that structure concept is compatible with thin cell/filter systems.

9.5 Material Tests

9.5.1 Tensile Test of Electroformed Nickel

Tensile properties of electroformed nickel will be established throughout the development studies to insure the process variables are being kept under control and that the design properties are consistent.

It is not possible to electroform tensile specimens at the same time the structures are being electroformed; therefore, tensile specimens are fabricated before and after the structures. This gives a reliable indication of the before/after properties of the electroforming bath.

Specimens were run before and after the Phase I test specimens; results are discussed in Section 6.

Specimens will also be run before and after the Phase II samples and before and after the demonstration panels. The tensile specimens will be plated to a somewhat greater thickness than the 2-mil hollow core structure to facilitate machining and testing to ASTM E-8.

9.5.2 Bonding of Thermal Control Paint, (RTV-60), and Dielectric Adhesive to Nickel and H-Film

A series of tests will be conducted to verify that the RTV-60, thermal control paint, and the dielectric adhesive develop full bond strength when applied to nickel and H-film surfaces. The test procedure will be to apply the various coatings to each of the two materials. The coated nickel and H-film are then to be subjected to thermal shocks. If the test specimen coating exhibits no flaking or peeling, the material combination will be qualified. The tests are not meant to space-qualify the individual materials; material selection is based on use of space-proved materials.

The tests are to serve a second purpose in that they will develop application techniques for achieving minimum weight before development of the demonstration panel.

Two types of thermal control paints are to be evaluated on nickel strips and electroformed hollow core samples. One paint

is a polyurethane base type with a high-gloss black finish (Laminar X-500). The other is a flat black epoxy base type (Cat-a-Lac 463-3-8). Both materials have been used successfully on aluminum alloys for the Ranger and Mariner programs.

The cell adhesive to be evaluated on H-film is RTV-60. This adhesive has been used on many space programs.

The H-film dielectric will be bonded to the nickel hollow core with the following adhesives:

1. RTV-60
2. Epon 934A&B
3. General Electric SR-585
4. American Cyanamid Co. FM-1000

9.6 Electroforming

The supporting substrate for the solar cells is a nickel hollow core structure fabricated by an electroforming process. This subsection details the three-phase process development studies which are being performed to produce the hollow core solar panel. The three-phase study consists of:

1. Phase I - Fabrication of buckling specimens
2. Phase II - Full-scale plating tests
3. Phase III - Fabrication of demonstration panel

The first phase of this study, already completed, has shown that the nickel hollow core structure capable of carrying the required design loads can be fabricated to a weight of 0.066 lb/ft². Phase II, now in progress, will establish the process requirements for the full-scale panel. Phase III will result in production of a demonstration panel to verify the fabrication process, weight, and design allowances for the solar panel. Each of the phases is discussed in the following paragraphs.

9.6.1 Phase I - Fabrication of Buckling Specimens

The purpose of this study was to fabricate several specimens of various hollow core designs that would (1) establish feasibility of the fabrication process and (2) provide test data to establish the validity of the design analysis.

During Phase I, 41 hollow core specimens were fabricated from 6 different designs. These designs are shown in Figs. 9-9 through 9-13.

Two aluminum mandrels were fabricated for each pattern design so that structures of both 1-mil and 2-mil nickel could be fabricated. The specimens were fabricated by drilling and reaming 0.100-in.-thick 6061-T-6 aluminum. After the mandrels were prepared they were placed in the electroforming bath as shown in Fig. 9-14. The plating parameters used were:

1. Bath type -- Nickel sulfamate, consisting of analysis nickel (9.3 oz/gal), nickel chloride (0.41 oz/gal), and boric acid (5.3 oz/gal)
2. pH -- 4.2 to 4.8
3. Bath temperature -- 130 to 135°F
4. Stress -- 5-15 compressive

All specimens electroformed without difficulty. After electroforming, the specimens were immersed in a 30 percent solution of muriatic acid to etch out the aluminum mandrel. During this operation several of the 1-mil samples failed. The few that did successfully pass the etching operation subsequently failed during the cutting and casting operations. These problems did not develop with the 2-mil specimens, however. Because of these failures, the 1-mil specimens were dropped from further evaluations.

The samples were cut to size after etching, as shown in Fig. 9-15. To load the specimens from the edges in compression, a loading foot was cast along two edges from epoxy resin. A completed specimen ready for testing is shown in Fig. 9-16.

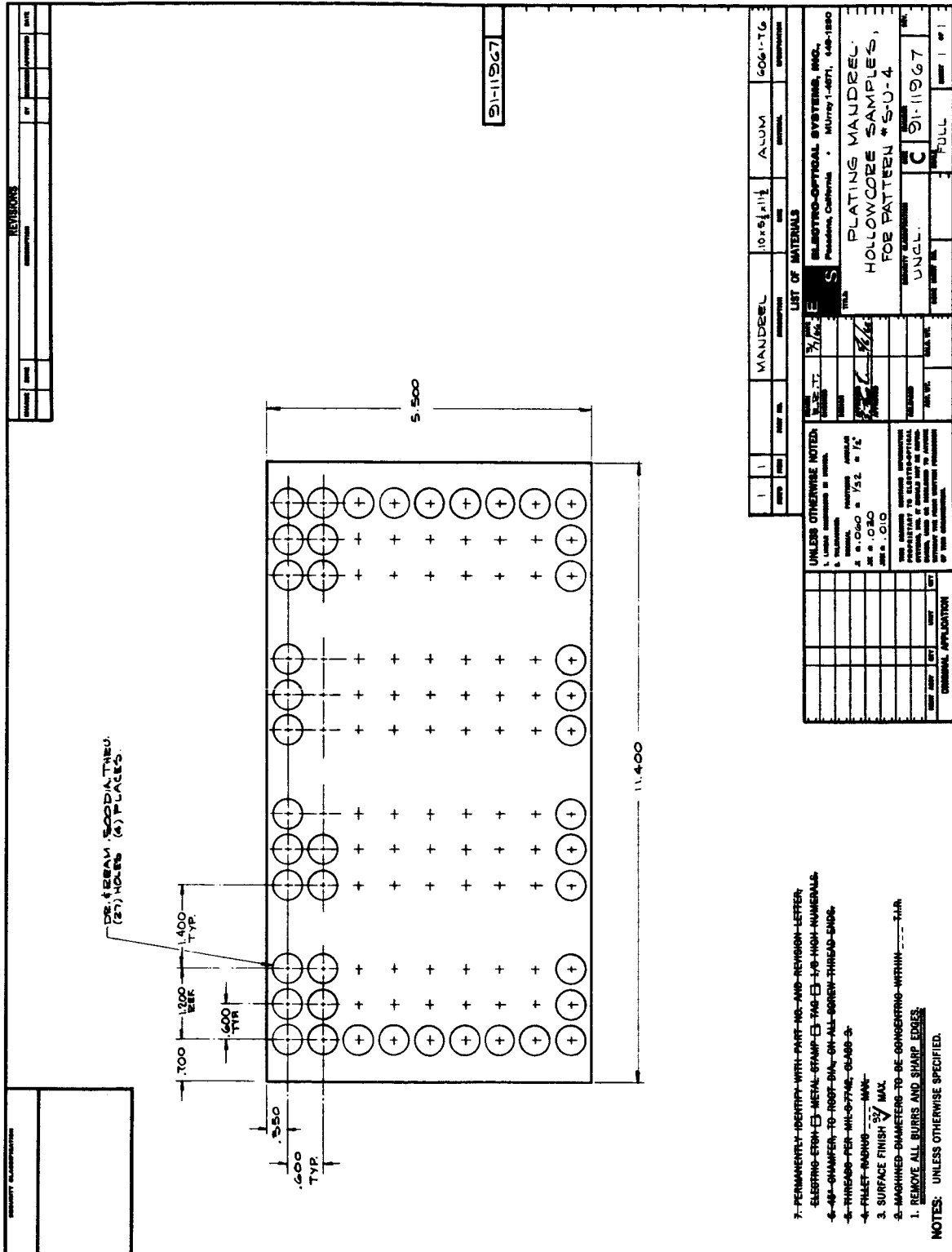
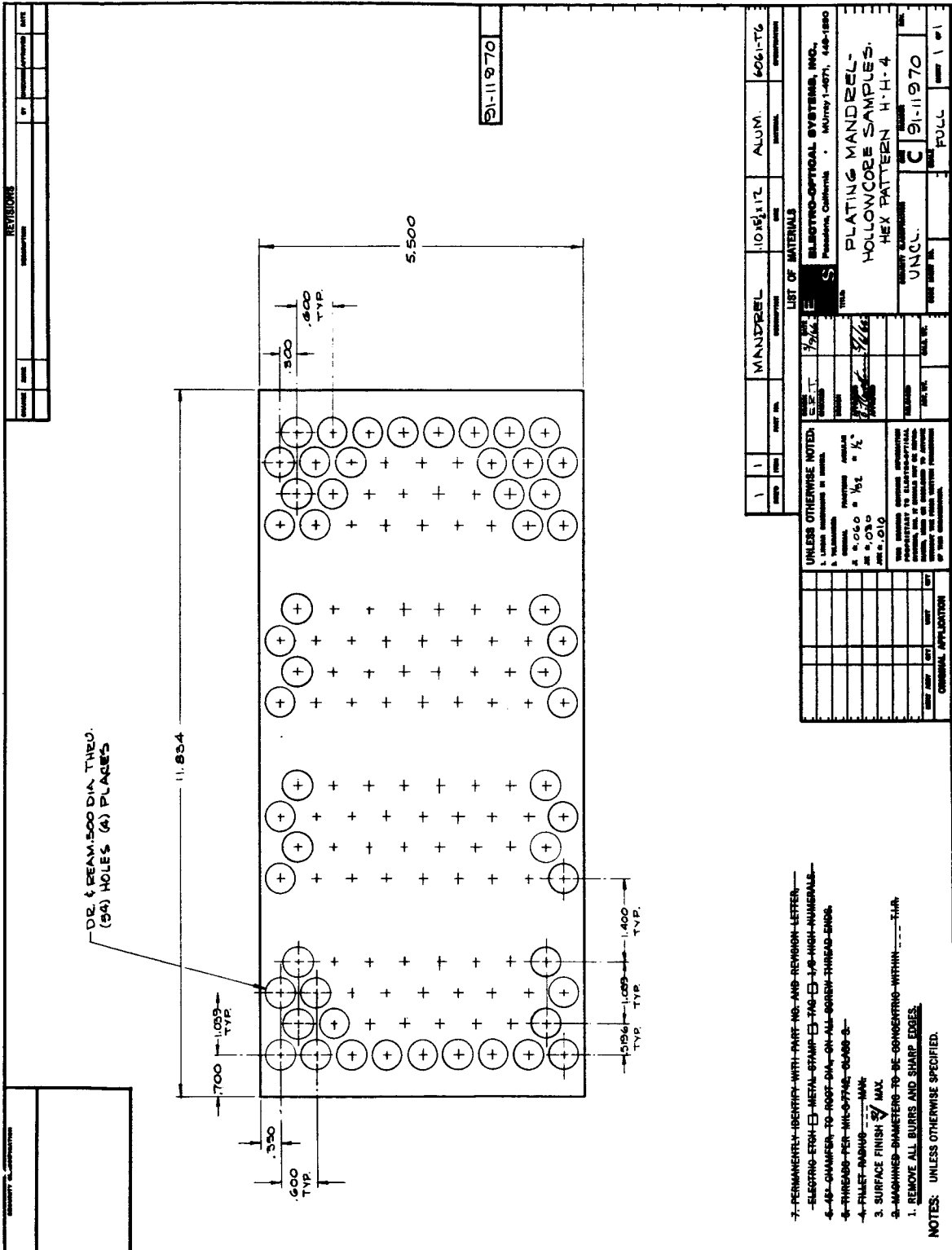


FIG. 9-10



REVISIONS	
NO.	DESCRIPTION

PROPERTY IDENTIFICATION	
NO.	DESCRIPTION

9-11-970

QTY	UNIT	DESCRIPTION	DATE	BY	CHKD
1	MANDREL	ALUM.	6061-T6		

LIST OF MATERIALS	
QTY	DESCRIPTION
1	MANDREL

UNLESS OTHERWISE NOTED	
QTY	DESCRIPTION
1	MANDREL

PROPERTY IDENTIFICATION	
NO.	DESCRIPTION

- 7- PERMANENTLY IDENTIFY WITH PART NO. AND REVISION LETTER—
 - ELECTRO-ETCH — METAL STAMP — TAG — 1/8" HIGH NUMERALS —
 - 4-45° CHAMFER TO ROOT DIA. ON ALL BORE THREAD ENDS.
 - 4- RINGGROOVE PER MIL-S-7742 — 60-60° — 3-
 - 4- FILLET RADIUS — 1/16" MAX.
 - 3- SURFACE FINISH — 32/ MAX.
 - 2- MACHINED DIMETERS TO BE CONCENTRIC WITHIN ±.010.
 - 1- REMOVE ALL BURRS AND SHARP EDGES.
- NOTES: UNLESS OTHERWISE SPECIFIED.

FIG. 9-12

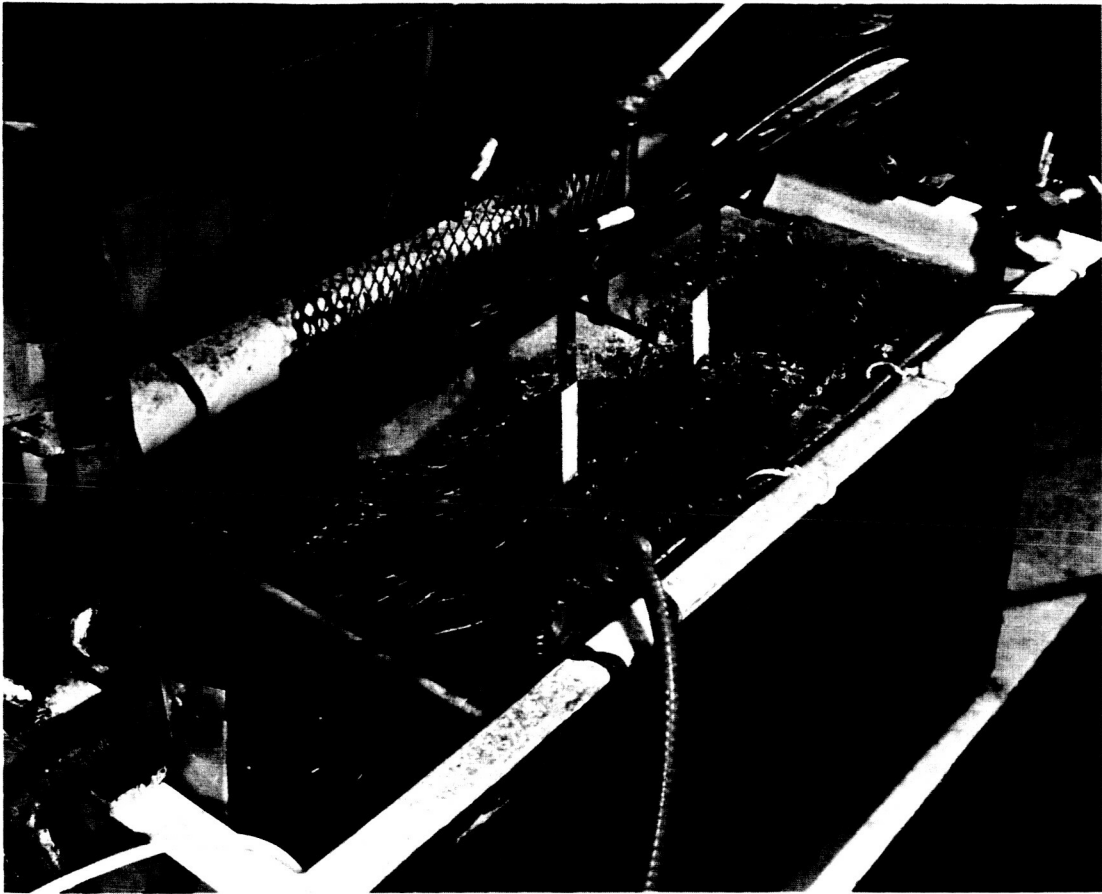


FIG. 9-14 ELECTROFORMING BATH SETUP — BUCKLING SPECIMENS

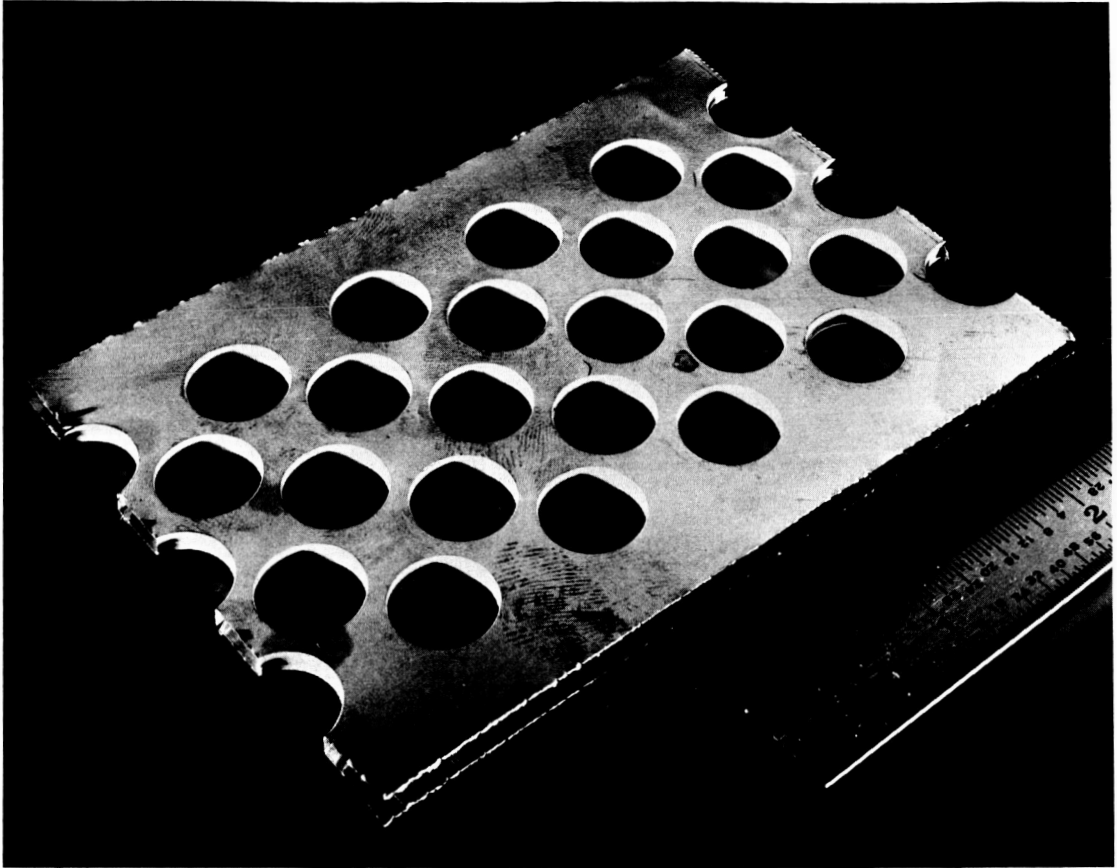


FIG. 9-15 NICKEL HOLLOW CORE STRUCTURE AFTER CUTTING AND ETCHING



FIG. 9-16 NICKEL HOLLOW CORE BUCKLING SPECIMEN READY FOR TEST

Test results for these specimens are detailed in Subsection 9.3.1 of this report. The fabrication and test of these specimens has definitely shown the feasibility of producing the hollow core structure by the electroforming process and that the nickel hollow core can meet the design load and weight requirements.

9.6.2 Phase II -- Full-Scale Plating Tests

This development study is required to establish the exact masking and plating parameters that will be used in plating the full-scale demonstration panel. Experience has shown that scale-up of masking and anode placement does not always prove successful.

This study will establish the full-scale plating bath and the masking and anode placements to be used. An etching study will also be made on a full-scale panel. These studies will be made using a commercially available perforated aluminum sheet for the mandrel. The mandrel will have hole sizes of 7/8 in. dia spaced on 1-1/8 in. staggered centers. The mandrel will give approximately 55 percent open area. The mandrel will be reamed and chamfered to give the required plating surface. If the forming tool for the demonstration panel mandrels is completed in time, the perforated mandrels will be formed to the contour before the plating tests are run; if not, the mandrels will be plated flat. The major tasks that will be performed under this study are:

1. Set up the full-scale plating bath, consisting of agitation, reciprocation, establishing and monitoring bath parameters, and determination of mask and anode arrangement.
2. Fabricate sample panels. This effort includes completion of perforated screen mandrel, electroforming, performance of etch study and conducting section and thickness checks.

9.6.3 Phase III -- Model Demonstration Panel

The final phase of the process development studies is the fabrication of a demonstration model panel. This panel will be fabricated using the processes developed under the Phase I and II studies. The fabrication will be controlled with a structure manufacturing process specification developed from the Phase I and II data. (The preliminary specification is included as Appendix A. It will be changed as required by the Phase II study data.)

Three mandrels will be fabricated to insure attainment of the demonstration panel. The three mandrels will be produced by stack drilling. The major tasks in this phase will be:

1. Fabricate mandrels. Effort involves drilling, reaming, and polishing; fabrication of forming mold; and forming of mandrels.
2. Electroform mandrels
3. Etch aluminum mandrels
4. Bond hollow core structure to supporting frame

9.7 Structural Bond (Frame to Frame and Substrate to Clip Bracket)

Tests are to be conducted to evaluate the physical properties and viscoelastic damping effect of the FM-1000 epoxy adhesive used to bond the frame section together and to bond the hollow core to the attachment clip. The tests will evaluate the amount of damping added and the pull and peel strength of the nickel-to-aluminum and aluminum-to-aluminum interfaces. The tests will be conducted to determine shear strength on tensile shear samples and evaluate internal damping on cantilevered laminated prismatic beams.

The test results will define process specifications to achieve specific strength of material characteristics; they will also determine bond line thickness requirements to obtain maximum structural damping for minimum weight.

APPENDIX A

MANUFACTURING PROCESS SPECIFICATION OUTLINES

APPENDIX A
MANUFACTURING PROCESS SPECIFICATION OUTLINES

This appendix contains outlines for the manufacturing process specifications written for the fabrication and assembly of the demonstration panel. The purpose of these specifications is to serve as a record of the critical areas of manufacturing of this new concept in solar arrays. The electroforming of large hollow core substrates, the assembly of thin 4-mil cells into submodules, and their attachment to the substrate are the particular processes to be documented. The specifications define the innovations in tooling and fabrication techniques required to achieve a structurally and electrically sound solar panel.

A1 Preliminary Hollow Core Structure--Process Specification Outline

1.0 Mandrel

- 1.1 Material - Aluminum 6061-T6 (QQA 327)
- 1.2 Hole pattern - per EOS Drawing 1100317
- 1.3 Contour - per EOS Drawing 1100317

2.0 Electroforming

- 1.1 Material - Electroformed nickel
- 1.2 Bath - Sulfamate nickel
(Ni-9.3 oz/gal; NiCl₂-0.41 oz/gal; HBO₃-5.5 oz/gal)
- 1.3 Plating parameters:
 - pH = 4.2 to 4.8
 - current density = 60 amp/ft²
 - bath temperature = 130 - 135°F
 - stresses = 5-15 compressive
 - time = as required by thickness

- 1.4 Tensile panel before electroforming panel
(thickness 0.010 in.)
- 1.5 Tensile panel after electroforming panel
- 1.6 Handling of panel after electroform (use white gloves)
- 3.0 Etch aluminum mandrel (white gloves)
 - 3.1 Solution - 30 percent (by vol) muriatic acid
 - 3.2 Position - vertical (remove and reimmerse as required)
 - 3.3 Time - until reaction stops
 - 3.4 Change solution
 - 3.5 Check for further reaction
- 4.0 Bonding to support frame
(process to be developed)

A2 Demonstration Panel Electrical Assembly Process Specification Outline

- 1.0 Solar cell grading
 - 1.1 Cell and filter handling and storage
 - 1.2 Grading test procedure
 - 1.3 Tooling and facilities requirements
- 2.0 Submodule Assembly
 - 2.1 Interconnector and cell assembly
 - 2.2 Application of filter
 - 2.3 Testing of submodule
 - 2.4 Tooling and facilities requirements
- 3.0 Dielectric and thermal control application to demonstration panel
 - 3.1 Application of dielectric
 - 3.2 Application of thermal control coating
 - 3.3 Tooling and facilities requirements
- 4.0 Submodule assembly on demonstration panel
 - 4.1 Bonding submodules to dielectric
 - 4.2 Tab and interconnection soldering
 - 4.3 Cabling of demonstration panel
 - 4.4 Tooling and facilities requirements

5.0 Performance testing of demonstration panel

5.1 Test facilities and instrumentation

5.2 Demonstration panel handling

APPENDIX B
ANALYSIS OF STRUCTURAL CONCEPTS (TRADE STUDIES)

APPENDIX B
ANALYSIS OF STRUCTURAL CONCEPTS (TRADE STUDIES)

B.1 STRUCTURE TRADE STUDIES

Considerable effort has been expended upon studies and evaluations of various solar panel structures for use on the demonstration panel. Analysis associated with this effort may be found in the attached sections. It was found that the electroformed biconvex construction lends itself readily to application involving environments described in the design criteria, with weight estimates equal to or less-than the other concepts evaluated. Five different design concepts were picked for evaluation in this study: 3 rigid and 2 semi-rigid designs. These designs are described in the following subsections.

B.1.1 Conventional Flat Plate Construction

The solar panel substrate is of sandwich construction with corrugated reinforcement on the backside. The substrate is attached to box beams carrying the load back to the spacecraft. Both aluminum and beryllium alloys were evaluated; the latter was found optimum with an average specific weight W of

$$W = 0.4129 \text{ lb/ft}^2 \text{ (including cells)}$$

B.1.2 Prestressed Tapes

In this concept, narrow, thin fiber glass tapes are stretched in a "beach chair" arrangement over a frame structure. The tapes are arranged such that the solar cells are supported along the edges and open over the remaining area. The prestress precludes significant additional loading caused by environment. The frame must withstand both the prestress and environmental loads during boost phase. This report indicates an average weight of

$$W = 0.374 \text{ lb/ft}^2 \text{ (including cells)}$$

B.1.3 Prestressed Diaphragm

In this concept a thin membrane is used instead of the inter-laced tapes. The diaphragm will be able to transmit shear better than in the tape concept. In addition, a reduced prestress can be used, thus reducing the size of the frame assembly. This report indicates an average specific weight of:

$$W = 0.3054 \text{ lb/ft}^2$$

The frame must be reinforced to withstand the boost phase environment, increasing the frame weight:

$$W = 0.345 \text{ lb/ft}^2$$

B.1.4 Honeycomb Construction

This design is similar to the one of Subsection B.1.1, with the only difference being that the substrate is of double-sheet construction with honeycomb core bonded between the sheets. Beryllium sheets of 0.002 inch will be used for the facing sheet and aluminum sheets of 0.0006 inch for the core, bonded into an assembly. The substructure will be similar to that in Subsection B.1.1. The average specific weight will be

$$W = 0.4148 \text{ lb/ft}^2$$

B.1.5 Hollow Core Biconvex Solar Panel

This design incorporates the inherent rigidity of the curved panel as well as its membrane-type loading characteristic. All the unnecessary material has been removed from the panel surface; the panel is supported along the edges by flexible clips to assure simple support, minimizing any induced moment in the structure. The clips are attached firmly to a rigid frame structure, thus assuring complete edge support of the hollow core.

The analysis of this concept is included in Appendixes C and D. The average specific weight has been calculated to be

$$W = 0.3397 \text{ lb/ft}^2$$

B.2 Concept Analyses

The following pages comprise documentation on the analyses for the five concepts considered.

CALCULATION SHEET

By _____

Subject _____ Checked By _____ Date _____

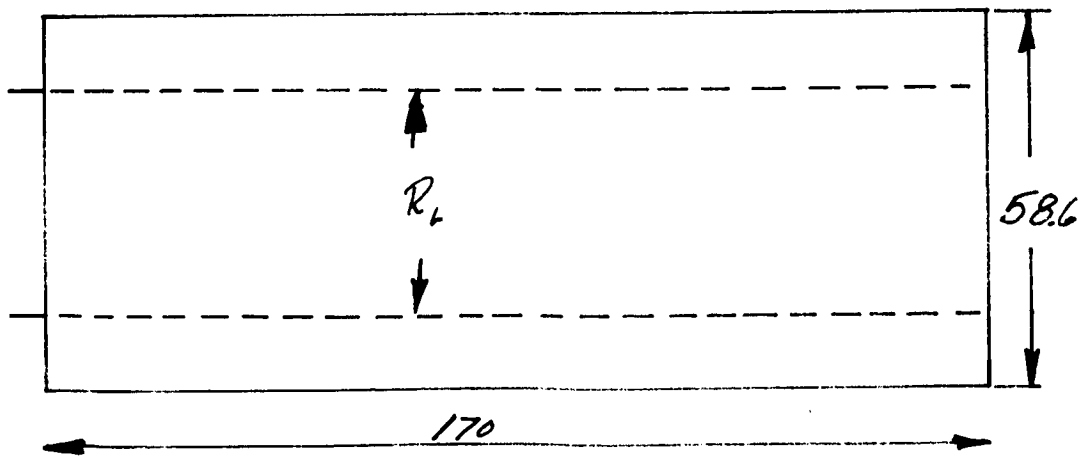
ELECTRO-OPTICAL SYSTEMS, INC.

STRUCTURAL STUDIES

5 DESIGNS HAVE BEEN CONSIDERED IN THE STUDY AND EACH WILL BE EVALUATED FOR ITS MERITS.

1. FLAT PLATE WITH CORRUGATED BACK STRUCTURE AND STRUCTURAL BEAMS
2. PRESTRESSED TAPES
3. PRESTRESSED DIAPHRAGM
4. HONEY COMB STRUCTURE
5. BICONVEX HOLLOW-CORE CONSTRUCTION.

10.4.1.1.1 FLAT PLATE CORRUGATIONS



SOLAR CELL WEIGHT : 0.160 ^{lb}/FT²

BY PLACING THE SUPPORT BEAMS AT $R_L = 0.55 \cdot 58.6$

THE MOMENT IS MINIMIZED

OVER HANG $M = \frac{w}{g} 0.022 l^2 \ddot{\delta} Q$

7027-IDR

EOS Form No. 6303 (7/64-200)

E.4

CALCULATION SHEET

By _____

Subject _____ Checked By _____ Date _____

ELECTRO-OPTICAL SYSTEMS, INC.

$$W = \text{WEIGHT PER UNIT AREA}$$

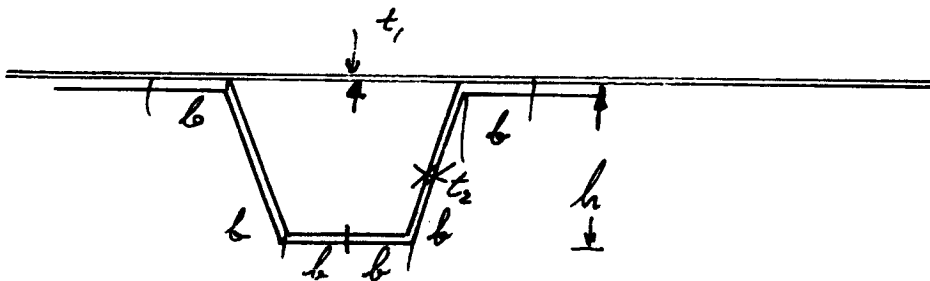
$$= W_{\text{SOLAR CELL}} + W_{\text{STRUCTURE}}$$

$$\ddot{S} = \text{INPUT ACCELERATION} = 1.5g$$

$$Q = \text{GAIN} = \frac{40}{\text{e}}$$

$$L = 58.6 \text{ IN}$$

$$M = W_f \cdot 0.022 \cdot 58.6^2 \cdot 1.5 \cdot 40 = \underline{\underline{4533 \text{ W}}}$$



$$\text{PITCH} = 6b$$

PER PITCH :

$$W_f = (6b \cdot t_1 + 4b \cdot t_2 + 2\sqrt{b^2 + h^2} t_2) \rho$$

$$= b(6t_1 + 4t_2 + 2\sqrt{1 + (\frac{h}{b})^2} t_2) \rho$$

$$I_{\text{PITCH}} = 4bt_2 \cdot (\frac{h}{2})^2 + \frac{7}{12} \sqrt{b^2 + h^2} t_2^3 \approx \underline{\underline{bh^2 t_2}}$$

TOP SHEET IN EFFECTIVE.

$$\underline{t_1 = 0.005 \text{ IN}}$$

PER INCH:

$$W_{\text{FIN}} = \frac{1}{6} \rho (6t_1 + 4t_2 + 2\sqrt{1 + (\frac{h}{b})^2} t_2) \rho$$

$$= (t_1 + \frac{2}{3} t_2 + \frac{1}{3} \sqrt{1 + (\frac{h}{b})^2} t_2) \rho$$

CALCULATION SHEET

By _____

Subject _____ Checked By _____ Date _____

ELECTRO-OPTICAL SYSTEMS, INC.

$$I = \frac{1}{6} b \cdot b h^2 t_2 = \underline{\underline{\frac{1}{6} h^2 t_2}}$$

$$f = \frac{M}{\frac{I}{c}} = \underline{\underline{\frac{4533 \left(\frac{0.160}{144} + \left(t_1 + \frac{2}{3} t_2 + \frac{1}{3} \sqrt{1 + \left(\frac{t_1}{b} \right)^2} t_2 \right) \right)}{\frac{1}{3} h t_2}}}$$

$F_{CR} =$ $A_L = 64000 \text{ PSI}$ $B_E = 40000 \text{ PSI}$

$$F_{CR \text{ BUCKLING}} = \frac{0.8 \cdot 5.41 \cdot \pi^2 \cdot E}{12(1-\nu^2)} \frac{t^2}{b^2} = 3.912 \frac{E t^2}{b^2}$$

ASSUME 5 MIL IS MINIMUM SHEET GAGE TO USE:

$$F_{CR} = \underline{\underline{97.792 \frac{E}{b^2} 10^{-6}}}$$

$$F_{CRAL} = \underline{\underline{977.92 \frac{1}{b^2}}}$$

$$F_{CRBE} = \underline{\underline{2738 \frac{1}{b^2}}}$$

ASSUME $h = 0.50 \text{ IN}$ $t_1 = t_2 = 0.005 \text{ IN}$

$$f = \frac{5.037 + 12.103 + 2.43 \sqrt{1 + \left(\frac{0.5}{b} \right)^2}}{\frac{1}{3} 0.5 \cdot 0.005} = \underline{\underline{20568 + 2916 \sqrt{1 + \left(\frac{0.5}{b} \right)^2}}}$$

$F_{CRAL} \quad b = 0.160 \text{ IN}$

$F_{CRAL} = \underline{\underline{38200 \text{ PSI}}}$

$F_{CRBE} \quad b = 0.265 \text{ IN}$

$F_{CRBE} = \underline{\underline{39000 \text{ PSI}}}$

B-6

CALCULATION SHEET

By _____

Subject _____ Checked By _____ Date _____

ELECTRO-OPTICAL SYSTEMS, INC.

CHECKS

$$H.S. \gamma = \underline{\underline{+}}$$

$$W_{ST} = 144 \left(0.005 + \frac{2}{3} 0.005 + \frac{1}{3} \sqrt{1 + \left(\frac{0.5}{l}\right)^2} 0.005 \right) g$$

#

$$W_{STAL} = 14.4 \left(0.005 + 0.0033 + \frac{1}{3} \sqrt{1 + \frac{0.5}{0.16} = 0.005} \right)$$

$$= \underline{\underline{0.1987}} \text{ #/FT}^2$$

$$W_{STBE} = 14.4 \cdot 0.756 \left(0.005 + 0.0033 + \frac{1}{3} \sqrt{1 + \left(\frac{0.5}{0.265}\right)^2} \right)$$

$$= \underline{\underline{0.1292}} \text{ #/FT}^2$$

BEAMS

$$M = 0.13 W l^2 \ddot{\theta} Q$$



W = WEIGHT OF SUBSTRATE AND BEAM.

$\ddot{\theta}$ = INPUT $g = 1.5g$

$Q = 10$

$l = 170 \text{ IN}$

$$M = 0.13 \cdot 170^2 \cdot 1.5 \cdot 10 W = \underline{\underline{56355 W}}$$

$$W_{SUBSTRATE} = \frac{1}{2} 58.6 \frac{W_{ST} + W_{SC}}{144} = \underline{\underline{0.073}} \text{ AL}$$

$$\underline{\underline{0.059}} \text{ BE}$$

B-7

CALCULATION SHEET

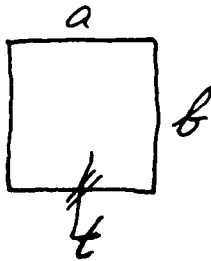
By _____

Subject _____ Checked By _____ Date _____

ELECTRO-OPTICAL SYSTEMS, INC.

**E
O
S**

BOX BEAM



$$I = 2at \cdot \left(\frac{b}{2}\right)^2 = \underline{\underline{\frac{1}{2} ab^2 t}}$$

$$A = \underline{\underline{2(a+b)t}}$$

THERE ARE GOING TO BE HOLES IN THE SIDE OF THE BEAM.

$$W_{BEAM} = 2(a+b)t \cdot \rho$$

USE $a = 1$ IN

$b = \underline{\underline{1.5}}$ IN

$$W_{BEAM} = \underline{\underline{5t\rho}}$$

$$I = \underline{\underline{1.125t}}$$

$$M = \underline{\underline{56355 \left(\frac{0.073}{0.059} + 5t\rho \right)}}$$

$$f = \frac{M}{\frac{I}{c}} = \frac{56355 \left(\frac{0.073}{0.059} + 5t\rho \right)}{\frac{1.125t}{0.75}} = 37570 \left(5.8 + \frac{t}{0.059} \right)$$

$$F_{CE} = \frac{0.8 \cdot 5.41 \cdot 10^{12} E}{12(1-\nu^2)} \left(\frac{t}{b}\right)^2 = \underline{\underline{3.912 Et^2}}$$

$$F_{CRAL} = \underline{\underline{39.12 t^2 \cdot 10^6}} \quad t = \underline{\underline{0.050}}$$

$$F_{CRBF} = 109.536 t^2 \cdot 10^6 \quad t = \underline{\underline{0.064}}$$

CALCULATION SHEET

By _____

Subject _____ Checked By _____ Date _____

ELECTRO-OPTICAL SYSTEMS, INC.

WEIGHT:

BEAM PER INCH: AL 549 = $5 \cdot 0.05 \cdot 0.1 = \underline{0.025 \text{ #/IN}}$

BE 57 0.0752 = $5 \cdot 0.064 \cdot 0.0752 = 0.024 \text{ #/IN}$

PANEL WEIGHT

ALUMINUM
SUBSTR. $170 \cdot 58.6 \frac{1}{144} (0.160 + 0.1987) = \underline{24.815 \text{ LBS}}$

BEAMS: $2 \cdot 170 \cdot 0.025 = \underline{8.500 \text{ LBS}}$

NET $\underline{33.315 \text{ LBS}}$

PER FT² = $\underline{0.481 \text{ #/FT}^2}$ ALUMINUM

PER FT² = $0.160 + 0.1292 + 0.1237 = \underline{0.4129 \text{ #/FT}^2}$

BERYLLIUM.

CALCULATION SHEET

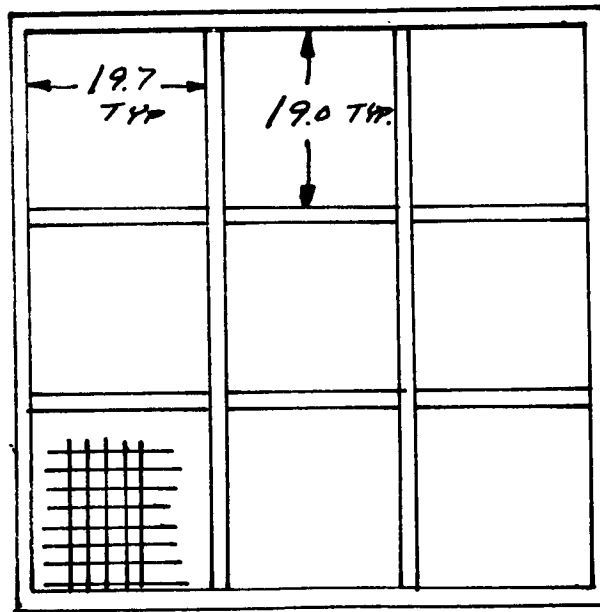
By _____

Subject _____ Checked By _____ Date _____

ELECTRO-OPTICAL SYSTEMS, INC.

PRESTRESSED TAPES.

PRESTRESSED FIBERGLASS-REINFORCED TAPES ARE STRUNG OVER A FRAME NETWORK AS SHOWN BELOW.



FIBERGLASS : 0.003 THICK X 0.200 WIDE , PITCH
0.800 IN

$F_{tu} = 140000 \text{ PSI}$

$E = 6.2 \cdot 10^6$

$P = 90^\circ/\text{IN}$

FRAME : LOCKALLOY

$F_{tu} = 53000 \text{ PSI}$

$F_{ty} = 40000 \text{ PSI}$

$\rho = 0.0756 \text{ \%/IN}^2$

$E = 28 \cdot 10^6 \text{ PSI}$

7027-IDR

B-10

EOS Form No. 6303 (7/64-200)

CALCULATION SHEET

By _____

Subject _____ Checked By _____ Date _____

ELECTRO-OPTICAL SYSTEMS, INC.

PRESSTRESSED TAPE : 90 #/IN

$$f = \frac{90}{\frac{0.003 \times 0.2}{0.8}} = \underline{\underline{120\,000\text{ PSI}}}$$

MAXIMUM TAPE STRESS SHOULD BE

$$P = 84 \#/\text{IN}$$

FRAME MOMENT :

$$M = \frac{1}{2} P \cdot 19.7^2 = \frac{1}{2} 84 \cdot 19.7^2 = \underline{\underline{2717\text{ INCHES}}}$$

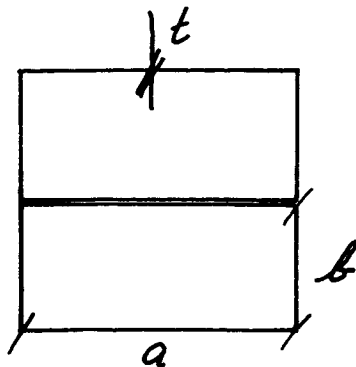
$$P_c = 19 \cdot \frac{1}{2} \cdot 84 = \underline{\underline{798\text{ LBS}}}$$

BY USING AN UPPER AND LOWER FRAME
WE HAVE :

$$A = 2(2(a+b)) \cdot t = \underline{\underline{4(a+bt)}}$$

$$I = 4bt \cdot \left(\frac{a}{2}\right)^2 + \frac{4}{12} a^3 t$$

$$= \underline{\underline{a^2 t \left(b + \frac{1}{3}a\right)}}$$



$$r = \sqrt{\frac{I}{A}} = a \sqrt{\frac{3b+a}{12(a+b)}}$$

$$= \underline{\underline{\frac{a}{2} \sqrt{\frac{3b+a}{3(a+b)}}}}$$

$$F_{CR\text{ BUCKLING}} = \frac{\pi^2 0.8 \cdot 698 \cdot 28 \cdot 10^6}{12(1-0.3^2)} \left(\frac{t}{b}\right)^2 = \underline{\underline{40\,000\text{ PSI}}}$$

$$\left(\frac{t \cdot 10^3}{b}\right)^2 = 283.06 = 283.06$$

$$t \cdot 10^3 = \underline{\underline{16.95\text{ b}}}$$

CALCULATION SHEET

By _____

Subject _____ Checked By _____ Date _____

ELECTRO-OPTICAL SYSTEMS, INC.

$b = 0.2$	$t = 0.003$
$b = 0.3$	$t = 0.005$
$b = 0.4$	$t = 0.007$
$b = 0.5$	$t = 0.0085$
$b = 0.6$	$t = 0.010$
$b = 0.7$	$t = 0.012$
$b = 0.75$	$t = \underline{\underline{0.013}}$

$$F_{CR} = \frac{\pi^2 E}{\left(\frac{cL}{r}\right)^2} = \frac{2\pi^2 E}{\left(\frac{L}{r}\right)^2}$$

FOR $b = 0.75$

$$a = 2.00$$

$$r = 1000 \sqrt{\frac{3 \cdot 0.75 + 2.00}{3(2.75)}} = \underline{\underline{.718 \text{ in}}}$$

$$F_{CR} = \frac{2 \cdot 9.86959 \cdot 28.10^6}{\left(\frac{19.7}{0.718}\right)^2} = \underline{\underline{\text{HIGH}}}$$

$$b = 0.6$$

$$a = 1.2$$

$$r = \underline{\underline{0.447}}$$

FACE BUCKLING MORE CRITICAL

FOR $b = 0.6$ $a = 1.2$ $t = 0.010 \text{ in}$

$$A = 4(0.6 + 1.2)t = \underline{\underline{0.072 \text{ in}^2}}$$

7027-IDR

EOS Form No. 6303 (7/64-200)

$$I = 1.2^2 \cdot 0.01 (0.6 + 0.4) = \underline{\underline{0.0144 \text{ in}^4}}$$

B-12

CALCULATION SHEET

By _____

Subject _____ Checked By _____ Date _____

ELECTRO-OPTICAL SYSTEMS, INC.

X SECTION IS TOO SMALL
SELECT 2 x 0.75 BOX

$$I = a^2 t \left(b + \frac{1}{3} a \right) = \underline{\underline{5.666 t}}$$

$$A = 4(2.75)t = \underline{\underline{11t}}$$

$$f_c = \frac{P}{A} = \frac{798}{11t} = \frac{72.5}{t}$$

$$f_b = \frac{Mc}{I} = \frac{2717}{5.666t} = \frac{479.5}{t}$$

$$f = f_c + f_b = \frac{1}{t} (72.5 + 479.5) = \frac{552}{t}$$

$$t = \left(\frac{40000}{552} \right)^{-1} = 0.0138 \sim \underline{\underline{0.014 \text{ IN}}}$$

Box 2 x 0.75 x 0.014 IN

FRAME WEIGHT:

$$W = 11t \cdot 0.075 \cdot (64.1 + 64.1 + 62.0 + 62.0)$$

$$= \underline{\underline{2.936 \#}}$$

STIFFENERS

$$L = 19.7 \text{ IN}$$

box c x d

$$c = 0.75 \text{ IN}$$

$$F_{CR} = 40000 = \frac{27 \times 10^6 E}{\left(\frac{L}{r} \right)^2} \quad \left(\frac{L}{r} \right)^2 = \frac{2 \cdot 9.86958 \cdot 28 \times 10^6}{40000}$$

CALCULATION SHEET

By _____

Subject _____ Checked By _____ Date _____

ELECTRO-OPTICAL SYSTEMS, INC.

$$\left(\frac{l}{r}\right)^2 = 13817$$

$$r^2 = \frac{19.7^2}{13817} = 0.028$$

$$r = \underline{0.168 \text{ IN}}$$

Box 0.75 x 0.75

$$r = \frac{a}{2} \sqrt{\frac{3b+a}{3(a+b)}} = \frac{a\sqrt{2}}{2\sqrt{3}} = \underline{0.307 \text{ IN}}$$

STIFFENER 0.75 x 0.75 x t ONE ON EACH SIDE.

$$A = 4 \cdot 0.75 \cdot t \times 2 = 6.0 t$$

$$P = 19.7 \times 84 = \underline{\underline{1654.8 \text{ LBS}}}$$

$$f = \frac{P}{A} = \frac{1654.8}{t \cdot 6} = \underline{\underline{275.8 \frac{1}{t}}}$$

$$t = \underline{\underline{0.007 \text{ IN}}}$$

IN CASE OF UNEVEN LOADING

$$t = \frac{3}{2} \cdot 0.007 = \underline{\underline{0.011 \text{ IN}}}$$

STIFFENER WEIGHT.

$$W = 6.0 t \cdot 0.0756 (6 \cdot 19.7 + 120) = \underline{\underline{1.1885 \text{ *}}}$$

FRAME WEIGHT:

$$W = 2.936 + 1.189 + 0.1(2.936 + 1.189) = \underline{\underline{4.538 \text{ LBS}}}$$

L-14

$$7027\text{-IDR } W_x = \frac{4.538}{23.91} = \underline{\underline{0.198 \text{ #/FT}^2}}$$

EOS

CALCULATION SHEET

ELECTRO-OPTICAL SYSTEMS, INC.

STRAP WEIGHT

$$W = \underline{\underline{0.015}} \text{ #/FT}^2$$

TOTAL STRUCTURE WEIGHT MUST INCLUDE
ADHESIVE : USE 1.5 MIL

$$W = 0.028$$

$$W_x = 0.00122 \text{ #/FT}^2$$

$$W_x = 0.015 + 0.00122 + 0.198 = \underline{\underline{0.214}} \text{ #/FT}^2$$

EXCLUDING CELLS:

$$W_T = 0.214 + 0.160 = \underline{\underline{0.374}} \text{ #/FT}^2$$

6-15

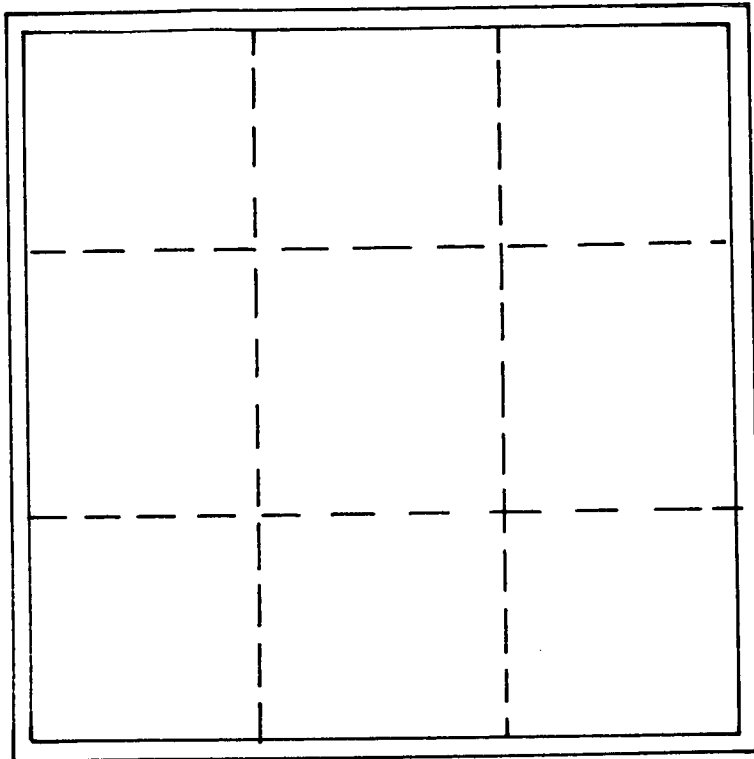
CALCULATION SHEET

By _____

Subject _____ Checked By _____ Date _____

ELECTRO-OPTICAL SYSTEMS, INC.

PRESTRESSED DIAPHRAGM



$$T_1(T_p + T_1)^2 = \frac{1.48}{6} W_0^2 \left(\frac{2}{\pi} g_0 + g_{STAT} \right)^2 \left(\frac{b}{2} \right)^3 \cdot t \cdot E$$

$W_0 =$ WEIGHT PER SQUARE INCH.

$$g_0 = 1.5 \cdot 40 = 60 g.$$

$$b = n \cdot b_1$$

$$a = n \cdot a_1$$

b = 1.6

**E
O
S**

CALCULATION SHEET

By _____

Subject _____ Checked By _____ Date _____

ELECTRO-OPTICAL SYSTEMS, INC.

$$T_i (T_p + T_i)^2 = \frac{1+\nu}{6} W_0^2 (2/\pi 60 + 0)^2 \left(\mu \frac{b}{2} \right)^3 t \cdot E$$

$$W_0 = \frac{0.160}{144} + W_s = \underline{\underline{0.00121}}$$

$$\nu = 0.3$$

$$b = 30.25 \cdot 2$$

$$\mu = \frac{1}{3}$$

$$t = 0.001$$

$$E = 2 \cdot 10^6, 10 \cdot 10^6, 6.2 \cdot 10^6 \quad 10^5$$

$$T_i (T_p + T_i)^2 = \frac{1.3}{6} \left(0.00121 \cdot \frac{120}{3.14159} \right)^2 \left(\frac{1}{3} \frac{60.5}{2} \right)^3 0.001 \cdot E$$

$$= \underline{\underline{475.15 E \cdot 10^{-6}}}$$

FOR BERYLLIUM

$$T_i (T_p + T_i)^2 = 13304$$

$$T_p = 10, 15, 20, 25, 30$$

$$T_i = 18, 15, 13, 11, 9$$

FOR ALUMINUM

$$T_i (T_p + T_i)^2 = 4751.5$$

$$T_p = 10, 20, 30, 40, 50, 60, 70$$

$$T_i = 11, 6.5, 4.1, 2.7, 1.8, 1.3$$

B-17

ELECTRO-OPTICAL SYSTEMS, INC.

USING A PRESTRESS OF 30 #/IN
WILL PRODUCE :

MAX 39 #/IN IN BERYLLIUM
34.1 #/IN IN ALUMINUM

MEMBRANE WILL IN ALL CASES PRODUCE
MARGIN OF SAFETY.

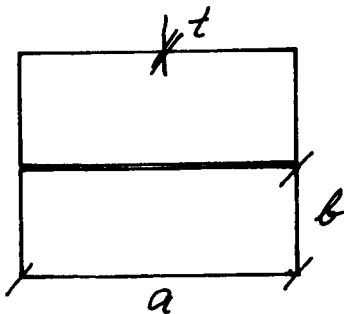
WEIGHT OF MEMBRANE:

$$t = 0.001$$

$$W = 0.144 \cdot S = \frac{0.0144 \text{ #/FT}^2}{0.0109 \text{ #/FT}^2}$$

FRAME:

DOUBLE BOX SECTION WILL BE USED. AS FOR 6.2.1.2



$$A_{TOT} = 2(2(a+b)t) = \underline{4(a+b)t}$$

$$I = a^2 t (b + \frac{1}{3}a)$$

$$r = \sqrt{\frac{I}{A}} = \frac{a}{2} \sqrt{\frac{3b+a}{3(a+b)}}$$

$$F_{CR} = \eta \frac{\pi^2 E \cdot K}{12(1-\nu^2)} \left(\frac{t}{b}\right)^2$$

FACE BUCKLING

$$F_{CR} = \eta \frac{\pi^2 E}{\left(\frac{c \cdot l}{r}\right)^2}$$

COLUMN BUCKLING

B-18

CALCULATION SHEET

By _____

Subject _____ Checked By _____ Date _____

ELECTRO-OPTICAL SYSTEMS, INC.

$$F_{CRB} = 0.8 \frac{\pi^2 \cdot E (6.98)}{12(1-0.3^2)} \left(\frac{t}{b}\right)^2 = \underline{\underline{5.047 E \left(\frac{t}{b}\right)^2}}$$

FOR BERYLLIUM

$$F_{CR} = \underline{\underline{141.312 \left(\frac{t}{b}\right)^2 \cdot 10^6}} \quad F_{CY} = \underline{\underline{40000 \text{ PSI}}}$$

ALUMINUM

$$F_{CR} = 50.47 E \left(\frac{t}{b}\right)^2 \cdot 10^6 \quad F_{CY} = \underline{\underline{35000 \text{ PSI}}}$$

b	t_{BE}	t_{AL}			
0.1	0.002	0.003			
0.2	0.004	0.006			
0.3	0.005	0.008			
0.4	0.007	0.011			
0.5	0.009	0.013			
0.6	0.010	0.016			
0.7	0.012	0.019			
0.75	0.013	0.020			

LOADING ON FRAME :

$$T = \underline{\underline{39 \text{ #/IN}}}$$

ASSUME CROSS SECTION

$$\underline{\underline{0.6 \times 0.20 \text{ IN}}}$$

$$P = T \cdot l_{eff.}$$

$$M = \frac{1}{2} T l^2$$

USE 2 STIFFENERS IN BOTH DIRECTIONS.

$$l = 19.7 \text{ IN}$$

$$l_{eff} = \frac{1}{2} \cdot 19$$

CALCULATION SHEET

By _____

Subject _____ Checked By _____ Date _____

ELECTRO-OPTICAL SYSTEMS, INC.

$$P = \underline{370.5 \text{ LBS}}$$

$$M = \frac{1}{12} 39 \cdot 19.7^2 = \underline{1261 \text{ INLBS}}$$

$$r_{0.6 \times 1.2} = 0.447 \text{ IN}$$

$$F_{CR} = \frac{\pi^2 \cdot E}{\left(\frac{0.707 \cdot 19.7}{0.447}\right)^2} = 10.16583 \cdot 10^{-3} E = \frac{284640 \text{ PSI} \cdot BE}{101660 \text{ PSI} \cdot AL}$$

$$A = 4(0.6 + 1.2)t = \underline{7.2 t}$$

$$I = 1.2^2 t (0.6 + 0.4) = \underline{1.44 t}$$

$$f_c = \frac{P}{A} = \frac{370.5}{7.2 t} = \frac{51.458}{t}$$

$$f_b = \frac{1261 \cdot 0.6}{1.44 t} = \frac{525.417}{t}$$

$$t \text{ REQ'D} \quad BE \quad t \geq 0.01 \text{ IN.}$$

$$AL \quad t \geq 0.016 \text{ IN.}$$

$$f = \frac{576.875}{t} = \frac{57687.5 \text{ PSI}}{36050 \text{ PSI}} \quad \begin{matrix} BE \\ AL. \end{matrix}$$

USE 0.016 IN FOR BE.

0.018 IN FOR AL.

CALCULATION SHEET

By _____

Subject _____ Checked By _____ Date _____

ELECTRO-OPTICAL SYSTEMS, INC.

WEIGHT OF FRAME:

	BE	AL
OUTER	243.4 AP <u>2.120"</u>	<u>3.154"</u>

STIFFENERS:

$$P = Tl = 39.19.7 = \underline{768.3 \text{ LBS}}$$

0.6 x 0.6 x t SIZE

$$V = \frac{a}{2} \sqrt{\frac{3b+t}{3(a+b)}} = \frac{0.6}{2} \sqrt{\frac{4}{6}} = \underline{0.245 \text{ IN}}$$

$$F_{CR} = \frac{\pi^2 E \cdot 2}{\left(\frac{19.7}{0.245}\right)^2} = \underline{3.053 E \cdot 10^{-3}} \quad \text{ADEQUATE}$$

$$F_{CR} = 85480 \text{ PSI BE}$$

$$30530 \text{ PSI AL}$$

ALLOWABLE
68380 PSI
24420 PSI

FOR $t = 0.010 \text{ IN}$ FOR BE 0.016 FOR AL

$$f = \frac{P}{2A}$$

$$A = 4 \cdot 0.6 \cdot t = 2.4t$$

$$f = \frac{768.3}{4.8t} = \frac{160.0625}{t} \quad \frac{16000 \text{ PSI BE}}{10000 \text{ PSI AL}}$$

MAY USE $t = 0.008$ FOR BE $t = 0.014$ FOR AL.

E-21

CALCULATION SHEET

By _____

Subject _____ Checked By _____ Date _____

ELECTRO-OPTICAL SYSTEMS, INC.

STIFFENER WEIGHT.

$$W = 234.6 \cdot 4.849 \quad \begin{matrix} BE \\ 0.681 \# \end{matrix} \quad \begin{matrix} AL \\ \underline{1.577 \#} \end{matrix}$$

ALUMINUM TOO HEAVY

FRAME WEIGHT:

$$BE : \quad 2.120 + 0.681 + 0.286 = \underline{3.081 \#}$$

$$AL : \quad 3.154 + 1.577 + 0.473 = \underline{5.204 \#}$$

$$W_{PBE} = \underline{0.1345 \# / FT^2} \quad \text{FRAME}$$

$$W_{PAL} = 0.2271 \# / FT^2 \quad \text{FRAME}$$

$$W_{PBE} = 0.0109 \# / FT^2 \quad \text{DIAPHRAGM}$$

$$W_{PAL} = 0.0144 \# / FT^2 \quad \text{DIAPHRAGM.}$$

$$W_{BE} = 0.1345 + 0.0109 = \underline{0.1454 \# / FT^2}$$

$$W_{AL} = 0.2271 + 0.0144 = 0.2415 \# / FT^2$$

INCLUDING CELLS:

HEAVIER FRAME 2x0.75

$$W_{BE} = \underline{0.3054 \# / FT^2}$$

$$\underline{0.346 \# / FT^2}$$

$$W_{AL} = \underline{0.4015 \# / FT^2}$$

7027-IDR

EOS Form No. 6303 (7/64-200)

B-22

E
S

CALCULATION SHEET

By _____

Subject _____ Checked By _____ Date _____

ELECTRO-OPTICAL SYSTEMS, INC.

FREQUENCY OF DIAPHRAGM

$$\begin{aligned}
 f &= \frac{1}{2} \sqrt{\frac{T_g}{s} \left(\left(\frac{1}{a}\right)^2 + \left(\frac{1}{b}\right)^2 \right)} \\
 &= \frac{1}{2} \sqrt{\frac{30.3864}{0.4709} \cdot 144 \left(\left(\frac{1}{19.7}\right)^2 + \left(\frac{1}{19.0}\right)^2 \right)} \\
 &= \frac{12}{2} \sqrt{\frac{11592}{0.0109} \left(5.3468 \right) 10^{-3}} = \underline{\underline{114 \text{ CPS}}}
 \end{aligned}$$

B-23

CALCULATION SHEET

By _____

Subject _____ Checked By _____ Date _____

ELECTRO-OPTICAL SYSTEMS, INC.

EOS

HONEY COMB SOLAR PANELS

USE ONLY BE FASE SHEETS.

$$F_{CY} = \underline{40000} \text{ PSI}$$

CELL SIZE :

$$F_{CR} = 0.8 \cdot \frac{\pi^2 \cdot 6.98}{12(1-0.3^2)} \cdot 28 \cdot 10^6 \left(\frac{t}{b}\right)^2$$

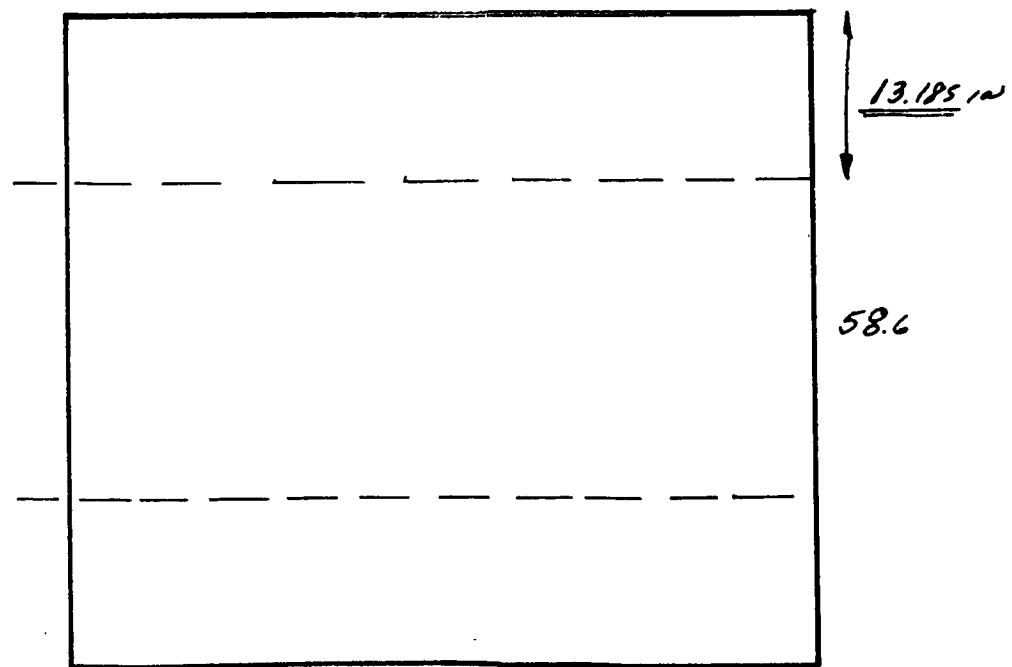
$$t = 0.001 \text{ in.}$$

$$F_{CR} = \underline{\underline{141.312}} \left(\frac{t}{b}\right)^2 \cdot 10^6 = \underline{\underline{\frac{141.312}{b^2}}}$$

$$F_{CR} = 4020 \text{ PSI} \quad \underline{b = \frac{3}{16}}$$

$$F_{CR} = 9044 \text{ PSI} \quad \underline{b = \frac{1}{8}}$$

CORE WEIGHT: 2.1 #/FT³



B. 24

CALCULATION SHEET

By _____

Subject _____ Checked By _____ Date _____

ELECTRO-OPTICAL SYSTEMS, INC.

SKIN WEIGHT

$$A = 288 \text{ IN}^2 \text{ PER FT}^2$$

$$W = 288 \cdot t \cdot S = \underline{21.773 \text{ #/FT}^2} \times t$$

$$t = 0.001 \quad = 0.0218 \text{ #/FT}^2$$

$$t = 0.0015 \quad = 0.0327 \text{ #/FT}^2$$

$$t = 0.002 \quad = 0.0436 \text{ #/FT}^2$$

CORE WEIGHT

$$W = 2.1 \frac{1}{12} h \text{ #/FT}^2$$

$$h = 0.250 \text{ IN} \quad 0.04375 \text{ #/FT}^2$$

$$h = 0.375 \text{ IN} \quad 0.065625 \text{ #/FT}^2$$

$$h = 0.500 \text{ IN} \quad 0.08750 \text{ #/FT}^2$$

$$h = 0.750 \text{ IN} \quad 0.13125 \text{ #/FT}^2$$

CRITICAL BUCKLING STRENGTH

$$b =$$

$$0.250 \quad 0.1875 \quad 0.125$$

$$t = 0.001 \quad 4020 \text{ PSI.} \quad 9044 \text{ PSI.}$$

$$t = 0.0015 \quad 9045 \text{ PSI.} \quad 20350 \text{ PSI.}$$

$$t = 0.002 \quad 18080 \text{ PSI.} \quad 36180 \text{ PSI.}$$

$$M = 4533 \text{ W}_{\text{IN}^2} = \underline{\underline{31.479 \text{ W}_{\text{FT}^2}}}$$

B-25-

CALCULATION SHEET

By _____

Subject _____ Checked By _____ Date _____

ELECTRO-OPTICAL SYSTEMS, INC.

t	CORE HEIGHT		$W =$	
	0.250	0.375	0.500	0.750
0.001	0.22555	0.24743	0.26930	0.31305
0.0015	0.23645	0.25833	0.28020	0.32395
0.0020	0.24735	0.26923	0.2911	0.33485
0.0030	0.26915	$\frac{\#}{FT^2}$ 0.29103	0.31290	0.35665

$M =$	IN LB/IN			
0.001	7.100	7.79	8.48	9.85
0.0015	7.44	8.13	8.82	10.20
0.002	7.79	8.48	9.16	10.54
0.003	8.47	9.16	9.85	11.23

$$f = \frac{2M}{t h^2}$$

$f =$	PSI.			
0.001	227200	110790	67840	35022
0.0015	158720	77080	47040	24180
0.002	124640	60300	36640	18740
0.003	90350	43430	26270	13310

PANEL HEIGHT : 0.500 $t = 0.002$ in

$$W_{ST} = \underline{0.1311} \frac{\#}{FT^2}$$

7027-IDR

B-26

EOS

CALCULATION SHEET

By _____

Subject _____ Checked By _____ Date _____

ELECTRO-OPTICAL SYSTEMS, INC.

BEAMS: AS FOR

$$W_t = \underline{\underline{0.025 \text{ #/IN}}}$$

$$W_B = \underline{\underline{0.1237 \text{ #/FT}^2}}$$

$$W_T = 0.160 + 0.1311 + 0.1237 = \underline{\underline{0.4148 \text{ #/FT}^2}}$$

B-27

CALCULATION SHEET

By _____

Subject _____ Checked By _____ Date _____

ELECTRO-OPTICAL SYSTEMS, INC.

DEMONSTRATION PANEL DESIGN CRITERIA.

INPUT DYNAMIC LOAD FACTOR 1.5g

STRUCTURE GAIN:

40 - HOLLOW CORE

10 - FRAME

MATERIAL STRENGTH. PER MIL HDBK 5
MIL HDBK 17

HOLLOW CORE THEORY (FROM APPENDIX 10.4.2)

STRUCTURE WEIGHT

$$W_p = \left[2 - \left[\frac{\pi}{4} \left(\frac{d}{a} \right)^2 - \frac{\pi}{2} \left(\frac{d}{a} \right) \left(\frac{h}{a} \right) \right] \cot \alpha \right] t \cdot g$$

EFFECTIVE PRESSURE

$$p = \left[\frac{W_{SC}}{144} + \left[2 - \left(\frac{\pi}{4} \left(\frac{d}{a} \right)^2 - \frac{\pi}{2} \left(\frac{d}{a} \right) \left(\frac{h}{a} \right) \right) \cot \alpha \right] t \cdot g \right] \left[g_{STAT} + 0.707g \right]$$

MEMBRANE STRESS:

$$f_m = \frac{\left[\frac{W_{SC}}{144} + \left[2 - \left(\frac{\pi}{4} \left(\frac{d}{a} \right)^2 - \frac{\pi}{2} \left(\frac{d}{a} \right) \left(\frac{h}{a} \right) \right) \cot \alpha \right] t \cdot g \right] \left[g_{STAT} + 0.707g \right] \cdot C \left[2 - \frac{C \sin \alpha}{B \sin \alpha} \right]}{2 \left(2 - \left(\frac{d}{a} \right) \cos \theta + \frac{h}{a} \right) t \sin \alpha}$$

CRIPPLING

$$F_{CR} = \frac{0.8 K \cdot \pi^2 E}{12(1-\nu^2)} \left(\frac{t}{b} \right)^2 \quad \text{PER NACA TN 3781}$$

PANEL BUCKLING

$$p_{CR} = - \frac{D (\lambda_m^2 + \mu_m^2)^2 + \frac{E h}{R}}{\frac{R}{2} (\lambda_m^2 + \mu_m^2)}$$

D = EI

h = PANEL THICKNESS (AREA OF CROSS SECTION)

B-28

CALCULATION SHEET

By _____

Subject _____ Checked By _____ Date _____

ELECTRO-OPTICAL SYSTEMS, INC.

$$\lambda_m = m \frac{\pi}{\alpha_0}$$

$$\mu_m = m \frac{\pi}{\beta_0}$$

$$\alpha_0 = \text{LENGTH } \left. \vphantom{\alpha_0} \right\} \text{ OF PANEL}$$

$$\beta_0 = \text{WIDTH}$$

FREQUENCY OF THE PANEL

$$f = \left[\frac{1}{4\pi^2} \cdot \frac{1}{\rho h} \left[D(\lambda_m^2 + \mu_m^2)^2 + E h \left(\frac{\frac{\lambda_m^2}{R_1} + \frac{\mu_m^2}{R_2}}{\lambda_m^2 + \mu_m^2} \right)^2 \right] \right]^{\frac{1}{2}}$$

$$\rho = \text{MASS OF CROSS-SECTION } \left(\frac{w}{g} \right)$$

CALCULATION SHEET

By

Subject Checked By Date

ELECTRO-OPTICAL SYSTEMS, INC.

PRESTRESSED DIAPHRAGM. (SEE APPENDIX 10.4.2)

7.2.3.1 *FREQUENCY*

$$f = \frac{1}{2} \sqrt{\frac{T \cdot g}{S} \left(\left(\frac{m}{a} \right)^2 + \left(\frac{m}{b} \right)^2 \right)}$$

NOTATIONS AS IN THE APPENDIX.

7.2.3.2 *STRESS*

$$f = \frac{T_p + T_i}{t}$$

FRAME (SEE APPENDIX 10.4.2)

7.2.4.1 *STRESS*

$$f = \frac{1}{12} T l_2^2 \frac{C_2}{I_2} + \frac{1}{2} T \frac{l_1}{A_2}$$

COLUMN STRENGTH

$$F_{ce} = \frac{0.8 \pi^2 E}{\left(\frac{c \cdot l}{r} \right)^2}$$

CRITICAL COLUMN LOADING

$$\frac{f_b}{F_b} = \sqrt{1 - \frac{F_c}{F_{cr}}}$$

FACE BUCKLING

$$F_{ce} = \frac{0.8 K \cdot \pi^2 E}{12(1 - \nu^2)} \left(\frac{t}{b} \right)^2$$

B-30

CALCULATION SHEET

By _____

Subject _____ Checked By _____ Date _____

ELECTRO-OPTICAL SYSTEMS, INC.

VERTICAL LOADING

C.G., AREA, MOMENT OF INERTIA FROM 10.4.2

$$f = \frac{p_{TOT} \cdot l^2 \cdot c}{8 I_y}$$

$$p_{TOT} = \text{FROM 10.4.2}$$

$$I_y = \text{FROM 10.4.2}$$

NATURAL FREQUENCY

$$f = \frac{22.4}{27.7 l^2} \sqrt{\frac{EI}{\mu}} \quad \text{PER VIBRATION MANUAL FOR ENGINEERS}$$

O.T.S PB 131785

THERMAL STRESS (SEE SECTION 10.4.2)

STRAIN DIFFERENCE

$$\Delta = \alpha_1 (T_1 - T_0) - \alpha_2 (T_2 - T_0)$$

DISCONTINUITY FORCE

$$H = \frac{E \phi_0}{W_a} (\alpha_1 (T_1 - T_0) - \alpha_2 (T_2 - T_0)) R \sin \theta$$

B-31

EOS

CALCULATION SHEET

By _____

Subject _____ Checked By _____ Date _____

ELECTRO-OPTICAL SYSTEMS, INC.

HOLLOW CORE SOLAR PANEL.

$W_{SC} = \underline{0.160} \text{ #/FT}^2$ SOLAR CELLS

$W_{ST} = 0.066 \text{ #/FT}^2$ STRUCTURAL PANEL (NUKROL HOLLOW CORE).

CLIPS : $W = \underline{0.231} \text{ #}$

ADHESIVE = $\underline{0.016} \text{ #}$

BEAMS : $W = \underline{2.112} \text{ #}$

ADHESIVE $W = 0.016 \text{ #}$

CORNER Pcs. $W = \underline{0.230} \text{ #}$

$W_{FRAME} \quad \underline{2.605} \text{ #}$

$W_F = \underline{0.1137} \text{ #/FT}^2$

$W_T = 0.160 + 0.066 + 0.1137 = \underline{0.3397} \text{ #/FT}^2$

B-32

7027-IDR

APPENDIX C

STRUCTURAL ANALYSIS OF HOLLOW CORE SUBSTRATE

APPENDIX C
STRUCTURAL ANALYSIS OF HOLLOW CORE SUBSTRATE

The weight of the hollow core substrate is dependent on a number of variables, such as skin thickness, hole size, depth of section, percent of open area, etc. The choice of the specific design is dependent on the frame used, attachment point, environment, and other design conditions. To handle the large number of design parameters and arrive at an optimum substrate structure, a computer program was derived and used in the analysis.

This appendix provides a record of the equations used in the analysis and presents some of the results of this analysis. The computer program is now checked out and available for further design calculations.

CALCULATION SHEET

By _____

Subject TRADE STUDY Checked By _____ Date _____

ELECTRO-OPTICAL SYSTEMS, INC.

IT WAS NECESSARY TO SIMPLIFY THE EXPRESSIONS TO EXPEDITE PROGRAMMING.

ALL THE COMPUTER RUNS WERE FOR SQUARE PATTERN HOLE LAYOUT.

IN THIS CASE

$$\phi = 45^\circ$$

$$\theta = 0^\circ$$

NET CROSS SECTION

$$t_{eq} = (2 - \frac{d}{a})t$$

APPLYING THESE AND CONSOLIDATING:

$$\frac{\left[\left(2 - \frac{\pi}{4} \left(\frac{d}{a} \right)^2 + \frac{\pi}{2} \left(\frac{d}{a} \right) \left(\frac{d}{a} \right) \right) t \cdot \rho + \frac{N_{sc}}{144} \left(g_{ST} + g_0 \cdot 0.707 \right) \cdot C \left(2 - \frac{C}{B} \right) \right]}{2 \left(2 - \frac{d}{a} \right) t \sin \alpha}$$

$$= \frac{0.8 K \pi^2 E}{12(1-\nu^2)} \frac{t^2}{a^2 \left(2 - \frac{d}{a} \right)^2}$$

$$\left[\frac{N_{sc}}{144} a^2 + \left(\left(2 - \frac{\pi}{4} \left(\frac{d}{a} \right)^2 \right) a^2 + \frac{\pi}{2} \left(\frac{d}{a} \right) a \right) t \cdot \rho \right] \frac{g_{ST} + 0.707 g_0}{t \sin \alpha} \cdot C \left(2 - \frac{C}{B} \right)$$

$$= \frac{0.8 K \pi^2 E}{12(1-\nu^2)} \frac{2 \cdot t^3}{\left(2 - \frac{d}{a} \right)}$$

7027-IDR

CALCULATION SHEET

By _____

Subject _____ Checked By _____ Date _____

ELECTRO-OPTICAL SYSTEMS, INC.

HERE

 W_{sc} = WEIGHT OF SOLAR CELLS #/FT² d/a = SELECTED PARAMETER a = HOLE HALF SPACING d = HOLE DIAMETER h = PANEL THICKNESS t = SKIN THICKNESS g = SKIN DENSITY g_{st} = STATIC ACCELERATION g_o = DYNAMIC " INCLUDING AMPLIFICATION α = PANEL HALF ANGLE C = PANEL HALF WIDTH B = PANEL HALF LENGTH. K = EMPIRICAL BUCKLING COEFFICIENT E = MATERIAL MODULUS OF ELASTICITY ν = POISSON'S RATIO.

FOR THE FIRST COMPUTER RUN THE FOLLOWING
INPUTS WERE GIVEN.

$$W_{sc} = 0.160 \text{ #/FT}^2$$

$$d/a = 1.4 \longleftrightarrow 1.0 \quad \text{RANGE}$$

$$t = 0.002 \longleftrightarrow 0.0002 \quad \text{RANGE}$$

$$h = 0.3 \longleftrightarrow 0.1 \quad \text{RANGE.}$$

$$g_o = g_{dyn} \times g = 1.5 \cdot 40$$

$$g_{stat} = 0$$

CALCULATION SHEET

By _____

Subject _____ Checked By _____ Date _____

ELECTRO-OPTICAL SYSTEMS, INC.

$\rho = 0.321 \text{ #/IN}^3 \text{ Ni}$ 0.100 #/IN AL.
 $g = 386.4 \text{ IN}^2/\text{SEC}^2$
 $\alpha = 10^\circ$
 $\nu = 0.3$

PANEL SIZE

SQUARE:

C	10	20	25	30	35	40	IN
B	10	20	25	30	35	40	IN

RECTANGULAR

C	10	20	25	30	35	40	IN
B	20	40	50	60	70	80	IN

BUCKLING COEFFICIENT
 SQUARE RECTANGULAR
 $K = 5.3$ 4.24

$E = 25 \cdot 10^6 \text{ NICKEL}$ $10 \cdot 10^6 \text{ ALUMINUM}$

4 DIFFERENT CASES RUN

- CASE 1 SQUARE PANEL - NICKEL - $g = 40$
- CASE 2 SQUARE PANEL - NICKEL - $g = 20$
- CASE 3 ~~SQUARE~~ RECTANGULAR PANEL - NICKEL - $g = 40$
- CASE 4 SQUARE PANEL - ALUMINUM - $g = 40$.

EOS

CALCULATION SHEET

By _____

Subject _____ Checked By _____ Date _____

ELECTRO-OPTICAL SYSTEMS, INC.

THE FOLLOWING FIGURES SHOW:

HOLE HALF SPACING VS SKIN THICKNESS.
MINIMUM WEIGHT SELECTED FOR EACH POINT
WEIGHTS ARE FOR $k = 0.1, 0.2, 0.3, 0.4$.
FOR SKIN THICKNESSES FROM $0.0002 - 0.002$ IN.
PANEL IS 60×60 IN² WITH HALF ANGLE OF 10° .

SUBSTRATE STRUCTURE WEIGHT VS
SKIN THICKNESS
(ABOVE NOTE DESCRIBES THIS FIGURE ALSO)

INERTIA EFFECT (PRESSURE) VS
SKIN THICKNESS (NOTE FOR FIG. 5.2.1
HOLDS FOR THIS FIGURE ALSO).

PANEL CRITICAL PRESSURE VS
SKIN THICKNESS (SEE NOTE UNDER FIG. 5.2.1)

CRITICAL FREQUENCY VS SKIN THICKNESS.

d/a RATIO VS PANEL STRUCTURE WEIGHT
VS d/a RATIO.

FOR PANEL 60×60 IN² $\alpha = 10^\circ$.
STRUCTURE WEIGHT (HOLLOW CORE)
VS.

PANEL SIZE
FOR $d/a = 1.0, 1.1, 1.2, 1.3, 1.4, 1.5$
 $k = 0.1$

FOR $k = 0.2, 0.3, 0.4$ FOR $d/a = 1.3$

SQUARE PANEL.

1-5

CALCULATION SHEET

By _____

Subject _____ Checked By _____ Date _____

ELECTRO-OPTICAL SYSTEMS, INC.

Weight of PANEL STRUCTURE (HOLLOW CORE)

VS

PANEL WIDTH.

- 1. RECTANGULAR PANEL : 2:1 $\frac{g}{b} = 40$
- 2. SQUARE PANEL : 1:1 $\frac{g}{b} = 40$
- 3. SQUARE PANEL : 1:1 $\frac{g}{b} = 20$

ALL ABOVE FABRICATED FROM NICKEL

4 SQUARE PANEL FABRICATED FROM ALUMINUM.

~~HOW~~ HOLLOW CORE STRUCTURE WEIGHT

VS

PANEL ARC HALF ANGLE

FROM $3^\circ \rightarrow 20^\circ$

FOR $h = 0.02$ IN 0.05 IN & 0.10 IN.

$d/a = 1.2, 1.3, 1.4$

HOLLOW CORE NATURAL FREQUENCY

VS.

PANEL ARC HALF ANGLE

FROM $3^\circ \rightarrow 20^\circ$

FOR $h = 0.02, 0.05, 0.10$ IN.

$d/a = 1.2, 1.3 \& 1.4$.

CRITICAL STRENGTH (PRESSURE) AND

INERTIA PRESSURE

VS

PANEL ARC HALF ANGLE.

HOLLOW CORE STRUCTURES WEIGHT

VS

PANEL WIDTH

FOR RECTANGULAR PANEL 1: 1.25

$h = 0.02, 0.05, 0.10$ IN.

CALCULATION SHEET

By _____

Subject _____ Checked By _____ Date _____

ELECTRO-OPTICAL SYSTEMS, INC.

NATURAL FREQUENCY

VS

PANEL WIDTH FOR RECTANGULAR PANEL
(1:1.25).FOR $h = 0.02, 0.05, 0.10$ IN
 $\alpha/\theta = 1.2, 1.3 \text{ \& } 1.4$ INERTIA EQUIVALENT PRESSURE IF
PANEL CRITICAL PRESSURE

VS

PANEL WIDTH (RECTANGULAR 1:1.25)

FOR $h = 0.02, 0.05, 0.10$ IN.
 $\alpha/\theta = 1.3.$

THE COMPUTER ANALYSIS SHOW:

1. THERE IS A DEFINITE ^{OPTIMUM} ~~MINIMUM~~ CONFIGURATION FOR EACH PARAMETER SELECTION.
WEIGHT INCREASES ON EITHER SIDE
2. THE WEIGHT PENALTY, CAUSED BY DEVIATING FROM THE MINIMUM POINT IS SMALL ON THE RIGHT HAND SIDE.
3. THE PANEL WEIGHT INCREASES FOR INCREASING SIZE.
4. THE PANEL WEIGHT INCREASES FOR DECREASING HALF ANGLE.
5. THE PANEL WEIGHT INCREASES FOR INCREASING PANEL THICKNESS

CALCULATION SHEET

By _____

Subject _____ Checked By _____ Date _____

ELECTRO-OPTICAL SYSTEMS, INC.

THE SELECTION OF APPLICABLE PANEL DESIGN MUST ^{CONSIDER} IN ADDITION TO THE ABOVE POINTS,

1. ELECTRIC EFFICIENCY
2. FABRICATION OF MANDREL
3. HANDLING OF MANDREL IN AND OUT OF BATH.

THE SQUARE PATTERN DOES NOT GIVE THE MOST EFFICIENT DESIGN. ONE MUST REMEMBER THAT THERE IS CONSERVATISM IN THE ABOVE ANALYSIS, SUCH THAT THE MARGIN OF SAFETY IN THE TRUE DESIGN EXCEEDS THE ANALYTICAL DESIGN.

BY USING A TRIANGULAR DESIGN $\phi = 60^\circ$ AND EFFECTIVE MATERIAL AREA ONE CAN OBTAIN ADDITIONAL WEIGHT SAVINGS.

$$A_{pin} = 1 - \frac{\pi}{8} \left(\frac{d}{a}\right)^2 \cot \phi$$

SQUARE PATTERN (ROUND HOLES ONLY)
UNIFORM SIZE HOLES.

$$\frac{d}{a} \text{ MAX} = \underline{1.414} \quad (\text{TOUCHING})$$

$$\phi = 45^\circ$$

$$A_{pin} = 1 - \frac{\pi}{8} \left(\frac{d}{a}\right)^2$$

$\frac{d}{a} =$	1.0	1.1	1.2	1.3	1.414
$A_{pin} =$	0.607	0.525	0.434	0.336	0.2146
$\frac{A_p}{A=1.0} \cdot 100$	60.7%	52.5%	43.4%	33.6%	21.46%

CALCULATION SHEET

By _____

Subject _____ Checked By _____ Date _____

ELECTRO-OPTICAL SYSTEMS, INC.

TRIANGULAR

$$A_{pin} = 1 - \frac{\pi}{8} \left(\frac{d'}{a}\right)^2 \cotan 60^\circ$$

$$= 1 - \frac{\pi}{8} \left(\frac{d'}{a}\right)^2 0.57735 = \underline{\underline{1 - 0.22672 \left(\frac{d'}{a}\right)^2}}$$

d'/a	1.5	1.6	1.7	1.8	1.9	2.0
A_{pin}	0.490	0.420	0.345	0.265	0.182	0.093
$\frac{A_{pin}}{A}$	49%	42%	34.5%	26.5%	18.2%	9.3%

ONE MAY BE ABLE TO WORK IN THE

 $d'/a = 1.3$ RANGE FOR SQUARE PATTERN $d'/a = 1.9$ RANGE FOR TRIANGULAR PATTERN.

IT IS EVIDENT THAT MORE MATERIAL CAN BE REMOVED WITH TRIANGULAR PATTERN.

TRIANGULAR PATTERN:

$$\left[\frac{1532}{144} a^3 + \left[2a^3 - \left(\frac{\pi}{4} \left(\frac{d'}{a}\right)^2 a^3 - \frac{\pi}{2} \left(\frac{d'}{a}\right) h a^2 \right) \cotan \phi \right] t g_1 \right] (g_1 + 0.707 g_2) e^{(2 - \frac{C \sin \alpha}{t \sin \alpha})}$$

$$= \frac{0.8 K E \pi^2}{12(1 - \nu^2)} \left(\frac{t}{h}\right)^2 2 \cdot \left(2a - \frac{d'}{a} \cos \theta \cdot a + h\right) t \sin \alpha$$

FOR THE CASE AT HAND

$h = 0.1 \text{ IN}$

$\phi = 60^\circ$

$0.001 < t < 0.003$

$\theta = 30^\circ$

$E = 25 \cdot 10^6 \text{ PSI}$

$g_1 = 0$

$\nu = 0.3$

$g_2 = 1.5$

$K = 8.5$

$g = 40$

$C = 29.3$

7027-IRD

EOS Form No. 6303 (7/64-200)

$b = 4 \left(1 - 0.433 \frac{d'}{a}\right) a$

CALCULATION SHEET

By _____

Subject _____ Checked By _____ Date _____

ELECTRO-OPTICAL SYSTEMS, INC.

$$\rho = \underline{0.321} \text{ #/IN}^3$$

$$W_{sc} = 0.160 \text{ #/FT}^2$$

$$\left[\frac{0.160}{144} a^3 + \left[2a^3 - \left(\frac{\pi}{4} \left(\frac{d}{a} \right)^2 a^3 - 0.1 \cdot \frac{\pi}{2} \left(\frac{d}{a} \right) a^2 \right) 0.57735 \right] t \cdot 0.321 \right] 1.5 \cdot 40 \cdot 0.707 \cdot 29.3$$

$$= \frac{0.8 \cdot 8.5 \cdot 25 \cdot 10^6 \cdot \pi^2 t^3}{12(1-0.3^2) \left(4 \left(1 - 0.433 \frac{d}{a} \right) \right)^2} \left(2 \left(2a - 0.86603 \left(\frac{d}{a} \right) + 0.1 \right) 0.17947 \right.$$

$$\left. 1.381 a^3 + \left[797.946 a^2 - 180.915 \left(\frac{d}{a} \right)^2 a^3 + 36.183 \frac{d}{a} a^2 \right] t \right)$$

$$= 3.4469 \cdot 10^6 \frac{t^3}{\left(1 - 0.433 \frac{d}{a} \right)^2} \left(a \left(2 - 0.86603 \frac{d}{a} \right) + 0.1 \right)$$

$$t_1 = \underline{2a - d}$$

$$W_{ST} = \left[2 - \left(\frac{\pi}{4} \left(\frac{d}{a} \right)^2 + \frac{\pi}{2} \frac{d}{a} \frac{h}{a} \right) \cot \text{ angle } \phi \right] t \cdot \rho \cdot 144$$

$$= 46.224 \left[2 - 0.45345 \left(\frac{d}{a} \right)^2 + 0.09069 \left(\frac{d}{a} \right) \frac{1}{a} \right] t$$

EOS

CALCULATION SHEET

By _____

Subject _____ Checked By _____ Date _____

ELECTRO-OPTICAL SYSTEMS, INC.

t			$d/\lambda = 1.95$	1.90	1.85	1.80	1.75	1.70
0.001	Q	IN	0.240	0.219	0.202	0.188	0.176	0.167
	t_1	IN	0.012	0.022	0.030	0.038	0.044	0.050
	W_{ST}	#/FT ²	0.047	0.053	0.059	0.065	0.070	0.075
0.0012	Q	IN.	0.297	0.271	0.250	0.232	0.217	0.205
	t_1	IN.	0.015	0.027	0.038	0.046	0.054	0.062
	W_{ST}	#/FT ²	0.048	0.055	0.062	0.069	0.075	0.080
0.0014	Q	IN	0.357	0.325	0.299	0.278	0.260	0.245
	t_1	IN	0.018	0.033	0.045	0.056	0.065	0.073
	W_{ST}	#/FT ²	0.050	0.058	0.065	0.072	0.079	0.085
0.0016	Q	IN	0.418	0.381	0.357	0.326	0.304	0.286
	t_1	IN	0.021	0.038	0.053	0.065	0.076	0.086
	W_{ST}	#/FT ²	0.052	0.060	0.069	0.076	0.084	0.091
0.0018	Q	IN	0.483	0.439	0.404	0.375	0.350	0.329
	t_1	IN	0.024	0.044	0.061	0.075	0.088	0.099
	W_{ST}	#/FT ²	0.053	0.063	0.072	0.080	0.089	0.096
0.0020	Q	IN	0.549	0.500	0.460	0.426	0.397	0.375
	t_1	IN	0.027	0.050	0.069	0.085	0.099	0.112
	W_{ST}	#/FT ²	0.055	0.065	0.075	0.0845	0.094	0.102
0.0025	Q	IN	0.725	0.658	0.603	0.557		
	t_1	IN	0.036	0.066	0.090	0.111		
	W_{ST}	#/FT ²	0.060	0.072	0.084	0.095		
0.0030	Q	IN	0.912	0.825	0.755			
	t_1	IN	0.046	0.083	0.113			
	W_{ST}	#/FT ²	0.065	0.0793	0.093			

2-11

CALCULATION SHEET

Page 11 of _____

By _____

Subject _____ Checked By _____ Date _____

ELECTRO-OPTICAL SYSTEMS, INC.

COMPARING FIGURE 6-2-21 TO THE WEIGHT CURVES FOR THE SQUARE PATTERN, ONE CAN DRAW THE CONCLUSION THAT A WEIGHT SAVING MAY BE OBTAINED BY USING A TRIANGULAR HOLE PATTERN
i.e. $\phi = 60^\circ$.

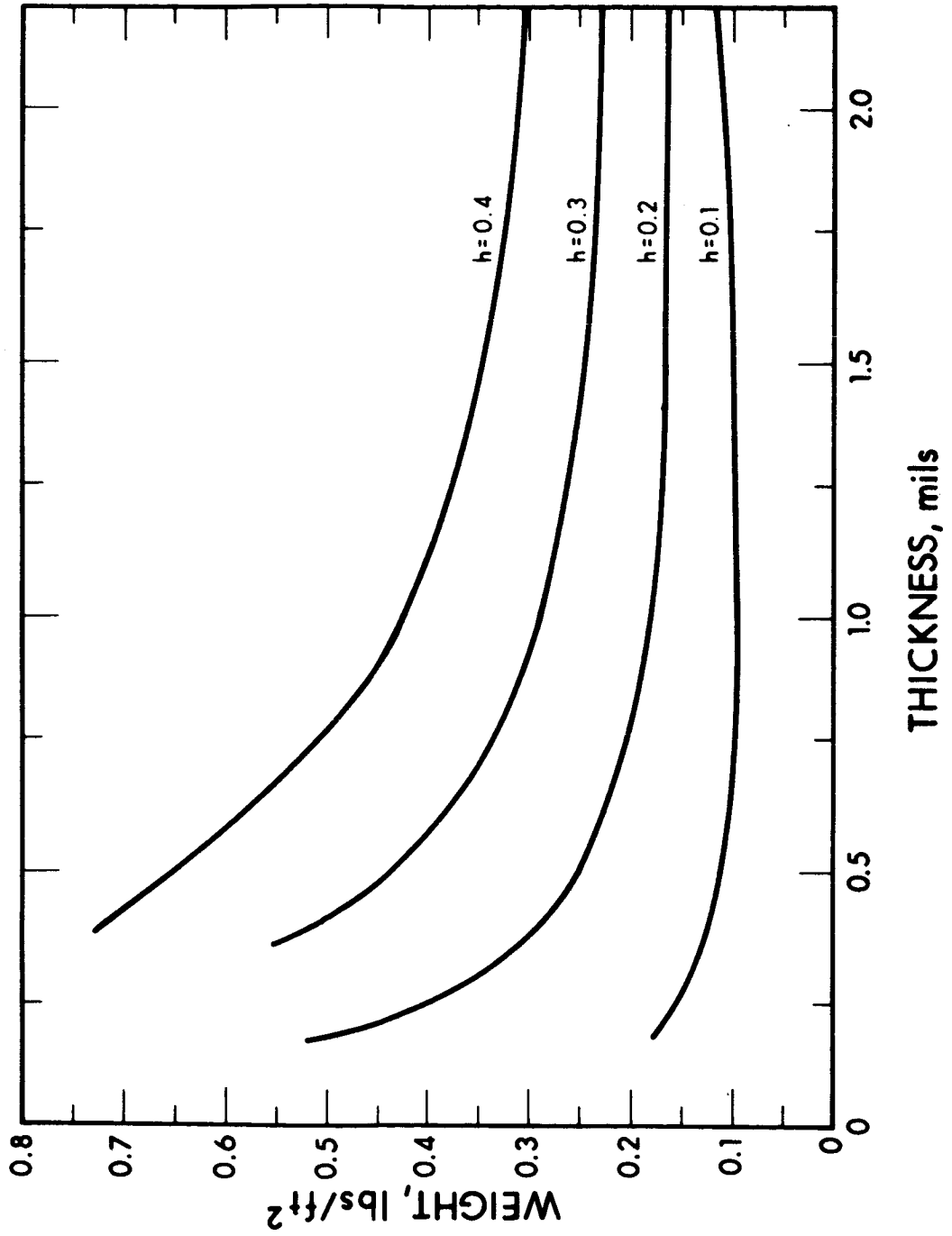
THE FABRICATORS RECOMMEND A MINIMUM SPACING BETWEEN THE HOLES OF 0.050 IN THEN FROM FIGURE 6-2-21 THE OPTIMUM DESIGN CAN BE DETERMINED.

$$t = 0.002 \text{ IN}$$

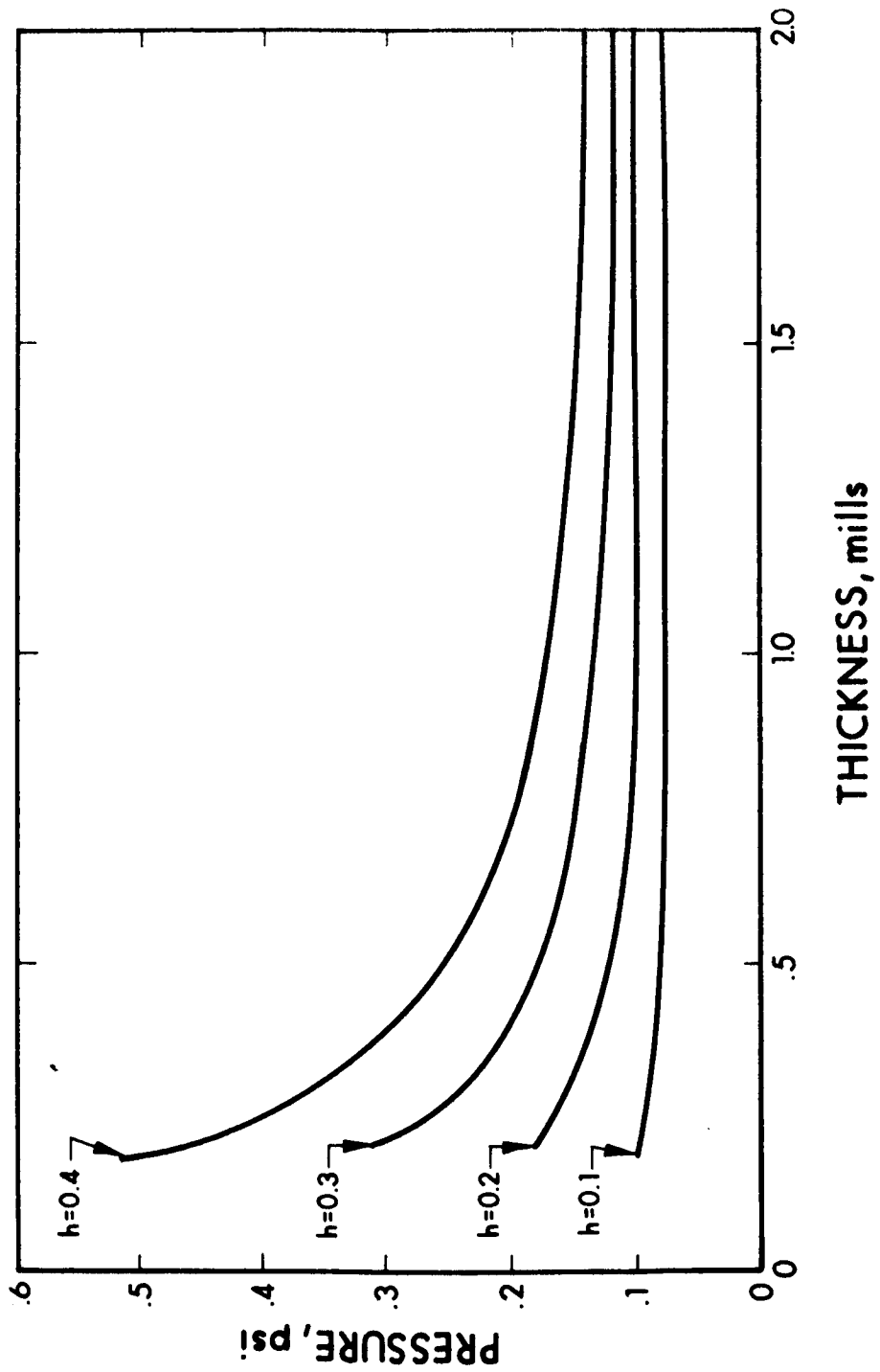
$$q = 0.500 \text{ IN}$$

$$d = 0.950 \text{ IN}$$

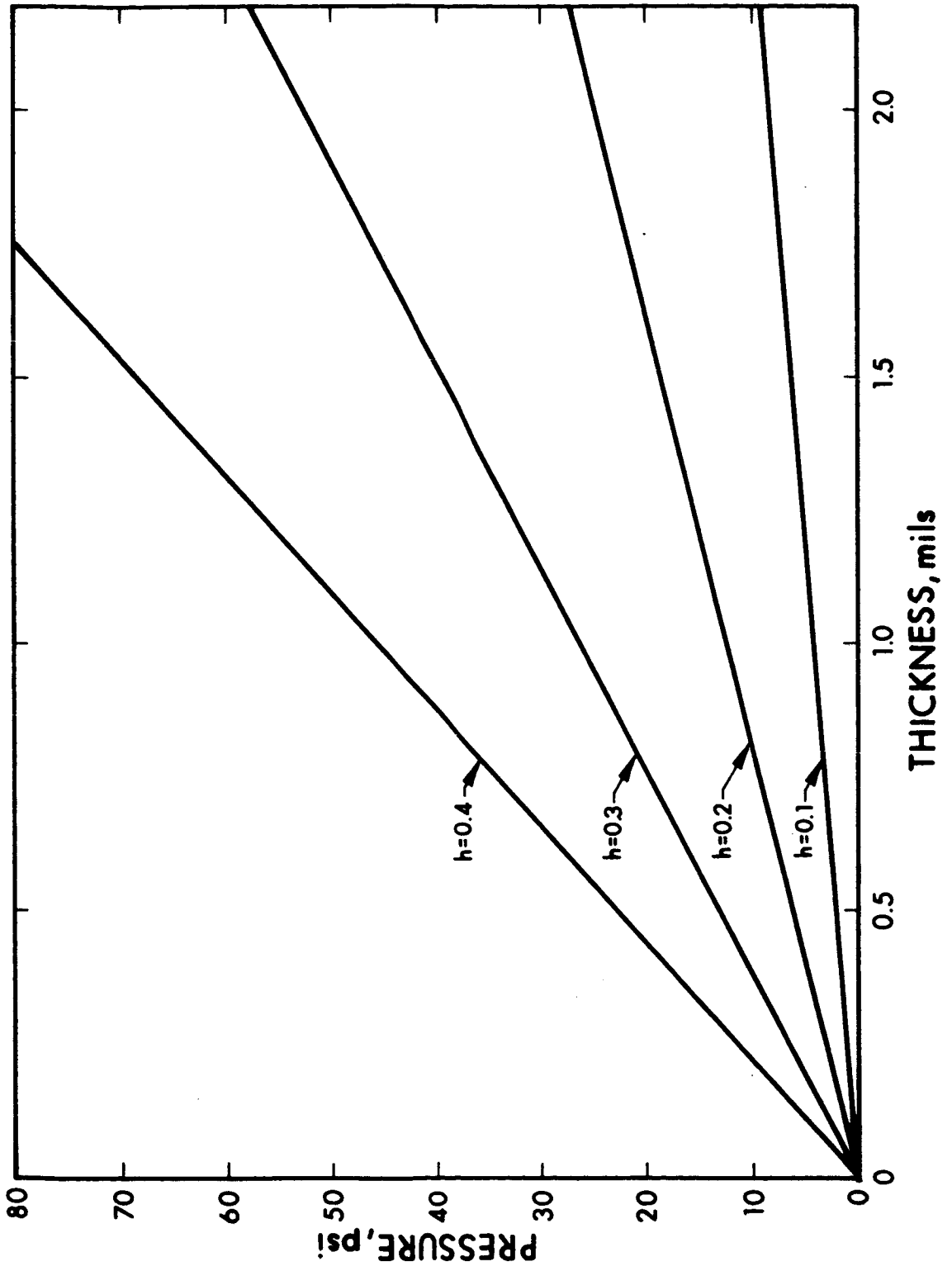
$$W_{ST} = \underline{0.065} \text{ #/FT}^2$$



7027-IDR

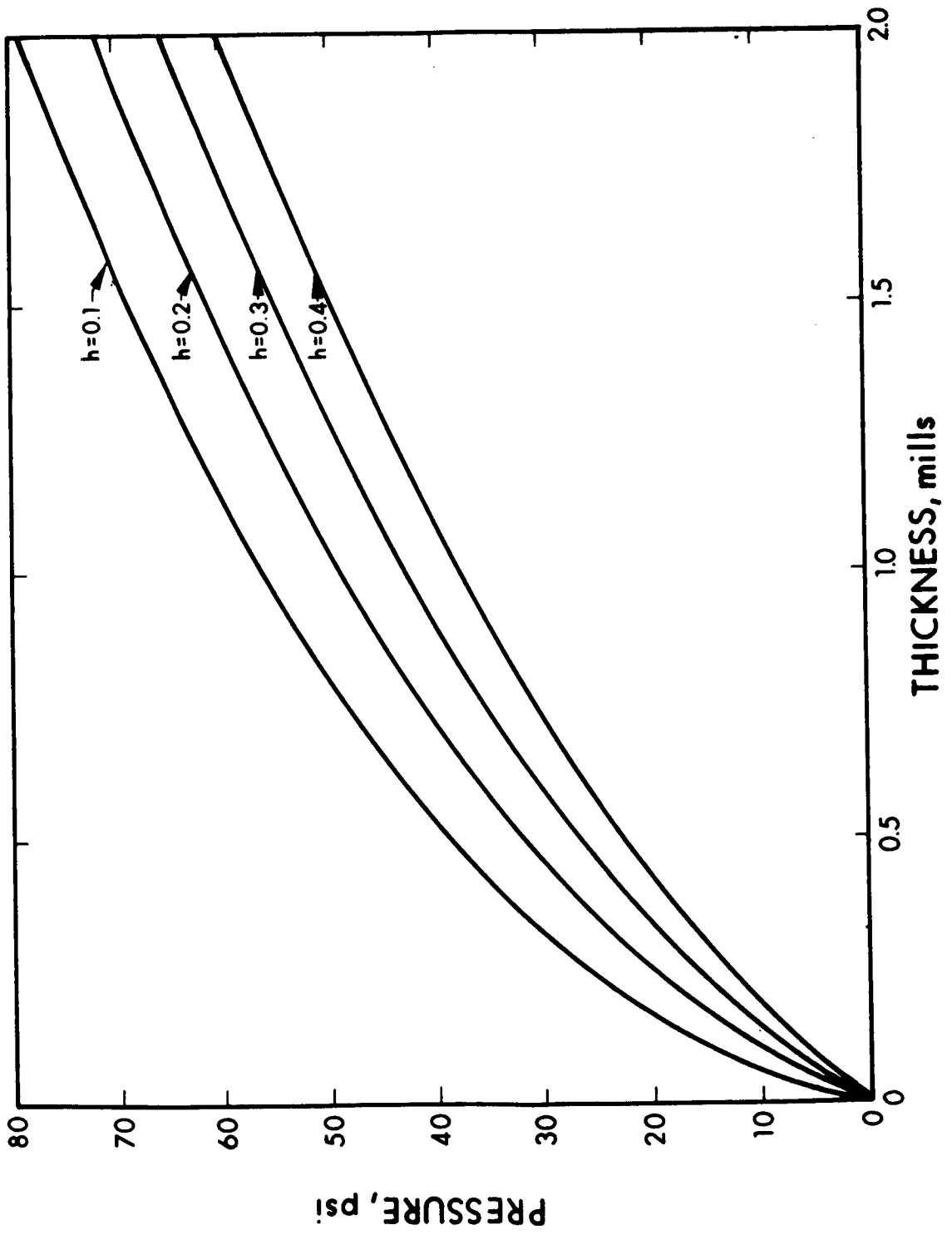


7027-IDR



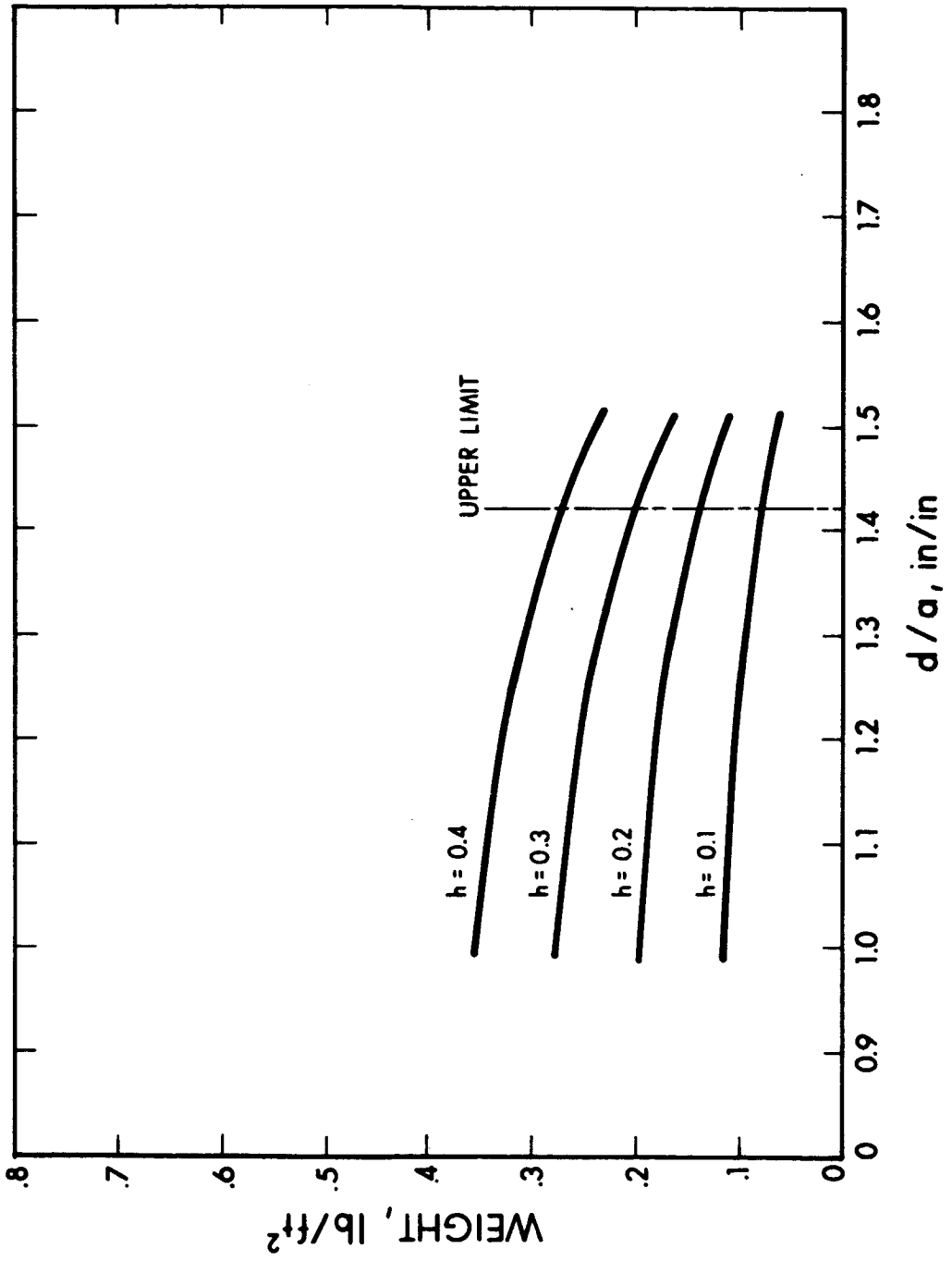
7027-IDR

215-

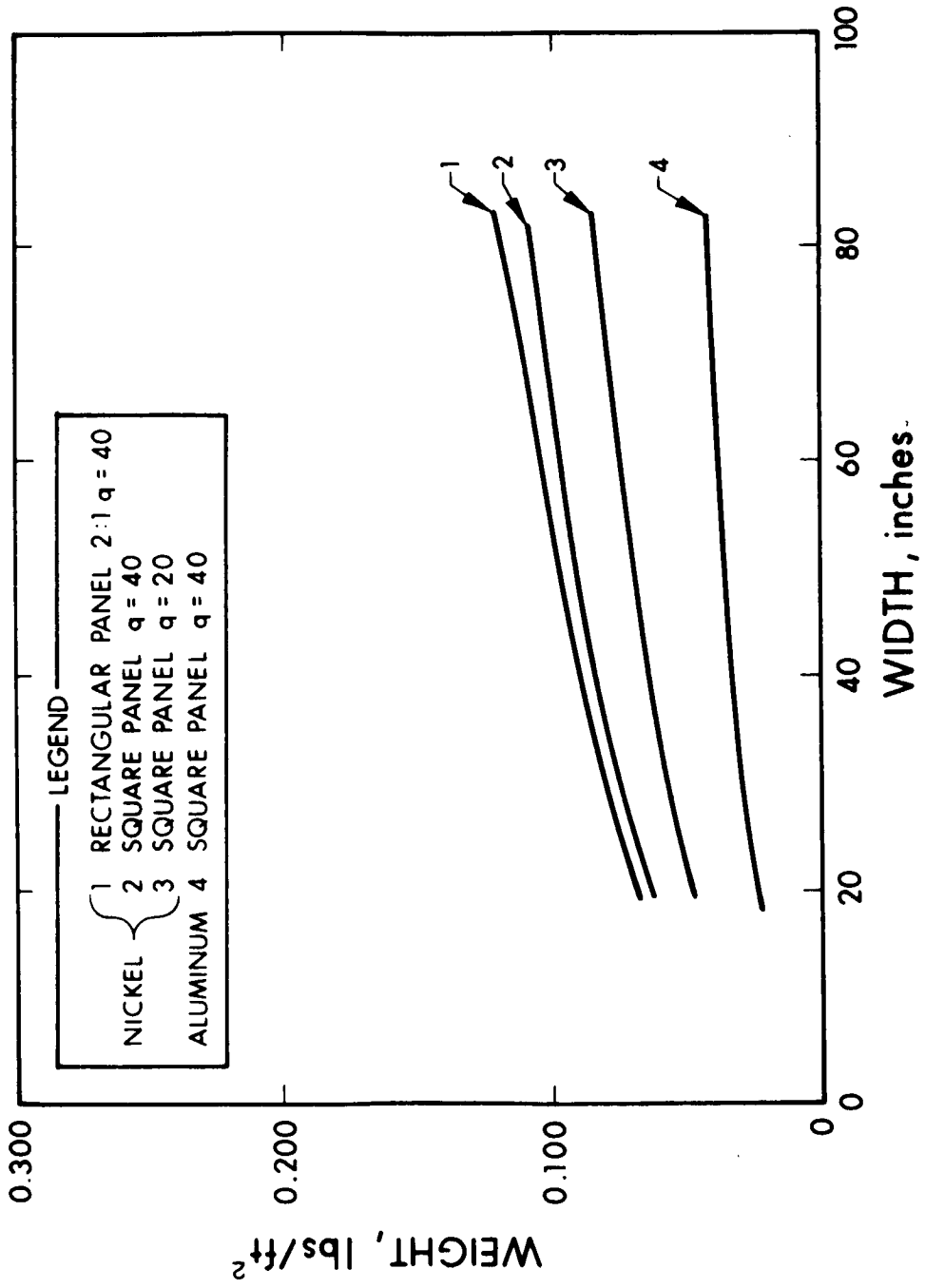


7027-IDR

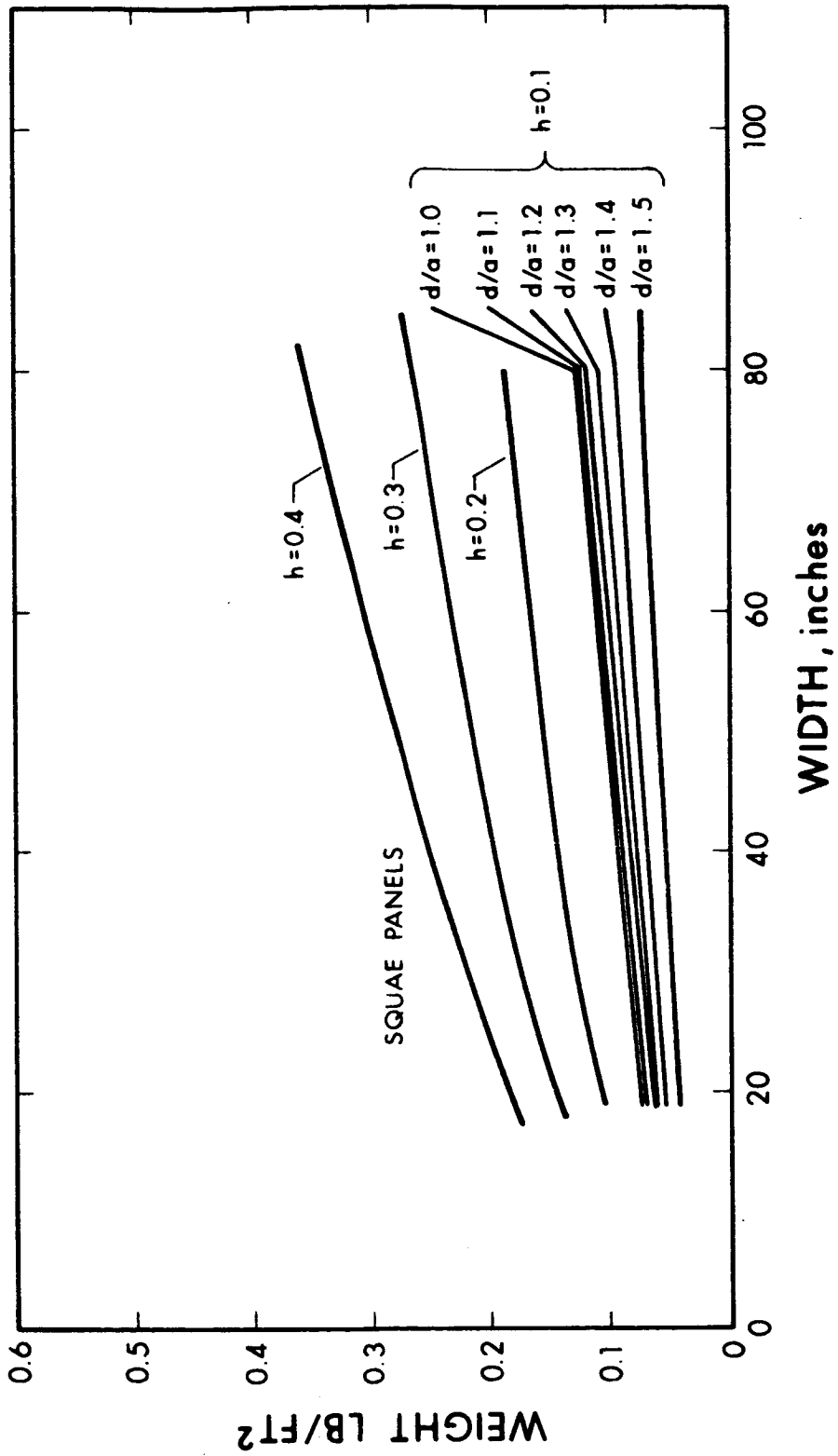
910

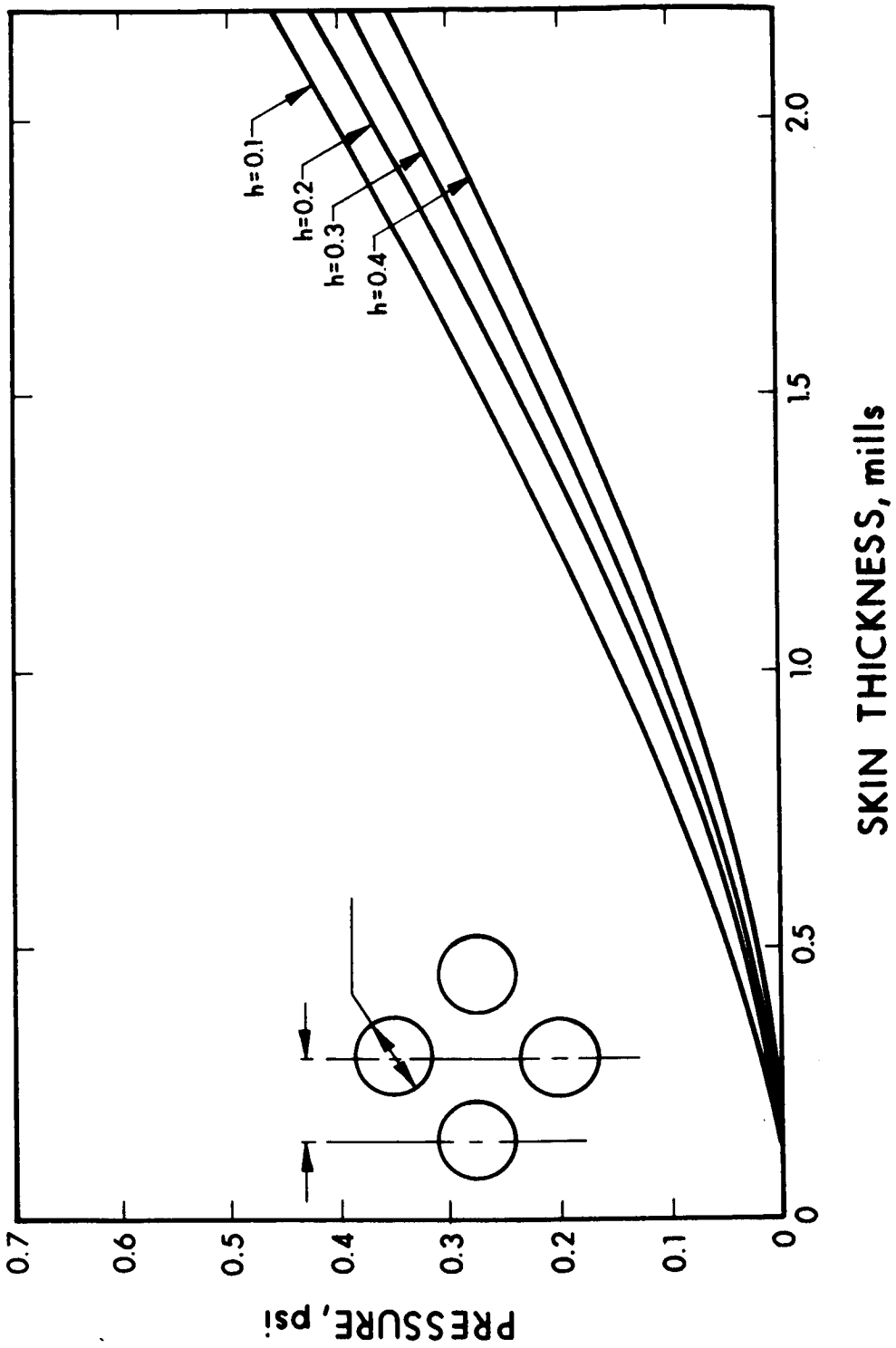


7027-IDR



7027-IDR





7027-IDR

APPENDIX D

EQUATION DERIVATIONS FOR STRUCTURAL ANALYSIS
OF DEMONSTRATION PANEL

APPENDIX D
EQUATION DERIVATIONS FOR STRUCTURAL ANALYSIS
OF DEMONSTRATION PANEL

This appendix contains the detailed stress analysis of the demonstration panel. The derivations for the equations used to analyze the biconvex substrate are presented on the following pages.

CALCULATION SHEET

By _____

Subject _____ Checked By _____ Date _____

ELECTRO-OPTICAL SYSTEMS, INC.

STRUCTURE STRESS ANALYSIS.

DESIGN CRITERIA

THEORY OF DOUBLY CURVED PANELS.

PANEL FREQUENCY.

PANEL BUCKLING.

PANEL CRIPPLING.

PANEL WEIGHT

PANEL INERTIA.

MEMBRANE STRESS

BUCKLING COEFFICIENTS.

THEORY OF PRESTRESSED DIAPHRAGM

FREQUENCY

STRESS

FRAME ANALYSIS

STRESS

STRENGTH.

D-2

CALCULATION SHEET

By B.T.

Subject STRUCTURAL ANALYSIS Checked By _____ Date _____

ELECTRO-OPTICAL SYSTEMS, INC.

STRUCTURAL ANALYSIS OF BICONVEX SOLAR PANELS.

DESIGN CRITERIA

INFORMATION TAKEN FROM:
 DESIGN CRITERIA AND REQUIREMENTS SPECIFICATIONS
 JANUARY 1966 (EOS DOCUMENT)
 SIGNED BY R.L. MOORE.

GROUND HANDLING & TRANSPORTATION

THE ASSEMBLY SHALL BE HANDLED IN SUITABLE TRANSPORT-PACKAGE TO MAINTAIN LOADS BELOW FLIGHT CONDITIONS.

VIBRATION ENVIRONMENT - STOWED

ONLY AFT ATTACHMENT POINT WILL BE USED.

SINUSOIDAL

$2 \leq f \leq 10$	1.5 g	R.M.S
$10 \leq f \leq 20$	1.5 g	"
$20 \leq f \leq 50$	1.5 g	"
$50 \leq f \leq 200$	2.0 g	"

VIBRATION INPUT IN ONE PLANE AT A TIME (NOT COMBINED)

RANDOM GAUSSIAN VIBRATION

0.2 g^2/cps 200 CPS → 2000 CPS

STATIC ENVIRONMENT STOWED

18 g LONGITUDINAL
 1 g LATERAL

DYNAMIC CHARACTERISTICS

FIRST MODE LESS THAN 10 CPS OR
 GREATER THAN 25 CPS

EOS

CALCULATION SHEET

By _____

Subject _____ Checked By _____ Date _____

ELECTRO-OPTICAL SYSTEMS, INC.

ACOUSTIC ENVIRONMENT

MAXIMUM 146 db OVERALL

THERMAL ENVIRONMENT

NO DEGRADATION TAKES PLACE DURING STOWED CONDITION.

DEPLOYED CONDITION

THERMAL GRADIENTS CAUSED BY SOLAR INPUT OF 360 W/FT²

STEADY STATE ACCELERATION

$3 \times 10^{-5} g$ AT 45° TO PLANE OF ARRAY

PITCHING

2×10^{-5} RADIANS / SEC²

ARRAY DYNAMIC CHARACTERISTICS

$f > 0.04$ CPS.

MATERIAL CONSIDERATIONS

MATERIALS USED IN PRIMARY STRUCTURES SHALL HAVE PROPERTIES AS SPECIFIED IN MIL HDBK 5 FOR METALLIC MATERIALS

MIL HDBK 17 FOR PLASTICS.

MATERIALS NOT ^{INCLUDED} IN ABOVE ~~■~~ MUST BE TESTED TO OBTAIN 0.999 RELIABILITY WITH A CONFIDENCE LEVEL OF 90.76.

4

**E
O
S**

Page 3 of _____

CALCULATION SHEET

By _____

Subject _____ Checked By _____ Date _____

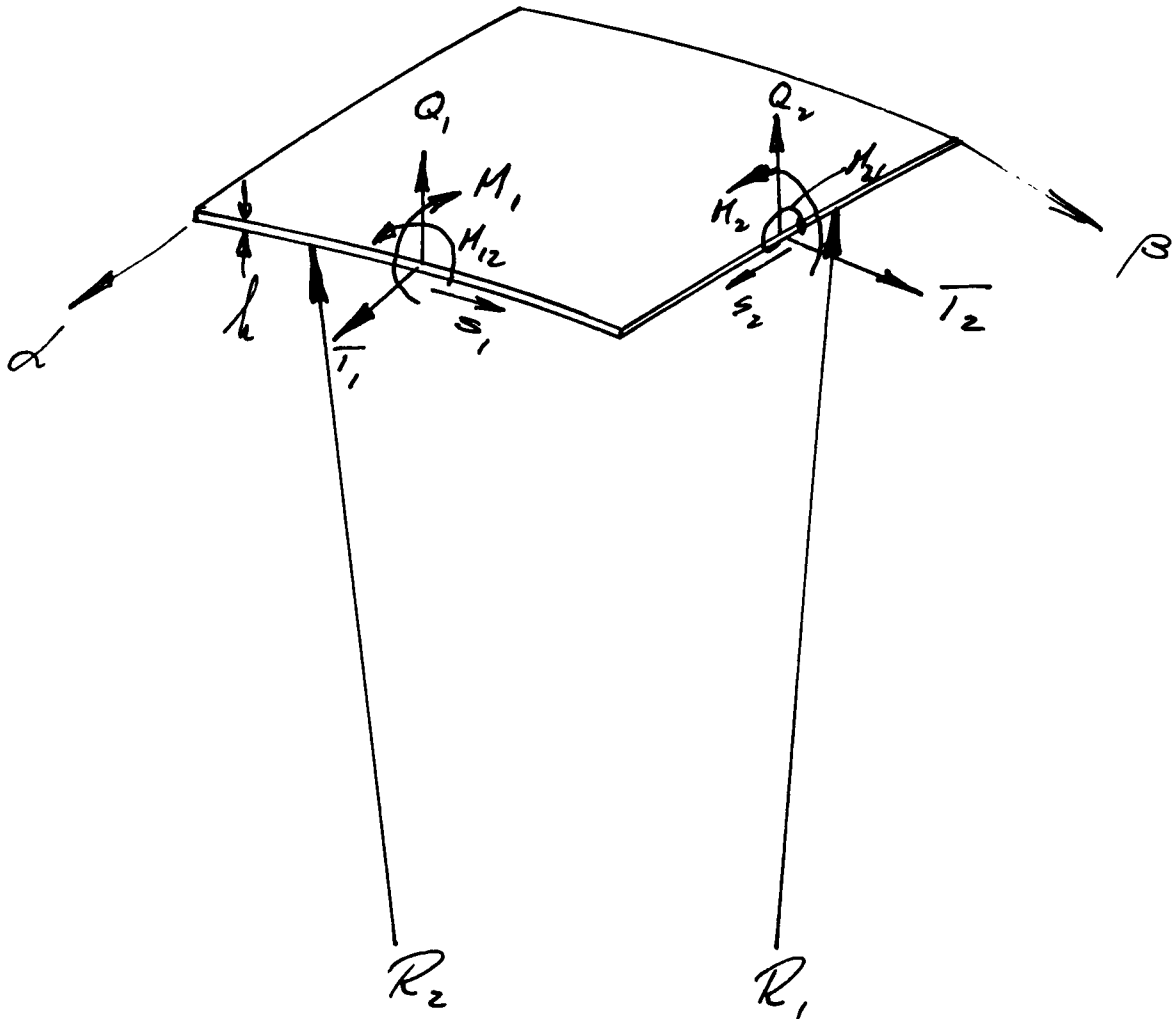
ELECTRO-OPTICAL SYSTEMS, INC.

*POLYMERIC MATERIALS TO BE SHIELDED OR SELECTED
TO WITHSTAND DEEP SPACE ENVIRONMENT*

7027-IDR

EOS Form No. 6303 (7/64-200)

THEORY OF DOUBLY CURVED PANELS.



- $M_1 \ \& \ M_2$ = APPLIED MOMENT
- $Q_1 \ \& \ Q_2$ = SHEAR
- $T_1 \ \& \ T_2$ = MEMBRANE LOAD
- $S_1 \ \& \ S_2$ = SHEAR
- $H_{12} \ \& \ H_{21}$ = TORQUE
- $\alpha \ \& \ \beta$ = ARC DIMENSIONS
- $R_1 \ \& \ R_2$ = PANEL CURVATURE GENERATORS.

CALCULATION SHEET

By _____

Subject _____ Checked By _____ Date _____

ELECTRO-OPTICAL SYSTEMS, INC.

TO MAINTAIN RADIAL EQUILIBRIUM:

$$1) \frac{1}{R_2} \frac{\partial^2 \phi}{\partial \alpha^2} + \frac{1}{R_1} \frac{\partial^2 \phi}{\partial \beta^2} + D \nabla^4 W + \rho h \frac{\partial^2 W}{\partial t^2} = 0$$

DISPLACEMENT COMPATIBILITY

$$2) \frac{1}{Eh} \nabla^4 \phi - \frac{1}{R_2} \frac{\partial^2 W}{\partial \alpha^2} - \frac{1}{R_1} \frac{\partial^2 W}{\partial \beta^2} = 0$$

HERE

 ϕ = STRESS FUNCTION

W = DISPLACEMENT FUNCTION

$$T_1 = \frac{\partial^2 \phi}{\partial \alpha^2}$$

$$T_2 = \frac{\partial^2 \phi}{\partial \beta^2}$$

$$S = - \frac{\partial^2 \phi}{\partial \alpha \cdot \partial \beta}$$

$$D = EI \frac{1}{1-\nu^2}$$

 ρ = MASS DENSITY

E = MODULUS OF ELASTICITY

I = MATERIAL MOMENT OF INERTIA

h = MATERIAL THICKNESS (EQUIVALENT)

MOMENTS & SHEARS CAN BE DETERMINED BY

DISPLACEMENT W.

$$M_1 = D \left(\frac{\partial^2 W}{\partial \alpha^2} + \nu \frac{\partial^2 W}{\partial \beta^2} \right)$$

$$M_2 = D \left(\frac{\partial^2 W}{\partial \beta^2} + \nu \frac{\partial^2 W}{\partial \alpha^2} \right)$$

CALCULATION SHEET

By _____

Subject _____ Checked By _____ Date _____

ELECTRO-OPTICAL SYSTEMS, INC.

$$H = - D (1 - \nu) \frac{d^2 W}{d\alpha \cdot d\beta}$$

$$Q_1 = - D \frac{\partial}{\partial \alpha} \nabla^2 W$$

$$Q_2 = - D \frac{\partial}{\partial \beta} \nabla^2 W$$

KIRCHHOFF SHEARS

$$Q_1^* = Q_1 + \frac{\partial H}{\partial \alpha} = - D \left[\frac{\partial^3 W}{\partial \alpha^3} + (2 - \nu) \frac{\partial^3 W}{\partial \alpha \partial \beta^2} \right]$$

$$Q_2^* = Q_2 + \frac{\partial H}{\partial \beta} = - D \left[\frac{\partial^3 W}{\partial \beta^3} + (2 - \nu) \frac{\partial^3 W}{\partial \beta \partial \alpha^2} \right]$$

NORMAL DISPLACEMENTS CAN BE OBTAINED FROM

$$T_1 = \frac{Eh}{1 - \nu^2} (\epsilon_\alpha + \nu \epsilon_\beta)$$

$$T_2 = \frac{Eh}{1 - \nu^2} (\epsilon_\beta + \nu \epsilon_\alpha)$$

$$\epsilon_\alpha = \frac{\partial u}{\partial \alpha} + \frac{W}{R_1}$$

ROTATION + EXTENSION

$$\epsilon_\beta = \frac{\partial v}{\partial \beta} + \frac{W}{R_2}$$

$$\epsilon_{\alpha\beta} = \frac{\partial u}{\partial \beta} + \frac{\partial v}{\partial \alpha}$$

$$S_1 = \frac{Eh}{2(1 + \nu)} \epsilon_{\alpha\beta}$$

CALCULATION SHEET

By _____

Subject _____ Checked By _____ Date _____

ELECTRO-OPTICAL SYSTEMS, INC.

IF WE CAN ASSUME SIMPLE SUPPORT OF EDGES THEN

$$W = V = H_1 = T_1 = 0 \quad \text{ON } \alpha = 0 \quad ; \quad \alpha = \alpha_0$$

$$W = U = H_2 = T_2 = 0 \quad \text{ON } \beta = 0 \quad ; \quad \beta = \beta_0$$

WE CAN THEN ASSUME:

$$\phi = \sum_m \sum_n A_{mn} \sin \lambda_m \alpha \cdot \sin \mu_n \beta \cdot \sin \omega_{mn} t$$

$$W = \sum_m \sum_n B_{mn} \sin \lambda_m \alpha \cdot \sin \mu_n \beta \cdot \sin \omega_{mn} t$$

$$\lambda_m = m \frac{\pi}{\alpha_0}$$

$$\mu_n = n \frac{\pi}{\beta_0}$$

$$\frac{\partial \phi}{\partial \alpha} = - \sum_m \sum_n A_{mn} \lambda_m \cos \lambda_m \alpha \cdot \sin \mu_n \beta \cdot \sin \omega_{mn} t$$

$$\frac{\partial^2 \phi}{\partial \alpha^2} = - \sum_m \sum_n A_{mn} \lambda_m^2 \sin \lambda_m \alpha \cdot \sin \mu_n \beta \cdot \sin \omega_{mn} t$$

$$\frac{\partial^3 \phi}{\partial \alpha^3} = + \sum_m \sum_n A_{mn} \lambda_m^3 \cos \lambda_m \alpha \cdot \sin \mu_n \beta \cdot \sin \omega_{mn} t$$

$$\frac{\partial \phi}{\partial \beta} = - \sum_m \sum_n A_{mn} \mu_n \sin \lambda_m \alpha \cdot \cos \mu_n \beta \cdot \sin \omega_{mn} t$$

$$\frac{\partial^2 \phi}{\partial \beta^2} = - \sum_m \sum_n A_{mn} \mu_n^2 \sin \lambda_m \alpha \cdot \sin \mu_n \beta \cdot \sin \omega_{mn} t$$

$$\frac{\partial^3 \phi}{\partial \beta^3} = + \sum_m \sum_n A_{mn} \mu_n^3 \sin \lambda_m \alpha \cdot \cos \mu_n \beta \cdot \sin \omega_{mn} t$$

CALCULATION SHEET

By _____

Subject _____ Checked By _____ Date _____

ELECTRO-OPTICAL SYSTEMS, INC.

$$\frac{\partial \phi}{\partial t} = - \sum_m \sum_n A_{mn} \omega_{mn} \sin \lambda_m \alpha \cdot \sin \mu_n \beta \cdot \cos \omega_{mn} t$$

$$\frac{\partial^2 \phi}{\partial t^2} = - \sum_m \sum_n A_{mn} \cdot \omega_{mn}^2 \sin \lambda_m \alpha \cdot \sin \mu_n \beta \cdot \cos \omega_{mn} t$$

$$\nabla^2 = \frac{\partial^2}{\partial \alpha^2} + \frac{\partial^2}{\partial \beta^2}$$

SIMILAR EXPRESSION TO ONES ABOVE MAY BE OBTAINED FOR W

INSERTING INTO (1) & (2) AND SOLVE SIMULTANEOUSLY

WE OBTAIN:

$$(3) \quad \omega_{mn}^2 = \frac{1}{8h} \left[D(\lambda_m^2 + \mu_n^2)^2 + Eh \left(\frac{\frac{\lambda_m^2}{R_2} + \frac{\mu_n^2}{R_1}}{\lambda_m^2 + \mu_n^2} \right)^2 \right]$$

$$\sum_m \sum_n A_{mn} = - \left(\frac{\lambda_m^2}{R_2} + \frac{\mu_n^2}{R_1} \right)$$

$$\sum_m \sum_n B_{mn} = \frac{1}{Eh} (\lambda_m^2 + \mu_n^2)^2$$

BY EXAMINING THE TERMS IN (3) WE SEE THAT THE FIRST TERM

$D(\lambda_m^2 + \mu_n^2)^2$ IS THE FLAT PLATE TERM

$Eh \left(\frac{\frac{\lambda_m^2}{R_2} + \frac{\mu_n^2}{R_1}}{\lambda_m^2 + \mu_n^2} \right)^2$ IS THE CURVATURE EFFECT.

CALCULATION SHEET

By _____

Subject _____ Checked By _____ Date _____

ELECTRO-OPTICAL SYSTEMS, INC.

$$M_1 = D \left[- \sum_{m,n} \frac{1}{\lambda_{mn}^2} + \left(- \sum_{m,n} \frac{1}{\mu_{mn}^2} \right) \right] \text{ (Note: } \lambda_{mn}^2 \text{ and } \mu_{mn}^2 \text{ are } \frac{1}{R_2} \text{ and } \frac{1}{R_1} \text{ respectively)}$$

$$= - \frac{D}{Eh} \left(\lambda_{mn}^2 + \mu_{mn}^2 \right)^2 \left(\lambda_{mn}^2 + \sqrt{\mu_{mn}^2} \right)$$

$$M_2 = - \frac{D}{Eh} \left(\lambda_{mn}^2 + \mu_{mn}^2 \right)^2 \left(\mu_{mn}^2 + \sqrt{\lambda_{mn}^2} \right)$$

FREQUENCY

THE CRITICAL FREQUENCY CAN BE OBTAINED FROM

$$f = \frac{\omega}{2\pi}$$

$$f_{mn} = \left[\frac{1}{4\pi^2} \frac{1}{gh} \left[D \left(\lambda_{mn}^2 + \mu_{mn}^2 \right)^2 + Eh \left(\frac{\lambda_{mn}^2}{R_2} + \frac{\mu_{mn}^2}{R_1} \right)^2 \right] \right]^{\frac{1}{2}}$$

PANEL BUCKLING

TO DETERMINE PANEL BUCKLING WE MUST

ADD FORCES TO FREQUENCY EQUATION TO MAKE

$$\omega_{mn} \rightarrow 0$$

$$\omega_{mn}^2 = \frac{1}{gh} \left[D \left(\lambda_{mn}^2 + \mu_{mn}^2 \right)^2 + Eh \left(\frac{\lambda_{mn}^2}{R_2} + \frac{\mu_{mn}^2}{R_1} \right)^2 + \lambda_{mn}^2 T_1 + \mu_{mn}^2 T_2 \right]$$

FOR $\omega_{mn} = 0$

$$D \left(\lambda_{mn}^2 + \mu_{mn}^2 \right)^2 + Eh \left(\frac{\lambda_{mn}^2}{R_2} + \frac{\mu_{mn}^2}{R_1} \right)^2 + \lambda_{mn}^2 T_1 + \mu_{mn}^2 T_2 = 0$$

FOR A BODY OF REVOLUTION:

7027-IDR

CALCULATION SHEET

By _____

Subject _____ Checked By _____ Date _____

ELECTRO-OPTICAL SYSTEMS, INC.

$$T_1 = \frac{p R_1}{2}$$

$$T_2 = \frac{p R_1}{2} \left(2 - \frac{R_1}{R_2} \right)$$

$$p \frac{R_1}{2} \left(\lambda_m^2 + \mu_m^2 \left(2 - \frac{R_1}{R_2} \right) \right) = \left[D(\lambda_m^2 + \mu_m^2)^2 + E h \left(\frac{\lambda_m^2 + \mu_m^2}{\lambda_m^2 + \mu_m^2} \right) \right]^{1/2}$$

$$p = - \frac{D(\lambda_m^2 + \mu_m^2)^2 + E h \left(\frac{\lambda_m^2 + \mu_m^2}{\lambda_m^2 + \mu_m^2} \right)^2}{\frac{R_1}{2} \left(\lambda_m^2 + \mu_m^2 \left(2 - \frac{R_1}{R_2} \right) \right)}$$

FOR SPHERICAL SURFACE

$$R_1 = R_2 = R$$

$$f = \frac{1}{2\pi} \left[\frac{1}{5h} \left(D(\lambda_m^2 + \mu_m^2)^2 + \frac{E h}{R} \right) \right]^{1/2}$$

$$p = - \frac{D(\lambda_m^2 + \mu_m^2)^2 + \frac{E h}{R}}{\frac{R}{2} (\lambda_m^2 + \mu_m^2)}$$

CALCULATION SHEET

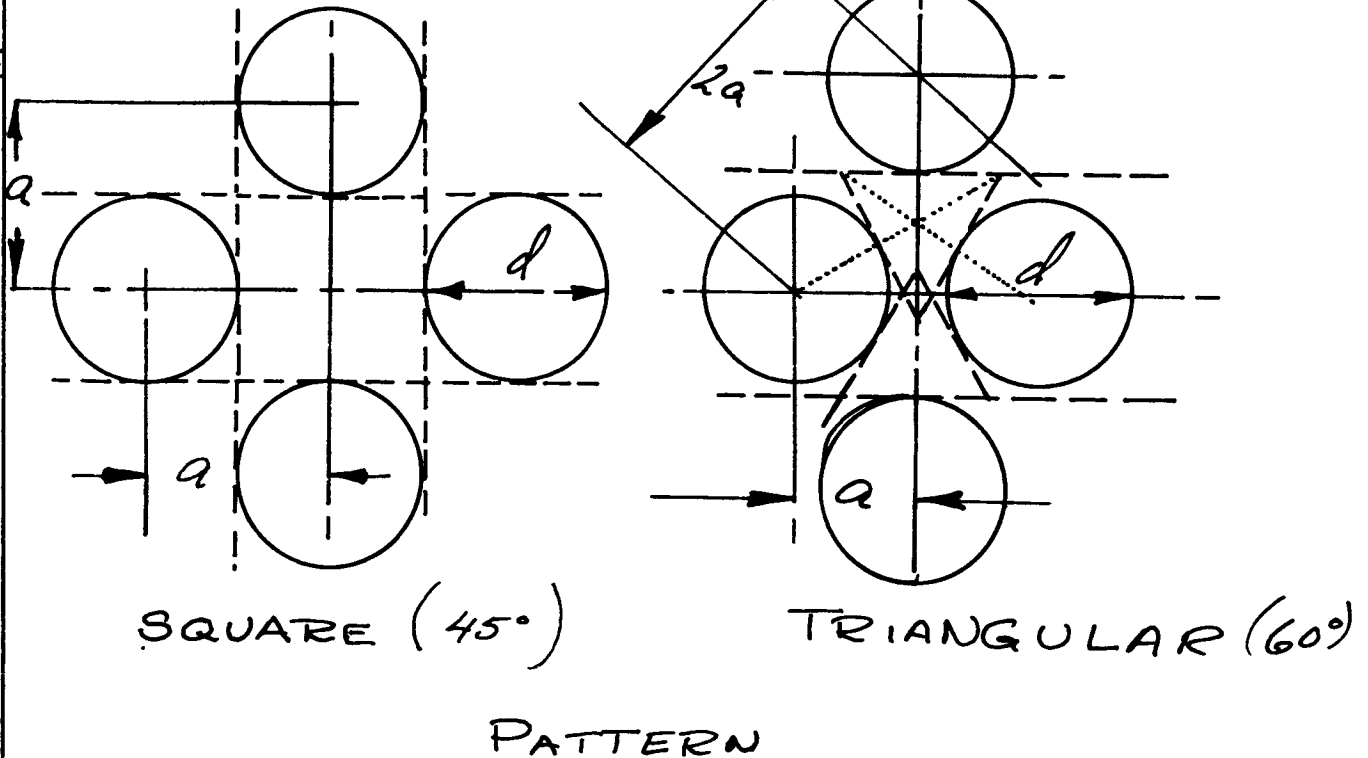
By _____

Subject _____ Checked By _____ Date _____

ELECTRO-OPTICAL SYSTEMS, INC.

THERE MAY EXIST A CONDITION OF CRIPPLING OF THE TOP SURFACES.

CRIPPLING



THE EFFECTIVE PANELS WILL BE AS SHOWN ABOVE.

SQUARE PATTERN:

SIDE : $S = \frac{2a - d}{2}$

LIMIT : $\sqrt{a^2 + a^2} - d = 0 \quad 1.414a - d = 0$

or $\frac{d}{a} = 1.414$

AT THIS POINT THE CIRCLE TOUCHES EACH OTHER.

$$\tau_{CR} = K_s \frac{\pi^2 E}{12(1-\nu^2)} \left(\frac{t}{2a-d} \right)^2$$

K = EMPIRICAL BUCKLING COEFFICIENT PER NASA TN 3781

E = MODULUS OF ELASTICITY

CALCULATION SHEET

By _____

Subject _____ Checked By _____ Date _____

ELECTRO-OPTICAL SYSTEMS, INC.

ν = POISSON'S RATIO ~ 0.3

t = SKIN THICKNESS

$2a$ = HOLE SPACING

d = DIAMETER OF HOLES.

TRIANGULAR PATTERN

$$S = 4a - d \tan 60^\circ = \underline{\underline{4a - 1.732d}}$$

$$\tau_{CR} = K_T \frac{\pi^2 E}{12(1-\nu^2)} \left(\frac{t}{4a - 1.732d} \right)^2$$

LIMIT $2a = d$

$$\underline{\underline{d/a = 2.00}} \quad \text{TOUCHING!}$$

CALCULATION SHEET

By _____

Subject _____ Checked By _____ Date _____

ELECTRO-OPTICAL SYSTEMS, INC.

HOLLOW CORE WEIGHT.

PROJECTED SURFACE

$$A_p = 2a \cdot a \tan \phi - \frac{\pi}{4} d^2$$

$$= 2a^2 \tan \phi - \frac{\pi}{4} d^2$$

Per IN²

$$A_{PIN} = \frac{1}{2a^2 \tan \phi} \left[2a^2 \tan \phi - \frac{\pi}{4} d^2 \right]$$

$$\underline{\underline{A_{PIN} = 1 - \frac{\pi}{8} \left(\frac{d}{a}\right)^2 \cot \phi}}$$

WEIGHT PER RUNNING INCH

$$W_{PIN} = \frac{1}{2a^2 \tan \phi} \left[4a^2 \tan \phi - \frac{\pi}{2} d^2 + \pi d h \right] t \rho$$

WHERE

 h = PANEL HEIGHT t = SKIN THICKNESS ρ = MATERIAL DENSITY

$$\underline{\underline{W_{PIN} = \left[2 - \left(\frac{\pi}{4} \left(\frac{d}{a}\right)^2 - \frac{\pi}{2} \left(\frac{d}{a}\right) \left(\frac{h}{a}\right) \right) \cot \phi \right] t \rho}}$$

SQUARE PATTERN

$$W_{PIN45} = \left[2 - \frac{\pi}{4} \left(\frac{d}{a}\right)^2 + \frac{\pi}{2} \left(\frac{d}{a}\right) \frac{h}{a} \right] t \rho$$

TRIANGULAR PATTERN

$$W_{PIN60} = \left[2 - 0.45345 \left(\frac{d}{a}\right)^2 - 0.9069 \left(\frac{d}{a}\right) \frac{h}{a} \right] t \rho$$

CALCULATION SHEET

By _____

Subject _____ Checked By _____ Date _____

ELECTRO-OPTICAL SYSTEMS, INC.

d/a	$h=0.05$	$h=0.100$	$h=0.150$		DISTANCE BETW. HOLES	Q
1.0	0.981	1.185	1.385	} $\times 10^{-3}$	0.104	0.250
1.0	0.914	1.049	1.183		0.155	0.375
1.0	0.881	0.981	1.082		0.207	0.500
1.0	0.860	0.941	1.022		0.259	0.625
1.1	0.896	1.118	1.339		0.079	0.250
1.1	0.821	0.970	1.118		0.118	0.375
1.1	0.785	0.896	1.007		0.157	0.500
1.1	0.763	0.857	0.946		0.196	0.625
1.2	0.800	1.042	1.284		0.054	0.250
1.2	0.719	0.881	1.042		0.080	0.375
1.2	0.679	0.800	0.921		0.107	0.500
1.2	0.655	0.752	0.848		0.134	0.625
1.3	0.694	0.956	1.218		0.029	0.250
1.3	0.606	0.781	0.952		0.043	0.375
1.3	0.523	0.694	0.825		0.057	0.500
1.3	0.537	0.642	0.746		0.071	0.625
1.35	0.637	0.910	1.182		0.016	0.250
1.35	0.546	0.728	0.910		0.024	0.375
1.35	0.501	0.637	0.773		0.032	0.500
1.35	0.474	0.583	0.692		0.040	0.625
1.40	0.578	0.866	1.143	0.004	0.250	
1.40	0.483	0.672	0.860	0.005	0.375	
1.40	0.437	0.578	0.719	0.007	0.500	
1.40	0.376	0.522	0.635	0.009	0.625	
1.414	0.521	0.846	1.131	0	0.250	
1.414	0.465	0.652	0.846	0	0.375	
1.414	0.418	0.521	0.703	0	0.500	
1.414	0.390	0.504	0.618	0	0.625	

#/IN²

IN

$$W_p = \left[2 - \frac{\pi}{4} \left(\frac{d}{a}\right)^2 + \frac{\pi}{2} \left(\frac{d}{a} \times \frac{h}{a}\right) \right] t \rho$$

W_p IN^{45°}

$t = 0.002$ IN

$\rho = 0.321$ #/IN³

CALCULATION SHEET

By _____

Subject _____ Checked By _____ Date _____

ELECTRO-OPTICAL SYSTEMS, INC.

TRIANGULAR PATTERN

$$W_{P \text{ in } 60^\circ} = \left[2 - 0.45345 \left(\frac{d}{a} \right)^2 + 0.9069 \left(\frac{d}{a} \right) \left(\frac{h}{a} \right) \right] t \cdot \rho$$

$$d/a = 2.00, 1.95, 1.90, 1.80, 1.70, 1.60, 1.50$$

$$h/a = 0.05, 0.10, 0.150$$

$$Q = 0.250, 0.375, 0.500, 0.625$$

h/a	0.05	0.10	0.150	0.03
$Q = 0.250$	0.2	0.4	0.6	0.120
$Q = 0.3125$	0.16	0.320	0.48	0.096
$Q = 0.375$	0.133	0.266	0.40	0.080
$Q = 0.4375$	0.114	0.228	0.343	0.069
$Q = 0.500$	0.100	0.200	0.300	0.060
$Q = 0.5625$	0.089	0.178	0.267	0.053
$Q = 0.625$	0.080	0.160	0.240	0.048

SEE FIGURES 2.4.6 THROUGH 2.4.13 FOR
PLOTTED DATA. ATTACHED TABLE SHOWS CALCULATED
WEIGHTS.

$$W_p = \left[2 - 0.45345 \left(\frac{d}{a} \right)^2 + 0.9069 \left(\frac{d}{a} \right) \left(\frac{h}{a} \right) \right] 92.449 \cdot 10^{-3}$$

	0.25	0.375	0.375	0.4375	0.500	0.5625	0.625		h	distance
2.00	37.3	33.3	30.6	28.8	27.3	26.1	25.3		0.030	0
	50.8	44.0	39.6	36.3	34.0	32.1	30.6		0.050	0
	84.3	70.9	61.8	55.4	50.8	47.1	44.0		0.100	0
	117.8	97.7	84.3	74.7	67.5	62.0	57.5		0.150	0
	0	0	0	0	0	0	0			56305 1.76311
1.90	52.7	48.9	46.3	44.6	43.1	42.0	41.2		0.03	
	65.4	59.1	54.7	51.7	49.5	47.7	46.3		0.05	
	97.3	84.5	85.9	69.9	65.4	61.9	59.1		0.100	
	129.1	110.0	97.3	88.2	81.4	76.1	71.8		0.150	
	0.025	0.031	0.038	0.044	0.050	0.056	0.063			53082 1.6242
1.8	67.2	63.6	61.1	59.5	58.1	57.1	56.3		0.03	0
	79.3	73.2	69.2	66.3	64.2	62.5	61.1		0.05	
	109.4	97.4	89.2	83.5	79.3	75.9	73.2		0.10	
	139.6	121.5	109.4	100.8	94.3	89.4	85.3		0.15	
										668953 1.51173
1.7	80.8	77.4	75.1	73.6	72.3	71.3	70.6		0.03	
	92.3	86.5	82.7	80.0	78.0	76.4	75.1		0.05	
	120.8	104.4	101.7	96.2	92.3	89.1	86.5		0.10	
	149.3	132.2	120.8	112.6	106.5	101.8	98.0		0.15	
										149247 1.45104
1.6	93.7	90.5	88.3	86.8	85.6	84.7	84.0		0.03	
	104.4	97.0	95.4	92.9	91.0	89.5	88.3		0.05	
	131.2	120.5	113.3	108.2	104.4	101.5	99.0		0.10	
	158.1	142.0	131.2	123.6	117.8	113.4	109.8		0.15	697974 1.36035
1.5	105.7	102.6	100.6	99.3	98.1	97.2	96.6		0.03	
	115.7	110.7	107.3	104.9	103.2	101.8	100.6		0.05	
	146.9	130.8	124.0	119.2	115.7	113.0	110.7		0.10	
	166.6	152.9	140.9	133.7	128.3	124.2	120.8		0.15	
	①	②	3	4	5	6	7			

18-18

CALCULATION SHEET

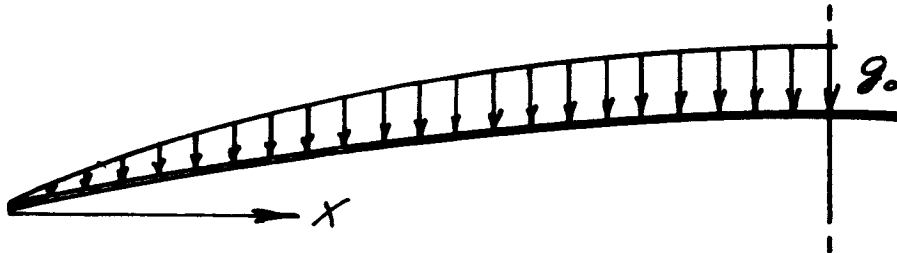
By _____

Subject _____ Checked By _____ Date _____

ELECTRO-OPTICAL SYSTEMS, INC.

PANEL INERTIA.

THE PANEL GAIN WILL BE INCREASING FROM THE EDGES TOWARDS THE PANEL CENTER.



$$g = g_0 \cdot \sin \frac{\pi}{l} x$$

DYNAMIC

$l =$ PANEL WIDTH

$$g_{ave} = 0.707 g_0$$

EFFECTIVE PRESSURE

$$p = W_t \cdot g = \left[2 - \left(\frac{\pi}{4} \left(\frac{d}{a} \right)^2 - \frac{\pi}{2} \left(\frac{d}{a} \right) \left(\frac{h}{a} \right) \right) \right] (g)$$

$$g = g_{STATIC} + g_{DYNAMIC} \cdot g$$

$$= g_{STAT} + g_0 \sin \frac{\pi}{l} x \cdot g$$

$g =$ AMPLIFICATION FACTOR.

$$p = \left[2 - \left(\frac{\pi}{4} \left(\frac{d}{a} \right)^2 - \frac{\pi}{2} \left(\frac{d}{a} \right) \left(\frac{h}{a} \right) \right) \cotan \phi \right] \left[g_{STAT} + g_0 \sin \frac{\pi}{l} x \right]$$

TO SIMPLIFY THE EXPRESSION g_{ave} WILL BE USED

$$p = \left[2 - \left(\frac{\pi}{4} \left(\frac{d}{a} \right)^2 - \frac{\pi}{2} \left(\frac{d}{a} \right) \left(\frac{h}{a} \right) \right) \cotan \phi \right] \left[g_{STAT} + 0.707 g_0 \right]$$

$$P_{sc} = \left[\frac{W_{sc}}{144} \right] \left[g_{STAT} + g_0 \cdot 0.707 \right]$$

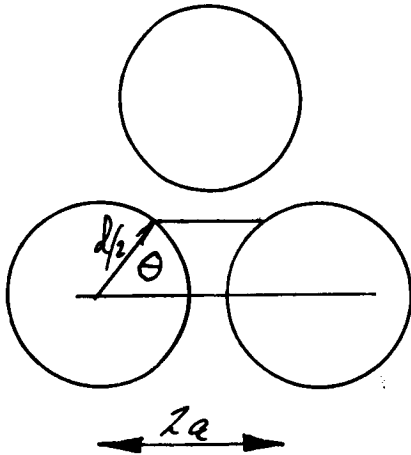
MEMBRANE STRESS

SINCE THE PANEL IS SPHERICAL IN CURVATURE

$$f = \frac{pR}{2t_{eff}}$$

R = RADIUS OF CURVATURE

t_{eff} = EFFECTIVE MATERIAL THICKNESS.



$$t_{eff} = \frac{1}{2a} (2a - 2 \cdot \frac{d}{2} \cos \theta + 2h) t$$

$$= 2 \left(1 - \frac{1}{2} \frac{d}{a} \cos \theta \right) + \frac{h}{a} t = \left(2 - \frac{d}{a} \cos \theta + \frac{h}{a} \right) t$$

RADIUS OF CURVATURE



$$R_1 = \frac{c}{\sin \alpha}$$

$$R_2 = \frac{B}{\sin \beta}$$

CALCULATION SHEET

By _____

Subject _____ Checked By _____ Date _____

ELECTRO-OPTICAL SYSTEMS, INC.

STRESS

$$p_t = p_{sr} + p_{sc}$$

$$= \left[\frac{w_{sc}}{144} + \left[2 - \left(\frac{\pi(d)}{4(a)} \right)^2 - \frac{\pi}{2} \left(\frac{d}{a} \right) \left(\frac{h}{a} \right) \right] \cot \alpha \right] t g \left[g_{stat} + \frac{g_{air}}{1000} \right]$$

$$f_m = \frac{p_t R}{2 t_{eq}}$$

$$R = \frac{C}{\sin \alpha} \quad \text{OR} \quad \frac{B}{\sin \beta}$$

$$t_{eq} = \left(2 - \frac{d}{a} \cos \theta + \frac{h}{a} \right) t$$

$$f_m = \frac{\left[\frac{w_{sc}}{144} + \left[2 - \left(\frac{\pi(d)}{4(a)} \right)^2 - \frac{\pi}{2} \left(\frac{d}{a} \right) \left(\frac{h}{a} \right) \cot \alpha \right] t g \left[g_{stat} + 0.707 g_{air} \right] c \left[2 - \frac{C \sin \beta}{B \sin \alpha} \right]}{2 \left(2 - \frac{d}{a} \cos \theta + \frac{h}{a} \right) t \sin \alpha}$$

CALCULATION SHEET

By _____

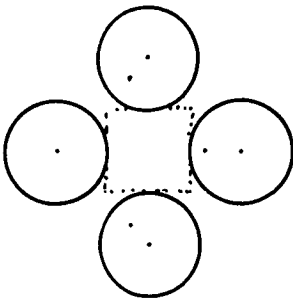
Subject _____ Checked By _____ Date _____

ELECTRO-OPTICAL SYSTEMS, INC.

BUCKLING COEFFICIENTS (CRIPPLING)

THE LOADING IS IN ALL CASES BIDIRECTIONAL

SQUARE PATTERN HOLE LAY OUT.



THE PANEL EDGES WILL HAVE 0 ROTATION AND DEFLECTION AND MAY THUS BE ASSUMED FIXED.

FROM : NORTH AMERICAN AVIATION

STRUCTURES MANUAL P.P 6.60.05

E 6.60.08

WE CAN COLLECT THE FOLLOWING EMPIRICAL DATA :

$$\sigma_{x,CR} = K_x \frac{\pi^2 E}{12(1-\nu^2)} \left(\frac{t}{b}\right)^2 \quad \sigma_{y,CR} = K_y \frac{\pi^2 E}{12(1-\nu^2)} \left(\frac{t}{b}\right)^2$$

HERE K_x AND K_y MAY BE SELECTED SUCH THAT

$$\frac{\sigma_x}{f_1} = \frac{\sigma_y}{f_2} \quad a/b = 1$$

	SIMPLE SUPPORT		FIXED SUPPORT	
	K_x	K_y	K_x	K_y
1	-3	7	-0.7	11
2	-2	6	0	10.35
3	-1	5	1	9.40
4	0	4	2	8.45
5	1	3	3	7.50
6	2	2	4	6.55
7	3	1	5	5.62
8	4	0	6	4.65
9	4.9	-1	7	3.60
10	5.45	-2	8	2.48
11	6.00	-3	9	1.35
12	6.50	-4	10	-0.2
13	6.92	-5	11	-2.0

CALCULATION SHEET

By _____

Subject _____ Checked By _____ Date _____

ELECTRO-OPTICAL SYSTEMS, INC.

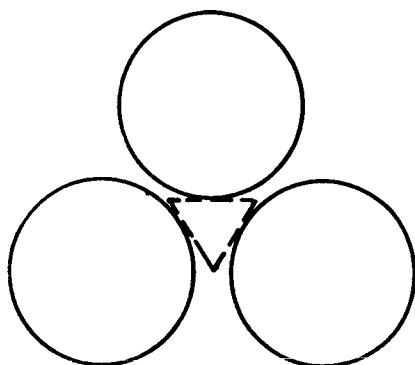
E = MODULUS OF ELASTICITY

ν = POISSON'S RATIO.

t = SKIN THICKNESS

$l = (2a - d)$ NOTATIONS AS USED IN REPORT

TRIANGULAR HOLE PATTERN

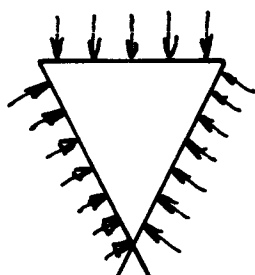


THE STRESS IN THE CRITICAL SECTION WILL BE BIDIRECTIONAL

PER NACA TN 3781

BUCKLING OF FLAT PLATES

$K = 12$



A CRIPPLING FACTOR OF 8.5 WILL BE USED IN DETERMINING CRITICAL STRENGTH

$K = 0.707 \times 12 = \underline{\underline{8.5}}$

TO INCLUDE THE EFFECT OF BIDIRECTIONAL STRESS.

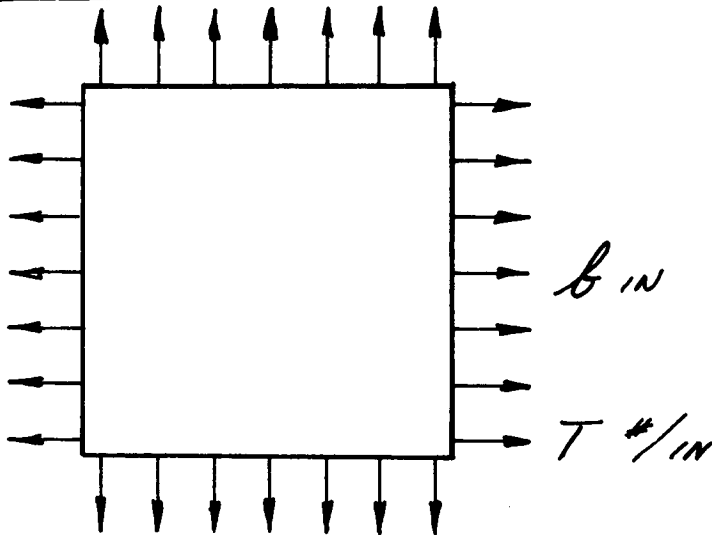
RATIOED FROM SQUARE PANELS.

B-23

CALCULATION SHEET

By _____

Subject _____ Checked By _____ Date _____

ELECTRO-OPTICAL SYSTEMS, INC.THEORY OF PRESTRESSED DIAPHRAGMFREQUENCY

$$\frac{\partial^2 z}{\partial t^2} = \sqrt{\frac{T \cdot g}{S}} \left(\frac{\partial^2 z}{\partial x^2} + \frac{\partial^2 z}{\partial y^2} \right)$$

T = TENSION

$$g = 386.4 \text{ IN/SEC}^2$$

S = WEIGHT PER IN²

ASSUME :

$$Z(x, y, t) = \sum_{m=1}^{\infty} \sum_{n=1}^{\infty} B_{mn} \cdot \sin\left(\frac{m\pi}{a} x\right) \cdot \sin\left(\frac{n\pi}{b} y\right) \cdot \cos \omega_{mn} t$$

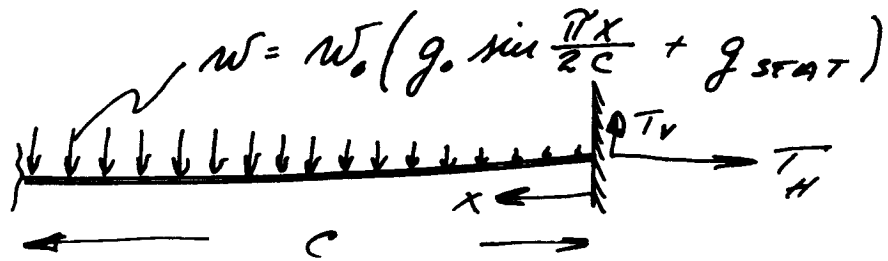
$$\omega_{mn} = \pi \sqrt{\frac{Tg}{S}} \sqrt{\frac{m^2}{a^2} + \frac{n^2}{b^2}}$$

$$f = \frac{\omega_{mn}}{2\pi} = \frac{1}{2} \sqrt{\frac{Tg}{S} \left(\left(\frac{m}{a}\right)^2 + \left(\frac{n}{b}\right)^2 \right)}$$

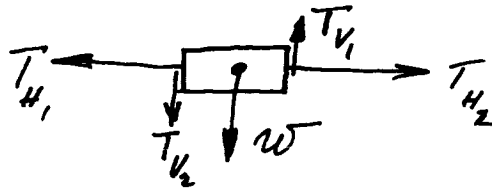
CALCULATION SHEET

By _____

Subject _____ Checked By _____ Date _____

ELECTRO-OPTICAL SYSTEMS, INC.STRESS

$$y = \frac{x^2}{T_H} w$$



$$T_{H1} - T_{H2} = 0 \quad T_{H1} = T_{H2}$$

$$T_{V2} + w = T_{V1}$$

T_{V2} IS ZERO AT $x = c$

$$T_V = \sum_{x=0}^{x=c} w_0 \left(g_0 \sin \frac{\pi x}{2c} + g_{STAT} \right) dx$$

$$= w_0 \int_0^c \left(g_0 \sin \frac{\pi x}{2c} + g_{STAT} \right) dx$$

$$= w_0 \left(\frac{2c}{\pi} g_0 + c \cdot g_{STAT} \right) = \underline{\underline{c \cdot w_0 \left(\frac{2}{\pi} g_0 + g_{STAT} \right)}}$$

CALCULATION SHEET

By _____

Subject _____ Checked By _____ Date _____

ELECTRO-OPTICAL SYSTEMS, INC.

PRESTRESS IS T_p

$$T_H = T_p + T_1$$

$$S = \text{ARC LENGTH} = \chi + \frac{1}{6} \frac{\chi^3}{a^2} + \dots$$

STRAIN IS THEN

$$\Delta S = \chi + \frac{1}{6} \frac{\chi^3}{a^2} + \dots - \chi$$

$$= \frac{1}{6} \frac{\chi^3}{a^2}$$

$$T_1 = \Delta S \cdot t \cdot E = \frac{1}{6} \frac{\chi^3}{a^2} t \cdot E$$

$$a = \frac{T_H}{W} = \frac{T_p + T_1}{W}$$

$$T_1 = \frac{1}{6} \frac{\chi^3}{(T_p + T_1)^2} W^2 t \cdot E$$

$$T_1 (T_p + T_1)^2 = \frac{1}{6} C^3 W^2 t \cdot E$$

$$T_1 (T_p + T_1)^2 = \frac{1}{6} W_0^2 \left(\frac{2}{\pi} g_0 + g_{\text{STAT}} \right)^2 C^3 t \cdot E$$

THIS INDICATES THAT THE GREATER THE PRESTRESS THE SMALLER THE DEFLECTION AND T_1 AND THE GREATER THE FREQUENCY.

$$T_{1 \text{ MAX}} = \sqrt[3]{\frac{1}{6} W_0^2 \left(\frac{2}{\pi} g_0 + g_{\text{STAT}} \right)^2 C^3 t \cdot E}$$

FOR BIDIRECTIONAL STRESS:

$$E \cdot \epsilon_1 = f_\theta - \nu f_\theta$$

$$E \cdot \epsilon_2 = f_\theta - \nu f_\theta$$

A. 26

CALCULATION SHEET

Page 26 of _____

By _____

Subject _____ Checked By _____ Date _____

ELECTRO-OPTICAL SYSTEMS, INC.

FOR A TRU STRESS THE EQUIVALENT UNIDIRECTIONAL STRAIN MUST BE USED

$$\epsilon_1 = \frac{1}{E} (f_\theta - \nu f_\theta)$$

$$\epsilon_2 = \frac{1}{E} (f_\theta - \nu f_\theta)$$

IF WE CAN ASSUME $f_\theta = \mu \cdot f_\theta$

$$\underline{\underline{\epsilon_{1EQ} = \frac{f_\theta}{E} (1 + \nu \mu)}}$$

THEN

$$T_1 (T_P + T_1)^2 = \frac{1 + \nu \mu}{6} \omega_0^2 \left(\frac{2}{\pi} g_0 + g_{STAT} \right)^2 C^3 \cdot t \cdot E$$

$$\underline{\underline{f = \frac{T_P + T_1}{t}}}$$

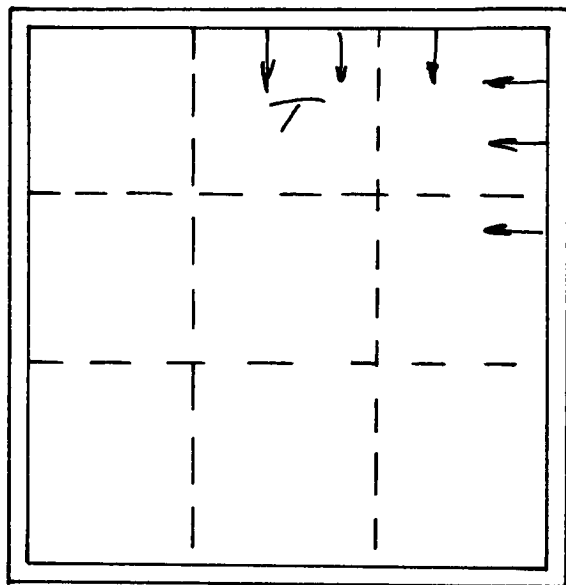
CALCULATION SHEET

By _____

Subject _____ Checked By _____ Date _____

ELECTRO-OPTICAL SYSTEMS, INC.

FRAME



THE FRAME FOR BOTH HOLLOW CORE AND PRESTRESSED DIAPHRAGM WILL BE SIMILAR IN DESIGN, CONSISTING OF ONE UPPER AND ONE LOWER SECTION. THE MAJOR LOADING WILL COME FROM MEMBRANE.

STRESS B

IN PLANE LOADING IS T

l = BEAM LENGTH (UNSUPPORTED)

$$l_1 = \frac{C}{M}$$

$$l_2 = \frac{B}{M}$$

$M \frac{1}{2} M$ NUMBER OF STIFFENERS.

$$M = \frac{1}{12} T l_1^2 \quad \text{OR} \quad \frac{1}{12} T l_2^2$$

$$P = \frac{1}{2} T l_2 \quad \text{OR} \quad \frac{1}{2} T l_1$$

$$f_1 = \frac{Mc}{I} + \frac{P}{A} = \frac{1}{12} T l_1^2 \frac{C_1}{I_1} + \frac{1}{2} \frac{T l_2}{A_1}$$

CALCULATION SHEET

By _____

Subject _____ Checked By _____ Date _____

ELECTRO-OPTICAL SYSTEMS, INC.

$$f_2 = \frac{1}{12} T l_2^2 \frac{C_2}{I_2} + \frac{1}{2} \frac{T l_1}{A_2}$$

COLUMN STRENGTH.

THE CRITICAL LOADING OCCURS WHEN MEMBRANE IS IN TENSION, FRAME IN COMPRESSION.

$$F_{CR} = \frac{\pi^2 E}{\left(\frac{C l}{r}\right)^2}$$

E = FRAME MODULUS OF ELASTICITY

C = FITTING FACTOR 0.707 IN CASES ANALYZED

l = FREE LENGTH

r = RADIUS OF GYRATION.

ONE MAY ASSUME THAT ONLY OUTER AND INNER SURFACE CARRY LOAD.

CRITICAL COLUMN LOADING :

$$\frac{f_c}{F_c} + \frac{f_b}{F_B \left(1 - \frac{f_c}{F_c}\right)} = 1$$

f_c = COMPRESSIVE STRESS $\left(\frac{P}{A}\right)$

f_b = BENDING STRESS $\frac{M_c}{I}$

F_c = CRITICAL STRENGTH IN COMPRESSION

F_B = CRITICAL STRENGTH IN BENDING.

$$\frac{f_c}{F_c} + \frac{\frac{f_b}{F_B}}{1 - \frac{f_c}{F_c}} = 1$$

CALCULATION SHEET

By _____

Subject _____ Checked By _____ Date _____

ELECTRO-OPTICAL SYSTEMS, INC.

$$\frac{f_c}{F_c} \left(1 - \frac{f_c}{F_c} \right) + \frac{f_b}{F_B} = 1 - \frac{f_c}{F_c}$$

$$\frac{f_c}{F_c} - \left(\frac{f_c}{F_c} \right)^2 + \frac{f_b}{F_B} - 1 + \frac{f_c}{F_c} = 0$$

$$- \left(\frac{f_c}{F_c} \right)^2 + 2 \left(\frac{f_c}{F_c} \right) - 1 + \frac{f_b}{F_B} = 0$$

$$- \left(\frac{f_c}{F_c} - 1 \right)^2 + \frac{f_b}{F_B} = 0$$

$$\frac{f_b}{F_B} = \sqrt{1 - \frac{f_c}{F_c}}$$

FACE BUCKLING
IT IS MORE LIKELY THAT THE FACE WILL
BUCKLE :

$$F_{CR} = K \frac{\pi^2 E}{12(1-\nu^2)} \left(\frac{t}{b} \right)^2 \quad \text{NACA TN 3781}$$

K = EMPIRICAL BUCKLING CONSTANT

E = MODULUS OF ELASTICITY

t = THICKNESS OF FLANGE.

b = WIDTH OF FLANGE

ν = POISSON'S RATIO.

K = 6.98 a/b → ∞

L 30

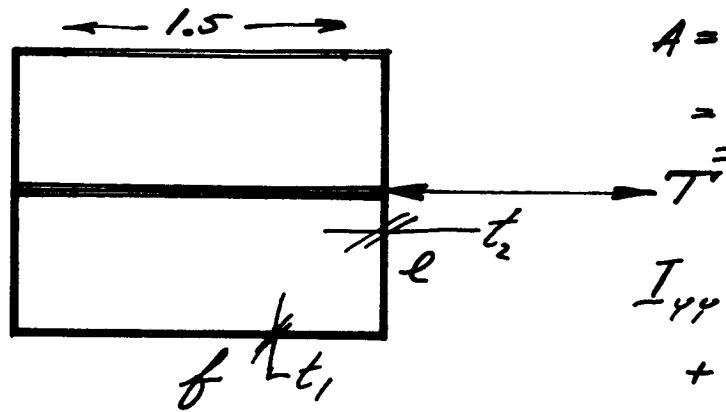
CALCULATION SHEET

By _____

Subject _____ Checked By _____ Date _____

ELECTRO-OPTICAL SYSTEMS, INC.

THE TOP SKINS ARE PERFORATED TO LIGHTEN ASSEMBLY.



$$A = 4et_2 + 8 \cdot 0.25 \cdot t_1$$

$$= \underline{\underline{4et_2 + 2t_1}}$$

$$I_{yy} = 2 \left(2e \cdot t_2 \cdot \left(\frac{f}{2}\right)^2 \right)$$

$$+ 0.25 \cdot t_1 \cdot \left(\frac{f}{2} - 0.125\right)^2 \cdot 8$$

$$\underline{\underline{I_{yy} = et_2 f^2 + 2t_1 \left(\frac{f}{2} - \frac{1}{8}\right)^2}}$$

$$I_{xx} = \frac{2}{12} (2e)^2 t_2 + 2(2 \cdot 0.25) e^2 t_1 = \frac{2}{3} e^2 t_2 + e^2 t_1$$

$$= \underline{\underline{e^2 \left(\frac{2}{3} t_2 + t_1\right)}}$$

THE RADIUS OF GYRATION IS:

$$\bar{r} = \sqrt{\frac{I}{A}} = \sqrt{\frac{et_2 f^2 + 2t_1 \left(\frac{f}{2} - \frac{1}{8}\right)^2}{4et_2 + 2t_1}}$$

$$= \sqrt{\frac{ef^2 + 2 \frac{t_1}{t_2} \left(\frac{f}{2} - \frac{1}{8}\right)^2}{4e + 2 \frac{t_1}{t_2}}}$$

2-31

CALCULATION SHEET

By _____

Subject _____ Checked By _____ Date _____

ELECTRO-OPTICAL SYSTEMS, INC.STRESS

$$f_{MAX} = \frac{1}{12} T l_1^2 \frac{C_1}{I_1} + \frac{1}{2} \frac{T l_2}{A_1}$$

$$f_{MAX} = \frac{1}{12} T l_2^2 \frac{C_2}{I_2} + \frac{1}{2} \frac{T l_1}{A_2}$$

$$f_{MAX} = \frac{1}{12} T l_1^2 \frac{f}{e t_2 f^2 + 2 t_1 \left(\frac{f}{2} - \frac{l_1}{8}\right)^2} + \frac{T l_2}{2(4 e t_2 + 2 t_1)}$$

$$= \frac{T l_1^2 f}{24(e t_2 f^2 + 2 t_1 \left(\frac{f}{2} - \frac{l_1}{8}\right)^2)} + \frac{T l_2}{2(4 e t_2 + 2 t_1)}$$

STRENGTH

$$F_{EU} = F_{CU}$$

$$\underline{f_{MAX} \leq 0.8 F_{TU}}$$

OR

$$\underline{f_{MAX} \leq 0.8 F_{CB} \quad \text{COLUMN BUCKLING}}$$

OR

$$\underline{f_{MAX} \leq 0.8 \frac{6.98 \pi^2 E}{12(1-\nu^2)} \left(\frac{t}{b}\right)^2}$$

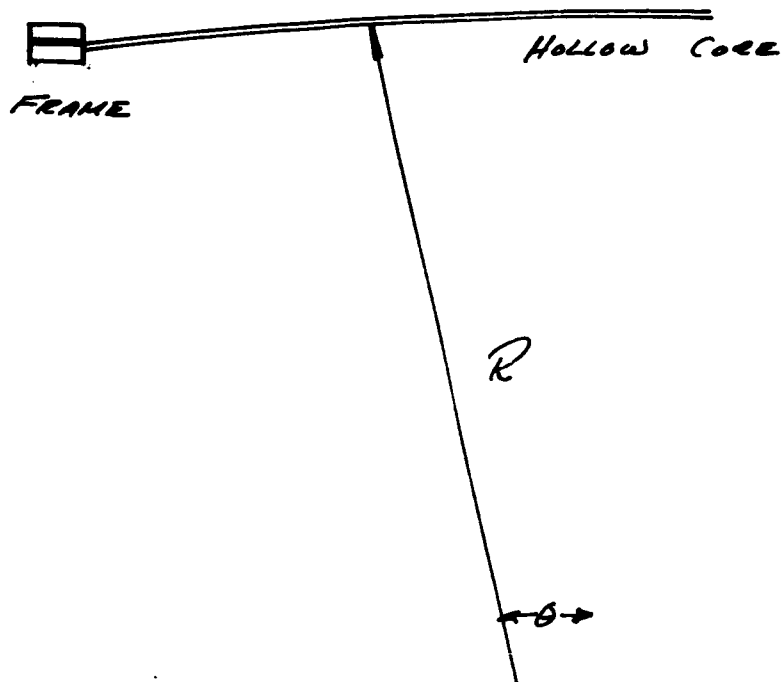
WHICH
EVER
IS
MORE
CRITICAL.

A-32

CALCULATION SHEET

By _____

Subject _____ Checked By _____ Date _____

ELECTRO-OPTICAL SYSTEMS, INC.VERTICAL LOADING

CENTER OF GRAVITY

HOLLOW CORE :

$$\bar{X} = \frac{2}{3\theta} \left[b + \frac{a^2}{b+a} \right] \sin \theta$$

FOR $b \approx a$

$$\bar{X}_P = \frac{\sin \theta}{\theta} \cdot R$$

$$\bar{X}_F = R \cos \theta \quad \text{FRAME}$$

AREA

HOLLOW CORE

$$A_P = \left(2 - \left(\frac{d}{a} \right) + \frac{b}{a} \right) t \cdot 2\pi R$$

NOTATIONS AS IN
EARLIER SECTIONS.

FRAME

$$A = 2(e+f)t_2 \cdot 2 = \underline{\underline{4(e+f)t_2}}$$

CALCULATION SHEET

By _____

Subject _____ Checked By _____ Date _____

ELECTRO-OPTICAL SYSTEMS, INC.

ACTUALLY :

$$A_F = 4(e t_1 + f t_2) = \underline{\underline{(8e + 4f) t_2}}$$

ASSEMBLY CENTER OF GRAVITY :

$$\bar{X} = \frac{2(2 - \frac{d}{e} + \frac{1}{2}) t R \theta \cdot \frac{\sin \theta}{\theta} R + 2(8e + 4f) t_2 \cdot R \cos \theta}{2(2 - \frac{d}{e} + \frac{1}{2}) t R \theta + 2(8e + 4f) t_2}$$

INDIVIDUAL MOMENTS OF INERTIA.

HOLLOW CORE

$$I_{YP} = \frac{1}{4} (b^4 - a^4) (\theta + \sin \theta \cos \theta) - \frac{4}{9} \sin^2 \theta \frac{(b^3 - a^3)^2}{b^2 - a^2}$$

$b \approx a$

$$b - a = t$$

PER: AEROJET STRUCTURES MANUAL
P. 3-12.05

NOTATIONS AS PER REFERENCE.

$$\begin{aligned} I_{YP} &= b^3 t \left[\theta + \sin \theta \cos \theta - 2 \frac{\sin^2 \theta}{\theta} \right] \\ &= R^3 t \left[\theta + \sin \theta \cos \theta - 2 \frac{\sin^2 \theta}{\theta} \right] \\ &= R^3 \left(2 - \frac{d}{e} + \frac{1}{2} \right) t \left[\theta + \sin \theta \cos \theta - 2 \frac{\sin^2 \theta}{\theta} \right] \end{aligned}$$

FRAME :

$$\begin{aligned} I_{YF} &= 4 \cdot \frac{1}{12} (e t_1)^3 t_1 + 4 \frac{1}{2} f t_2 e^2 + \\ &= \frac{1}{3} (e t_1)^3 (2 t_1) + 2 f t_2 e^2 + \\ &= \underline{\underline{e^2 t_2 \left(\frac{16}{3} e + 2 f \right)}} \end{aligned}$$

CALCULATION SHEET

By _____

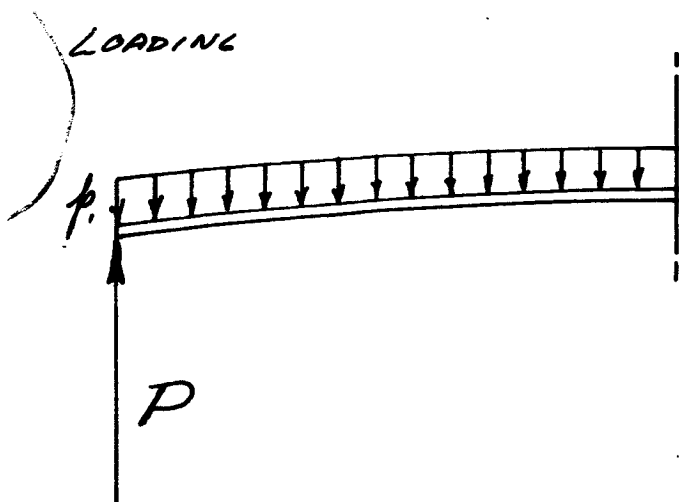
Subject _____ Checked By _____ Date _____

ELECTRO-OPTICAL SYSTEMS, INC.

ASSEMBLY MOMENT OF INERTIA.

$$I_{yTOT} = R^3 \left(2 - \left(\frac{d}{a}\right) + \frac{b}{a} \right) t \left[\theta + \sin \theta \cos \theta - 2 \frac{\sin^2 \theta}{\theta} \right] \\ + 2e^2 t_2 \left(\frac{16}{3} e + 2f \right) + 2 \left(2 - \left(\frac{d}{a}\right) + \left(\frac{b}{a}\right) \right) t R \theta \left(\frac{\sin \theta}{\theta} R - \bar{x} \right)^2 \\ + 2.4 (2e + f) t_2 \left(\bar{x} - R \cos \theta \right)^2$$

$$I_{yTOT} = R^3 t \left(2 - \left(\frac{d}{a}\right) + \left(\frac{b}{a}\right) \right) t \left[\theta + \sin \theta \cos \theta - 2 \frac{\sin^2 \theta}{\theta} + 2 \cdot \theta \left(\frac{\sin \theta}{\theta} - \frac{\bar{x}}{R} \right)^2 \right] \\ + 2e^2 t_2 \left(\frac{16}{3} e + 2f \right) + 2.4 (2e + f) t_2 \left(\bar{x} - R \cos \theta \right)^2$$



A CONSERVATIVE APPROACH IS TO ASSUME LOADING AS SHOWN

$$p_i = (p_{HOLLOW CORE} + p_{FRAME}) \times width. EFFECT.$$

FRAME AND HOLLOW CORE DOES NOT RESONATE AT SAME FREQUENCY.

CALCULATION SHEET

By _____

Subject _____ Checked By _____ Date _____

ELECTRO-OPTICAL SYSTEMS, INC.

CASE 1 : HOLLOW CORE RESONATING.

$$p_{HC} = \left[\frac{W_{SC}}{144} + \left[2 - \left(\frac{d}{a} \right)^2 - \frac{2}{\pi} \left(\frac{d}{a} \right) \left(\frac{h}{a} \right) \cot \alpha \right] t \cdot \rho \right] (g_{STAT} + 0.767 \frac{g_0}{g})$$

$W_{SC} = 0.160 \text{ #/FT}^2$

$\frac{d}{a} = 1.905$

$\frac{h}{a} = \frac{0.1}{0.525} = 0.1905$

$\theta = 60^\circ$

$t = 0.002$

$\rho = 0.321$

$g_{STAT} = 0$

$g_0 = 1.5$

$g = 40$

$p_{HC} = \underline{0.066} \text{ PSI. X L}$ (THIS LOADING VARIES)
 ONLY CENTER SECTION SEE THIS LOADING

CASE 2
 HOLLOW CORE NOT RESONATING

$p_{H.C} = \underline{1.55586 \cdot 10^{-3}} \cdot g_{STAT} \times L$

$g_0 = 0$
 $g_{STAT} = \text{INPUT FROM FRAME}$

FRAME CASE 1.

$p = 2 \cdot (8e + 4f) t_2 \cdot \rho \cdot g_{INPUT}$

CASE 2

$p = 2(8e + 4f) t_2 \cdot \rho \cdot g_0 \cdot \sin\left(\frac{\pi}{l} X\right)$

X = DISTANCE FROM SUPPORT

l = PANEL LENGTH.

CALCULATION SHEET

By _____

Subject _____ Checked By _____ Date _____

ELECTRO-OPTICAL SYSTEMS, INC.

CASE 1

$$p = 0.066 \cdot \sin\left(\frac{\pi}{2} x\right) + 2(8e + 4f)t_2 \rho \cdot g_0$$

CASE 2

$$p = 0.00155586 \cdot b \cdot g_0 \cdot g \cdot \sin\left(\frac{\pi}{2} x\right) + 2(8e + 4f)t_2 \cdot g \cdot g_0 \cdot \sin\left(\frac{\pi}{2} x\right)$$

$$= \left[0.00155586 b + 2(8e + 4f)t_2 \cdot g \right] g_0 \cdot \sin\left(\frac{\pi}{2} x\right)$$

WHICHEVER IS GREATER SHOULD BE USED.

STRESS

$$f = \frac{\frac{1}{8} p_{TOT} \cdot l^2 \cdot c}{I_y}$$

$\frac{1}{8} p_{TOT} \cdot l^2$ MOMENT FOR UNIFORM LOAD

$$M = \int_0^l p dx$$

$$f = \frac{\int_0^l p dx \cdot c}{I_y}$$

$$M.S. = \frac{F}{f} - 1$$

8-37

CALCULATION SHEET

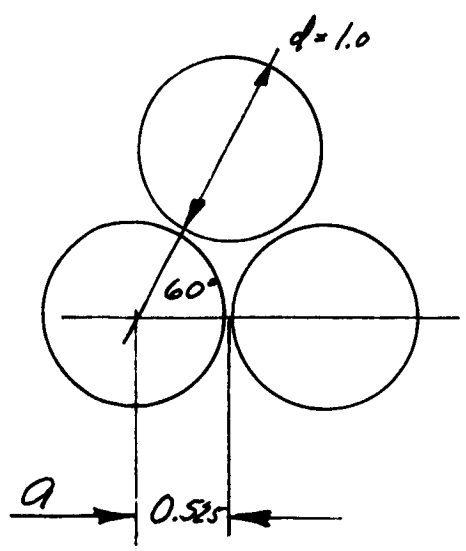
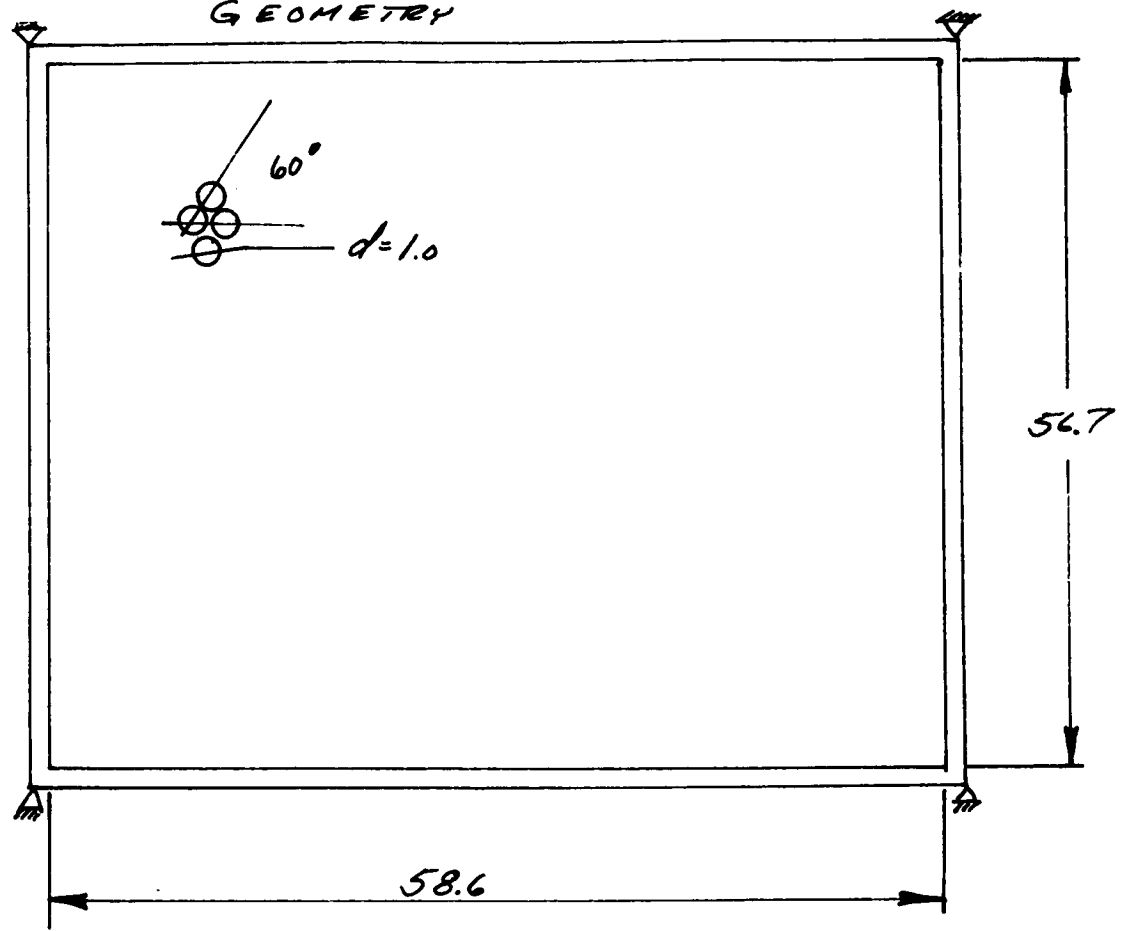
By _____

Subject _____ Checked By _____ Date _____

ELECTRO-OPTICAL SYSTEMS, INC.

DEMONSTRATION PANEL ANALYSIS.

GEOMETRY



PANEL THICKNESS : 0.100 IN.
 PANEL CURVATURE : $R_c = 163.25$ IN
SPM
 SKIN THICKNESS : $t = 0.002$ IN
 FRAME :
 DOUBLE BOX $\frac{3}{4} \times 20$ IN
 $t = 0.010$ IN

2-38

CALCULATION SHEET

By _____

Subject _____ Checked By _____ Date _____

ELECTRO-OPTICAL SYSTEMS, INC.

HOLLOW CORE.

$$g_0 = 1.5 g$$

$$g = 40$$

$$d/a = \frac{1.000}{0.525} = \underline{1.905}$$

$$h = 0.1 \text{ IN}$$

$$t = 0.002 \text{ IN}$$

MEMBRANE STRESS

FROM 7.2.2.6.3

$$f_m = \frac{\left[\frac{w_{stat}}{144} + \left[2 - \left(\frac{\pi}{4} \left(\frac{d}{a} \right)^2 - \frac{\pi}{2} \left(\frac{d}{a} \right) \left(\frac{h}{a} \right) \right] \cot \alpha \right] t \cdot g \left[g_{STAT} + g_{90.707} \right] C \left[2 - \frac{C_{11}}{C_{22}} \right]}{2 \left(2 - \frac{d}{a} \cos \theta + \frac{h}{a} \right) t \sin \alpha}$$

BUCKLING TESTS HAVE CONFIRMED THAT THE PANEL AVERAGE STRESS IS THE CRITICAL STRESS.

$$\theta = 30^\circ$$

$$f_m = \frac{\left[\frac{0.160}{144} + \left[2 - \left(\frac{\pi}{4} (1.905)^2 - \frac{\pi}{2} 1.905 \frac{0.1}{0.525} \right) 0.57735 \right] 0.002 \cdot 0.321 \right] 0.707 \cdot 1.540}{2 \left(2 - 1.905 \cdot 0.86603 + \frac{0.1}{0.525} \right) 0.002 \cdot 0.17947} \cdot 29.3$$

$$g_{STAT} = 0$$

$$f_m = \underline{4963 \text{ PSI}}$$

7.2.5.2.2 CRIPPLING STRENGTH

FROM 7.2.2.3

$$F_{CR} = \frac{0.8 \cdot K_T \cdot \pi^2 E}{12(1-\nu^2)} \left(\frac{t}{4a - 1.732d} \right)^2$$

7027-IDR

CALCULATION SHEET

By _____

Subject _____ Checked By _____ Date _____

ELECTRO-OPTICAL SYSTEMS, INC.

$$F_{CR} = \frac{0.8 \cdot 8.5 \cdot \pi^2 \cdot 28 \cdot 10^6}{12(1 - 0.3^2)} \left(\frac{0.002}{4 \cdot 0.525 - 1.732 \cdot 1.0} \right)^2 =$$

$$F_{CR} = \underline{\underline{5084 \text{ PSI}}}$$

$$F_{t4} = \underline{\underline{30000 \text{ PSI}}} \text{ MINIMUM FOR NICKEL ALLOY}$$

$$M.S. = \frac{1}{R} - 1 = \frac{1}{\frac{4963}{5084}} - 1 = \underline{\underline{0.02}}$$

ACTUALLY THE CRITICAL BUCKLING STRESS WILL BE LOWER THAN THE ONE SHOWN, THIS INCREASING THE MARGIN OF SAFETY.

CRIPPLING TESTS HAVE SHOWN THAT THE CRIPPLED SECTION IS ABLE TO CARRY THE FULL LOAD, THEREFORE THE 80% OF BUCKLING STRENGTH CAN ALSO BE RAISED.

CALCULATION SHEET

By _____

Subject _____ Checked By _____ Date _____

ELECTRO-OPTICAL SYSTEMS, INC.

PANEL BUCKLING:

FROM 7.2.2.2

$$p_{cr} = - \frac{D (\lambda_m^2 + \mu_m^2)^2 + \frac{Eh}{R^2}}{\frac{R}{2} (\lambda_m^2 + \mu_m^2)}$$

$$\lambda_m = m \frac{\pi}{\alpha_0}$$

$$\mu_m = m \frac{\pi}{\beta_0}$$

$$m = n = 1$$

$$\alpha_0 = \text{PANEL WIDTH} = 56.7 \text{ IN}$$

$$\beta_0 = \text{PANEL LENGTH} = 58.6 \text{ IN}$$

$$p_{cr} = - \frac{D \left(\frac{\pi^2}{56.7^2} + \frac{\pi^2}{58.6^2} \right)^2 + \frac{Eh}{R^2}}{\frac{R}{2} \left(\frac{\pi^2}{56.7^2} + \frac{\pi^2}{58.6^2} \right)}$$

$$p_{cr} = - \frac{D (0.00594)^2 + \frac{Eh}{R^2}}{0.00594 \cdot \frac{R}{2}}$$

$$D = \frac{E}{1-\nu^2} \left(2 - \frac{d}{a} \cos \theta \right) \frac{h^2 t}{4}$$

$$E = 28 \cdot 10^6 \text{ PSI}$$

$$\nu = 0.3$$

$$\frac{d}{a} = 1.905$$

$$\theta = 30^\circ$$

$$h = 0.1$$

$$t = 0.002 \text{ IN}$$

7027-IDR

EOS Form No. 6303 (7/64-200)

41

CALCULATION SHEET

By _____

Subject _____ Checked By _____ Date _____

ELECTRO-OPTICAL SYSTEMS, INC.

$$D = \frac{28 \cdot 10^6}{1 - 0.3^2} (2 - 1.905 \cdot 0.96603) \frac{0.1^2 \cdot 0.002}{4}$$

$$= \underline{\underline{53.878}}$$

$$h = (2 - \frac{d}{2} \cos \theta + \frac{h}{a}) t = \underline{\underline{0.00108 \text{ IN}}}$$

$$R = 163.25 \text{ IN}$$

$$P_{CR} = \frac{53.878 \cdot (0.00594)^2 + \frac{28 \cdot 10^6 \cdot 0.001080}{163.25^2}}{0.00594 \cdot \frac{163.25}{2}}$$

$$= \underline{\underline{2.732 \text{ PSI}}}$$

APPLIED PRESSURE

$$p = \left[\frac{W_{sc}}{144} + \left[2 - \left(\frac{\pi}{4} \left(\frac{d}{a} \right)^2 - \frac{\pi}{2} \left(\frac{d}{a} \right) \frac{h}{a} \right) \cos \theta \right] t \right] \rho_{STAT} + 0.707 g \cdot g$$

$$= \left(\frac{160}{144} + \left(2 - \left(\frac{\pi}{4} 1.905^2 - \frac{\pi}{2} 1.905 \frac{0.1}{0.5325} \right) 0.57735 \right) 0.002 \cdot 0.321 \right) (0.707 \cdot 1.5 \cdot 40)$$

$$= 0.047 + 0.019 = \underline{\underline{0.066 \text{ PSI}}}$$

$$M.S.P = \frac{2.732}{0.066} - 1 = \underline{\underline{+ HIGH}}$$

E
O
S

CALCULATION SHEET

By _____

Subject _____ Checked By _____ Date _____

ELECTRO-OPTICAL SYSTEMS, INC.

FREQUENCY

$$f_m = \frac{1}{2\pi} \left(\frac{1}{\rho h} \left[D(\lambda_m^2 + \mu_m^2)^2 + \frac{Eh}{R^2} \right] \right)^{\frac{1}{2}}$$

FROM 7.2.2.1

SPHERICAL SURFACE.

$D = 53.878$

$R = 163.25$

$h = 0.00108$

$(\lambda_m^2 + \mu_m^2) = (0.00594)$

$$\rho = \frac{W}{g} = \frac{0.160}{144} + \frac{2 - \left(\frac{\pi}{4} \left(\frac{d}{a} \right)^2 - \frac{\pi}{2} \left(\frac{d}{a} \times \frac{b}{a} \right) \cot \phi \right) t \cdot g}{386.4}$$

$$= \frac{1.111 \cdot 10^{-3} + 0.43878 \cdot 10^{-3}}{386.4} = \frac{1.54989 \cdot 10^{-3}}{386.4}$$

$$f = \frac{1}{2\pi} \left(\frac{1}{\frac{1.54989 \cdot 10^{-3}}{386.4}} \left(53.878 \cdot (0.00594)^2 + \frac{28 \cdot 10^6 \cdot 0.00108}{163.25^2} \right) \right)^{\frac{1}{2}}$$

$$= \frac{1}{2\pi} \left(\frac{386400}{1.54989} (0.00190 + 1.13468) \right)^{\frac{1}{2}}$$

$$= \underline{\underline{84.7 \text{ CPS}}}$$

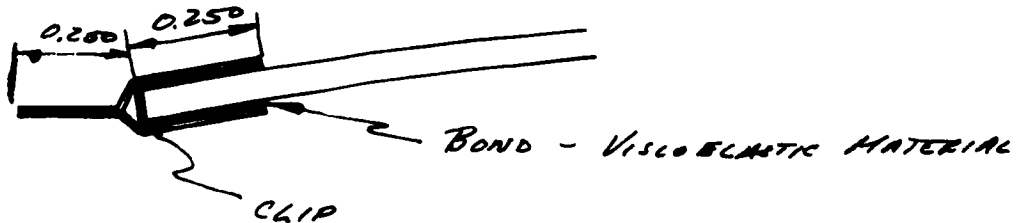
CALCULATION SHEET

By _____

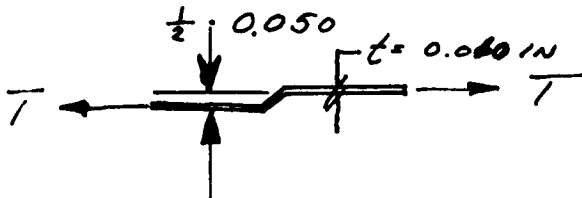
Subject _____ Checked By _____ Date _____

ELECTRO-OPTICAL SYSTEMS, INC.

HOLLOW CORE CLIP



THE CLIP IS FABRICATED FROM
ALUMINUM ALLOY 6061-T6



$$T = \frac{pR}{2} = \frac{0.066 \times 163.25}{2} = \underline{\underline{5.4 \text{ #/IN}}}$$

DIRECT STRESS :

$$f = \frac{pR}{2A} = \frac{5.4}{2 \times 0.010} = \underline{\underline{270 \text{ PSI}}}$$

$$F_{LY} = \underline{\underline{35000 \text{ PSI}}}$$

BENDING :

$$M = T \cdot 0.030 = 5.4 \cdot 0.030 = \underline{\underline{0.162 \text{ IN-LB/IN}}}$$

$$f_b = \frac{Mc}{I} = \frac{6M}{t^2} = \frac{6 \cdot 0.162}{(0.010)^2} = \underline{\underline{9720 \text{ PSI}}}$$

$$M.S. = \frac{1}{\frac{f_b}{F_{LY}} + \frac{f}{F_b}} - 1 = \frac{35000}{9720 + 270} - 1 = \underline{\underline{2.5}}$$

EOS

CALCULATION SHEET

By _____

Subject _____ Checked By _____ Date _____

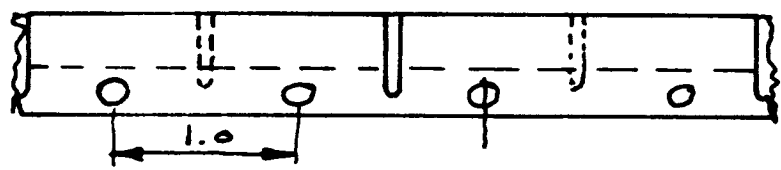
ELECTRO-OPTICAL SYSTEMS, INC.

RIVETS :

USE $\frac{1}{8}$ IN. RIVETS DIMPLED SHEETS.

$F_{50} = 28000 \text{ PSI}$ 5056 -

LOAD PER RIVET : 5.4 LBS



$P_{RIVET} = 363 \#$ MIL HDBK - 5 P. 8.1

M.S. = $\frac{363}{5.4} - 1 = + \text{HIGH}$

BEARING :

$f_{br} = \frac{P}{A} = \frac{5.4}{0.125 \times 0.010} = \underline{4320 \text{ PSI}}$

EVEN WITH SMALLEST RIVET ($d = 0.063 \text{ IN}$)

$f_{br} = \underline{8640 \text{ PSI}}$

M.S. = $\frac{50000}{4320} - 1 = + \text{HIGH}$

1045

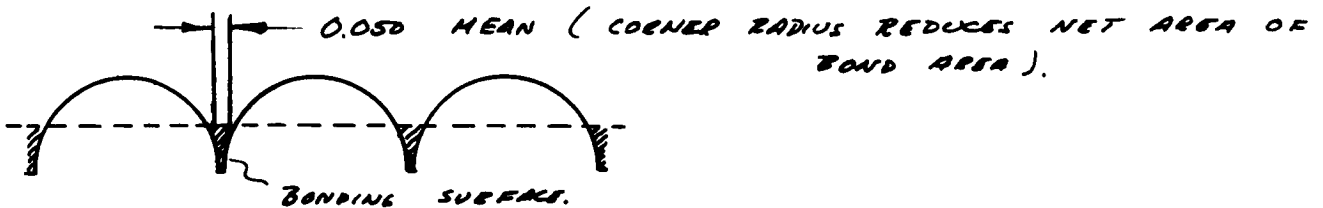
CALCULATION SHEET

By _____

Subject _____ Checked By _____ Date _____

ELECTRO-OPTICAL SYSTEMS, INC.

BOND



$$\text{BOND AREA : } 0.050 \times 0.250 = \underline{\underline{0.0125 \text{ IN}^2/\text{IN}}}$$

$$\text{BOND LOAD : } \underline{\underline{P = 5.4 \text{ LB/IN}}}$$

$$f = \frac{\frac{1}{2}P}{\frac{1}{2} \cdot 0.0125} = \frac{5.4}{0.0125} = \underline{\underline{432 \text{ LB/IN}^2}}$$

HALF OF LOADING ON TOP SKIN, HALF ON BOTTOM.
 BOND IS ASSUMED 50% EFFECTIVE.

A NYLON - EPOXY MATERIAL SUCH AS
 FM 1000 WILL BE USED

$$F_{50} = \underline{\underline{7000 \text{ PSI}}} \text{ PER VENDOR}$$

$$M.S. = \frac{7000}{1.25 \cdot 432} - 1 = \underline{\underline{+ HIGH}}$$

10-46

7027-IDR

EOS Form No. 6303 (7/64-200)

CALCULATION SHEET

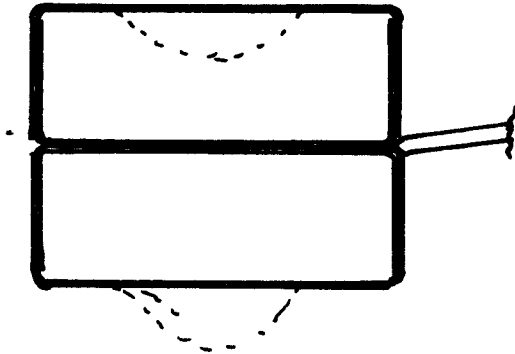
By _____

Subject _____ Checked By _____ Date _____

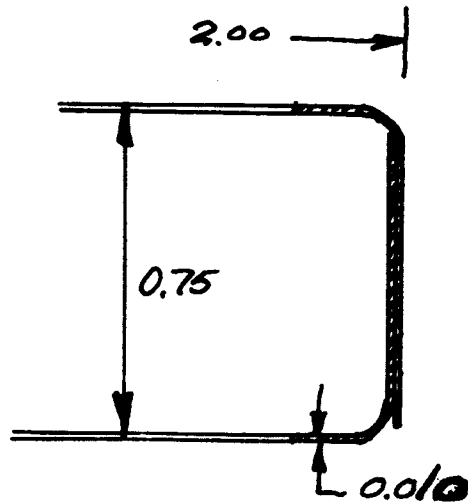
ELECTRO-OPTICAL SYSTEMS, INC.

FRAME

GEOMETRY



THE FRAME IS BOX SHAPED FABRICATED FROM 0.010 IN ALUMINUM ALLOY 6061-T6, CONSISTING OF 2 MATING CHANNEL SECTIONS. THERE IS A DIMPLED GROOVE ON TOP AND BOTTOM TO PROVIDE A TONGUE AND GROOVE ARRANGEMENT FOR SHEAR TRANSFER IN THE STOWED POSITION. THIS EFFECT WILL BE NEGLECTED, SINCE A REINFORCEMENT WILL BE EXPECTED.



MINIMUM AREA:

$$A = 2(.750 + 2 - 1.25 + 0.750)t$$

$$= \underline{0.045 \text{ IN}^2 \text{ PER BOX}}$$

$$A_T = \underline{0.090 \text{ IN}^2}$$

$$I = 4 \cdot (0.750 \times 0.01^3 + 0.375 \cdot 0.01 \cdot 0.875^2 \cdot 2)$$

$$I_{\text{Box}} = (0.0075 + 0.0057)4 = \underline{0.0528 \text{ IN}^4}$$

47

CALCULATION SHEET

By _____

Subject _____ Checked By _____ Date _____

ELECTRO-OPTICAL SYSTEMS, INC.**E
O
S**STRESS

$$M = \frac{1}{2} T l^2 = \frac{1}{2} \cdot 5.4 \cdot 58.6^2 = \underline{\underline{1545 \text{ IN LBS}}}$$

$$f_b = \frac{M \cdot c}{I} = \frac{1545 \cdot 1}{0.0528} = \underline{\underline{29260 \text{ PSI}}}$$

$$F_B = \underline{\underline{35000 \text{ PSI}}} \quad \text{PER MIL HDBK 5} \\ \text{P. 3.2.6.0}$$

$$R_b = \frac{f_b}{F_B} = \frac{29260}{35000} = \underline{\underline{0.836}}$$

DIRECT STRESS

$$f_c = \frac{P}{A}$$

$$P = \frac{1}{2} T l_2 = \frac{1}{2} \cdot 5.4 \cdot 56.7 = \underline{\underline{153 \text{ LBS}}}$$

$$f_c = \frac{153}{0.090} = \underline{\underline{1700 \text{ PSI}}}$$

STRENGTH

$$F_{CR} = \frac{\pi^2 E}{\left(\frac{0.707 l}{r}\right)^2}$$

$$E = 10 \cdot 10^6 \text{ PSI}$$

$$l = 58.6 \text{ IN}$$

$$r = \sqrt{\frac{I}{A}} = \sqrt{\frac{0.0528}{0.090}} = \underline{\underline{0.766}}$$

$$F_{CR} = \frac{9.86959 \cdot 10^7}{\left(\frac{0.707 \cdot 58.6}{0.766}\right)^2} = \underline{\underline{33738 \text{ PSI}}}$$

A-48

7027-IDR

CALCULATION SHEET

By _____

Subject _____ Checked By _____ Date _____

ELECTRO-OPTICAL SYSTEMS, INC.

$$R_c = \frac{f_c}{F_{ce}} = \frac{1700}{33738} = \underline{\underline{0.05}}$$

$$M.S. = \frac{1}{R_b + R_c} - 1 =$$

$$= \frac{1}{0.766 + 0.05} - 1 = \underline{\underline{0.23}}$$

PER MIL HDBK 5
P. 1.5.35

FLAT PANEL BUCKLING:

$$F_{cr} = \eta K \frac{E \pi^2}{12(1-\nu^2)} \left(\frac{t}{b}\right)^2$$

$$= 0.8 \frac{6.98 \cdot 10^7 \cdot 9.86959}{12(1-0.3^2)} \left(\frac{0.010 \cdot 2}{0.750}\right)^2 =$$

$$F_{cr} = \underline{\underline{35890}} > F_{Ly}$$

49

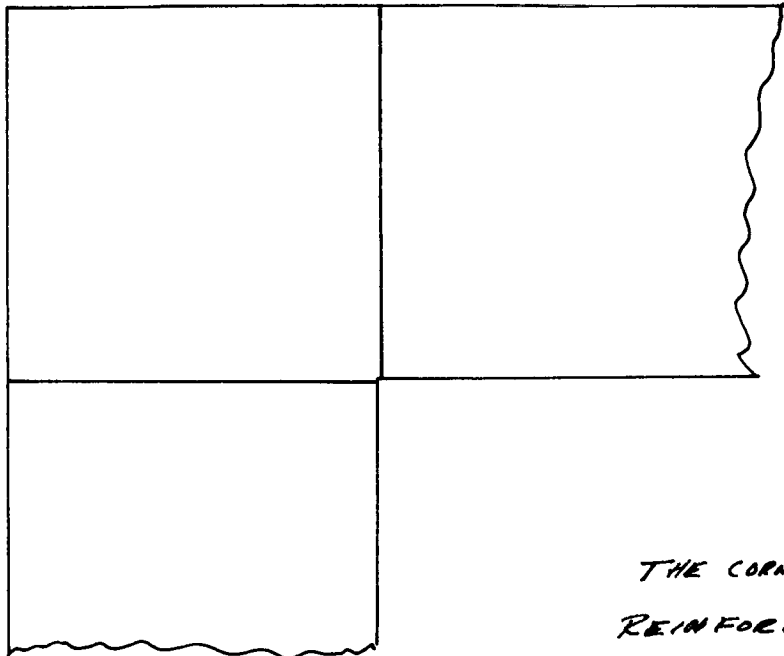
CALCULATION SHEET

By _____

Subject _____ Checked By _____ Date _____

ELECTRO-OPTICAL SYSTEMS, INC.

CORNER REINFORCEMENT



THE CORNERS WILL BE
REINFORCED WITH CLEVIS
ATTACHMENT

$$M = \frac{1}{12} T L_1^2$$

$$P = \frac{1}{2} T L_2$$

$$I_1 = 2 \left(\frac{2}{12} t h^3 \right) = 2 \cdot \frac{2}{12} \cdot 0.016 \cdot 2^3 = \underline{\underline{0.04266 \text{ IN}^4}}$$

$$I_2 = 4 (0.625 \cdot 0.016 \cdot 1^2) = \underline{\underline{0.04000 \text{ IN}^4}}$$

$$I_T = 0.04266 + 0.04000 = \underline{\underline{0.08266 \text{ IN}^4}}$$

$$f_b = \frac{1545}{0.08266} = \underline{\underline{18690 \text{ PSI}}}$$

$$f_c = \frac{153}{2 \cdot 2 \cdot 0.016 + 2 \cdot 0.625 \cdot 0.016} = \underline{\underline{1820 \text{ PSI}}}$$

$$M.S. = \frac{35000}{18690 + 1820} - 1 = \underline{\underline{0.706}}$$

7027-IDR

EOS Form No. 6303 (7/64-200)

CALCULATION SHEET

ELECTRO-OPTICAL SYSTEMS, INC.

FRAME CONTINUED.

VERTICAL LOADING.

IT WILL BE ASSUMED THAT THE FRAME CARRY THE SHEAR, EVEN THOUGH THE HOLLOW CORE ADDS CONSIDERABLE STIFFNESS.

$$p_{cr} = 0.066 \cdot \sin\left(\frac{\pi}{2} x\right) \cdot 58.6 + 2(8.175 + 4 \cdot 0.5) \cdot 0.01 \cdot 0.1 \cdot 1.5$$

$$= \underline{\underline{3.8676 \sin\left(\frac{\pi}{2} x\right) + 0.024}}$$

$$p_{cc} = [0.09117 + 0.086] \cdot 1.5 \cdot 10 \cdot \sin\left(\frac{\pi}{2} x\right)$$

$$= \underline{\underline{1.60755 \sin\left(\frac{\pi}{2} x\right)}}$$

UPPER CASE MORE CRITICAL

$$p_{cr} = 3.8676 \sin\left(\frac{\pi}{2} x\right) + 0.024$$

$$P_{cr} = \int_0^{\frac{l}{2}} p_{cr} \cdot dx = 3.8676 \frac{l}{\pi} \left(-\cos\left(\frac{\pi}{2} x\right)\right) + 0.024 \frac{l}{2}$$

$$= 3.8676 \frac{l}{\pi} + 0.024 \frac{l}{2} = \underline{\underline{73 \#}}$$

$$M = P x - \int_0^x p_{cr} \cdot dx \cdot x$$

$$= 73 \cdot \frac{58.6}{2} - 3.8676 \frac{l^2}{\pi^2} - 0.024 \frac{l^2}{8}$$

$$= 2138.9 - 1259.8 - 9.6 = \underline{\underline{869.5 \text{ IN LBS}}}$$

2-51

CALCULATION SHEET

By _____

Subject _____ Checked By _____ Date _____

ELECTRO-OPTICAL SYSTEMS, INC.

$$I_y = e^2 t_2 \left(\frac{16}{3} e + 2 f \right) \quad \text{PER BEAM}$$

$$e = 0.75 \text{ IN}$$

$$f = 0.500 \text{ IN (MEAN)}$$

$$t_2 = 0.010 \text{ IN.}$$

$$I_y = 0.75^2 \cdot 0.01 \left(\frac{16}{3} \cdot 0.75 + 2 \times 0.50 \right) = \underline{\underline{0.02813 \text{ IN}^4}}$$

$$f_b = \frac{M_c}{2I_y} = \frac{869.5 \cdot 0.75}{2 \cdot 0.02813} = \underline{\underline{23180 \text{ PSI}}}$$

SINCE THE ENTIRE FRAME - HOLLOW CORE ACT AS A UNIT THE BENDING STRESS WILL BE LESS.

STRESS MAXIMUM AT CENTER.

$$f_{b1} = 23180 \text{ PSI.}$$

HOLLOW CORE EFFECT

$$f_{bc} = \frac{1}{2} 29260 = \underline{\underline{14630 \text{ PSI}}}$$

$$F_{bu} = k \cdot F_{tu}$$

$$k = \frac{2 Q_c}{I} \quad (\text{CONVAIR STRUCTURES MANUAL})$$

P. 17-21.17

$$F_{bu} = \underline{\underline{39400 \text{ PSI}}}$$

1.52

CALCULATION SHEET

By _____

Subject _____ Checked By _____ Date _____

ELECTRO-OPTICAL SYSTEMS, INC.

$$M.S.Y = \frac{39400}{\frac{1}{2} 23180 + 14630} - 1 = \underline{\underline{0.502}}$$

NATURAL FREQUENCY OF FRAME MEMBERS.

$$f_1 = \frac{22.4}{2\pi l^2} \sqrt{\frac{EI}{\mu}}$$

l = BEAM LENGTH

E = MODULUS OF ELASTICITY

$$I = l^2 t_2 \left(\frac{16}{3} e + 2f \right) = 0.02813 \text{ IN}^4$$

$$g \cdot \mu = (8 \cdot 0.75 + 4 \cdot 0.5) 0.01 \cdot 0.1 = \underline{\underline{0.008 \text{ #/IN}}}$$

$$f = \frac{22.4}{2\pi \cdot l^2} \sqrt{\frac{10 \cdot 10^6 \text{ #/IN}^2 \cdot 0.02813 \text{ IN}^4}{\frac{0.008 \text{ #/IN}}{386.4 \text{ IN/SEC}^2}}}$$

$$l = 58.6 \text{ IN}$$

$$f = \underline{\underline{121 \text{ CPS}}}$$

CALCULATION SHEET

By _____

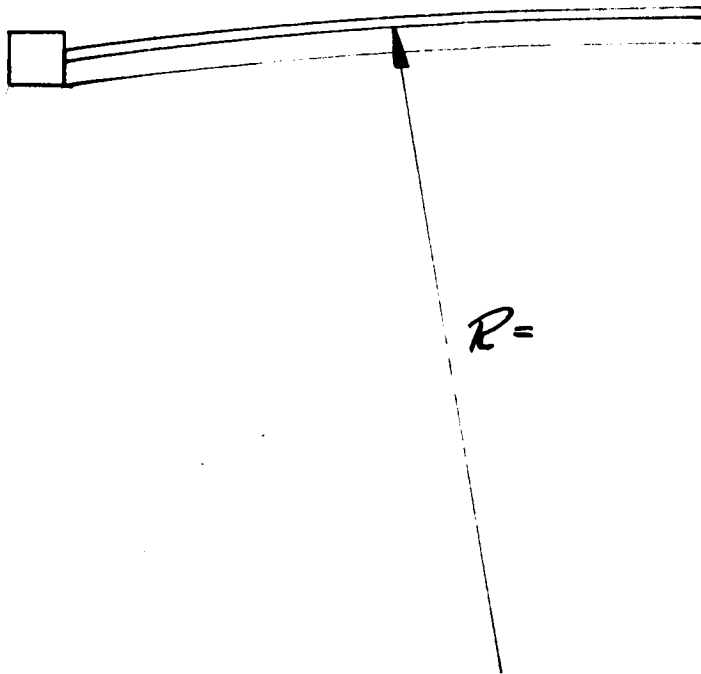
Subject _____ Checked By _____ Date _____

ELECTRO-OPTICAL SYSTEMS, INC.

THERMAL STRESS

THE SUBSTRATE IS FABRICATED FROM NICKEL
AND THE FRAME IS FABRICATED FROM ALUMINUM.
THUS FOR A TEMPERATURE CHANGE OR DIFFERENCE
A DIFFERENCE IN GROWTH WILL RESULT.
FOR THE GENERAL CASE.

STRAIN DIFFERENCE



FOR UNIFORM TEMPERATURE:

T_0 = STARTING TEMPERATURE.

T = INSTANTANEOUS TEMPERATURE.

α = COEFFICIENT OF THERMAL EXPANSION

FREE GROWTH OF PANEL:

7027-IDR

EOS Form No. 6303 (7/64-200)

CALCULATION SHEET

By _____

Subject _____ Checked By _____ Date _____

ELECTRO-OPTICAL SYSTEMS, INC.

$$\Delta_{TA} = \alpha_1 (T_1 - T_0) \cdot R \cdot \theta \quad \text{ALONG ARC}$$

$$\Delta_T = \alpha_1 (T_1 - T_0) \cdot R \sin \theta \quad \text{NORMAL TO AXIS.}$$

ALONG EDGES $\theta = \theta_0$

$$\underline{\underline{\Delta_T = \alpha_1 (T_1 - T_0) \cdot R \sin \theta_0}}$$

FRAME GROWTH

$T_2 =$ INSTANTANEOUS FRAME TEMPERATURE.

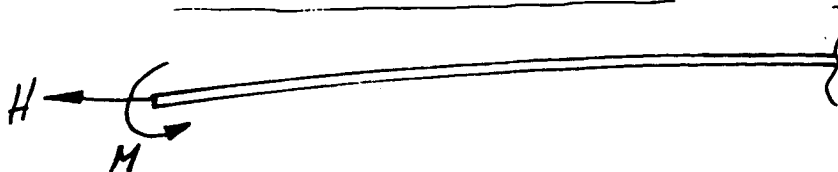
$$\Delta_F = \alpha_2 (T_2 - T_0) \cdot R \sin \theta_0$$

DIFFERENCE IN STRAIN IS

$$\underline{\underline{\Delta = \Delta_F - \Delta_T = (\alpha_1 (T_1 - T_0) - \alpha_2 (T_2 - T_0)) R \sin \theta_0}}$$

IF WE CAN ASSUME THAT MOST OF THE DEFLECTION MUST BE TAKEN BY HOLLOW CORE, THEN WE HAVE:

DISCONTINUITY FORCE.



FROM AERJET-GENERAL STRUCTURES MANUAL: P.P.

6.22.09 - 6.22.60

CALCULATION SHEET

By _____

Subject _____ Checked By _____ Date _____

ELECTRO-OPTICAL SYSTEMS, INC.

$$\frac{d^4 Q_\phi}{d\phi^4} + \frac{2}{\phi} \frac{d^3 Q_\phi}{d\phi^3} - \frac{3}{\phi^2} \frac{d^2 Q_\phi}{d\phi^2} + \frac{3}{\phi^3} \frac{d Q_\phi}{d\phi} - \frac{3}{\phi^4} Q_\phi + 4\lambda^4 Q_\phi$$

$$\lambda^4 = 3(1-\nu^2) \frac{a^2}{t^2} \quad (\text{ESLINGER APPROXIMATION})$$

a = RADIUS

t = THICKNESS

THERE IS SIMPLE SUPPORT ALONG EDGES

THEREFORE $M=0$

THEN

$$\frac{W_a}{E\phi_0} \cdot H = (\alpha_1(T_1 - T_0) - \alpha_2(T_2 - T_0)) R \sin\phi$$

$$\phi_0 = \theta_0$$

$$W_a = - \frac{K_{12}}{\sqrt{12(1-\nu^2)}} \left[(\lambda\sqrt{2}\phi_0)^3 (\psi_1^2 + \psi_2^2) - \right.$$

$$\left. 2(\lambda\sqrt{2}\phi_0)(\psi_1'\psi_2 - \psi_2'\psi_1) + (1-\nu^2)(\lambda\sqrt{2}\phi_0)(\psi_1'^2 + \psi_2'^2) \right]$$

 ψ_1, ψ_2 SCHLEICHER FUNCTIONS ψ_1', ψ_2' DERIVATIVES OF ABOVE W_a HAS BEEN CALCULATED AND LISTED IN REFERENCE DOCUMENT FOR VARIOUS $\lambda\sqrt{2}\phi$ VALUES.

THEN

$$H = \frac{E\phi_0}{W_a} (\alpha_1(T_1 - T_0) - \alpha_2(T_2 - T_0)) R \sin\phi$$

7027-IDR

EOS Form No. 6303 (7/64-200)

EOS

CALCULATION SHEET

By _____

Subject _____ Checked By _____ Date _____

ELECTRO-OPTICAL SYSTEMS, INC.

SOLVING H ONE MAY DETERMINE

$$N_{\phi} = (m_1 C_{1H} + m_2 C_{2H}) H$$

$$N_{\theta} = (\eta_1 C_{1H} + \eta_2 C_{2H}) H$$

$$M_{\phi} = (m_1 C_{1H} + m_2 C_{2H}) H \cdot t_e$$

$$M_{\theta} = \nu M_{\phi} + (k_1 C_{1H} + k_2 C_{2H}) H t_e$$

NOMENCLATURE AS PER REFERENCE.

$$t_e = \left(2 - \frac{d}{a} + \frac{h}{a}\right) t$$

THEN ADDITIONAL STRESS IS:

$$f_{\text{DIRECT}} = \frac{N_{\phi}}{\left(2 - \frac{d}{a} + \frac{h}{a}\right) t}$$

$$f_{\text{DIRECT}} = \frac{N_{\theta}}{\left(2 - \frac{d}{a} + \frac{h}{a}\right) t}$$

$$f_{\text{BEND}} = \frac{M_{\phi} \cdot c}{I} = \frac{M_{\phi}}{\left(2 - \frac{d}{a}\right) t \frac{h}{2}}$$

$\frac{d}{a}$ = RATIO GIVEN

t = SKIN THICKNESS

h = PANEL THICKNESS

657

APPENDIX E
DYNAMIC ANALYSIS AND EQUATION DERIVATIONS

APPENDIX E
DYNAMIC ANALYSIS AND EQUATION DERIVATIONS

This appendix shows the equations for analyzing the biconvex structure mode shapes and natural frequencies.

The substrate frequencies are defined in Appendix D. A calculation is included here to indicate substrate deflection for the boost conditions; the deployed array minimum resonant frequencies are also estimated in this appendix.

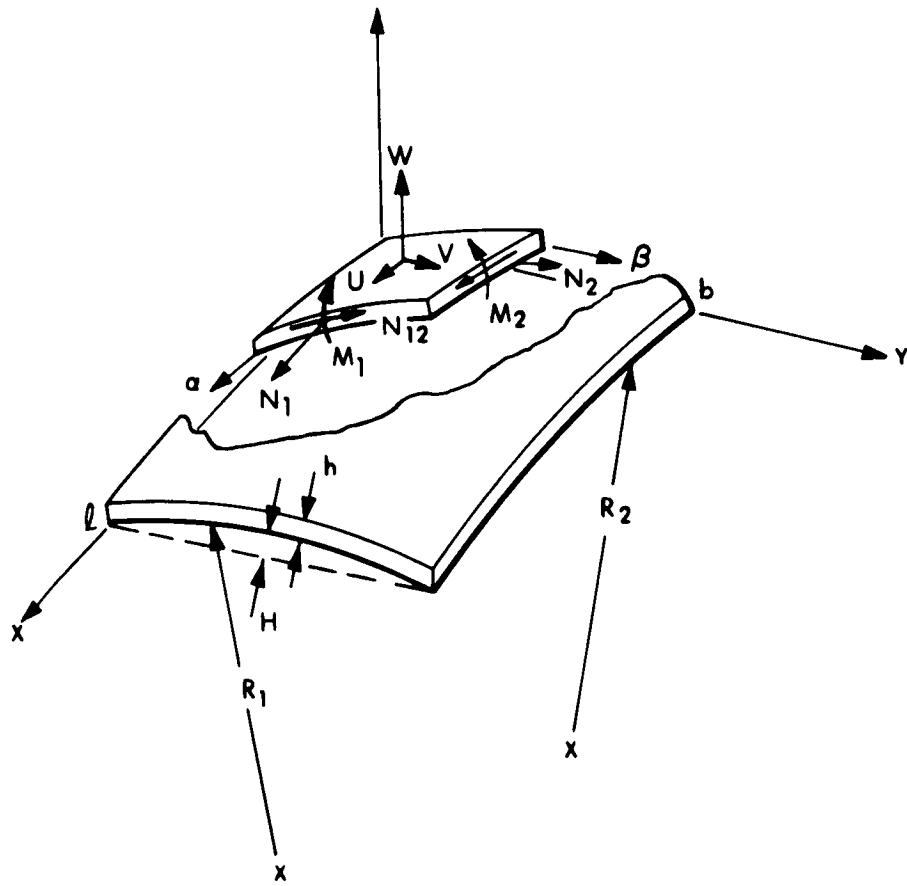
The internal loads for the biconvex substrate can be obtained from the derived equations once the mode shapes are determined. Equation complexity dictates that the mode shapes must be determined by test.

Also discussed here is a method of analysis to determine the effect and optimum design of viscoelastic adhesive damped structures.

E.1 Prediction of Natural Frequencies and Mode Shapes of the Substrate

The mathematical model of the thin shell of the panel shown in Fig. E-1 will be developed from the shallow shell theory presented by Marguerre (Ref. 1). The quantities $1/R_1$ and $1/R_2$ represent the principal curvatures of the panel; α and β are orthogonal curvilinear coordinates along the principal directions; U , V , and W are displacements of the shell midsurface along the principal and radial directions. The sign conventions for membrane stresses and moments are also shown in Fig. E-1.

The shallow shell theory, as written in terms of a stress function ϕ and the radial displacement W takes the following form if the radial inertia is included



$$\frac{1}{R_2} \frac{\partial^2 \phi}{\partial \alpha^2} + \frac{1}{R_1} \frac{\partial^2 \phi}{\partial \beta^2} + D \nabla^4 W + \rho h \frac{\partial^2 W}{\partial t^2} = 0 \quad (1)$$

$$\frac{1}{Eh} \nabla^4 \phi - \frac{1}{R_2} \frac{\partial^2 W}{\partial \alpha^2} - \frac{1}{R_1} \frac{\partial^2 W}{\partial \beta^2} = 0 \quad (2)$$

Equation 1 is the condition for radial equilibrium of the shell and Eq. 2 is the condition for compatibility of the displacements. D is a stiffness parameter given by

$$D = \frac{Eh^3}{12(1 - \nu^2)}$$

where E is the modulus of elasticity and ν is Poisson's ratio. ρ is the mass density of the shell.

Other relations which are required to formulate the boundary conditions are:

1. The membrane stress relations

$$N_1 = \frac{\partial^2 \phi}{\partial \beta^2}$$

$$N_2 = \frac{\partial^2 \phi}{\partial \alpha^2}$$

$$N_{12} = \frac{\partial^2 \phi}{\partial \alpha \partial \beta}$$

2. The moment and shear relations

$$M_1 = D \left(\frac{\partial^2 W}{\partial \alpha^2} + \nu \frac{\partial^2 W}{\partial \beta^2} \right)$$

$$M_2 = D \left(\frac{\partial^2 W}{\partial \beta^2} + \nu \frac{\partial^2 W}{\partial \alpha^2} \right)$$

$$H_{12} = -D (1 - \nu) \frac{\partial^2 W}{\partial \alpha \partial \beta}$$

$$Q_1 = -D \frac{\partial}{\partial \alpha} \nabla^2 W$$

$$Q_2 = -D \frac{\partial}{\partial \beta} \nabla^2 W$$

The stress-strain relations from which the displacements U and V can be found are:

$$N_1 = \frac{Eh}{1-\nu^2} (\epsilon_\alpha + \nu \epsilon_\beta)$$

$$N_2 = \frac{Eh}{1-\nu^2} (\epsilon_\beta + \nu \epsilon_\alpha)$$

$$N_{12} = \frac{Eh}{2(1+\nu)} \epsilon_{\alpha\beta}$$

where

$$\epsilon_\alpha = \frac{\partial U}{\partial \alpha} + \frac{W}{R_1}$$

$$\epsilon_\beta = \frac{\partial V}{\partial \alpha} + \frac{W}{R_2}$$

$$\epsilon_{\alpha\beta} = \frac{\partial U}{\partial \beta} + \frac{\partial V}{\partial \alpha}$$

Boundary conditions for demonstration panel.

The support condition for the demonstration panel will be such that

$$W = V = M_1 = N_1 = 0 \quad \text{on} \quad \alpha = 0, \alpha = \alpha_0$$

$$U = W = M_2 = N_2 = 0 \quad \text{on} \quad \beta = 0, \beta = \beta_0$$

Mode Shapes and Frequency Equations

The form of the series solutions which satisfy the boundary conditions above are:

$$\phi = \sum_{m=1}^{\infty} \sum_{n=1}^{\infty} A_{mn} \sin \lambda_n \alpha \sin \mu_m \beta \sin \omega_{mn} t \quad (3)$$

$$W = \sum_{m=1}^{\infty} \sum_{n=1}^{\infty} B_{mn} \sin \lambda_n \alpha \sin \mu_m \beta \sin \omega_{mn} t \quad (4)$$

where

$$\lambda_n = \frac{n\pi}{\alpha_0} \quad \text{and} \quad \mu_m = \frac{m\pi}{\beta_0}$$

Substitution of Eqs. 3 and 4 in 1 and 2 leads to the following set of algebraic equations in A_{mn} and B_{mn}

$$\left(\frac{1}{R_2} \lambda_n^2 + \frac{1}{R_1} \mu_m^2 \right) A_{mn} + \left[D (\lambda_n^2 + \mu_m^2)^2 + \rho h \omega_{mn}^2 \right] B_{mn} = 0$$

$$\frac{1}{Eh} (\lambda_n^2 + \mu_m^2)^2 A_{mn} - \left(\frac{1}{R_2} \lambda_n^2 + \frac{1}{R_1} \mu_m^2 \right) B_{mn} = 0$$

The condition which must be satisfied for a solution for A_{mn} and B_{mn} to exist is that the determinant of the coefficients vanishes. That is

$$-\left(\frac{1}{R_2} \lambda_n^2 + \frac{1}{R_1} \mu_m^2 \right)^2 - \frac{1}{Eh} (\lambda_n^2 + \mu_m^2)^2 \left[D (\lambda_n^2 + \mu_m^2)^2 + \rho h \omega_{mn}^2 \right] = 0$$

which may be solved for ω_{mn}^2

$$\omega_{mn}^2 = \frac{1}{\rho h} \left[D \left(\lambda_n^2 + \mu_m^2 \right)^2 + Eh \frac{\left(\frac{\lambda_n^2}{R_2} + \frac{\mu_m^2}{R_1} \right)^2}{\left(\lambda_n^2 + \mu_m^2 \right)^2} \right] \quad (5)$$

For the special case of the demonstration panel $R_1 = R_2 = R$ and the frequency equation becomes

$$\omega_{mn}^2 = \frac{1}{\rho h} \left[D \left(\lambda_n^2 + \mu_m^2 \right)^2 + \frac{Eh}{R^2} \right]$$

whereas for a flat plate $R_1 = R_2 = \infty$ the frequency equation becomes

$$\omega_{mn}^2 = \frac{D}{\rho h} \left(\lambda_n^2 + \mu_m^2 \right)^2$$

It is interesting to note that at the lower frequencies, i.e., small m and n , the term due to the panel curvature, Eh/R^2 , is the predominate term in the frequency equation whereas for large m and n , high frequencies, the frequencies of the doubly curved panel approach those of a flat plate as is expected. This substantial increase in the fundamental and lower natural frequencies of the panel is the inherent advantage of the curved panel over the flat panel.

Some interesting conclusions about the nature of the vibration of the panel can be drawn from the form of the solutions Eqs. 3 and 4 and the resulting frequency Eq. 5. The solutions are expansions in a set of generalized coordinates which are the normal modes of the system each of which is associated with a frequency ω_{mn} . For a square panel, that is for $\alpha_0 = \beta_0$ and $R_1 = R_2 = R$ the frequency equation is symmetric in m and n which means that the initial conditions (or forcing function) may be chosen in a way where for $m \neq n$

$$W = \left[A_{mn} \sin \frac{m\pi}{\alpha_0} \sin \frac{n\pi}{\beta_0} + A_{nm} \sin \frac{n\pi}{\alpha_0} \sin \frac{m\pi}{\beta_0} \right] \sin t$$

with A_{mn} and A_{nm} completely arbitrary and still have motion at the natural frequency ω_{mn} . For examples of the different types of natural vibration which can occur at a given frequency, ω_{mn} , see Ref. 2.

E.2 Response of Substrate to Sinusoidal and Random Input

Where the panel is excited by moving supports, the total displacement at $\alpha = 0$, $\alpha = \alpha_0$, $\beta = 0$, and $\beta = \beta_0$ is

$$W_s = W_0 \sin \omega_s t.$$

Assume that the displacement of the panel relative to the supports is given by

$$W = \bar{W}(\alpha, \beta) q(t)$$

$$W = q_0 \sin \frac{n\pi}{\alpha_0} \alpha \sin \frac{m\pi}{\beta_0} \beta \sin \omega_{mn} t$$

$$q(t) = q_0 \sin \omega_{mn} t$$

that is, assume $\omega_s = \omega_{mn} = \omega_{11}$ and that the response is primarily the fundamental mode of the panel. The total displacement is then given by

$$Z = \bar{W} q(t) + W_s$$

Lagrange's equations for a nonconservative system may be written as

$$\frac{d}{dt} \left(\frac{\partial T}{\partial \dot{q}} \right) + \frac{\partial D}{\partial \dot{q}} + \frac{\partial V}{\partial q} = 0 \quad (6)$$

where

$$T = \frac{1}{2} \rho \int_0^{\beta_0} \int_0^{\alpha_0} (\bar{W} \dot{q} + \dot{W}_s)^2 d\alpha d\beta$$

$$V = \frac{1}{2} K_E q^2$$

$$D = \frac{1}{2} C_E \dot{q}^2$$

K_E = Effective Stiffness

C_E = Effective Damping

Performing the operations indicated in Eq. 6 gives

$$-\omega_{11}^2 W_0 \int_0^{\beta_0} \int_0^{\alpha_0} \rho \bar{w}(\alpha, \beta) d\alpha d\beta - \omega_{11}^2 q_0 \int_0^{\beta_0} \int_0^{\alpha_0} [\bar{w}(\alpha, \beta)]^2 d\alpha d\beta + C_E i \omega_{11} q_0 + K_E q_0 = 0 \quad (7)$$

Let

$$I_1 = \int_0^{\beta_0} \int_0^{\alpha_0} \rho \bar{w}(\alpha, \beta) d\alpha d\beta$$

$$I_2 = \int_0^{\beta_0} \int_0^{\alpha_0} \rho [\bar{w}(\alpha, \beta)]^2 d\alpha d\beta$$

Then Eq. 7 becomes

$$-\omega_{11}^2 q_0 I_2 + (C_E i \omega_{11} + K_E) q_0 = \omega_{11}^2 W_0 I_1 \quad (8)$$

at resonance $\omega_s \cong \omega_{11}$ and the panel spring forces balance the inertia i.e.,

$$K_E q_0 = \omega_{11}^2 q_0 I_2$$

so that Eq. 8 becomes

$$\frac{q_0}{W_0} = -i \frac{I_1}{C_E} \omega_{11}$$

or neglecting phase

$$\frac{q_o}{W_o} = \frac{I_1}{C_E} \omega_{11} \quad (9)$$

but the critical damping coefficient is given by

$$C_C = 2 \sqrt{I_2 K_E}$$

and since

$$\omega_{11} = \sqrt{\frac{K_E}{I_2}}$$

$$C_C = 2I_2 \omega_{11} \quad (10)$$

and the dynamic magnification factor for the panel is

$$Q = \frac{1}{\eta} = \frac{1}{2 C_E / C_C} \quad (11)$$

where η is the structural damping coefficient for the first mode; substituting Eq. 10 and 11 in 9 gives

$$\frac{q_o}{W_o} = \frac{I_1}{I_2} Q$$

then

$$W = \frac{I_1}{I_2} Q \bar{W}(\alpha, \beta) W_s$$

and

$$\dot{W} = \frac{I_1}{I_2} Q \bar{W}(\alpha, \beta) \dot{W}_s$$

or

$$W = \frac{I_1 Q}{I_2 \omega_{11}^2} \bar{W}(\alpha, \beta) \ddot{W}_s$$

$$I_1 = \int_0^{\beta_0} \int_0^{\alpha_0} \rho \sin \frac{\pi}{\alpha_0} \alpha \sin \frac{\pi}{\beta_0} \beta \, d\alpha \, d\beta = \frac{4\alpha_0 \beta_0}{\pi^2} \rho$$

$$I_2 = \int_0^{\beta_0} \int_0^{\alpha_0} \rho \sin^2 \frac{\pi}{\alpha_0} \alpha \sin^2 \frac{\pi}{\beta_0} \beta \, d\alpha \, d\beta = \frac{\alpha_0 \beta_0}{4} \rho$$

so that

$$W = \frac{16}{\pi^2} \frac{Q}{\omega_{11}^2} \bar{W}(\alpha, \beta) \ddot{W}_s \quad (12)$$

Maximum Deflection of Demonstration Panel - Sinusoidal Input

Assume an input acceleration of 1.5 g's to the substrate e.g., no amplification in the frame. From Eq. 10 of Subsection E.1

$$\omega_{11}^2 = 32,000$$

assume $\eta = 0.04$; $Q = 25$; for maximum W , $\alpha = \alpha_0/2$, $\beta = \beta_0/2$

$$W = \frac{(16)(25)(1.5)(387)}{\pi^2 (32,000)} = \frac{232,200}{315,826}$$

$W = 0.735$ inches at the center of the panel

Consideration of Random Vibration Environment

The random vibration environment is band limited between 200 and 2000 cps and is not expected to produce critical design loads since the solar panel structure will have its primary resonances well below 200 cps.

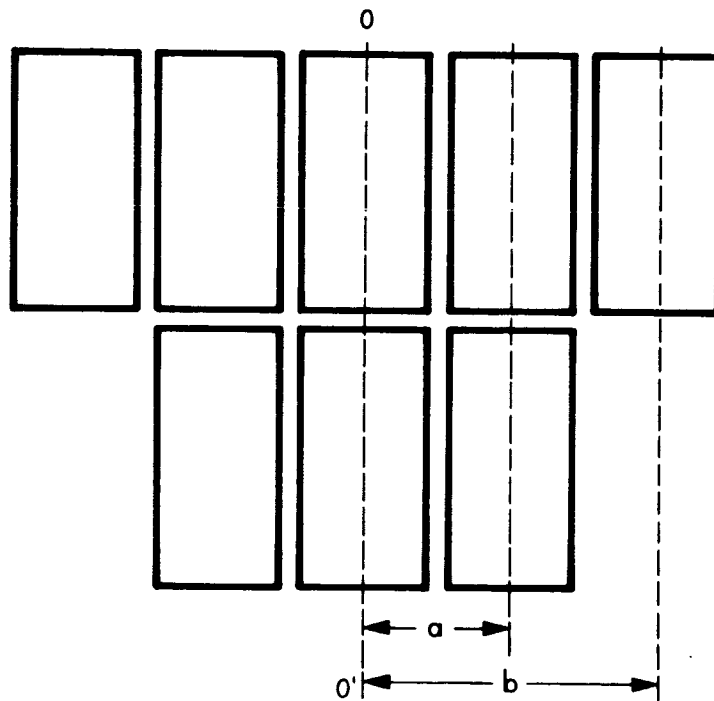
E.3 Dynamics of Deployed Array

E.3.1 Estimate of Lower Bound of Natural Frequencies of the Deployed Array

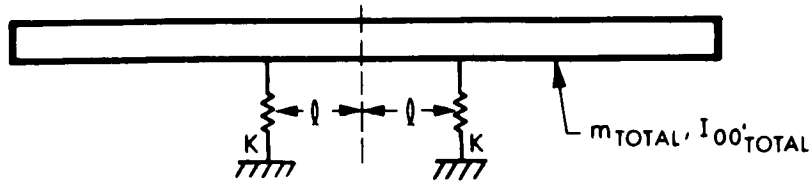
An estimate of the lowest natural frequencies of the deployed array has been made based on the following assumptions.

1. All the load is carried by the two frame members which attach to the spacecraft as cantilever beams.
2. The stiffness added to the structure by the panels is neglected.
3. The mass and mass moment of inertia is uniformly distributed along the beams.
4. The torsional frequency is calculated based on differential bending of the cantilever beams, neglecting the torsional stiffness of the box beams and cross members.

All of these assumptions will lead to estimates of natural frequencies which are conservatively low.



The array shown above is reduced to the model shown on the following page.



$$M_{total} = 8 \times m = 8 \times 0.06476 = 0.51808 \text{ lb sec}^2/\text{in}$$

$$I_{00}'_{total} = 2I_{00}' + 4(I_{00}' + ma^2) + 2(I_{00}' + mb^2)$$

$$I_{00}' = 17.7 \text{ lb-in-sec}^2$$

$$I_{00}'_{total} = 2913.4 \text{ lb-in-sec}^2$$

$$K = \frac{8EI}{L^3}$$

$$E = 10^7 \text{ psi}$$

$$L = 360 \text{ in}$$

$$l = 30 \text{ in}$$

$$I = 0.0528 \text{ in}^4 \text{ (section moment of inertia of frame)}$$

$$K = \frac{8(10^7)(0.0528)}{(3.6)^3 \times 10^6} = 0.0905 \text{ lb/in}$$

The fundamental cantilever frequency is given by

$$f = \frac{1}{2\pi} \sqrt{\frac{2K}{m_{total}}} = 0.094 \text{ cps}$$

the first torsional frequency is given by

$$f = \frac{1}{2\pi} \sqrt{\frac{2Kl^2}{I_{00}'_{total}}} = 0.038 \text{ cps}$$

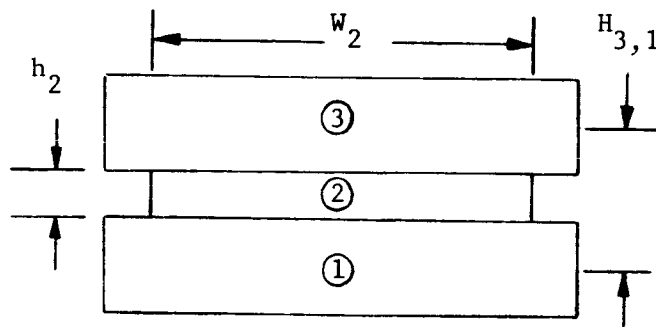
E.3.2 Mathematical model of Deployed Array - Stiffness Matrix Analysis

The test results from the demonstration panel will be used to deduce a stiffness matrix and a damping matrix for the deployed array from which the frequencies, mode shapes, and frequency response can be calculated.

E.4 Analysis of Viscoelastic Damping in Composite Structures

In order to minimize the dynamic magnification factor of the frame structure, the feasibility of incorporating a frame design which uses composite beams with constrained layers of viscoelastic material is being investigated. The constrained layer approach was chosen over a free layer arrangement since the former provides more damping with less added weight than the latter.

Consider a general composite beam which has cross section as shown



① and ③ Primary Structure

② Viscoelastic Layer

h_2 is thickness of the viscoelastic material

W_2 is width of the viscoelastic material

$H_{3,1}$ is the distance between the neutral axes of sections 1 and 3 of the composite beam.

The loss factor for the composite beam is given in Ref. 3.

$$\eta = \frac{\beta Y X}{1 + (2+Y)X + (1+Y)(1+\beta^2) X^2} \quad (13)$$

Where Y is a geometry parameter given by

$$Y = \frac{H_{3,1}^2}{\frac{1}{E_1 A_1} + \frac{1}{E_3 A_3} (E_1 I_1 + E_3 I_3)} \quad (14)$$

and X is a parameter given by

$$X = \frac{G_2 W_2}{h_2} \left(\frac{\lambda}{2\pi} \right)^2 \left(\frac{1}{E_1 A_1} + \frac{1}{E_3 A_3} \right) \quad (15)$$

where

β = loss factor of viscoelastic material in shear

E = modulus of elasticity, psi

A = cross sectional area, in²

I = section moment of inertia

G = shear modulus, psi

λ = wavelength, in = $\sqrt{E/\rho}/f$

for a given geometry of the primary structure, Y, and a given loss factor, β , Eq. 13 may be maximized by adjusting X.

$$X_{\text{optimum}} = \frac{1}{\sqrt{(1+Y)(1+\beta^2)}} \quad (16)$$

the maximum loss factor for the composite beam is

$$\eta_{\text{max}} = \frac{\beta Y}{2 + Y + \frac{2}{X_{\text{opt}}}} \quad (17)$$

REFERENCES

1. Marguerre, K. Fur Theorie Der Gekrumnten Platte Grosser Formanderung, Proc. 5th International Congress of Applied Mechanic, (1938), p. 93
2. Byerly, W. E., An Elementary Treatise on Fourier's Series and Spherical, Cylindrical and Ellipsoidal Harmonics with Applications to Problems in Mathematical Physics. Dover Publications, Inc., New York, New York, pages 128-134
3. Ungar, Eric E., "A Guide to Designing Highly Damped Structures Using Layers of Viscoelastic Material," Machine Design, Feb 14, 1963

APPENDIX F
THERMAL ANALYSIS AND DERIVATIONS

APPENDIX F
THERMAL ANALYSIS AND DERIVATIONS

F.1 Thermal Analysis of Hollow Core Substrate

The steady-state equilibrium temperature distribution within a typical section of the hollow core nickel substrate has been determined through the use of a digital computer program and an IBM 7094 computer. The conducting material is first divided into a number of nodal areas used to approximate the continuous region such that a simple heat balance equation can be written for each node:

$$R_i = \sum C_{ji} (T_j - T_i) + \sum S_{ji} (T_j^4 - T_i^4) + Q_i$$

The conductance between the i th node and any other (j) node is given as C_{ji} , the corresponding radiation coefficient is S_{ji} , and the heat source of the i th node is Q_i . At steady-state equilibrium, the residual, R_i , is zero for each node. The digital computer program uses Newton's formula and a numerical relaxation technique to establish each of the temperatures such that each residual is reduced to zero.

The conductance between nodes is calculated for each mutual conducting boundary as:

$$C_{ji} = \frac{k A_{ji}}{X_{ji}}$$

where k is the thermal conductivity of the material, A_{ji} is the cross-sectional area of the boundary between i and j , and X_{ji} is the length between these two node centers. The radiation coefficients, S_{oi} , in

the problem under consideration, are between exterior surface elements and deep space. With specularly reflecting walls on the substrate holes, the radiation coefficient can be calculated as $\sigma A_i \epsilon_i$. In the case of segments radiating from two sides, ϵ_i can be replaced with the sum of the top and bottom emissivities. The solar radiation absorbed was included as heat source terms, $Q_i = A_i S \alpha$.

F.2 Predicted Temperature Distribution

The predicted temperature distribution for earth-space solar radiation intensities is given in the data below.

<u>Node</u>	<u>Area (ft x 10⁴)</u>	<u>Emissivity (ϵ)</u>	<u>Heat Absorbed (Btu/hr x 10⁴)</u>	<u>Temperature (°F)</u>
1-3	0.015	1.7	5.4	126.1
4-6	0.046	1.7	16.5	126.1
7-9	0.076	1.7	26.9	126.1
10-12	0.106	1.7	37.6	126.1
13-15	0.137	1.7	48.7	126.1
16-18	0.167	1.7	59.2	126.1
19-21	0.197	1.7	70.0	126.1
22-24	0.228	1.7	80.8	126.1
25-27	0.261	0.8	93.0	126.2
28	0.360	0.8	128.0	126.7
29-31	-	0	0	126.1
32-34	-	0	0	125.7
35-37	-	0	0	125.4
38-40	-	0	0	125.1
41-43	-	0	0	124.8
44-46	0.261	0.9	0	123.8
47	0.360	0.9	0	121.2

Conductance (Btu/hr-°F)

C ₁	0.0047	C ₇	0.0188
C ₂	0.155	C ₈	0.0388
C ₃	0.0094	C ₉	0.0236
C ₄	0.0775	C ₁₀	0.0309
C ₅	0.0142	C ₁₁	0.0283
C ₆	0.0515		

C₁, for instance, is C₁₄ = C₄₁ = C₂₅ = C₅₂ = C₃₆ = C₆₃; C₂ is C₁₂ = C₂₁ = C₂₃ = C₃₂, etc.

APPENDIX G
PROGRAM DRAWING LIST AND DETAIL DRAWINGS

APPENDIX G

PROGRAM DRAWING LIST AND DETAIL DRAWINGS

G.1 Drawing List

The drawings related to this program are listed in the table below. The detail drawings for the demonstration panel are also listed in this appendix.

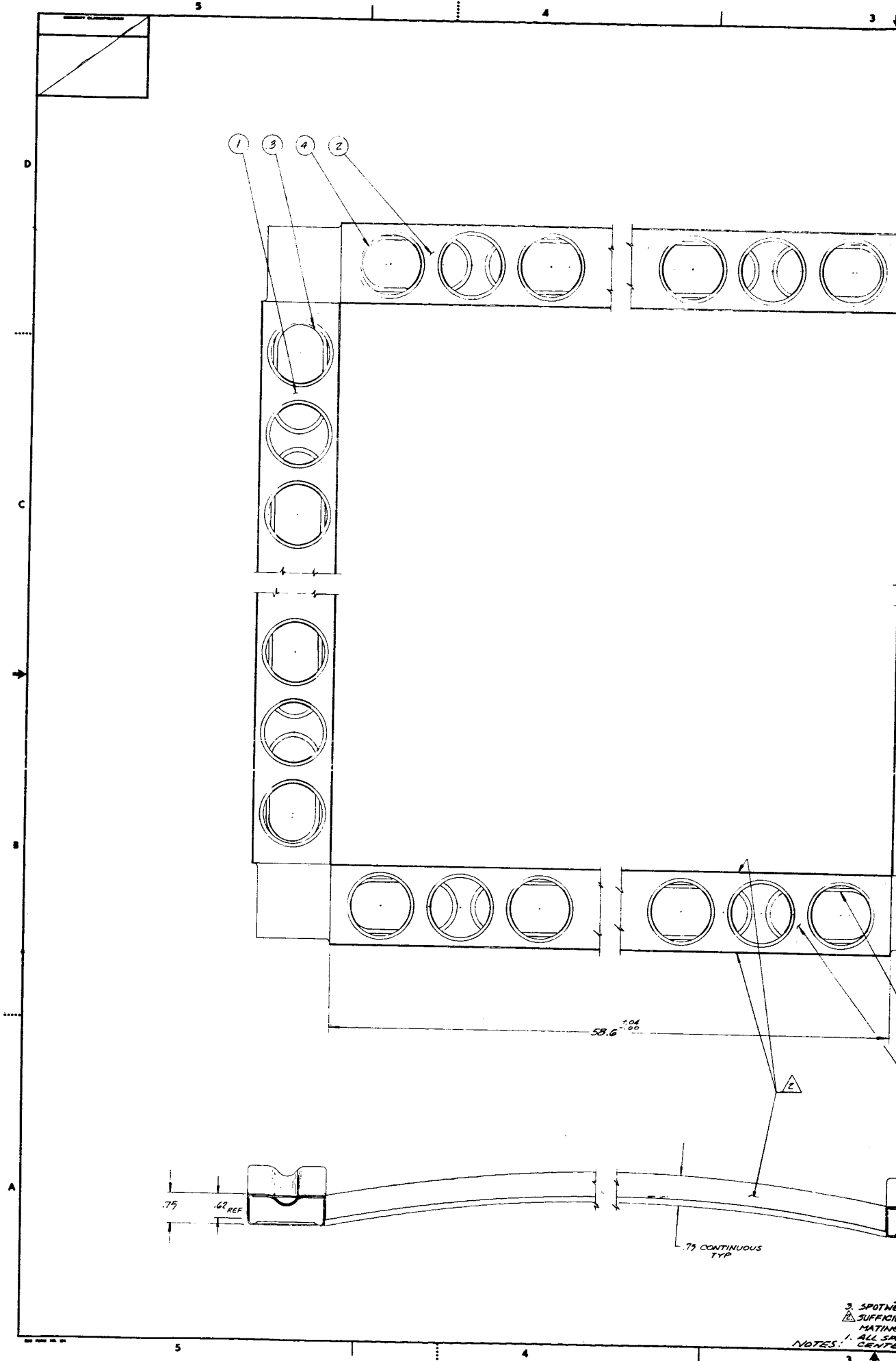
<u>EOS Drawing Number</u>	<u>Title</u>
1100300	Solar Panel Assembly, Demonstration
1100301	Substrate Assembly
*1100302	Upper Frame Assembly
*1100303	Lower Frame Assembly
*1100304	Clip - Substrate - Upper
*1100305	Clip - Substrate - Lower
*1100306	Channel - Lower - 58.6
*1100307	Channel - Lower - 56.7
*1100308	Channel - Upper - 58.6
*1100309	Channel - Upper - 56.7
*1100310	Hinge Bracket
*1100311	Upper Corner Bracket
*1100312	Bottom Corner Bracket
*1100313	Frame (46)
*1100314	Frame (45)
*1100315	Frame (44)
*1100316	Frame (43)
*1100317	Hollow Core Substrate
1100318	Molding, Proposed Cross Section
1100319	Molding, Proposed Cross Section
*1100320	Frame, Proposed Cross Section

<u>EOS Drawing Number</u>	<u>Title</u>
1100321	Array Studies
1100322	Array Studies
1100323	Art Work "P" Bus Bar
1100324	Art Work "N" Bus Bar
1100325	Art Work "P" Bus Bar
1100326	Art Work "N" Bus Bar Module
1100327	Prototype Solar Panel Assembly
*1100328	P Bus Bar, Detail
*1100329	N Bus Connection, Detail
*1100330	N Bus Bar, Detail
*1100331	P Bus Connection, Detail
1100332	Photovoltaic Assembly, Demonstration Panel
1100333	not used
1100334	Proposed Current Flow in Eight Sub-panels for 1000 sq. ft. Array
1100335	Assembly - Stowed Configuration
1100336	Stowed Configuration 1000 sq. ft.
1100337	Solar Panel Deployment 1000 sq. ft.
1100338	Hinge - Spring - Damper Configuration
*1100339	Hinge - Latch - Configuration
*1100340	Hinge Configuration
*1100341	Hinge Configuration
*1100342	Panel Latch
1100343	Pin Puller
*1100344	Bus Connector and Crossover
1100345	Assembly - Stowed Configuration With Band
1100346	Stowed Configuration 500 sq. ft.
1100347	10 kW Solar Panel, Electric Propulsion, Jupiter Fly-By
1100348	not used

<u>EOS Drawing Number</u>	<u>Title</u>
1100349	not used
1100350	not used
91-11966	Plating Mandrel, Hollow Core Sample, Pattern for Part HH-
91-11967	Plating Mandrel, Hollow Core Sample, Pattern for Part SU-
91-11968	Plating Mandrel, Hollow Core Sample, Pattern for Part SC-
91-11970	Plating Mandrel, Hollow Core Sample, Pattern for Part H-H-4
91-11985	Plating Mandrel, Hollow Core Sample, Pattern for Part H-H-8

G.2 Miscellaneous Drawings

The following pages comprise drawings, astericked in the above list, for the demonstration panel which have not been referenced in this report.



3 SPOTWELDS
 SUFFICIENT
 MATING
 1. ALL SPOTWELDS
 CENTERED
 NOTES:

SECURITY CLASSIFICATION

5

4

3

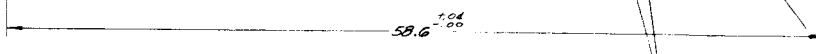
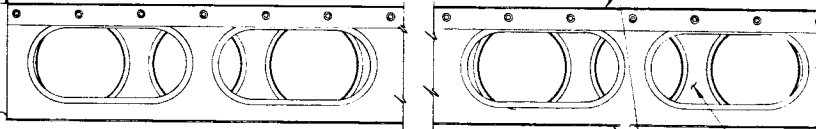
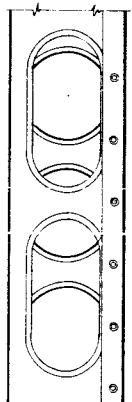
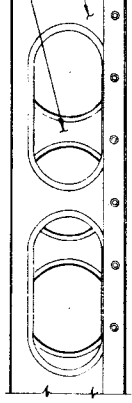
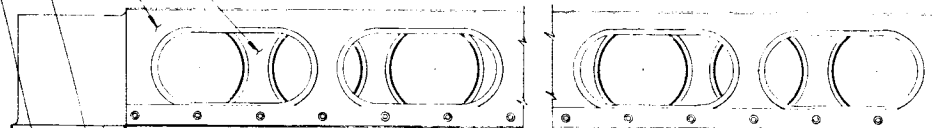
D

C

B

A

3 1 2 4

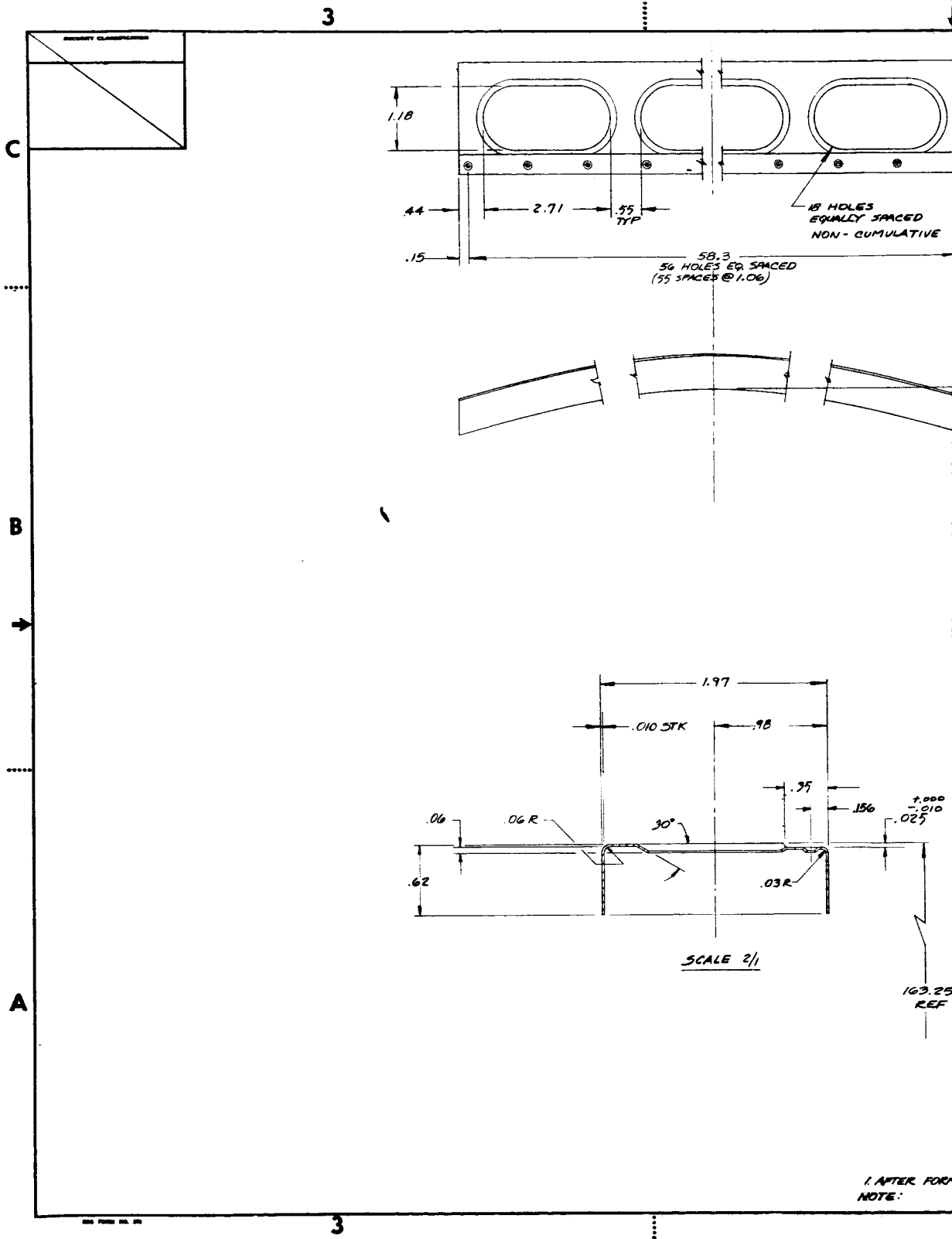


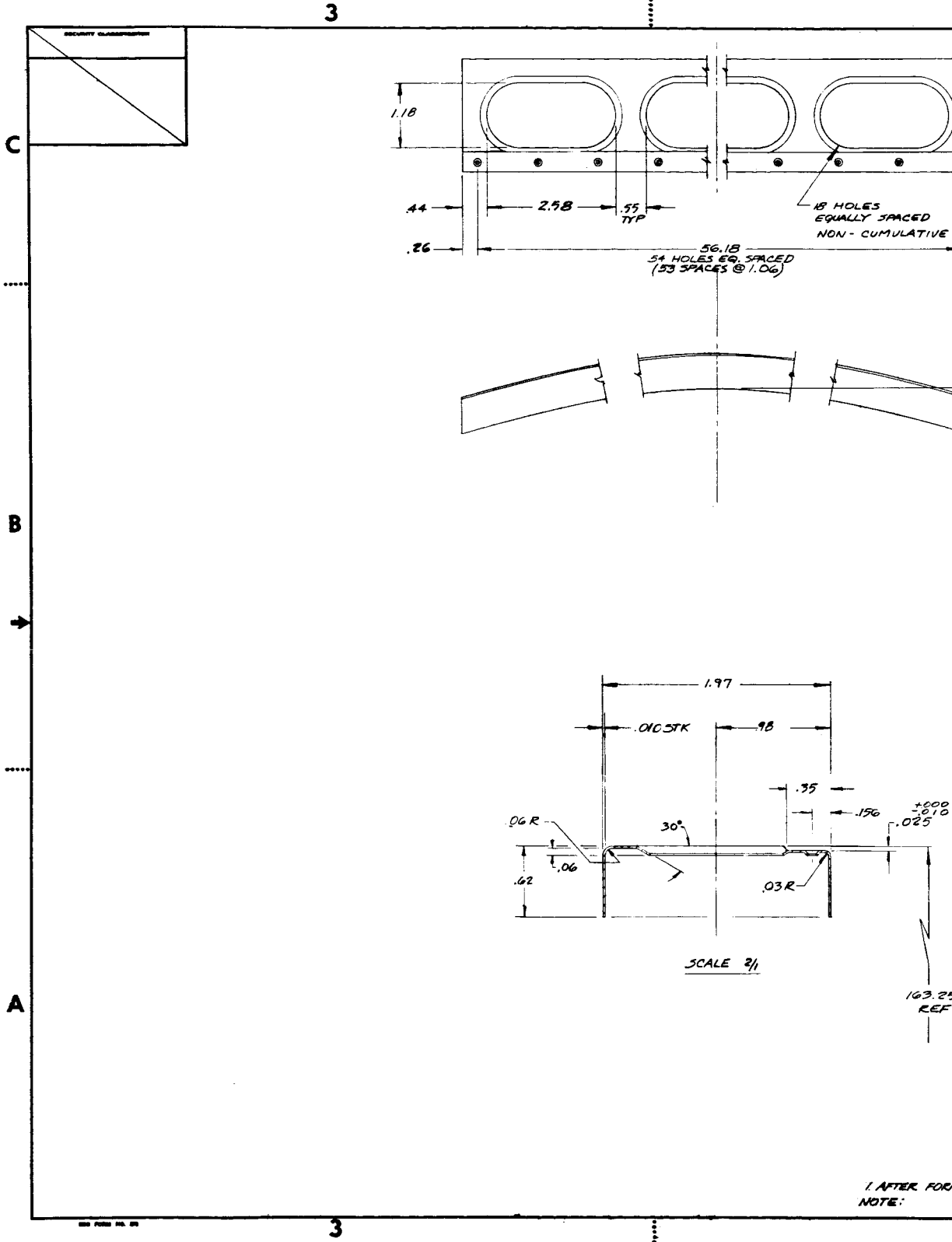
3 SPOT
2 BUFF
1 MAT
1 ALL
75 CA
NOTES:

5

4

3





SECURITY CLASSIFICATION

C

B

A

3

3

163.25 REF

+000
-010
.025

SCALE 3/4

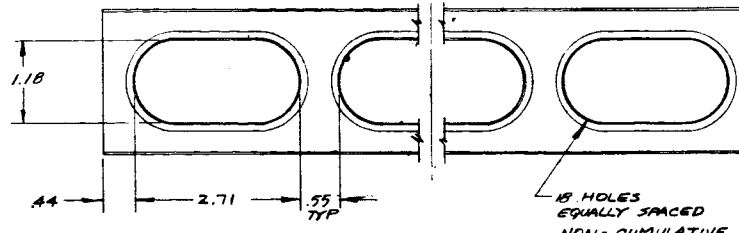
1. AFTER FOR NOTE:

1

PROPERTY CLASSIFICATION
/

C

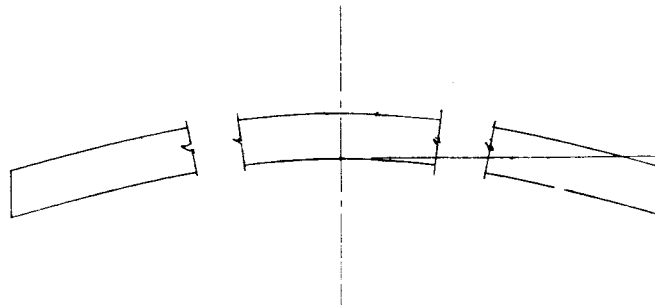
3



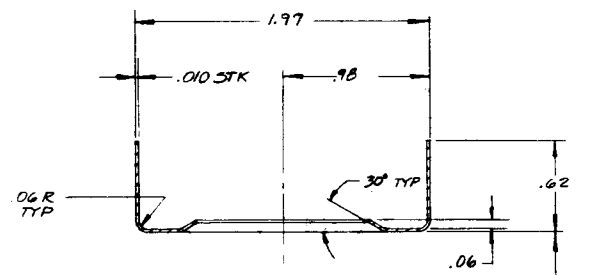
.....

B

→



.....



A

SCALE 2/1

163.25 REF

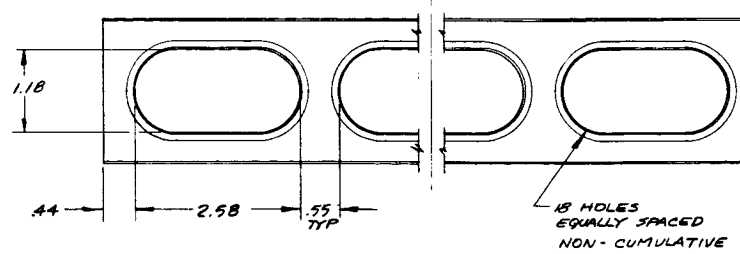
3

T' AFTER FORMING
NOTE:

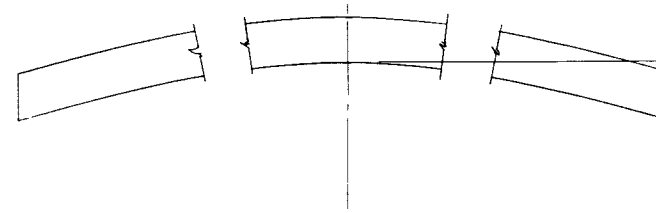
SECURITY CLASSIFICATION

3

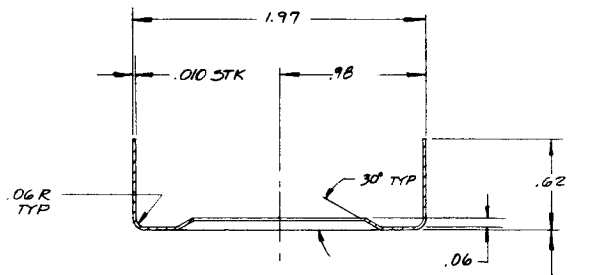
C



B



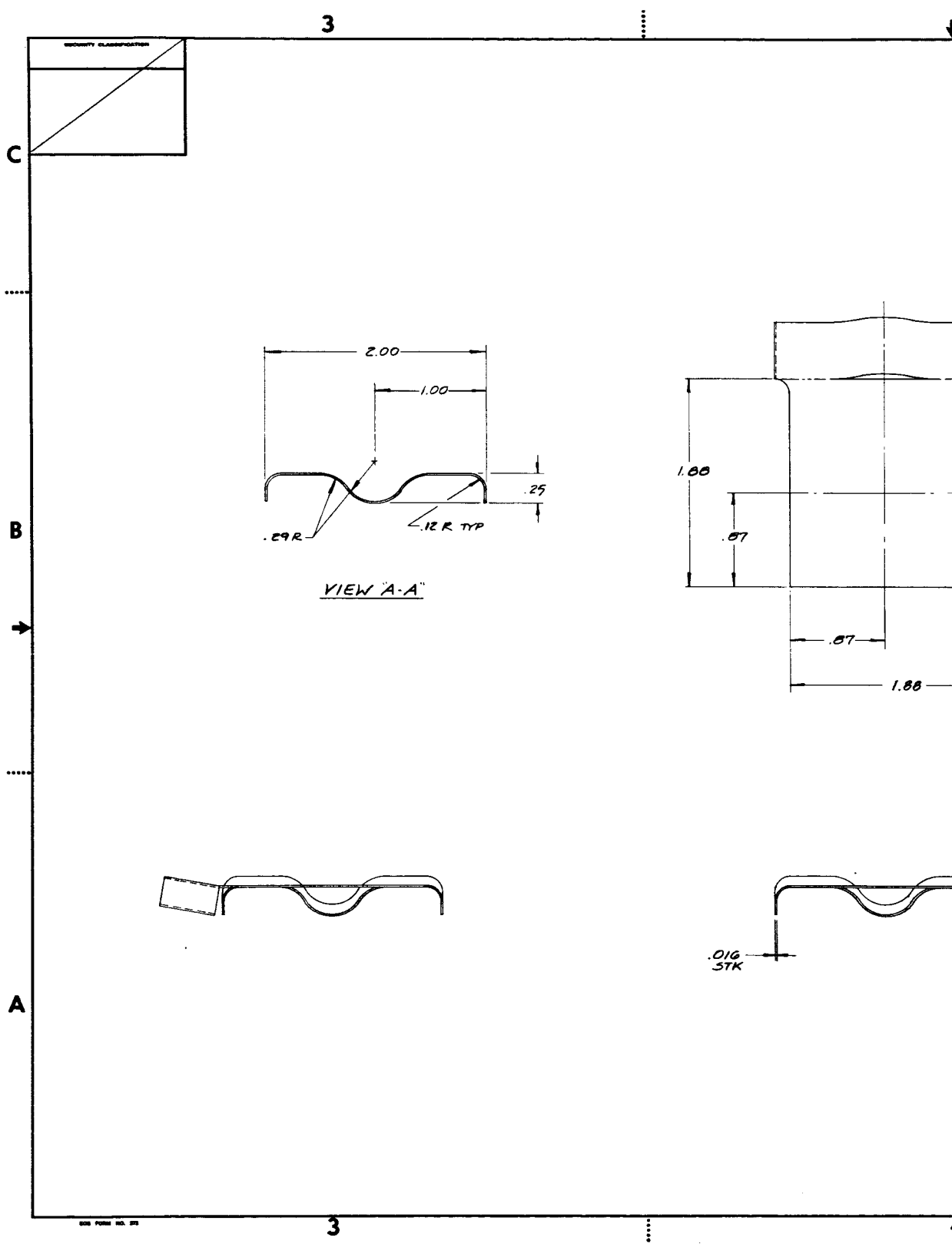
A



SCALE 3/4

163.25 REF

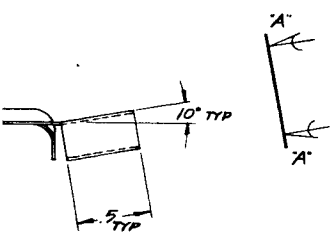
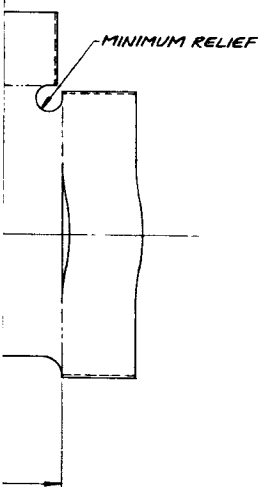
1 AFTER FORMING
NOTE:



1

1

REVISIONS				
CHANGE	DATE	DESCRIPTION	BY	APPROVED



C

B

1100311 -

A

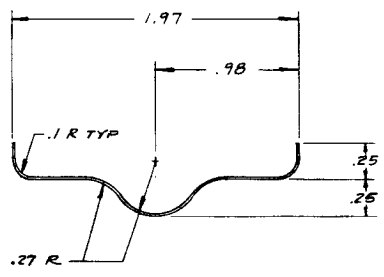
BRACKET		SHOWN	6061-T6 AL ALY	RR-A-327
REV. NO.	DATE	DESCRIPTION	BY	APPROVED
LIST OF MATERIALS				
UNLESS OTHERWISE NOTED:		DESIGNER	DATE	
1. LARGEST DIMENSION IN DIMENSIONS		LAZ	4/21/64	E
2. VOLUMES				
3. DIMENSIONS: FRACTIONS ANGULAR				
A = .030"				
B = .015"				
C = .015"				
D = .015"				
E = .015"				
F = .015"				
G = .015"				
H = .015"				
I = .015"				
J = .015"				
K = .015"				
L = .015"				
M = .015"				
N = .015"				
O = .015"				
P = .015"				
Q = .015"				
R = .015"				
S = .015"				
T = .015"				
U = .015"				
V = .015"				
W = .015"				
X = .015"				
Y = .015"				
Z = .015"				
AA = .015"				
AB = .015"				
AC = .015"				
AD = .015"				
AE = .015"				
AF = .015"				
AG = .015"				
AH = .015"				
AI = .015"				
AJ = .015"				
AK = .015"				
AL = .015"				
AM = .015"				
AN = .015"				
AO = .015"				
AP = .015"				
AQ = .015"				
AR = .015"				
AS = .015"				
AT = .015"				
AU = .015"				
AV = .015"				
AW = .015"				
AX = .015"				
AY = .015"				
AZ = .015"				
BAA = .015"				
BAB = .015"				
BAC = .015"				
BAD = .015"				
BAE = .015"				
BAF = .015"				
BAG = .015"				
BAH = .015"				
BAI = .015"				
BAJ = .015"				
BAK = .015"				
BAL = .015"				
BAM = .015"				
BAN = .015"				
BAO = .015"				
BAQ = .015"				
BAR = .015"				
BAS = .015"				
BAT = .015"				
BAU = .015"				
BAV = .015"				
BAW = .015"				
BAX = .015"				
BAZ = .015"				
CBA = .015"				
CBB = .015"				
CBC = .015"				
CBD = .015"				
CBE = .015"				
CBF = .015"				
CBG = .015"				
CBH = .015"				
CBI = .015"				
CBJ = .015"				
CBK = .015"				
CBL = .015"				
CBM = .015"				
CBN = .015"				
CBO = .015"				
CBQ = .015"				
CBR = .015"				
CBS = .015"				
CBT = .015"				
CBU = .015"				
CBV = .015"				
CBW = .015"				
CBX = .015"				
CBZ = .015"				
CCA = .015"				
CCB = .015"				
CCC = .015"				
CCD = .015"				
CCE = .015"				
CCF = .015"				
CCG = .015"				
CCH = .015"				
CCI = .015"				
CCJ = .015"				
CCK = .015"				
CCL = .015"				
CCM = .015"				
CCN = .015"				
CCO = .015"				
CCQ = .015"				
CCR = .015"				
CCS = .015"				
CCT = .015"				
CCU = .015"				
CCV = .015"				
CCW = .015"				
CCX = .015"				
CCZ = .015"				
CDA = .015"				
CDB = .015"				
CDC = .015"				
CDD = .015"				
CDE = .015"				
CDF = .015"				
CDG = .015"				
CDH = .015"				
CDI = .015"				
CDJ = .015"				
CDK = .015"				
CDL = .015"				
CDM = .015"				
CDN = .015"				
CDO = .015"				
CDQ = .015"				
CDR = .015"				
CDS = .015"				
CDT = .015"				
CDU = .015"				
CDV = .015"				
CDW = .015"				
CDX = .015"				
CDZ = .015"				
CEA = .015"				
CEB = .015"				
CEC = .015"				
CED = .015"				
CEE = .015"				
CEF = .015"				
CEG = .015"				
CEH = .015"				
CEI = .015"				
CEJ = .015"				
CEK = .015"				
CEL = .015"				
CEM = .015"				
CEN = .015"				
CEO = .015"				
CEQ = .015"				
CER = .015"				
CES = .015"				
CET = .015"				
CEU = .015"				
CEV = .015"				
CEW = .015"				
CEX = .015"				
CEZ = .015"				
CEA = .015"				
CEB = .015"				
CEC = .015"				
CED = .015"				
CEE = .015"				
CEF = .015"				
CEG = .015"				
CEH = .015"				
CEI = .015"				
CEJ = .015"				
CEK = .015"				
CEL = .015"				
CEM = .015"				
CEN = .015"				
CEO = .015"				
CEQ = .015"				
CER = .015"				
CES = .015"				
CET = .015"				
CEU = .015"				
CEV = .015"				
CEW = .015"				
CEX = .015"				
CEZ = .015"				
CEA = .015"				
CEB = .015"				
CEC = .015"				
CED = .015"				
CEE = .015"				
CEF = .015"				
CEG = .015"				
CEH = .015"				
CEI = .015"				
CEJ = .015"				
CEK = .015"				
CEL = .015"				
CEM = .015"				
CEN = .015"				
CEO = .015"				
CEQ = .015"				
CER = .015"				
CES = .015"				
CET = .015"				
CEU = .015"				
CEV = .015"				
CEW = .015"				
CEX = .015"				
CEZ = .015"				
CEA = .015"				
CEB = .015"				
CEC = .015"				
CED = .015"				
CEE = .015"				
CEF = .015"				
CEG = .015"				
CEH = .015"				
CEI = .015"				
CEJ = .015"				
CEK = .015"				
CEL = .015"				
CEM = .015"				
CEN = .015"				
CEO = .015"				
CEQ = .015"				
CER = .015"				
CES = .015"				
CET = .015"				
CEU = .015"				
CEV = .015"				
CEW = .015"				
CEX = .015"				
CEZ = .015"				
CEA = .015"				
CEB = .015"				
CEC = .015"				
CED = .015"				
CEE = .015"				
CEF = .015"				
CEG = .015"				
CEH = .015"				
CEI = .015"				
CEJ = .015"				
CEK = .015"				
CEL = .015"				
CEM = .015"				
CEN = .015"				
CEO = .015"				
CEQ = .015"				
CER = .015"				
CES = .015"				
CET = .015"				
CEU = .015"				

SECURITY CLASSIFICATION

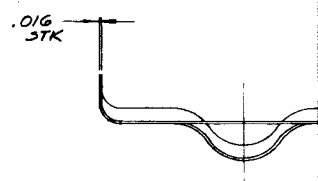
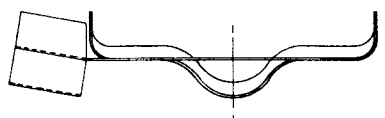
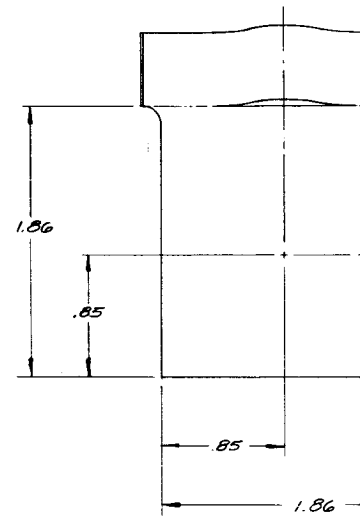
C

B

A



VIEW "A-A"

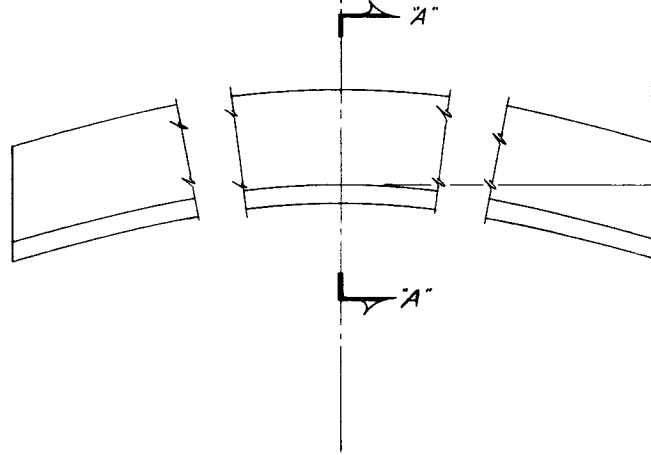
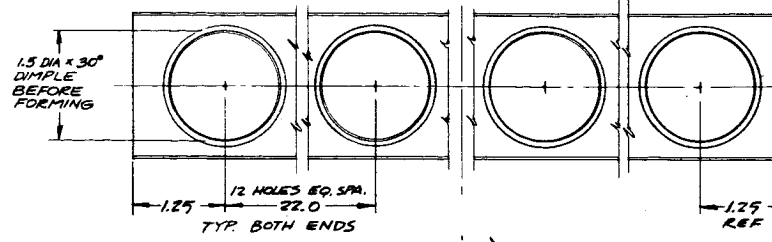


1

3

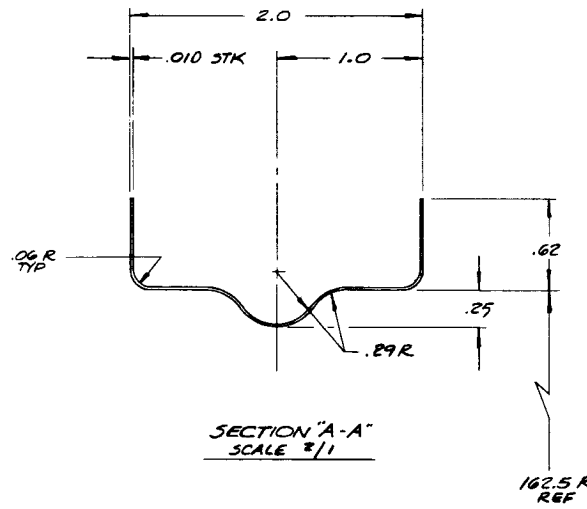
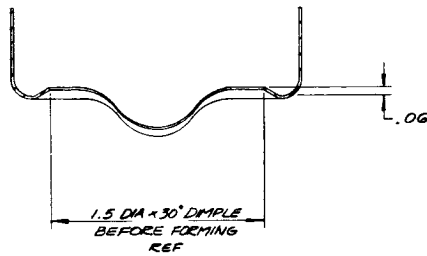
SECURITY CLASSIFICATION

C



B

→

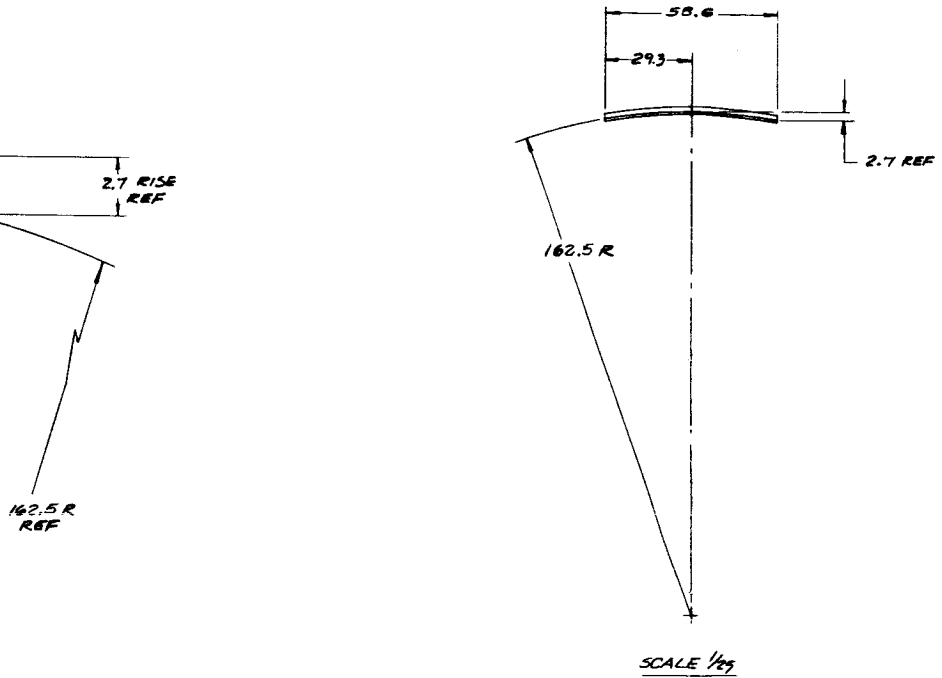


A

1. AFTER FORM
NOTE:

3

REVISIONS				
CHANGE	DATE	DESCRIPTION	BY	APPROVED



1100313 -

			FRAME	SHOWN	6061-T4 AL ALY	Q9-A-327
--	--	--	-------	-------	----------------	----------

LIST OF MATERIALS						
UNLESS OTHERWISE NOTED: 1. LISTED DIMENSIONS IN DECIMALS. 2. VELDRENGTH: 3. MATERIAL: 6061-T4 AL ALY 4. THICKNESS: .030 5. FINISH: .015			DRAWN: LAI 3/9/62 CHECKED: [Signature] APPROVED: [Signature]	ELECTRO-OPTICAL SYSTEMS, INC. Pasadena, California - A Subsidiary of Xerox Corp.	TITLE: FRAME 58.6	QUANTITY CLASSIFICATION: D
THIS DRAWING CONTAINS INFORMATION PROPRIETARY TO ELECTRO-OPTICAL SYSTEMS, INC. IF DISCLOSED MUST BE APPROVED IN WRITING BY THE PERSONNEL OF THIS CORPORATION.			DATE: 3/9/62 SHEET NO.: 12705	PART NO.: 1100313	ALL NOTES: 1 of 1	ORIGINAL APPLICATION

ING, AGE TO "T6" CONDITION.

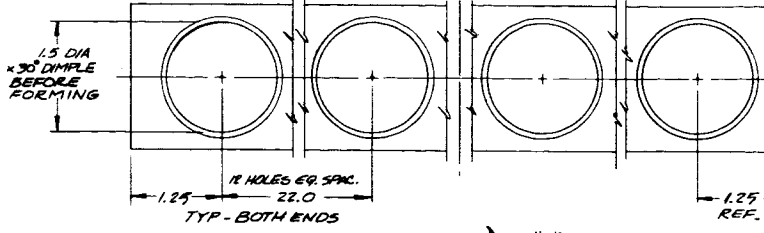
1 W.D. 7028 NAS 7. 928

2

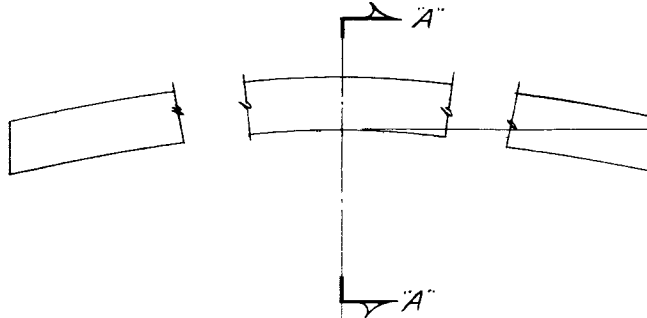
SECURITY CLASSIFICATION

3

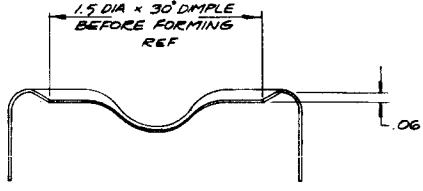
C



.....



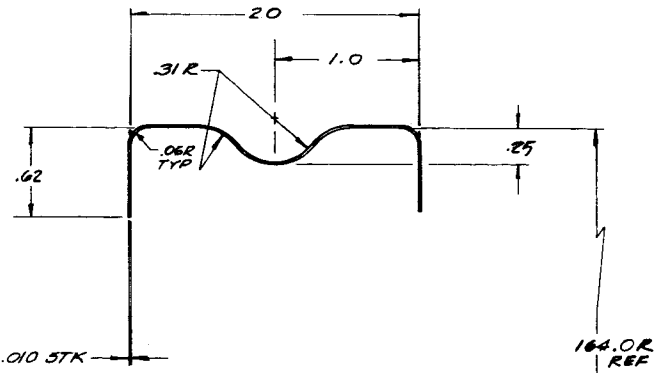
B



→

.....

A



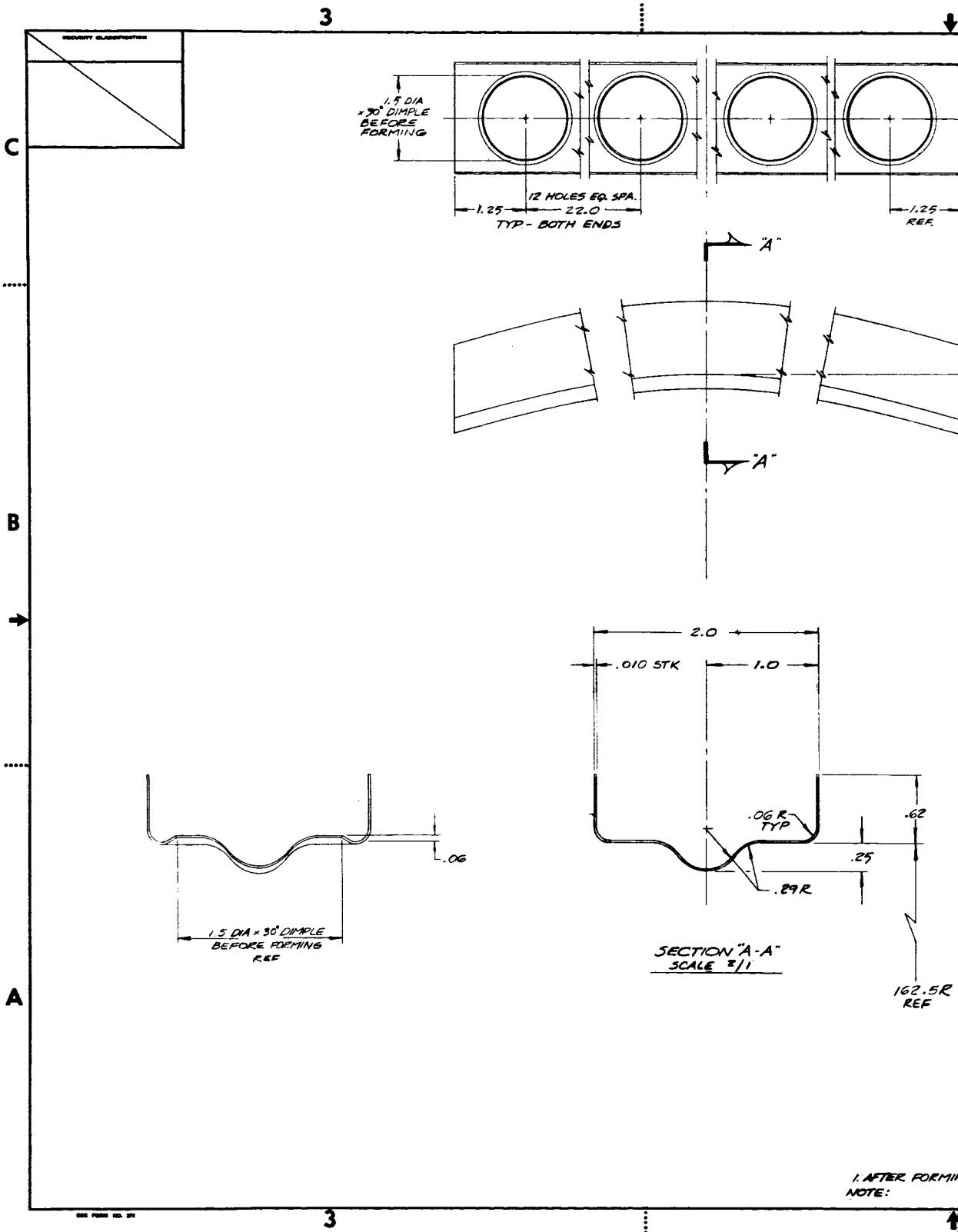
SECTION "A-A"
SCALE 3/1

1. AF
NOTE:

3

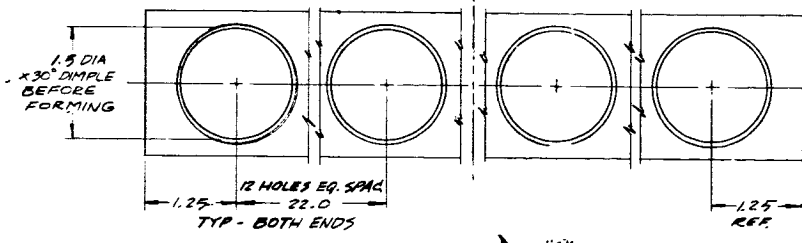
500 FORM NO. 37

1

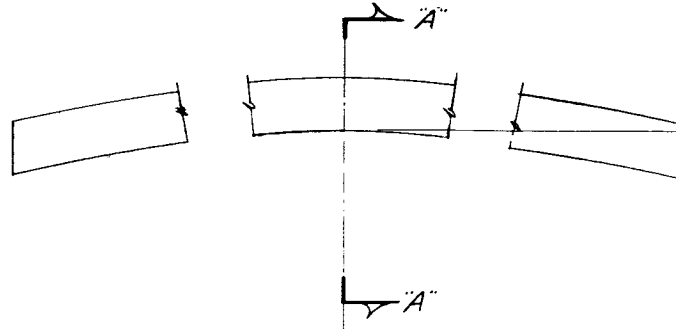


SECURITY CLASSIFICATION

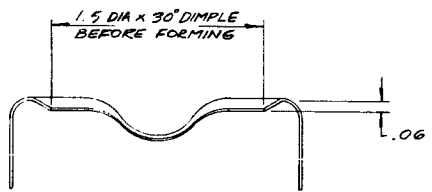
3



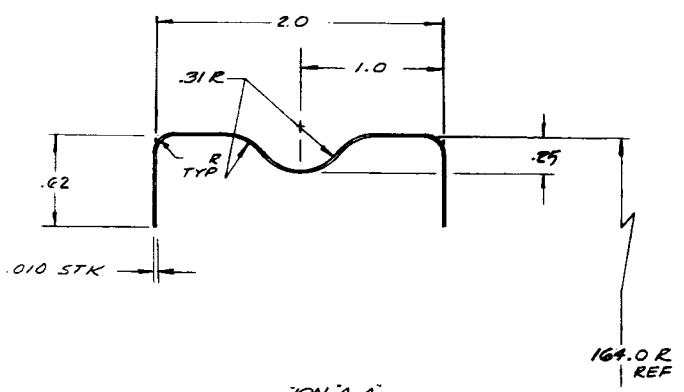
C



B



A



1.0 AFTER NOTE

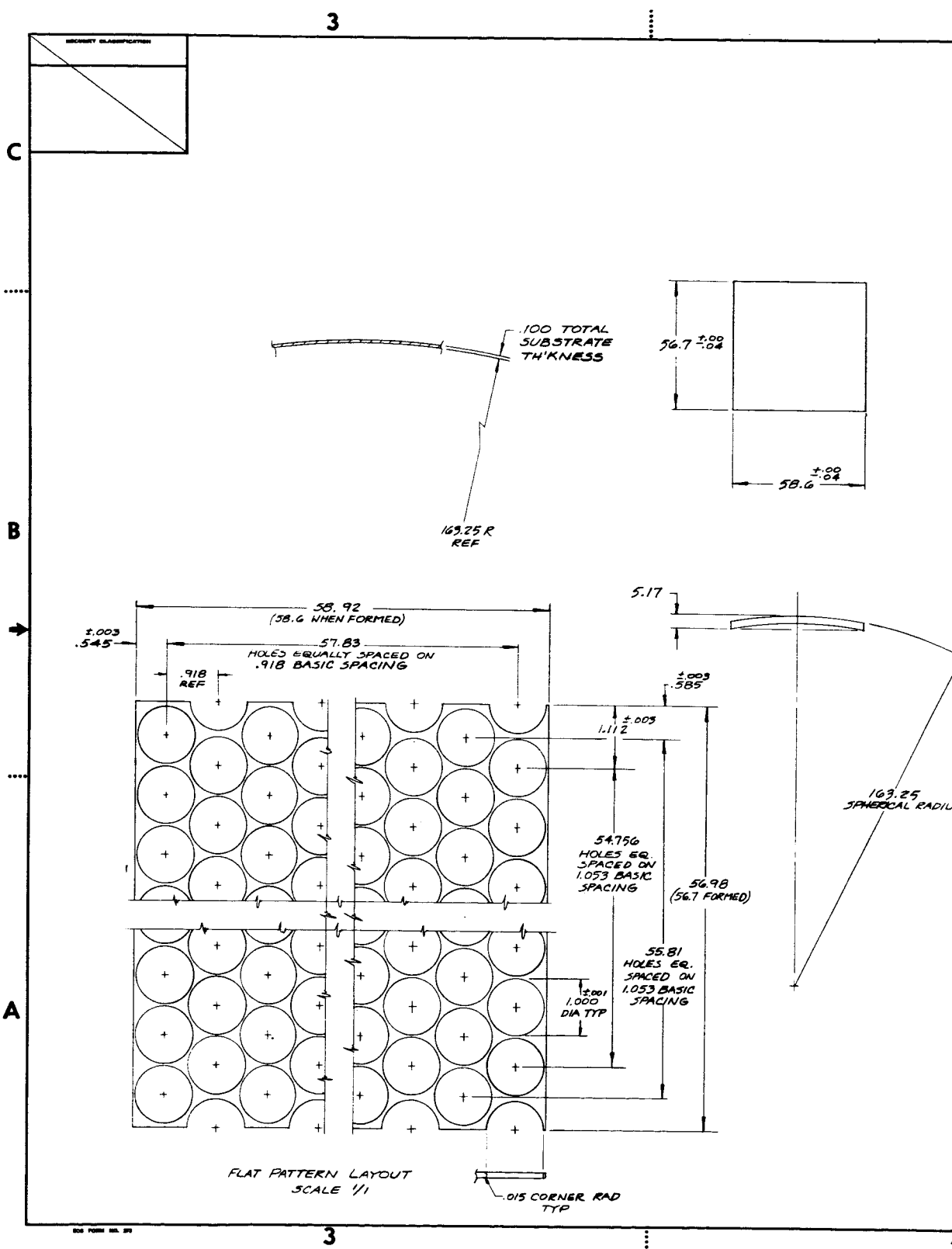
164.0 R REF

1.0 AFTER NOTE

See Form No. 87

3



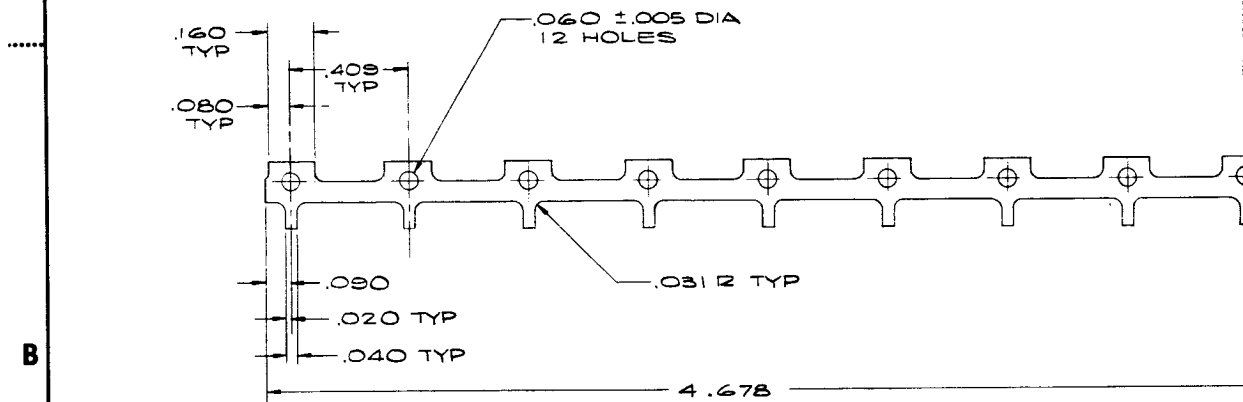


1

3

SECURITY CLASSIFICATION

C



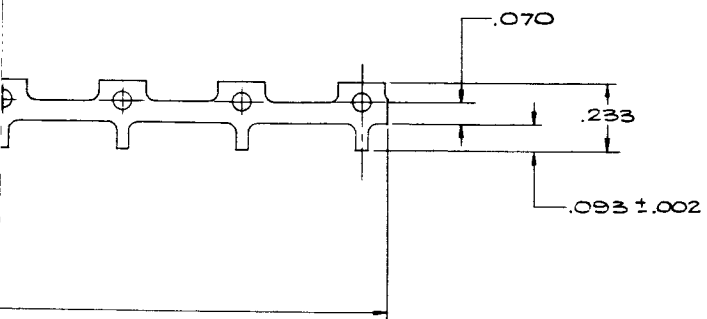
B

A

3

1

REVISIONS					
CHANGE	DATE	DESCRIPTION	BY	CHECKED	APPROVED



C
B
A

1100328

DATE	ITEM	QUANTITY	DESCRIPTION	UNIT	REMARKS
			BUS BAR	.001 THK	MOLYBDENUM SILVER PLATED

UNLESS OTHERWISE NOTED:
 1. LINEAR DIMENSIONS IN DECIMALS.
 2. TOLERANCES:
 DECIMAL FRACTIONS ANGULAR
 X X X X X X X X X X
 DEC X .005

THIS DRAWING REMAINS PROPRIETARY TO ELECTRO-OPTICAL SYSTEMS, INC. IT SHALL NOT BE REPRODUCED, COPIED OR DISCLOSED TO ANYONE WITHOUT THE WRITTEN PERMISSION OF THIS ORGANIZATION.

DATE: 8-5-66
 APPROVED: [Signature]

SECURITY CLASSIFICATION: S
 PART NUMBER: 1100328
 QUANTITY: 4/1

1 W.A. 7027-01-03

2

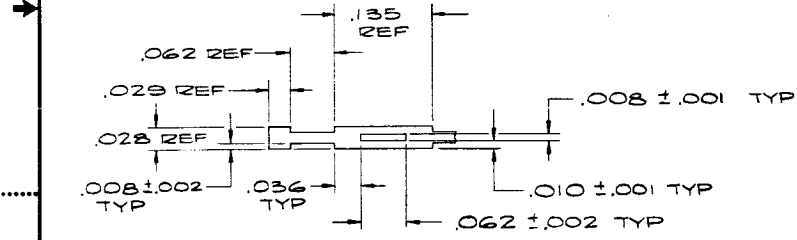
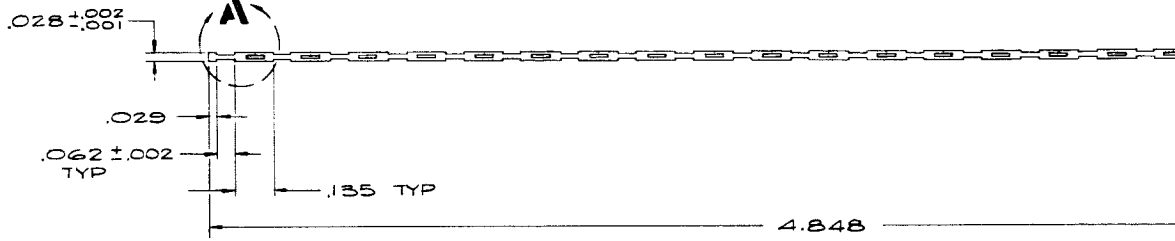
3

SECURITY CLASSIFICATION

C

B

A



DETAIL -A-
SCALE: 10/1

3

808 FORM NO. 272

1

REVISIONS						
CHANGE	DATE	DESCRIPTION	BY	CHECKED	APPROVED	DATE

C

B

A

1100329

QTY	UNIT	DESCRIPTION	QTY	UNIT	DESCRIPTION
		"N" BUS CONNECTION			

QTY	UNIT	DESCRIPTION	QTY	UNIT	DESCRIPTION

UNLESS OTHERWISE NOTED:

1. LISTED DIMENSIONS IN INCHES.

2. TOLERANCES:

 FRACTIONS DECIMALS

 .005 .005

3. THIS DRAWING CONTAINS INFORMATION PROPRIETARY TO ELECTRO-OPTICAL SYSTEMS, INC. IT SHOULD NOT BE REPRODUCED, USED OR DISCLOSED TO ANYONE WITHOUT THE WRITTEN PERMISSION OF THIS CORPORATION.

DATE: 12/7/54
BY: [Signature]

LIST OF MATERIALS

1. QUANTITY: 1

2. DATE: 12/7/54

3. DRAWING: 1100329

4. TITLE: "N" BUS CONNECTION

5. SECURITY CLASSIFICATION: **E**

6. ISSUE: **D**

7. PART NUMBER: 1100329

8. DATE: 12/7/54

9. SHEET: 4/1 OF 4

1

W.A. 7027-01-03

2

SECURITY CLASSIFICATION

3

C

B



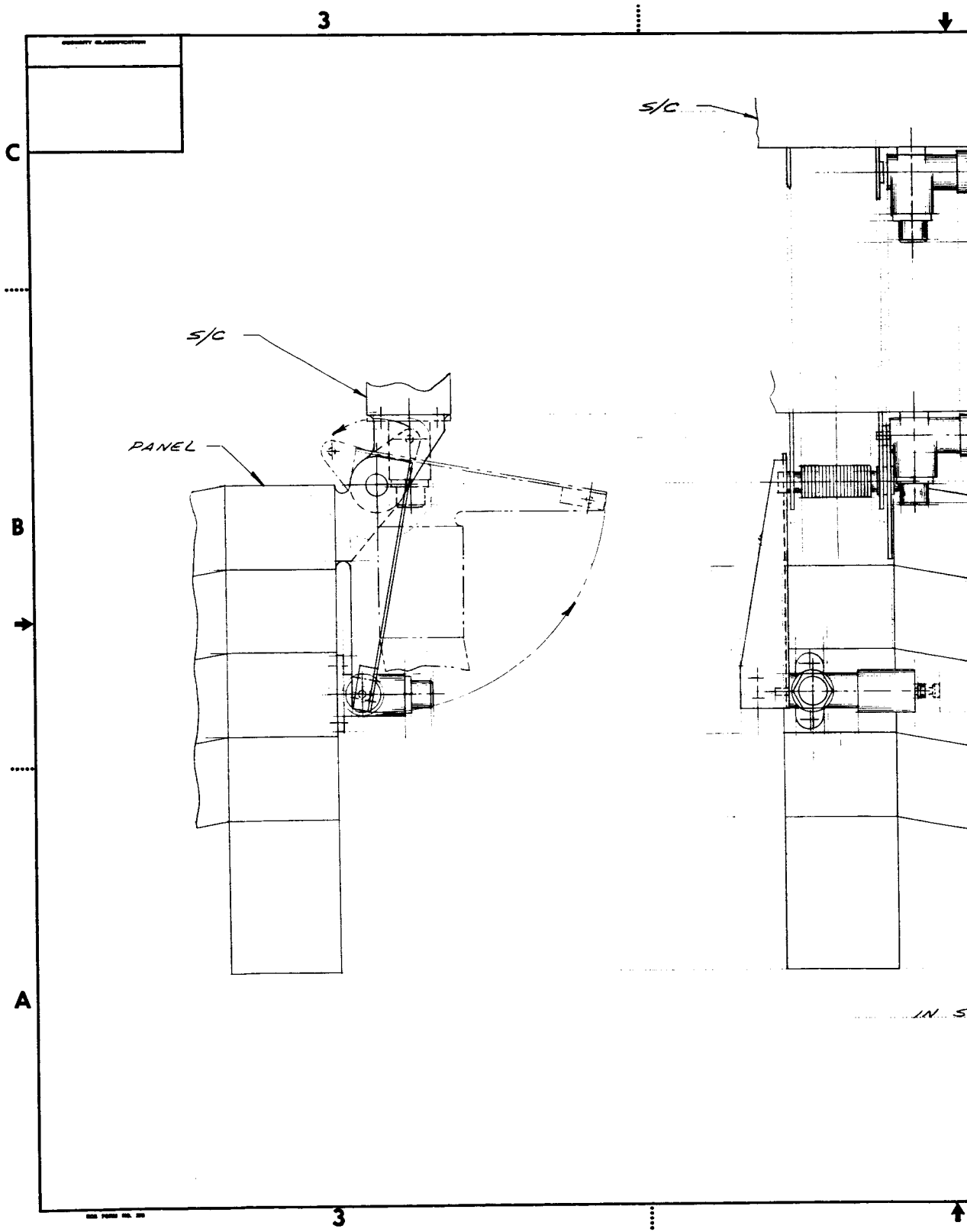
A

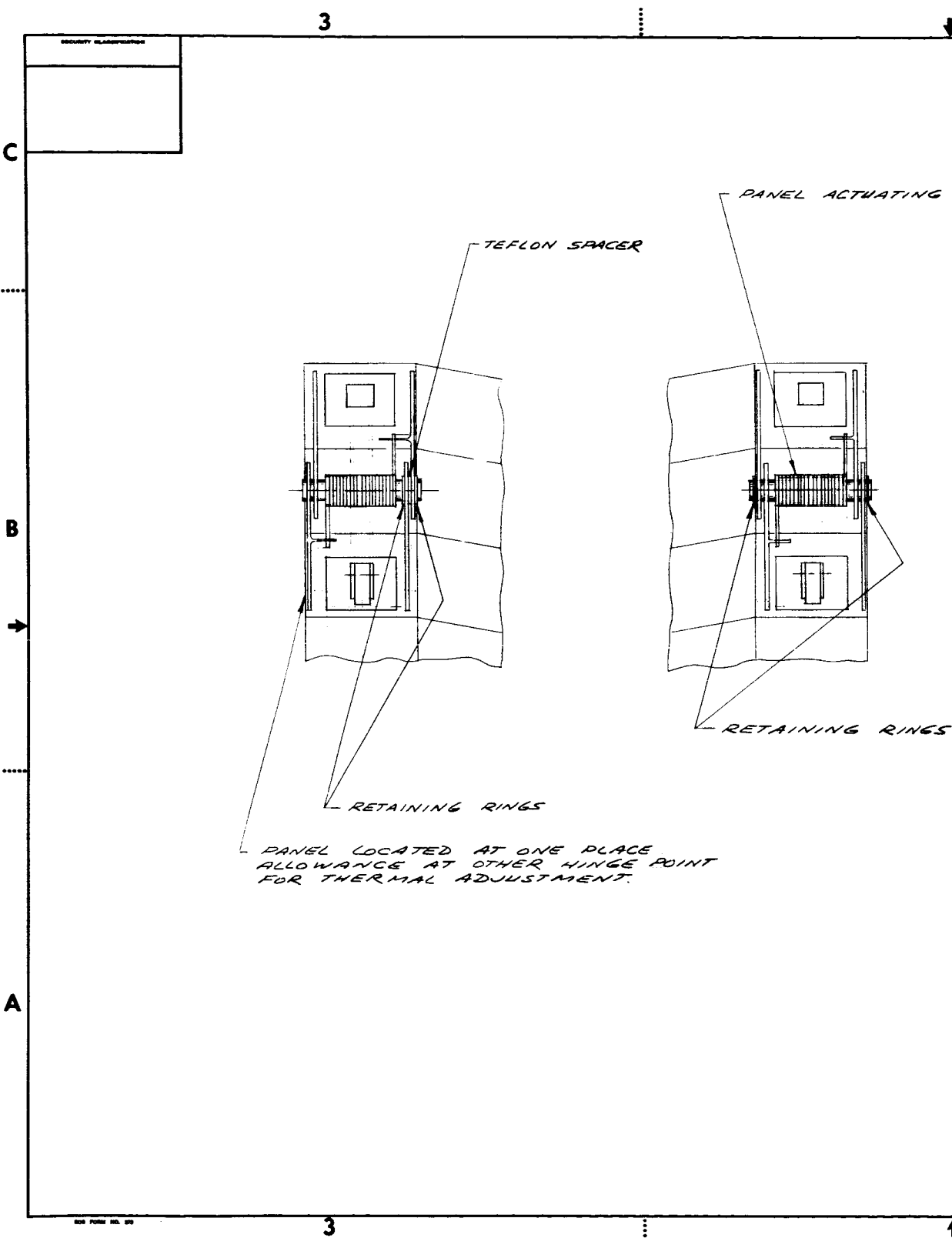
4.738

DD FORM NO. 101

3







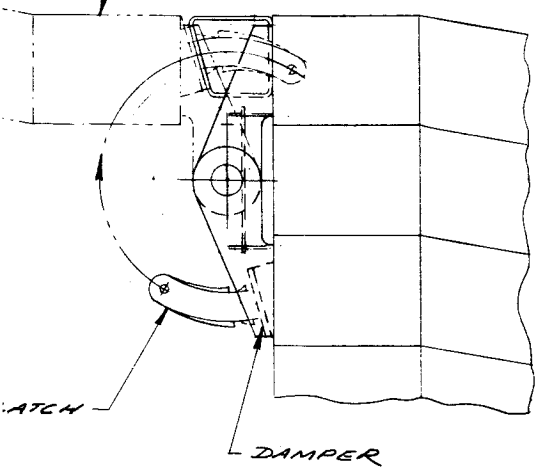
1

1

REVISIONS				
CHANGE	DATE	DESCRIPTION	BY	APPROVED

SPRING

PANEL IN STOWED POSITION



C

B

A

1100340

QTY	UNIT	DESCRIPTION	REVISION	DATE	BY	APPROVED
LIST OF MATERIALS						
UNLESS OTHERWISE NOTED: 1. Length dimensions in inches. 2. Tolerances: DIMENSION FINISHES ALLOWED ± .010 .005 .0025 ± .015 .0075 .00375 ± .020 .010 .0050			DRAWN: <i>UK</i> CHECKED: <i>[Signature]</i> DATE: <i>5/5/66</i>	E ELECTRO-OPTICAL SYSTEMS, INC., Poway, California - A Subsidiary of Xerox Corp. S HINGE CONFIGURATION		
QTY	UNIT	DESCRIPTION	REVISION	DATE	BY	APPROVED
ORIGINAL APPLICATION		SECURITY CLASSIFICATION		DATE	BY	APPROVED
				D	1100340	
				12705		

W.O. 7027 NAS 7-428

2

3

SECURITY CLASSIFICATION

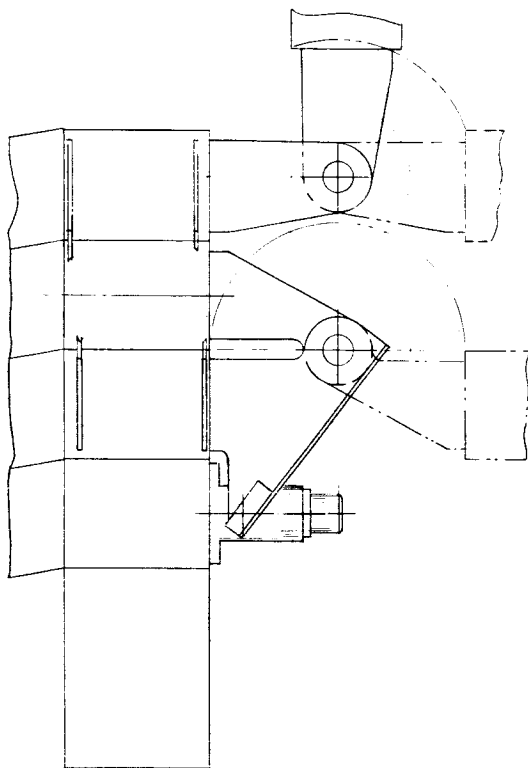
C

RETAINING RINGS

B



A

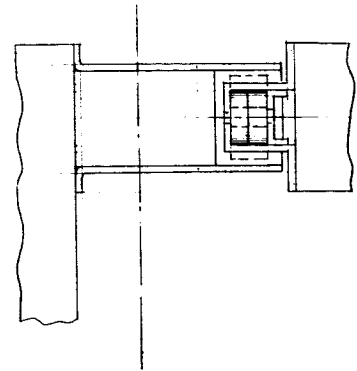


1

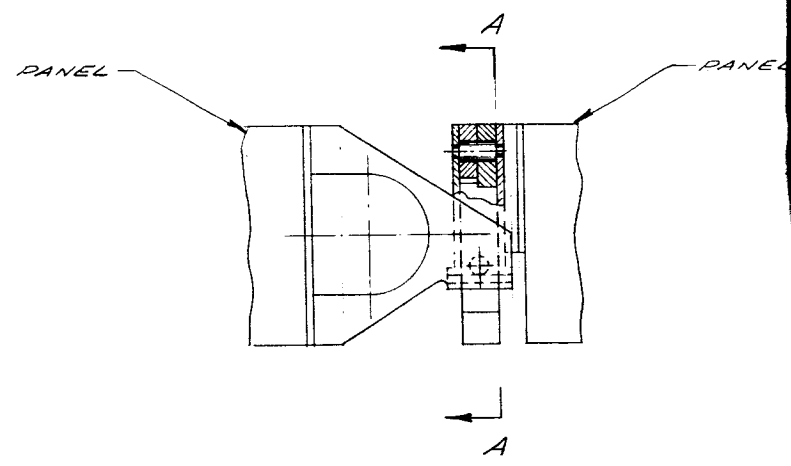
3

SECURITY CLASSIFICATION

C



B



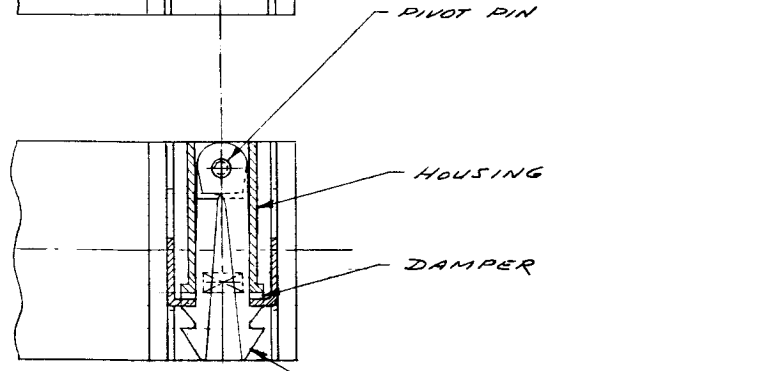
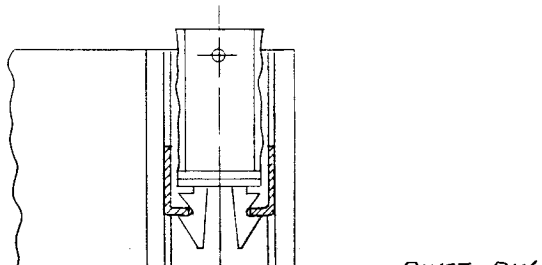
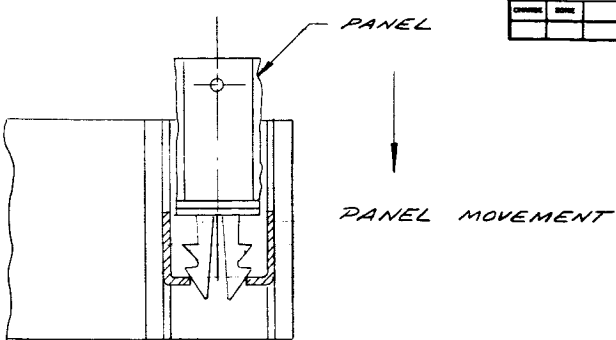
A

DD FORM NO. 12

3

1

REVISIONS				
CHANGE	DATE	DESCRIPTION	BY	APPROVED



IN STOWED POSITION

SECTION A-A

REV	DATE	DESCRIPTION	BY	APPROVED

DRAWN		CHECKED		DATE		BY		APPROVED	

LIST OF MATERIALS									
UNLESS OTHERWISE NOTED:					E				
1. LARGEST DIMENSION IN INCHES					S				
2. TOLERANCES:					ELECTRO-OPTICAL SYSTEMS, INC.,				
					Pasadena, California - A Subsidiary of Keros Corp.				
					PART NO. 1100342				
					TITLE PANEL LATCH				
					REV. D				
					1100342				
					12705				
					3/1				
					1 of 1				

1 N.O. 7027 NAS 7.428

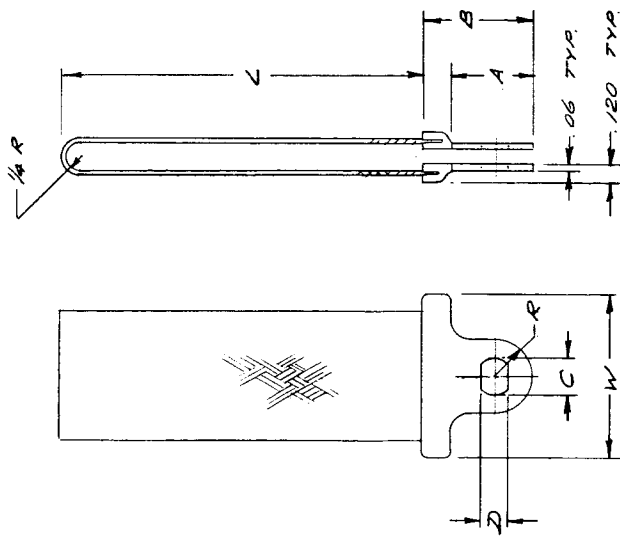
2

REVISIONS			
NO.	DATE	BY	DESCRIPTION

AMPS	WIRE SIZE	LENGTH	WIRE TYPE
6.25	18.75	1875	CIRCULAR MILS
12.5	"	3750	"
18.75	"	5625	"
50	"	15000	"

PART	A	B	C	D	R	W
-1	.625	1/4	.251	.187	.312	1
-2	.750	1/2	.253	.234	.375	1/2

1100344



TUBULAR WEAVE FLATTENED.
 TERMINAL CONTACT AREA TO BE
 FREE FROM SCALE OR DITS AND
 METAL FINISH BRIGHT.
 MATERIAL: TINNED COPPER.

REV.	DATE	BY	DESCRIPTION

UNLESS OTHERWISE NOTED:	
1.	Unless otherwise noted, all dimensions are in inches.
2.	Unless otherwise noted, all tolerances are ± .005.
3.	Unless otherwise noted, all surfaces are to be smooth.
4.	Unless otherwise noted, all surfaces are to be tinned copper.
5.	Unless otherwise noted, all surfaces are to be bright.

LIST OF MATERIALS	
ITEM NO.	DESCRIPTION
1	TUBULAR WEAVE FLATTENED
2	TERMINAL CONTACT AREA TO BE FREE FROM SCALE OR DITS AND METAL FINISH BRIGHT
3	MATERIAL: TINNED COPPER

REV.	DATE	BY	DESCRIPTION

ELECTRO-OPTICAL SYSTEMS, INC.	
Pasadena, California - A Subsidiary of Avco Corp.	
ITEM NO.	1100344
REV.	C
DATE	12705
BY	